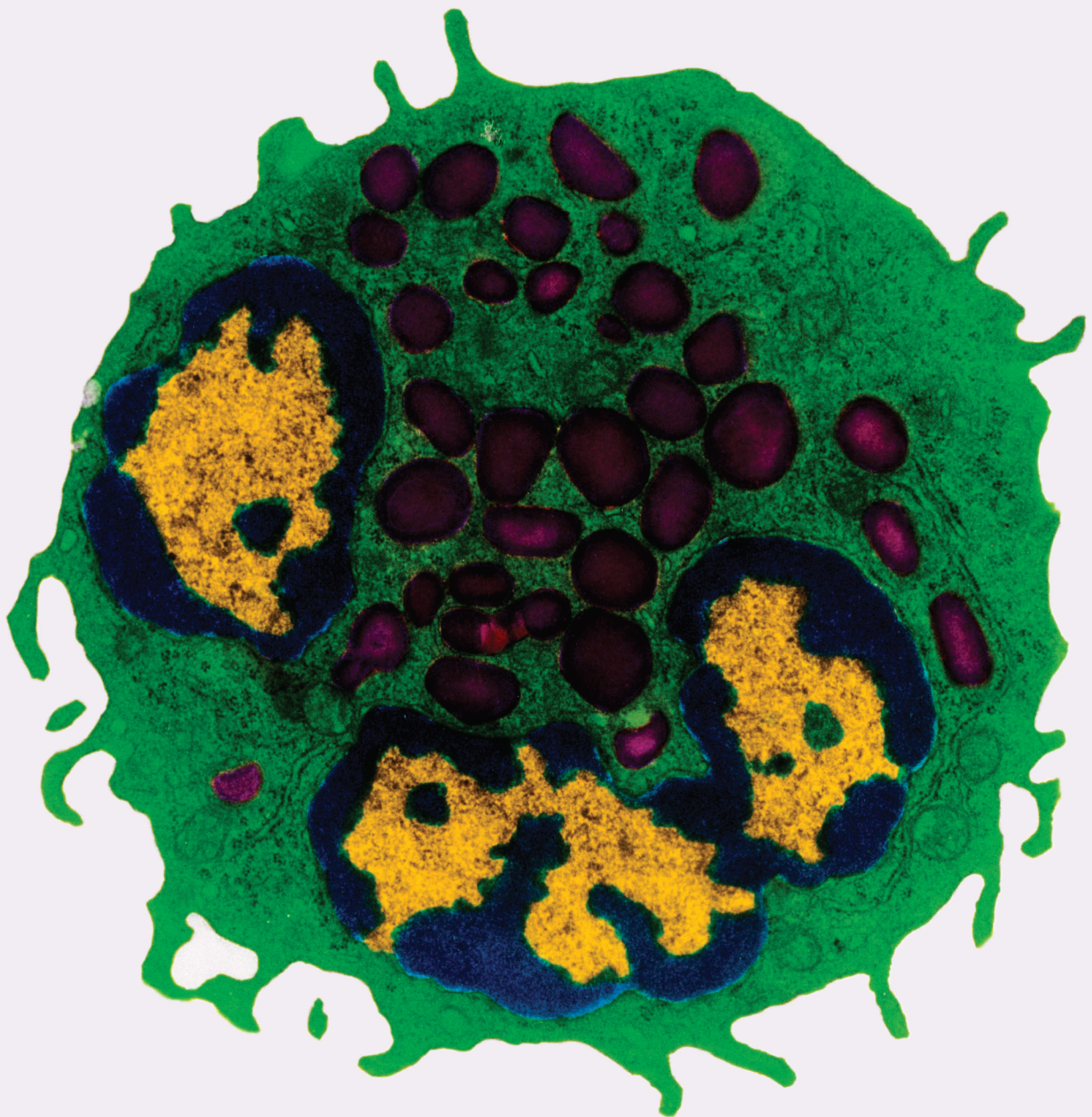# Inflammatory Mediators in Musculoskeletal Disorders

Lead Guest Editor: Wenyuan Ding
Guest Editors: Guoyong Yin, Shibao Lu, Sidong Yang, and Xiaolong Chen

Inflammatory Mediators in Musculoskeletal Disorders

Inflammatory Mediators in Musculoskeletal Disorders

Lead Guest Editor: Wenyuan Ding
Guest Editors: Guoyong Yin, Shibao Lu, Sidong Yang, and Xiaolong Chen

Contents

Research Article

PLCG2 and IFNAR1: The Potential Biomarkers Mediated by Immune Infiltration and Osteoclast Differentiation of Ankylosing Spondylitis in the Peripheral Blood

Bo Han [iD],[1,2,3,4] **Qiaobo Xie** [iD],[2,5,6] **Weishi Liang,**[1,2,3,4] **Peng Yin,**[1,2,3,4] **Xianjun Qu** [iD],[2,5] and **Yong Hai** [iD][1,2,3,4]

[1]*Department of Orthopedics, Beijing Chao-Yang Hospital, Capital Medical University, GongTiNanLu 8#, Chao-Yang District, Beijing 100020, China*
[2]*Joint Laboratory for Research and Treatment of Spinal Cord Injury in Spinal Deformity, Capital Medical University, Beijing, China*
[3]*Clinical Center for Spinal Deformity, Capital Medical University, Beijing, China*
[4]*Department of Orthopaedics, Capital Medical University, Beijing, China*
[5]*Department of Pharmacology, School of Basic Medical Sciences, Capital Medical University, Beijing, China*
[6]*Capital Institute of Pediatrics, Beijing 100020, China*

Correspondence should be addressed to Xianjun Qu; qxj@ccmu.edu.cn and Yong Hai; yong.hai@ccmu.edu.cn

Bo Han and Qiaobo Xie contributed equally to this work.

Objectives. Ankylosing spondylitis (AS) is a chronic inflammatory rheumatic disease characterized by chronic spinal inflammation, arthritis, gut inflammation, and enthesitis. We aimed to identify the key biomarkers related to immune infiltration and osteoclast differentiation in the pathological process of AS by bioinformatic methods. *Methods.* GSE25101 from the Gene Expression Omnibus was used to obtain AS-associated microarray datasets. We performed bioinformatics analysis using R software to validate different expression levels. The purpose of the GO and KEGG enrichment analyses of DEGs was to exclude key genes. Using weighted correlation network analysis (WGCNA), we examined all expression profile data and identified differentially expressed genes. The objective was to investigate the interaction between genetic and clinical features and to identify the essential relationships underlying coexpression modules. The CIBERSORT method was used to make a comparison of the immune infiltration in whole blood between the AS group and the control group. The WGCNA R program from Bioconductor was used to identify hub genes. RNA extraction reverse transcription and quantitative polymerase chain reaction were conducted in the peripheral blood collected from six AS patients and six health volunteers matched by age and sex. *Results.* 125 DEGs were identified, consisting of 36 upregulated and 89 downregulated genes that are involved in the cell cycle and replication processes. In the WGCNA, modules of MCODE with different algorithms were used to find 33 key genes that were related to each other in a strong way. Immune infiltration analysis found that naive CD4+ T cells and monocytes may be involved in the process of AS. PLCG2 and IFNAR1 genes were obtained by screening genes meeting the conditions of immune cell infiltration and osteoclast differentiation in AS patients among IGF2R, GRN, SH2D1A, LILRB3, IFNAR1, PLCG2, and TNFRSF1B. The results demonstrated that the levels of PLCG2 mRNA expression in AS were considerably higher than those in healthy individuals ($P = 0.003$). IFNAR1 mRNA expression levels were considerably lower in AS than in healthy individuals ($P < 0.0001$). *Conclusions.* Dysregulation of PLCG2 and IFNAR1 are key factors in disease occurrence and development of AS through regulating immune infiltration and osteoclast differentiation. Explaining the differences in immune infiltration and osteoclast differentiation between AS and normal samples will contribute to understanding the development of spondyloarthritis.

1. Introduction

Ankylosing spondylitis (AS), as a subtype of spondyloarthritis [1], is a chronic inflammatory rheumatic disease that is characterized by chronic spinal inflammation, arthritis, gut inflammation, and enthesitis [2]. Patients with fixed and kyphotic deformities caused by AS may face the problems such as impaired horizontal gaze, severe neck pain, and

TABLE 1: Patients' information and specimens' source of GSE25101.

| | Patient information | | | | Source of specimen | |
| | Age (years, mean $\pm$ SD) | Sex | | Family history | Tissue | Cell type |
		Male	Female			
AS patients ($n = 18$)	45.9 ± 12.9	10	8	5	Whole blood	PBMC
AS control ($n = 16$)	NA	NA	NA	NA	Whole blood	PBMC

sagittal imbalance [3]. A combination of multistep surgery and digital planning is often required in complex AS deformities, which is a real challenge for spine surgeons [4]. AS is a considerable burden to patients and society because of deformity, pain, and disability [5].

Although the exact etiology and pathogenesis of AS are still unknown, mainly five hypotheses, including arthritogenic peptides, an unfolded protein response, human leucocyte antigen (HLA)-B27, homodimer formation, malfunctioning endoplasmic reticulum aminopeptidases, gut inflammation, and dysbiosis to explain the pathogenesis exist [6]. Genetic studies suggest that genetic factors account for about 90% of the pathogenesis of AS, and the genetic risk factors involved are major histocompatibility complex (MHC) and non-MHC gene loci [7]. Numerous studies have also shown that immune cell and osteoclast differentiation were crucial mechanisms and findings in the pathogenesis of AS [8–10].

Many studies focused on the key genes in the progression of AS by integrated bioinformatics analysis. However, there is no bioinformatics analysis related to the immune infiltration and osteoclast differentiation to analyze the function and regulation of differential genes. Hence, we conducted this investigation to identify the main biomarkers associated with immune infiltration and osteoclast development in the pathological process of AS utilizing bioinformatic techniques.

2. Materials and Methods

2.1. Data Download. In our study, microarray data were retrieved from the Gene Expression Omnibus database (https://www.ncbi.nlm.nih.gov/geo/) [11] by using keywords "spondylitis, ankylosing" (All Fields) OR "Ankylosing Spondylitis" (all fields). The GPL6947 Illumina HumanHT-12 V3.0 expression bead chip serves as the foundation for this dataset. This chip comprises a total of 32 samples split between two groups. Under the comprehensive consideration, we finally selected GSE25101 as the research object. Patients' information and specimens' source of GSE25101 were outlined in Table 1. The dataset was obtained using R's "GEOquery" package (3.6.3) [12]. The workflow is shown in Figure 1.

2.2. Differential Expression Analysis. The "limma" package was applied to standardize and analyze patient and control data differences [13]. Differentially expressed genes (DEGs) were selected using the Benjamini–Hochberg adjusted P value <0.05.

2.3. Functional Annotation of DEGs. Gene ontology (GO) terms include biological process (BP), cellular component (CC), and molecular function (MF). The false discovery rate (FDR) <0.05 was significantly enriched. To reveal the
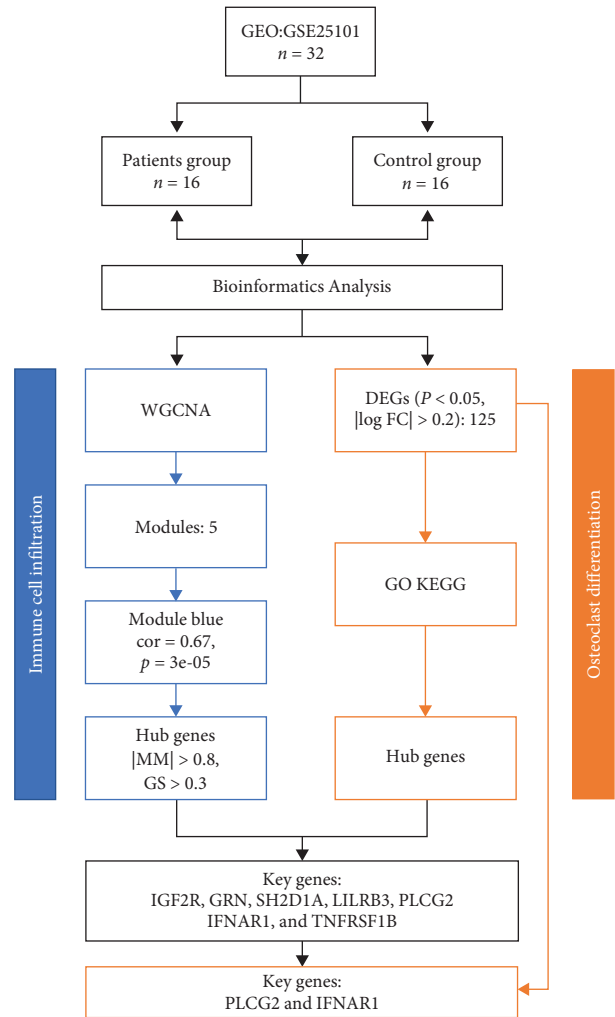
FIGURE 1: A flow-process chart shows the analysis steps in this study.

function of the network, the "clusterProfiler" packages were used to perform GO and Kyoto Encyclopedia of Genes and Genomes (KEGG) analyses [14].

2.4. Construction of Weighted Gene Coexpression Network Analysis (WGCNA). WGCNA is a systems biology approach that detects patterns of genetic linkage between diverse samples. Based on connectedness and relationship between genomes and phenotypes, it can reveal highly synergistic genomes, alternative biomarker genes, or therapeutic targets [15]. The "hclust" function was initially employed for hierarchical clustering analysis. Then, during module creation, we applied "pickSoftThreshold" to filter the soft thresholds and select the right power levels. To create the coexpression

TABLE 2: PCR primers.

Gene	Forward primer sequence	Reverse primer sequence
IFNAR1	5′-TGTCCGCAGCCGCAGGTG-3′	5′-CCCGACAGACTCATCGCTCCTG-3′
PLCG2	5′-GGACATAGAGCTGGCTTCCC-3′	5′-GTTCAGTTCTTCTTGCCGCC-3′
Actin	5′-ACCGCGAGAAGATGACCCA-3′	5′-GGATAGCACAGCCTGGATAGCAA-3′

network, we employ the "WGCNA" program. Label each module with a distinct color, and then filter out the modules with the most interconnections. Using the "clusterProfiler" program and Metascape [16] (http://metascape.org), GO and KEGG analyses were performed on the genes in the modules. The screening criteria for crucial genes were gene significance (GS) > 0.70 and module membership (MM) > 0.80. We intersected the pivotal genes obtained from WGCNA with DEGs associated with osteoclast differentiation to obtain the essential genes. These genes make a significant contribution to the progression of AS.

2.5. Immune Infiltration Analysis. The immune cell infiltration matrix was produced by uploading gene expression profile data to CIBERSORT (https://cibersort.stanford.edu/) [17]. To visualize the differences in immune cell infiltration between control and patient groups, two-dimensional PCA clustering maps and violin plots were generated using the "ggplot2" software package. Heat maps of 22 infiltrating immune cells were generated using "pheatmap" (version 1.0.8) software [18]. Finally, differences in immune cell infiltration between the high and low-expression groups were analyzed and visualized according to the median expression levels of key genes.

2.6. RNA Extraction and Reverse Transcription and Quantitative Real-Time Polymerase Chain Reaction (qRT-PCR). The peripheral blood was collected from six AS patients and six health volunteers matched by age and sex at the Beijing Chaoyang Hospital, Capital Medical University.

The inclusion criteria were as follows: (1) the patient was diagnosed with AS, (2) the age of patients ranging from 18 to 35-year old, (3) without osteoporosis or osteopenia, (4) early stage of the AS disease, (5) not associated with infectious diseases, and (6) the patient agrees and signs the informed consent form; The exclusion criteria were as follows: (1) medication was started, (2) with other rheumatic immune diseases, (3) with other chronic diseases, (4) with cancer in any system, (5) history of orthopedic surgery and diseases, and (6) no definite diagnosis of AS. All human specimens were acquired under the approval of the institutional review board of Beijing Chaoyang Hospital, Capital Medical University (2017-KE-67, Beijing, China). Under the guidance of the World Medical Association Declaration of Helsinki, we obtained informed consent from each patient.

The RNAprep Pure Hi-Blood Kit (Tiangen Biotech, China) was used to perform the reverse transcription of the extracted RNA. Using Nanodrop, the purity and amount of isolated RNA were evaluated. (Thermo Fisher Scientific, USA). cDNA was synthesized using reverse transcriptase (TIANGEN, Beijing, China). On an ABI 7500 Real-Time PCR System (Applied Biosystems), the SYBR Green Real-time PCR Master Mix (TOYOBO, Japan) was employed for quantitative PCR of hub genes. β-Actin was utilized as an internal control. All the primers

(Sangon, China) used in this study are listed in Table 2. Normalization and calculation of relative mRNA expression were accomplished using the comparative Ct method ($2^{-\Delta\Delta Ct}$). The data are shown as a fold change in expression relative to normal tissue. Comparisons were carried out through a one-way ANOVA, and $P < 0.05$ indicated that there were statistically significant differences.

2.7. Statistical Analysis. R software (3.6.3) was utilized to carry out the statistical analysis. Mean ± standard deviation (SD) was calculated for each and every set of numbers. Using the "limma" software tool, the difference in DEGs between control and the patients' groups were determined.

3. Results

3.1. Research Design Summary. Figure 1 shows the study's flowchart. Having screened for DEGs in AS using microarray data from the GEO database, we then screened for immune cells linked with AS using CIBERSORT. WGCNA and related techniques were utilized to identify genes focused on immune cells. The relationship between central gene expression and the clinical characteristics of AS was demonstrated using qRT-PCR.

3.2. DEGs between the Patients and Control Groups. The data on the expression profiles of the patients and the control group were compared and screened using a threshold of P less than 0.05 and a |logFC| value <0.2. We acquired a total of 125 DEGs, 36 of which were upregulated and 89 of which were downregulated among the genes (Figure 2(a)).

3.3. Enrichment Analysis of DEGs. The KEGG data revealed the enriched pathways for the related genes (Figure 2(b)). The findings of the GO analysis revealed that the DEGs were primarily abundant in BPs (Figure 2(c)). Intracellular transport, cellular macromolecule localization, the biological process involved in symbiotic interaction, and cell activation involved in immune response were among the substantially enriched BP keywords for the DEGs. Catalytic complex, nuclear protein-containing complex, and ribonucleoprotein complex were among the significantly enriched CC keywords for the DEGs (Figure 2(d)). Among the significantly enriched MF keywords for the DEGs, enzyme binding, RNA binding, and transcription factor binding were outlined as the first three (Figure 2(e)).

3.4. Immune Microenvironment Characteristics of AS. To gain a more comprehensive understanding of the immune environment present in AS, distinct immune cell types were analyzed using the CIBERSORT technique. After deleting cells with an immunological abundance value of "0," the results showed that 17 different types of immune cells were examined, and it was found that the levels of naive CD4+ T cells and Monocytes were considerably higher in AS ($P < 0.05$; Figure 3(a)). Further

(a)

(b)

(c)

(d)

FIGURE 2: Continued.

–log10 (FDR)

(e)

FIGURE 2: Functional annotation of DEGs. (a) DEGs were identified using a volcano plot, where red represents upregulated genes and blue represents downregulated genes. (b) KEGG pathway enrichment analysis for DEGs. (c–e) GO analysis of DEGs in (c) BP, (d) CC, and (e) MF.

research into the CIBERSORT scores revealed a strong positive association between B cells, Tregs, and M2 macrophages. This was illustrated by the correlation-based heatmap (corheatmap), which can be found in Figure 3(b). On the other hand, the infiltration of CD4+ T cells, NK cells, and M0 macrophages was found to relate to one another negatively. Together, as part of a joint process, the aberrant infiltration of immune cells seen in AS might have particular guiding relevance in the clinical management of the condition.

3.5. Identification of Immune Cell-Related Genes.
The WGCNA was applied to identify differentially expressed immune cell-related genes and explore the network's phenotype and hub genes (Figure 4(a)–4(c)). Twenty-five genes were selected by the correlation test. Cytoscape was used to create the interaction network that was comprised of these 25 genes as well as the genes that they were targeting. The WGCNA hub

genes were intersected. Different colors were then used to differentiate these DEGs (Figures 4(b) and 4(c)). One of the four gene modules we assessed was tightly connected with immune cells (Figure 4(c)). The blue module had a strong positive correlation of 0.67 with naive CD4+ T cells, and $P < 0.001$ (Figure 4(d)). Based on the selection of the 30 most significantly elevated genes and the 33 most important genes, heat maps were generated (Figure 4(e)).

3.6. The Identification of Candidate Biomarkers.
Twenty-five different gene modules were obtained due to the creation of the coexpression matrix (Figure 4(d)). Twelve genes satisfied the preselection criteria and were chosen based on relevant tests (Figures 5(a) and 5(b)). Finally, IGF2R, GRN, SH2D1A, LILRB3, IFNAR1, PLCG2, and TNFRSF1B were identified as key genes. After that, as depicted in Figures 5(c) and 5(d), we utilized metascape to collect more information on these
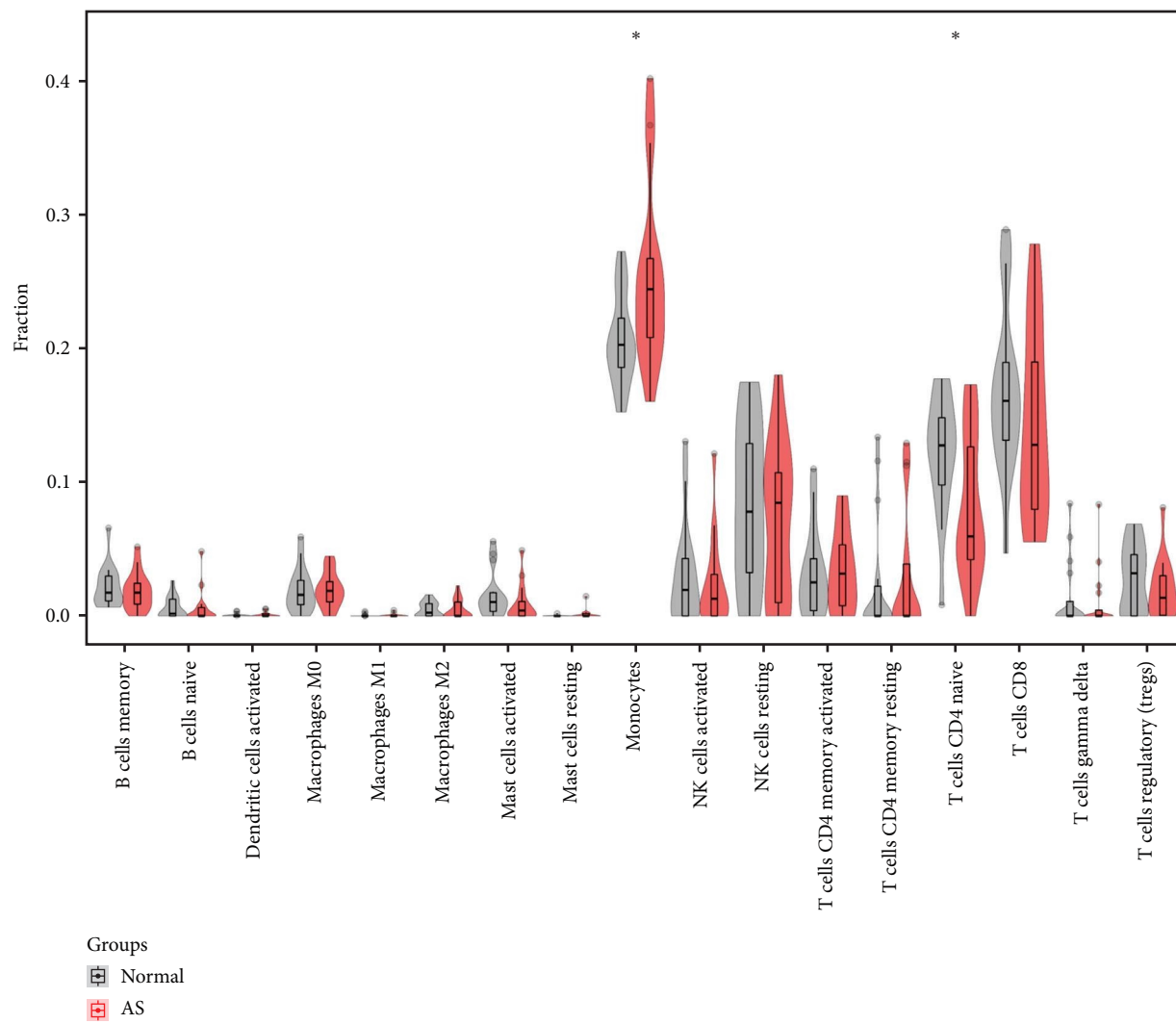
(a)

FIGURE 3: Continued.

(b)
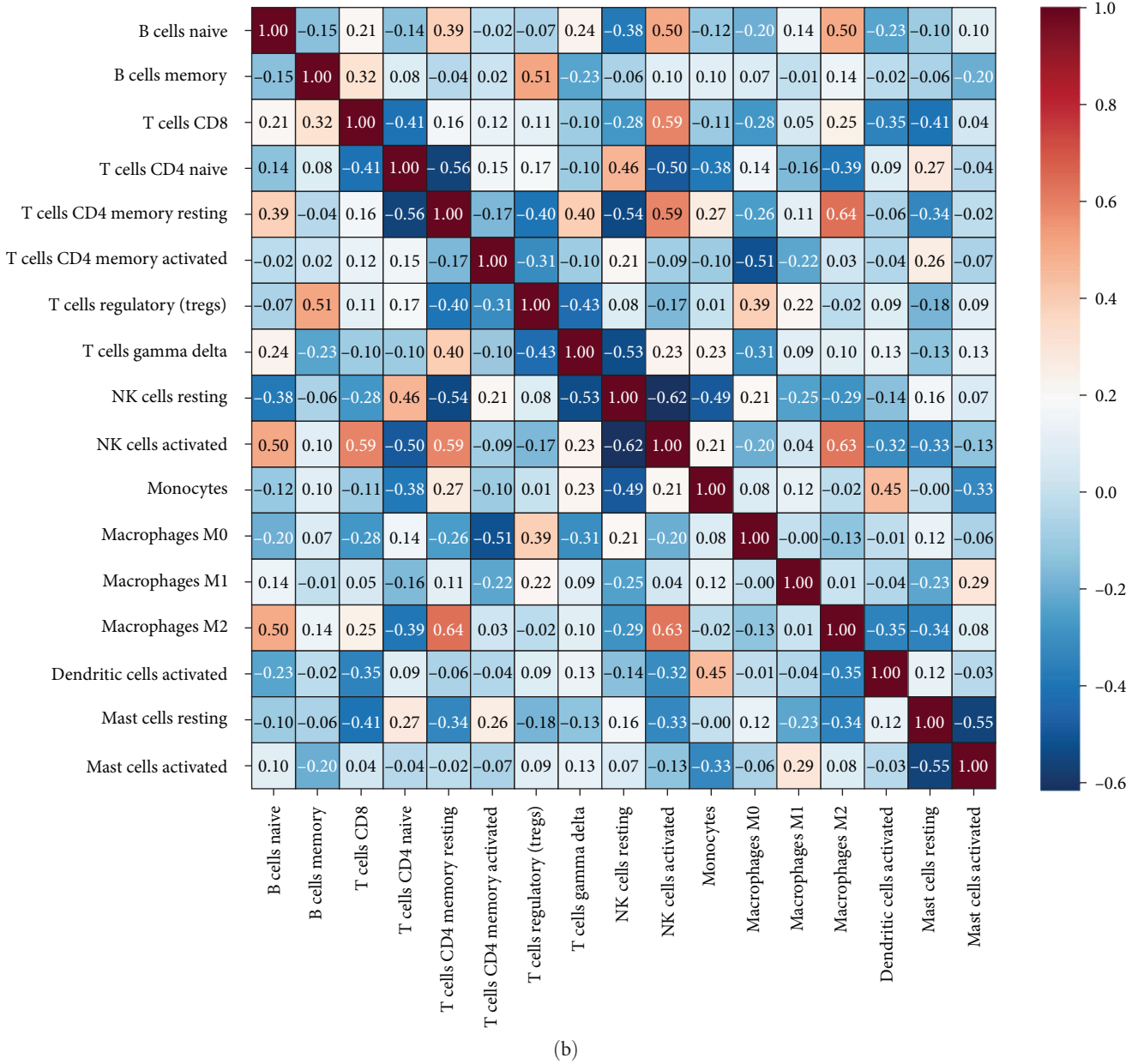
FIGURE 3: Immune infiltration landscape in whole blood. (a) Immune infiltration differences between patients and control group. (b) Correlation matrix of 22 immune cell type proportions. Some of the immune cells had a negative relation, denoted by the color blue, while others had a positive relation, represented by the color red. Compared to the lighter color, the association was much more robust ($P < 0.05$).

genes and analyze their functions. Genes were enriched in essential biological processes, such as inflammatory response, chemokine signaling pathway, cytokine-mediated signaling pathway, regulation of neuroinflammatory response, leukocyte migration, and natural killer cell-mediated cytotoxicity.

According to the findings, most of the genes significantly enriched in pathways associated with immune response were the blue module.

We intersected the hub genes screened by WGCNA and the genes in osteoclast differentiation and obtained two genes: IFNAR1 and PLCG2.

3.7. qRT-PCR Validation of Data. qRT-PCR experiments were performed to verify the bioinformatics results. The

characteristics of patients and healthy volunteers are shown in Table 3. The results revealed that the mRNA expression levels of PLCG2 in AS were significantly higher than that in the normal person ($P = 0.003$). The mRNA expression levels of IFNAR1 in AS were significantly lower than that in the normal person ($P < 0.0001$). All of the above results indicate that the outcomes of bioinformatics analysis are very competent and have considerable research value. (Figures 6(a) and 6(b)).

4. Discussion

AS is a common chronic inflammatory autoimmune disease in which axial inflammation, bone destruction, and new bone formation are the key events [19]. From 2005 to 2019

Sample clustering to detect outliers

(a)

Cluster Dendrogram

(b)

Module–trait relationships

(c)
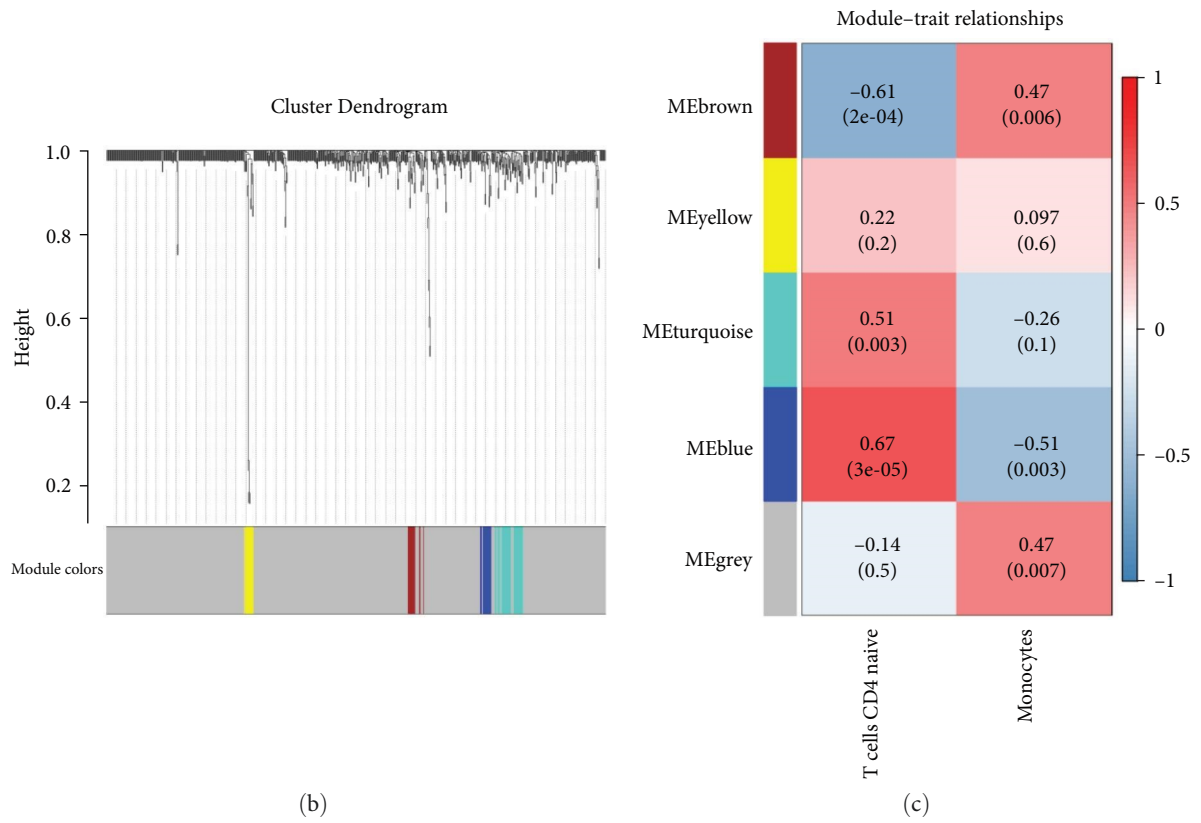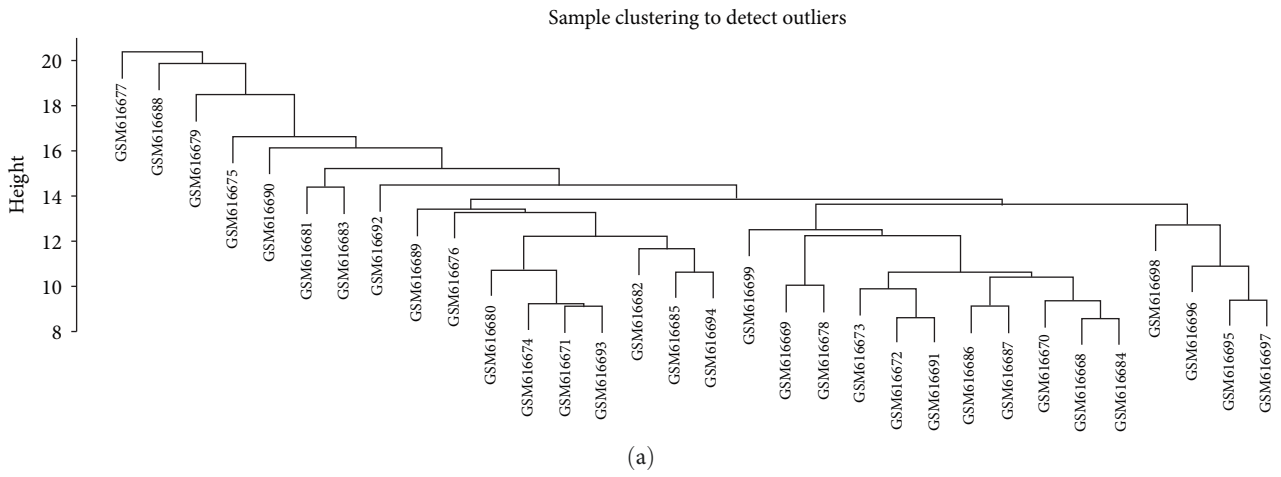
FIGURE 4: Continued.
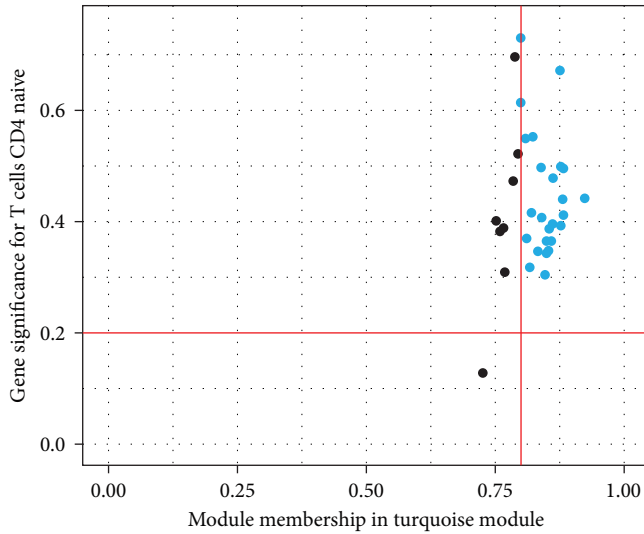
(d)
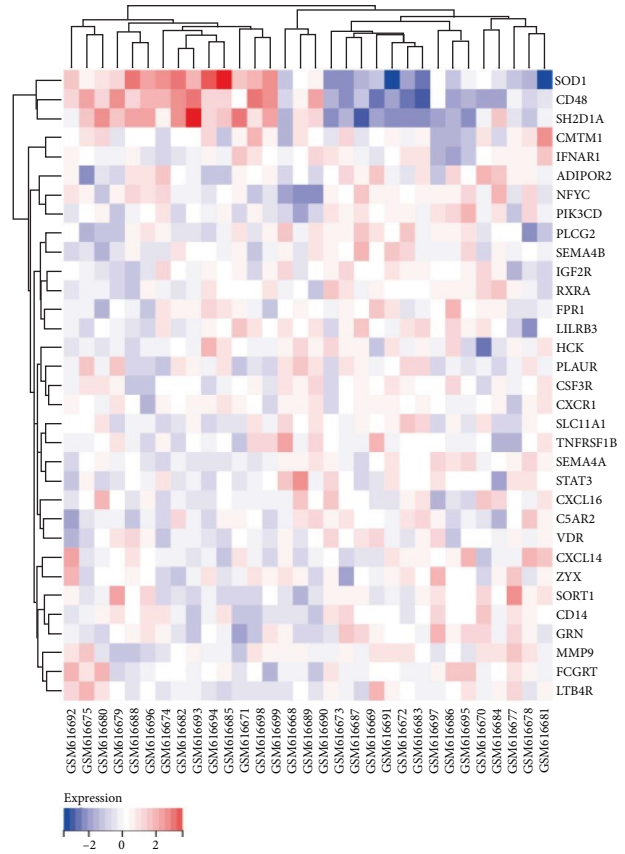
(e)

FIGURE 4: Identification of the immune infiltration-related genes in Ankylosing Spondylitis. (a) A clustering tree for the coexpression network module is created. (b) Feature of each combined module's relationship, with distinct colors denoting different parts. Each row represents a module. Each column shows how that module relates to the qualities, and each individual unit consists of both the *P*-value and the correlation coefficient. (c) Genes that belong to the blue module that was selected. (d) The blue portion of the collected genes. (e) A heat map of hub genes.

in China, the total prevalence of AS was 0.29%, among which there were 0.42% in males and 0.15% in females [20]. The mean AS prevalence was 0.24% in Europe, 0.17% in Asia, 0.32% in North America, 0.10% in Latin America, and 0.07% in Africa [21]. The most common symptoms of AS are chronic back pain and spinal stiffness, but peripheral and musculoskeletal manifestations are also frequently present [22].

In this study, we acquired a total of 125 DEGs, 36 of which were upregulated and 89 downregulated among the genes. IGF2R, GRN, SH2D1A, LILRB3, IFNAR1, PLCG2, and TNFRSF1B were identified as key genes enriched in the inflammatory response, chemokine signaling pathway, cytokine-mediated signaling pathway, regulation of neuroinflammatory response, leukocyte migration, and natural killer (NK) cell-mediated cytotoxicity. In terms of the inflammatory response, Guggino et al. [23] evaluated the activation and functional relevance of inflammasome pathways in AS patients and presented that inflammasomes drove type III cytokine production with an IL-1β-dependent mechanism in AS patients. The free heavy chain of HLA-B 27 may induce inflammation via T cells, NK cells, and bone marrow cells [24]. As is the case with AS, vascular endothelial cells respond to TNF by experiencing various pro-inflammatory alterations. The effectiveness of TNF-blocking medications in the treatment of AS

demonstrates that TNF plays an essential part in inflammation [25]. In 17 different types of immune cells, we found naive CD4+ T cells and monocytes were considerably higher in AS. Zheng et al. [26] The AS contained a higher proportion of CD8+ T cells, naive CD4+ T cells, and neutrophils among CIBERSORT results. There was a strong positive association between B cells, Tregs, and M2 macrophages, while the infiltration of CD4+ T cells, NK cells, and M0 macrophages was found to relate to one another negatively. Zhang et al. [27] reported negative correlations in CD8+ T cells and neutrophils activated memory CD4+ T cells, which was similar to our results. Multiple immune cells control the activity of bone cells and the size of bones through the release of cytokines and signaling pathways. DCs and their subtypes play crucial roles in numerous autoimmune and chronic inflammatory diseases [28]. Increased plasmacytoid DCs have been found in the bone marrow and peripheral blood of AS patients, which has been linked to higher levels of inflammatory cytokines such as trafficking molecules, CCR6 and CCL20, TNF-, IL-6, and IL-23 [29]. The pathophysiology of AS can be better understood if the association between the immune and skeletal systems is further examined.

The phospholipase C gamma 2 (PLCG2) gene is responsible for encoding phospholipase Cγ2 [30]. PLCG2 can regulate various cells' immune, inflammatory, and allergic

(a)

(b)

Figure 5: Continued.

- ■ Chemotaxis
- ■ Neutrophill degranulation
- ■ Inflammatory response
- ■ Chemokine signaling pathway
- ■ Cytokine-mediated signaling pathway
- ■ Regulation of neuroinflammatory response
- ■ Leukocyte migration
- ■ Natural killer cell mediated cytotoxicity
- ■ Negative regulation of response to external stimulus
- ■ Cytokine-cytokine receptor interaction
- ■ Adipocytokine signaling pathway
- ■ Response to lipopolysaccharide
- ■ Respiratory burst
- ■ Lipid and atherosclerosis
- ■ PID AMB2 NEUTROPHILS PATHWAY
- ■ Receptor-mediated endocytosis
- ■ Positive regulation of response to biotic stimulus
- ■ Response to wounding
- ■ Spinal cord injury
- ■ Lysosomal transport

(c)

logFC

0   0

GO Terms
- ■ Osteoclast differentiation
- ■ Hepatitis C
- ■ Non-small cell lung cancer
- ■ Chemokine signaling pathway
- ■ Adipocytokine signaling pathway
- ■ Lipid and atherosclerosis
- ■ JAK-STAT signaling pathway
- ■ Acute myeloid leukemia
- ■ Hepatitis B

(d)

Osteoclast differentiation   Module membership genes

IFNAR1
PLCG2

74   2   31

(e)

FIGURE 5: (a) The hub gene expression levels in different groups. (b) Matrix of expression correlations for each hub gene in AS. (c) The meta scale was used to enhance the functional enrichment of the correlated genes. Symbols "*", "**", and "ns," respectively, stand for $P < 0.05$, $P < 0.01$, and nonsignificance. (d) Chord plots demonstrate key roles in hub genes. (e) Venn diagram showing the intersection of hub genes in the blue module in WGCNA and genes in the osteoclast differentiation signal pathway.

TABLE 3: The characteristics of patients and healthy volunteers.

Characteristic	Group AS	Group control	P
Age (yr)	30.2 ± 4.7	26.5 ± 4.8	0.21
Male sex-no. (%)	5 (83.33)	5 (83.33)	0.77
BMI (Kg/m^2)	23.83 ± 4.17	23.17 ± 3.87	0.78
Race-Asian no. (%)	6 (100)	6 (100)	1
Positive for HLA-B27-no. (%)	6 (100)	/	
Time (Mons)	6.50 ± 3.27	/	/
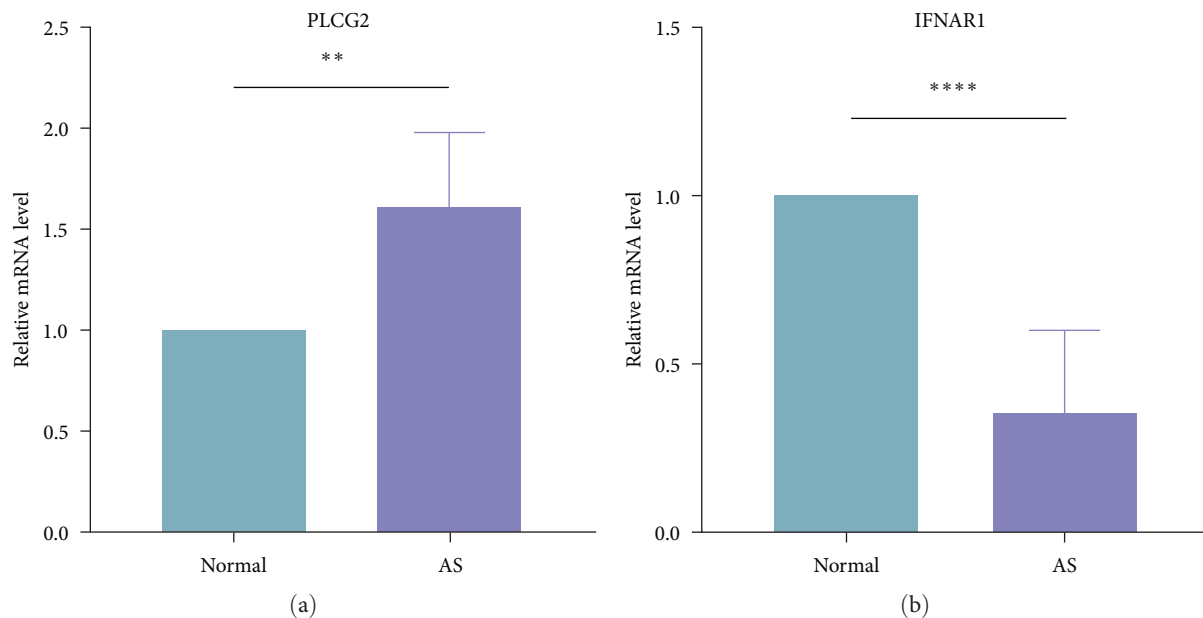
FIGURE 6: qRT-PCR validation in the peripheral blood. (a) The mRNA expression levels of PLCG2 in ankylosing spondylitis were significantly higher than that in the normal person ($P = 0.003$). (b) The mRNA expression levels of IFNAR1 in ankylosing spondylitis were significantly lower than that in the normal person ($P < 0.0001$). ($P < 0.05$, $^{**}P < 0.01$, and $^{****}P < 0.0001$).

responses through NFAT, NF-κB, and MAPK signaling pathways [30, 31]. Yu et al. [32] found a point mutation in the mouse PLCG2 gene, which leads to hyperreactive external calcium entry in B cells and expansion of innate inflammatory cells, leading to severe spontaneous inflammation and autoimmunity. In humans, point mutations of PLCG2 can lead to autoimmune inflammation, resulting in arthralgia and inflammatory bowel disease, suggesting that point mutations of PLCG2 are an essential mechanism for inducing immune inflammation [33]. The destruction of bone and cartilage and local osteoporosis are important pathological manifestations of AS, among which osteoclasts play an essential role. Therefore, exploring the genes related to osteoclasts formation is of great significance. Studies have shown that PLCG2 mediator can induce osteoclasts while blocking PLCG2 enzyme activity can limit the development and function of early osteoclasts [34]. Normal bone remodeling requires a balance between the metabolic processes of bone-resorbing cells, osteoclasts, and bone-forming cells [35]. Jeong et al. [36] also found that betulinic acid could significantly inhibit the generation of osteoclasts by inhibiting the phosphorylation of PLCG2. Under the influence of promoting bone resorption factors, the multinucleated

osteoclasts were formatted by the fusion and differentiation of monocyte progenitors, which could regulate osteoblast differentiation and bone formation [37].

IFN can stimulate the differentiation of immune cells and enhance immunological function, which may be an influential variable element in the pathogenesis of AS illness [38]. IFN can play an immunomodulatory role only when it binds to the interferon-α/β receptor (IFNAR). Studies have shown that IFN-γ polymorphisms are positively associated with the risk of AS [38]. Santiago-Raber et al. [39] found in NZB mice that a reduced number of IFNα/β receptors affected the incidence of immune lupus disease, suggesting the role of IFNAR in rheumatic diseases. However, the mechanism of IFNAR in the immune inflammation of AS remains unclear. It was reported that induction of IFN-B through the STING signaling pathway could restrai osteoclast differentiation and bone resorption, so it is speculated that decreased IFNAR can promote osteoclast differentiation [40].

In our study, PLCG2 and IFNAR genes were obtained by screening genes meeting the conditions of immune cell infiltration and osteoclast differentiation in AS patients. The above analysis indicated that inhibition of PLCG2 may inhibit the immune inflammatory response and osteoclast

formation in patients with AS. In contrast, the increased expression of IFNAR may inhibit the immune inflammatory response and osteoclast formation.

Limitations of our study still remain. First, we used the GEO database instead of our patient data, and there was unknown bias such as duration of medication, the severity of AS, and race of patients. Second, data validation is not sufficient relatively and qRT-PCR should be used to show the link between hub gene expression and AS clinical characteristics. Based on our existing samples, we will subsequently integrate more samples and conduct in-depth research in peripheral blood, bone tissue, and single cells.

5. Conclusions

Dysregulation of PLCG2 and IFNAR1 are key factors in disease occurrence and development of AS through regulating immune infiltration and osteoclast differentiation. Investigating the differences between AS and normal samples in immune cell infiltration and osteoclast differentiation would contribute to a better comprehension of the root cause of spondyloarthritis and therapeutic methods.

Data Availability

The data of this study are available from the corresponding author.

Conflicts of Interest

The authors declare that they have no conflicts of interest.

Authors' Contributions

Bo Han and Qiaobo Xie contributed equally to this work.

References

[1] J. Sieper and D. Poddubnyy, "Axial spondyloarthritis," *The Lancet*, vol. 390, no. 10089, pp. 73–84, 2017.

[2] T.-J. Kim and T.-H. Kim, "Clinical spectrum of ankylosing spondylitis in Korea," *Joint Bone Spine*, vol. 77, no. 3, pp. 235–240, 2010.

[3] S. L. Zuckerman, J. L. Goldberg, and K. D. Riew, "Multilevel anterior cervical osteotomies with uncinatectomies to correct a fixed kyphotic deformity associated with ankylosing spondylitis: technical note and operative video," *Neurosurgical Focus*, vol. 51, no. 4, Article ID E11, 2021.

[4] Y. Zhang, Y. Hai, Y. Liu et al., "The reliability of computer-assisted three-dimensional surgical simulation of posterior osteotomies in thoracolumbar kyphosis secondary to ankylosing spondylitis patients," *Mediators of Inflammation*, vol. 2022, Article ID 8134242, 10 pages, 2022.

[5] K. Krüger, U. von Hinüber, F. Meier et al., "Ankylosing spondylitis causes high burden to patients and the healthcare system: results from a German claims database analysis," *Rheumatology International*, vol. 38, pp. 2121–2131, 2018.

[6] A. Sharip and J. Kunz, "Understanding the pathogenesis of spondyloarthritis," *Biomolecules*, vol. 10, no. 10, Article ID 1461, 2020.

[7] D. Ellinghaus, L. Jostins, S. L. Spain et al., "Analysis of five chronic inflammatory diseases identifies 27 new associations and highlights disease-specific patterns at shared loci," *Nature Genetics*, vol. 48, pp. 510–518, 2016.

[8] T. Yu, J. Zhang, W. Zhu et al., "Chondrogenesis mediates progression of ankylosing spondylitis through heterotopic ossification," *Bone Research*, vol. 9, Article ID 19, 2021.

[9] M. Gengenbacher, H.-J. Sebald, P. M. Villiger, W. Hofstetter, and M. Seitz, "Infliximab inhibits bone resorption by circulating osteoclast precursor cells in patients with rheumatoid arthritis and ankylosing spondylitis," *Annals of the Rheumatic Diseases*, vol. 67, no. 5, pp. 620–624, 2008.

[10] R. Wilbrink, A. Spoorenberg, G. M. P. J. Verstappen, and F. G. M. Kroese, "B cell involvement in the pathogenesis of ankylosing spondylitis," *International Journal of Molecular Sciences*, vol. 22, no. 24, Article ID 13325, 2021.

[11] T. Barrett, S. E. Wilhite, P. Ledoux et al., "NCBI GEO: archive for functional genomics data sets—update," *Nucleic Acids Research*, vol. 41, no. D1, pp. D991–D995, 2012.

[12] S. Davis and P. S. Meltzer, "GEOquery: a bridge between the gene expression omnibus (GEO) and BioConductor," *Bioinformatics*, vol. 23, no. 14, pp. 1846-1847, 2007.

[13] M. E. Ritchie, B. Phipson, D. Wu et al., "limma powers differential expression analyses for RNA-sequencing and microarray studies," *Nucleic Acids Research*, vol. 43, no. 7, Article ID e47, 2015.

[14] G. Yu, L.-G. Wang, Y. Han, and Q.-Y. He, "clusterProfiler: an R package for comparing biological themes among gene clusters," *OMICS: A Journal of Integrative Biology*, vol. 16, no. 5, pp. 284–287, 2012.

[15] S. Horvath and J. Dong, "Geometric interpretation of gene coexpression network analysis," *PLoS Computational Biology*, vol. 4, no. 8, Article ID e1000117, 2008.

[16] Y. Zhou, B. Zhou, L. Pache et al., "Metascape provides a biologist-oriented resource for the analysis of systems-level datasets," *Nature Communications*, vol. 10, Article ID 1523, 2019.

[17] A. M. Newman, C. L. Liu, M. R. Green et al., "Robust enumeration of cell subsets from tissue expression profiles," *Nature Methods*, vol. 12, no. 5, pp. 453–457, 2015.

[18] K. Hu, "Become competent in generating RNA-Seq heat maps in one day for novices without prior R experience," in *Nuclear Reprogramming*, vol. 2239 of *Methods in Molecular Biology*, pp. 269–303, Humana, New York, NY, 2021.

[19] D. Poddubnyy and J. Sieper, "Mechanism of new bone formation in axial spondyloarthritis," *Current Rheumatology Reports*, vol. 19, no. 9, Article ID 55, 2017.

[20] J. Zhao, C. Huang, H. Huang et al., "Prevalence of ankylosing spondylitis in a Chinese population: a systematic review and meta-analysis," *Rheumatology International*, vol. 40, pp. 859–872, 2020.

[21] L. E. Dean, G. T. Jones, A. G. MacDonald, C. Downham, R. D. Sturrock, and G. J. Macfarlane, "Global prevalence of ankylosing spondylitis," *Rheumatology*, vol. 53, no. 4, pp. 650–657, 2014.

[22] A. Watad, C. Bridgewood, T. Russell, H. Marzo-Ortega, R. Cuthbert, and D. McGonagle, "The early phases of ankylosing spondylitis: emerging insights from clinical and basic science," *Frontiers in Immunology*, vol. 9, Article ID 2668, 2018.

[23] G. Guggino, D. Mauro, A. Rizzo et al., "Inflammasome activation in ankylosing spondylitis is associated with gut dysbiosis," *Arthritis & Rheumatology*, vol. 73, no. 7, pp. 1189–1199, 2021.

[24] S. J. Pedersen and W. P. Maksymowych, "The pathogenesis of ankylosing spondylitis: an update," *Current Rheumatology Reports*, vol. 21, Article ID 58, 2019.

[25] J. R. Bradley, "TNF-mediated inflammatory disease," *The Journal of Pathology*, vol. 214, no. 2, pp. 149–160, 2008.

[26] Y. Zheng, B. Cai, C. Ren et al., "Identification of immune related cells and crucial genes in the peripheral blood of ankylosing spondylitis by integrated bioinformatics analysis," *PeerJ*, vol. 9, Article ID e12125, 2021.

[27] D. Zhang, B. Li, R. Guo et al., "*RAB5C, SYNJ1*, and *RNF19B* promote male ankylosing spondylitis by regulating immune cell infiltration," *Annals of Translational Medicine*, vol. 9, no. 12, Article ID 1011, 2021.

[28] S. Smolinska, D. Groeger, and L. O'Mahony, "Biology of the microbiome 1: interactions with the host immune response," *Gastroenterology Clinics of North America*, vol. 46, no. 1, pp. 19–35, 2017.

[29] L. Liu, Y. Yuan, S. Zhang, J. Xu, and J. Zou, "Osteoimmunological insights into the pathogenesis of ankylosing spondylitis," *Journal of Cellular Physiology*, vol. 236, no. 9, pp. 6090–6100, 2021.

[30] J. T. Jackson, E. Mulazzani, S. L. Nutt, and S. L. Masters, "The role of PLCγ2 in immunological disorders, cancer, and neurodegeneration," *Journal of Biological Chemistry*, vol. 297, no. 2, Article ID 100905, 2021.

[31] Y. Baba and T. Kurosaki, "Impact of Ca^{2+} signaling on B cell function," *Trends in Immunology*, vol. 32, no. 12, pp. 589–594, 2011.

[32] P. Yu, R. Constien, N. Dear et al., "Autoimmunity and inflammation due to a gain-of-function mutation in phospholipase Cγ2 that specifically increases external Ca^{2+} entry," *Immunity*, vol. 22, no. 4, pp. 451–465, 2005.

[33] Q. Zhou, G.-S. Lee, J. Brady et al., "A hypermorphic missense mutation in *PLCG2*, encoding phospholipase Cγ2, causes a dominantly inherited autoinflammatory disease with immunodeficiency," *The American Journal of Human Genetics*, vol. 91, no. 4, pp. 713–720, 2012.

[34] D. Mao, H. Epple, B. Uthgenannt, D. V. Novack, and R. Faccio, "PLCγ2 regulates osteoclastogenesis via its interaction with ITAM proteins and GAB2," *Journal of Clinical Investigation*, vol. 116, no. 11, pp. 2869–2879, 2006.

[35] R. Baum and E. M. Gravallese, "Impact of inflammation on the osteoblast in rheumatic diseases," *Current Osteoporosis Reports*, vol. 12, no. 1, pp. 9–16, 2014.

[36] D. H. Jeong, S. C. Kwak, M. S. Lee, K.-H. Yoon, J.-Y. Kim, and C. H. Lee, "Betulinic acid inhibits RANKL-induced osteoclastogenesis via attenuating Akt, NF-κB, and PLCγ2-Ca^{2+} signaling and prevents inflammatory bone loss," *Journal of Natural Products*, vol. 83, no. 4, pp. 1174–1182, 2020.

[37] K. Matsuo and N. Irie, "Osteoclast–osteoblast communication," *Archives of Biochemistry and Biophysics*, vol. 473, no. 2, pp. 201–209, 2008.

[38] H. Xu and B. Li, "Effect of interferon-γ polymorphisms on ankylosing spondylitis: a case–control study," *Medical Science Monitor*, vol. 23, pp. 4126–4131, 2017.

[39] M.-L. Santiago-Raber, R. Baccala, K. M. Haraldsson et al., "Type-I interferon receptor deficiency reduces lupus-like disease in NZB mice," *Journal of Experimental Medicine*, vol. 197, no. 6, pp. 777–788, 2003.

[40] Y. Kwon, O.-J. Park, J. Kim, J.-H. Cho, C.-H. Yun, and S. H. Han, "Cyclic dinucleotides inhibit osteoclast differentiation through STING-mediated interferon-β signaling," *Journal of Bone and Mineral Research*, vol. 34, no. 7, pp. 1366–1375, 2019.

Hindawi

Research Article

TMEM100 Regulates Neuropathic Pain by Reducing the Expression of Inflammatory Factors

Huifei Cui [iD],[1] **Zhaoyang Guo** [iD],[1,2] **Zhu Guo** [iD],[1] **Zuoran Fan** [iD],[1] **Nana Shen** [iD],[3] **Xiaoying Qi** [iD],[4] **Yuanye Ma** [iD],[1] **Youfu Zhu** [iD],[1] **Xiaolin Wu** [iD],[1] **Bohua Chen** [iD],[1] **and Hongfei Xiang** [iD][1]

[1]*Department of Orthopedics, The Affiliated Hospital of Qingdao University, Qingdao 266003, China*
[2]*Department of Orthopedics, The Second Affiliated Hospital of Chongqing Medical University, Chongqing 400010, China*
[3]*Department of Rehabilitation, The Affiliated Hospital of Qingdao University, Qingdao 266000, China*
[4]*Department of Gynecology, The Affiliated Hospital of Qingdao University, Qingdao 266003, China*

Correspondence should be addressed to Xiaolin Wu; fyqs01@126.com, Bohua Chen; bhchen@hotmail.com and Hongfei Xiang; xianghf@qdu.edu.cn

There is no effective treatment for peripheral nerve injury-induced chronic neuropathic pain (NP), which profoundly impacts the quality of life of those affected. Transmembraneprotein100 (TMEM100) is considered to be a pain regulatory protein and is expressed in the dorsal root ganglion (DRG) of rats. However, the mechanism of pain regulation and the expression of TMEM100 following various peripheral nerve injuries are unclear. In this study, we constructed two pain models of peripheral nerve injury: tibial nerve injury (TNI) and chronic constriction injury (CCI). This study found that the Paw Withdrawal Mechanical Threshold (PWMT) and Paw Withdraw Thermal Latency (PWTL) of the rats in the two pain models decreased significantly, and the expression of TMEM100 in the DRG of two groups also decreased significantly. Furthermore, the decrease in the CCI group was more obvious than in the TNI group. There was no significant statistical significance ($P > 0.05$). We constructed an adeno-associated virus 6 (AAV6) vector expressing recombinant fluorescent TMEM100 protein and injected it into the sciatic nerve (SN) of two pain models: CCI and TNI. PWMT and PWTL were significantly increased in the two groups, along with the expression of TMEM100 in the spinal cord and DRG. It also significantly inhibited the activation of microglia, astrocytes, and several inflammatory mediators (TNF-α, IL-1β, and IL-6). In summary, the results of this study suggested that TMEM100 might be a promising molecular strategy for the treatment of NP, and its anti-inflammatory effects might play an important role in pain relief.

1. Introduction

The term neuropathic pain (NP) refers to the pain caused by a primary lesion or dysfunction of the nervous system [1, 2]. It is a common clinical problem that usually manifests as persistent pain (burning, squeezing, and compression) or paroxysmal pain (shock-like sensations and tingling), resulting in paresthesia and dysesthesia (tingling and needles) [3]. NP affects approximately 7%–10% of the general population globally, primarily in patients over 50 [2, 4]. The pathogenesis of NP is complex. Previous studies have found that NP is associated with structural and functional changes in nociceptive pathways such as peripheral nerve injury sites, spinal cord, and dorsal root ganglia (DRG) [3]. These diseases are associated with various peripheral or central nervous system lesions [5]. NP can be divided into peripheral and central NP based on the anatomy of injury and disease [6]; the former is more common in clinical practice [7, 8]. Although peripheral nerve injury frequently causes chronic NP, the underlying mechanisms are often uncertain [9]. There are currently no adequate and effective treatments for NP, while numerous studies have focused on discovering new drug targets and their impact on pain behavior.

Transmembraneprotein100 (TMEM100) has been found to have many biological functions, expressed in vascular, lung, and gastrointestinal tissues, and plays an imperative role in arterial endothelial differentiation, vascular integrity, cancer cell, and proliferation [10–13]. Recently, it has been

found that TMEM100 is also expressed in DRG [9, 14] as a pain signal modulator expressed by nociceptive neurons. It regulates pain by regulating the interaction between TRPA1 and TRPV1, and plays an important role in pain and the nervous system [14]. DRG is an important part of the peripheral nervous system. It is reported that TMEM100 is mainly located in mouse DRG and ganglion cell peptidergic neurons [14, 15], but its expression in NP is uncertain [15]. There may be differences in gene expression between inflammatory pain and NP [16–19].

Studies have shown that chronic pain is caused by interference with the decomposition of neuroinflammation [20–23]. Typical features of neuroinflammation under chronic pain conditions include infiltration of immune cells into the sciatic nerve (SN) and DRG, activation of glial cells: microglia and astrocytes, production and secretion of pro-inflammatory cytokines and chemokines (TNF, IL-1 β, IL-6, CCL2, and CXCL1) [20]. Previous studies have reported that TMEM100 has an inhibitory role in the secretion of inflammatory cytokines in liver inflammation [24]. Therefore, we investigated the contribution of TMEM100 in the inception of inflammation in nerve tissue.

AAV6 is now considered one of the most useful vectors for gene therapy due to its less immunogenicity and toxicity. Gene delivery to the DRG has been shown to be possible. It has been reported that retrograde transfection of AAV6 into neurons by SN injection can achieve higher transfection efficiency of DRG neurons than other transfection methods (intravenous, intramuscular, and intrathecal).

AAV6 is now considered one of the most useful vectors for gene therapy due to its less immunogenicity and toxicity [25]. Gene delivery to the DRG has been shown to be possible [26, 27]. It has been reported that retrograde transfection of AAV6 into neurons by SN injection can achieve higher transduction efficiency of DRG neurons than other transduction methods (intravenous, intramuscular, and intrathecal) [28, 29].

This study aimed to explore the effect of TMEM100 on NP and the therapeutic potential of TMEM100 as a target for treating chronic NP. In this study, we constructed an adeno-associated virus (AAV6) -TMEM100 overexpression vector and injected it into the SN of the rats, and analyzed the differential expression of TMEM100 and pain behavior in rats. In addition, the pro-inflammatory cytokines causing pain in rat DRG were evaluated.

2. Methods and Materials

2.1. Animals.
This study used clean, healthy male Sprague–Dawley (SD) rats aged 7–10 weeks, weighing 200–300 g. The indoor temperature was maintained at $23 \pm 2°C$, the relative humidity was 60%–70%. The rats were fed in separate cages and drank and ate freely. The Qingdao University Experimental Animal Center in Shandong Province provided all the experimental animals. The experimental operation met the requirements of Animal Protection Association and the user Committee of Qingdao University and was consistent with the guidelines of National Animal Protection Institute.

2.2. Establishing Animal Models.
According to the method of Bennett [30], a rat model of chronic constriction injury (CCI) was established: we used 4% isoflurane for induction and 2% for maintenance of anesthesia, then made the rat prone on the operating table, and the right hind limb was shaved for preparation. The skin was sterilized with 10% iodophor solution, followed by the incision at the sciatic tubercle and blunt dissection of each layer of muscle to expose the SN; 4–0 catgut was used to make four loose fit junctions, with a spacing of about 1 mm, to obtain a damaged SN of length 4–5 mm. The ligation strength was based on the mild compression of epineurial artery under the dissecting microscope, while the blood flow was not completely interrupted. When the rat exhibited typical NP signs: reduced hindlimb weight, paw contracture, licking, and no motor function limitation such as lameness, the model was judged to be successful.

According to the method of Lee et al. [31] a rat model of permanent tibial nerve injury (TNI) was established: the steps of anesthesia, skin preparation, and disinfection were the same as the CCI model. The SN and its three branches were exposed and separated from the surrounding soft tissue with a nerve dissection. The SN stem and three branches were carefully isolated. The tibial nerve branches were carefully identified, and the tibial nerve was tightly ligated with 4–0 chrome catgut and cut to a length of approximately 5 mm, leaving the common peroneal and sural nerves intact. The success sign was the same as CCI.

2.3. Experimental Grouping.
A total of 80 male SD rats were included in this study and randomly divided into eight groups: normal; Sham; CCI; TNI; CCI, AAV6-GFP; TNI, AAV6-GFP; CCI, AAV6-TMEM100; and TNI, AAV6-TMEM100 group with 10 each. The description of groups is as follows.

Nothing was done to the normal group. In the Sham group, SN was exposed but not ligated. Surgical modeling was done in CCI and TNI groups, but no injection was administered. While in CCI, AAV6-GFP, and TNI, AAV6-GFP groups; AAV6-GFP (10* 1,012 viral particles each) were injected into the SN. Furthermore, in CCI, AAV6-TMEM100, and TNI, AAV6-TMEM100 groups, AAV6-TMEM100 (10* 1,012 viral particles each) were injected into the SN during modeling. AAV6-TMEM100 and AAV6-TMEM100 were designed and synthesized by Biomedicine Biotech (Chongqing, China).

2.4. Behavioral Analysis.
Paw Withdrawal Mechanical Threshold (PWMT) test was conducted one day before modeling, and 1, 3, 5, 7, 10, 14, 21, and 28 days after modeling, according to the up–down method [32, 33], using von Frey filaments to determine mechanical allodynia by foot withdrawal. The rat was placed on a metal mesh frame, and the cilia were stabbed vertically through the mesh into the skin of rat's hind limbs until they were slightly bent into an S shape. The duration of each stimulation was 3–5 s, and the interval was 10–15 s. Reaction: if the rat displayed foot withdrawal, it was marked as "+"; if there was no response, it was marked as "−"; if "+" appeared, the adjacent cilia with decreasing force were used for stimulation; if negative, the adjacent increasing force was used for stimulation. Stimulation was stopped if

TABLE 1: The primers used for qPCR detection.

Gene name	Forward	Reverse
TMEM100	GTCTTCATCACCGGGATCGT	TGTTCCTTTGTCTCACCTTCCA
GAPHD	ATGCCGCCTGGAGAAACC	GCATCAAAGGTGGAAGAATGG
IL-1β	CCCAAGCACCTTCTTTTCCTT	TCAGACAGCACGAGGCATTT
IL-6	CTGATTGTATGAACAGCGATGATG	GGTAGAAACGGAACTCCAGAAGAC
TNF-α	CAAGAGCCCTTGCCCTAAGG	CGGACTCCGTGATGTCTAAGTACTT
GFAP	GAGATCGCCACCTACAGGAAATT	CTTTACCACGATGTTCCTCTTGAG
Iba1	GGAGGCCTTCAAGACGAAGTAC	GAGCCACTGGACACCTCTCTAATT

there was no positive response to the maximum stimulation intensity of cilia. After the first positive reaction, the up–down method was used to repeat the measurement six times with a 10 min rest; the extreme values on both sides were removed, and the average of remaining values was taken as the PWMT value of rat.

Paw Withdraw Thermal Latency (PWTL) determination was done one day before modeling, and 1, 3, 5, 7, 10, 14, 21, and 28 days after modeling, according to the paw withdrawal latency (PWL) method [34]. The thermal radiation exposure time limit was set to 20 s, the rat was placed on the glass plate while the temperature of glass plate was maintained at $26 \pm 0.5°C$, and the irradiation light source under the glass plate was adjusted to aim at the palm of hind paw of the rat. When the foot withdrawal reaction occurred or the irradiation time reached 20 s or more (20 s was the irradiation limit), the light source was turned off and recorded. The measurement was repeated six times with a 10 min rest; the extreme values on both sides were removed, and the average was recorded as PWTL.

2.5. Immunofluorescence.

After the pain behavior measurement, rats in each group were dissected at L4, L5, and L6 lumbar vertebrae and the DRG, and the DRG tissue was quickly removed and dissected. The L4–L6 spine was exposed, and the spinal cord was separated from the middle with a tool. The removed tissues were postfixed in 4% paraformaldehyde at 4°C for 8 hr, embedded in paraffin, and serially sectioned at 4 μm. Immunofluorescence tristaining was done to characterize cellular specificity and distribution of target molecules in sections. Four micrometer thick sections were deparaffinized in xylene, rehydrated by graded alcohols, and treated by heat-induced epitope retrieval in 10 mM citrate buffer (Elabscience). We used a 5% BSA (Solarbio, Beijing, China) blocking solution for 1 hr at room temperature of 37°C, following the addition of primary antibody diluted with antibody diluent (dilution ratio was according to the antibody instructions) dropwise and the wet box was placed in a 4°C refrigerator to incubate overnight. Two fluorescent secondary antibodies (Elabscience) were added and incubated at room temperature at 37°C for 1 hr. After each incubation, wash the polyvinylidene fluoride (PVDF) membrane three times with TBST solution on a shaker for 10 min/time. Then, the nuclei were counterstained with the fluorescent dye DAPI (blue), and dropwise an antifluorescence quencher was added. Coverslips were placed in a low-temperature freezer at 4°C for later use. After the preparation, the slices were observed under a confocal microscope, and the tissue images were photographed using Image-Pro Plus (version 6.0.0.260, Media Cybernetics Corporation, USA). Images were finally analyzed.

2.6. Quantitative Real-Time Polymerase Chain Reaction (qRT–PCR).

After the removal of specimen, it was put into an enzyme-free EP tube (containing 1 ml Trizol (Elabscience) and steel ball) followed by shaker grinding at 60 rpm for 30 s, six times. After standing, chloroform was added to extract mRNA. It was then reverse transcribed into cDNA using the Evo M-MLV RT Kit for qPCR (Accurate Biology). The qPCR amplification reaction was performed on a PCR instrument according to the kit manufacturer's instructions (SYBR® Green Premix Pro Taq HS qPCR Kit (Accurate Biology)) with the following conditions: 95°C for 30 s, then 95°C for 5 s, and 60°C for 30 s for 40 cycles. The primer sequences used in this study are displayed in Table 1. The obtained data were analyzed using the 2(−$\Delta\Delta$Ct) algorithm to acquire the results.

2.7. Western Blot Analysis.

Proteins were extracted by lysing tissues with radioimmunoprecipitation (RIPA) lysis buffer (Solarbio, Beijing, China) containing 1 mM phenylmethanesulfonyl fluoride (PMSF). The concentration of extracted protein was determined with a bicinchoninic acid (BCA) kit (Solarbio, Beijing, China). Protein and loading buffer were mixed at a ratio of 4 : 1 (V/V) and boiled at 99°C for 10 min. Separated by sodium dodecyl sulfate-polyacrylamide gel electrophoresis (SDS-PAGE) and transferred to PVDF membrane. PVDF membranes were blocked with 5% nonfat dry milk at room temperature. Membranes were then incubated with primary antibodies overnight at 4°C (Table 2). After overnight, the membrane was incubated with horseradish peroxidase (HRP)-labeled secondary antibody (Elabscience) for 1 hr, and then the ECL kit (Elabscience) was used for luminescence observation. The acquired images were analyzed using a developing instrument (Odyssey® XF).

2.8. Statistical Analysis.

Statistical analysis was performed on the data collected, detected, and sorted. Continuous data were presented as mean ± standard deviation, while nonparametric data were presented as median and interquartile range. Comparisons between groups were performed using one-way analysis of variance (ANOVA) followed by the Kruskal–Wallis test. A comparison of parameters between parallel groups was performed using the t-test. $P < 0.05$ was

TABLE 2: Primary antibodies and IgG controls used in this study.

Antibody*	Host	Supplier/catalog number	Dilution
TMEM100	Rabbit polyclonal	Millipore/ABN1721	1 : 100(IHC), 1 : 500(Wb)
TMEM100	Mouse monoclonal	Origene/TA500532	1 : 100(IHC), 1 : 500(Wb)
GFAP	Mouse monoclonal	Elabscience/E-AB-22022	1 : 200(IHC), 1 : 1000(Wb)
Iba1	Rabbit polyclonal	Abcam/ab178846	1 : 100(IHC), 1 : 1000(Wb)
IL-1β	Rabbit polyclonal	Affinity/AF5103	1 : 1000(Wb)
IL-6	Rabbit polyclonal	Affinity/DF6087	1 : 1000(Wb)
TNF-α	Rabbit polyclonal	Abcam/ab215188	1 : 1000(Wb)
β-actin	Rabbit polyclonal	Elabscience/E-AB-20058	1 : 1000(Wb)
Tubulin	Rabbit polyclonal	Elabscience/E-AB-20070	1 : 200(IHC)
IgG control	Mouse	Elabscience/E-AB-1001	1 : 2000(Wb)
IgG control	Rabbit	Elabscience/E-AB-1003	1 : 5000(Wb)
IgG control	Mouse	Elabscience/E-AB-1015	1 : 100(IHC)
IgG control	Rabbit	Elabscience/E-AB-1014	1 : 100(IHC)

*TMEM100, transmembraneprotein100; GFAP, glial fibrillary acidic protein; Iba1, ionized calcium binding adaptor molecule 1; IL-1β, interleukin-1β; IL-6, interleukin-6; TNF-α, tumor necrosis factor α; GAPDH, glyceraldehyde 3-phosphate dehydrogenase; Tubulin, β-tubulin; IgG, immunoglobulin G.

considered statistically significant. Statistical analysis was performed, and statistical graphs were drawn using GraphPad Prism 8 (GraphPad Software, USA) software.

3. Results

3.1. Decreased TMEM100 Expression in the Two NP Models

3.1.1. The Two Groups of Rat Pain Models Exhibited a Significant Decrease in Behavioral Pain Tests. The postoperative condition of rats was good overall; and there was no autophagy of limbs, and typical spontaneous hyperalgesia gradually appeared. The right limb of rat was involved, dragged, or suspended, and there was obvious walking and lameness. We first conducted pain studies on the rats in the normal, Sham, CCI, and TNI groups: PWMT and PWTL test results revealed that the values of normal and Sham groups were the same each time, and there was no significant change ($P > 0.05$). Compared with the normal group, the PWMT and PWTL of the CCI and the TNI group decreased at each time point after the operation, and they decreased significantly on the first day and lasted until the 28th day after the operation ($P < 0.01$, Figures 1(a) and 1(b)).

3.1.2. Painful Rats Transfected with Adenovirus Demonstrated Significant Relief in Pain Behavior. During modeling, we injected AAV6-GFP and AAV6-TMEM100 into the SN of CCI and TNI rats. The results indicated that the AAV6-TMEM100 group had a lesser decrease in PWMT and PWTL than the AAV6-GFP group, and in the last seven days after the operation, there were different degrees of increase ($P < 0.01$), with the highest level at 28 days ($P < 0.01$, Figure 1 (c)–1(f).

3.1.3. Decreased TMEM100 Expression of DRG in Peripheral NP. After 4 weeks of modeling, the rats were sacrificed, and their DRG tissues were dissected. Normal and Sham groups were compared using Western blot, qRT–PCR, and immunofluorescence. Moreover, DRG tissues of CCI and TNI groups were compared. The expression of TMEM100 gene

varied, and the expression of TMEM100 in normal and Sham groups were detectable. The expression of TMEM100 was significantly attenuated in CCI and TNI groups compared to normal and Sham groups, with statistical significance ($P < 0.01$). The TNI group had slightly higher expression levels than the CCI group, but the difference was not statistically significant ($P > 0.05$, Figure 2(a)). The qRT–PCR results were consistent with western blot results. The expression in CCI and TNI groups was significantly decreased than in the normal and Sham groups ($P < 0.01$). CCI group histone expression was slightly lower than TNI ($P > 0.05$). Normal and Sham groups had similar histone expressions ($P > 0.05$, Figure 2(b)).

Immunofluorescence staining yielded identical outcomes described previously. The fluorescence intensity of CCI and TNI groups was lower than normal and Sham groups ($P < 0.05$), TNI group was slightly higher than CCI group ($P > 0.05$), and there were no significant differences between the other groups ($P > 0.05$, Figure 3). By constructing two pain models, CCI and TNI, we discovered that TMEM100 expression was downregulated in the DRGs of both models. We speculated that TMEM100 might be involved in the occurrence of pain, as its expression exhibited a downward trend.

3.2. Minimally Invasive Injection of AAV6-TMEM100 into CCI and TNI Rats Could Reverse the Decrease in TMEM100 and Relieve NP. Pain models: CCI and TNI were transfected with TMEM100 mediated by adenovirus, and the same experimental group was set up as a normal group and virus transfection group (AAV6-GFP and AAV6-TMEM100 groups). Four weeks after transfection, qRT–PCR detection was performed. The results revealed that AAV6-TMEM100 had significantly increased expression compared to AAV6-GFP group with a statistical difference ($P < 0.05$, Figure 4).

Western blotting detected that CCI, AAV6-TMEM100, and TNI, AAV6-TMEM100 groups had significantly enhanced protein expression compared with the AAV6-GFP group with statistical differences ($P < 0.05$, Figures 5(a), 5(c), and 5(d)).
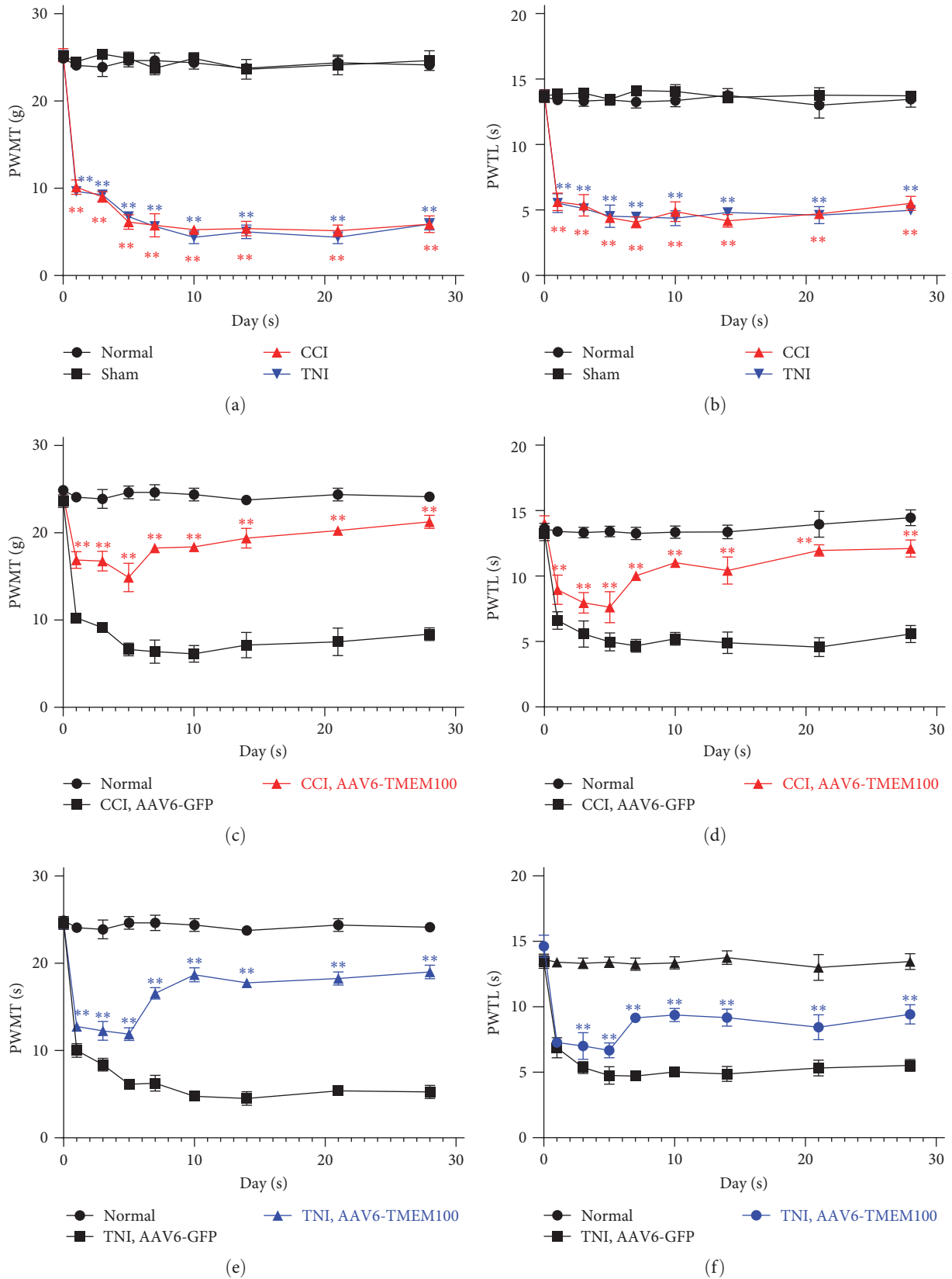
FIGURE 1: (a) Changes of PWMT in CCI and TNI groups at different times. **$P < 0.01$ vs. normal group; (b) changes in PWTL in CCI and TNI groups. **$P < 0.01$ vs. normal group; (c) PWMT changes of rats in CCI group at different times after transfection; (d) changes of PWTL of rats in CCI group after transfection at different times; (e) rats in TNI group after transfection at different times; (f) changes in PWTL in TNI group rats at different times after transfection; **$P < 0.01$ vs. AAV6-GFP group.

(a)　　　　　　　　　　　　　　　　　　　　　(b)
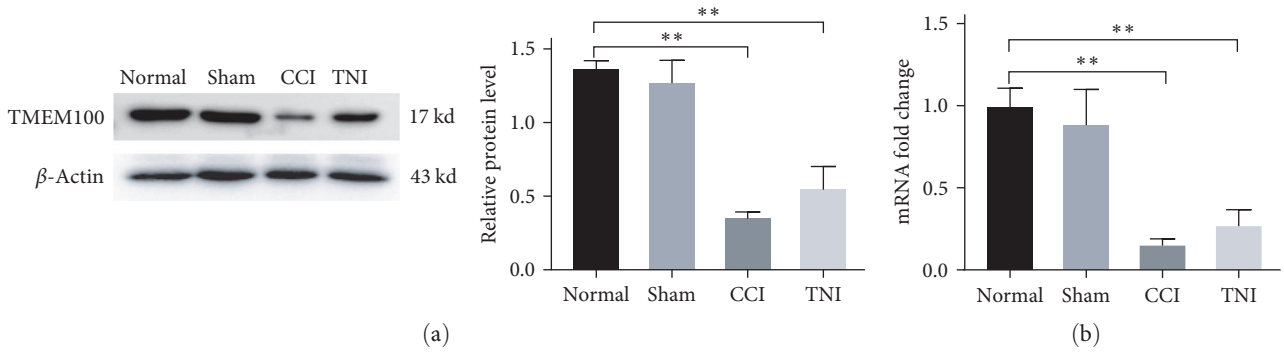
FIGURE 2: (a) Western blot used to detect the expression of TMEM100 protein in CCI and TNI groups; (b) qRT–PCR was used to detect the mRNA of TMEM100 in CCI and TNI groups. **$P < 0.01$.
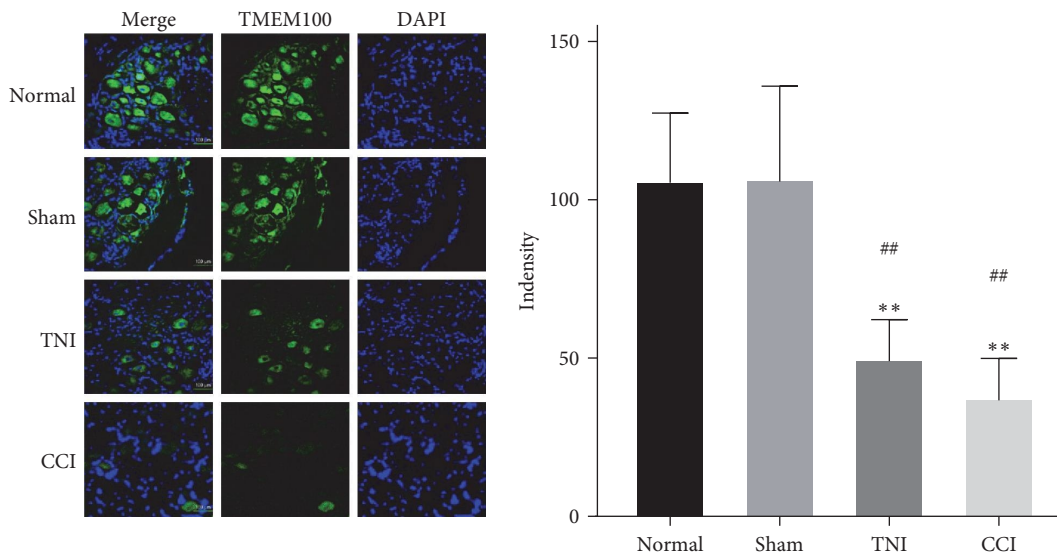
FIGURE 3: The relative fluorescence intensity of TMEM100 expression in DRG of CCI and TNI groups was detected by immunofluorescence. **$P < 0.01$ vs. normal group; ##$P < 0.01$ vs. normal group.

Simultaneously, we extracted and tested the spinal cords of rats' modeled side (R) and the unmodeled side (L) in each group, obtaining comparable results with the former. There was a statistical difference ($P < 0.05$). Furthermore, in CCI, the expression of TMEM100 in the modeled side of spinal cord of the rats in AAV6-TMEM100 group was higher than the unmodeled side, with a statistical difference between the two ($P < 0.05$). The expression of TMEM100 in the spinal cord of rats in the TNI and AAV6-TMEM100 groups was higher than on the nonmodeled side, but there was no significant difference between the two ($P > 0.05$, Figures 5(b), 5(e), and 5(f)).

Immunofluorescence staining yielded similar results as mentioned above. The AAV6-TMEM100 group exhibited a statistically significant enhanced fluorescence intensity compared to the AAV6-GFP group ($P < 0.05$, Figures 6(a) and 6(b)). This suggested TMEM100 as a crucial protein that regulates pain and immunity and plays a crucial role in NP. Transfection with adenovirus carrying TMEM100 could reverse discogenic

pain and achieve the therapeutic effect. It could serve as gene therapy for discogenic pain. Sexual pain provides a good theoretical basis and a prerequisite for later animal experiments.

3.3. Reversal of TMEM100 Expression Reduces the Elevated Expression of Glial Cells and Inflammatory Mediators Caused by Peripheral NP. This study investigated the relationship between TMEM100 and microglia (Iba-1), astrocytes (GFAP), and inflammatory mediators (TNF-α, IL-6, and IL-1β) after peripheral NP. Western blot, qPCR, and immunofluorescence were used to detect the expression levels of each index in the normal and the virus-injected groups. The qPCR demonstrated that the expressions of Iba-1, GFAP, TNF-α, IL-6, and IL-1β in the AAV6-GFP group were increased to varying degrees compared to the normal group ($P < 0.05$). The AAV6-TMEM100 group had significantly lower expression than the AAV6-GFP group ($P < 0.05$, Figure 7). Similar results were obtained by the western blot ($P < 0.05$, Figure 8).
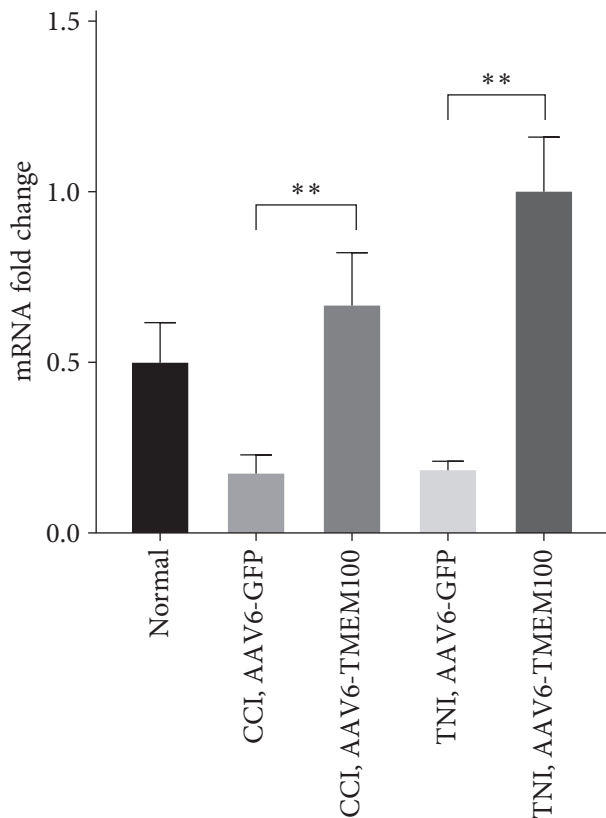
FIGURE 4: Relative expression of mRNA in normal group and virus transfection group $^{**}P<0.01$.

We further verified the expression of Iba-1 and GFAP by immunofluorescence, and the results were consistent with those obtained by qPCR and Western blot (Figure 9).

These results indicated that TMEM100 might relieve pain by reducing the expression of glial cells and inflammatory factors in NP.

4. Discussion

This study aimed to determine the expression of TMEM100 in NP and to explore the possible role of TMEM100 in pain relief. We found that the expression of TMEM100 was significantly reduced in the DRG of rats with peripheral NP by creating two different pain models: CCI and TNI. We established an AAV6 vector encoding recombinant fluorescent TMEM100 and transfected it into the DRG proximal to the peripheral nerve injury. We found that the expression of TMEM100 in the DRG of transfected rats was significantly higher than that of model rats alone, and the pain behavior of rats was significantly improved. Moreover, we discovered that reversing the expression of TMEM100 inhibited NP and microglia (Iba-1), astrocytes (GFAP), and inflammatory mediators (IL-1β, TNF-α, and IL-6). Overall, the findings of this study direct that TMEM100 is an important pain-regulating protein that plays an important role in NP and may alleviate pain by reducing inflammatory mediators.

TMEM100 is a two-transmembrane protein that is widely distributed in various tissues. It has been reported that TMEM100 is expressed in blood vessels, notochords, and other tissues and is related to kidney development, angiogenesis, and lung cancer metastasis [10, 35, 36]. The expression of TMEM100 has recently been found in the nervous system [14]. However, the expression and role of TMEM100 in NP are still unclear.

To further determine the association between TMEM100 and pain, we established two pathological pain models: CCI and TNI. The CCI model is a well-established [30] and the most used pain model in research. Pain is induced by the compression of four thread knots of the SN trunk, and rats may experience paresthesia, mechanical allodynia, and caloric allodynia in the operated limb, similar to the characteristics of human NP [37]. The TNI model is an optimized derivative type of spared nerve injury (SNI). It has the typical characteristics of SNI class and some advantages. Lee et al. [31] found that simultaneous transection of the tibial and sural nerves or a single TNI resulted in more severe pain threshold changes. The tibial nerve may play an important role in the pain process [38]. Therefore, researchers believed single TNI to be a more stable and efficient model of peripheral NP than classic SNI [39].

We performed behavioral tests on rats with two different pain models and evaluated the expression of TMEM100 in each group. We found that the pain production was accompanied by changes in the TMEM100 expression in the DRG of rats in the two pain models. The expression of TMEM100 was significantly reduced in the two groups, so we hypothesized a close relation of TMEM100 in the generation or regulation of pain. Interestingly, although the expression of TMEM100 was significantly decreased in both CCI and TNI groups compared to the normal group, the decrease in TMEM100 was more pronounced in the CCI model. Many studies have demonstrated that [9] the downregulation of TMEM100 may be related to the proliferation of astrocytes and microglia after nerve injury. By detecting astrocyte-specific marker (GFAP) and microglia-specific marker (Iba-1), we discovered that there were different degrees of elevation in both pain models; in the CCI model, the elevation of GFAP and Iba-1 was more pronounced than that of TNI, which explained the decrease of TMEM100 in NP, and lower expression of TMEM100 in CCI compared to TNI model.

The function of TMEM100 is implicated in many aspects of biology. For example, TMEM100 is involved in the control of developmental proliferation and differentiation [40]. It plays a role in cell development and differentiation through pathways such as transforming growth factor-bone morphogenic protein in the enteric nervous system. It has essential functions in maintaining vascular integrity as well as in the formation of blood vessels. Meanwhile, TMEM100 acts as a tumor suppressor in various tumor cells to inhibit metastasis and proliferation [41]. Pan et al. [24] demonstrated that TMEM100 is crucial for the secretion of inflammatory factors and found that TNF-α had an inhibitory effect on the expression of TMEM100, while decreased TMEM100 expression could significantly
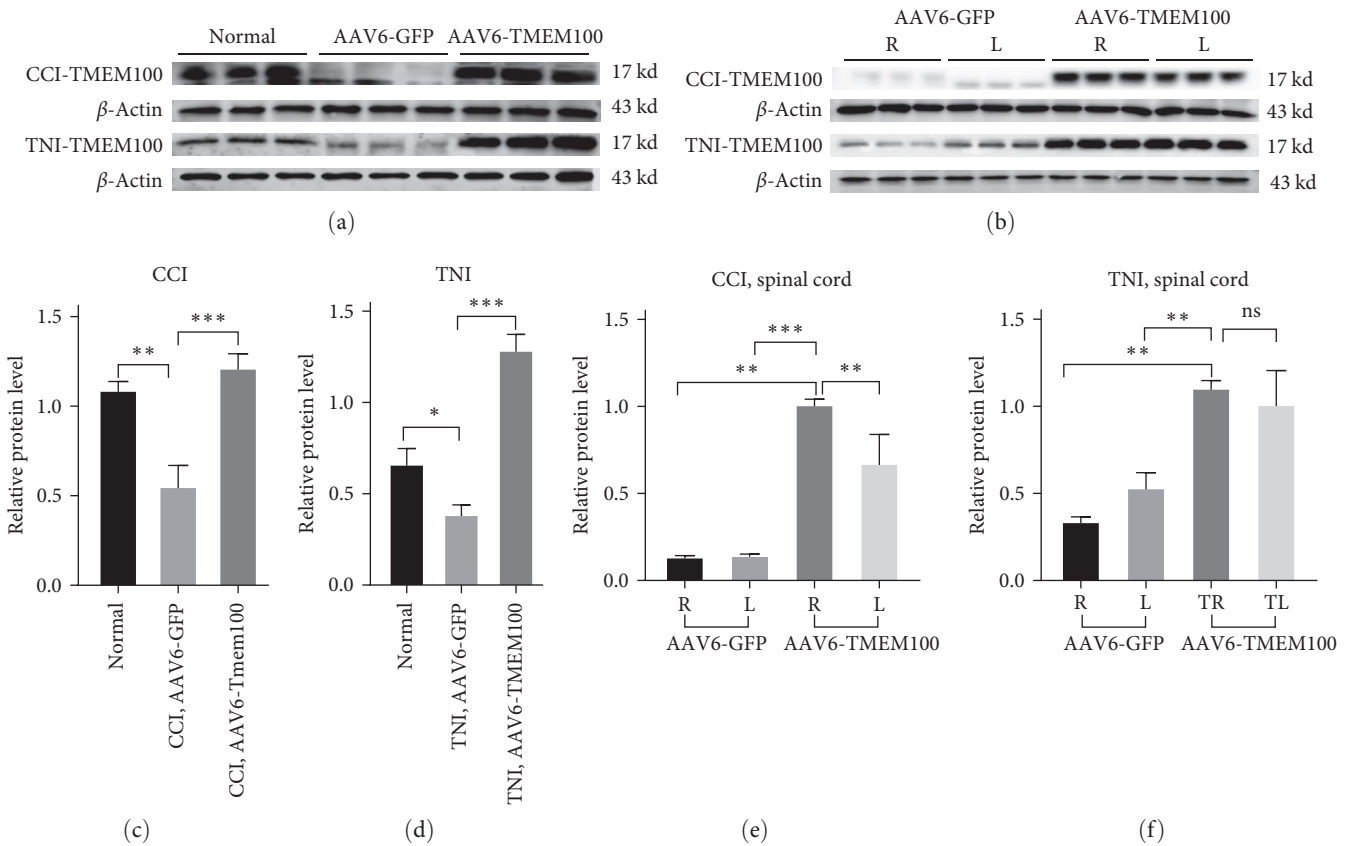
FIGURE 5: (a) The expression of TMEM100 protein in normal group and virus transfection group (AAV6-GFP and AAV6-TMEM100 groups). (b) The expression of CCI and TNI rat spinal cord in virus transfection group. The expression of TMEM100 protein on the model side (R) and the unmodeled side (L). (c) The histogram of expression of TMEM100 protein of CCI in the virus transfection group. (d) The expression of TMEM100 protein of TNI in the virus transfection group. The histogram of expression level. (e) The histogram of expression level of TMEM100 protein in the spinal cord of CCI rats in the virus transfection group. (f) The histogram of expression level of TMEM100 protein in the spinal cord of TNI rats in the virus transfection group; $^*P < 0.05$ and $^{**}P < 0.01$.

reduce the secretion of inflammatory factors such as IL-1β and IL-6. This is consistent with the findings of our study that the expression of TNF-α, IL-1β, and IL-6 in DRG of CCI and TNI rats decreased after overexpression of TMEM100. The release of inflammatory mediators (TNF-α, IL-1β, and IL-6) is closely related to the pathogenesis of NP. These inflammatory mediators contribute to central spinal cord sensitization, thereby enhancing the development of NP [42, 43].

Activation of glial cells and interactions between these cells and neurons may be involved in nociception in the central and peripheral nervous systems [44]. Glial cells, including astrocytes and microglia, are involved in the induction and maintenance of NP [45]. The vital role astrocytes play upon activation may be related to the production of cytokines after injury [46]. It has been suggested that upregulation of GFAP, a marker of astrocyte activation following injury, has a role in the maintenance of NP [47]. One study found that upregulation of GFAP persisted from 3 to 21 days after nerve injury [48]. This study showed that GFAP levels increased in the

groups of CCI and TNI models injected with empty virus (AAV6-GFP group). In contrast, the group injected with a virus carrying TMEM100 (AAV6-TMEM100) exhibited attenuated GFAP levels in CCI and TNI models.

Furthermore, the activation of microglia has a key role in the central sensitization of NP [49]. The pathological condition of NP results in microglia activation: microglia release many pro-inflammatory cytokines, such as TNF-α, along with glutamate release, excess reactive oxygen, and apoptosis. In this study, we detected different degrees of elevation of Iba-1, a marker of microglia activation, among the rats of AAV6-GFP group in the CCI and TNI models. The levels of Iba-1 in the AAV6-TMEM100 group were significantly decreased. Yu et al. [9] proved through in vitro experiments that overexpression of TMEM100 in astrocytes and microglia cell lines significantly inhibited their proliferation and found through animal experiments that TMEM100 may play a role in the control of satellite glial cells (SGCs) proliferation. It is believed that glial cell proliferation in animals after nerve injury may be the reason for the

(a)

(b)
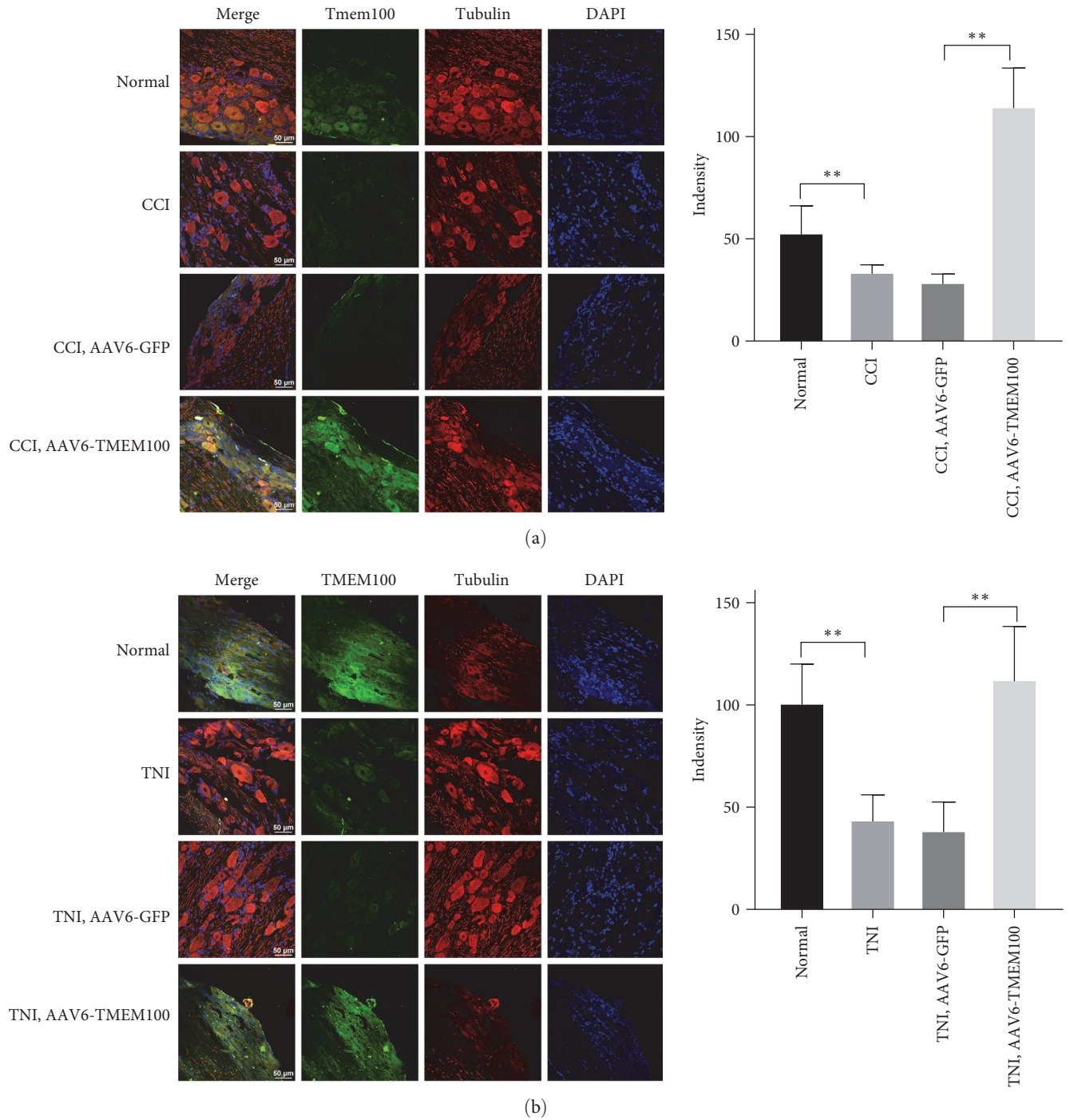
FIGURE 6: (a) Immunofluorescence detection of relative fluorescence intensity of TMEM100 in CCI rat normal group and virus transfection group (AAV6-GFP and AAV6-TMEM100 groups); (b) immunofluorescence detection of TNI rats. The relative fluorescence intensity expression difference of TMEM100 between normal group and virus transfection group (AAV6-GFP and AAV6-TMEM100 groups) $**P < 0.01$.
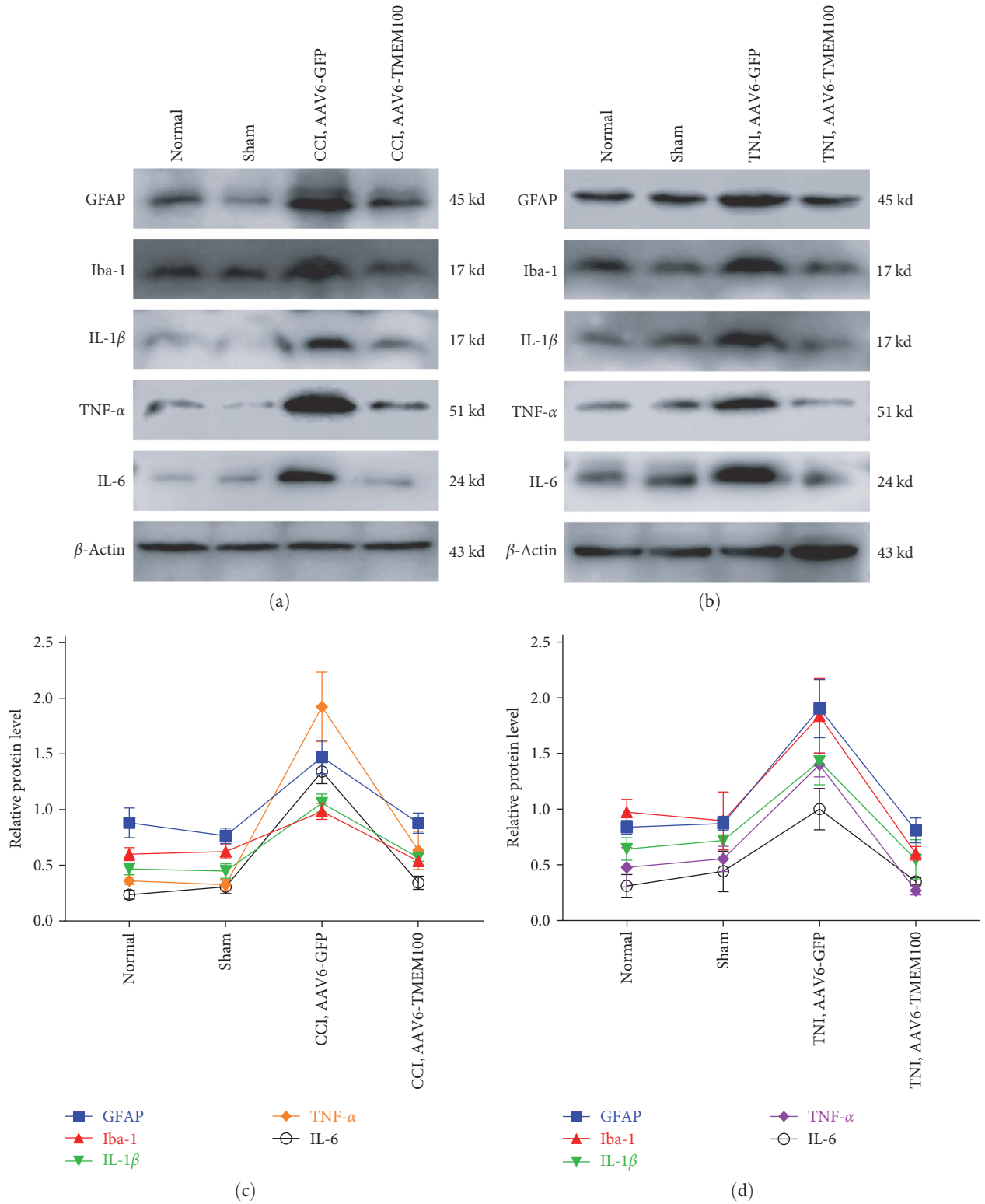
FIGURE 7: Western blot was used to detect the difference of protein expression of microglia (Iba-1), astrocytes (GFAP), and inflammatory mediators (TNF- α, IL-6, and IL-1 β) between CCI (a) and TNI (b) groups (AAV6-GFP group and AAV6-TMEM100 group). (c) Histogram of protein expression in CCI group; (d) histogram of protein expression in TNI group.

(a)

(b)

(c)

(d)

(e)
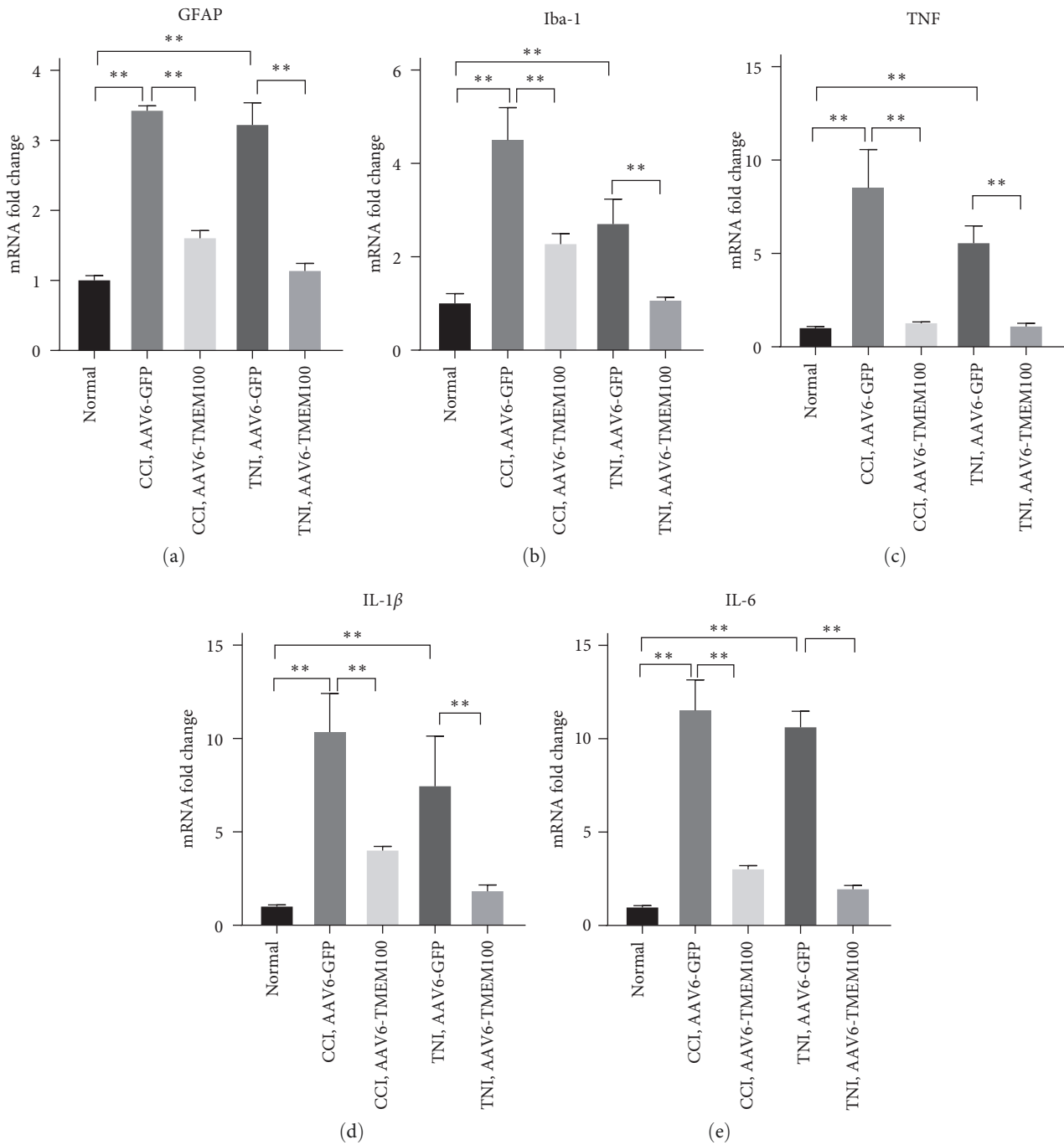
Figure 8: Detecting microglia (Iba-1), astrocytes (GFAP), and inflammatory mediators in virus-transfected groups (AAV6-GFP and AAV6-TMEM100 groups) in CCI and TNI groups by qRT–PCR detection (TNF-α, IL-6, and IL-1β) mRNA expression differences. $**P < 0.01$.

downregulation of TMEM100 expression, which is consistent with our findings.

After we injected AAV6-TMEM100 into SN of rats, the expression of TMEM100 in both CCI and TNI rats was significantly increased, and the expression of pain behavior was significantly improved, which also reflected the potential therapeutic mechanism of analgesic effect of TMEM100. Therefore, AAV6-mediated DRG-targeted delivery of TMEM100 has the potential to be translated into clinical use for treating patients with NP, although long-term safety requires further study.

5. Conclusions

This study found that the expression level of TMEM100 was decreased in NP. By upregulating the expression of
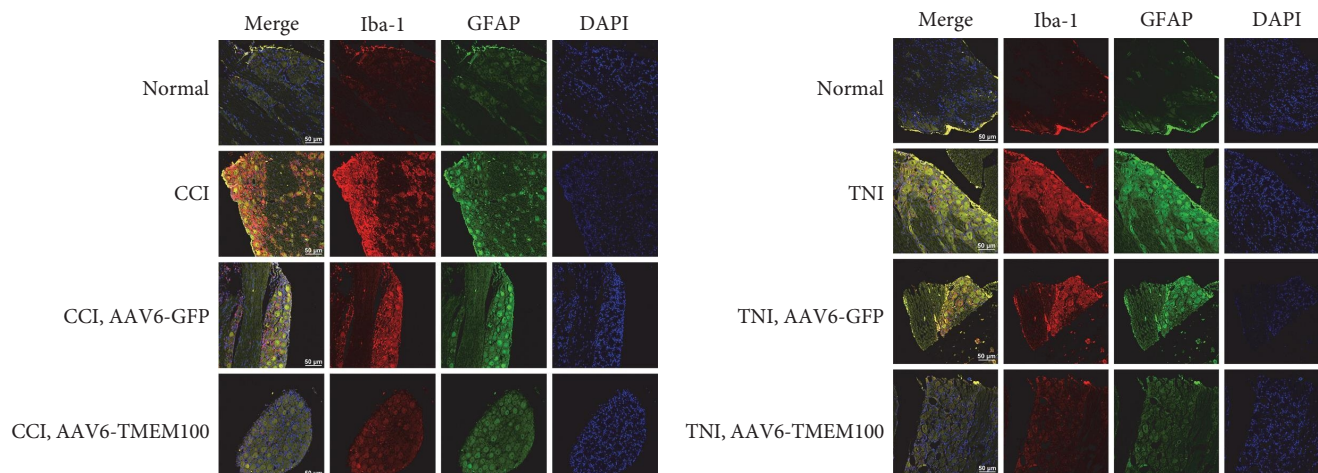
FIGURE 9: Detecting microglia (Iba-1), astrocytes (GFAP), and inflammatory mediators in virus-transfected groups (AAV6-GFP and AAV6-TMEM100 groups) in CCI and TNI groups by immunofluorescence detection (TNF-α, IL-6, and IL-1β) fluorescence intensity expression difference.

TMEM100, the activation of glial cells and inflammatory mediators can be reduced to relieve pain. We believe that TMEM100 may be helpful in the treatment of NP.

Data Availability

All the data and material can be available from Zhaoyang Guo, Zhu Guo, Zuoran Fan, Hongfei Xiang, Xiaolin Wu, and Bohua Chen for reasonable request.

Disclosure

A preprint has previously been published [https://www.researchsquare.com/article/rs-2358317/v1] [50].

Conflicts of Interest

The authors declare that they have no conflicts of interest.

Authors' Contributions

Xiaolin Wu, Zhu Guo, Bohua Chen, and Hongfei Xiang contributed in design of experiments, Youfu Zhu and Zuoran Fan contributed in literature search, Zhaoyang Guo, Huifei Cui, Yuanye Ma, and Zuoran Fan contributed in conducting the experiments, Huifei Cui, Zhu Guo, Xiaolin Wu, and Nana Sheng contributed in data analysis, Zhaoyang Guo, Zhu Guo, and Hongfei Xiang contributed in manuscript writing, and Xiaolin Wu, Hongfei Xiang, Nana Shen, Xiaoying Qi, and Bohua Chen contributed in manuscript review. Huifei Cui, Zhaoyang Guo, and Zhu Guo contributed equally to this study.

Acknowledgments

References

[1] T. S. Jensen, R. Baron, M. Haanpää et al., "A new definition of neuropathic pain," *Pain*, vol. 152, no. 10, pp. 2204-2205, 2011.

[2] L. Colloca, T. Ludman, D. Bouhassira et al., "Neuropathic pain," *Nature Reviews Disease Primers*, vol. 3, Article ID 17002, 2017.

[3] A. Truini, L. Garcia-Larrea, and G. Cruccu, "Reappraising neuropathic pain in humans—how symptoms help disclose mechanisms," *Nature Reviews Neurology*, vol. 9, pp. 572–582, 2013.

[4] D. Szok, J. Tajti, A. Nyári, L. Vécsei, and L. Trojano, "Therapeutic approaches for peripheral and central neuropathic pain," *Behavioural Neurology*, vol. 2019, Article ID 8685954, 13 pages, 2019.

[5] C. Toth, J. Lander, and S. Wiebe, "The prevalence and impact of chronic pain with neuropathic pain symptoms in the general population," *Pain Medicine*, vol. 10, no. 5, pp. 918–929, 2009.

[6] T.-Y. Yeh, I.-W. Luo, Y.-L. Hsieh, T.-J. Tseng, H. Chiang, and S.-T. Hsieh, "Peripheral neuropathic pain: from experimental models to potential therapeutic targets in dorsal root ganglion neurons," *Cells*, vol. 9, no. 12, Article ID 2725, 2020.

[7] T. S. Jensen and N. B. Finnerup, "Allodynia and hyperalgesia in neuropathic pain: clinical manifestations and mechanisms," *The Lancet Neurology*, vol. 13, no. 9, pp. 924–935, 2014.

[8] S. P. Cohen and J. Mao, "Neuropathic pain: mechanisms and their clinical implications," *BMJ*, vol. 348, Article ID f7656, 2014.

[9] H. Yu, S. M. Shin, F. Wang et al., "Transmembrane protein 100 is expressed in neurons and glia of dorsal root ganglia and is reduced after painful nerve injury," *PAIN Reports*, vol. 4, no. 1, Article ID e703, 2019.

[10] S. T. Eisenman, S. J. Gibbons, R. D. Singh et al., "Distribution of TMEM100 in the mouse and human gastrointestinal tract—a novel marker of enteric nerves," *Neuroscience*, vol. 240, pp. 117–128, 2013.

[11] E.-H. Moon, Y. S. Kim, J. Seo, S. Lee, Y. J. Lee, and S. P. Oh, "Essential role for TMEM100 in vascular integrity but limited contributions to the pathogenesis of hereditary haemorrhagic telangiectasia," *Cardiovascular Research*, vol. 105, no. 3, pp. 353–360, 2015.

[12] S. Somekawa, K. Imagawa, H. Hayashi et al., "*Tmem100*, an ALK1 receptor signaling-dependent gene essential for arterial endothelium differentiation and vascular morphogenesis," *Proceedings of the National Academy of Sciences*, vol. 109, no. 30, pp. 12064–12069, 2012.

[13] E. Frullanti, F. Colombo, F. S. Falvella et al., "Association of lung adenocarcinoma clinical stage with gene expression pattern in noninvolved lung tissue," *International Journal of Cancer*, vol. 131, no. 5, pp. E643–E648, 2012.

[14] H.-J. Weng, K. N. Patel, N. A. Jeske et al., "Tmem100 is a regulator of TRPA1–TRPV1 complex and contributes to persistent pain," *Neuron*, vol. 85, no. 4, pp. 833–846, 2015.

[15] M.-K. Chung, J. Park, J. Asgar, and J. Y. Ro, "Transcriptome analysis of trigeminal ganglia following masseter muscle inflammation in rats," *Molecular Pain*, vol. 12, 2016.

[16] M. L. LaCroix-Fralish, J. S. Austin, F. Y. Zheng, D. J. Levitin, and J. S. Mogil, "Patterns of pain: meta-analysis of microarray studies of pain," *Pain*, vol. 152, no. 8, pp. 1888–1898, 2011.

[17] B. Luchting, J. Heyn, T. Woehrle et al., "Differential expression of P2X7 receptor and IL-1β in nociceptive and neuropathic pain," *Journal of Neuroinflammation*, vol. 13, Article ID 100, 2016.

[18] T. Rouwette, J. Sondermann, L. Avenali, D. Gomez-Varela, and M. Schmidt, "Standardized profiling of the membrane-enriched proteome of mouse dorsal root ganglia (DRG) provides novel insights into chronic pain," *Molecular & Cellular Proteomics*, vol. 15, no. 6, pp. 2152–2168, 2016.

[19] Q. Xu and T. L. Yaksh, "A brief comparison of the pathophysiology of inflammatory versus neuropathic pain," *Current Opinion in Anaesthesiology*, vol. 24, no. 4, pp. 400–407, 2011.

[20] Y. Huh, R.-R. Ji, and G. Chen, "Neuroinflammation, bone marrow stem cells, and chronic pain," *Frontiers in Immunology*, vol. 8, Article ID 1014, 2017.

[21] R.-R. Ji, A. Chamessian, and Y.-Q. Zhang, "Pain regulation by non-neuronal cells and inflammation," *Science*, vol. 354, no. 6312, pp. 572–577, 2016.

[22] G. Littlejohn, "Neurogenic neuroinflammation in fibromyalgia and complex regional pain syndrome," *Nature Reviews Rheumatology*, vol. 11, pp. 639–648, 2015.

[23] C. Sommer, M. Leinders, and N. Üçeyler, "Inflammation in the pathophysiology of neuropathic pain," *Pain*, vol. 159, no. 3, pp. 595–602, 2018.

[24] L.-X. Pan, L.-Y. Li, H. Zhou et al., "TMEM100 mediates inflammatory cytokines secretion in hepatic stellate cells and its mechanism research," *Toxicology Letters*, vol. 317, pp. 82–91, 2019.

[25] C.-X. Zheng, S.-M. Wang, Y.-H. Bai et al., "Lentiviral vectors and adeno-associated virus vectors: useful tools for gene transfer in pain research," *The Anatomical Record*, vol. 301, no. 5, pp. 825–836, 2018.

[26] M. Glatzel, E. Flechsig, B. Navarro et al., "Adenoviral and adeno-associated viral transfer of genes to the peripheral nervous system," *Proceedings of the National Academy of Sciences*, vol. 97, no. 1, pp. 442–447, 2000.

[27] Y. Xu, Y. Gu, G.-Y. Xu, P. Wu, G.-W. Li, and L.-Y. M. Huang, "Adeno-associated viral transfer of opioid receptor gene to primary sensory neurons: a strategy to increase opioid antinociception," *Proceedings of the National Academy of Sciences*, vol. 100, no. 10, pp. 6204–6209, 2003.

[28] C. Towne, M. Pertin, A. T. Beggah, P. Aebischer, and I. Decosterd, "Recombinant adeno-associated virus serotype 6 (rAAV2/6)-mediated gene transfer to nociceptive neurons through different routes of delivery," *Molecular Pain*, vol. 5, Article ID 52, 2009.

[29] L. Vulchanova, D. J. Schuster, L. R. Belur et al., "Differential adeno-associated virus mediated gene transfer to sensory neurons following intrathecal delivery by direct lumbar puncture," *Molecular Pain*, vol. 6, 2010.

[30] G. J. Bennett and Y.-K. Xie, "A peripheral mononeuropathy in rat that produces disorders of pain sensation like those seen in man," *Pain*, vol. 33, no. 1, pp. 87–107, 1988.

[31] B. H. Lee, R. Won, E. J. Baik, S. H. Lee, and C. H. Moon, "An animal model of neuropathic pain employing injury to the sciatic nerve branches," *NeuroReport*, vol. 11, no. 4, pp. 657–661, 2000.

[32] M.-K. Chung, A. D. Güler, and M. J. Caterina, "TRPV1 shows dynamic ionic selectivity during agonist stimulation," *Nature Neuroscience*, vol. 11, pp. 555–564, 2008.

[33] S. R. Chaplan, F. W. Bach, J. W. Pogrel, J. M. Chung, and T. L. Yaksh, "Quantitative assessment of tactile allodynia in the rat paw," *Journal of Neuroscience Methods*, vol. 53, no. 1, pp. 55–63, 1994.

[34] K. Hargreaves, R. Dubner, F. Brown, C. Flores, and J. Joris, "A new and sensitive method for measuring thermal nociception in cutaneous hyperalgesia," *Pain*, vol. 32, no. 1, pp. 77–88, 1988.

[35] Z. Han, T. Wang, S. Han et al., "Low-expression of TMEM100 is associated with poor prognosis in non-small-cell lung cancer," *American Journal of Translational Research*, vol. 9, no. 5, pp. 2567–2578, 2017.

[36] E.-H. Moon, M.-J. Kim, K. S. Ko et al., "Generation of mice with a conditional and reporter allele for Tmem100," *Genesis*, vol. 48, no. 11, pp. 673–678, 2010.

[37] A. A. A. Pradhan, X. H. Yu, and J. M. A. Laird, "Modality of hyperalgesia tested, not type of nerve damage, predicts pharmacological sensitivity in rat models of neuropathic pain," *European Journal of Pain*, vol. 14, no. 5, pp. 503–509, 2010.

[38] A. F. Bourquin, M. Süveges, M. Pertin et al., "Assessment and analysis of mechanical allodynia-like behavior induced by spared nerve injury (SNI) in the mouse," *Pain*, vol. 122, no. 1, pp. 14e1–14e14, 2006.

[39] D. Li, H. Yang, B. A. Meyerson, and B. Linderoth, "Response to spinal cord stimulation in variants of the spared nerve injury pain model," *Neuroscience Letters*, vol. 400, no. 1-2, pp. 115–120, 2006.

[40] T. Yamazaki, M. Muramoto, O. Okitsu, N. Morikawa, and Y. Kita, "Discovery of a novel neuroprotective compound, AS1219164, by high-throughput chemical screening of a newly identified apoptotic gene marker," *European Journal of Pharmacology*, vol. 669, no. 1–3, pp. 7–14, 2011.

[41] H. J. You, H.-Y. Park, J. Kim et al., "Integrative radiogenomic analysis for genomic signatures in glioblastomas presenting leptomeningeal dissemination," *Medicine*, vol. 95, no. 27, Article ID e4109, 2016.

[42] L. Zhang, X. Chen, L. Wu et al., "Ameliorative effects of escin on neuropathic pain induced by chronic constriction injury of sciatic nerve," *Journal of Ethnopharmacology*, vol. 267, Article ID 113503, 2021.

[43] K. Ren and R. Dubner, "Interactions between the immune and nervous systems in pain," *Nature Medicine*, vol. 16, pp. 1267–1276, 2010.

[44] R.-R. Ji, T. Berta, and M. Nedergaard, "Glia and pain: is chronic pain a gliopathy?" *Pain*, vol. 154, pp. S10–S28, 2013.

[45] J. V. Berger, R. Deumens, S. Goursaud et al., "Enhanced neuroinflammation and pain hypersensitivity after peripheral nerve injury in rats expressing mutated superoxide dismutase 1," *Journal of Neuroinflammation*, vol. 8, Article ID 33, 2011.

[46] X. Zhang, Y. Chen, C. Wang, and L.-Y. M. Huang, "Neuronal somatic ATP release triggers neuron–satellite glial cell communication in dorsal root ganglia," *Proceedings of the National Academy of Sciences*, vol. 104, no. 23, pp. 9864–9869, 2007.

[47] D.-S. Kim, K. W. Figueroa, K.-W. Li, A. Boroujerdi, T. Yolo, and D. Z. Luo, "Profiling of dynamically changed gene expression in dorsal root ganglia post peripheral nerve injury and a critical role of injury-induced glial fibrillary acidic protein in maintenance of pain behaviors," *Pain*, vol. 143, no. 1, pp. 114–122, 2009.

[48] W. Wang, W. Wang, Y. Wang, J. Huang, S. Wu, and Y.-Q. Li, "Temporal changes of astrocyte activation and glutamate transporter-1 expression in the spinal cord after spinal nerve ligation-induced neuropathic pain," *The Anatomical Record*, vol. 291, no. 5, pp. 513–518, 2008.

[49] E. D. Milligan and L. R. Watkins, "Pathological and protective roles of glia in chronic pain," *Nature Reviews Neuroscience*, vol. 10, pp. 23–36, 2009.

[50] Z. Guo, Z. Guo, Z. Fan et al., "TMEM100 regulates neuropathic pain by reducing the expression of inflammatory factors," PREPRINT (Version 1) available at Research Square, 2022.

Hindawi

Research Article

Safety and Efficacy of Polyetheretherketone (PEEK) Cages and Cadaveric Allografts in Transforaminal Lumbar Interbody Fusion (TLIF) for Treating Lumbar Pyogenic Spondylodiscitis

Huo-Liang Zheng [iD], **Bo Li** [iD], **Shao-Kuan Song** [iD], **Peng-Bo Chen** [iD], **Xin-Feng Zheng** [iD], **Lei-Sheng Jiang** [iD], **and Sheng-Dan Jiang** [iD]

Department of Clinic of Spine Center, Xinhua Hospital, Shanghai Jiao Tong University School of Medicine, Shanghai 200092, China

Correspondence should be addressed to Lei-Sheng Jiang; jiangleisheng@xinhuamed.com.cn
and Sheng-Dan Jiang; jiangshengdan@xinhuamed.com.cn

Purpose. There have been many studies in the operative management of pyogenic spondylodiscitis with foreign materials. However, it still remains an issue of debate on whether the allografts may be used in pyogenic spondylodiscitis. This study sought to evaluate the safety and effectiveness of PEEK cages and the cadaveric allograft in transforaminal lumbar interbody fusion (TLIF) for treating lumbar pyogenic spondylodiscitis. *Methods.* From January 2012 to December 2019, 56 patients underwent surgery for lumbar pyogenic spondylodiscitis. The posterior debridement of all patients and their fusion with allografts, local bone grafts, and bone chip cages were performed before posterior pedicle screw fusion. An assessment of the residual pain, the grade of neurological injury, and the resolution of infection was conducted on 39 patients. The clinical outcome was evaluated using a visual analog scale (VAS) and the Oswestry Disability Index (ODI), and neurological outcomes were appraised based on Frankel grades. The radiological outcomes were evaluated via focal lordosis, lumbar lordosis, and the state of the fusion. *Results.* Staphylococcus aureus and Staphylococcus epidermidis were the most common causative organisms. The mean preoperative focal lordosis was $-1.2°$ ($-11.4°$ to $5.7°$), and the mean postoperative focal lordosis increased to $10.3°$ ($4.3°–17.2°$). At the final follow-up, there were five cases with subsidence of the cage, no case of recurrence, and no case with cage and screw loosening or migration. The mean preoperative VAS and ODI scores were 8.9 and 74.6%, respectively, and improvements in VAS and ODI were 6.6 ± 2.2 and $50.4 \pm 21.3\%$, respectively. The Frankel grade D was found in 10 patients and grade C in 7. Following the final follow-up, only one patient improved from Frankel grade C to grade D while the others recovered completely. *Conclusion.* The PEEK cage and cadaveric allograft combined with local bone grafts is a safe and effective choice for intervertebral fusion and restoring sagittal alignment without increased incidence of relapse for treating lumbar pyogenic spondylodiscitis.

1. Introduction

Pyogenic spondylitis continues to represent a worldwide problem. Pyogenic spondylitis is relatively rare with an incidence between 0.4 and 2.0 cases per 100,000 each year but can be severe and life-threatening [1, 2]. A conservative strategy, primarily antibiotic therapy and bracing may be effective in managing spondylodiscitis that does not lead to osseous destruction and subsequent instability. Surgical treatment is necessary in more advanced states, especially those with significant instability, deformity, and/or neurological deficits [3]. Today's gold standard of care includes instrumentation of the posterior pedicle screw, radical disc debridement, and intervertebral fusion with titanium cages or autologous bone grafts [4–7].

In terms of the fusion rate, titanium cages are reliable, but the incidence of subsidence and secondary kyphotic deformity remains controversial [5, 6, 8, 9]. Biocompatible

polyetheretherketone (PEEK) cages are used extensively in various degenerative spinal diseases as biocompatible alternatives to metal implants. Although some studies have reported that PEEK cages are safe for patients with pyogenic spondylodiscitis [10], the implementation and modification of PEEK cages still need to be further explored.

Local bone grafts from the facet or lamina, however, may be insufficient for satisfied intervertebral fusion in lumbar pyogenic spondylodiscitis. Despite widespread acceptance of tricortical bone grafting for intervertebral fusion, postoperative pain and fracture at the donor site remain serious management issues. Allografts appear to be a promising option, but it still remains an issue of debate whether the allografts could be used in active spinal infection. Few studies have focused on the application of cadaveric allografts and PEEK cages for treating lumbar pyogenic spondylodiscitis. As a consequence, we aimed to determine whether the use of PEEK cages and cadaveric allografts for treating lumbar pyogenic spondylodiscitis was safe and effective.

2. Materials and Methods

Fifty-six patients underwent surgery for lumbar pyogenic spondylodiscitis from January 2012 to December 2019, and 39 patients were assessed in this study. The surgical indications included medical treatment failure, severe pain, vertebral destruction resulting in segmental kyphosis, instability, or neurological deficits. All patients were treated with a posterior debridement and fusion with cadaveric allograft and a PEEK cage loaded with bone chips, prior to posterior pedicle screw fixation. In this study, follow-up time for patients averaged 28.3 months, lasting for at least 2 years.

Clinical presentation; imaging findings including X-ray, CT, and MRI; and hematological examinations were used to formulate the diagnosis of lumbar pyogenic spondylodiscitis. An acute spinal hematogenous infection was diagnosed in all patients. Each patient's intraoperative specimens were processed for Gram staining, aerobic and anaerobic culture and sensitivity, fungal culture, and acid-fast staining.

In the surgical strategy, instrumentation of the posterior pedicle screw was followed by intervertebral disc resection, bony debridement, and an intervertebral fusion. A normal saline irrigation was performed after removing the infected tissue from the disc space. Subsequently, cadaveric allografts and local bone grafts were inserted into the disc space, and then, the intervertebral PEEK cage filled with bone chips was implanted obliquely to bridge the endplates in a unilateral TLIF technique. There was no harvesting of the iliac crest bone in any of the patients. Afterwards, a standard single-layer closure was utilized to close the wound.

VAS and ODI were used to evaluate clinical outcomes, while the Frankel scale was used to evaluate neurological results. Postoperatively, lateral X-ray and CT were used to assess the interbody fusion, subsidence, segmental lordosis, and lumbar lordosis. The following criteria were used to determine if fusion was successful: the contiguous bony bridge that connects the instrumented vertebrae, absence of the radiolucency around the cages, and no implant failure. Subsidence is defined as more than 5 mm of sinking of the cage or disc space compared with immediate postoperative imaging. Based on preoperative and follow-up radiographs, segmental lordosis of the fusion level was assessed.

A short period of broad-spectrum intravenous antibiotic therapy was followed by adjustment based on the antibiogram. After surgery, all patients received intravenous antibiotics for a minimum of four weeks, followed by oral antibiotics for at least four weeks or until the CRP and ESR levels returned to normal [11]. In cases without positive cultures, vancomycin and meropenem are given to eliminate both gram-positive and gram-negative bacteria until ESR and CRP levels back to normal.

Patients were evaluated for infection resolution, residual pain, neurological grade, Cobb angle, lumbar lordosis, and fusion and implant statuses at their follow-up visits. Macnab's criteria were used to assess clinical outcome.

SPSS (version 20.0) was used to analyze the data. One-way repeated measure analysis of variance (ANOVA) was used to compare the indicators in the same group at different time points, while the Friedman test was used for data that does not fit Gaussian distribution. We set a statistical significance threshold at less than 0.05.

3. Results

In this study, the median patient age was 63 years old, and females predominated (64.1%). All patients had back pain, eight patients (20.5%) had radicular pain, and only seventeen patients (43.6%) had a fever upon presentation. It took an average of 1.8 months (0.5 to 4 months) from symptom onset to diagnosis. There were 14 patients with infection at L4/5 (35.9%), followed by L3/4 in 11 patients (28.2%), L5/S1 in 9 patients (23.1%), and L2/3 in 5 patients (12.8%) (Table 1).

The duration of operation was 106 ± 24.3 minutes. Blood loss during the operation was 205 ± 84.1 ml. Histopathological examination of the intraoperative biopsy confirmed the diagnosis, demonstrating an infiltration of inflammatory cells and vascular proliferation associated with granulation tissue. Bacteria cultures were conducted on all observed specimens taken from the infected site during operation, but only thirty-three positive cultures were found. Staphylococcus aureus was the most common causative organism, detected in twenty-three patients. Of the twenty-three patients, two were positive with methicillin-resistant Staphylococcus aureus. Six patients had Staphylococcus epidermidis, one patient had Streptococcus suis, one patient had Escherichia coli, one patient had Acinetobacter baumannii, and one patient had Corynebacterium (Table 2).

3.1. Radiological Outcomes. The extent of the lesion was determined via preoperative MRI scans. Bony destruction, instability, and deformity were assessed via preoperative X-rays and CT scans. Focal lordosis and lumbar lordosis were measured by using the Cobb method on preoperative and postoperative radiographs. As shown in Table 3, the mean preoperative focal lordosis was $-1.2°$ ($-11.4°$ to $5.7°$), and the mean postoperative focal lordosis significantly increased to $10.3°$ ($4.3°$–$17.2°$). The mean two-year postoperative focal

TABLE 1: Basic data of patients ($x \pm s$, $n = 39$).

Characteristics	
Age at surgery	63.0 ± 12.7
Sex	
Male	14 (35.9%)
Female	25 (64.1%)
Infected level	
L2/3	5 (12.8%)
L3/4	11 (28.2%)
L4/5	14 (35.9%)
L5/S1	9 (23.1%)
Fever	17 (43.6%)
Operation time (min)	106.0 ± 24.3
Blood loss (ml)	205.0 ± 84.1
Follow-up period (month)	28.3 ± 8.5

TABLE 2: Organisms from specimen culture findings.

Organism	Number of patients
Staphylococcus aureus	21
Methicillin-resistant Staphylococcus aureus	2
Staphylococcus epidermidis	6
Streptococcus suis	1
Escherichia coli	1
Acinetobacter baumannii	1
Corynebacterium	1
Not identified	6

lordosis was maintained at 9.8° (4.1°–16.9°). Mean preoperative lumbar lordosis was 21.6° (13.6°–27.5°), and the mean postoperative lumbar lordosis significantly increased to 31.5° (26.1°–37.2°). The mean two-year postoperative lumbar lordosis was maintained at 30.6° (24.9°–36.8°). During the final follow-up, thirty-eight patients had bone bridging across the fusion site, indicating a definitive fusion (Figure 1). At the final follow-up, one patient was suspected to have pseudoarthrosis, five cases showed cage subsidence, and one case showed cage and screw migration or loosening.

3.2. Neurological Function. In 17 patients, lower-extremity weakness or sensory changes were noted, although they were rarely severe. Frankel grade D was found in 10 patients and grade C in 7. At the final follow-up, 16 patients recovered completely, while only 1 patient with grade C improved to grade D.

3.3. Clinical Outcomes. There was a mean preoperative VAS score of 8.9 and a mean ODI score of 74.6% among all patients. In the two-year follow-up, VAS and ODI scores improved by 6.6 ± 2.2 and $50.4 \pm 21.3\%$, respectively (Table 4).

On the final follow-up, all infections had been cleared. Overall, thirty-three patients (84.6%) had complete pain relief, while six (15.4%) had slight residual pain that did not limit daily activity or need frequent analgesic use. Based on Macnab's criteria [12], thirty-three patients (84.6%) had excellent results, five patients had (12.8%) good results, and only one patient (2.6%) had a fair result.

4. Discussion

Although imaging, microbiology, and histopathology techniques have improved, the early diagnosis of pyogenic spondylosis remains challenging. There is always a delay of diagnosis as reported in some studies [13, 14]. Similarly, a median delay of 1.8 months was observed before the correct diagnosis in our series. Two factors might account for this delay of diagnosis. One is that there was no specific symptom in the early stage of lumbar pyogenic spondylodiscitis except for back pain, and the other is that our hospital serves as a tertiary care center for a large region, where patients usually present after failing to receive successful treatment elsewhere. The delay in diagnosis always leads to greater tissue destruction, spinal instability, local kyphotic deformity, and worsening neurological deficits.

Several strategies have been described for the treatment of lumbar pyogenic spondylodiscitis. It was found that autologous bone grafting after debridement proved to be the most efficient and safe method of treating active infections, irrespective of the organism causing the infection, according to Wiltberger in 1952 [15, 16]. Nevertheless, complications, such as pain at the donor site, frequently occur, so grafting with other materials has been introduced. As an additional material, the cadaveric allograft was widely used in treating degenerative spinal disorders, whereas only a minority of the studies reported the cadaveric allograft for interbody fusion in pyogenic spinal infection [17–19]. The application and generalization of the cadaveric allograft in lumbar pyogenic spondylodiscitis still needs to be further confirmed.

Aside from this, some authors claim that grafting with foreign material may reduce antibiotic efficiency and increase the adhesion of bacteria [16, 20]. In comparison to stainless steel, titanium has proven less prone to bacterial colonization [21]. Pee et al. [8] reported the efficacy of titanium cages, titanium mesh cages, and PEEK cages in treating pyogenic spondylodiscitis. They compared clinical and radiological results between patients with pyogenic spondylodiscitis who were treated with cages and struct bone grafts for interbody fusion and found that the struct group had a higher subsidence rate. Cages provided a stronger stability than the struct grafts, which was more favorable for bony fusion. Moreover, studies have shown that PEEK cages do not affect the radiological outcome and increase the risk of reinfection compared to titanium cages [9]. Shiban et al. demonstrated that the use of PEEK cages for interbody fusion is feasible and safe in patients suffering from a pyogenic spinal infection [10]. Similarly, Tschöke et al. [22] proved the efficacy of PEEK interbody cages in treating lumbar pyogenic spondylodiscitis, allowing a stable and solid bony fusion through the posterior TLIF approach. In this study of thirty-nine cases suffering from lumbar pyogenic spondylodiscitis, we reviewed the primary radiological and clinical outcomes. The foreign materials including PEEK and the cadaveric allograft did not seem to affect the clinical

TABLE 3: Focal and lumbar lordosis before and after surgery ($x \pm s$, $n = 39$).

Parameters	Preoperative	1-month postoperative	2-year postoperative	p
Focal lordosis	-1.2 ± 5.3	10.3 ± 3.7^a	9.8 ± 3.8^a	<0.001
Lumbar lordosis	21.6 ± 4.3	31.5 ± 3.6^a	30.6 ± 3.7^a	<0.001

Note: comparison between preoperative and postoperative parameters; $^a p < 0.05$.
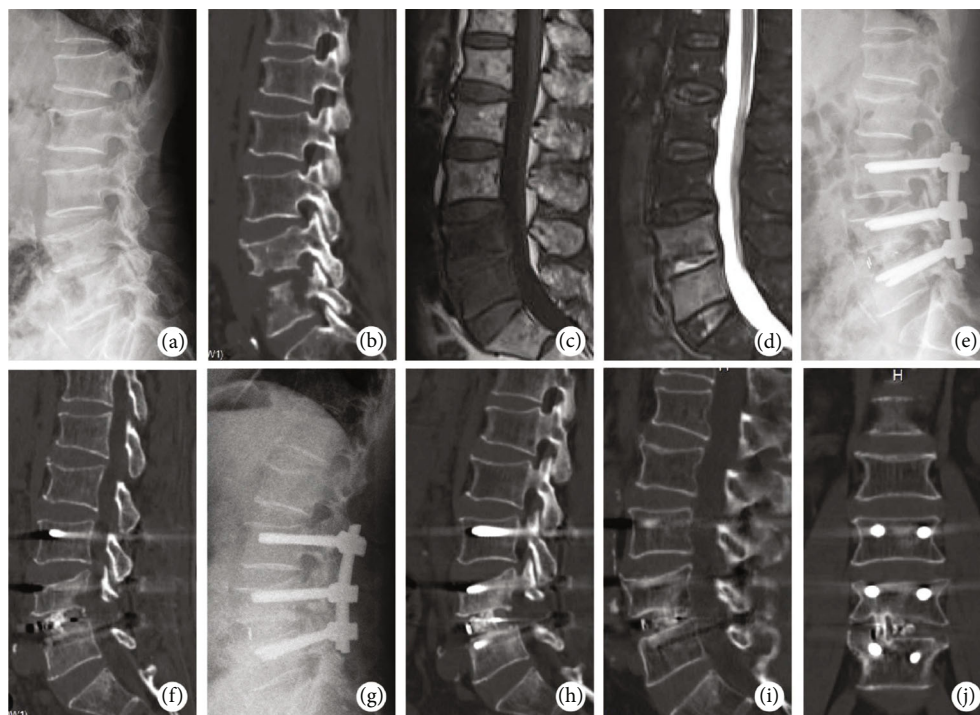
FIGURE 1: A 68-year-old male with lumbar pyogenic spondylodiscitis. (a) Preoperative lumbar spine X-ray. (b) Preoperative lumbar CT image. (c) T1-weighted image showed hypointensity of L4–L5 vertebral body. (d) T2-weighted fat-suppression sequence showed relative homogeneous enhancement of vertebral bodies and remarkable hyperintensity of the disc. (e, f) Postoperative lumbar radiological images. (g, h) Radiological images at 3 months postoperatively. (i, j) The CT scan showed solid interbody fusion at 1 year after surgery.

TABLE 4: VAS and ODI scores before and after surgery ($x \pm s$, $n = 39$).

Parameters	Preoperative	1-month postoperative	2-year postoperative	p
VAS	8.9 ± 1.1	4.3 ± 1.3^a	2.3 ± 1.7^a	<0.001
ODI	74.6 ± 11.8	39.7 ± 9.4^a	24.2 ± 13.9^a	<0.001

Note: VAS: visual analog scale; ODI: Oswestry Disability Index. Comparison between preoperative and postoperative parameters; $^a p < 0.05$.

outcome and the risk of reinfection. In the present study, we were able to demonstrate that there were no cases of recurring inflammation in patients treated with the PEEK material and allograft after a minimum follow-up of 24 months.

Spinal instrumentation has proven to be safe and effective when used in the presence of active infection [23–25]. Biofilms that bind organisms to implants do not appear to pose any significant clinical risks. According to Hee et al., patients with or without posterior instrumentation had differing outcomes [26]. In comparison to patients who underwent anterior fusion alone, the posterior instrumentation significantly corrected sagittal alignment by 6.2 times (11.1∘±7.4∘ compared with 1.8∘±4.6∘, $p = 0.005$). Our study also found that the patients treated with additional instrumentation obtained an 11.5° correction of the sagittal alignment postoperatively that was maintained at final follow-up. In comparison with noninstrumented cases, posterior instrumentation provides greater sagittal balance, little loss of correction, and more satisfied fusion rates.

A 97% fusion rate was achieved in our series. Kim et al. [17] reported that 93.3% of patients (14 of 15) using the cadaveric allograft showed osseous union while only 83.3% of patients using the titanium cage showed union. The cadaveric allograft in combination with the PEEK cage may explain the higher fusion rate in our series. On the one hand, the amount of the bone graft for fusion is sufficient because of the cadaveric allograft. On the other hand, the PEEK cage increases the stability and benefits bone fusion.

The PEEK cage can restore and maintain sagittal alignment in treating lumbar pyogenic spondylodiscitis, and the cadaveric allograft can be a useful adjunct for intervertebral fusion. The posterior interbody fusion with the cadaveric allograft and PEEK cage followed by the pedicle screw fixation does not increase relapse rates and is a safe and effective surgical option for treating pyogenic spondylodiscitis.

Data Availability

The datasets analyzed in the current study are available from the corresponding authors.

Ethical Approval

The study was approved by the Ethics Committee of the Xinhua Hospital affiliated to the Shanghai Jiao Tong University School of Medicine.

Consent

All individual participants have provided consent to participate in the study.

Conflicts of Interest

The authors declare that they have no competing interests.

Authors' Contributions

Huo-Liang Zheng and Bo Li wrote the article. Shao-Kuan Song and Peng-Bo Chen were responsible for the data collection and analysis. Xin-Feng Zheng were responsible for reviewing the data. Lei-Sheng Jiang and Sheng-Dan Jiang were responsible for reviewing and revising the article. Huo-Liang Zheng and Bo Li have contributed equally to this work.

Acknowledgments

We acknowledge all the participants in this study.

References

[1] K. Sato, K. Yamada, K. Yokosuka et al., "Pyogenic spondylitis: clinical features, diagnosis and treatment," *The Kurume Medical Journal*, vol. 65, no. 3, pp. 83–89, 2019.

[2] M. Babic and C. S. Simpfendorfer, "Infections of the spine," *Infectious Disease Clinics of North America*, vol. 31, no. 2, pp. 279–297, 2017.

[3] J. S. Butler, M. J. Shelly, M. Timlin, W. G. Powderly, and J. M. O'Byrne, "Nontuberculous pyogenic spinal infection in adults: a 12-year experience from a tertiary referral center," *Spine*, vol. 31, no. 23, pp. 2695–2700, 2006.

[4] P. Korovessis, G. Petsinis, G. Koureas, P. Iliopoulos, and S. Zacharatos, "Anterior surgery with insertion of titanium mesh cage and posterior instrumented fusion performed sequentially on the same day under one anesthesia for septic spondylitis of thoracolumbar spine: is the use of titanium mesh cages safe?," *Spine*, vol. 31, no. 9, pp. 1014–1019, 2006.

[5] Y. Robinson, S. K. Tschoeke, T. Finke, R. Kayser, W. Ertel, and C. E. Heyde, "Successful treatment of spondylodiscitis using titanium cages: a 3-year follow-up of 22 consecutive patients," *Acta Orthopaedica*, vol. 79, no. 5, pp. 660–664, 2008.

[6] Y. Robinson, S. K. Tschoeke, R. Kayser, H. Boehm, and C. E. Heyde, "Reconstruction of large defects in vertebral osteomyelitis with expandable titanium cages," *International Orthopaedics*, vol. 33, no. 3, pp. 745–749, 2009.

[7] M. Ruf, D. Stoltze, H. R. Merk, M. Ames, and J. Harms, "Treatment of vertebral osteomyelitis by radical debridement and stabilization using titanium mesh cages," *Spine*, vol. 32, no. 9, pp. E275–E280, 2007.

[8] Y. H. Pee, J. D. Park, Y. G. Choi, and S. H. Lee, "Anterior debridement and fusion followed by posterior pedicle screw fixation in pyogenic spondylodiscitis: autologous iliac bone strut versus cage," *Journal of Neurosurgery. Spine*, vol. 8, no. 5, pp. 405–412, 2008.

[9] M. Schomacher, T. Finger, D. Koeppen et al., "Application of titanium and polyetheretherketone cages in the treatment of pyogenic spondylodiscitis," *Clinical Neurology and Neurosurgery*, vol. 127, pp. 65–70, 2014.

[10] E. Shiban, I. Janssen, P. R. da Cunha et al., "Safety and efficacy of polyetheretherketone (PEEK) cages in combination with posterior pedicel screw fixation in pyogenic spinal infection," *Acta Neurochirurgica*, vol. 158, no. 10, pp. 1851–1857, 2016.

[11] J. P. Rutges, D. H. Kempen, M. van Dijk, and F. C. Oner, "Outcome of conservative and surgical treatment of pyogenic spondylodiscitis: a systematic literature review," *European Spine Journal*, vol. 25, no. 4, pp. 983–999, 2016.

[12] I. Macnab, "Negative disc exploration," *The Journal of Bone and Joint Surgery*, vol. 53, no. 5, pp. 891–903, 1971.

[13] S. E. Emery, D. P. Chan, and H. R. Woodward, "Treatment of hematogenous pyogenic vertebral osteomyelitis with anterior debridement and primary bone grafting," *Spine*, vol. 14, no. 3, pp. 284–291, 1989.

[14] G. D. Sundararaj, N. Babu, R. Amritanand et al., "Treatment of haematogenous pyogenic vertebral osteomyelitis by single-stage anterior debridement, grafting of the defect and posterior instrumentation," *The Journal of Bone and Joint Surgery*, vol. 89-B, no. 9, pp. 1201–1205, 2007.

[15] R. A. McGuire and F. J. Eismont, "The fate of autogenous bone graft in surgically treated pyogenic vertebral osteomyelitis," *Journal of Spinal Disorders*, vol. 7, no. 3, pp. 206–215, 1994.

[16] F. A. Waldvogel and P. S. Papageorgiou, "Osteomyelitis: the past decade," *The New England Journal of Medicine*, vol. 303, no. 7, pp. 360–370, 1980.

[17] H. W. Kim, J. I. Ryu, and K. H. Bak, "The safety and efficacy of cadaveric allografts and titanium cage as a fusion substitutes in pyogenic osteomyelitis," *Journal of Korean Neurosurgical Society*, vol. 50, no. 4, pp. 348–356, 2011.

[18] T. C. Chung, S. C. Yang, H. S. Chen, Y. H. Kao, Y. K. Tu, and W. J. Chen, "Single-stage anterior debridement and fibular allograft implantation followed by posterior instrumentation for complicated infectious spondylitis: report of 20 cases and review of the literature," *Medicine*, vol. 93, no. 27, article e190, 2014.

[19] D. C. Lu, V. Wang, and D. Chou, "The use of allograft or autograft and expandable titanium cages for the treatment of vertebral osteomyelitis," *Neurosurgery*, vol. 64, no. 1, pp. 122–129, 2009.

[20] M. Oga, Y. Sugioka, C. D. Hobgood, A. G. Gristina, and Q. N. Myrvik, "Surgical biomaterials and differential colonization by *Staphylococcus epidermidis*," *Biomaterials*, vol. 9, no. 3, pp. 285–289, 1988.

[21] C. C. Chang and K. Merritt, "Infection at the site of implanted materials with and without preadhered bacteria," *Journal of Orthopaedic Research*, vol. 12, no. 4, pp. 526–531, 1994.

[22] S. K. Tschöke, H. Fuchs, O. Schmidt, J. Gulow, N. H. von der Hoeh, and C. E. Heyde, "Single-stage debridement and spinal fusion using PEEK cages through a posterior approach for eradication of lumbar pyogenic spondylodiscitis: a safe treatment strategy for a detrimental condition," *Patient Safety in Surgery*, vol. 9, no. 1, p. 35, 2015.

[23] J. Kim, J. H. Lee, S. W. Kim, J. K. Oh, Y. W. Kim, and T. H. Kim, "Outcomes of additional instrumentation in elderly patients with pyogenic vertebral osteomyelitis and previous spinal instrumentation," *The Spine Journal*, vol. 19, no. 9, pp. 1498–1511, 2019.

[24] H. Q. Zhang, Y. X. Wang, J. H. Wu, and J. Chen, "Debridement and interbody graft using titanium mesh cage, posterior monosegmental instrumentation, and fusion in the surgical treatment of monosegmental lumbar or lumbosacral pyogenic vertebral osteomyelitis via a posterior-only approach," *World Neurosurgery*, vol. 135, pp. e116–e125, 2020.

[25] W. H. Chen, L. S. Jiang, and L. Y. Dai, "Surgical treatment of pyogenic vertebral osteomyelitis with spinal instrumentation," *European Spine Journal*, vol. 16, no. 9, pp. 1307–1316, 2007.

[26] H. T. Hee, M. E. Majd, R. T. Holt, and D. Pienkowski, "Better treatment of vertebral osteomyelitis using posterior stabilization and titanium mesh cages," *Journal of Spinal Disorders & Techniques*, vol. 15, no. 2, pp. 149–156, 2002.

Hindawi

Review Article

Regulatory Effect of Inflammatory Mediators in Intervertebral Disc Degeneration

Zhangfu Li ⓘ, Honghao Yang ⓘ, Yong Hai ⓘ, and Yunzhong Cheng ⓘ

Department of Orthopedic Surgery, Beijing Chao-Yang Hospital, Capital Medical University, Beijing 100020, China

Correspondence should be addressed to Yong Hai; yong.hai@ccmu.edu.cn and Yunzhong Cheng; chengyunzhong@163.com

Intervertebral disc degeneration (IDD) is a major contributor to back, neck, and radicular pain. It is related to changes in tissue structure and function, including the breakdown of the extracellular matrix (ECM), aging, apoptosis of the nucleus pulposus, and biomechanical tissue impairment. Recently, an increasing number of studies have demonstrated that inflammatory mediators play a crucial role in IDD, and they are being explored as potential treatment targets for IDD and associated disorders. For example, interleukins (IL), tumour necrosis factor-α (TNF-α), chemokines, and inflammasomes have all been linked to the pathophysiology of IDD. These inflammatory mediators are found in high concentrations in intervertebral disc (IVD) tissues and cells and are associated with the severity of LBP and IDD. It is feasible to reduce the production of these proinflammatory mediators and develop a novel therapy for IDD, which will be a hotspot of future research. In this review, the effects of inflammatory mediators in IDD were described.

1. Introduction

Intervertebral disc degeneration (IDD) is a disease of the discs that link adjacent vertebrae, with structural damage leading to a degeneration of the discs and surrounding areas. The intervertebral disc (IVD) is a fibrocartilage tissue that joins the adjacent vertebral bodies in the spine. The nucleus pulposus (NP) is the central component of the IVD and is rich in elastic colloidal compounds, including proteoglycans and type II collagen [1]. IDD can be diagnosed and graded by conventional T2-weighted magnetic resonance images, in which the colour and homogeneity of the disc, distinction of nucleus and annulus, disc signal intensity, and disc height are the basis for grading [2]. IDD is associated with disc herniation, spondylosis, lumbar spinal stenosis, sagittal imbalance of the spinal-pelvic complex, and neurological symptoms, such as low back pain (LBP), limb numbness, and decreased muscle strength [3–5]. The most common symptom of IDD is LBP, which impacts the quality of life of middle-aged and elderly individuals while increasing the economic burden on families and society [6, 7]. Although current evidence-based medicine has identified IDD as the

result of a variety of genetic, traumatic, inflammatory, lifestyle, aging, and nutritional variables, the pathogenic processes implicated in the development of IDD remain unclear [8–14]. Currently, treatment options include noninvasive therapy such as medications, multiple physical modalities, and multidisciplinary biopsychosocial rehabilitation; interventional treatments, such as intradiscal radiofrequency and epidural injections; regeneration by injecting solutions of papain and methylene blue into the disc; and surgical approaches, such as intervertebral fusion or artificial disc replacement. Despite advances in pain relief therapies, they provide only temporary relief and are associated with complications [15].

IDD progresses due to cellular and biochemical changes in the IVD microenvironment, resulting in progressive functional and structural damage. The main pathological features of IDD include the production of proinflammatory mediators, progressive loss of ECM, increased cellular senescence and apoptosis, and phenotypic changes in healthy NP cells [13, 14, 16, 17]. Many molecular biology studies have demonstrated increased expression of inflammatory mediators such as IL-1β, TNF-α, IL-6, IL-8, and IL-20 in degenerative

IVD [18–23]. Increased plasma inflammatory mediator concentrations are related to the degree of IDD and the severity of LBP [24]. Advances in inflammatory mediator mechanisms will significantly promote the translation of molecular research into clinical practice, offering new paths for developing IDD medication. This review is aimed at discussing the research on the potential function of inflammatory mediators in IDD.

2. Upstream and Downstream Regulatory Networks

Disc degeneration was derived from several initializing factors, such as genetics, mechanical stress, aging, trauma, and environmental factors [25–29]. These initializing factors lead to morphological changes in the disc tissue and surrounding structures, including a series of changes such as rupture of the annulus fibrosus (AF), NP herniation, and calcification of the cartilage endplates (CE). Since the intervertebral disc is a nearly wholly enclosed avascular tissue with few sources of nutrition, accumulation of degraded organelles and waste materials that are difficult to metabolize occurs, and a closed acidic environment gradually develops, leading to an imbalance in the internal and external environment, which propagates inflammatory signals and causes a massive release of inflammatory mediators [1], including IL-1α, IL-1β, IL-2, IL-6, IL-8, IL-9, IL-10, IL-17, TNF-α, chemokines, the NLRP3 inflammasome, and nitric oxide. These inflammatory mediators can activate signalling pathways, such as the NF-κB, PI3-K/Akt/mTOR, TGF-β, JAK-STAT, Wnt/β-catenin, and MAPK pathways, resulting in a range of pathological responses within the IVD, including an enhanced inflammatory response, promote ECM degradation, accelerate cellular senescence, increased intracellular ROS, promotion of apoptosis or pyroptosis, regulation of NP cell proliferation, and increased angiogenesis and neoinnervation. Ultimately, this process exacerbates the development of IDD. A schematic diagram of this pathological process is shown in Figure 1.

3. Sources of Inflammatory Mediators

Inflammatory mediators can be secreted by endogenous intervertebral disc cells and exogenous immune cells [30]. The normal aging process associated with genetic susceptibility leads to degeneration of the IVD, causing alterations in the ECM, such as a reduced number of functional cells, reduced proteoglycan content, malnutrition, dehydration, matrix breakdown, and calcification. Modifications in the ECM affect the typical response of the IVD to mechanical loading. The IVD becomes prone to microfissures and consequent ingrowth of nerve tissue and blood vessels. Fragments and microcrystals of the ECM may internally cause an inflammatory response, stimulating endogenous IVD cells to produce proinflammatory mediators such as IL-1β, IL-6, and IL-8, further promoting a chain reaction of tissue degeneration. In addition, NP is recognized by the immune system as nonself when exposed to tissues, such as through microfissures or protrusions, thereby recruiting inflamma-

tory cells such as macrophages, endothelial cells, B cells, and T cells. These inflammatory cells can secrete inflammatory mediators. A brief overview of the various cells expressing different cytokines is presented in Figure 2.

4. Inflammatory Mediators

Table 1 shows the inflammatory mediators associated with IDD.

4.1. Interleukin (IL)

4.1.1. IL-1α. IL-1α is a critical inflammatory mediator primarily released by monocytes, macrophages, dendritic cells, and endothelial cells [31]. IL-1α and IL-1β act in the same way, and their receptors share the same ligand binding and signal transduction pathways [32]. However, unlike IL-1β, IL-1α activity is not dependent on the inflammasome caspase-1 pathway [33]. Several studies have found that IL-1α levels in degenerative lumbar disc tissue are elevated compared with those in normal lumbar disc tissue and that IL-1α levels are positively associated with the severity of IDD [31, 34]. Previous meta-analyses revealed that the IL-1α (+889C/T) polymorphism was related to the increased incidence of IDD in Caucasian and Chinese Han populations [35, 36]. IL-1α has been found to accelerate IDD development by increasing extracellular matrix-degrading enzyme production and inhibiting extracellular matrix synthesis [37, 38]. IL-1α may also play a role in cartilage endplate degeneration by regulating MMP-3 and TIMP-3[39]. Furthermore, IL-1α could contribute to LBP by inducing IVDs to produce prostaglandin E2 and other inflammatory chemicals [40]. The sensitivity of bradykinin can be enhanced by IL-1α, which directly irritates nerve roots and hence contributes to IDD-induced neuralgia [41]. The synthesis and signal transduction pathways of IL-1α and IL-1β are shown in Figure 3. In conclusion, IL-1α is of paramount importance in the development of IDD.

Two distinct genes encode IL-1α and IL-1β. Both proteins are produced as propeptide precursors (pro-IL-1α and pro-IL-1β). Pro-IL-1α is a physiologically active molecule with intracellular and extracellular effects. Pro-IL-1α has a nuclear localization sequence at its N-terminus and exists in high quantities in the nucleus. Pro-IL-1α is also produced as a membrane-bound cytokine after myristoylation, where it is most likely engaged in cell–cell interactions. Less frequently, the precursor form can be cleaved by a calpain-like protease to generate secreted IL-1α and an N-terminal peptide. Pro-IL-1α and the N-terminal peptide can be physiologically active after nuclear translocation. Caspase 1 cleaves pro-IL-1β into IL-1β, which may be released as a soluble, functional protein. Pro-IL1α, IL-1α, and IL-1β can all bind to IL1R1, allowing the recruitment of the IL1RAcP coreceptor. A series of events downstream of the IL-1R complex activate essential signalling proteins, such as mitogen-activated kinases (JNK, p38, and ERK1/2) and transcription factors, such as NF-κB (p65 and p50 subunits) and c-Jun (an AP-1 subunit), which regulate the expression
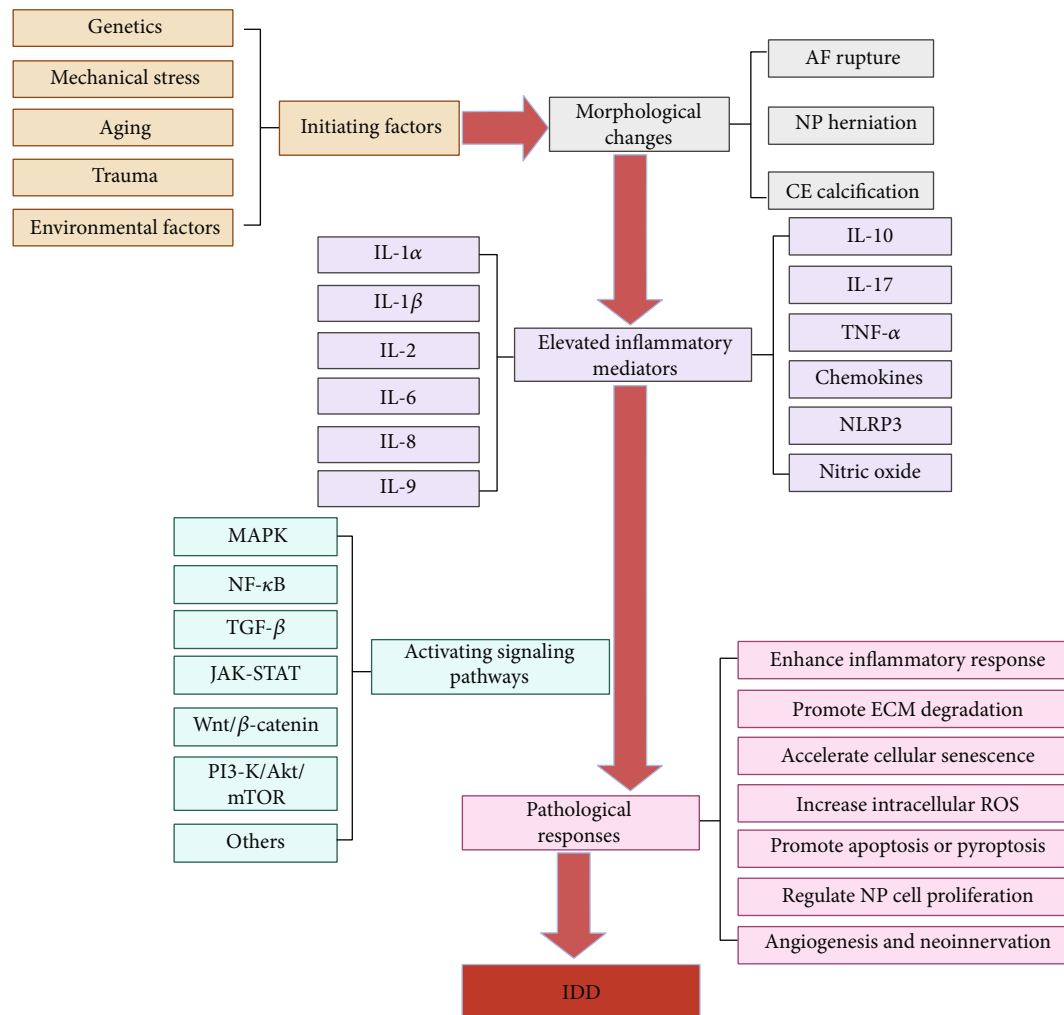
FIGURE 1: Diagram of IDD upstream and downstream regulation networks.

of several inflammatory and catabolic genes. Signalling through the IL-1R complex can be modulated by the inhibitory effects of IL-1R2, sIL-1R2, sIL-1RAcP, and IL-1Ra.

4.1.2. IL-1β. IL-1β is a crucial inflammatory mediator with a wide range of actions and activities on various cells that can lead to various inflammatory processes. Systemically, IL-1β signalling generates an acute phase response, hypotension, vasodilation, and fever; locally, IL-1β signalling leads to an increase in adhesion molecules, which increases lymphocyte recruitment and amplifies the inflammatory response [42]. IL-1β expression has been demonstrated to be significantly increased in degenerative IVDs and is related to symptoms of LBP [43–46].

As shown in Figure 4, IL-1β may influence the development of IDD through several mechanisms. First, IL-1β can enhance the inflammatory response of the IVD by increasing the production of inflammatory mediators, such as IL-6, IL-8, IL-17, prostaglandin E2, chemokines, and the NLRP3 inflammasome [47–50]. Second, IL-1β regulates ADAMTS and MMP production in the IVD, resulting in ECM degradation [38, 51–53]. Third, the output of senescence-associated-

galactosidase (SA-β-Gal) can be enhanced by IL-1β, indicating that this inflammatory mediator may accelerate IDD development by hastening cellular senescence [54–57]. Fourth, IL-1β can promote apoptosis and pyroptosis in NP cells by regulating the NF-κB and MAPK pathways, which hastens the development of IDD [50, 53, 58, 59]. Fifth, it was demonstrated that IL-1β regulated NP cell proliferation leading to the development of IDD [56, 60]. Additionally, IL-1β increases intracellular reactive oxygen species (ROS), and excessive ROS accumulation can lead to oxidative stress and the progression of IDD [61–63]. Finally, IL-1β might increase angiogenesis and neoinnervation inside IVDs by increasing the synthesis of vascular endothelial growth factor (VEGF), nerve growth factor (NGF), and BDNF [64, 65]. In conclusion, IL-1β plays a significant role in IDD and may be a promising therapeutic target.

4.1.3. IL-2. IL-2, found on 4q27, is mainly generated by mature T cells and acts as a growth factor for T and B cells, playing a role in their growth. IL-2 is increased in individuals with lumbar disc herniation and influences human NPC proliferation, apoptosis, and ECM degradation through
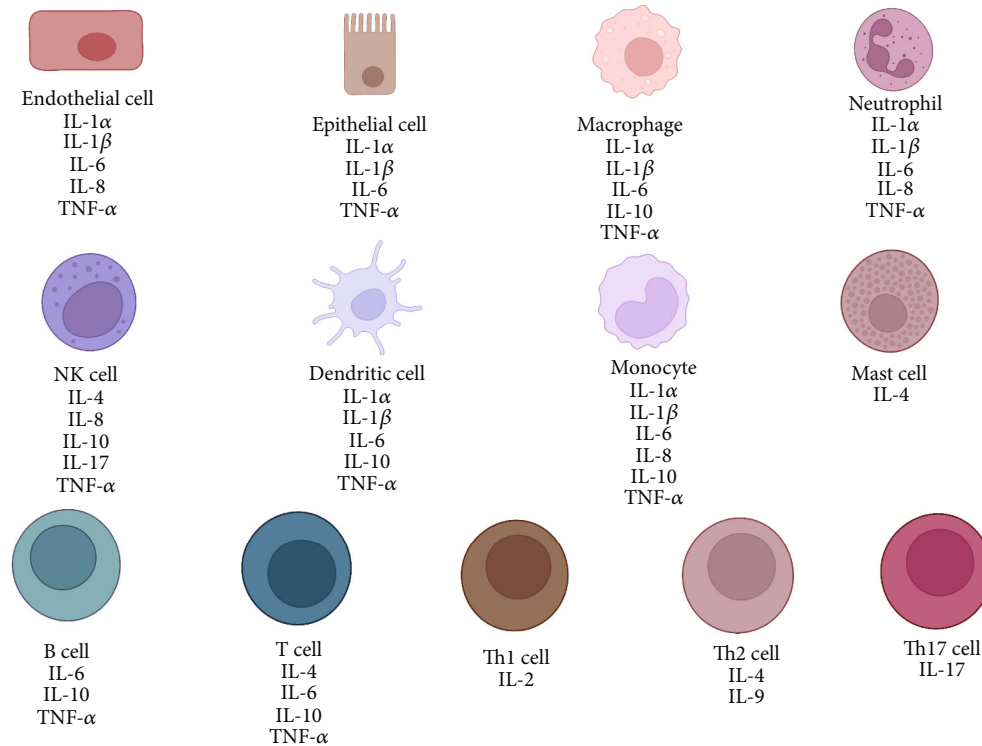
Figure 2: Schematic illustration of different cells expressing various cytokines.

the MAPK pathway [66]. Furthermore, IL-2 gene variations have been revealed as susceptibility factors for IDD, indicating that IL-2 may play a role in the development of IDD [67]. In conclusion, IL-2 has a function in IDD, but the exact mechanism is still unclear.

4.1.4. IL-4. IL-4 is a cytokine produced by T cells that regulates the activity of various immune cells. IL-4 is primarily generated by immune cells, but its receptors are found in various cell types and promote cell proliferation and differentiation, tissue regeneration, and neurological function. It was discovered that IL-4 expression was significantly higher in IDD patients than in healthy controls [68–70]. Interestingly, unlike IL-1, IL-4 exhibits direct anti-inflammatory actions by binding to the IL-4RA receptor on 16p12.1 and blocking the induction pathway of IL-1 and TNF-α [71–75]. In conclusion, IL-4 performs an anti-inflammatory function in IDD and can be used to treat this disorder.

4.1.5. IL-6. IL-6 is an important cytokine that can be secreted by T cells, macrophages, and NP cells. According to research, patients with disc degeneration have higher serum IL-6 levels than healthy controls [76, 77]. It has also been demonstrated that increased serum IL-6 levels are associated with disc degeneration-related LBP [78, 79]. Furthermore, IL-6 levels are linked to the degree of disc degeneration and pain intensity [80–83]. There are multiple potential mechanisms for IL-6 involvement in IDD. IL-6 accelerates the course of IDD by increasing the catabolic effects of IL-1β and TNF-α on NP cells through the JAK/STAT signalling pathway [84]. Moreover, IL-6 promotes apoptosis of neu-

rons in the dorsal root ganglion, resulting in sensory impairment [85]. Furthermore, IL-6 promotes the degeneration of NP cells by blocking miR-10a-5p and hence the IL-6R signalling pathway, which in turn encourages chondrocyte ferrogenesis [86]. In conclusion, IL-6 plays an essential role in IDD and may be a target for future therapy.

4.1.6. IL-8. IL-8 is a chemokine with a distinct CXC amino acid sequence [87]. IL-8 expression is considerably higher in the disc tissue of IDD patients, indicating that it may have a role in the disease [88–90]. IL-8 can activate microglia in the spinal cord, promote the upregulation of neuroinflammatory markers such as IL-1β and TNF-α, and exacerbate the inflammatory response, aggravating the development of IDD [91]. IL-8 can also regulate angiogenesis by enhancing extracellular matrix survival, proliferation, and MMP-2 production through the MAPK signalling pathway, thereby affecting IDD progression [87, 92, 93].

4.1.7. IL-9. IL-9 is a polymorphic cytokine that regulates the Th2 inflammatory response [94]. IL-9 was shown to upregulate TNF-α and PGE2 production in NP cells, and its blood levels were positively associated with the degree of disc degeneration in IDD patients [95]. Therefore, IL-9 may play a role in the autoimmune inflammatory process in IDD, but the exact mechanism is not yet clear.

4.1.8. IL-10. Interleukin-10 (IL-10) is an important immune system regulator that regulates inflammation and tissue hemostasis [96]. IL-10 SNPs have been linked to IDD, suggesting that genetic alterations in IL-10 may lead to

Table 1: Inflammatory mediators associated with IDD progression.

Name	Size (amino acids)	Chromosomal location	Gene	Origins	Receptor	Function in IDD	Signaling pathways
IL-1α	271	2q14	IL1A (IL1F1)	Neutrophil; macrophage; monocyte; endothelial cell; epithelial cell; dendritic cell	IL1R1; IL1R2	Inhibit ECM synthesis; enhance inflammatory response; enhance bradykinin sensitivity	TGF-β; MAPK; NF-κB; Wnt/β-catenin; PI3K/Akt/mTOR
IL-1β	269	2q14	IL1B (IL1F2)	Neutrophil; macrophage; monocyte; endothelial cell; epithelial cell; dendritic cell	IL1R1; IL1R2	Enhance inflammatory response; promote ECM degradation; accelerate cellular senescence; promote apoptosis and pyroptosis; regulate NP cell proliferation; increase angiogenesis and neoinnervation	TGF-β; MAPK; NF-κB; Wnt/β-catenin; PI3K/Akt/mTOR
IL-2	153	4q26-q27	IL2	Th1 cell	IL2RA; IL2RB; IL2RG	Regulate NP cell proliferation; promote apoptosis; promote ECM degradation	PI3K/Akt/mTOR; MAPK; JAK-STAT
IL-4	153	5q31.1	IL4	Th2 cell; NK cell; T cell; mast cell	IL4R	Inhibit inflammatory processes	JAK-STAT
IL-6	212	7p21	IL6 (IFNB2)	Neutrophil; macrophage; T cell; B cell; monocyte; endothelial cell; epithelial cell; dendritic cell	IL6R	Enhance inflammatory response; promote apoptosis of neurons in the dorsal root ganglion; promote chondrocyte ferrogenesis	JAK-STAT; MAPK; PI3K/Akt/mTOR
IL-8	99	4q13-q21	CXCL8 (IL8)	Neutrophil; NK cell; endothelial cell; monocyte	CXCR1; CXCR2	Enhance inflammatory response; regulate angiogenesis	MAPK; JAK-STAT; NF-κB; PI3K/Akt/mTOR
IL-9	144	5q31.1	IL9	Th2 cell	IL9R	Enhance inflammatory response	MAPK; JAK-STAT
IL-10	178	1q31-q32	IL10	Macrophage; T cell; B cell; NK cell; monocyte; dendritic cell	IL10R1; IL10R2	Enhance inflammatory response	MAPK; JAK-STAT; NF-κB
IL-17A	155	6p12	IL17A (CTLA8, IL17)	Th17 cell; NK cell	IL17RA; IL17RC	Enhance inflammatory response; promote ECM degradation; block autophagy in degenerating NP cells	MAPK; NF-κB; C/EBPβ/δ
TNF-α	233	6p21.33	TNF (TNFA, TNFSF2)	Endothelial cell; epithelial cell; macrophage; neutrophil; NK cell; dendritic; monocyte; B cell; T cell	TNFR1; TNFR2	Enhance inflammatory response;↑ promote ECM degradation;↑ accelerate cellular senescence;↑ promote apoptosis;↑ regulate NP cell proliferation;↑ increase angiogenesis and neoinnervation	MAPK; NF-κB; Notch; UPR/XBP1

TABLE 1: Continued.

Name	Size (amino acids)	Chromosomal location	Gene	Origins	Receptor	Function in IDD	Signaling pathways
Chemokines	-	-	-	Endothelial cell; epithelial cell; B cell; T cell; NK cell	CR; CCR; CXCR; CX3CR	Enhance inflammatory response; promote ECM degradation; promote apoptosis; Increase angiogenesis and neoinnervation	NF-κB; PI3K/Akt/mTOR
NLRP3	1036	1q44	NLRP3 (C1orf7, CIAS1, NALP3, PYPAF1)	Neutrophil; macrophage	-	Enhance inflammatory response; promote apoptosis	NF-κB
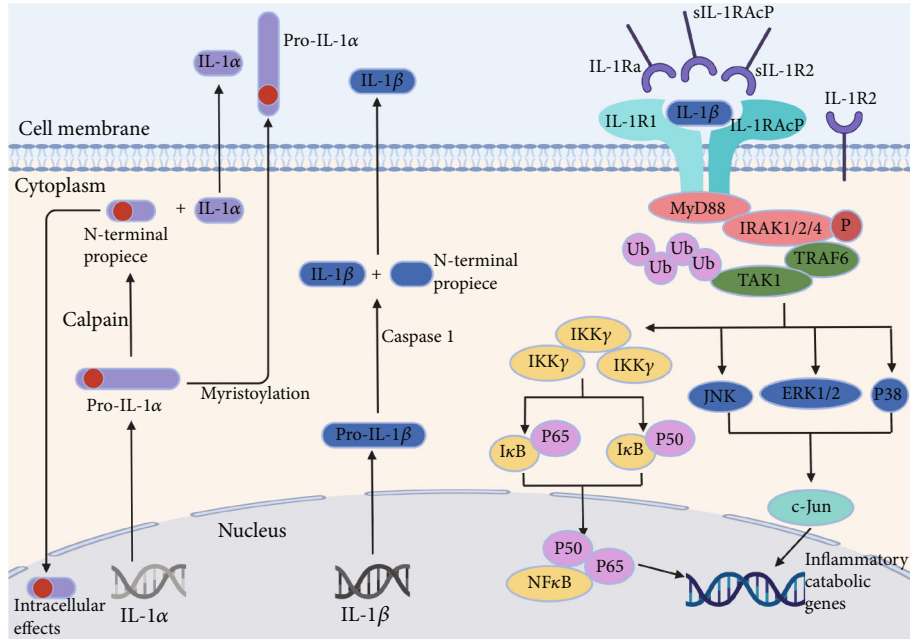
FIGURE 3: IL-1α and IL-1β synthesis and signal transduction pathways.
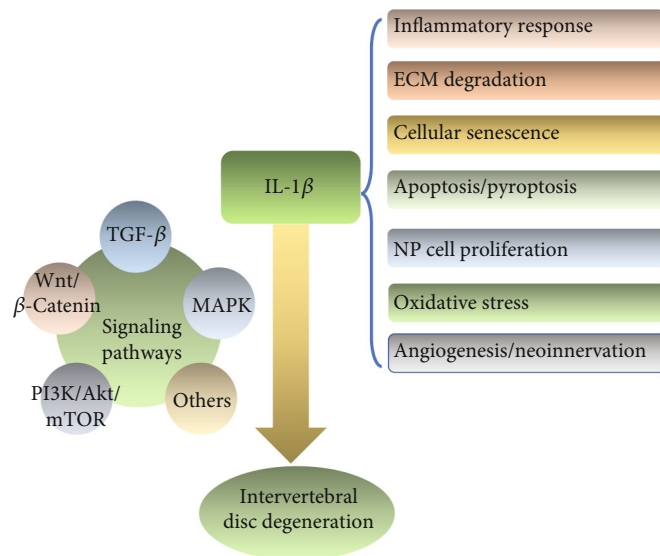
FIGURE 4: IL-1β is involved in multiple pathological processes of intervertebral disc degeneration.

intervertebral disc imbalances and degeneration [97]. The expression of IL-10 is considerably higher in IDD patients, indicating the close relationship between this inflammatory cytokine and the disorder [70, 77]. Furthermore, in IDD animal models, IL-10 expression levels in several spinal components (bone, discs, and ligaments) were dramatically upregulated [98]. According to previous studies, IL-10 may hasten IDD development by intensifying the inflammatory response [99, 100]. To summarize, IL-10 plays a role in the degenerative process of IDD and can potentially be a new therapeutic target.

4.1.9. IL-17A. IL-17 is a cytokine primarily generated by the T helper 17 subsets of CD4+ T cells and plays a vital role in various inflammatory disorders [101, 102]. It has six members in its family, from IL-17A to IL-17F [103]. IL-17A, one of the most important members of the IL family, has been related to a range of degenerative illnesses [104, 105]. It has been demonstrated that IL-17A is more abundant in degenerative disc tissue than in normal tissue [96, 106, 107]. There are various probable theories for the mechanism of action. In NP cells, IL-17A can increase the production of inflammatory markers, such as IL-6, COX-2, MMPs, IFN-γ,
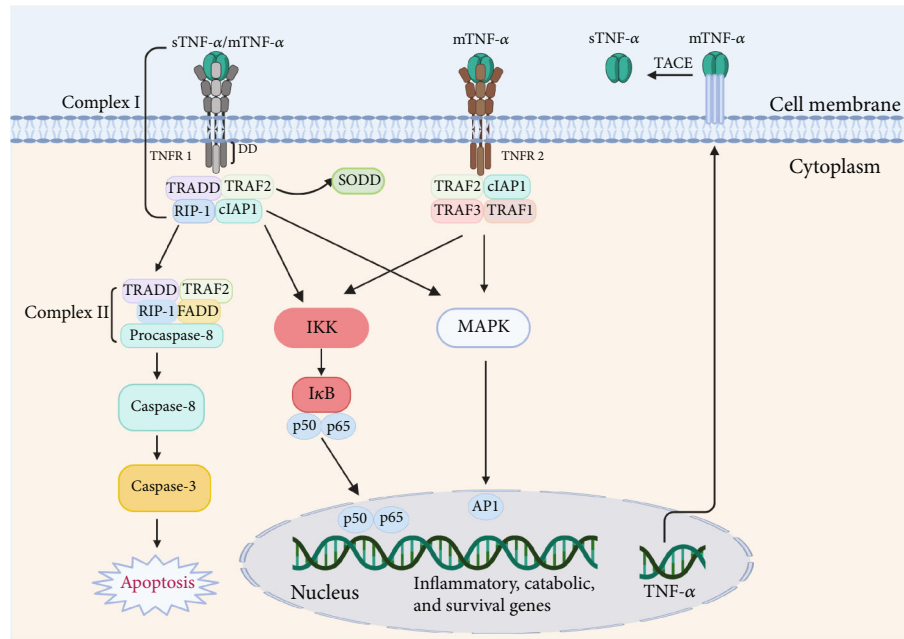
FIGURE 5: TNF-α signalling pathway.

and TNF-α [106, 108–110]. IL-17A has been found to regulate the development of IDD by modulating the ECM metabolism balance linked with ADAMTS-7 expression [107, 111, 112]. In addition, IL-17A may accelerate the development of IDD by blocking autophagy in human degenerative NP cells through stimulation of the PI3K/Akt/Bcl-2 signalling pathway [113, 114]. To summarize, the involvement of IL-17 in IDD is significant, and it may be an essential target for IDD treatment.

4.2. TNF-α. Tumour necrosis factor-alpha (TNF-α), located at 6p21.33, is mainly synthesized as a transmembrane protein and is turned into an active molecule following processing by specific enzymes, including TNF-α converting enzymes [115]. TNF-α is a proinflammatory cytokine linked to some pathological illnesses, including infections, autoimmune diseases, cancer, atherosclerosis, Alzheimer's disease, and inflammatory bowel disease [116–121]. TNF-α also regulates various developmental and immunological processes, including inflammation, differentiation, lipid metabolism, and apoptosis [122–124]. TNF-α has been linked to almost every component of the human immune system [125].

Studies have shown that TNF-α expression is upregulated in degenerative disc tissue more than in normal tissue [126–129]. TNF-α levels were also found to be positively associated with the severity of IDD [129–131]. In the absence of substantial deterioration, transgenic mice overexpressing human TNF-α exhibited early onset spontaneous disc herniation [132]. In a porcine model, lumbar discs treated with exogenous TNF-α displayed degenerative alterations, including annular fissures, loss of NP matrix, vascularization, and expression of IL-1β in the outer annulus, indicating that TNF-α is a driver of disc degeneration [133].

As shown in Figure 5, TNF-α binds to two receptors: TNF receptor type 1 (TNFR1) and TNF receptor type 2

(TNFR2). TNF-α may be implicated in IDD in many ways. TNF-α has been demonstrated in multiple studies to trigger IVDs by releasing many proinflammatory cytokines, including IL-1, IL-6, IL-8, IL-17, NO, and PGE2, and chemokines, which further exacerbate the inflammatory response of discs [134–137]. TNF-α also increases the synthesis of substance P, NGF, and VEGF, all of which can cause pain by sensitizing the nervous system and driving neurovascular development toward IVD [138, 139]. Furthermore, TNF-α stimulates ECM breakdown mostly via the NF-κB/MAPK signalling pathway [140–144]. TNF-α also interacts with its receptor and affects the JNK/ERK-MAPK and NF-κB signalling pathways in NPCs during IDD, upregulating proapoptotic proteins and downregulating antiapoptotic proteins, resulting in apoptosis [145–149]. Furthermore, TNF-α has been shown to cause premature senescence in NPCs [150, 151]. Additionally, TNF-α can affect the proliferation of NP cells via the JNK, NF-κB, Notch, UPR/XBP1, and p38 MAPK signalling pathways [152–156].

TNF-α is generally found as a stable homotrimer known as mTNF-α. TACE, a metalloproteinase, can convert mTNF-α to sTNF-α. TNF-α works via two distinct receptors, TNFR1 and TNFR2. sTNF-α or mTNF-α may bind to transmembrane TNFR1, resulting in a conformational shift and release of the inhibitory SODD protein. Bound TNFR1 recruits several factors, including TRADD, RIP1, TRAF2, and cIAP 1 and 2, to form complex I, which signals via the NF-κB or MAPK pathway, and activate p65 or AP1. Complex I signalling causes inflammation (through chemokines and cytokines) and activates stromal catabolic genes (MMPs and ADAMTSs), as well as survival-promoting genes (cIAP1 and 2, cFLIP, TRAF1, and TRAF2). In addition, mTNF-α may also activate TNFR2, resulting in a similar complex and downstream signaling cascade. In specific circumstances, TNFR1 bound to sTNF-α may be internalized into

complex II, causing procaspase 8 to be converted into caspase 8 and then caspase 3 to be activated, eventually leading to apoptosis.

4.3. Chemokines.

Chemokines are significant second-order cytokines produced in response to stimuli and play an essential role in acute and chronic inflammation [134]. Based on the primary cysteine residues involved in disulphide bonding, chemokines have been categorized as C, CC, CXC, and CX3C [157]. According to a bioinformatics study, numerous chemokine genes may have a role in the development of IDD caused by inflammatory reactions [158]. CCL2, CCL5, CXCL6, CXCL12, CXCL20, C-X-C receptor 4 (CXCR4), and stromal cell-derived factor 1 (SDF1) expression is considerably elevated in IDD tissues [159–163]. Serum CCL3, CXCL12, and SDF1 levels have also been demonstrated to be positively associated with the degree of IDD [137, 162, 164, 165]. Chemokines may have a role in IDD through a variety of pathways. Zhang et al. [166] discovered that the CCL20/CCR6 pathway attracts IL-17-producing cells to degenerate IVDs and that IL-17 is implicated in the autoimmune process of IDD in a rat model. Furthermore, CXCL12 promotes ECM disintegration and enhances MMP production in human disc endplate chondrocytes [167]. SDF1/CXCR4 was discovered to be higher in degenerating intervertebral discs, and it promotes apoptosis of NPCs via the NF-B pathway, leading to IDD [168]. Furthermore, the SDF1/CXCR4 axis, via the PI3K/AKT pathway, can regulate VEC survival, migration, tube formation, and angiogenesis in human degenerative discs [169–171].

4.4. The NLRP3 Inflammasome.

The NLRP3 inflammasome is a multiprotein complex in the cytoplasm that consists of a receptor, adaptor, and effector [172]. NLRP3 expression in IDD was observed to be considerably higher than that in normal disc tissue [173, 174]. There is further evidence from MRI and histology that NLRP3 is linked to the progression of IDD [175]. It has been demonstrated that overactivation of the NLRP3 inflammasome results in the overproduction of downstream IL-1, which is vital in the development of IDD [173]. Activation of the NLRP3 inflammasome can also cause apoptosis in NP cells [176, 177]. In addition, *Propionibacterium acnes* can activate the NLRP3 inflammasome via the TXNIP-NLRP3 pathway, causing pyroptosis of NP cells and IDD [178]. In summary, the NLRP3 inflammasome plays a crucial role in IDD, and more research is needed to discover its mechanism of action.

4.5. Nitric Oxide.

NP cells can create nitric oxide (NO), and it was shown that NO production is enhanced in IDD and that its synthesis relies on nitric oxide synthase (NOS) [131]. TNF-α, IL-1β, lipopolysaccharide, and interferon-γ were discovered to promote NO production [89, 179]. Nitric oxide has proinflammatory effects, and its role as a vasodilator promotes vascular leakage, inhibits proteoglycans, and induces neuropathic pain, all of which contribute to IDD [180]. In addition, NO is regarded as a member of the ROS superfamily due to its similar effects to those of ROS,

and ROS hasten intervertebral disc degeneration. The specific mechanism is shown in Figure 6.

ROS alter the ECM of IVDs through oxidative modification, eventually impairing the structure of IVDs. ROS activate multiple signaling pathways, such as the MAPK and NF-κB pathways, thereby regulating autophagy, apoptosis, senescence, and the phenotype of IVD cells, thus reinforcing matrix degradation and inflammation and enhancing the decrease in the number of functional IVD cells. Ultimately, ROS/oxidative stress promotes the progression of IDD.

5. Therapeutic Prospects for IDD by Targeting Inflammation

The inflammatory response that mediates the degenerative cascade in IVDs is being targeted as a potential therapeutic or prognostic strategy. Currently, the main goals of therapies are to manage degenerated IVDs and relieve symptoms. The conventional approaches include systemic medicine and surgical decompression/discectomy. However, these methods are not aimed at the pathogenesis of IDD. In this section, we focused on reviewing and providing more information on novel anti-inflammation therapies for IDD, including intradiscal injections, gene therapies, MSC-based therapies, and exosome-based therapies.

5.1. Intradiscal Injections.

Injecting medications into the IVD is one of the most straightforward ways to regulate inflammation in IVDs. TNF-α inhibitors are examples of medications administered in this way [181]. TNF inhibitors, such as infliximab and Atsttrin, have been shown to decrease the inflammatory response [182, 183]. Infliximab is an antibody against TNF-α. Injecting infliximab into the IVD of rats alleviated discomfort compared with the control groups [184]. Atsttrin is an inflammatory-related growth factor consisting of three pieces of progranulin. In a mouse model, this protein inhibited TNF-initiated inflammatory signaling by binding directly to TNF-α receptors [185]. Additionally, Atsttrin suppressed TNF-induced inflammatory cytokine production, including production of MMP-13, COX-2, iNOS, and IL-17, causing concomitant catabolic alterations in cartilage, disc height, and NP cells in ex vivo cultured rat discs [183].

The IL-1 inhibitor, IL-1 receptor antagonist (IL-1Ra), binds to the IL-1 receptor (IL-1R) and blocks the transmission of inflammatory signals [141]. IL-1Ra may have a therapeutic role in IDD, according to previous studies [38, 186, 187]. Injection of IL-1Ra into both degenerative and nondegenerative human IVD tissues reduced the production of matrix breakdown proteases, such as type II collagenase, gelatinase, and caseinase [38]. Another study revealed the therapeutic efficacy of IL-1Ra by applying polylactic-co-glycolic acid (PLGA) microspheres as a delivery vehicle. In NP cell cultures, IL-1Ra-PLGA microspheres attenuated the degradative effects of IL-1β on NP cells by suppressing NO production while restoring the levels of iNOS, IL-6, ADAMTS-4, and MMP-13 [186].

COX-2, which controls PGE2 production in inflammatory circumstances, is also a target for suppressing
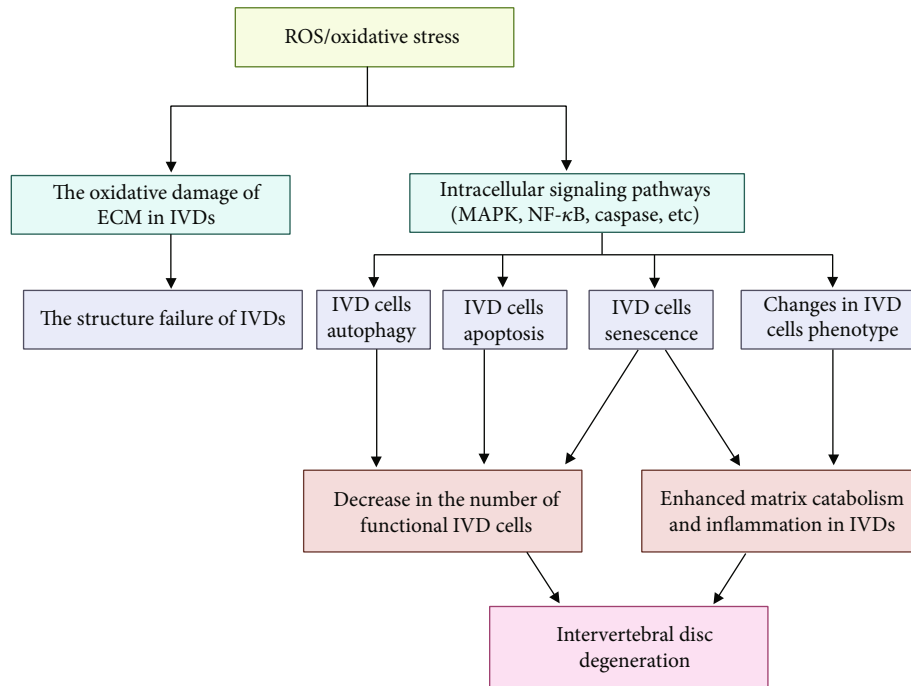
FIGURE 6: The role of ROS/oxidative stress in the development of IDD.

inflammation in IVDs [188]. In a rat model of disc herniation, epidural injections of COX-2 inhibitors resulted in satisfactory pain relief [189]. Additionally, the inhibitor of IkB kinase-b (IKKb), which is involved in NF-kB activation, is a novel candidate for treating inflammation in IVD. Intradiscal injection of IKKb downregulated the expression of TNF-α, IL-1β, and IL-6 in degenerative discs and neuropeptides in dorsal root ganglion neurons [190]. Despite promising results, injection of such molecules in IVDs may be ineffective owing to their short half-life and the complicated microenvironment of degenerative IVDs [30]. Furthermore, the potential risk of IDD caused by puncturing should be noted.

The injection of phytochemicals derived from medicinal plants has been researched in recent years because of its cost-effectiveness and biological functions. According to previous in vivo and in vitro studies, various phytochemicals, including resveratrol [191], mangiferin [192], epigallocatechin-3-gallate [177], chlorogenic acid [193], celastrol [194], isofraxidin [195], higenamine [196], sesamin [197, 198], honokiol [176], naringin [199, 200], baicalein [201], berberine [53], wogonin [52], and luteoloside [202]. Most of these phytochemicals inhibit the IL-1β-induced or TNF-α-induced inflammatory response and extracellular matrix degradation in NP cells. Although satisfactory therapeutic effects of phytochemicals in IDD have been reported, the metabolic processes, organ distribution, and toxicity of different doses still need to be investigated.

5.2. Gene Therapies.

With the ability of locally modifying the expression of a certain gene and production of the corresponding protein, gene therapy offers longer sustained effects in IDD [203]. A study published in 1997 proposed genetic modifications as a positional treatment for IDD [204]. In this study, a retrovirus vector was developed to transduce IL-1Ra into bovine chondrocyte cells. Injection of cells overexpressing IL-1Ra significantly downregulated MMP3 for 14 days in degenerative IVD tissue, reducing IL-1-mediated matrix degradation and halting the deterioration of IDD. In a rabbit model, NP cells transfected with TGF-β1 demonstrated increased proteoglycan production [205]. Consistent with this finding, TGF-β1-transfected senescent NP cells of humans also enhanced the synthesis of proteoglycan and collagen [206, 207].

The safety of gene therapy may restrict its application in clinical settings. For the treatment of chronic IDD, high dosage exposure and long-term usage may induce oncogenesis, which is a critical concern [208]. Improvement in the reliability of viral vector designs and expression control of transgenes might allow the safe use of gene therapy.

5.3. MSC-Based Therapies.

In recent years, many cell-based treatments to regenerate IVDs have been developed [209, 210]. Among the candidates, MSCs have the best potential for IVD regeneration, which is attributed to their autologous transplantation ability [211]. MSCs boosted collagen type II expression and slowed the apoptosis process of NP cells [212]. Additionally, IVD tissue survived for 6 months in rabbits with the concomitance of MSCs [213]. However, the number of transplanted MSCs is important [214]. In addition to their multidifferentiation capability, the immunomodulatory role of MSCs has been revealed [215, 216]. MSCs participate in inflammation by releasing cytokines, which directly interact with degenerative NP cells [217]. In vitro studies showed that MSCs cocultured with rat NP cells inhibited the expression of proinflammatory cytokines,

including IL-3, IL-6, IL-11, IL-15, and TNF-α [218]. In a clinical trial, LBP was significantly alleviated by three months of MSC injection, and the authors concluded that MSCs stimulated the regeneration of IVD and had immunomodulatory characteristics [219]. In another 2-year follow-up study, after the injection of umbilical cord-derived MSCs into IVDs, LBP and lumbar function were improved and maintained during the duration of follow-up [220]. Although benefits and promising outcomes of MSC-based therapies have been observed, the mechanisms have still not been clearly elucidated by animal experiments, and most of the clinical studies were case reports with limited sample sizes.

5.4. *Exosome-Based Therapies.* Exosomes and exosomal miRNAs have been the focus of IDD therapy in recent years. The potential mechanisms reported in previous studies could be categorized as angiogenesis of the ECM, senescence, metabolic homeostasis, proliferation, apoptosis, and oxidative stress [221]. Additionally, exosomes and exosomal miRNAs also play an important role in the regulation of inflammation in IVDs [222]. By downregulating LRG1, BMSC-derived exosomal miR-129-5p attenuated the activation of the p38 MAPK pathway to inhibit macrophage polarization from the M1 to M2 phenotype, which resulted in the release of anti-inflammatory mediators and prevented apoptosis of NP cells as well as degradation of ECM [223]. NLRP3, a member of the inflammasome, is a crucial component of innate immunity and participates in several proinflammatory processes [224]. NLRP3 can be extremely upregulated in the development of IDD [225]. By blocking the NLRP3/caspase-1 pathway, MSC-derived exosomal miR-410 reversed the expression of IL-1β and IL-18, reducing LPS-induced pyroptosis in NP cells [226]. Similarly, human umbilical cord mesenchymal stem cell- (hucMSC-) derived miR-26a-5p affected mRNA methyltransferase (METTL14) and m6A methylation in NP cells, which downregulated the expression of NLRP3, leading to the inhibition of pyroptosis and the release of proinflammatory cytokines [227]. As a novel therapy, more studies focused on the role of exosomes in IDD treatment are expected.

6. Conclusion

IDD is a prevalent musculoskeletal illness that produces LBP and negatively impacts quality of life. Recent research has revealed that various inflammatory mediators, such as IL-1β, TNF-α, IL-6, IL-17, chemokines, and the NLRP3 inflammasome, play an essential role in IDD. Most research has found that inflammatory mediators have a role in the development of IDD primarily through the control of the inflammatory response, IVD cell proliferation, senescence, apoptosis, pyroptosis, autophagy, ECM degradation, and oxidative stress. Targeting these inflammatory mediators may lead to future optimum IDD treatment. Clinical investigations have recently revealed that inhibiting IL-1β and TNF-α is a promising future therapy for IDD. More research into IDD-related inflammatory mediators is needed to help us understand the molecular pathophysiology of IDD and provide novel ideas for future IDD therapy based on inflammatory mediators.

Data Availability

The data used to support the findings of this study are available from the corresponding authors upon request.

Conflicts of Interest

The authors declare that they have no competing interests.

Authors' Contributions

Zhangfu Li and Honghao Yang collected the documents and finished the manuscript. Yong Hai and Yunzhong Cheng supervised and revised the manuscript. All authors have read and approved the content of the manuscript. Zhangfu Li and Honghao Yang are co-first authors of this article, contributing equally to the design and drafting of the manuscript.

References

[1] S. Roberts, H. Evans, J. Trivedi, and J. Menage, "Histology and pathology of the human intervertebral disc," *Journal of Bone and Joint Surgery*, vol. 88, Supplement 2, pp. 10–14, 2006.

[2] C. W. Pfirrmann, A. Metzdorf, M. Zanetti, J. Hodler, and N. Boos, "Magnetic resonance classification of lumbar intervertebral disc degeneration," *Spine*, vol. 26, no. 17, pp. 1873–1878, 2001.

[3] C. Barrey, J. Jund, O. Noseda, and P. Roussouly, "Sagittal balance of the pelvis-spine complex and lumbar degenerative diseases. A comparative study about 85 cases," *European Spine Journal*, vol. 16, no. 9, pp. 1459–1467, 2007.

[4] D. Gopal, A. L. Ho, A. Shah, and J. H. Chi, "Molecular basis of intervertebral disc degeneration," in *Advances in Experimental Medicine and Biology*, pp. 114–133, Springer, 2012.

[5] D. Sakai, "Future perspectives of cell-based therapy for intervertebral disc disease," *European Spine Journal*, vol. 17, Supplement 4, pp. 452–458, 2008.

[6] P. P. Vergroesen, I. Kingma, K. S. Emanuel et al., "Mechanics and biology in intervertebral disc degeneration: a vicious circle," *Osteoarthritis and Cartilage*, vol. 23, no. 7, pp. 1057–1070, 2015.

[7] Z. Liao, X. Wu, Y. Song et al., "Angiopoietin-like protein 8 expression and association with extracellular matrix metabolism and inflammation during intervertebral disc degeneration," *Journal of Cellular and Molecular Medicine*, vol. 23, no. 8, pp. 5737–5750, 2019.

[8] M. Teraguchi, N. Yoshimura, H. Hashizume et al., "Progression, incidence, and risk factors for intervertebral disc degeneration in a longitudinal population-based cohort: the Wakayama Spine Study," *Osteoarthritis and Cartilage*, vol. 25, no. 7, pp. 1122–1131, 2017.

[9] A. B. Dario, M. L. Ferreira, K. M. Refshauge, T. S. Lima, J. R. Ordoñana, and P. H. Ferreira, "The relationship between obesity, low back pain, and lumbar disc degeneration when genetics and the environment are considered: a systematic review of twin studies," *The Spine Journal*, vol. 15, no. 5, pp. 1106–1117, 2015.

[10] S. S. Sivan, E. Wachtel, and P. Roughley, "Structure, function, aging and turnover of aggrecan in the intervertebral disc," *Biochimica et Biophysica Acta*, vol. 1840, no. 10, pp. 3181–3189, 2014.

[11] M. Hangai, K. Kaneoka, S. Kuno et al., "Factors associated with lumbar intervertebral disc degeneration in the elderly," *The Spine Journal*, vol. 8, no. 5, pp. 732–740, 2008.

[12] Y. X. J. Wang, "Postmenopausal Chinese women show accelerated lumbar disc degeneration compared with Chinese men," *Journal of Orthopaedic Translation*, vol. 3, no. 4, pp. 205–211, 2015.

[13] M. A. Adams and P. J. Roughley, "What is intervertebral disc degeneration, and what causes it?," *Spine*, vol. 31, no. 18, pp. 2151–2161, 2006.

[14] S. Z. Wang, Y. F. Rui, Q. Tan, and C. Wang, "Enhancing intervertebral disc repair and regeneration through biology: platelet-rich plasma as an alternative strategy," *Arthritis Research & Therapy*, vol. 15, no. 5, p. 220, 2013.

[15] L. Zhao, L. Manchikanti, A. D. Kaye, and A. Abd-Elsayed, "Treatment of discogenic low back pain: current treatment strategies and future options-a literature review," *Current Pain and Headache Reports*, vol. 23, no. 11, p. 86, 2019.

[16] P. J. Roughley, "Biology of intervertebral disc aging and Degeneration," *Spine*, vol. 29, no. 23, pp. 2691–2699, 2004.

[17] P. Priyadarshani, Y. Li, and L. Yao, "Advances in biological therapy for nucleus pulposus regeneration," *Osteoarthritis and Cartilage*, vol. 24, no. 2, pp. 206–212, 2016.

[18] S. Suzuki, N. Fujita, T. Fujii et al., "Potential involvement of the IL-6/JAK/STAT3 pathway in the pathogenesis of intervertebral disc degeneration," *Spine*, vol. 42, no. 14, pp. E817–e824, 2017.

[19] M. V. Risbud and I. M. Shapiro, "Role of cytokines in intervertebral disc degeneration: pain and disc content," *Nature Reviews Rheumatology*, vol. 10, no. 1, pp. 44–56, 2014.

[20] J. G. Burke, R. W. G. Watson, D. McCormack, F. E. Dowling, M. G. Walsh, and J. M. Fitzpatrick, "Intervertebral discs which cause low back pain secrete high levels of proinflammatory mediators," *Journal of Bone and Joint Surgery. British Volume*, vol. 84-B, no. 2, pp. 196–201, 2002.

[21] M. Doita, T. Kanatani, T. Harada, and K. Mizuno, "Immunohistologic study of the ruptured intervertebral disc of the lumbar spine," *Spine*, vol. 21, no. 2, pp. 235–241, 1996.

[22] K. Y. Huang, R. M. Lin, W. Y. Chen, C. L. Lee, J. J. Yan, and M. S. Chang, "IL-20 may contribute to the pathogenesis of human intervertebral disc herniation," *Spine*, vol. 33, no. 19, pp. 2034–2040, 2008.

[23] H. Takahashi, T. Suguro, Y. Okazima, M. Motegi, Y. Okada, and T. Kakiuchi, "Inflammatory cytokines in the herniated disc of the lumbar spine," *Spine*, vol. 21, no. 2, pp. 218–224, 1996.

[24] A. Lai, A. Moon, D. Purmessur et al., "Annular puncture with tumor necrosis factor-alpha injection enhances painful behavior with disc degeneration in vivo," *The Spine Journal*, vol. 16, no. 3, pp. 420–431, 2016.

[25] L. A. Nasto, K. Ngo, A. S. Leme et al., "Investigating the role of DNA damage in tobacco smoking-induced spine degeneration," *The Spine Journal*, vol. 14, no. 3, pp. 416–423, 2014.

[26] N. Vo, H. Y. Seo, A. Robinson et al., "Accelerated aging of intervertebral discs in a mouse model of progeria," *Journal of Orthopaedic Research*, vol. 28, no. 12, pp. 1600–1607, 2010.

[27] C. H. Moon, L. Jacobs, J. H. Kim et al., "Part 2: quantitative proton T2 and sodium magnetic resonance imaging to assess intervertebral disc degeneration in a rabbit model," *Spine*, vol. 37, no. 18, pp. E1113–E1119, 2012.

[28] D. Samartzis, J. Karppinen, D. Chan, K. D. Luk, and K. M. Cheung, "The association of lumbar intervertebral disc degeneration on magnetic resonance imaging with body mass index in overweight and obese adults: a population-based study," *Arthritis and Rheumatism*, vol. 64, no. 5, pp. 1488–1496, 2012.

[29] G. Livshits, M. Popham, I. Malkin et al., "Lumbar disc degeneration and genetic factors are the main risk factors for low back pain in women: the UK Twin Spine Study," *Annals of the Rheumatic Diseases*, vol. 70, no. 10, pp. 1740–1745, 2011.

[30] M. Molinos, C. R. Almeida, J. Caldeira, C. Cunha, R. M. Gonçalves, and M. A. Barbosa, "Inflammation in intervertebral disc degeneration and regeneration," *Journal of the Royal Society Interface*, vol. 12, no. 104, article 20141191, 2015.

[31] P. B. Li, W. J. Tang, K. Wang, K. Zou, and B. Che, "Expressions of IL-1alpha and MMP-9 in degenerated lumbar disc tissues and their clinical significance," *European Review for Medical and Pharmacological Sciences*, vol. 21, no. 18, pp. 4007–4013, 2017.

[32] H. Wesche, C. Korherr, M. Kracht, W. Falk, K. Resch, and M. U. Martin, "The interleukin-1 receptor accessory protein (IL-1RAcP) is essential for IL-1-induced activation of interleukin-1 receptor-associated kinase (IRAK) and stress-activated protein kinases (SAP kinases)," *The Journal of Biological Chemistry*, vol. 272, no. 12, pp. 7727–7731, 1997.

[33] A. Kwak, Y. Lee, H. Kim, and S. Kim, "Intracellular interleukin (IL)-1 family cytokine processing enzyme," *Archives of Pharmacal Research*, vol. 39, no. 11, pp. 1556–1564, 2016.

[34] F. Cai, L. Zhu, F. Wang et al., "The paracrine effect of degenerated disc cells on healthy human nucleus pulposus cells is mediated by MAPK and NF-κB pathways and can be reduced by TGF-β1," *DNA and Cell Biology*, vol. 36, no. 2, pp. 143–158, 2017.

[35] Z. Wang, Z. Qu, C. Fu et al., "Interleukin 1 polymorphisms contribute to intervertebral disc degeneration risk: a meta-analysis," *PLoS One*, vol. 11, no. 6, article e0156412, 2016.

[36] Y. Chen, H. Ma, D. Bi, and B. Qiu, "Association of interleukin 1 gene polymorphism with intervertebral disc degeneration risk in the Chinese Han population," *Bioscience Reports*, vol. 38, no. 4, 2018.

[37] S. Solovieva, S. Kouhia, P. Leino-Arjas et al., "Interleukin 1 polymorphisms and intervertebral disc degeneration," *Epidemiology*, vol. 15, no. 5, pp. 626–633, 2004.

[38] K. L. E. Phillips, N. Jordan-Mahy, M. J. Nicklin, and C. L. Le Maitre, "Interleukin-1 receptor antagonist deficient mice provide insights into pathogenesis of human intervertebral disc degeneration," *Annals of the Rheumatic Diseases*, vol. 72, no. 11, pp. 1860–1867, 2013.

[39] J. F. Zhang, G. L. Wang, Z. J. Zhou, X. Q. Fang, S. Chen, and S. W. Fan, "Expression of matrix metalloproteinases, tissue inhibitors of metalloproteinases, and interleukins in vertebral cartilage endplate," *Orthopaedic Surgery*, vol. 10, no. 4, pp. 306–311, 2018.

[40] F. Rannou, M. T. Corvol, C. Hudry et al., "Sensitivity of anulus fibrosus cells to interleukin 1β: comparison with articular chondrocytes," *Spine*, vol. 25, no. 1, pp. 17–23, 2000.

[41] K. Olmarker, M. Nutu, and R. Storkson, "Changes in spontaneous behavior in rats exposed to experimental disc herniation are blocked by selective TNF-alpha inhibition," *Spine*, vol. 28, no. 15, pp. 1635–1641, 2003.

[42] S. E. Navone, G. Marfia, A. Giannoni et al., "Inflammatory mediators and signalling pathways controlling intervertebral disc degeneration," *Histology and Histopathology*, vol. 32, no. 6, pp. 523–542, 2017.

[43] Y. Wang, M. Che, J. Xin, Z. Zheng, J. Li, and S. Zhang, "The role of IL-1β and TNF-α in intervertebral disc degeneration," *Biomedicine & Pharmacotherapy*, vol. 131, article 110660, 2020.

[44] F. J. Lyu, H. Cui, H. Pan et al., "Painful intervertebral disc degeneration and inflammation: from laboratory evidence to clinical interventions," *Bone Research*, vol. 9, no. 1, p. 7, 2021.

[45] I. Altun, "Cytokine profile in degenerated painful intervertebral disc: variability with respect to duration of symptoms and type of disease," *The Spine Journal*, vol. 16, no. 7, pp. 857–861, 2016.

[46] M. Schroeder, L. Viezens, C. Schaefer et al., "Chemokine profile of disc degeneration with acute or chronic pain," *Journal of Neurosurgery: Spine*, vol. 18, no. 5, pp. 496–503, 2013.

[47] J. Jia, L. Nie, and Y. Liu, "Butyrate alleviates inflammatory response and NF-kappaB activation in human degenerated intervertebral disc tissues," *International Immunopharmacology*, vol. 78, article 106004, 2020.

[48] F. Chen, G. Jiang, H. Liu et al., "Melatonin alleviates intervertebral disc degeneration by disrupting the IL-1β/NF-κB-NLRP3 inflammasome positive feedback loop," *Bone Research*, vol. 8, p. 10, 2020.

[49] F. J. Brand, M. Forouzandeh, H. Kaur, F. Travascio, and J. P. de Rivero Vaccari, "Acidification changes affect the inflammasome in human nucleus pulposus cells," *Journal of Inflammation*, vol. 13, no. 1, p. 29, 2016.

[50] Z. Ma, P. Tang, W. Dong et al., "SIRT1 alleviates IL-1β induced nucleus pulposus cells pyroptosis via mitophagy in intervertebral disc degeneration," *International Immunopharmacology*, vol. 107, article 108671, 2022.

[51] S. Zhan, K. Wang, Y. Song et al., "Long non-coding RNA HOTAIR modulates intervertebral disc degenerative changes via Wnt/β-catenin pathway," *Arthritis Research & Therapy*, vol. 21, no. 1, p. 201, 2019.

[52] W. Fang, X. Zhou, J. Wang et al., "Wogonin mitigates intervertebral disc degeneration through the Nrf2/ARE and MAPK signaling pathways," *International Immunopharmacology*, vol. 65, pp. 539–549, 2018.

[53] L. Lu, J. Hu, Q. Wu et al., "Berberine prevents human nucleus pulposus cells from IL1beta induced extracellular matrix degradation and apoptosis by inhibiting the NF-κB pathway," *International Journal of Molecular Medicine*, vol. 43, no. 4, pp. 1679–1686, 2019.

[54] C. Q. Zhao, L. M. Wang, L. S. Jiang, and L. Y. Dai, "The cell biology of intervertebral disc aging and degeneration," *Ageing Research Reviews*, vol. 6, no. 3, pp. 247–261, 2007.

[55] M. Yang, Y. Peng, W. Liu, M. Zhou, Q. Meng, and C. Yuan, "Sirtuin 2 expression suppresses oxidative stress and senescence of nucleus pulposus cells through inhibition of the p53/p21 pathway," *Biochemical and Biophysical Research Communications*, vol. 513, no. 3, pp. 616–622, 2019.

[56] X. Li, F. Lin, Y. Wu et al., "Resveratrol attenuates inflammation environment-induced nucleus pulposus cell senescence in vitro," *Bioscience Reports*, vol. 39, no. 5, 2019.

[57] Z. B. Chen, Y. B. Yu, Q. B. Wa, J. W. Zhou, M. He, and Y. Cen, "The role of quinazoline in ameliorating intervertebral disc degeneration by inhibiting oxidative stress and anti-inflammation via NF-κB/MAPKs signaling pathway," *European Review for Medical and Pharmacological Sciences*, vol. 24, no. 4, pp. 2077–2086, 2020.

[58] K. Wang, T. Chen, X. Ying et al., "Ligustilide alleviated IL-1β induced apoptosis and extracellular matrix degradation of nucleus pulposus cells and attenuates intervertebral disc degeneration in vivo," *International Immunopharmacology*, vol. 69, pp. 398–407, 2019.

[59] K. Zhang, W. Ding, W. Sun et al., "Beta1 integrin inhibits apoptosis induced by cyclic stretch in annulus fibrosus cells via ERK1/2 MAPK pathway," *Apoptosis*, vol. 21, no. 1, pp. 13–24, 2016.

[60] S. L. Wang, Y. L. Yu, C. L. Tang, and F. Z. Lv, "Effects of TGF-β1 and IL-1β on expression of ADAMTS enzymes and TIMP-3 in human intervertebral disc degeneration," *Experimental and Therapeutic Medicine*, vol. 6, no. 6, pp. 1522–1526, 2013.

[61] L. A. Nasto, A. R. Robinson, K. Ngo et al., "Mitochondrial-derived reactive oxygen species (ROS) play a causal role in aging-related intervertebral disc degeneration," *Journal of Orthopaedic Research*, vol. 31, no. 7, pp. 1150–1157, 2013.

[62] G. Hou, H. Lu, M. Chen, H. Yao, and H. Zhao, "Oxidative stress participates in age-related changes in rat lumbar intervertebral discs," *Archives of Gerontology and Geriatrics*, vol. 59, no. 3, pp. 665–669, 2014.

[63] Q. Liu, L. Jin, F. H. Shen, G. Balian, and X. J. Li, "Fullerol nanoparticles suppress inflammatory response and adipogenesis of vertebral bone marrow stromal cells-a potential novel treatment for intervertebral disc degeneration," *The Spine Journal*, vol. 13, no. 11, pp. 1571–1580, 2013.

[64] Y. H. Hsu, R. M. Lin, Y. S. Chiu, W. L. Liu, and K. Y. Huang, "Effects of IL-1β, IL-20, and BMP-2 on intervertebral disc inflammation under hypoxia," *Journal of Clinical Medicine*, vol. 9, no. 1, 2020.

[65] W. K. Kwon, H. J. Moon, T. H. Kwon, Y. K. Park, and J. H. Kim, "The role of hypoxia in angiogenesis and extracellular matrix regulation of intervertebral disc cells during inflammatory reactions," *Neurosurgery*, vol. 81, no. 5, pp. 867–875, 2017.

[66] Z. Wang, G. Wang, X. Zhu, D. Geng, and H. Yang, "Interleukin-2 is upregulated in patients with a prolapsed lumbar intervertebral disc and modulates cell proliferation, apoptosis and extracellular matrix metabolism of human nucleus pulposus cells," *Experimental and Therapeutic Medicine*, vol. 10, no. 6, pp. 2437–2443, 2015.

[67] S. Hanaei, S. Abdollahzade, M. Sadr et al., "Association of interleukin 2, interleukin 12, and interferon-γ with intervertebral disc degeneration in Iranian population," *BMC Medical Genetics*, vol. 21, no. 1, p. 143, 2020.

[68] S. Hanaei, S. Abdollahzade, M. Sadr et al., "The role of interleukin 4 and IL-4RA in intervertebral disc degeneration: investigation of single nucleotide polymorphisms in genes and a systematic review & meta-analysis of IL-4 expression level," *British Journal of Neurosurgery*, vol. 34, no. 1, pp. 66–71, 2020.

[69] K. Wang, J. P. Bao, S. Yang et al., "A cohort study comparing the serum levels of pro- or anti-inflammatory cytokines in patients with lumbar radicular pain and healthy subjects," *European Spine Journal*, vol. 25, no. 5, pp. 1428–1434, 2016.

[70] S. Akyol, B. S. Eraslan, H. Etyemez, T. Tanriverdi, and M. Hanci, "Catabolic cytokine expressions in patients with degenerative disc disease," *Turkish Neurosurgery*, vol. 20, no. 4, pp. 492–499, 2010.

[71] A. A. Te Velde, J. P. Klomp, B. A. Yard, J. E. De Vries, and C. G. Figdor, "Modulation of phenotypic and functional properties of human peripheral blood monocytes by IL-4," *Journal of Immunology*, vol. 140, no. 5, pp. 1548–1554, 1988.

[72] A. J. Schuerwegh, E. J. Dombrecht, W. J. Stevens, J. F. Van Offel, C. H. Bridts, and L. S. De Clerck, "Influence of pro-inflammatory (IL-1α, IL-6, TNF-α, IFN-γ) and anti-inflammatory (IL-4) cytokines on chondrocyte function," *Osteoarthritis and Cartilage*, vol. 11, no. 9, pp. 681–687, 2003.

[73] T. T. Chowdhury, D. L. Bader, and D. A. Lee, "Anti-inflammatory effects of IL-4 and dynamic compression in IL-1β stimulated chondrocytes," *Biochemical and Biophysical Research Communications*, vol. 339, no. 1, pp. 241–247, 2006.

[74] P. S. Rachakonda, M. F. Rai, K. Manning, and M. F. Schmidt, "Expression of canine interleukin-4 in canine chondrocytes inhibits inflammatory cascade through STAT6," *Cytokine*, vol. 44, no. 1, pp. 179–184, 2008.

[75] E. Assirelli, L. Pulsatelli, P. Dolzani et al., "Human osteoarthritic cartilage shows reduced in vivo expression of IL-4, a chondroprotective cytokine that differentially modulates IL-1β-stimulated production of chemokines and matrix-degrading enzymes in vitro," *PLoS One*, vol. 9, no. 5, article e96925, 2014.

[76] K. T. Weber, D. O. Alipui, C. P. Sison et al., "Serum levels of the proinflammatory cytokine interleukin-6 vary based on diagnoses in individuals with lumbar intervertebral disc diseases," *Arthritis Research & Therapy*, vol. 18, p. 3, 2016.

[77] M. Xiaogang, H. Quanshan, Z. Liping, and H. Kaken, "The expression of cytokine and its significance for the intervertebral disks of Kazakhs," *Journal of Clinical Laboratory Analysis*, vol. 31, no. 5, 2017.

[78] L. M. Pedersen, E. Schistad, L. M. Jacobsen, C. Røe, and J. Gjerstad, "Serum levels of the pro-inflammatory interleukins 6 (IL-6) and -8 (IL-8) in patients with lumbar radicular pain due to disc herniation: a 12-month prospective study," *Brain, Behavior, and Immunity*, vol. 46, pp. 132–136, 2015.

[79] X. Deng, F. Zhao, B. Kang, and X. Zhang, "Elevated interleukin-6 expression levels are associated with intervertebral disc degeneration," *Experimental and Therapeutic Medicine*, vol. 11, no. 4, pp. 1425–1432, 2016.

[80] E. I. Schistad, A. Espeland, L. M. Pedersen, L. Sandvik, J. Gjerstad, and C. Røe, "Association between baseline IL-6 and 1-year recovery in lumbar radicular pain," *European Journal of Pain*, vol. 18, no. 10, pp. 1394–1401, 2014.

[81] Y. Guo, C. Li, B. Shen et al., "Is there any relationship between plasma IL-6 and TNF-α levels and lumbar disc degeneration? A retrospective single-center study," *Disease Markers*, vol. 2022, Article ID 6842130, 8 pages, 2022.

[82] Y. Guan, S. Wang, J. Wang et al., "Gene polymorphisms and expression levels of interleukin-6 and interleukin-10 in lumbar disc disease: a meta-analysis and immunohistochemical study," *Journal of Orthopaedic Surgery and Research*, vol. 15, no. 1, p. 54, 2020.

[83] A. Hiyama, K. Suyama, D. Sakai, M. Tanaka, and M. Watanabe, "Correlational analysis of chemokine and inflammatory cytokine expression in the intervertebral disc and blood in patients with lumbar disc disease," *Journal of Orthopaedic Research*, vol. 40, no. 5, pp. 1213–1222, 2022.

[84] R. K. Studer, N. Vo, G. Sowa, C. Ondeck, and J. Kang, "Human nucleus pulposus cells react to IL-6: independent actions and amplification of response to IL-1 and TNF-α," *Spine*, vol. 36, no. 8, pp. 593–599, 2011.

[85] Y. Murata, B. Rydevik, U. Nannmark et al., "Local application of interleukin-6 to the dorsal root ganglion induces tumor necrosis factor-alpha in the dorsal root ganglion and results in apoptosis of the dorsal root ganglion cells," *Spine*, vol. 36, no. 12, pp. 926–932, 2011.

[86] S. Bin, L. Xin, Z. Lin, Z. Jinhua, G. Rui, and Z. Xiang, "Targeting miR-10a-5p/IL-6R axis for reducing IL-6-induced cartilage cell ferroptosis," *Experimental and Molecular Pathology*, vol. 118, article 104570, 2021.

[87] A. Li, M. L. Varney, J. Valasek, M. Godfrey, B. J. Dave, and R. K. Singh, "Autocrine role of interleukin-8 in induction of endothelial cell proliferation, survival, migration and MMP-2 production and angiogenesis," *Angiogenesis*, vol. 8, no. 1, pp. 63–71, 2005.

[88] J. D. Kang, H. I. Georgescu, L. McIntyre-Larkin, M. Stefanovic-Racic, W. F. Donaldson III, and C. H. Evans, "Herniated lumbar intervertebral discs spontaneously produce matrix metalloproteinases, nitric oxide, interleukin-6, and prostaglandin E2," *Spine*, vol. 21, no. 3, pp. 271–277, 1996.

[89] M. F. Shamji, L. A. Setton, W. Jarvis et al., "Proinflammatory cytokine expression profile in degenerated and herniated human intervertebral disc tissues," *Arthritis and Rheumatism*, vol. 62, no. 7, pp. 1974–1982, 2010.

[90] Y. Zhang, A. Chee, P. Shi et al., "Intervertebral disc cells produce interleukins found in patients with back pain," *American Journal of Physical Medicine & Rehabilitation*, vol. 95, no. 6, pp. 407–415, 2016.

[91] S. E. Navone, M. Peroglio, L. Guarnaccia et al., "Mechanical loading of intervertebral disc modulates microglia proliferation, activation, and chemotaxis," *Osteoarthritis and Cartilage*, vol. 26, no. 7, pp. 978–987, 2018.

[92] H. J. Moon, T. Yurube, T. P. Lozito et al., "Effects of secreted factors in culture medium of annulus fibrosus cells on microvascular endothelial cells: elucidating the possible pathomechanisms of matrix degradation and nerve in-growth in disc degeneration," *Osteoarthritis and Cartilage*, vol. 22, no. 2, pp. 344–354, 2014.

[93] A. Li, S. Dubey, M. L. Varney, B. J. Dave, and R. K. Singh, "IL-8 directly enhanced endothelial cell survival, proliferation, and matrix metalloproteinases production and regulated angiogenesis," *Journal of Immunology*, vol. 170, no. 6, pp. 3369–3376, 2003.

[94] H. P. Hauber, C. Bergeron, and Q. Hamid, "IL-9 in allergic inflammation," *International Archives of Allergy and Immunology*, vol. 134, no. 1, pp. 79–87, 2004.

[95] Y. Zhang, Y. Zhao, J. Li et al., "Interleukin-9 promotes TNF-α and PGE2 release in human degenerated intervertebral disc tissues," *Spine*, vol. 41, no. 21, pp. 1631–1640, 2016.

[96] E. S. Banimostafavi, M. Fakhar, S. Abediankenari et al., "Determining serum levels of IL-10 and IL-17 in patients with low back pain caused by lumbar disc degeneration," *Infectious Disorders Drug Targets*, vol. 21, no. 5, 2021.

[97] S. Hanaei, S. Abdollahzade, M. Sadr, M. H. Mirbolouk, A. Khoshnevisan, and N. Rezaei, "Association of *IL10* and *TGFB* single nucleotide polymorphisms with intervertebral disc degeneration in Iranian population: a case control study," *BMC Medical Genetics*, vol. 19, no. 1, p. 59, 2018.

[98] S. Holm, Z. Mackiewicz, A. K. Holm et al., "Pro-inflammatory, pleiotropic, and anti-inflammatory TNF-α, IL-6, and IL-10 in experimental porcine intervertebral disk degeneration," *Veterinary Pathology*, vol. 46, no. 6, pp. 1292–1300, 2009.

[99] J. Chen, Z. Mei, B. Huang et al., "IL-6/YAP1/β-catenin signaling is involved in intervertebral disc degeneration," *Journal of Cellular Physiology*, vol. 234, no. 5, pp. 5964–5971, 2019.

[100] H. Kim, J. Y. Hong, J. Lee, W. J. Jeon, and I. H. Ha, "IL-1β promotes disc degeneration and inflammation through direct injection of intervertebral disc in a rat lumbar disc herniation model," *The Spine Journal*, vol. 21, no. 6, pp. 1031–1041, 2021.

[101] H. Park, Z. Li, X. O. Yang et al., "A distinct lineage of CD4 T cells regulates tissue inflammation by producing interleukin 17," *Nature Immunology*, vol. 6, no. 11, pp. 1133–1141, 2005.

[102] J. S. Kim and M. S. Jordan, "Diversity of IL-17-producing T lymphocytes," *Cellular and Molecular Life Sciences*, vol. 70, no. 13, pp. 2271–2290, 2013.

[103] S. Liu, X. Song, B. A. Chrunyk, S. Shanker, and L. R. Hoth, "Crystal structures of interleukin 17A and its complex with IL-17 receptor A," *Nature Communications*, vol. 4, p. 1888, 2013.

[104] C. T. Weaver, R. D. Hatton, P. R. Mangan, and L. E. Harrington, "IL-17 family cytokines and the expanding diversity of effector T cell lineages," *Annual Review of Immunology*, vol. 25, pp. 821–852, 2007.

[105] T. A. Moseley, D. R. Haudenschild, L. Rose, and A. H. Reddi, "Interleukin-17 family and IL-17 receptors," *Cytokine & Growth Factor Reviews*, vol. 14, no. 2, pp. 155–174, 2003.

[106] M. A. Gabr, L. Jing, A. R. Helbling et al., "Interleukin-17 synergizes with IFNγ or TNFα to promote inflammatory mediator release and intercellular adhesion molecule-1 (ICAM-1) expression in human intervertebral disc cells," *Journal of Orthopaedic Research*, vol. 29, no. 1, pp. 1–7, 2011.

[107] P. Tian, Z. J. Li, X. Fu, and X. L. Ma, "Role of interleukin-17 in chondrocytes of herniated intervertebral lumbar discs," *Experimental and Therapeutic Medicine*, vol. 10, no. 1, pp. 81–87, 2015.

[108] Z. Yao, W. C. Fanslow, M. F. Seldin et al., "Herpesvirus saimiri encodes a new cytokine, IL-17, which binds to a novel cytokine receptor," *Immunity*, vol. 3, no. 6, pp. 811–821, 1995.

[109] J. K. Li, L. Nie, Y. P. Zhao et al., "IL-17 mediates inflammatory reactions via p38/c-Fos and JNK/c-Jun activation in an AP-1-dependent manner in human nucleus pulposus cells," *Journal of Translational Medicine*, vol. 14, p. 77, 2016.

[110] K. Suyama, D. Sakai, N. Hirayama et al., "Effects of interleukin-17A in nucleus pulposus cells and its small-molecule inhibitors for intervertebral disc disease," *Journal of Cellular and Molecular Medicine*, vol. 22, no. 11, pp. 5539–5551, 2018.

[111] Z. H. Ouyang, W. J. Wang, Y. G. Yan, B. Wang, and G. H. Lv, "The PI3K/Akt pathway: a critical player in intervertebral disc degeneration," *Oncotarget*, vol. 8, no. 34, pp. 57870–57881, 2017.

[112] S. S. Wang, W. Zhang, Y. Q. Zhang et al., "IL-17A enhances ADAMTS-7 expression through regulation of TNF-α in human nucleus pulposus cells," *Journal of Molecular Histology*, vol. 46, no. 6, pp. 475–483, 2015.

[113] B. Hu, J. Wang, X. Wu, Y. Chen, W. Yuan, and H. Chen, "Interleukin-17 upregulates vascular endothelial growth factor by activating the JAK/STAT pathway in nucleus pulposus cells," *Joint, Bone, Spine*, vol. 84, no. 3, pp. 327–334, 2017.

[114] W. S. He, M. X. Zou, Y. G. Yan et al., "Interleukin-17A promotes human disc degeneration by inhibiting autophagy through the activation of the phosphatidylinositol 3-kinase/Akt/Bcl2 signaling pathway," *World Neurosurgery*, vol. 143, pp. e215–e223, 2020.

[115] B. E. Bachmeier, A. G. Nerlich, C. Weiler, G. Paesold, M. Jochum, and N. Boos, "Analysis of tissue distribution of TNF-α, TNF-α-receptors, and the activating TNF-α-converting enzyme suggests activation of the TNF-α system in the aging intervertebral disc," *Annals of the New York Academy of Sciences*, vol. 1096, pp. 44–54, 2007.

[116] R. M. Locksley, N. Killeen, and M. J. Lenardo, "The TNF and TNF receptor superfamilies: integrating mammalian biology," *Cell*, vol. 104, no. 4, pp. 487–501, 2001.

[117] B. B. Aggarwal, "Signalling pathways of the TNF superfamily: a double-edged sword," *Nature Reviews Immunology*, vol. 3, no. 9, pp. 745–756, 2003.

[118] I. Dichamp, A. Bourgeois, C. Dirand, G. Herbein, and D. Wendling, "Increased nuclear factor-kappaB activation in peripheral blood monocytes of patients with rheumatoid arthritis is mediated primarily by tumor necrosis factor-alpha," *The Journal of Rheumatology*, vol. 34, no. 10, pp. 1976–1983, 2007.

[119] S. M. Ragab, M. A. Safan, O. M. Obeid, and A. S. Sherief, "Lipoprotein-associated phospholipase A2 (Lp-PLA2) and tumor necrosis factor-alpha (TNF-α) and their relation to premature atherosclerosis in β-thalassemia children," *Hematology*, vol. 20, no. 4, pp. 228–238, 2015.

[120] W. Swardfager, K. Lanctôt, L. Rothenburg, A. Wong, J. Cappell, and N. Herrmann, "A meta-analysis of cytokines in Alzheimer's disease," *Biological Psychiatry*, vol. 68, no. 10, pp. 930–941, 2010.

[121] J. Brynskov, P. Foegh, G. Pedersen et al., "Tumour necrosis factor α converting enzyme (TACE) activity in the colonic mucosa of patients with inflammatory bowel disease," *Gut*, vol. 51, no. 1, pp. 37–43, 2002.

[122] D. Wallach, "The TNF family: only the surface has been scratched," *Seminars in Immunology*, vol. 26, no. 3, pp. 181-182, 2014.

[123] G. Herbein, U. Mahlknecht, F. Batliwalla et al., "Apoptosis of CD8$^+$ T cells is mediated by macrophages through interaction of HIV gp120 with chemokine receptor CXCR4," *Nature*, vol. 395, no. 6698, pp. 189–194, 1998.

[124] B. B. Aggarwal, S. C. Gupta, and J. H. Kim, "Historical perspectives on tumor necrosis factor and its superfamily: 25 years later, a golden journey," *Blood*, vol. 119, no. 3, pp. 651–665, 2012.

[125] D. Wallach, "The TNF cytokine family: one track in a road paved by many," *Cytokine*, vol. 63, no. 3, pp. 225–229, 2013.

[126] C. L. Le Maitre, J. A. Hoyland, and A. J. Freemont, "Catabolic cytokine expression in degenerate and herniated human

intervertebral discs: IL-1β and TNFα expression profile," *Arthritis Research & Therapy*, vol. 9, no. 4, p. R77, 2007.

[127] S. Ohtori, G. Inoue, Y. Eguchi et al., "Tumor necrosis factor-α-immunoreactive cells in nucleus pulposus in adolescent patients with lumbar disc herniation," *Spine*, vol. 38, no. 6, pp. 459–462, 2013.

[128] P. Andrade, V. Visser-Vandewalle, M. Philippens et al., "Tumor necrosis factor-α levels correlate with postoperative pain severity in lumbar disc hernia patients: opposite clinical effects between tumor necrosis factor receptor 1 and 2," *Pain*, vol. 152, no. 11, pp. 2645–2652, 2011.

[129] H. Liang, X. Yang, C. Liu, Z. Sun, and X. Wang, "Effect of NF-kB signaling pathway on the expression of MIF, TNF-α, IL-6 in the regulation of intervertebral disc degeneration," *Journal of Musculoskeletal & Neuronal Interactions*, vol. 18, no. 4, pp. 551–556, 2018.

[130] C. Weiler, A. G. Nerlich, B. E. Bachmeier, and N. Boos, "Expression and distribution of tumor necrosis factor alpha in human lumbar intervertebral discs: a study in surgical specimen and autopsy controls," *Spine*, vol. 30, no. 1, pp. 44–53, 2005.

[131] J. Y. Park, S. U. Kuh, H. S. Park, and K. S. Kim, "Comparative expression of matrix-associated genes and inflammatory cytokines-associated genes according to disc degeneration: analysis of living human nucleus pulposus," *Journal of Spinal Disorders & Techniques*, vol. 24, no. 6, pp. 352–357, 2011.

[132] D. J. Gorth, I. M. Shapiro, and M. V. Risbud, "Transgenic mice overexpressing human TNF-α experience early onset spontaneous intervertebral disc herniation in the absence of overt degeneration," *Cell Death & Disease*, vol. 10, no. 1, p. 7, 2018.

[133] R. Kang, H. Li, K. Rickers, S. Ringgaard, L. Xie, and C. Bünger, "Intervertebral disc degenerative changes after intradiscal injection of TNF-α in a porcine model," *European Spine Journal*, vol. 24, no. 9, pp. 2010–2016, 2015.

[134] H. E. Gruber, G. L. Hoelscher, J. A. Ingram, S. Bethea, M. Cox, and E. N. Hanley Jr., "Proinflammatory cytokines modulate the chemokine CCL2 (MCP-1) in human annulus cells in vitro: CCL2 expression and production," *Experimental and Molecular Pathology*, vol. 98, no. 1, pp. 102–105, 2015.

[135] H. J. Moon, J. H. Kim, H. S. Lee et al., "Annulus fibrosus cells interact with neuron-like cells to modulate production of growth factors and cytokines in symptomatic disc degeneration," *Spine*, vol. 37, no. 1, pp. 2–9, 2012.

[136] C. K. Kepler, D. Z. Markova, A. S. Hilibrand et al., "Substance P stimulates production of inflammatory cytokines in human disc cells," *Spine*, vol. 38, no. 21, pp. E1291–E1299, 2013.

[137] J. Wang, Y. Tian, K. L. E. Phillips et al., "Tumor necrosis factor α- and interleukin-1β-dependent induction of CCL3 expression by nucleus pulposus cells promotes macrophage migration through CCR1," *Arthritis and Rheumatism*, vol. 65, no. 3, pp. 832–842, 2013.

[138] Y. Abe, K. Akeda, H. S. An et al., "Proinflammatory cytokines stimulate the expression of nerve growth factor by human intervertebral disc cells," *Spine*, vol. 32, no. 6, pp. 635–642, 2007.

[139] T. Ohba, H. Haro, T. Ando et al., "TNF-alpha-induced NF-kappaB signaling reverses age-related declines in VEGF induction and angiogenic activity in intervertebral disc tissues," *Journal of Orthopaedic Research*, vol. 27, no. 2, pp. 229–235, 2009.

[140] S. Yang, L. Li, L. Zhu et al., "Aucubin inhibits IL-1β- or TNF-α-induced extracellular matrix degradation in nucleus pulposus cell through blocking the miR-140-5p/CREB1 axis," *Journal of Cellular Physiology*, vol. 234, no. 8, pp. 13639–13648, 2019.

[141] J. A. Hoyland, C. Le Maitre, and A. J. Freemont, "Investigation of the role of IL-1 and TNF in matrix degradation in the intervertebral disc," *Rheumatology*, vol. 47, no. 6, pp. 809–814, 2008.

[142] C. Wang, X. Yu, Y. Yan et al., "Tumor necrosis factor-α: a key contributor to intervertebral disc degeneration," *Acta Biochimica et Biophysica Sinica Shanghai*, vol. 49, no. 1, pp. 1–13, 2017.

[143] J. S. Kim, M. B. Ellman, D. Yan et al., "Lactoferricin mediates anti-inflammatory and anti-catabolic effects via inhibition of IL-1 and LPS activity in the intervertebral disc," *Journal of Cellular Physiology*, vol. 228, no. 9, pp. 1884–1896, 2013.

[144] J. Wang, D. Markova, D. G. Anderson, Z. Zheng, I. M. Shapiro, and M. V. Risbud, "TNF-α and IL-1β Promote a Disintegrin-like and Metalloprotease with Thrombospondin Type I Motif-5-mediated Aggrecan Degradation through Syndecan-4 in Intervertebral Disc," *The Journal of Biological Chemistry*, vol. 286, no. 46, pp. 39738–39749, 2011.

[145] J. Zhang, X. Wang, H. Liu et al., "TNF-α enhances apoptosis by promoting chop expression in nucleus pulposus cells: role of the MAPK and NF-κB pathways," *Journal of Orthopaedic Research*, vol. 37, no. 3, pp. 697–705, 2019.

[146] W. Yu, J. Fu, Y. Liu, Y. Wu, and D. Jiang, "Osteogenic protein-1 inhibits nucleus pulposus cell apoptosis through regulating the NF-κB/ROS pathway in an inflammation environment," *Bioscience Reports*, vol. 38, no. 6, 2018.

[147] H. E. Gruber, G. L. Hoelscher, S. Bethea, and E. N. Hanley Jr., "Mitochondrial membrane potential and nuclear and gene expression changes during human disc cell apoptosis: in vitro and in vivo annulus findings," *Spine*, vol. 40, no. 12, pp. 876–882, 2015.

[148] Z. Guo, W. S. Gao, Y. F. Wang, F. Gao, W. Wang, and W. Y. Ding, "MiR-502 Suppresses TNF-α-Induced Nucleus Pulposus Cell Apoptosis by Targeting TARF2," *BioMed Research International*, vol. 2021, Article ID 5558369, 11 pages, 2021.

[149] H. Zhu, B. Sun, and Q. Shen, "TNF-α induces apoptosis of human nucleus pulposus cells via activating the TRIM14/NF-κB signalling pathway," *Artif Cells Nanomed Biotechnol*, vol. 47, no. 1, pp. 3004–3012, 2019.

[150] D. Purmessur, B. A. Walter, P. J. Roughley, D. M. Laudier, A. C. Hecht, and J. Iatridis, "A role for TNFα in intervertebral disc degeneration: A non-recoverable catabolic shift," *Biochemical and Biophysical Research Communications*, vol. 433, no. 1, pp. 151–156, 2013.

[151] J. Xie, B. Li, P. Zhang, L. Wang, H. Lu, and X. Song, "Osteogenic protein-1 attenuates the inflammatory cytokine-induced NP cell senescence through regulating the ROS/NF-κB pathway," *Biomedicine & Pharmacotherapy*, vol. 99, pp. 431–437, 2018.

[152] X. Lin and Q. Lin, "MiRNA-495-3p attenuates TNF-α induced apoptosis and inflammation in human nucleus pulposus cells by targeting IL5RA," *Inflammation*, vol. 43, no. 5, pp. 1797–1805, 2020.

[153] S. Cheng, X. Li, Z. Jia et al., "The inflammatory cytokine TNF-α regulates the biological behavior of rat nucleus pulposus mesenchymal stem cells through the NF-κB signaling

pathway in vitro," *Journal of Cellular Biochemistry*, vol. 120, no. 8, pp. 13664–13679, 2019.

[154] H. Wang, Y. Tian, J. Wang et al., "Inflammatory Cytokines Induce NOTCH Signaling in Nucleus Pulposus Cells:," *The Journal of Biological Chemistry*, vol. 288, no. 23, pp. 16761–16774, 2013.

[155] L. Chen, Z. Y. Xie, L. Liu et al., "Nuclear factor-kappa B-dependent X-box binding protein 1 signalling promotes the proliferation of nucleus pulposus cells under tumour necrosis factor alpha stimulation," *Cell Proliferation*, vol. 52, no. 2, article e12542, 2019.

[156] X. H. Wang, X. Hong, L. Zhu et al., "Tumor necrosis factor alpha promotes the proliferation of human nucleus pulposus cells via nuclear factor-κB, c-Jun N-terminal kinase, and p38 mitogen-activated protein kinase," *Experimental Biology and Medicine*, vol. 240, no. 4, pp. 411–417, 2015.

[157] K. Beider, M. Abraham, and A. Peled, "Chemokines and chemokine receptors in stem cell circulation," *Frontiers in Bioscience*, vol. 13, pp. 6820–6833, 2008.

[158] N. Fan, S. Yuan, Y. Hai et al., "Identifying the potential role of IL-1β in the molecular mechanisms of disc degeneration using gene expression profiling and bioinformatics analysis," *Journal of Orthopaedic Surgery*, vol. 30, no. 1, 2022.

[159] G. Pattappa, M. Peroglio, D. Sakai et al., "CCL5/RANTES is a key chemoattractant released by degenerative intervertebral discs in organ culture," *European Cells & Materials*, vol. 27, 2014.

[160] S. Grad, C. Bow, J. Karppinen et al., "Systemic blood plasma CCL5 and CXCL6: potential biomarkers for human lumbar disc degeneration," *European Cells & Materials*, vol. 31, pp. 1–10, 2016.

[161] H. Zhong, Z. Zhou, L. Guo et al., "The miR-623/CXCL12 axis inhibits LPS-induced nucleus pulposus cell apoptosis and senescence," *Mechanisms of Ageing and Development*, vol. 194, article 111417, 2021.

[162] H. Zhang, L. Zhang, L. Chen, W. Li, F. Li, and Q. Chen, "Stromal cell-derived factor-1 and its receptor CXCR4 are upregulated expression in degenerated intervertebral discs," *International Journal of Medical Sciences*, vol. 11, no. 3, pp. 240–245, 2014.

[163] N. Willems, A. R. Tellegen, N. Bergknut et al., "Inflammatory profiles in canine intervertebral disc degeneration," *BMC Veterinary Research*, vol. 12, p. 10, 2016.

[164] Z. J. Er, C. F. Yin, W. J. Wang, and X. J. Chen, "Serum CXCL12/SDF-1 level is positively related with lumbar intervertebral disc degeneration and clinical severity," *Innate Immunity*, vol. 26, no. 5, pp. 341–350, 2020.

[165] Y. L. Zhang, B. Li, and Z. H. Zhou, "A cross-sectional study: serum CCL3/MIP-1α levels may reflect lumbar intervertebral disk degeneration in Han Chinese people," *Journal of Pain Research*, vol. 11, pp. 497–503, 2018.

[166] Y. Zhang, L. Liu, S. Wang et al., "Production of CCL20 on nucleus pulposus cells recruits IL-17-producing cells to degenerated IVD tissues in rat models," *Journal of Molecular Histology*, vol. 47, no. 1, pp. 81–89, 2016.

[167] H. Zhang, T. Zhu, L. Zhang, and Q. Wu, "Stromal cell-derived factor-1 induces matrix metalloproteinase expression in human endplate chondrocytes, cartilage endplate degradation in explant culture, and the amelioration of nucleus pulposus degeneration in vivo," *International Journal of Molecular Medicine*, vol. 41, no. 2, pp. 969–976, 2018.

[168] Z. Liu, C. Ma, J. Shen, D. Wang, J. Hao, and Z. Hu, "SDF-1/CXCR4 axis induces apoptosis of human degenerative nucleus pulposus cells via the NF-κB pathway," *Molecular Medicine Reports*, vol. 14, no. 1, pp. 783–789, 2016.

[169] H. Zhang, P. Wang, X. Zhang, W. Zhao, H. Ren, and Z. Hu, "SDF1/CXCR4 axis facilitates the angiogenesis via activating the PI3K/AKT pathway in degenerated discs," *Molecular Medicine Reports*, vol. 22, no. 5, pp. 4163–4172, 2020.

[170] H. Zhang, P. Wang, X. Zhang, W. Zhao, H. Ren, and Z. Hu, "SDF1/CXCR7 signaling axis participates in angiogenesis in degenerated discs via the PI3K/AKT pathway," *DNA and Cell Biology*, vol. 38, no. 5, pp. 457–467, 2019.

[171] H. Zhang and B. He, "SDF1/CXCR4 axis plays a role in angiogenesis during the degeneration of intervertebral discs," *Molecular Medicine Reports*, vol. 20, no. 2, pp. 1203–1211, 2019.

[172] O. Gross, C. J. Thomas, G. Guarda, and J. Tschopp, "The inflammasome: an integrated view," *Immunological Reviews*, vol. 243, no. 1, pp. 136–151, 2011.

[173] Z. H. Chen, S. H. Jin, M. Y. Wang et al., "Enhanced NLRP3, caspase-1, and IL-1β levels in degenerate human intervertebral disc and their association with the grades of disc degeneration," *The Anatomical Record*, vol. 298, no. 4, pp. 720–726, 2015.

[174] P. Tang, R. Zhu, W. P. Ji et al., "The NLRP3/Caspase-1/Interleukin-1β axis is active in human lumbar cartilaginous endplate degeneration," *Clinical Orthopaedics and Related Research*, vol. 474, no. 8, pp. 1818–1826, 2016.

[175] W. Zhang, G. Li, R. Luo et al., "Cytosolic escape of mitochondrial DNA triggers cGAS-STING-NLRP3 axis- dependent nucleus pulposus cell pyroptosis," *Experimental & Molecular Medicine*, vol. 54, no. 2, pp. 129–142, 2022.

[176] P. Tang, J. M. Gu, Z. A. Xie et al., "Honokiol alleviates the degeneration of intervertebral disc via suppressing the activation of TXNIP-NLRP3 inflammasome signal pathway," *Free Radical Biology & Medicine*, vol. 120, pp. 368–379, 2018.

[177] Y. Tian, Z. Bao, Y. Ji, X. Mei, and H. Yang, "Epigallocatechin-3-Gallate protects H_2O_2-Induced nucleus pulposus cell apoptosis and inflammation by inhibiting cGAS/Sting/NLRP3 Activation," *Drug Design, Development and Therapy*, vol. 14, pp. 2113–2122, 2020.

[178] D. He, M. Zhou, Z. Bai, Y. Wen, J. Shen, and Z. Hu, "*Propionibacterium acnes* induces intervertebral disc degeneration by promoting nucleus pulposus cell pyroptosis via NLRP3-dependent pathway," *Biochemical and Biophysical Research Communications*, vol. 526, no. 3, pp. 772–779, 2020.

[179] H. Hashizume, M. Kawakami, H. Nishi, and T. Tamaki, "Histochemical demonstration of nitric oxide in herniated lumbar discs. A clinical and animal model study," *Spine*, vol. 22, no. 10, pp. 1080–1084, 1997.

[180] C. M. De Geer, "Cytokine involvement in biological inflammation related to degenerative disorders of the intervertebral disk: a narrative review," *Journal of Chiropractic Medicine*, vol. 17, no. 1, pp. 54–62, 2018.

[181] P. Goupille, D. Mulleman, G. Paintaud, H. Watier, and J. P. Valat, "Can sciatica induced by disc herniation be treated with tumor necrosis factor alpha blockade?," *Arthritis and Rheumatism*, vol. 56, no. 12, pp. 3887–3895, 2007.

[182] M. Likhitpanichkul, O. M. Torre, J. Gruen, B. A. Walter, A. C. Hecht, and J. C. Iatridis, "Do mechanical strain and TNF-α interact to amplify pro-inflammatory cytokine production

in human annulus fibrosus cells?," *Journal of Biomechanics*, vol. 49, no. 7, pp. 1214–1220, 2016.

[183] H. Ding, J. Wei, Y. Zhao, Y. Liu, L. Liu, and L. Cheng, "Progranulin derived engineered protein Atsttrin suppresses TNF-α-mediated inflammation in intervertebral disc degenerative disease," *Oncotarget*, vol. 8, no. 65, pp. 109692–109702, 2017.

[184] T. W. Evashwick-Rogler, A. Lai, H. Watanabe et al., "Inhibiting tumor necrosis factor-alpha at time of induced intervertebral disc injury limits long-term pain and degeneration in a rat model," *JOR Spine*, vol. 1, no. 2, article e1014, 2018.

[185] W. Tang, Y. Lu, Q. Y. Tian et al., "The growth factor progranulin binds to TNF receptors and is therapeutic against inflammatory arthritis in mice," *Science*, vol. 332, no. 6028, pp. 478–484, 2011.

[186] D. J. Gorth, R. L. Mauck, J. A. Chiaro et al., "IL-1ra delivered from poly(lactic-co-glycolic acid) microspheres attenuates IL-1beta-mediated degradation of nucleus pulposus in vitro," *Arthritis Research & Therapy*, vol. 14, no. 4, p. R179, 2012.

[187] G. Swamy, P. Salo, N. Duncan, F. Jirik, and J. Matyas, "IL-1Ra deficiency accelerates intervertebral disc degeneration in C57BL6J mice," *JOR Spine*, vol. 5, no. 2, article e1201, 2022.

[188] I. Bjarnason, "The impact of recent data on our understanding of the roles of COX-1 and COX-2 in gastrointestinal pathophysiology," *Clinical Drug Investigation*, vol. 27, Supplement 1, pp. 7–13, 2007.

[189] M. Kawakami, T. Matsumoto, H. Hashizume, K. Kuribayashi, and T. Tamaki, "Epidural injection of cyclooxygenase-2 inhibitor attenuates pain-related behavior following application of nucleus pulposus to the nerve root in the rat," *Journal of Orthopaedic Research*, vol. 20, no. 2, pp. 376–381, 2002.

[190] S. Kobori, M. Miyagi, S. Orita et al., "Inhibiting IκB Kinase-β downregulates inflammatory cytokines in injured discs and neuropeptides in dorsal root ganglia innervating injured discs in rats," *Spine (Phila Pa 1976)*, vol. 39, no. 15, pp. 1171–1177, 2014.

[191] K. Wuertz, L. Quero, M. Sekiguchi et al., "The red wine polyphenol resveratrol shows promising potential for the treatment of nucleus pulposus-mediated pain in vitro and in vivo," *Spine (Phila Pa 1976)*, vol. 36, no. 21, pp. E1373–E1384, 2011.

[192] H. Yu, G. Hou, J. Cao, Y. Yin, Y. Zhao, and L. Cheng, "Mangiferin Alleviates Mitochondrial ROS in Nucleus Pulposus Cells and Protects against Intervertebral Disc Degeneration via Suppression of NF-κB Signaling Pathway," *Oxidative Medicine and Cellular Longevity*, vol. 2021, Article ID 6632786, 27 pages, 2021.

[193] Q. Ge, J. Ying, Z. Shi et al., "Chlorogenic Acid retards cartilaginous endplate degeneration and ameliorates intervertebral disc degeneration *via* suppressing NF-κB signaling," *Life Sciences*, vol. 274, article 119324, 2021.

[194] J. Chen, J. Xuan, Y. T. Gu et al., "Celastrol reduces IL-1β induced matrix catabolism, oxidative stress and inflammation in human nucleus pulposus cells and attenuates rat intervertebral disc degeneration in vivo," *Biomedicine & Pharmacotherapy*, vol. 91, pp. 208–219, 2017.

[195] X. Su, B. Liu, F. Gong et al., "Isofraxidin attenuates IL-1β-induced inflammatory response in human nucleus pulposus cells," *Journal of Cellular Biochemistry*, vol. 120, no. 8, pp. 13302–13309, 2019.

[196] X. Bai, W. Ding, S. Yang, and X. Guo, "Higenamine inhibits IL-1β-induced inflammation in human nucleus pulposus cells," *Bioscience Reports*, vol. 39, no. 6, 2019.

[197] K. Li, Y. Li, B. Xu, L. Mao, and J. Zhao, "Sesamin inhibits lipopolysaccharide-induced inflammation and extracellular matrix catabolism in rat intervertebral disc," *Connective Tissue Research*, vol. 57, no. 5, pp. 347–359, 2016.

[198] K. Li and C. Lv, "Intradiscal injection of sesamin protects from lesion-induced degeneration," *Connective Tissue Research*, vol. 61, no. 6, pp. 594–603, 2020.

[199] G. Gao, F. Chang, T. Zhang et al., "Naringin protects against interleukin 1β (IL-1β)-Induced human nucleus pulposus cells degeneration via downregulation nuclear factor kappa B (NF-κB) pathway and p53 expression," *Medical Science Monitor*, vol. 25, pp. 9963–9972, 2019.

[200] R. Chen, S. Gao, H. Guan et al., "Naringin protects human nucleus pulposus cells against TNF-α-induced inflammation, oxidative stress, and loss of cellular homeostasis by enhancing autophagic flux via AMPK/SIRT1 activation," *Oxidative Medicine and Cellular Longevity*, vol. 2022, Article ID 7655142, 17 pages, 2022.

[201] H. Jin, Q. Wang, J. Wu et al., "Baicalein inhibits the IL-1β-Induced inflammatory response in nucleus pulposus cells and attenuates disc degeneration in vivo," *Inflammation*, vol. 42, no. 3, pp. 1032–1044, 2019.

[202] J. Lin, J. Chen, Z. Zhang et al., "Luteoloside inhibits IL-1β-Induced apoptosis and catabolism in nucleus pulposus cells and ameliorates intervertebral disk degeneration," *Frontiers in Pharmacology*, vol. 10, p. 868, 2019.

[203] S. Chen, M. Luo, H. Kou, G. Shang, Y. Ji, and H. Liu, "A review of gene therapy delivery systems for intervertebral disc degeneration," *Current Pharmaceutical Biotechnology*, vol. 21, no. 3, pp. 194–205, 2020.

[204] P. Wehling, K. P. Schulitz, P. D. Robbins, C. H. Evans, and J. A. Reinecke, "Transfer of genes to chondrocytic cells of the lumbar spine. Proposal for a treatment strategy of spinal disorders by local gene therapy," *Spine (Phila Pa 1976)*, vol. 22, no. 10, pp. 1092–1097, 1997.

[205] K. Nishida, J. D. Kang, L. G. Gilbertson et al., "Modulation of the biologic activity of the rabbit intervertebral disc by gene therapy: an in vivo study of adenovirus-mediated transfer of the human transforming growth factor beta 1 encoding gene," *Spine (Phila Pa 1976)*, vol. 24, no. 23, pp. 2419–2425, 1999.

[206] Y. J. Lee, M. H. Kong, K. Y. Song, K. H. Lee, and S. H. Heo, "The relation between Sox9, TGF-beta1, and proteoglycan in human intervertebral disc cells," *Journal of Korean Neurosurgical Association*, vol. 43, no. 3, pp. 149–154, 2008.

[207] Y. Tan, Y. Hu, and J. Tan, "Extracellular matrix synthesis and ultrastructural changes of degenerative disc cells transfected by Ad/CMV-hTGF-beta 1," *Chinese Medical Journal*, vol. 116, no. 9, pp. 1399–1403, 2003.

[208] Y. Takeoka, T. Yurube, and K. Nishida, "Gene therapy approach for intervertebral disc degeneration: an update," *Neurospine*, vol. 17, no. 1, pp. 3–14, 2020.

[209] A. Hajiesmailpoor, O. Mohamadi, P. Emami, G. Farzanegan, and M. Ghorbani, "Overview of stem cell therapy in intervertebral disc disease: clinical perspectives," *Current Stem Cell Research & Therapy*, 2022.

[210] A. S. Croft, S. Illien-Jünger, S. Grad, J. Guerrero, S. Wangler, and B. Gantenbein, "The application of mesenchymal

stromal cells and their homing capabilities to regenerate the intervertebral disc," *International Journal of Molecular Sciences*, vol. 22, no. 7, p. 3519, 2021.

[211] F. Steffen, L. A. Smolders, A. M. Roentgen, A. Bertolo, and J. Stoyanov, "Bone marrow-derived mesenchymal stem cells as autologous therapy in dogs with naturally occurring intervertebral disc disease: feasibility, safety, and preliminary results," *Tissue Engineering. Part C, Methods*, vol. 23, no. 11, pp. 643–651, 2017.

[212] L. Qi, R. Wang, Q. Shi, M. Yuan, M. Jin, and D. Li, "Umbilical cord mesenchymal stem cell conditioned medium restored the expression of collagen II and aggrecan in nucleus pulposus mesenchymal stem cells exposed to high glucose," *Journal of Bone and Mineral Metabolism*, vol. 37, no. 3, pp. 455–466, 2019.

[213] T. Miyamoto, T. Muneta, T. Tabuchi et al., "Intradiscal transplantation of synovial mesenchymal stem cells prevents intervertebral disc degeneration through suppression of matrix metalloproteinase-related genes in nucleus pulposus cells in rabbits," *Arthritis Research & Therapy*, vol. 12, no. 6, p. R206, 2010.

[214] S. M. Richardson, G. Kalamegam, P. N. Pushparaj et al., "Mesenchymal stem cells in regenerative medicine: focus on articular cartilage and intervertebral disc regeneration," *Methods*, vol. 99, pp. 69–80, 2016.

[215] J. R. Ferreira, G. Q. Teixeira, E. Neto et al., "IL-1β-pre-conditioned mesenchymal stem/stromal cells' secretome modulates the inflammatory response and aggrecan deposition in intervertebral disc," *European Cells & Materials*, vol. 41, pp. 431–543, 2021.

[216] J. S. Heo, Y. Choi, H.-S. Kim, and H. O. Kim, "Comparison of molecular profiles of human mesenchymal stem cells derived from bone marrow, umbilical cord blood, placenta and adipose tissue," *International Journal of Molecular Medicine*, vol. 37, no. 1, pp. 115–125, 2016.

[217] I. Urits, A. Capuco, M. Sharma et al., "Stem cell therapies for treatment of discogenic low back pain: a comprehensive review," *Current Pain and Headache Reports*, vol. 23, no. 9, p. 65, 2019.

[218] X. Li, A. Wu, C. Han et al., "Bone marrow-derived mesenchymal stem cells in three-dimensional co-culture attenuate degeneration of nucleus pulposus cells," *Aging (Albany NY)*, vol. 11, no. 20, pp. 9167–9187, 2019.

[219] L. Orozco, R. Soler, C. Morera, M. Alberca, A. Sánchez, and J. García-Sancho, "Intervertebral disc repair by autologous mesenchymal bone marrow cells: a pilot study," *Transplantation*, vol. 92, no. 7, pp. 822–828, 2011.

[220] X. Pang, H. Yang, and B. Peng, "Human umbilical cord mesenchymal stem cell transplantation for the treatment of chronic discogenic low back pain," *Pain Physician*, vol. 17, no. 4, pp. E525–E530, 2014.

[221] Z. Li, Y. Wu, G. Tan, Z. Xu, and H. Xue, "Exosomes and exosomal miRNAs: a new therapy for intervertebral disc degeneration," *Frontiers in Pharmacology*, vol. 13, article 992476, 2022.

[222] B. Bhujel, H. E. Shin, D. J. Choi, and I. Han, "Mesenchymal stem cell-derived exosomes and intervertebral disc regeneration: review," *International Journal of Molecular Sciences*, vol. 23, no. 13, p. 7306, 2022.

[223] S. Cui and L. Zhang, "MicroRNA-129-5p shuttled by mesenchymal stem cell-derived extracellular vesicles alleviates intervertebral disc degeneration via blockade of LRG1-mediated p38 MAPK activation," *Journal of Tissue Engineering*, vol. 12, 14 pages, 2021.

[224] B. Z. Shao, Z.-Q. Xu, B.-Z. Han, D.-F. Su, and C. Liu, "NLRP3 inflammasome and its inhibitors: a review," *Frontiers in Pharmacology*, vol. 6, p. 262, 2015.

[225] G. Chao-Yang, C. Peng, and Z. Hai-Hong, "Roles of NLRP3 inflammasome in intervertebral disc degeneration," *Osteoarthritis and Cartilage*, vol. 29, no. 6, pp. 793–801, 2021.

[226] J. Zhang, J. Zhang, Y. Zhang et al., "Mesenchymal stem cells-derived exosomes ameliorate intervertebral disc degeneration through inhibiting pyroptosis," *Journal of Cellular and Molecular Medicine*, vol. 24, no. 20, pp. 11742–11754, 2020.

[227] X. Yuan, T. Li, L. Shi, J. Miao, Y. Guo, and Y. Chen, "Human umbilical cord mesenchymal stem cells deliver exogenous miR-26a-5p via exosomes to inhibit nucleus pulposus cell pyroptosis through METTL14/NLRP3," *Molecular Medicine*, vol. 27, no. 1, p. 91, 2021.

Research Article

Smurf1 Facilitates Oxidative Stress and Fibrosis of Ligamentum Flavum by Promoting Nrf2 Ubiquitination and Degradation

Yifei Gu, Jinquan Hu, Chen Wang, Min Qi, Yu Chen, Wenchao Yu, Zhanchao Wang [ID], **Xinwei Wang** [ID]**, and Wen Yuan** [ID]

Department of Orthopedics, Shanghai Changzheng Hospital, Naval Medical University, Shanghai 200003, China

Correspondence should be addressed to Xinwei Wang; orth.wang@263.net and Wen Yuan; ywspine@126.com

Lumbar spinal stenosis (LSS), which can lead to irreversible neurologic damage and functional disability, is characterized by hypertrophy and fibrosis in the ligamentum flavum (LF). However, the underlying mechanism is still unclear. In the current study, the effect of Smurf1, a kind of E3 ubiquitin ligase, in promoting the fibrosis and oxidative stress of LF was investigated, and its underlying mechanism was explored. The expression of oxidative stress and fibrosis-related markers was assessed in the tissue of lumbar spinal stenosis (LSS) and lumbar disc herniation (LDH). Next, the expression of the top 10 E3 ubiquitin ligases, obtained from Gene Expression Omnibus (GEO) dataset GSE113212, was assessed in LDH and LSS, and confirmed that Smurf1 expression was markedly upregulated in the LSS group. Furthermore, Smurf1 overexpression promotes the fibrosis and oxidative stress of LF cells. Subsequently, NRF2, an important transcription factor for oxidative stress and fibrosis, was predicted to be a target of Smurf1. Mechanistically, Smurf1 directly interacts with Nrf2 and accelerates Nrf2 ubiquitination and degradation. In conclusion, the current study suggests that Smurf1 facilitated the fibrosis and oxidative stress of LF and induced the development of LSS by promoting Nrf2 ubiquitination and degradation.

1. Introduction

Lumbar spinal stenosis (LSS) is one of the most common spinal disorders in aging patients and is closed related to lower back pain, limb numbness, and intermittent claudication [1, 2]. Compression of the cauda equina and lumbar nerve roots often results in sensory and motor dysfunction of the lower limbs, which can lead to severe disability [3]. LSS development has been attributed to a number of factors, including disc protrusion, facet joint degeneration, and hypertrophy of the ligamentum flavum (HLF) [4, 5]. In previous studies, fibrosis was considered to be the main pathology of HLF. Histologically, normal LF consists of approximately 20% collagen fibers and 80% elastic fibers [4, 6]. Conversely, HLF tissues exhibit fibrosis changes with an increase in collagen fibers and elastic fiber loss. Recently, several studies have reported the fibrosis of HLF at the cellular and histological levels. However, to date, the molecular mechanisms underlying the fibrosis of HLF are still unclear.

Reactive oxygen species (ROS) generation leads to oxidative stress when it surpasses the capacity of antioxidant enzymes, and excessive ROS production has been linked to a number of aging illnesses. [7, 8]. Strong inflammatory reactions and fibrosis of vital organs, including the heart, kidneys, lungs, and liver, can be induced by an excess of ROS. A previous study clarified that catalase expression was decreased in HLF tissue of LSS patients [9]. Another study reported that oxidative stress mediates age-related HLF by promoting fibrosis, inflammation, and apoptosis via promoting MAPK-AKT pathway [10]. Together, these studies confirmed that oxidative stress-mediated LF fibrosis plays an important role in the development of LSS, however the exact mechanism by which oxidative stress dysregulation in HLF occurs is still unclear.

Previous research has reported that ubiquitination contributes to the age-related diseases. Hunt et al. reported that antagonistic control of myofiber size and muscle protein quality is controlled by the ubiquitin ligase UBR4 during

aging [11]. Kong et al. reported that the prostaglandin D2/DP1 axis suppresses age-related Th1 activation and subsequent hypertensive response in male mice through an increase in NEDD4L-mediated T-bet degradation by ubiquitination [12]. Moreover, multiple lines of evidence indicate an important function of ubiquitination in regulating oxidative stress and fibrosis. Wang et al. reported that FBW7 regulates pulmonary epithelial stem cell senescence and fibrosis by regulating telomere uncapping [13]. However, the regulatory mechanisms of ubiquitination in the development of HLF are still unclear.

Nuclear factor-erythroid 2-related factor 2 (Nrf2) is an important regulator of many antioxidant enzymes [14]. Nrf2 regulates the balance of cell redox by facilitating the activity of antioxidant defense components, including heme oxygenase-1 (HO-1), superoxide dismutase (SOD), peroxidase (GSH-Px), and glutathione [15], and dysregulation of Nrf2 is associated with a variety of oxidative stress-related diseases, including neurodegenerative diseases [16], cardiovascular disorders [17], pulmonary diseases [18], and cancer [19]. In addition, Nrf2 activation prevents cell senescence, whereas inhibiting the activation of Nrf2 markedly accelerates cell senescence [20], suggesting that has an anti-aging impact. Additionally, Nrf2 expression and activity decreased with age. In the current study, the expression of Smurf1, an E3 ubiquitin ligase was found to be obviously increased in the LSS group, and Smurf1 overexpression accelerates oxidative stress and fibrosis of LF cells. Moreover, Smurf1 facilitates ubiquitination-mediated degradation of Nrf2.

2. Materials and Methods

2.1. Patients and Sample Harvest.
All experimental protocols were approved by the Ethics Committee of the Naval Medical University (2016SL-034-01). Ligamentum flavum samples were collected from 27 patients (10 females and 17 males) who underwent posterior lumbar decompression surgery with removal of LF tissue from June 2021 to December 2021 (Table 1). For the HLF group, 15 LF specimens were harvested from LSS patients with LF hypertrophy, and for the control group, 12 specimens were collected from individuals with uncomplicated lumbar disc herniation and no LF hypertrophy. The thickness of the LF was quantified at the facet joint level on T2-weighted magnetic resonance imaging (MRI) for all 27 patients using Picture Archiving and Communication Systems (PACS) software. An expert spine surgeon assessed the value three times for each patient, and the average value designated the LF thickness. According to previous studies, hypertrophy of LF was defined as LF thickness> 4 mm [21, 22]. Extensive or partial laminectomy with LF resection was performed in all patients during the operation. The resected ligamentum flavum was rinsed in 4°C physiological saline and then sent for examination immediately.

2.2. Bioinformatic Analysis.
The gene expression profile of data GSE113212 was obtained from the Gene Expression Omnibus (GEO) database (http://www.ncbi.nlm.nih.gov/geo/), National Center for Biotechnology Information (NCBI). This data set was based on the GPL17077 platform and contained a total of 8 samples, including 4 hypertrophic ligamentum flavum samples from the elderly individuals and 4 non-hypertrophic samples from the young individuals. The top 10 differentially expressed E3 ubiquitin ligase were obtained from this dataset to investigate the regulation of ubiquitination in the development of HLF. UbiBrowser (http://ubibrowser.ncpsb.org.cn/ubibrowser/), a target prediction tool was applied to predict the target of selected ubiquitin ligase.

2.3. Quantitative Real-Time PCR (qPCR).
About three cubic metres of ligamentum flavum tissue were homogenized in $800 \mu L$ of Trizol. Total RNA was isolated by Trizol reagent (Invitrogen, USA) according to the manufacturer's instructions, and further reverse transcribed by using the iScript cDNA Synthesis kit (bio-rad). Real-time PCR and analysis were performed as previously described [23]. The fold changes of target genes were analyzed by the 2-ΔΔCt method and 18 s was used as an internal control.

2.4. Western Blotting Analysis.
Western blotting was carried out as previous [23]. In brief, the total protein of tissue from LSS and LDH patients was extracted by using a commercial kit (BC3701, Solarbio, China), The following primary antibodies were used: anti-Collagen III (1 : 500, Abcam, ab6301); anti-Collagen I (1 : 1000, Abcam, ab138492); anti-a-SMA (0.5 μg/ml, Abcam, ab7817); anti-Smurf1 (1 : 1000, Abcam, ab57573); anti-Nrf2 (1 : 1000, Abcam, ab62352); anti-ubiquitin (1 : 1000, Abcam, ab140601); anti-GAPDH (1 : 5000, Abcam, ab9485).

2.5. Immunohistochemistry (IHC).
For IHC, LSS tissue that had been formalin-fixed and paraffin-embedded was divided into 5 m serial slices. IHC was performed as previously. Primary antibodies: anti-Collagen I (1 : 1500, Abcam, ab138492); anti-Collagen III (1 : 200, Abcam, ab6301); anti-a-SMA (0.05 μg/ml, Abcam, ab7817); anti-Smurf1 (1 : 1000, Abcam, ab57573).

2.6. Human LF Cell Isolation.
Ligamentum flavum cells were isolated as described previously [21, 24]. In brief, LF tissue was washed by PBS 3 times, cut into small pieces measuring around $0.5 mm^3$ and digested for one hour with 0.2% type I collagenase (Gibco), The digested fragments were then rinsed in DMEM (Gibco), supplemented with 10% FBS (Glpbio, USA), and 100 U/ml penicillin. Cells after the third passage were used for experiments.

TABLE 1: Patient demographics.

	LDH	HLF	p value
Number of cases	12	15	
Sex (female/male)	3/9	7/8	0.247
Age (years)	35.00 ± 10.18	69.27 ± 4.65	< 0.001
LF thickness (mm)	2.62 ± 0.56	5.37 ± 0.73	< 0.001

LDH: lumbar disc herniation; HLF: hypertrophy of the ligamentum flavum.
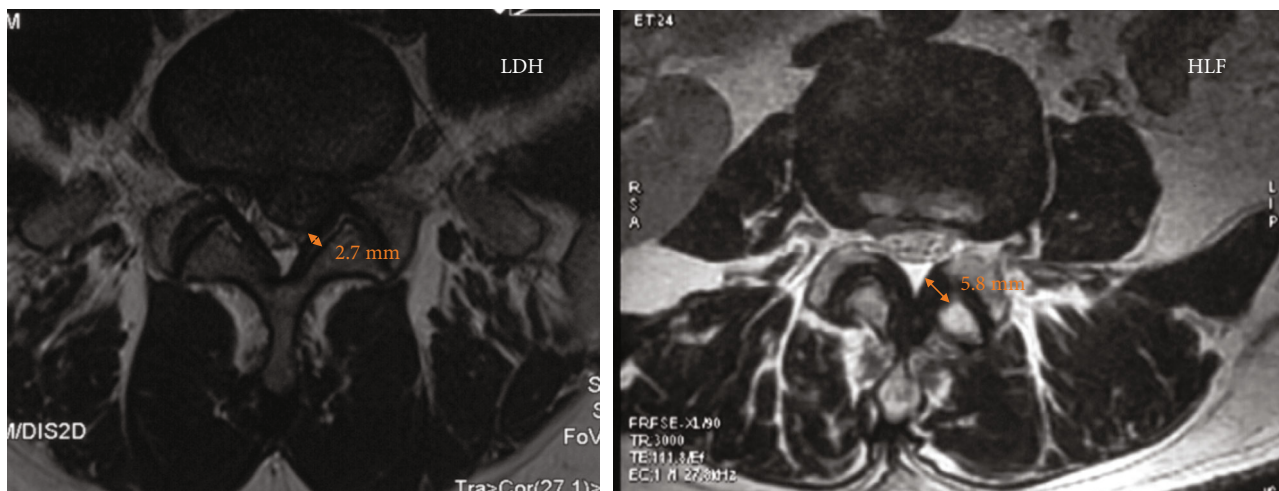
(a)
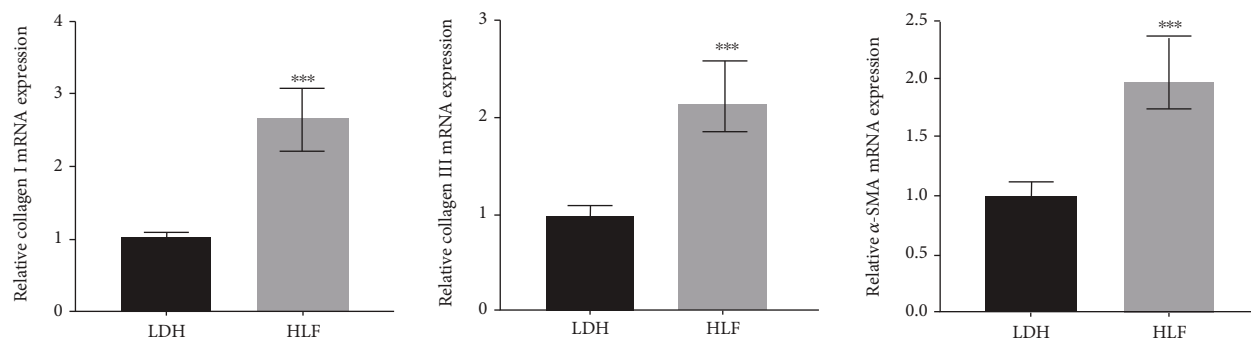
(b)
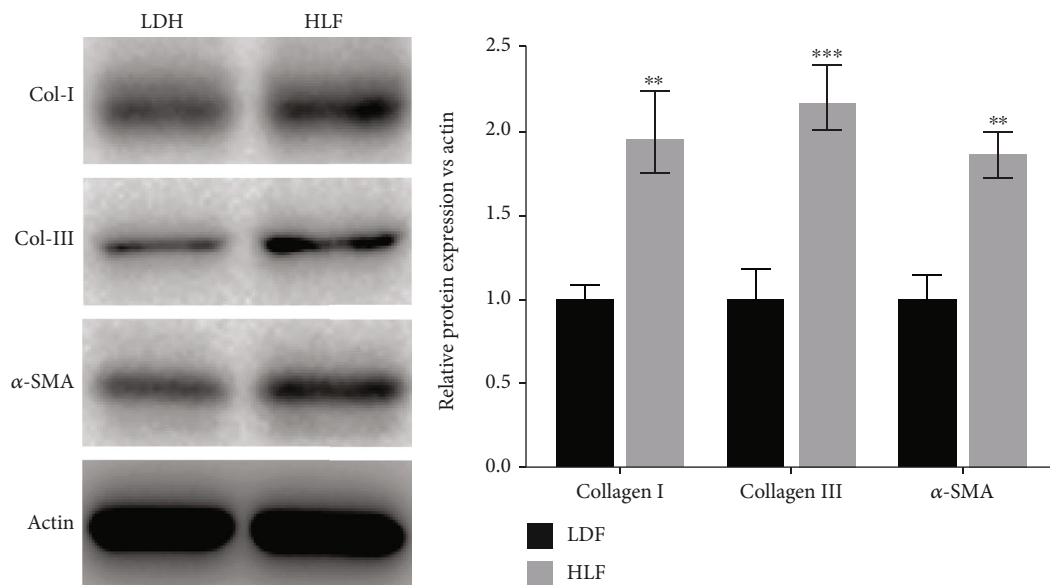
(c)

Figure 1: Continued.

(d)
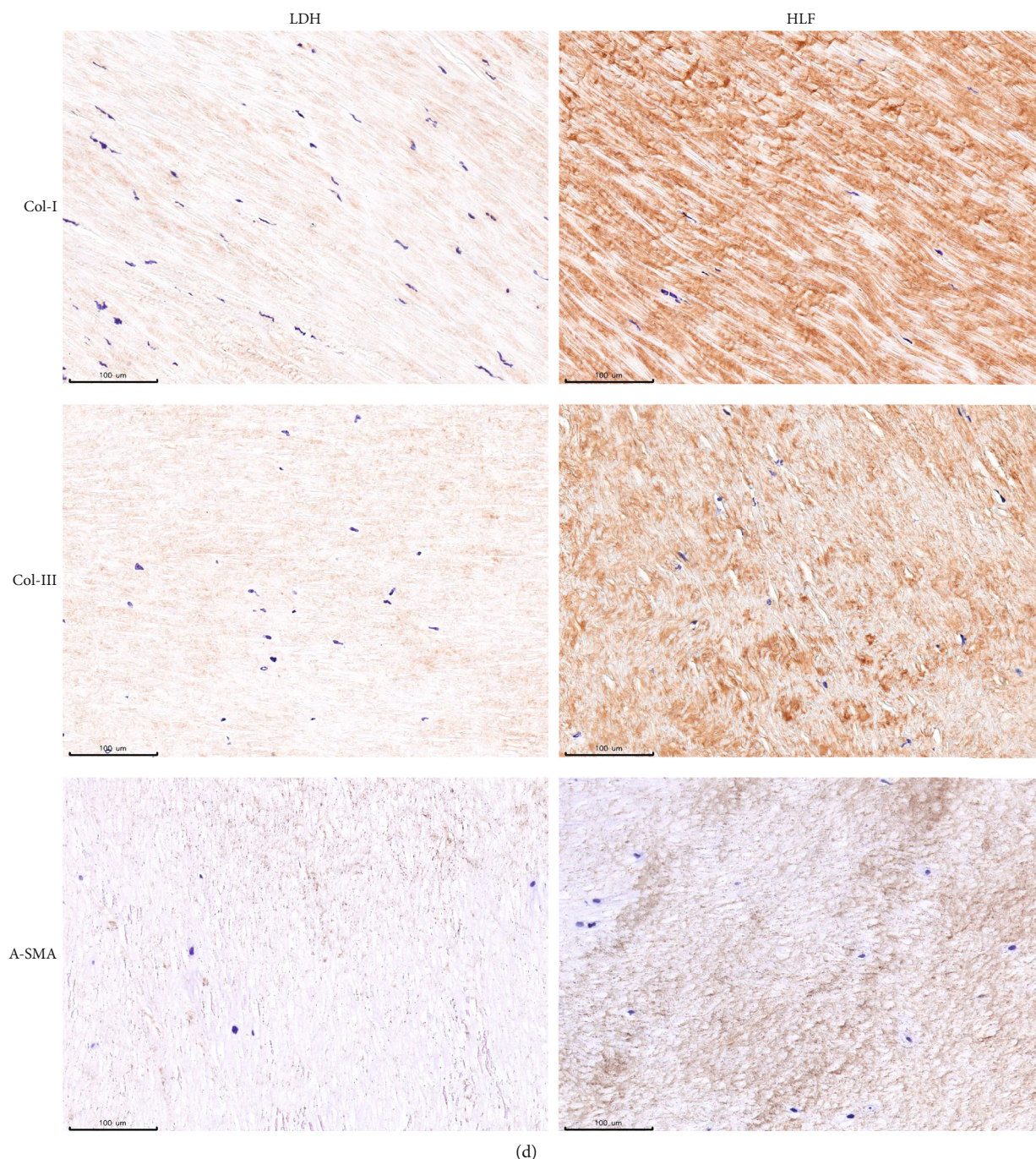
Figure 1: Fibrosis was upregulated in LF tissues from HLF patients. (a) Magnetic resonance imaging (MRI) shows axial views of the lumbar spinal canal in the LDH and HLF patients. (b) Collagen I, Collagen III, and α-SMA mRNA levels in the LDH and HLF patients were assessed by qRT-PCR ($n = 27$). $^{***}p < 0.001$. (c, d) Collagen I, Collagen III, and α-SMA protein expression in the LDH and HLF patients was assessed by western-blot and IHC ($n = 10$). $^{**}p < 0.01$, $^{***}p < 0.001$.

2.7. Reactive Oxygen Species (ROS) Assay. The level of ROS in LF tissue was assessed by a Tissue Reactive Oxygen Species (ROS) Detection Kit (Bestbio China) according to the instructions. The level of ROS in LF cells was assessed by a C11-BODIPY probe assay kit (Invitrogen) according to the instructions. 1×10^4 LF cells were seeded in 96-well plates and cultured for 30 minutes with $2 \mu M$ C11-BODIPY probe, and the amount of ROS was measured using a flow cytometer.

2.8. MDA and GSH Content. The MDA and GSH content in tissue homogenates and cell lysis were analyzed by a lipid peroxidation kit (Sigma, MAK085) and Glutathione Assay Kit (Sigma, CS0260) in accordance with the standard protocol.

2.9. Transfection. To overexpress Smurf1, lentivirus production of Smurf1 was purchased from GeneChem (Shanghai,

(a)

(b)
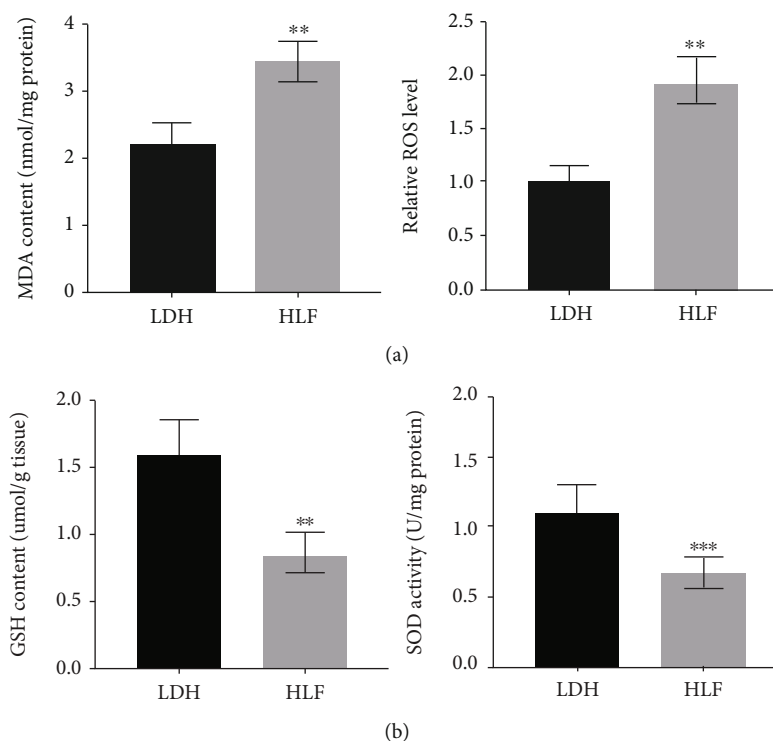
FIGURE 2: Oxidative stress was upregulated in LF tissues from HLF patients. (a) The ROS levels and malondialdehyde (MDA) were higher in the HLF group compared with the LDH group. ($n = 27$). $**p < 0.01$. (b) The glutathione (GSH) content, and superoxide dismutase (SOD) activity were decreased in the HLF group compared with the LDH group ($n = 27$). $**p < 0.01$, $***p < 0.001$.

China) and infected LF cells according to the instructions. After 24 hours of transfection, cells were grown for additional 24 hours after transfection and then extracted for the following experiment.

2.10. Co-Immunoprecipitation (co-IP). After being lysed in NP-40 lysis solution, LF cells lysate were added to the immunoprecipitation complex and rotated overnight at 4°C after being coated with anti-Smurf1 or anti-Nrf2 antibodies for 4 hours. The following day, PBS was used to rinse the Protein A/G beads three times. The immunoprecipitates complex was then examined using anti-Smurf1 or anti-NRF2 antibodies in western blotting.

2.11. Statistical Analysis. Data from every experiment are presented as mean ± SD. The statistical analyses were performed by SPSS 20.0. The student's *t*-test was used to assess the significance between two groups, and more than two groups was determined by one-way ANOVA followed by Tukey-Kramer multiple comparisons test was applied to determine the data for more than two groups. A statistically significant difference was defined as $p < 0.05$.

3. Results

3.1. Fibrosis and Oxidative Stress Were Upregulated in LF Tissues from HLF Patients. To clarify that the HLF is the major cause of LSS, the thickness of ligamentum flavum was assessed via MRI. Figure 1(a) showed that the thickness of LF was markedly increased in HLF patients. Meanwhile,

previous studies have confirmed that the importance of LF fibrosis in the pathological progression of LSS. Thus, the expression of Collagen I, Collagen III, and α-SMA was assessed by qRT-PCR and western blotting in the LF tissues of HLF and LDH. We found that the expression of Collagen I, Collagen III, and α-SMA was markedly increased in the HLF group (Figures 1(b) and 1(c)). Moreover, the result was further confirmed by IHC staining (Figure 1(d)). Given that oxidative stress regulates age-related HLF by promoting fibrosis, oxidative stress markers expression in the HLF group were determined by ELISA. Figures 2(a) and 2(b) showed that the MDA content and ROS level were significantly increased in the HLF group, whereas the GSH content and SOD activity were markedly decreased in the HLF group. These data demonstrated that oxidative stress and ligamentum flavum fibrosis were significantly increased in HLF.

3.2. Smurf1 Was Upregulated in LF Tissues from HLF Patients. To investigate the regulation of ubiquitination in the development of LSS, the top 10 (RNF67, HERC6, RNF218, SMURF1, NEDL2, WWP1, HERC4, SMURF2, RNF218, and RNF58) differentially expressed E3 ubiquitin ligase were obtained from GSE113212, and the expression of these 10 genes was assessed in HLF and LDH patients using qRT-PCR. Figures 3(a) and 3(b) showed that the mRNA level of RNF218 and Smurf1 was markedly increased in HLF patients. Given that the Smurf1 mRNA expression was most upregulated in the HLF group, the Smurf1 protein expression was further confirmed by western blotting and

(a)

(b)

(c)

(d)
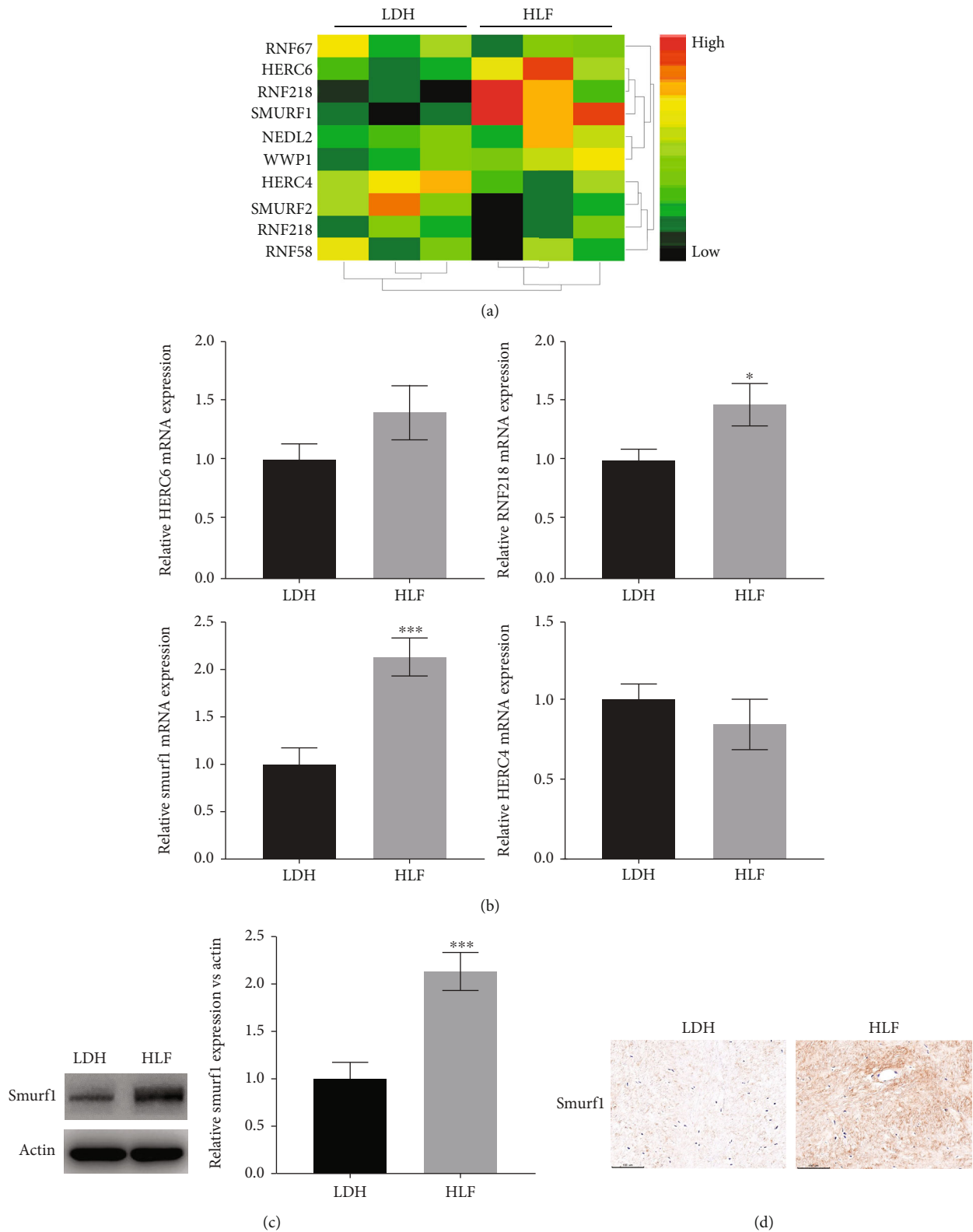
FIGURE 3: Smurf1 was upregulated in LF tissues from HLF patients. (a, b) The mRNA expression of the top ten E3 ligases was assessed by qRT-PCR array in the HLF and LDH group ($n = 27$). $^{*}p < 0.05$. $^{***}p < 0.001$. (c) Western blotting and semiquantification for Smurf1 expression in the HLF and LDH groups ($n = 10$). $^{***}p < 0.001$. (d) Immunohistochemistry for Smurf1 expression in the HLF and LDH groups.

(a)

(b)

(c)

(d)

(e)

FIGURE 4: Continued.

(f)
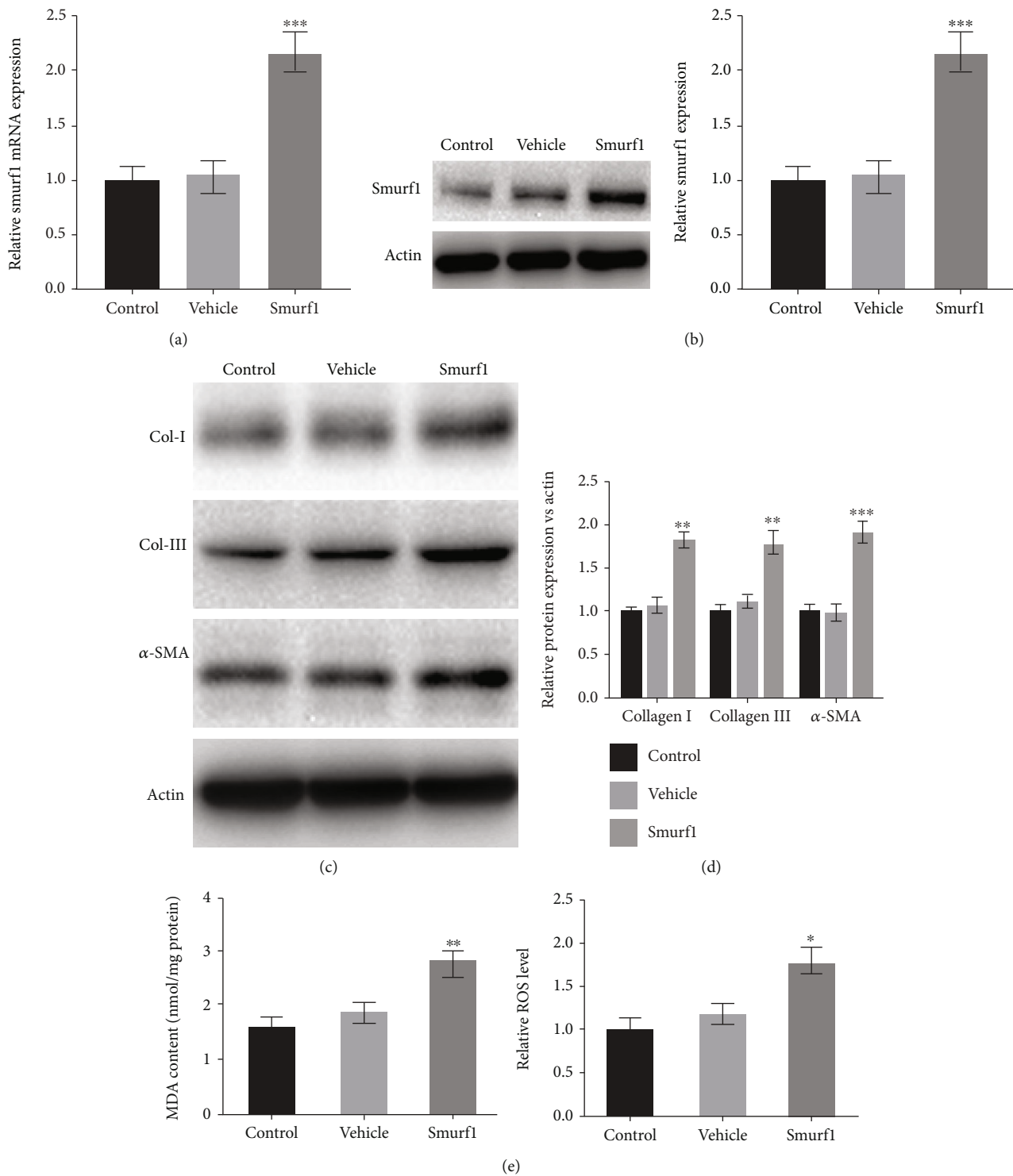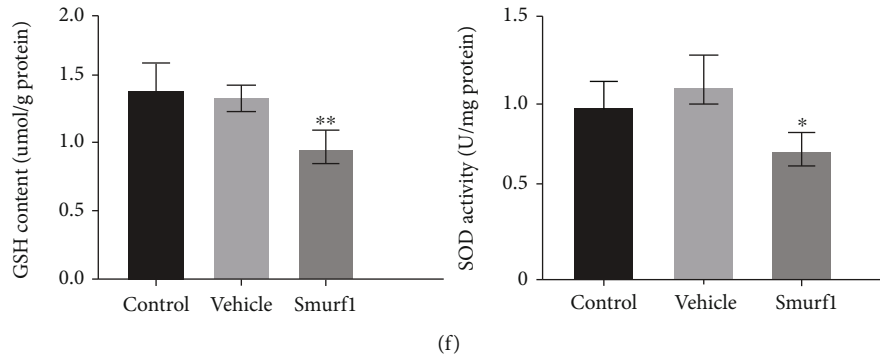
FIGURE 4: Smurf1 facilitated the fibrosis and oxidative stress of LF cells. (a, b) the transfection efficiency of Smurf1 was analyzed by qRT-PCR and western-blot. ***$p < 0.001$. (c, d) Western blotting and semiquantification for Collagen I, Collagen III, and α-SMA mRNA levels in the LF cells with or without Smurf1-OE). **$p < 0.01$. ***$p < 0.001$. (e) The ROS levels and MDA content was assessed in the LF cells with or without Smuf1-OE. *$p < 0.05$. **$p < 0.01$. (f) the Glutathione (GSH) content, and Superoxide dismutase (SOD) activity was assessed in the LF cells with or without Smuf1-OE. *$p < 0.05$. **$p < 0.01$.

(a)

(b)

(c)

(d)
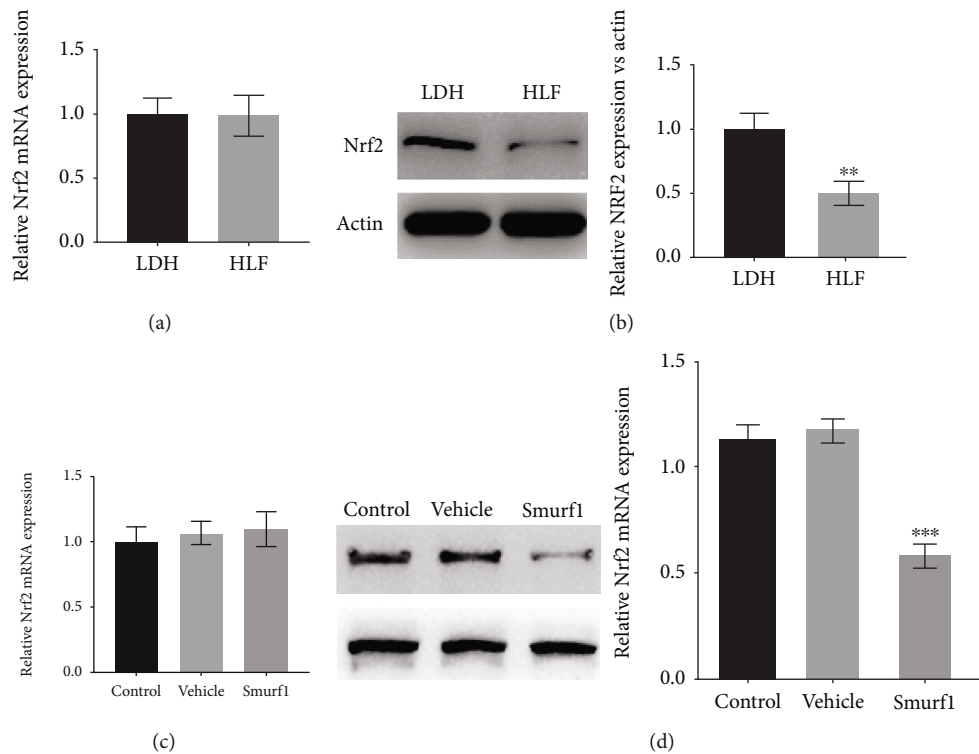
FIGURE 5: Nrf2 is the target of Smurf1. (a) Nrf2 mRNA level in the LDH and HLF patients was assessed by qRT-PCR ($n = 27$). (b) Western blotting and semiquantification for Nrf2 level in the LDH and HLF patients ($n = 10$). **$p < 0.01$. (c) qRT-PCR was used to determine the level of Nrf2 mRNA in LF cells with or without Smuf1-OE. (d) Western blotting and semiquantification for Collagen I, Collagen III, and α-SMA mRNA level in the LF cells with or without Smuf1-OE. ***$p < 0.001$.

IHC. Similar to the qRT-PCR results, western blotting and IHC data showed that the expressions of Smurf1 were significantly increased in HLF patients compared with LDH patients (Figures 3(c) and 3(d)), suggesting that Smurf1 may contribute to the development of HLF.

3.3. Smurf1 Facilitated the Fibrosis and Oxidative Stress of LF Cells. To investigate whether Smurf1 is critical for the fibrosis and oxidative stress of HLF, Smurf1 was forcefully

expressed by pcDNA-Smurf1, and the efficiency was determined by qRT-PCR and western blotting (Figures 4(a) and 4(b)). We next verify the function of Smurf1 on fibrosis and oxidative stress of LF cells. As expected, Collagen I, Collagen III, and α-SMA expression was significantly increased by Smurf1 (Figures 4(c) and 4(d)), suggesting that Smurf1 promoted the fibrosis of LF cells. Similarly, the oxidative stress of LF cells was upregulated by Smurf1 as evidenced by the upregulation of MDA content and ROS level

(a)

(b)

(c)
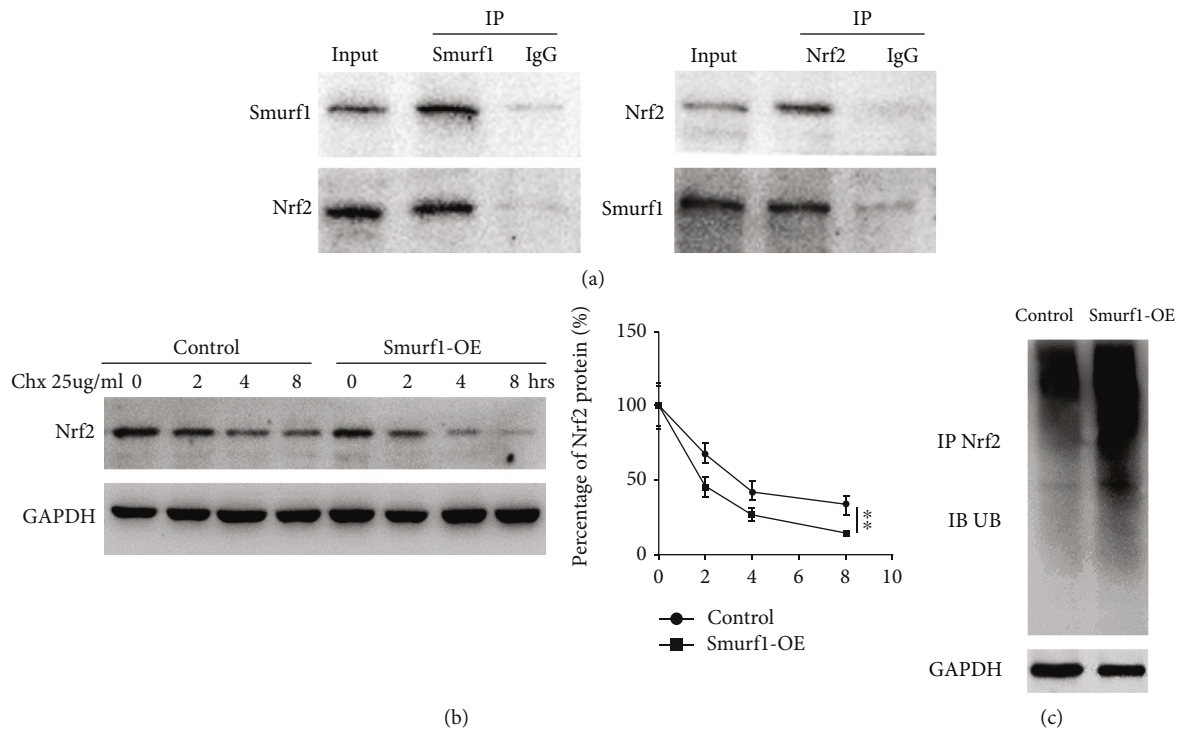
Figure 6: Smurf1 promotes the ubiquitination and degradation of Nrf2. (a) Smurf1 directly interacts with Nrf2 was assessed by CO-IP. (b, c) Western blot analysis of Nrf2 protein stability in Smurf1-OE LF cells treated with 25 ug/ml CHX for various times. $**p < 0.01$. (d) Cell lysates from control and Smurf1-OE LF cells was immunoprecipitated with anti-Nrf2 antibody, then assesed by western blot using antiubiquitin antibody.

(Figure 4(e)) and the downregulation of GSH content and SOD (Figure 4(f)). In conclusion, these data indicated that Smurf1 facilitated the fibrosis and oxidative stress of LF cells.

3.4. Smurf1 Facilitated the Fibrosis and Oxidative Stress of LF Cells by Promoting the Ubiquitination and Degradation of Nrf2. Previous studies found that Smurf1 promotes oxidative stress and fibrosis in the kidney by regulating the polyubiquitination of Nrf2 [25]. Given that Nrf2 is an important transcriptional inhibitor of oxidative stress and fibrosis, we speculated that Smurf1 might facilitate the fibrosis and oxidative stress of LF cells by regulating Nrf2. To this end, UbiBrowser was applied to predict the target of Smurf1 and Nrf2 (gene name: NFE2L2) was found to be a potential target of Smurf1 (Supplementary Figure 1). Next, the expression of Nrf2 was analyzed in LF tissues of HLF and LDH by qRT-PCR and western blotting. As shown in Figures 5(a) and 5(b), there was no significant difference in the mRNA level of Nrf2 between the LDH group and the HLF group, whereas the protein level of Nrf2 was significantly increased in the HLF group compared with the LDH group. Similarly, Smurf1 overexpression had no effect on NRF2 mRNA but decreased NRF2 protein expression (Figures 5(c) and 5(d)), suggesting that Nrf2 expression was regulated by Smurf1-mediated degradation.

A reciprocal co-immunoprecipitation assay was performed to further confirm Nrf2 status as the substrate of Smurf1. As shown in Figure 6(a), positive Nrf2 signal was detected in the protein complex pulled down by the anti-Smurf1 antibody. Similarly, a positive Smurf1 signal was also detected in the protein-complex pulled down by the anti-Nrf2 antibody, suggesting that Nrf2 is the direct target of Smurf1. Furthermore, the protein stability of Nrf2 was verified by the cycloheximide assay (CHX) in LF cells with or without Smurf1 overexpression. Figure 6(b) showed that Nrf2 protein stability was markedly decreased in the Smurf1 overexpression cell. Next, the ubiquitination of Nrf2 was analyzed by CO-IP with an anti-Nrf2 antibody and subsequent immunoblotting with an anti-ubiquitin antibody. Figure 6(c) showed that Smurf1-OE significantly increased the ubiquitination of Nrf2 in LF cells. Taken together, our data suggest that Smurf1 directly interacts with Nrf2 and accelerates its ubiquitination and degradation.

4. Discussion

Lumbar spinal stenosis (LSS) is one of the most common spinal disorders in aging patients, and is characterized by HLF. Previous studies showed that oxidative stress and fibrosis contribute to the progression of HLF [4]. However, the underlying mechanism is unclear. In the current study, we demonstrated that Smurf1 facilitates oxidative stress and fibrosis of ligamentum flavum by promoting Nrf2 ubiquitination and degradation, as evidenced by: (1) fibrosis and oxidative stress were upregulated in LF tissues from HLF patients; (2) Smurf1 was upregulated in LF tissues from HLF patients; (3) Smurf1 facilitated the fibrosis and oxidative stress of LF cells; (4) Smurf1 facilitated the fibrosis and

oxidative stress of LF cells by facilitating the ubiquitination and degradation of Nrf2. Fibrosis have been identified as a key process during the development of HLF [4]. As is known, oxidative stress is an important factor in aging-related diseases and usually contributes to the pathogenesis of many diseases by regulating tissue fibrosis [10]. Mohammed et al. reported that necroptosis-mediated inflammation contributes to the fibrosis of the liver and accelerated aging in a mouse model of increased oxidative stress [26]. Hecker et al. demonstrated that loss of cellular redox homeostasis accelerates profibrotic myofibroblast phenotypes that lead to persistent fibrosis associated with aging [27]. Wang et al. demonstrated that in response to oxidative stress, FBW7 regulates cell senescence and tissue fibrosis through telomere uncapping [13]. Similarly, Chuang et al. found that oxidative stress mediates age-related HLF by promoting fibrosis via activating MAPK and AKT pathways [10]. Consistent with previous studies, we also found that oxidative stress and fibrosis was markedly increased in HLF patients compared with LDH control. However, the regulatory mechanism of oxidative stress and fibrosis dysregulation in HLF is still unclear.

Previous studies suggest that protein ubiquitination is an important regulatory posttranslational modification controlling oxidative stress and fibrosis [28]. In the current study, we provide mechanistic insight that Smurf1 is involved in the development of HLF by regulating oxidative stress and fibrosis through Nrf2 ubiquitination. First, our data showed that Smurf1 was upregulated in HLF patients, and overexpression of Smurf1 promoted the oxidative stress and fibrosis of ligamentum flavum cells. Consistent with our findings, other studies have also clarified that Smurf1 promotes the development of multiple fibrosis-related diseases. Qi et al. reported that miR-129-5p targeted Smurf1 and repressed the ubiquitination of PTEN, thus improving the fibrosis and oxidative stress of cardiac in CHF rats [29]. Chen et al. demonstrated that connexin32 ameliorated kindey fibrosis in diabetic mice by accelerating polyubiquitination and degradation of Nox4 by inhibiting Smurf1 expression [30]. Second, our data showed that Nrf2 is the target of Smurf1, and Smurf1 promoting Nrf2 ubiquitination and degradation. Growing studies indicate that Nrf2 is an important negative regulator of oxidative stress and fibrosis. Mohs et al. demonstrated that the activation of Nrf2 in patients with NASH correlates with the grade of inflammation, and in vivo data suggested that NRF2 activation in chronic liver disease is protective by alleviating fibrogenesis and progression of HCC [31]. Marrone et al. reported that KLF2 upregulation profoundly alleviated fibrosis and oxidative stress of HSC partly via the activation of Nrf2 [32]. In addition, ubiquitination and proteasome-mediated degradation of Nrf2 have been documented. Liu et al. reported that BDH2 accelerated the ubiquitination and degradation of Nrf2 and increased the accumulation of ROS [33]. Chen et al. reported that IKK facilitates the ubiquitination of Nrf2 and further promotes oxidative stress-mediated injury of the kidney in obesity-related nephropathy [34]. Here, we reveal that Smurf1 promotes the ubiquitination and degradation of Nrf2, thus, promoting oxidative stress and fibrosis of LF.

5. Conclusions

In the current study, we clarify the regulatory mechanism of LF fibrosis and oxidative stress and uncovers a specific E3 ubiquitin ligase, Smurf1, in the development of HLF.

Data Availability

The raw data used to support the study's findings is given in the article's figures.

Ethical Approval

All experimental protocols were approved by the Ethics Committee of the Naval Medical University (2016SL-034-01).

Consent

All subjects signed the informed consent.

Conflicts of Interest

The authors declare no competing interests.

Authors' Contributions

Yifei Gu, Jinquan Hu, and Chen Wang contributed equally to the work.

Acknowledgments

Supplementary Materials

Nrf2 (gene name: NFE2L2) was found to be a potential target of Smurf1 using UbiBrowser. (Supplementary Materials)

References

[1] A. Andaloro, "Lumbar spinal stenosis," *JAAPA*, vol. 32, no. 8, pp. 49-50, 2019.

[2] J. Y. Lee, P. G. Whang, J. Y. Lee, F. M. Phillips, and A. A. Patel, "Lumbar spinal stenosis," *Instructional Course Lectures*, vol. 62, pp. 383–396, 2013.

[3] A. M. Lafian and K. D. Torralba, "Lumbar spinal stenosis in older adults," *Rheumatic Diseases Clinics of North America*, vol. 44, no. 3, pp. 501–512, 2018.

[4] C. Sun, H. Zhang, X. Wang, and X. Liu, "Ligamentum flavum fibrosis and hypertrophy: molecular pathways, cellular mechanisms, and future directions," *The FASEB Journal*, vol. 34, no. 8, pp. 9854–9868, 2020.

[5] D. J. Coughlin, G. N. Rymarczuk, and M. S. Dirks, "Noncalcified hypertrophic ligamentum flavum causing severe cervical stenosis and myelopathy: case report and review of the literature," *World Neurosurgery*, vol. 95, article 618.e21, 2016.

[6] H. Takeda, S. Nagai, D. Ikeda, S. Kaneko, T. Tsuji, and N. Fujita, "Collagen profiling of ligamentum flavum in patients with lumbar spinal canal stenosis," *Journal of Orthopaedic Science*, vol. 26, no. 4, pp. 560–565, 2021.

[7] P. Davalli, T. Mitic, A. Caporali, A. Lauriola, and D. D'Arca, "ROS, cell senescence, and novel molecular mechanisms in aging and age-related diseases," *Oxidative Medicine and Cellular Longevity*, vol. 2016, Article ID 3565127, 2016.

[8] D. S. A. Simpson and P. L. Oliver, "ROS generation in microglia: understanding oxidative stress and inflammation in neurodegenerative disease," *Antioxidants (Basel)*, vol. 9, no. 8, p. 743, 2020.

[9] S. C. Yucetas and T. Cakir, "Decreased catalase expression is associated with ligamentum flavum hypertrophy due to lumbar spinal canal stenosis," *Medicine (Baltimore)*, vol. 98, no. 15, article e15192, 2019.

[10] H. C. Chuang, K. L. Tsai, K. J. Tsai et al., "Oxidative stress mediates age-related hypertrophy of ligamentum flavum by inducing inflammation, fibrosis, and apoptosis through activating Akt and MAPK pathways," *Aging (Albany NY)*, vol. 12, no. 23, pp. 24168–24183, 2020.

[11] L. C. Hunt, B. Schadeberg, J. Stover et al., "Antagonistic control of myofiber size and muscle protein quality control by the ubiquitin ligase UBR4 during aging," *Nature Communications*, vol. 12, no. 1, p. 1418, 2021.

[12] D. Kong, Q. Wan, J. Li et al., "DP1 activation reverses age-related hypertension via NEDD4L-mediated T-bet degradation in T cells," *Circulation*, vol. 141, no. 8, pp. 655–666, 2020.

[13] L. Wang, R. Chen, G. Li et al., "FBW7 mediates senescence and pulmonary fibrosis through telomere uncapping," *Cell Metabolism*, vol. 32, no. 5, pp. 860–877, 2020.

[14] L. Rochette, J. Lorin, M. Zeller et al., "Nitric oxide synthase inhibition and oxidative stress in cardiovascular diseases: possible therapeutic targets?," *Pharmacology & Therapeutics*, vol. 140, no. 3, pp. 239–257, 2013.

[15] M. Dodson, R. Castro-Portuguez, and D. D. Zhang, "NRF2 plays a critical role in mitigating lipid peroxidation and ferroptosis," *Redox Biology*, vol. 23, article 101107, 2019.

[16] T. C. Kang, "Nuclear factor-erythroid 2-related factor 2 (Nrf2) and mitochondrial dynamics/mitophagy in neurological diseases," *Antioxidants (Basel)*, vol. 9, no. 7, p. 617, 2020.

[17] R. Vashi and B. M. Patel, "NRF2 in cardiovascular diseases: a ray of hope!," *Journal of Cardiovascular Translational Research*, vol. 14, no. 3, pp. 573–586, 2021.

[18] Q. Liu, Y. Gao, and X. Ci, "Role of Nrf2 and its activators in respiratory diseases," *Oxidative Medicine and Cellular Longevity*, vol. 2019, Article ID 7090534, 2019.

[19] K. Smolkova, E. Miko, T. Kovacs, A. Leguina-Ruzzi, A. Sipos, and P. Bai, "Nuclear factor erythroid 2-related factor 2 in regulating cancer metabolism," *Antioxidants & Redox Signaling*, vol. 33, no. 13, pp. 966–997, 2020.

[20] C. Yu and J. H. Xiao, "The Keap1-Nrf2 system: a mediator between oxidative stress and aging," *Oxidative Medicine and Cellular Longevity*, vol. 2021, Article ID 6635460, 2021.

[21] Z. Zheng, X. Ao, P. Li et al., "CRLF1 is a key regulator in the ligamentum flavum hypertrophy," *Frontiers in Cell and Developmental Biology*, vol. 8, p. 858, 2020.

[22] Y. Cao, Y. Zhan, S. Qiu et al., "Integrative analysis of genome-wide DNA methylation and single-nucleotide polymorphism identified ACSM5 as a suppressor of lumbar ligamentum flavum hypertrophy," *Arthritis Research & Therapy*, vol. 23, no. 1, p. 251, 2021.

[23] C. Xu, Y. Zhang, Q. Wang et al., "Long non-coding RNA GAS5 controls human embryonic stem cell self-renewal by maintaining NODAL signalling," *Nature Communications*, vol. 7, no. 1, article 13287, 2016.

[24] N. Specchia, A. Pagnotta, A. Gigante, G. Logroscino, and A. Toesca, "Characterization of cultured human ligamentum flavum cells in lumbar spine stenosis," *Journal of Orthopaedic Research*, vol. 19, no. 2, pp. 294–300, 2001.

[25] W. Gong, Z. Chen, Y. Zou et al., "CKIP-1 affects the polyubiquitination of Nrf2 and Keap1 via mediating Smurf1 to resist HG-induced renal fibrosis in GMCs and diabetic mice kidneys," *Free Radical Biology & Medicine*, vol. 115, pp. 338–350, 2018.

[26] S. Mohammed, E. H. Nicklas, N. Thadathil et al., "Role of necroptosis in chronic hepatic inflammation and fibrosis in a mouse model of increased oxidative stress," *Free Radical Biology & Medicine*, vol. 164, pp. 315–328, 2021.

[27] L. Hecker, N. J. Logsdon, D. Kurundkar et al., "Reversal of persistent fibrosis in aging by targeting Nox4-Nrf2 redox imbalance," *Science Translational Medicine*, vol. 6, no. 231, article 231ra247, 2014.

[28] D. Kong, Z. Zhang, L. Chen et al., "Curcumin blunts epithelial-mesenchymal transition of hepatocytes to alleviate hepatic fibrosis through regulating oxidative stress and autophagy," *Redox Biology*, vol. 36, article 101600, 2020.

[29] Y. Qi, Y. Tang, L. Yin et al., "miR-129-5p restores cardiac function in rats with chronic heart failure by targeting the E3 ubiquitin ligase Smurf1 and promoting PTEN expression," *Bioengineered*, vol. 13, no. 2, pp. 2371–2386, 2022.

[30] Z. Chen, X. Sun, Q. Chen et al., "Connexin32 ameliorates renal fibrosis in diabetic mice by promoting K48-linked NADPH oxidase 4 polyubiquitination and degradation," *British Journal of Pharmacology*, vol. 177, no. 1, pp. 145–160, 2020.

[31] A. Mohs, T. Otto, K. M. Schneider et al., "Hepatocyte-specific NRF2 activation controls fibrogenesis and carcinogenesis in steatohepatitis," *Journal of Hepatology*, vol. 74, no. 3, pp. 638–648, 2021.

[32] G. Marrone, R. Maeso-Diaz, G. Garcia-Cardena et al., "KLF2 exerts antifibrotic and vasoprotective effects in cirrhotic rat livers: behind the molecular mechanisms of statins," *Gut*, vol. 64, no. 9, pp. 1434–1443, 2015.

[33] J. Z. Liu, Y. L. Hu, Y. Feng et al., "BDH2 triggers ROS-induced cell death and autophagy by promoting Nrf2 ubiquitination in gastric cancer," *Journal of Experimental & Clinical Cancer Research*, vol. 39, no. 1, p. 123, 2020.

[34] Y. Y. Chen, H. Hong, Y. T. Lei, J. Zou, Y. Y. Yang, and L. Y. He, "IκB kinase promotes Nrf2 ubiquitination and degradation by phosphorylating cylindromatosis, aggravating oxidative stress injury in obesity-related nephropathy," *Molecular Medicine*, vol. 27, no. 1, p. 137, 2021.

Hindawi

Research Article

circRNA_17725 Promotes Macrophage Polarization towards M2 by Targeting FAM46C to Alleviate Arthritis

Chunjuan Yang,[1] **Biao Ni,**[2] **Chaoran Li,**[1] **Wenchang Sun,**[2] **Zhangxue Wang,**[1] **Hui Wang,**[2] **Xinyue Hou,**[2] **Shushan Yan** (ID),[3] **Xiaodong Wang** (ID),[4] **and Donghua Xu** (ID)[1,2]

[1]*Department of Rheumatology of the First Affiliated Hospital & the First Clinical College, Weifang Medical University, Weifang 261000, China*
[2]*Central Laboratory of the First Affiliated Hospital & the First Clinical College, Weifang Medical University, Weifang 261000, China*
[3]*Department of Gastrointestinal and Anal Diseases Surgery of the Affiliated Hospital, Weifang Medical University, Weifang 261000, China*
[4]*Department of Rheumatology of the Affiliated Hospital, Weifang Medical University, Weifang 261000, China*

Correspondence should be addressed to Shushan Yan; fyyanss@wfmc.edu.cn, Xiaodong Wang; wxdongdoctor@163.com, and Donghua Xu; flower322@163.com

Accumulating studies have implicated that circular RNAs (circRNAs) play vital roles in the pathogenesis of rheumatoid arthritis (RA). Dysregulation of macrophage polarization leads to immune homeostatic imbalance in RA. However, the altering effects and mechanisms of circRNAs on macrophages polarization and immune homeostatic balance remain largely unclear. We aimed to investigate the potential role of circRNA_17725 in RA. The high-throughput sequence was performed to identify the dysregulated circRNAs in RA. We confirmed the data by CCK-8, EdU, and Annexin V/PI staining to elucidate the proliferation and apoptosis. The expressions of M1/M2-associated markers were confirmed using real-time PCR and flow cytometry analysis. Luciferase reporter assay and RNA Binding Protein Immunoprecipitation (RIP) were used to demonstrate the underlying mechanism of circRNA_17725. The altering effect of circRNA_17725 on macrophages in vivo was evaluated using collagen-induced arthritis (CIA) mouse model. circRNA_17725 was demonstrated to be downregulated in peripheral blood mononuclear cells and CD14$^+$ monocytes from RA cases in contrast to healthy controls. The negative association between circRNA_17725 and the disease activity indexes (CRP, ESR, and DAS28) was observed, suggesting a vital role of circRNA_17725 in RA disease activity. Besides, after a coexpression analysis based on high-input sequencing and the bioinformatics analysis in MiRanda and TargetScan databases, a circRNA_17725-miR-4668-5p-FAM46C competing endogenous RNA (ceRNA) network was hypothesized. A series of cytology experiments *in vitro* have implicated that circRNA_17725 could inhibit the proliferation but enhance the apoptosis of macrophages. Decreased expression of TNF-α, IL-1β, and MMP-9 were observed in the supernatant of circRNA_17725-overexpressed Raw264.7 macrophages, implicating the inhibitory effect of circRNA_17725 on macrophage inflammatory mediators. Furthermore, circRNA_17725 could promote macrophage polarization towards M2 by targeting miR-4668-5p/FAM46C as a miRNA sponge. Additionally, circRNA_17725-overexpressed macrophages alleviated arthritis and protected against joint injuries and bone destruction by inducing macrophage polarization towards M2 in collagen-induced arthritis (CIA) mice. This study has suggested that circRNA_17725 regulated macrophage proliferation, apoptosis, inflammation, and polarization by sponging miR-4668-5p and upregulating FAM46C in RA.

1. Introduction

Rheumatoid arthritis (RA) is a common and chronic autoimmune disease. It can cause synovial hyperplasia, inflammation, cartilage injury, bone damage, and even disability [1]. The pathogenesis of RA is complex with dysregulated mononuclear macrophages, T cells, and B cells. It has been well-documented imbalance of M1/M2 macrophage, Th17/Treg, and other

immune cells leads to immune homeostatic imbalance. M1 macrophage is associated with enhanced inflammation and immune activation in specific tissues and organs in RA. It has been demonstrated that genetics, sex hormones, and infectious factors are closely related to RA [2]. Chronic inflammation affects the onset and progression of RA. In spite of great advance in RA diagnosis and treatment, illustrating the molecular mechanism underlying RA pathogenesis is essential for identifying more valuable therapeutic targets for RA. Exploring more effective immunotherapy based on immune cells and potential biological targets has always been the research focus in RA.

During the past few years, the role of noncoding RNAs (ncRNAs) in autoimmune diseases has been drawing more and more attention, primarily including circular RNA (circRNA), long chain noncoding RNAs (lncRNA), and microRNAs (miRNA) [3]. These ncRNAs play critical roles in maintaining the stability and normal expression of genes. Furthermore, ncRNAs regulate inflammation and autoimmunity through protein-RNA or RNA-RNA interactions. As a key type of ncRNA, circRNAs have been suggested to contribute to RA by a number of studies [4, 5]. Some studies have implicated that some circRNAs are specifically expressed in RA, such as circ_0008360, circ_0140271, and circ_0003972 [6–8], which are primarily involved in regulating inflammation and autoimmune disorders. circRNA is a new competitive endogenous RNA (ceRNA) with high stability. They are critical regulators in the immune system, and are specifically expressed in specific organs, tissues, or cells. Accumulating evidence has highlighted the crucial potentials of circRNAs as diagnostic and therapeutic markers in multiple autoimmune diseases, including systemic lupus erythematosus (SLE), multiple sclerosis (MS), and RA [9–11]. Nevertheless, little is known of the effects and mechanism of circRNAs in regulating immune cell polarization and immune homeostatic imbalance. As described previously [12], we have demonstrated several circRNAs are aberrantly expressed in RA, including circRNA_09505 and circRNA_17725. circRNA_09505 has been suggested to enhance inflammation injuries and bone damages in collagen-induced arthritis (CIA) mice by sponging miR-6089 as a ceRNA through the AKT1/NF-κB signaling pathway [12]. circRNA_17725 was significantly downregulated in RA with unclear regulatory effects and molecular mechanisms. Here, we focus on the altering effects of circRNA_17725 in RA pathogenesis and progression, particularly highlighting its potential use in RA as a key biomarker.

2. Materials and Methods

2.1. Sample Preparation and Cell Culture. The study regarding human subjects had been approved by the Institutional Ethics Committee of the First Affiliated Hospital, Weifang Medical University (2021YX076). Peripheral blood mononuclear cells (PBMCs) were isolated by use of Ficoll-Paque gradient centrifugation from 35 RA cases and 28 healthy controls adjusted by age and sex. They had all agreed with the written informed consent. Raw264.7 cells were incubated in DMEM adding with 10% fetal bovine serum (Sigma-Aldrich, USA) under 37°C and 5% CO_2. Cells were transfected by miRNA mimics and mimics

controls (Ruibo Biosciences, Guangzhou, China). Lentivirus plasmids overexpressing circRNA_17725 and plasmids of FAM46C-WT (wild-type) and FAM46C-MT (mutant) were constructed by OBiO Technology Corp., Ltd. (Shanghai, China). Raw264.7 macrophages were transfected by these plasmids and used for experiments. The luciferase activity in macrophages was estimated by the luminescence kit (Toyo Ink, Japan) according to the protocol as reported previously [12].

2.2. High-Throughput Sequencing Analysis. As described previously, we performed the high-throughput sequence to identify the dysregulated circRNAs in RA based on the platform of Oebiotech Company (Shanghai, China) [12]. The correlation coefficient was analyzed according to the complementary base pairs of circRNA_17725/mRNAs with shared miRNAs and the coexpression of circRNA_17725/mRNAs/miRNAs in RA PBMCs. circRNA was determined to have a positive coexpression correlation with mRNA, when the P value was less than 0.05 and the absolute value of Pearson's correlation coefficient was more than 0.7. Pairs of circRNAs-miRNAs-mRNAs were screened according to the principles of sharing miRNAs $\geq$ 3, Pearson's correlation index $\geq$ 0.7, and $P < 0.05$.

2.3. Cell Proliferation and Apoptosis. Briefly, Raw264.7 macrophages (2×10^5/well) were seeded into cell plate in fetal bovine serum-free DMEM overnight. Subsequently, the proliferation of macrophages at 24, 48, and 72 hours was estimated using CCK-8 kit (Vazyme Biotech, Nanjing, China). Besides, we used the 5-ethynyl-2′-deoxyuridine (EdU) kit to evaluate the proliferation of cells at 48 h according to the protocol of the reagent kit (RiboBio, Guangzhou, China). In addition, cells were pretreated with H_2O_2 (100 mmol/L) for 4 hours. Flow cytometry was carried out to estimate the impact of circRNA_17725 on the apoptosis of macrophage.

2.4. Real-Time Polymerase Chain Reaction (PCR). PBMCs from another 40 RA cases and 30 controls enrolled in hospital for health examination were purified by CD14$^+$ magnetic bead sorting (Miltenyi Biotec, San Diego, USA) after isolating by the Ficoll-Paque gradient centrifugation. The expression of circRNA_17725 in CD14$^+$ monocytes was also determined by real-time PCR. The association between circRNA_17725 and IL-10 and FAM46C and TNF-α was estimated. We applied TRIzol (Invitrogen, CA, USA) to isolate total RNAs, which were used for the synthesis of cDNA as template (0.5 μg) by use of RT kit (Vazyme, Nanjing China). cDNAs (5 ng) were used as templates for PCR using SYBR Green Mastermix kit (Vazyme, Nanjing China). The Novabio SYBR qPCR Mix kit (Novabio, Shanghai, China) was used to amplify circRNA. TaqMan miRNA PCR kit (ThermoFisher Scientific, USA) was applied for miRNA determination. Primers were as follows: circRNA_17725-f, AGGGAGAAAGCTTGATATGAGTTTG3, circRNA_17725-r, AGAAGTAATAAAGCCAGCAGGTACG3; human CD206-f, GGGTTGCTATCACTCTCTATGC, human CD206-r, TTTCTTGTCTGTTGCCGTAGTT; human IL-10-f, GACTTTAAGGGTTACCTGGGTTG, human IL-10-r, TCACATGCGCCTTGATGTCTG; human TNF-α-f, CCTCTCTCTAATCAGCCCTCTG, human

TNF-α-r, GAGGACCTGGGAGTAGATGAG; human GAPDH-f, GGAGCGAGATCCCTCCAAAAT, human GAPDH-r, GGCTGTTGTCATACTTCTCATGG; human FAM46C-f, GGCCACGTTTTGGTCAAAGAC, human FAM46C-r, GGGAACACAGAACCACATCTC; mouse FAM46C-f, AACTGGGATCAGGTTAGCCG, mouse FAM46C-r, CAACCCAAGCCGTTGTCTT; mouse CD11c-f, CTGGATAGCCTTTCTTCTGCTG, mouse CD11c-r, GCACACTGTGTCCGAACTCA; mouse CD163-f,GGTG GACACAGAATGGTTCTTC, mouse CD163-r, CCAGGA GCGTTAGTGACAGC; and mouse GAPDH-f, AGGTCG GTGTGAACGGATTTG, mouse GAPDH-r, TGTAGACCA TGTAGTTGAGGTCA.

2.5. Flow Cytometry Analysis.

Flow cytometry was carried out to determine the genotypes in Raw264.7 cells and mice spleen cells. 2×10^5 cells were resuspended in $100 \mu L$ PBS incubating with $5 \mu L$/anti-mouse CD14, HLA-DR, CD68, CD206, CD11c, and CD163 fluorescent-labeled antibodies (BioLegend, USA) for 30 min at room temperature. After washing twice using $300 \mu L$ PBS, cells were determined by flow cytometry. For apoptotic analysis, cells were stimulated by H_2O_2 ($100 \mu mol/L$) for 4 h and harvested by centrifugation. Then, cells were resuspended in $1 \times$ Binding Buffer plus apoptosis detection reagents ($5 \mu L$/tube) according to the protocol of Annexin V/PI Apoptosis Assay kit (Multisciences Biotech., Hangzhou, China). After incubation for 15 min at room temperature, the apoptosis status of cells was estimated by flow cytometry.

2.6. Enzyme-Linked Immunosorbent Assay (ELISA).

2×10^5/well Raw264.7 macrophage was seeded into 96-cell plate in serum-free DMEM at 37°C, 5% CO_2. Cells were stimulated by LPS ($1 \mu g/mL$) for 48 h. Cytokines in the cultural supernatant were detected by use of mouse TNF-α, IL-10, IL-1β (R&D Systems, USA), and MMP-9 (abcam, USA) ELISA kits according to the protocols, as decried previously [12]. In addition, TNF-α and IL-1β in the plasm samples from mice were also determined.

2.7. RNA Fluorescence In Situ Hybridization (FISH).

5×10^5/well Raw264.7 cells were seeded into plastic dish (35 mm, Thermo Scientific Nunc, USA) overnight adding with DMEM without fetal bovine serum. Subsequently, Raw264.7 cells were fixed with paraformaldehyde (4%) and dehydrated using ethanol. We carried out FISH to estimate the location of circRNA_17725 in Raw264.7 cells, which were labeled by fluorescent probe for circRNA_17725 during the process of hybridization.

2.8. Luciferase Reporter Assay.

5×10^5/well 293T cells seeded into cell culture plate, which were incubated until the cell confluence up to 70-80%. Then, cells were transfected by miRNA mimics, or mimics controls, or luciferase reporter plasmids of FAM46C-WT and FAM46C-MT by use of the lipofectamine 2000. At last, 293T cells were lysed. We applied the Picagene Dual SeaPansy luminescence kit (Toyo Ink, Japan) to detect the luciferase activity in cells according to the protocol.

2.9. RNA Binding Protein Immunoprecipitation (RIP).

RIP was performed to estimate the association between circRNA_17725 and miR-4668-5p. Briefly, $5 \sim 10 \times 10^6$ macrophages were lysed. Lysates were collected by centrifugation, followed by probe incubation based on the instructions of RIP Kit (Millipore, Bedford, USA). Ago2 and IgG were used for immunoprecipitation with cell lysates. Real-time PCR was conducted to determine the expression of circRNA_17725 and miR-4668-5p.

2.10. Collagen-Induced Arthritis (CIA) Mouse Model Construction and Estimation.

Animal experiments were conducted according to the guidelines of Institutional Animal Care and Use Committee of Weifang Medical University (2021SDL311). We used bovine type II collagen (4 mg/mL, Chondrex, Washington, USA) and the Freund's complete adjuvant (Sigma-Aldrich, USA) to construct CIA mice model by tail vein injection at the ratio of 1:1. There were 6 mice in each group. Mice were intravenously injected with Raw264.7 cells (10^6 cells in $200 \mu L$ PBS) on day 5 and day 15. Booster immunity was conducted by use of $100 \mu L$ emulsion solution on day 21. After estimating for 60 days from the first immunization, all mice were executed for determination. We carried out Hematoxylin-Eosin (H&E) and Safranin O/Solid green staining to estimate the status of mouse joints and tissues.

2.11. Statistical Analysis.

All data was analyzed by SPSS (v20.0) software and GraphPad Prism (v8.0) software. The data were analyzed by parametric or nonparametric tests according the homoscedasticity estimation and the adherence to the normal curve. The parametric tests were performed using one-way ANOVA or independent sample Student's T test. The nonparametric tests were conducted using Mann–Whitney U test or Kruskal-Wallis H test according to subgroups. Pearson's correlation analysis estimated the correlation between circRNA_17725 expression and clinical indexes of CRP, ESR, and DAS28. $P < 0.05$ was statistically significant.

3. Results

3.1. Expression of circRNA_17725 in the Peripheral Blood Mononuclear Cells and Its Association with Clinical Indexes.

In a previous study, we found that circRNA_17725 was significantly reduced in RA as implicated by gene sequencing analysis and real-time PCR [12]. In this study, circRNA_17725 was further demonstrated to be significantly decreased in RA patients' PBMCs (Figure 1(a)). Besides, the expression of circRNA_17725 was negatively associated with the disease activity indexes including CRP, ESR and DAS28 (Figures 1(b)–1(d)). Taken together, circRNA_17725 may play a critical role in the pathogenesis or disease progression of RA.

3.2. Potential Target Prediction of circRNA_17725 in Macrophage.

The bioinformatics analysis was conducted to evaluate the potential targets of circRNA_17725. Based on the expression value analysis of high-throughput sequencing, a positive coexpression relationship between circRNA_17725 and FAM46C was observed (Figure 2(a)), which was

(a)

(b)

(c)

(d)
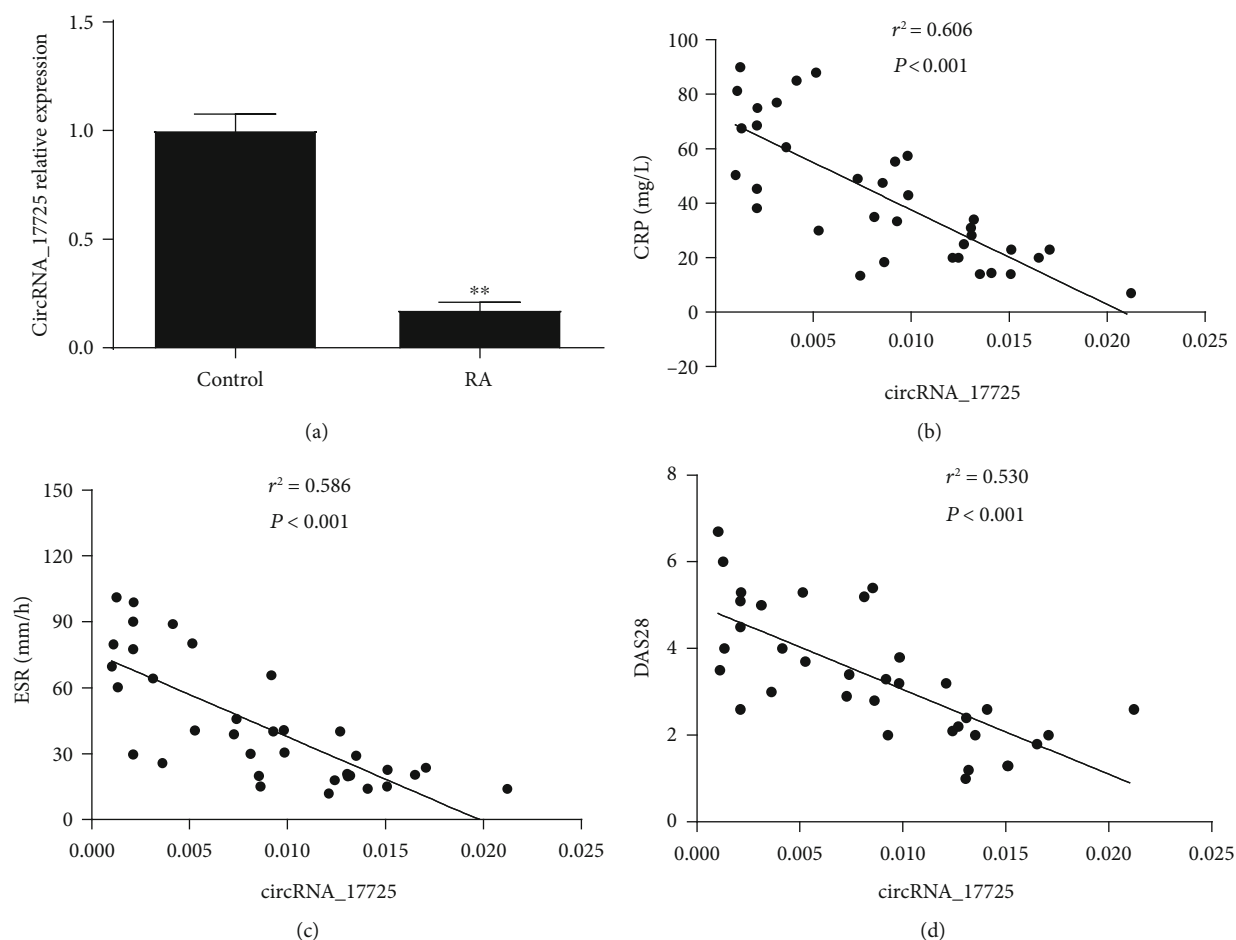
FIGURE 1: Expression of circRNA_17725 in the PBMCs and its association with the disease activity indexes of RA. (a) Expression of circRNA_17725 in the PBMCs from RA patients ($^{**}P < 0.01$; RA/control: 35/28). (b) Pearson's correlation analysis: relationship of circRNA_17725 with CRP ($n = 35$). (c) Pearson's correlation analysis: relationship of circRNA_17725 with ESR ($n = 35$). (d) Pearson's correlation analysis: relationship of circRNA_17725 with DAS28 ($n = 35$).

a macrophage polarization-associated molecule. However, whether circRNA_17725 directly binds to FAM46C needs further demonstration. Competing endogenous RNA (ceRNA) is the main mechanism for circRNA to exert biological effects. We subsequently found that circRNA_17725 and miR-4668-5p possessed 16 complementary base pairs with miR-4668-5p after scanning in MiRanda and TargetScan databases (Figure 2(b)). Moreover, miR-4668-5p was predicted to recognize the 3' untranslated region (UTR) of FAM46C scanned in TargetScan database (Figure 2(b)). Accordingly, we hypothesize that circRNA_17725 may serve as a ceRNA molecule competitively antagonizing miR-4668-5p and targeting macrophage polarization-related molecule, namely, FAM46C (Figure 2(c)). Whether the circRNA_17725/miR-4668-5p/FAM46C contributes to macrophage polarization and immune balance in RA warrants to be explored in subsequent experiments.

3.3. Positive Association between circRNA_17725 and FAM46C. FAM46C is a M2 macrophage polarization-related molecule. In this study, mRNAs of circRNA_17725 and FAM46C were both

significantly reduced in CD14$^+$ monocytes of RA patients compared with those in controls (Figures 3(a) and 3(b)). FAM46C was positively associated with circRNA_17725 demonstrated by Pearson's correlation analysis (Figure 3(c)). Moreover, the expression of circRNA_17725 was positively related to IL-10 and CD206, but negatively associated with TNF-α regarding their expression at mRNA levels (Figures 3(d)–3(f)). As mentioned before, IL-10, CD206, and FAM46C are typical markers for M2 cells, while TNF-α is a M1 maker. M2 macrophage can inhibit inflammation and exert immunoregulatory effects in maintaining homeostasis. Accordingly, we hypothesize that circRNA_17725 may contribute to M2 polarization by targeting FAM46C.

3.4. circRNA_17725 Location and Its Regulatory Effects on Macrophage Proliferation, Apoptosis, and Inflammation. Here, we have performed a series of experiments to elucidate the role and mechanism of circRNA_17725 on macrophage growth and functions. circRNA_17725 was overexpressed in Raw264.7 macrophages by use of lentivirus plasmids (Figure 4(a)). The test of FISH has suggested circRNA_17725
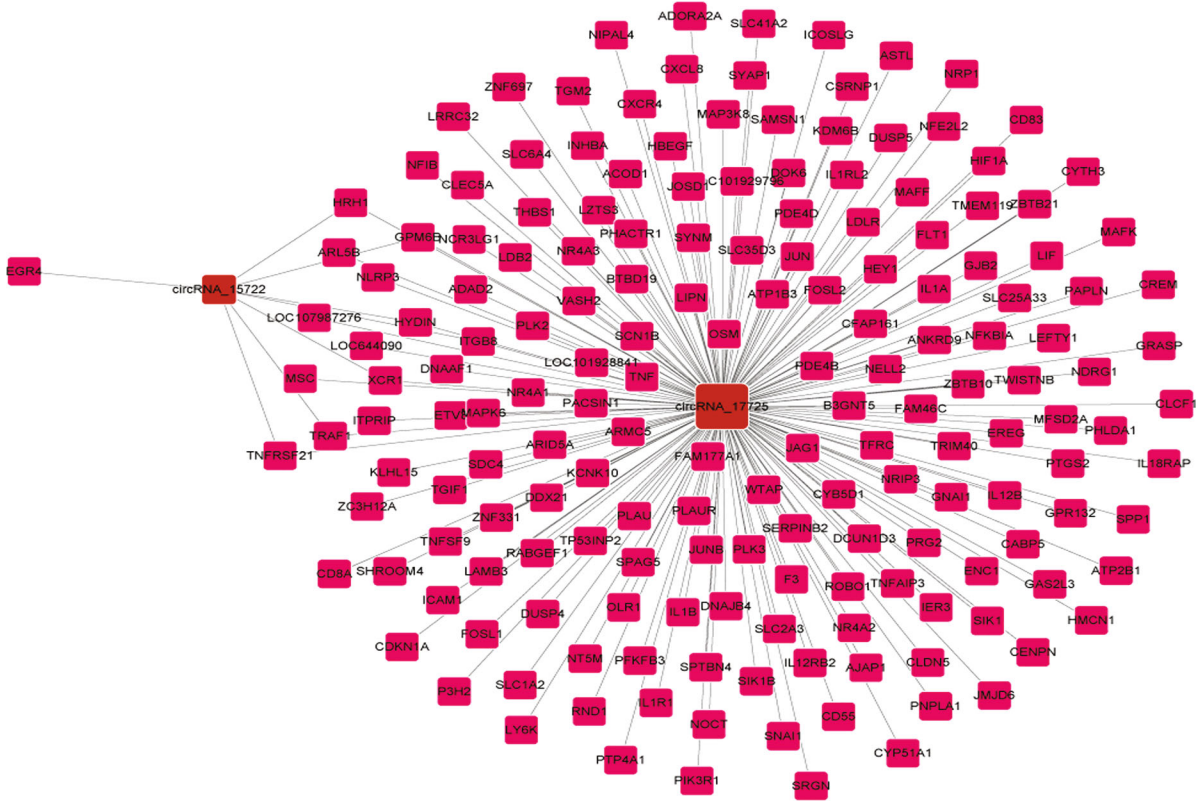
(a)

hsa-miR-4668-5p 3' cuGUUUAGGA-----AAAAAAAAAGGGa 5'
| | | | : : | | | | | | | | | | | |
circRNA_17725 5' gtCAAAGTTTGAGTTTGT TT TTCCCt 3'

hsa-miR-4668-5p 3' CUGUUUAGGAAAAAAAAAAAGGGA 5'
| | | | | | | | | | | | | |
FAM46C 3'UTR 5' UGCUUUUUUUUUUUUUUUUUCUCC 3'
(Position 127-138)

(b)

Figure 2: Continued.

(c)
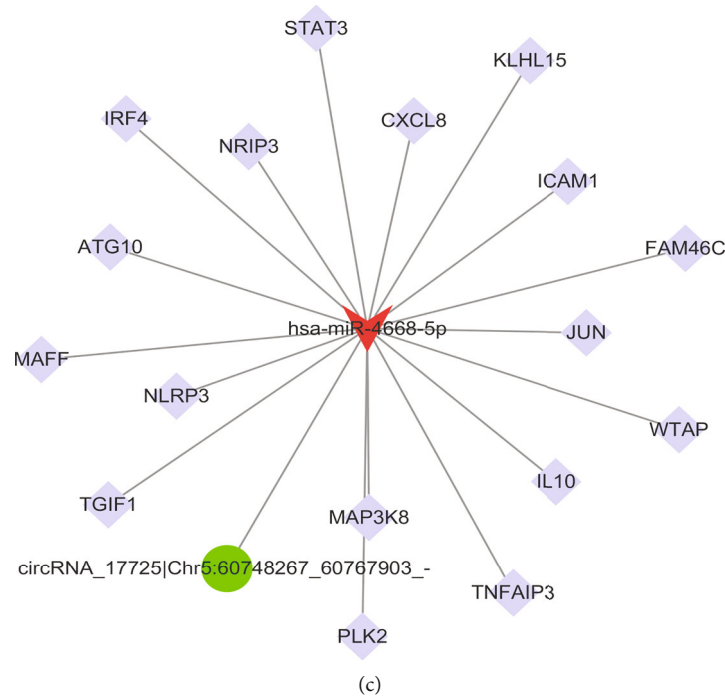
FIGURE 2: Potential targets prediction of circRNA_17725. (a) Positive coexpression association between circRNA_17725 and FAM46C and other factors implicated by high-throughput sequencing and bioinformatics analysis. (b) Complementary base pairs of circRNA_17725 and miR-4668-5p, plus miR-4668-5p, and FAM46C. (c) A predicted circRNA_17725/miR-4668-5p/FAM46C ceRNA network (the red shape represents miR-4668-5p, the purple squares represent targeted mRNAs including FAM46C, and the green circle represents circRNA_17725).

was primarily located in macrophage cytoplasm (Figure 4(b)). The apoptosis of Lv-circRNA_17725 plasmids-intervened macrophage was obviously promoted compared with that of Lv-control plasmid-treated cells, which was demonstrated by flow cytometry (Figure 5(a)). However, results of EdU and CCK-8 cell proliferation detections showed that circRNA_17725 significantly inhibited the proliferation of Raw264.7 macrophage in a time-dependent manner (Figures 5(b) and 5(c)). Moreover, inflammatory cytokines of IL-1β, TNF-α, and MMP-9 in the supernatant of Lv-circRNA_17725 plasmid-treated macrophage was significantly decreased, although they were activated by LPS, a classic stimulator for macrophage activation (Figure 5(d)). IL-10 was reversely enhanced in the cultural supernatant of Lv-circRNA_17725 plasmids treated macrophage (Figure 5(d)). Taken together, circRNA_17725 can regulate macrophage proliferation, apoptosis, and inflammatory response *in vitro*, suggesting a pivotal role of circRNA_17725 in macrophage-mediated inflammation in RA. Nonetheless, its altering effects on macrophage functional phenotypes and the potential molecular mechanism are needed to elucidate in the following experiments.

3.5. circRNA_17725 Promoted M2 Polarization via Targeting miR-4668-5p/FAM46C. As shown in Figures 6(a) and 6(b), IL-4 could induce M2 polarization of Raw264.7 cells. Overexpression of circRNA_17725 enhanced the percentages of CD206$^+$M2 and CD163$^+$M2 cells, but significantly inhibited HLA-DR$^+$M1 and CD68$^+$M1 cell percentages (Figures 6(a)

and 6(b)). Besides, the mRNA level of CD206 was elevated, while CD11c mRNA expression was obviously decreased in circRNA_17725-overexpressed macrophages (Figures 6(c) and 6(d)). As a result, circRNA_17725 promoted M2 polarization *in vitro*. Nonetheless, the underlying molecular mechanism of circRNA_17725 in regulating macrophage polarization was still not clear. We further performed the following experiments to elucidate the potential mechanism underlying macrophage differentiation and polarization. Previous bioinformatics analysis had suggested the circRNA_17725/miR-4668-5p/FAM46C ceRNA network (Figure 2). In this study, Lv-circRNA-transfected Raw264.7 macrophage had upregulated expression of FAM46C but decreased expression of miR-4668-5p compared with the Lv-control group (Figures 7(a)–7(c)). Besides, the luciferase reporter assay had implicated that miR-4668-5p significantly downregulated FAM46C at the post-transcriptional level in macrophages (Figure 7(d)). Moreover, the RIP test suggested circRNA_17725 could combine with miR-4668-5p and acting as a ceRNA in macrophages (Figures 7(e) and 7(f)). Taken together, circRNA_17725 is involved in regulating macrophage polarization by targeting FAM46C through the circRNA_17725-miR-4668-5p-FAM46C ceRNA network.

3.6. Overexpression of circRNA_17725 in Macrophage Alleviated Arthritis in CIA Mice by Promoting M2 Polarization. Figure 8(a) showed the flowchart for the construction and intervention of CIA mice. As shown in Figure 8(b), circRNA_
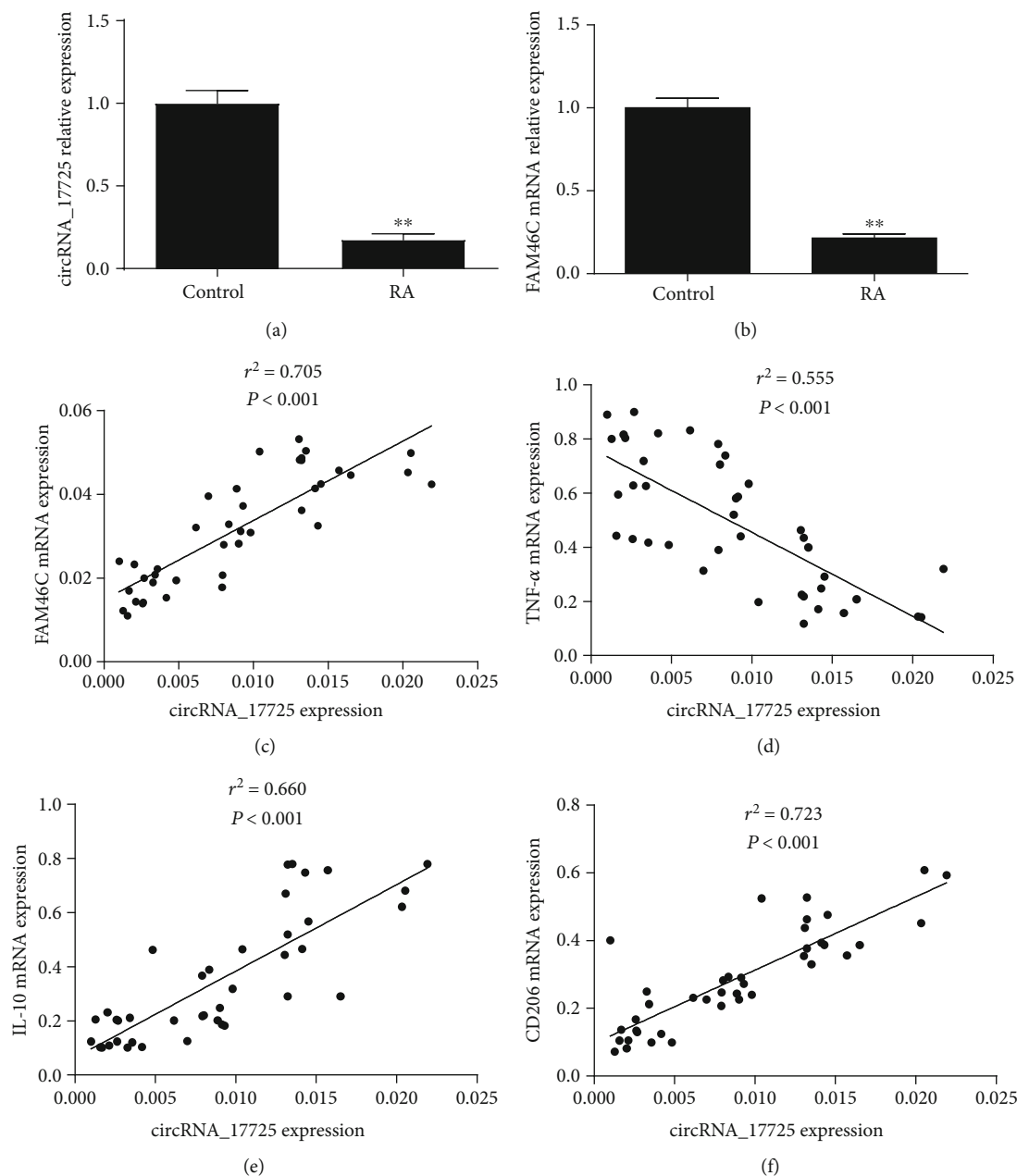
Figure 3: Association between circRNA_17725, FAM46C, TNF-α, IL-10, and CD206 in RA. (a) Expression of circRNA_17725 in CD14^{+}monocytes from RA patients in contrast to controls ([**]$P < 0.01$; RA/control: 40/30). (b) Expression of FAM46C in CD14^{+}monocytes from RA patients in contrast to controls ([**]$P < 0.01$; RA/control: 40/30). (c) Pearson's correlation analysis: relationship of circRNA_17725 with FAM46C ($n = 40$). (d) Pearson's correlation analysis: relationship of circRNA_17725 with TNF-α ($n = 40$). (e) Pearson's correlation analysis: relationship of circRNA_17725 with IL-10 ($n = 40$). (f) Pearson's correlation analysis: relationship of circRNA_17725 with CD206 ($n = 40$).

17725 decreased the mean score of arthritis and prolonged the time of arthritis first occurred in CIA mice treated by circRNA_17725-overexpressed Raw264.7 macrophages. Less redness and swelling of mouse joints were observed in CIA mice administrated by Lv-circRNA-intervened macrophages compared with those in control mice (Figure 8(c)). As demonstrated by HE staining, less subchondral bone erosions, synovitis, and inflammatory lymphocyte infiltration were found in the joint tissue slices of CIA mice intervened by circRNA_17725-overexpressed macrophages (Figure 8(d)). Besides, the Safranin O/Solid green staining had shown less severe cartilaginous injury and bone damages in the joint tissue slices of CIA mice treated by Lv-circRNA_17725-transfected macrophages compared with those in Lv-control-transfected macrophage-treated CIA mice (Figure 8(e)). Moreover, the flow cytometry analysis showed that increased CD163^{+} M2-type cells but decreased

(a)

(b)
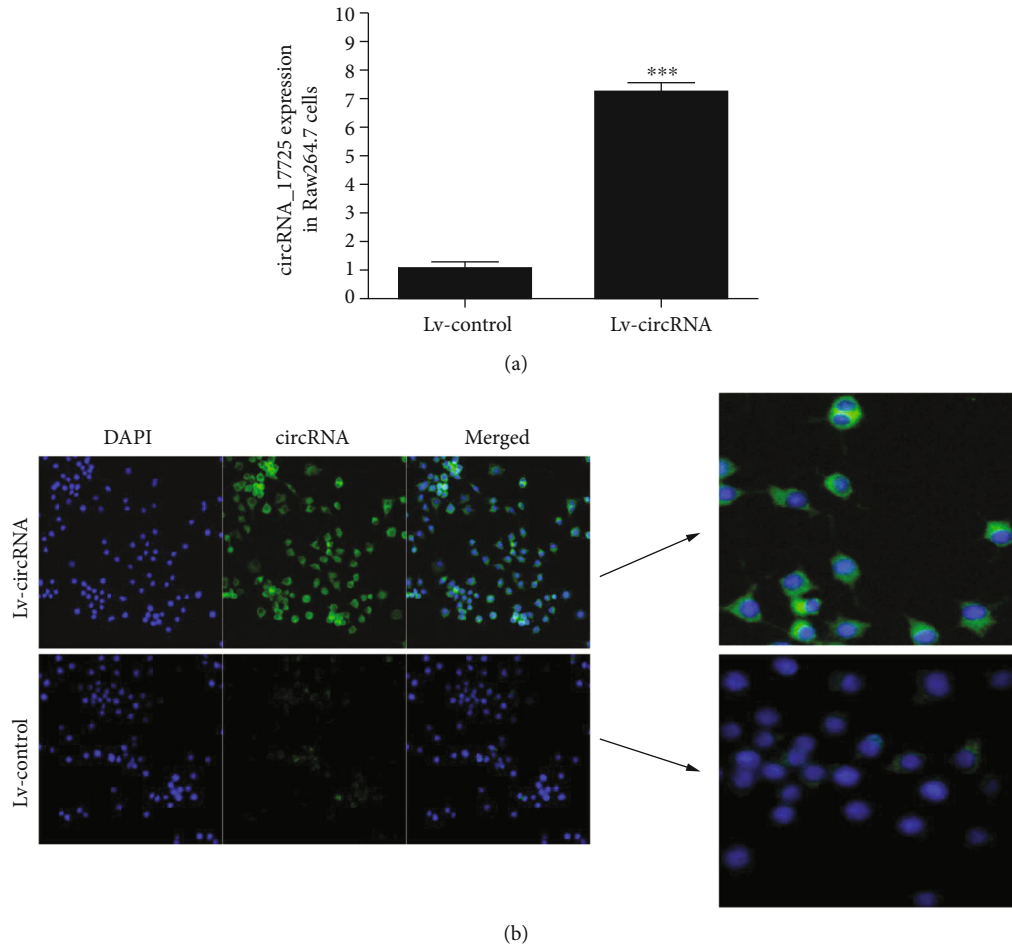
FIGURE 4: Location of circRNA_17725 in macrophages. (a) Real-time PCR: circRNA_17725 expression in Raw264.7 macrophages ($***P < 0.001$; $n = 3$). (b) FISH: location of circRNA_17725 in Raw264.7 macrophages (representative pictures; 20x).

CD11c^{+} M1-type cells were infiltrated in spleens of CIA mice treated by Lv-circRNA_17725-transfected macrophages (Figure 9(a)). Similarly, the real-time PCR had suggested lower levels of CD11c mRNA but higher levels of CD163 and FAM46C mRNAs in spleen mononuclear cells of macrophage-treated CIA mice compared with untreated CIA mice, which had been treated by Lv-circRNA control plasmid-transfected macrophages through tail intravenous injection (Figure 9(b)). Moreover, reduced production of TNF-α and IL-1β was observed in the plasm samples from Lv-circRNA_17725-transfected macrophage-treated CIA mice (Figure 9(c)). Taken together, circRNA_17725 protected against synovitis, joint injuries, and bone destruction in vivo by inducing macrophage polarization towards M2 through the circRNA_17725-miR-4668-5p-FAM46C signaling axis.

4. Discussion

With the progress of molecular biology techniques, the role of ncRNAs in autoimmune diseases, cancers, and inflammation-associated diseases has been elucidated, some of which may serve as ideal markers for disease diagnosis and treatment. In previous studies, the specific expression profiles of ncRNAs in RA patients have been identified, primarily including specific lncRNAs and miRNAs. Among them, lncRNA HIX003209, miR-6089, and miR-548a-3p have been demonstrated to be involved in regulating inflammation and autoimmunity [13–15]. In particular, lncRNA HIX003209 can sponge with miR-6089 and function as a ceRNA in macrophage response in RA [13]. Exosomes-delivering miR-6089 and miR-548a-3p can inhibit the generation of inflammatory mediators in macrophages, which thus alleviates arthritis [14, 15]. circRNAs are ncRNAs with closed circular structure, which account for the majority of ncRNAs. They are stably expressed and not easy to degradation. circRNAs play critical roles in various pathophysiological processes. Accumulating studies have reported that some specific circRNAs are dysregulated and associated with the disease activity of RA [16, 17]. We have also found that circRNA_09505 was upregulated in RA and participated in macrophage-mediated immune and inflammatory response in RA [12]. Accordingly, identification of novel circRNAs in RA may provide insight into the pathogenesis and biological therapy of RA.

Macrophages are heterogeneous cells with different phenotypes and functions, which can be differentiated into classically activated M1 and alternatively activated M2

(a)

(b)

(c)

(d)
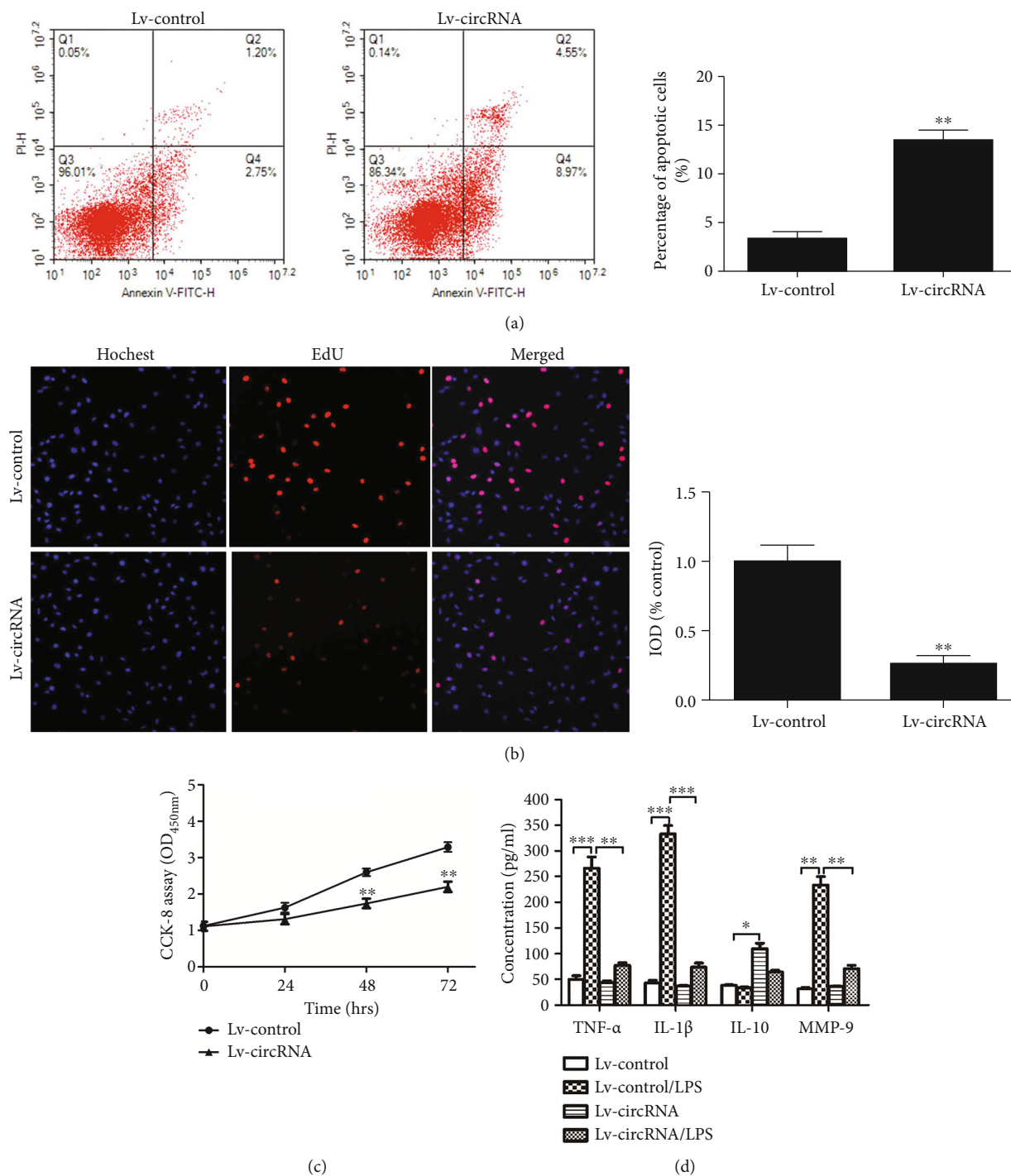
Figure 5: circRNA_17725 regulated macrophage proliferation, apoptosis, and inflammation. (a) Flow cytometry: Lv-circRNA_17725 plasmids promoted the apoptosis of macrophages induced by H_2O_2 at 4 h ($^{**}P < 0.01$; $n = 3$). (b) EdU: Lv-circRNA_17725 plasmids inhibited the proliferation of macrophages at 48 h (20x; $^{**}P < 0.01$; $n = 3$). (c) CCK-8: Lv-circRNA_17725 plasmids inhibited the proliferation of macrophages in a time-dependent way ($^{**}P < 0.01$; $n = 3$). (d) ELISA: Lv-circRNA_17725 plasmids decreased TNF-α, IL-1β, and MMP-9 but increased IL-10 in cells cultural supernatant ($^{*}P < 0.05$, $^{**}P < 0.01$, and $^{***}P < 0.001$; $n = 3$).

macrophages under the modifying effects of diverse mediators in the microenvironment. Increased levels of proinflammatory mediators from M1-type macrophages lead to inflammation and immune disorders, such as TNF-α, IL-6, and IL-1β [18]. It has been well established that M1/M2 imbalance was found in RA characterized by more M1 macrophages and fewer M2 macrophages in the immune microenvironment [19]. M1/M2 imbalance can promote Th1 and Th17 cell reactions, which thus exacerbates the immunoinflammatory response and causes synovial cell hyperplasia,

(a)

(b)

(c)

(d)
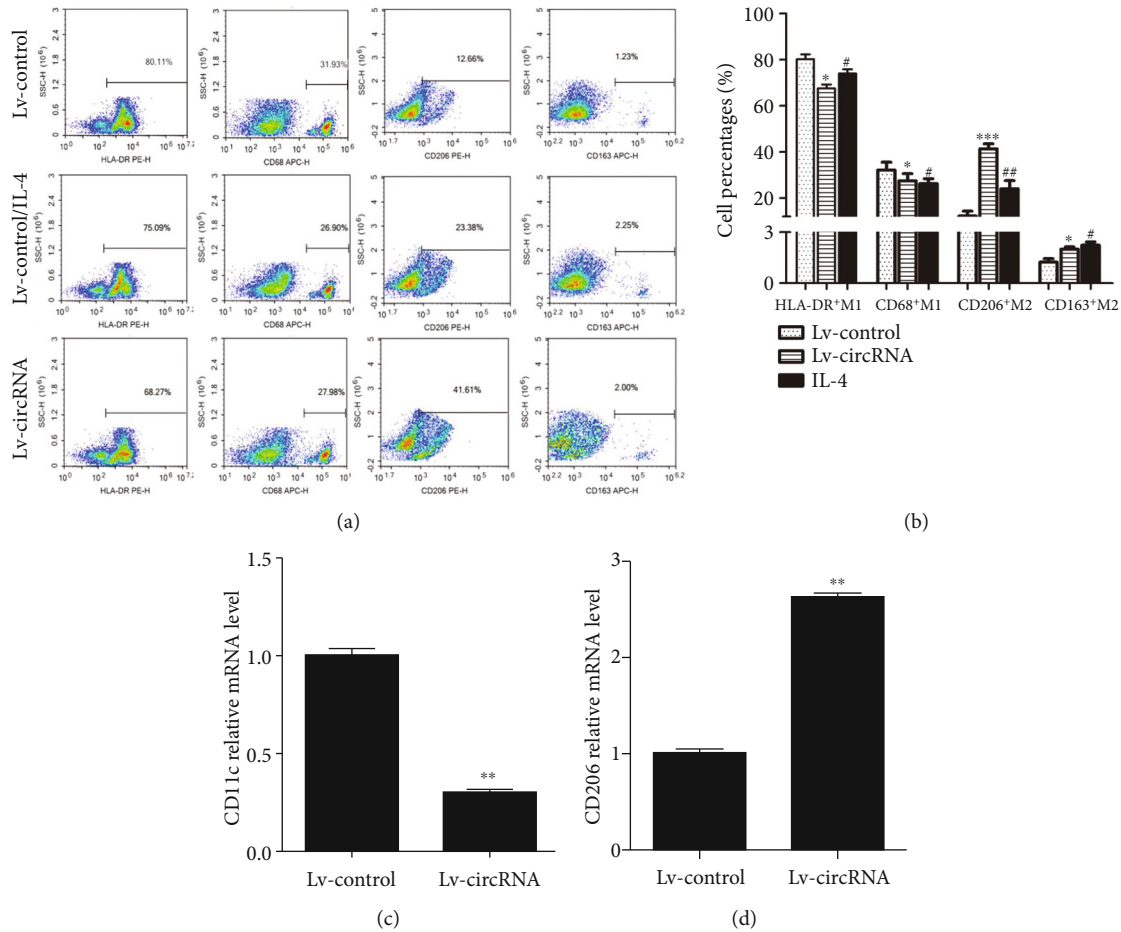
Figure 6: circRNA_17725 promoted macrophage polarization towards M2. (a) Flow cytometry: circRNA_17725 promoted CD206$^+$M2 and CD163$^+$M2 cells while inhibited HLA-DR$^+$M1 and CD68$^+$M1 cells polarization (representative pictures). (b) Cell percentages of CD206$^+$M2, CD163$^+$M2, HLA-DR$^+$M1, and CD68$^+$M1 cells determined by flow cytometry (vs. Lv-control: $^*P < 0.05$, $^{***}P < 0.001$; vs. Lv-control: $^\#P < 0.05$, $^{\#\#}P < 0.01$; $n = 3$). (c) CD11c mRNA expression was decreased in circRNA_17725-overexpressed Raw264.7 cells ($^{**}P < 0.01$; $n = 3$). (d) CD206 mRNA expression was increased in circRNA_17725-overexpressed macrophages ($^{**}P < 0.01$; $n = 3$).

synovial hypertrophy, osteoclast formation, and cartilage injury [20]. Accordingly, intervening the M1/M2 macrophage polarization balance effectively and maintaining the balance of immune microenvironment would be a promising therapeutic way for RA. It has been found that family with sequence similarity 46 member C (FAM46C), signaling, and signal transducer and activator of transcription 33 (STAT3) play important regulatory roles in regulating macrophage polarization [19, 21, 22]. Some ncRNAs have been demonstrated to regulate the macrophage phenotypic polarization and function by targeting STAT3 and other molecules associated with macrophage polarization, such as miR-221-3p and lncRNA NTT [23, 24]. Nonetheless, litter is known about the impact of circRNAs in regulating macrophage phenotypes in RA. In this study, we have found that circRNA_17725 could reduce macrophage proliferation but promote cell apoptosis. Besides, circRNA_17725 reduced the expression of inflammatory factors, such as TNF-α and IL-1β in RA. Moreover, circRNA_17725 played a protective role by promoting M2 polarization in vitro and in vivo, sug-

gesting the crucial effect of circRNA in regulating inflammation and autoimmunity in RA.

It has been demonstrated that the expression profile of circRNAs is different between M1 macrophage and M2 macrophage [25], suggesting the diverse and complicated regulatory effects of circRNAs on macrophage phenotypes and functions. M1/M2 bias leads to chronic inflammation and metabolic imbalance in SLE, which influences the balance of immune microenvironment in targeted organs including kidneys [26]. Song et al. have reported that circCdyl played a pivotal role in abdominal aortic aneurysm (AAA) by promoting M1 macrophage inflammatory response and inducing M1 polarization [27]. circ_0000518 has been demonstrated to promote macrophage/microglia M1 polarization in multiple sclerosis [28]. A recent study has also suggested the crucial role of circ_0005567 in inhibiting chondrocyte apoptosis and the progression of osteoarthritis by promoting M2 polarization via the miR-492/SOCS2 signaling axis [29]. However, the molecular mechanism of circRNA in regulating M1/M2 polarization in RA is rarely

(a)

(b)

(c)

(d)

(e)

(f)
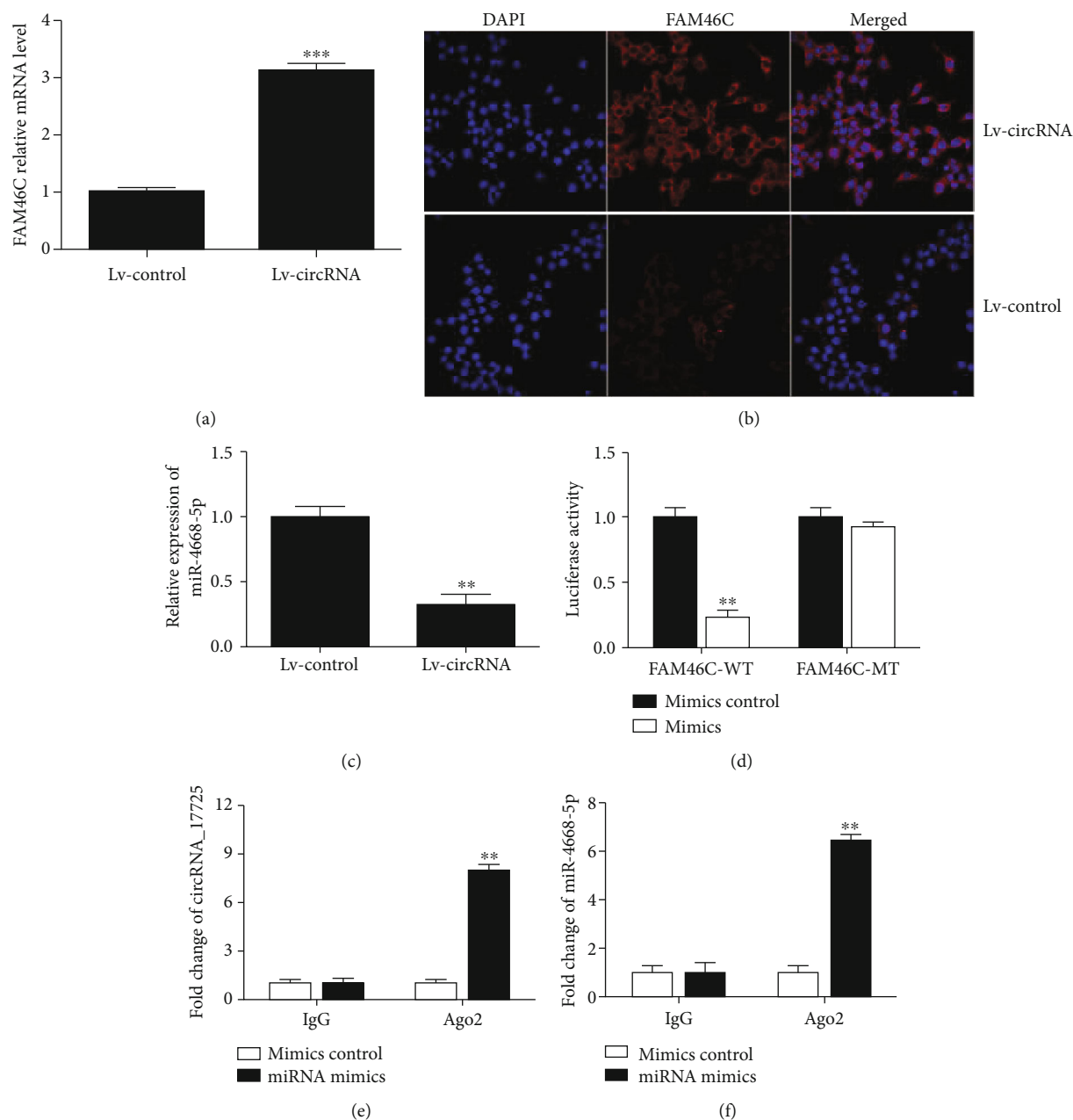
FIGURE 7: circRNA_17725 functioned as a ceRNA based on the circRNA_17725-miR-4668-5p-FAM46C network. (a) Real-time PCR: increased expression of FAM46C in Lv-circRNA-transfected Raw264.7 macrophages (***$P < 0.001$; $n = 3$). (b) Cell immunofluorescence: higher expression of FAM46C in Raw264.7 macrophages transfected by Lv-circRNA plasmids (representative pictures; 20x). (c) Real-time PCR: decreased miR-4668-5p in Lv-circRNA-treated cells (**$P < 0.01$; $n = 3$). (d) Luciferase reporter assay: miR-4668-5p mimics inhibited FAM46C expression in macrophages (**$P < 0.01$; $n = 3$). (e) RIP test: expression of circRNA_17725 in immunoprecipitions (**$P < 0.01$; $n = 3$). (f) RIP test: expression of miR-4668-5p in immunoprecipitions (**$P < 0.01$; $n = 3$).

reported. In this study, we have found that circRNA_17725 was significantly downregulated in RA. It was capable of inhibiting macrophage proliferation and inflammatory response, implicating a pivotal regulatory effect of circRNA_17725 on macrophage-mediated inflammation in RA. Moreover, it could elevate the expression of M2-associated molecule FAM46C and thus promote M2-type cell response in CIA mice by increasing CD163^{+} M2 macrophages but decreasing CD11c^{+} M1 macrophage infiltration in spleens of CIA mice. Taken together, this study has implicated the protective role of circRNA_17725 in RA and its critical effects on macrophage phenotypic plasticity.

The functions of circRNAs are different according to their localization in cells [30, 31]. Most circRNAs molecules are localized in the cytoplasm and exert effects by RNA-RNA interactions including sponging with miRNAs and antagonizing their posttranscriptional regulatory effects on the downstream mRNAs [32, 33]. Nonetheless, some

(a)

(b)

(c)

(d)

(e)
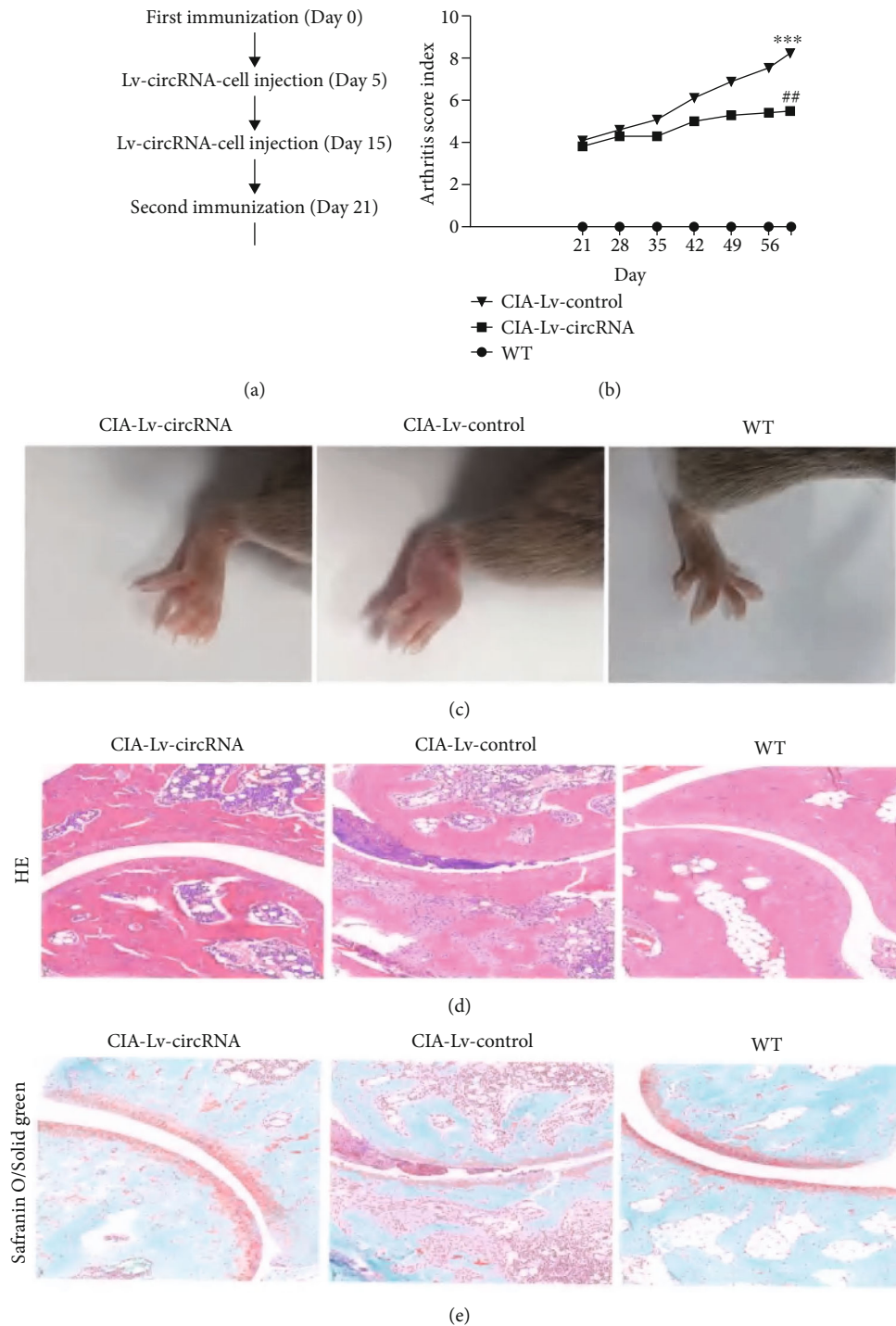
Figure 8: circRNA_17725-overexpressed macrophage alleviated arthritis in CIA mice. (a) CIA mouse model construction flowchart (6 mice/group). (b) Arthritis score: circRNA_17725-overexpressed macrophage-treated CIA mice had lower arthritis score (vs. the WT group, $***P < 0.001$; vs. the CIA-Lv-control group, $^{##}P < 0.01$). (c) Representative pictures: less redness, swelling, and alleviated arthritis of CIA mice treated by circRNA_17725-overexpressed macrophages. (d) Representative pictures of HE staining of joint tissues from CIA mice treated by circRNA_17725-overexpressed macrophages (20x). (e) Representative Safranin O/Solid green staining pictures: less severe cartilaginous injury and bone damages in the joint tissues of CIA mice treated by Lv-circRNA-transfected macrophages (20x).

circRNAs can function by directly binding to proteins through RNA-protein interactions [28, 34]. In a previous study, we found that circRNA_09505 could aggravate inflammation and joint damage by regulating macrophage-mediated immunoinflammatory response in CIA mice by acting as a ceRNA for miR-6089 via the AKT1/NF-κB axis [12], which suggests the pivotal mechanism of circRNA as a ceRNA molecule in immune cells. The altering effect of

(a)

(b)

(c)
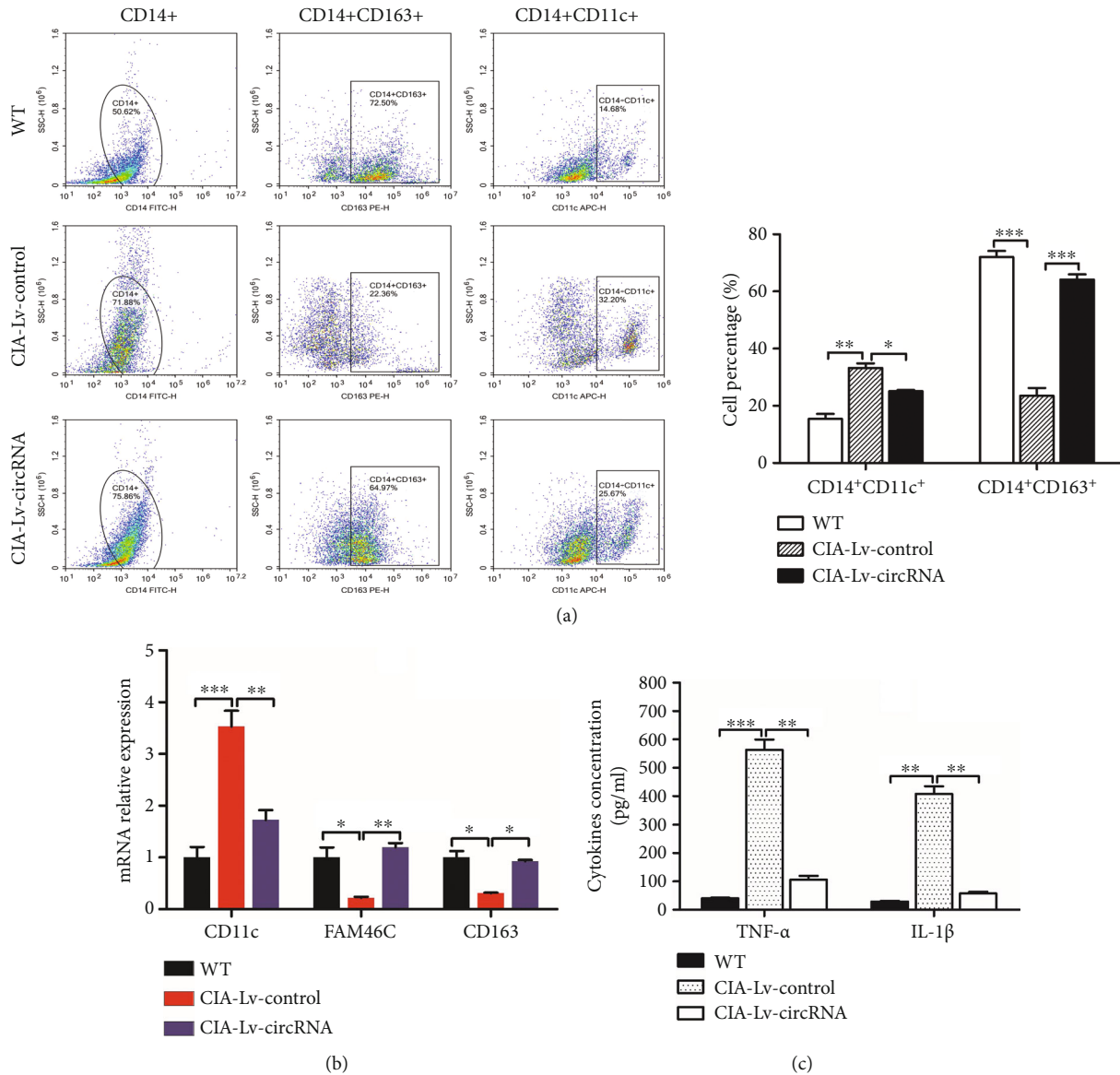
FIGURE 9: circRNA_17725 promoted M2 polarization in CIA mice. (a) Flow cytometry: CD14$^+$CD163$^+$ cells and CD14$^+$CD11c$^+$ cells infiltration in spleens from CIA mice ($^*P < 0.05$, $^{**}P < 0.01$, and $^{***}P < 0.001$; 6 mice/group, $n = 3$). (b) Real-time PCR: CD11c, CD163, and FAM46C mRNA expressions in spleen mononuclear cells of CIA mice ($^*P < 0.05$, $^{**}P < 0.01$, and $^{***}P < 0.001$; 6 mice/group, $n = 3$). (c) ELISA: decreased TNF-α and IL-1β in the plasm from Lv-circRNA-transfected macrophage-treated CIA mice ($^{**}P < 0.01$, $^{***}P < 0.001$; 6 mice/group, $n = 3$).

circRNA in regulating macrophage phenotypic polarization warrants in depth investigation. In this study, the findings have strongly supported that overexpression of circRNA_17725 could elevate CD206$^+$M2 and CD163$^+$M2 cells percentages, while significantly inhibit HLA-DR$^+$M1 and CD68$^+$M1 cells percentages. Besides, miR-4668-5p could downregulate the expression of FAM46C in macrophage, while circRNA_17725 served as a ceRNA by sponging miR-4668-5p and promoted FAM46C expression in macrophages. All the findings have shed some light on the pathogenesis of RA. It also provides novel ideas for investigating more promising immunotherapy for RA by targeting certain checkpoint molecules in this axis. Nevertheless, there are some drawbacks in this study. On the one hand, the role of circRNA_17725 in regulating macrophage polarization should be further evaluated in the local immune balance of joints. On the other hand, future studies are recommended to investigate the modifying effects of circRNA_17725 on influencing cartilage damages and articular repair. Last but not the least, the downstream signaling pathway and key checkpoints of circRNA_17725-miR-4668-5p-FAM46C axis warrant to be elucidated in the future.

In conclusion, this study has implicated that circRNA_17725 protected against synovitis, joint injuries and bone destruction by inducing macrophage polarization towards M2 through the circRNA_17725-miR-4668-5p-FAM46C signaling axis in RA. circRNA_17725 might be serve as a promising target for the biotherapy of RA.

Abbreviations

circRNAs: Circular RNAs
RA: Rheumatoid arthritis
RIP: RNA binding protein immunoprecipitation
CIA: Collagen-induced arthritis
ncRNAs: Noncoding RNAs
circRNA: Circular RNA
lncRNA: Long chain noncoding RNAs
miRNA: MicroRNAs
PBMCs: Peripheral blood mononuclear cells
ceRNA: Competitive endogenous RNA
SLE: Systemic lupus erythematosus
MS: Multiple sclerosis
FISH: RNA fluorescence in situ hybridization
FAM46C: Sequence similarity 46 member C
STAT3:   Signaling and signal transducer and activator of transcription 3
AAA: Abdominal aortic aneurysm.

Data Availability

All data and materials in this study have been included in this paper. Further inquiries can be directed to the corresponding authors.

Ethical Approval

The study regarding human subjects was approved by the Institutional Ethics Committee of the First Affiliated Hospital of Weifang Medical University. Besides, CIA mouse model experiments were performed based on the guidelines of Institutional Animal Care and Use Committee of Weifang Medical University.

Conflicts of Interest

The authors declare that they have no conflict of interest.

Authors' Contributions

D.X. and S.Y. conceived the project. C.Y., W.S., H.W., C.L., and X.H. performed the experiments and analyzed data. C.Y., W.S., D.X. and S.Y. wrote the manuscript. B.N., X.W., W.S., D.X., and S.Y. revised the manuscript. All authors had read and approved the final manuscript. Chunjuan Yang, Biao Ni, Chaoran Li, Wenchang Sun, and Zhangxue Wang contributed equally to this work.

Acknowledgments

References

[1] D. L. Scott, F. Wolfeand, and T. W. Huizinga, "Rheumatoid arthritis," *The Lancet*, vol. 376, no. 9746, pp. 1094–1108, 2010.

[2] D. Giannini, M. Antonucci, F. Petrelli, S. Bilia, A. Alunno, and I. Puxeddu, "One year in review 2020: pathogenesis of rheumatoid arthritis," *Clinical and Experimental Rheumatology*, vol. 38, no. 3, pp. 387–397, 2020.

[3] J. Wang, S. Yan, J. Yang, H. Lu, D. Xu, and Z. Wang, "Noncoding RNAs in rheumatoid arthritis: from bench to bedside," *Frontiers in Immunology*, vol. 10, p. 3129, 2020.

[4] X. Zhai, Y. Zhang, S. Xin, P. Cao, and J. Lu, "Insights into the involvement of circular RNAs in autoimmune diseases," *Frontiers in Immunology*, vol. 12, article 622316, 2021.

[5] X. Chen, T. Yang, W. Wang et al., "Circular rnas in immune responses and immune diseases," *Theranostics*, vol. 9, no. 2, pp. 588–607, 2019.

[6] J. Hao, Y. Chenand, and Y. Yu, "Circular RNA circ_0008360 inhibits the proliferation, migration, and inflammation and promotes apoptosis of fibroblast-like synoviocytes by regulating miR-135b-5p/HDAC4 axis in rheumatoid arthritis," *Inflammation*, vol. 45, no. 1, pp. 196–211, 2022.

[7] Y. Chen, X. Xu, X. Li et al., "Identification of circular RNAs hsa_circ_0140271 in peripheral blood mononuclear cells as a novel diagnostic biomarker for female rheumatoid arthritis," *Journal of Orthopaedic Surgery and Research*, vol. 16, no. 1, p. 647, 2021.

[8] J. Li, D. Liu, K. Wu, Q. Chen, and J. Lei, "Circ_0003972 promotes the proliferation and inflammation of fibroblast-like synovial cells in rheumatoid arthritis through regulation of the miR-654-5p/FZD4 axis," *Immunological Investigations*, vol. 51, no. 5, pp. 1437–1451, 2022.

[9] H. Liu, Y. Zou, C. Chen, Y. Tang, and J. Guo, "Current understanding of circular RNAs in systemic lupus erythematosus," *Frontiers in Immunology*, vol. 12, article 628872, 2021.

[10] A. E. Zurawska, M. P. Mycko, I. Selmaj, C. S. Raine, and K. W. Selmaj, "Multiple sclerosis: circRNA profile defined reveals links to b-cell function," *Neurology - Neuroimmunology Neuroinflammation*, vol. 8, no. 5, p. e1041, 2021.

[11] V. Lodde, G. Murgia, E. R. Simula, M. Steri, M. Floris, and M. L. Idda, "Long noncoding RNAs and circular RNAs in autoimmune diseases," *Biomolecules*, vol. 10, no. 7, p. 1044, 2020.

[12] J. Yang, M. Cheng, B. Gu, J. Wang, S. Yan, and D. Xu, "CircRNA_09505 aggravates inflammation and joint damage in collagen-induced arthritis mice via miR-6089/AKT1/NF-κB axis," *Cell Death & Disease*, vol. 11, no. 10, p. 833, 2020.

[13] S. Yan, P. Wang, J. Wang et al., "Long non-coding RNA hix003209 promotes inflammation by sponging mir-6089 via TLR4/NF-κB signaling pathway in rheumatoid arthritis," *Frontiers in Immunology*, vol. 10, p. 2218, 2019.

[14] Y. Wang, F. Zheng, G. Gao et al., "miR-548a-3p regulates inflammatory response via TLR4/NF-κB signaling pathway in rheumatoid arthritis," *Journal of Cellular Biochemistry*, vol. 120, no. 2, pp. 1133–1140, 2019.

[15] D. Xu, M. Song, C. Chai et al., "Exosome-encapsulated miR-6089 regulates inflammatory response via targeting TLR4," *Journal of Cellular Physiology*, vol. 234, no. 2, pp. 1502–1511, 2019.

[16] Q. Luo, J. Liu, B. Fu et al., "Circular RNAs hsa_circ_0002715 and hsa_circ_0035197 in peripheral blood are novel potential biomarkers for new-onset rheumatoid arthritis," *Disease Markers*, vol. 2019, Article ID 2073139, 12 pages, 2019.

[17] X. Yang, J. Li, Y. Wu, B. Ni, and B. Zhang, "Aberrant dysregulated circular RNAs in the peripheral blood mononuclear cells of patients with rheumatoid arthritis revealed by RNA sequencing: novel diagnostic markers for RA," *Scandinavian Journal of Clinical and Laboratory Investigation*, vol. 79, no. 8, pp. 551–559, 2019.

[18] Y. Liu, S. Luo, Y. Zhan et al., "Increased expression of PPAR-γ modulates monocytes into a M2-like phenotype in SLE patients: an implicative protective mechanism and potential therapeutic strategy of systemic lupus erythematosus," *Frontiers in Immunology*, vol. 11, article 579372, 2020.

[19] S. Tardito, G. Martinelli, S. Soldano et al., "Macrophage M1/M2 polarization and rheumatoid arthritis: a systematic review," *Autoimmunity Reviews*, vol. 18, no. 11, article 102397, 2019.

[20] S. Fukui, N. Iwamoto, A. Takatani et al., "M1 and m2 monocytes in rheumatoid arthritis: a contribution of imbalance of M1/M2 monocytes to osteoclastogenesis," *Frontiers in Immunology*, vol. 8, p. 1958, 2018.

[21] J. Tan, T. Sun, J. Shen et al., "Fam46c inhibits lipopolysaccharides-induced myocardial dysfunction via downregulating cellular adhesion molecules and inhibiting apoptosis," *Life Sciences*, vol. 229, pp. 1–12, 2019.

[22] P. Wang, Z. Wang, G. Liu et al., "miR-657 promotes macrophage polarization toward M1 by targeting FAM46C in gestational diabetes mellitus," *Mediators of Inflammation*, vol. 2019, Article ID 4851214, 9 pages, 2019.

[23] W. Liu, Q. Long, W. Zhang et al., "miRNA-221-3p derived from M2-polarized tumor-associated macrophage exosomes aggravates the growth and metastasis of osteosarcoma through SOCS3/JAK2/STAT3 axis," *Aging*, vol. 13, no. 15, pp. 19760–19775, 2021.

[24] C. A. Yang, J. P. Li, J. C. Yen et al., "lncRNA NTT/PBOV1 axis promotes monocyte differentiation and is elevated in rheumatoid arthritis," *International Journal of Molecular Sciences*, vol. 19, no. 9, p. 2806, 2018.

[25] Y. Zhang, X. Li, M. Zhang, X. Li, M. Zhang, and K. Lv, "Microarray analysis of circular rna expression patterns in polarized macrophages," *International Journal of Molecular Medicine*, vol. 39, no. 2, pp. 373–379, 2017.

[26] C. Jing, T. Castro-Dopico, N. Richoz et al., "Macrophage metabolic reprogramming presents a therapeutic target in lupus nephritis," *Proceedings of the National Academy of Sciences of the United States of America*, vol. 117, no. 26, pp. 15160–15171, 2020.

[27] H. Song, Y. Yang, Y. Sun et al., "Circular RNA Cdyl promotes abdominal aortic aneurysm formation by inducing M1 macrophage polarization and M1-type inflammation," *Molecular Therapy*, vol. 30, no. 2, pp. 915–931, 2022.

[28] F. Jiang, X. Liu, X. Cui et al., "Circ_0000518 Promotes Macrophage/Microglia M1 Polarization via the FUS/CaMKKβ/AMPK Pathway to Aggravate Multiple Sclerosis," *Neuroscience*, vol. 490, pp. 131–143, 2022.

[29] J. Zhang, F. Cheng, G. Rong, Z. Tang, and B. Gui, "Circular RNA hsa_circ_0005567 overexpression promotes M2 type macrophage polarization through miR-492/SOCS2 axis to inhibit osteoarthritis progression," *Bioengineered*, vol. 12, no. 1, pp. 8920–8930, 2021.

[30] M. Xu, F. Xie, X. Tang, T. Wang, and S. Wang, "Insights into the role of circular RNA in macrophage activation and fibrosis disease," *Pharmacological Research*, vol. 156, article 104777, 2020.

[31] D. Zhou, Y. Wu, S. Wang, J. Li, and J. Luan, "Harnessing noncoding RNA-based macrophage polarization: emerging therapeutic opportunities for fibrosis," *Immunity, Inflammation and Disease*, vol. 8, no. 4, pp. 793–806, 2020.

[32] Y. Tay, J. Rinnand, and P. P. Pandolfi, "The multilayered complexity of ceRNA crosstalk and competition," *Nature*, vol. 505, no. 7483, pp. 344–352, 2014.

[33] Z. Z. Liang, C. Guo, M. M. Zou, P. Meng, and T. T. Zhang, "CircRNA-miRNA-mRNA regulatory network in human lung cancer: an update," *Cancer Cell International*, vol. 20, no. 1, p. 173, 2020.

[34] Z. Zhou, R. Jiang, X. Yang et al., "CircRNA mediates silica-induced macrophage activation via HECTD1/ZC3H12A-dependent ubiquitination," *Theranostics*, vol. 8, no. 2, pp. 575–592, 2018.

Research Article

Circulating IGFBP-3 and Interleukin 6 as Predictors of Osteoporosis in Postmenopausal Women: A Cross-Sectional Study

Xiu Shi [1] **Jingjing Jiang,** [2] **Ru Hong,** [3,4] **Feng Xu** [3,4] **and Shouqian Dai** [3,4]

[1]*Department of Obstetrics and Gynecology, The First Affiliated Hospital, Soochow University, Suzhou 215006, China*
[2]*Department of Obstetrics and Gynecology, The Affiliated Huai'an Hospital of Xuzhou Medical University and Second People's Hospital of Huaian, Huai'an 223001, China*
[3]*Department of Emergency Medicine, The First Affiliated Hospital of Soochow University, Suzhou 215006, China*
[4]*National Regional Center for Trauma Medicine, The First Affiliated Hospital of Soochow University, Suzhou 215006, China*

Correspondence should be addressed to Shouqian Dai; daishouqian@suda.edu.cn

Objective. To explore the relationship between circulating IGFBP-3, IL-6, and bone mineral density and the potential diagnostic role of circulating IGFBP-3 and IL-6 in postmenopausal women with osteoporosis. *Methods.* Eighty-five postmenopausal women at Soochow University's First Affiliated Hospital, Osteoporosis and Menopause Clinics, were recruited. Forty-five of 85 women were diagnosed with osteoporosis. Circulating IL-6, PTH, 1,25(OH)2D3, osteocalcin (OST), IGF-1, IGFBP-3, and bone mineral density (BMD) of the lumbar spine (LS) and femoral neck (FN) were measured in 40 ordinary and 45 osteoporotic women. A simple regression analysis calculated the correlation between age, BMD, IL-6, and IGFBP-3. Multiple stepwise regression analyses were conducted to determine which variables were independently related to BMD. The potential role of IGFBP-3 and IL-6 in the diagnosis of postmenopausal osteoporosis was predicted using the area under the receiver operating characteristic curve (ROC, AUC). *Results.* Age, years since menopause, and circulating IL-6, PTH, and IGFBP-3 were significantly higher in the osteoporosis group compared to the normal group. Osteoporotic women had substantially lower BMDs of the LS and FN than normal women. Age-related increases were found for IGFBP-3 and IL-6, whereas age-related decreases were observed for LS/FN BMD. IGFBP-3 and IL-6 were both negatively correlated with LS and FN BMD. Stepwise multiple regression analysis showed that IGFBP-3 and IL-6 were strong predictors of BMD in postmenopausal women. AUC cut-off values (IGFBP-3: 3.65, IL-6: 0.205) were best evaluated for the diagnosis of postmenopausal women with osteoporosis, and the AUC for circulating IGFBP-3 and IL-6 were 0.706 (95% CI 0.594–0.818) and 0.685 (95% CI 0.571–0.798), respectively. *Conclusion.* In this cross-sectional study of postmenopausal women, IGFBP-3 and IL-6 were negatively related to BMD. Circulating IGFBP-3 and IL-6 might be essential predictors of postmenopausal osteoporosis and can help predict osteoporotic fracture.

1. Introduction

Postmenopausal osteoporosis is a relatively common metabolic disease in postmenopausal women, and the research regarding its pathogenesis is still sparse [1]. Studies have shown that estrogen deficiency is a fundamental cause of the disease [2]. The primary clinical basis for diagnosing postmenopausal osteoporosis is the bone mineral density (BMD) of the lumbar vertebrae and proximal femur. Postmenopausal women experience low back pain as their primary clinical symptom. Epidemiological surveys show that more than 10% of osteoporosis occurs in postmenopausal women, but fewer patients have fractures with the progression of the disease [3]. At the same time, the clinical manifestations of chronic pain in postmenopausal osteoporosis are not apparent, and there is a lack of sensitive indicators or predictors in early diagnosis [4].

However, in the past few years, some factors, particularly the IGF (insulin-like growth factor) system (IGF-I, IGF-II, and IGFBP- (IGF binding protein-) 1~6), have been proposed to play crucial roles in the pathogenesis of bone loss or osteoporosis in postmenopausal women. Especially,

IGF-1 and IGFBP-3 play essential roles in regulating bone metabolism. IGF-I is a synthetic growth hormone secreted by the liver. Its prominent role includes stimulating osteocyte proliferation and inhibiting collagen degradation, thereby promoting bone growth and development [5]. IGFBP-3 is a binding protein of IGF-I, which regulates the synthesis of IGF-I, prolongs the half-life of IGF-I in bone metabolism, regulates the metabolism of vitamin D, and promotes the utilization of calcium [6]. According to a study, circulating levels of IGF-I and IGFBP-3 were significantly lower in older adults than in the young population, and a low circulating IGF-I and IGFBP-3 level was associated with osteoporosis [7]. However, other researchers reported that IGFBP-3 is a potent inhibitor of IGF-I-medicated DNA synthesis [8], indicating that IGFBP-3 could counteract the physiological function of IGF-I to a certain extent. In addition, Eguchi et al. demonstrated that IGFBP-3 might help maintain bone mass in both an IGF-I-dependent or IGF-I-independent manner by inhibiting osteoblast differentiation via the BMP-2 signal pathway [9]. Therefore, the specific role of IGFBP-3 in bone metabolism and osteoporosis remains controversial.

IL-6, a multifunctional cytokine, is secreted by activation of T cells, B cells, mononuclear macrophages, fibroblasts, specific tumor stromal cells, and osteoblasts. Although the content of IL-6 is minimal, it can act locally through autocrine and paracrine and affect the function of bone cells. It can promote the growth of hematopoietic stem cells, thereby exerting various biological activities [10]. A study involving 45 postmenopausal women showed that the circulating levels of IL-1β, IL-6, and TNF-α in postmenopausal women with osteoporosis were significantly higher than those without osteoporosis. At the same time, neither group had significant differences in other parameters of bone metabolism [11]. Scheidt et al. found that in women with osteoporosis, circulating IL-6 levels were positively correlated with bone loss in the first ten days after menopause, most notably in the hip [12]. This evidence suggests that postmenopausal osteoporosis is associated with IL-6.

This cross-sectional study is aimed at exploring the relationship between circulating IGFBP-3, IL-6, and bone mineral density in postmenopausal women. In addition, the potential diagnostic role of circulating IGFBP-3 and IL-6 in the pathogenesis of postmenopausal osteoporosis in postmenopausal women was investigated.

2. Materials and Methods

2.1. Population. Eighty-five postmenopausal women attending the bone mineral density examination at Soochow University's First Affiliated Hospital, Osteoporosis and Menopause Clinics, participated in this study. The circulating estradiol content in all patients was less than 20 pg/ml. Both healthy and osteoporosis women were included in our study. The age of menopause, duration of lactation, parity, and age of menarche were recorded for each participant. All participants have been out of menstruation for more than one year. We excluded patients with hepatic or renal dysfunction, thyroid disorders, or systemic diseases affecting

bone metabolism. All participants gave informed written consent. The medical ethics committee of our hospital approved the study. All participants did not take medications known to affect bone metabolism.

2.2. BMD Measurements. The BMDs of the L2-L4 lumbar spine and femoral neck (g/cm^2) were measured in all postmenopausal women using a dual-energy X-ray absorptiometry (DXA) system (Discovery, Hologic, Waltham, MA, USA). Among 85 postmenopausal women, 45 had osteoporosis (DXA T scores less than -2.5 standard deviations) according to the WHO criteria [13–15]. According to the in vivo variation coefficients, the lumbar spine had a variation coefficient of 1.7%, while the femoral neck had a variation coefficient of 2.2%. The same operator tested all the participants to eliminate operator discrepancies. In order to calculate the body mass index (BMI), body weight (kg) was divided by the square of body height (m^2).

2.3. Biochemical Measurements. After an overnight fast, blood samples were collected, and serum was separated and stored at -20°C until testing. Standard automated techniques were used to perform routine serum determinations. The circulating IGF-I levels were measured using radioimmunoassay (RIA) after acid-ethanol extraction, and circulating IGFBP-3 levels were measured by RIA as described previously [16]. Circulating levels of parathyroid hormone (PTH), IL-6, osteocalcin (OST), and 1,25-dihydroxyvitamin D$_3$ [1,25(OH)$_2$D$_3$] were measured as previously described [13, 17, 18]. These measurements were subjected to intra-assay variation of 2-3% and intra-assay variation of 6-7%, respectively.

2.4. Statistical Analysis. Means and standard deviations were calculated for all variables. This study used SPSS 26.0 (SPSS Inc., Chicago, IL, USA) for all statistical analyses. Comparisons were made between the normal and osteoporosis groups using an independent-sample t-test. Using Pearson's correlation coefficient, we evaluated the correlation between age, BMD, IL-6, and IGFBP-3 and determined the linear relationship using simple regression analysis. In order to determine which variables were independently related to BMD, multiple stepwise regression analyses were conducted. In order to determine whether IGFBP-3 and IL-6 circulating levels indicate osteoporosis in postmenopausal women, a receiver-operating characteristic (ROC) curve was constructed, and cut-off levels were selected. All analyses were considered statistically significant if the p value was less than 0.05.

3. Results

3.1. Baseline Characteristics. In this study, 85 postmenopausal women met the eligibility criteria for participation. The demographics and baseline data of the enrolled patients are presented in Table 1. Compared to the normal women, age, years duration of menopause, and circulating IL-6, PTH, and IGFBP-3 were significantly higher in the osteoporosis women. Compared to normal women, osteoporotic women had substantially lower BMDs at the lumbar spine

TABLE 1: The demographics and baseline data of the participants in the normal group and osteoporosis group (mean and standard deviation).

Variables	Normal group ($n = 40$)	Osteoporosis group ($n = 45$)
Age (years)	60.9 ± 6.4	64.5 ± 7.6^a
Years since menopause (years)	9.8 ± 2.1	12.4 ± 2.8^c
BMI (kg/m^2)	22.6 ± 3.3	22.1 ± 2.9
IL-6 (IU/ml)	0.15 ± 0.08	0.21 ± 0.09^b
PTH (pg/ml)	29.4 ± 6.3	32.6 ± 7.1^a
1,25(OH)$_2$D$_3$ (pg/ml)	26.3 ± 5.8	25.8 ± 4.7
OST (ng/ml)	7.3 ± 2.6	7.9 ± 3.1
IGF-1 (ng/ml)	178.5 ± 54.8	157.3 ± 45.9
IGFBP-3 (μg/ml)	3.36 ± 0.56	3.87 ± 0.68^c
LS BMD (g/cm^2)	0.712 ± 0.108	0.636 ± 0.114^b
FN BMD (g/cm^2)	0.623 ± 0.086	0.568 ± 0.092^b

Significant at $^a p < 0.05$, $^b p < 0.01$, and $^c p < 0.001$. BMI: body mass index; IL-6: interleukin 6; PTH: parathyroid hormone; OST: osteocalcin; LS: lumbar spine; FN: femoral neck.

and femoral neck. However, no significant differences in BMI and circulating levels of 1,25(OH)$_2$D$_3$, OST, and IGF-1 were observed in the two groups.

3.2. Age-Related Changes. Correlations of age with IL-6, IGFBP-3, and LS/FN BMD in all study populations are presented in Figure 1. Age-related increases were found for IGFBP-3 ($r = 0.348$; $p = 0.001$) and IL-6 ($r = 0.337$; $p = 0.002$), whereas an age-related decrease was only observed for BMD of the lumbar spine ($r = -0.243$; $p = 0.025$). BMD of the femoral neck tended to decrease with age, but this correlation was not statistically significant ($r = 0.138$; $p = 0.207$).

3.3. Correlations with BMD. Correlations of LS/FN BMD with IGFBP-3 and IL-6 in all postmenopausal women are presented in Figure 2. IGFBP-3 was negatively correlated with LS BMD ($r = -0.286$; $p = 0.008$) and FN BMD ($r = 0.228$; $p = 0.036$). Similarly, IL-6 was also negatively correlated with LS BMD ($r = -0.267$; $p = 0.014$) and FN BMD ($r = -0.305$; $p = 0.005$).

3.4. Determinants of BMD. A stepwise multiple regression analysis was conducted to identify the determinants of BMD by including age, BMI, IGFBP-3, and IL-6 as independent variables (Table 2). The multiple regression model included variables whose p values were 0.2 or less. Multiple regression analysis showed that age ($\beta = -0.178$; $p = 0.015$) and circulating IGFBP-3 ($\beta = -0.304$; $p < 0.001$) and IL-6 ($\beta = -0.285$; $p = 0.004$) levels are independent predictors of BMD of the LS BMD ($R^2 = 0.38$). Meanwhile, age ($\beta = -0.126$; $p = 0.011$) and circulating IGFBP-3 ($\beta = -0.328$; $p = 0.003$) and IL-6 ($\beta = -0.301$; $p = 0.012$) levels were also independent predictors of BMD of the FN BMD ($R^2 = 0.32$). IGFBP-3 and IL-6 were the strongest predictors of BMD in postmenopausal women.

3.5. Diagnostic Values of IGFBP-3 and IL-6. The ROC curve determined diagnostic values of circulating IGFBP-3 and IL-6 levels for postmenopausal osteoporosis. As shown in Table 3, the AUC for circulating IGFBP-3 and IL-6 was 0.706 (95% CI 0.594–0.818) and 0.685 (95% CI 0.571–0.798), respectively. When circulating IGFBP-3 and IL-6 levels of 3.65 μg/ml and 0.205 IU/ml (Youden index 46.37 and 34.78) were taken as cut-off values, the sensitivity and specificity of their assay in the diagnosis of postmenopausal osteoporosis were 89.12% and 57.25% and 80.25% and 54.53%, respectively.

4. Discussion

The pathological features of osteoporosis include decreased bone formation, reduced bone mass and density, and destruction of bone microstructures. The main clinical symptoms are spinal deformity, diffuse bone pain, and fragility fractures. Currently, the risk factors of osteoporosis are relatively straightforward and multifactorial. Many studies have shown that smoking, lack of sunshine, a calcium-deficient diet, and some endocrine diseases increase the risk of osteoporosis in postmenopausal women [19]. However, there is no consensus on the relationship between circulating cytokines such as IGFBP-3 or IL-6 and new markers of bone turnover in postmenopausal women. This study compared the baseline characteristics of postmenopausal women in the normal and osteoporosis groups and found that the two groups had statistically significant differences in age; years since menopause; circulating IL-6, PTH, and IGFBP-3; LS BMD; and FN BMD. In our study, a significant correlation has also been found between circulating IGFBP-3, IL-6, and bone mineral density in postmenopausal women. Moreover, circulating IGFBP-3 and IL-6 levels were important potential diagnostic biomarkers for postmenopausal women with osteoporosis.

The estrogen hormone acts on the IL-6 promoter directly and on the IL-1 and TNF promoters indirectly and reduces the production of IL-1, IL-6, and TNF [20]. Postmenopausal osteoporosis is closely related to cellular senescence and inflammation caused by estrogen deficiency and is mainly characterized by enhanced osteoclast differentiation and bone resorption. Cellular inflammatory factors can regulate the formation of osteoclasts through the immune system and promote the occurrence and development of osteoporosis and pathological bone diseases. Previous studies have found that the knockout of the IL-6 gene could prevent bone loss after ovariectomy in mice. Applying IL-6 antagonists to transgenic mice with highly expressed IL-6 can prevent the occurrence of osteoporosis and growth retardation [21]. It has been reported that IL-6 can directly enhance osteoclast activity and inhibit its apoptosis, thereby prolonging osteoclast lifespan [22]. IL-6 can also promote osteoclastic activity and bone loss by activating the osteoprotegerin/receptor activator of nuclear factor kappa B ligand/ receptor activator of the nuclear factor kappa B (OPG/ RANKL/RANK) system, leading to osteoporosis [23]. In several animal models of chronic inflammation, estrogen can inhibit bone resorption and inflammation, reducing inflammation-mediated pain responses and the occurrence
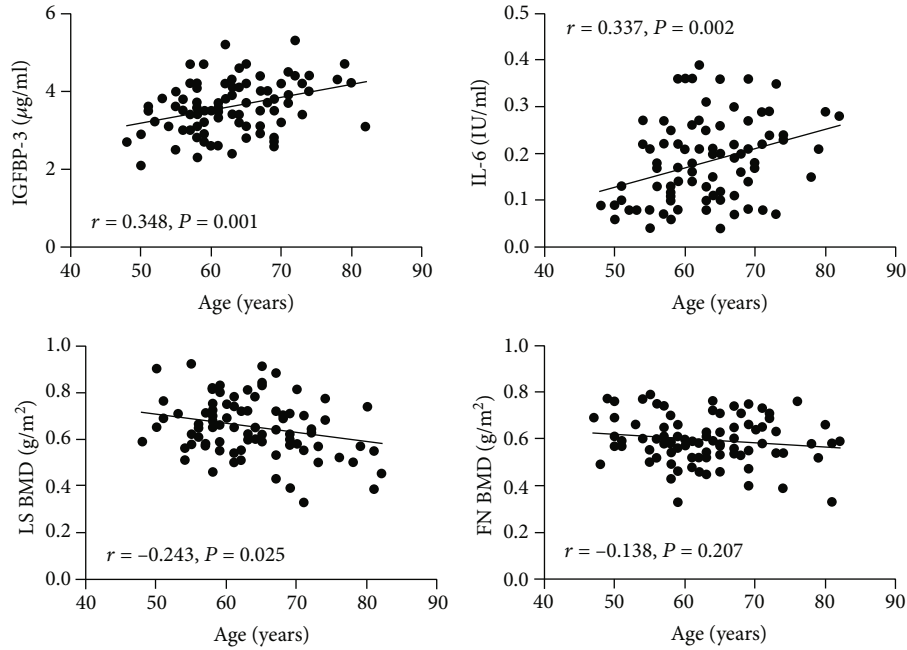
FIGURE 1: Correlations of age with IGFBP-3, IL-6, and BMD at the lumbar spine and femoral neck in all postmenopausal women. LS: lumbar spine; FN: femoral neck.
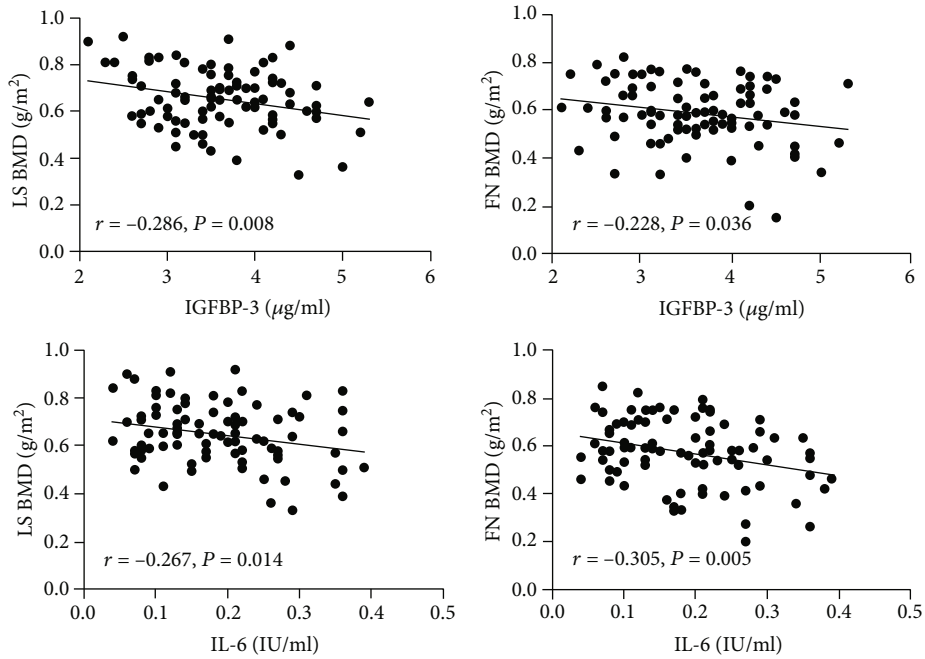
FIGURE 2: Correlations of LS BMD and FN BMD with IGFBP-3 and IL-6 in all postmenopausal women. LS: lumbar spine; FN: femoral neck.

TABLE 2: Stepwise multiple regression analysis between age, BMI, IGFBP-3, and IL-6 considering LS/FN BMD as dependent variables.

Variables	LS BMD			FN BMD		
	β	P	R^2	β	P	R^2
Age	-0.178	0.015	0.38	-0.126	0.011	0.32
IGFBP-3	-0.304	<0.001		-0.328	0.003	
IL-6	-0.285	0.004		-0.301	0.012	

BMI: body mass index; IL-6: interleukin 6; LS: lumbar spine; FN: femoral neck.

of neuroinflammatory diseases [24]. Our present findings are compatible with those of previous studies. There was a significant increase in IL-6 levels in the osteoporosis group compared to the control group in the current study. It was both negatively related to age and LS or FN BMD. Therefore, postmenopausal osteoporosis is significantly impacted by IL-6. Thus, exploring the relationship between IL-6, other inflammatory factors, and estrogen will deepen the understanding of the pathogenesis of osteoporosis.

TABLE 3: Diagnostic value of IGFBP-3 and IL-6 for osteoporosis ($n = 85$).

Variables	AUC (95% CI)	Cut-off values	Sensitivity	Specificity	Youden index
IGFBP-3	0.706 (0.594-0.818)	3.65	89.12	57.25	46.37
IL-6	0.685 (0.571-0.798)	0.205	80.25	54.53	34.78

AUC (95%): area under the receiver operating characteristic curve (95% confidence interval).

As one of the most abundant IGFBP families (IGFBP-1~6) in blood circulation, IGFBP-3 is primarily produced in the liver and can transport more than 75% of IGF [25]. The physiological functions of IGFBP-3 include IGF transport and the regulation of the interaction between IGF and its receptors. IGFBP-3 can regulate the bioavailability of IGF by increasing its half-life and altering its biological activity on target tissues, thereby exerting physiological effects in an IGF-1-dependent or IGF-1-independent manner [26]. IGF-1 is a growth-promoting peptide substance induced by growth hormone, and it is also the most abundant growth factor in osteoblasts. Previous studies found that IGFBP-3 can antagonize the effect of IGF by combining with IGF to reduce the amount of free IGF. Therefore, it has antiproliferative, antimitotic, and proapoptotic physiological effects [27]. Our results indicated that the osteoporosis group had significantly high levels of IGFBP-3 than the control group.

Meanwhile, the circulating level of IGFBP-3 increased with age and was negatively related to both LS BMD and FN BMD. However, the results of some previous studies were inconsistent with our findings. Yang et al. found that IGFBP-3 could activate the growth factor signaling pathway and exert its inhibitory effect on osteoclasts [28]. Govoni et al. reported that the expression level of IGFBP-3 was significantly reduced with the aggravation of postmenopausal osteoporosis in female patients [29]. IGFBP-3 has both protective and destructive effects on the maintenance of bone mass. First, IGFBP-3 can act on target cells, including osteoblasts, by inducing apoptosis or programmed cell death [25]. Second, IGFBP-3 can inhibit the osteoblast differentiation induced by BMP-2 [9]. In addition, the overexpression of IGFBP-3 caused by increased RNA stability might be associated with aging-induced osteoporosis [8]. These findings suggest that IGFBP-3 promotes osteoporosis differently, but the specific mechanism needs to be explored.

According to the current stepwise multiple regression analysis, the independent predictors of LS and FN BMD were circulating IGFBP-3 and IL-6, which indicated that circulating cytokines were essential for preventing bone loss and osteoporosis. Other variables, including age, years since menopause, and PTH, did not predict BMD in postmenopausal women. However, they were significantly different in the normal and osteoporosis groups. An analysis of ROC curves showed that circulating levels of IGFBP-3 and IL-6 could be identified as reliable diagnostic biomarkers for postmenopausal osteoporosis.

There were several limitations in our study. First, our cross-sectional research was only observational at a single time, and our correlative data cannot be treated as definitive evidence of a causal relationship. Second, our study involved only a Chinese population at a single hospital, and there is a potential for selection bias in larger groups. Last, our sample size was not large, which might limit multiple variable analysis. Therefore, a prospective study or randomized controlled trial with a large sample size is recommended.

5. Conclusions

In this cross-sectional study of postmenopausal women, we found negative correlations between IGFBP-3, IL-6, and BMD in the lumbar spine and femoral neck. Circulating levels of IGFBP-3 and IL-6 explained between 28.5% and 32.8% of the variation of LS/FN BMD. Circulating measurements of IGFBP-3 and IL-6 might be essential predictors of postmenopausal osteoporosis and could predict osteoporotic fracture.

Data Availability

The datasets used during the current study are available from the corresponding author on reasonable request.

Ethical Approval

The ethics committee of the First Affiliated Hospital of Soochow University approved this study.

Consent

Written informed consent for publication was obtained from patients.

Conflicts of Interest

All authors declare that they have no conflict of interest.

Authors' Contributions

Shouqian Dai contributed to the study design, Xiu Shi and Jingjing Jiang prepared the manuscript, Ru Hong collected the data, Feng Xu performed the data analysis, and all authors read and approved the manuscript. Xiu Shi, Jingjing Jiang, and Ru Hong contributed equally to this work. Xiu Shi, Jingjing Jiang, and Ru Hong are the co-first authors.

Acknowledgments

References

[1] J. Blake, F. A. Cosman, E. M. Lewiecki, M. R. McClung, J. Pinkerton, and M. Shapiro, "Management of osteoporosis in postmenopausal women: the 2021 position statement of the North American Menopause Society," *Menopause*, vol. 28, no. 9, pp. 973–997, 2021.

[2] Y. Miyauchi, Y. Sato, T. Kobayashi et al., "HIF1α is required for osteoclast activation by estrogen deficiency in postmenopausal osteoporosis," *Proceedings of the National Academy of Sciences of the United States of America*, vol. 110, no. 41, pp. 16568–16573, 2013.

[3] D. M. Black and C. J. Rosen, "Postmenopausal osteoporosis," *New England Journal of Medicine*, vol. 374, no. 3, pp. 254–262, 2016.

[4] S. Abdolalipour and M. Mirghafourvand, "Effect of education on preventive behaviors of osteoporosis in adolescents: a systematic review and meta-analysis," *International Quarterly of Community Health Education*, vol. 41, no. 3, pp. 325–347, 2021.

[5] A. Mancini, E. Vergani, C. Bruno et al., "Relationships between thyroid hormones, insulin-like growth factor-1 and antioxidant levels in hypothalamic amenorrhea and impact on bone metabolism," *Hormone and Metabolic Research*, vol. 51, no. 5, pp. 302–308, 2019.

[6] N. M. Al-Daghri, A. Manousopoulou, M. S. Alokail et al., "Sex-specific correlation of IGFBP-2 and IGFBP-3 with vitamin D status in adults with obesity: a cross-sectional serum proteomics study," *Nutrition & Diabetes*, vol. 8, no. 1, p. 54, 2018.

[7] J. Boker, H. Volzke, M. Nauck, A. Hannemann, and N. Friedrich, "Associations of insulin-like growth factor-I and insulin-like growth factor binding protein-3 with bone quality in the general adult population," *Clinical Endocrinology*, vol. 88, no. 6, pp. 830–837, 2018.

[8] S. Wang, E. J. Moerman, R. A. Jones, R. Thweatt, and S. Goldstein, "Characterization of IGFBP-3, PAI-1 and SPARC mRNA expression in senescent fibroblasts," *Mechanisms of Ageing and Development*, vol. 92, no. 2-3, pp. 121–132, 1996.

[9] K. Eguchi, Y. Akiba, N. Akiba, M. Nagasawa, L. F. Cooper, and K. Uoshima, "Insulin-like growth factor binding protein-3 suppresses osteoblast differentiation via bone morphogenetic protein-2," *Biochemical and Biophysical Research Communications*, vol. 507, no. 1-4, pp. 465–470, 2018.

[10] A. Latourte, C. Cherifi, J. Maillet et al., "Systemic inhibition of IL-6/Stat3 signalling protects against experimental osteoarthritis," *Annals of the Rheumatic Diseases*, vol. 76, no. 4, pp. 748–755, 2017.

[11] S. X. Zheng, Y. Vrindts, M. Lopez et al., "Increase in cytokine production (IL-1β, IL-6, TNF-α but not IFN-γ, GM-CSF or LIF) by stimulated whole blood cells in postmenopausal osteoporosis," *Maturitas*, vol. 26, no. 1, pp. 63–71, 1997.

[12] C. Scheidt-Nave, H. Bismar, G. Leidig-Bruckner et al., "Serum interleukin 6 is a major predictor of bone loss in women specific to the first decade past menopause," *The Journal of Clinical Endocrinology and Metabolism*, vol. 86, no. 5, pp. 2032–2042, 2001.

[13] J. A. Kanis, L. J. Melton 3rd, C. Christiansen, C. C. Johnston, and N. Khaltaev, "The diagnosis of osteoporosis," *Journal of Bone and Mineral Research*, vol. 9, no. 8, pp. 1137–1141, 1994.

[14] A. H. Alghadir, F. A. Aly, and S. A. Gabr, "Effect of moderate aerobic training on bone metabolism indices among adult humans," *Pakistan Journal of Medical Sciences*, vol. 30, no. 4, pp. 840–844, 2014.

[15] A. H. Alghadir, S. A. Gabr, E. S. Al-Eisa, and M. H. Alghadir, "Correlation between bone mineral density and serum trace elements in response to supervised aerobic training in older adults," *Clinical Interventions in Aging*, vol. 11, pp. 265–273, 2016.

[16] W. F. Blum, M. B. Ranke, K. Kietzmann, E. Gauggel, H. J. Zeisel, and J. R. Bierich, "A specific radioimmunoassay for the growth hormone (GH)-dependent somatomedin-binding protein: its use for diagnosis of GH deficiency," *The Journal of Clinical Endocrinology and Metabolism*, vol. 70, no. 5, pp. 1292–1298, 1990.

[17] T. Sugimoto, D. Nakaoka, M. Nasu, M. Kanzawa, T. Sugishita, and K. Chihara, "Effect of recombinant human growth hormone in elderly osteoporotic women," *Clinical Endocrinology*, vol. 51, no. 6, pp. 715–724, 1999.

[18] T. Sugimoto, D. Nakaoka, M. Nasu, M. Kanzawa, T. Sugishita, and K. Chihara, "Age-dependent changes in body composition in postmenopausal Japanese women: relationship to growth hormone secretion as well as serum levels of insulin-like growth factor (IGF)-I and IGF-binding protein-3," *European Journal of Endocrinology*, vol. 138, no. 6, pp. 633–639, 1998.

[19] L. M. M. Rossi, R. M. Copes, L. C. Dal Osto, C. Flores, F. V. Comim, and M. O. Premaor, "Factors related with osteoporosis treatment in postmenopausal women," *Medicine (Baltimore)*, vol. 97, no. 28, article e11524, 2018.

[20] R. Pacifici, "Estrogen, cytokines, and pathogenesis of postmenopausal osteoporosis," *Journal of Bone and Mineral Research*, vol. 11, no. 8, pp. 1043–1051, 1996.

[21] F. De Benedetti, P. Pignatti, M. Vivarelli et al., "In vivo neutralization of human IL-6 (hIL-6) achieved by immunization of hIL-6-transgenic mice with a hIL-6 receptor antagonist," *Journal of Immunology*, vol. 166, no. 7, pp. 4334–4340, 2001.

[22] O. A. Adebanjo, B. S. Moonga, T. Yamate et al., "Mode of action of interleukin-6 on mature osteoclasts. Novel interactions with extracellular Ca^{2+} sensing in the regulation of osteoclastic bone resorption," *The Journal of Cell Biology*, vol. 142, no. 5, pp. 1347–1356, 1998.

[23] Y. Y. Kong, H. Yoshida, I. Sarosi et al., "OPGL is a key regulator of osteoclastogenesis, lymphocyte development and lymph-node organogenesis," *Nature*, vol. 397, no. 6717, pp. 315–323, 1999.

[24] A. R. Gintzler, E. M. Storman, and N. J. Liu, "Estrogens as arbiters of sex-specific and reproductive cycle-dependent opioid analgesic mechanisms," *Vitamins and Hormones*, vol. 111, pp. 227–246, 2019.

[25] S. Jogie-Brahim, D. Feldman, and Y. Oh, "Unraveling insulin-like growth factor binding protein-3 actions in human disease," *Endocrine Reviews*, vol. 30, no. 5, pp. 417–437, 2009.

[26] M. Gao, B. Zhu, Z. Xu et al., "Association between acromegaly and a single nucleotide polymorphism (rs2854744) in the IGFBP3 gene," *BMC Medical Genetics*, vol. 19, no. 1, p. 182, 2018.

[27] M. B. Ranke, "Insulin-like growth factor binding-protein-3 (IGFBP-3)," *Best Practice & Research. Clinical Endocrinology & Metabolism*, vol. 29, no. 5, pp. 701–711, 2015.

[28] J. Yang, Q. He, Y. Wang et al., "Gegen Qinlian Decoction ameliorates type 2 diabetes osteoporosis via IGFBP3/MAPK/NFATc1 signaling pathway based on cytokine antibody array," *Phytomedicine*, vol. 94, article 153810, 2022.

[29] K. E. Govoni, D. J. Baylink, and S. Mohan, "The multifunctional role of insulin-like growth factor binding proteins in bone," *Pediatric Nephrology*, vol. 20, no. 3, pp. 261–268, 2005.

Research Article

Ameliorative Effect of Curcumin Nanoparticles against Monosodium Iodoacetate-Induced Knee Osteoarthritis in Rats

Hadeer M. Hamdalla [iD],[1] **Rasha R. Ahmed** [iD],[1] **Sanaa R. Galaly** [iD],[1] **Ibrahim A. Naguib** [iD],[2] **Badrah S. Alghamdi** [iD],[3,4] **Osama M. Ahmed** [iD],[5] **Ahmed Farghali** [iD],[6] **and Manal Abdul-Hamid** [iD][1]

[1]Cell Biology, Histology and Genetics Division, Department of Zoology, Faculty of Science, Beni-Suef University, P.O. Box 62521, Beni-Suef, Egypt
[2]Department of Pharmaceutical Chemistry, College of Pharmacy, Taif University, P.O. Box 11099, Taif 21944, Saudi Arabia
[3]Department of Physiology, Neuroscience Unit, Faculty of Medicine, King Abdulaziz University, Jeddah 22252, Saudi Arabia
[4]Pre-Clinical Research Unit, King Fahd Medical Research Center, King Abdulaziz University, Jeddah, Saudi Arabia
[5]Physiology Division, Zoology Department, Faculty of Science, Beni-Suef University, P.O. Box 62521, Beni-Suef, Egypt
[6]Department of Material Science and Nanotechnology, Faculty of Postgraduate Studies for Advanced Science, Beni-Suef University, Egypt

Correspondence should be addressed to Badrah S. Alghamdi; basalghamdi@kau.edu.sa
and Manal Abdul-Hamid; medo_bio@yahoo.com

Aim. This study is aimed at evaluating the use of curcumin-loaded polylactic-co-glycolic acid nanoparticles (CUR-loaded PLGA NPs) as a treatment against monosodium iodoacetate- (MIA-) induced knee OA. *Materials and Methods.* Eighteen rats were assigned to three groups ($n = 6$), namely, normal control group that received intra-articular injections (IAIs) of saline, an OA control group that received an IAIs of MIA ($2 \, mg/50 \, \mu L$), and a treatment group (MIA+CUR-loaded PLGA NPs) that received IAIs of CUR-loaded PLGA NPs ($200 \, mg/kg$ b.wt). *Results.* The CUR NP treatment against knee OA alleviated radiographic alternations and histopathological changes and inhibited the upregulation in the serum levels of interleukin-1β, tumor necrosis factor-α, interleukin-6, and transforming growth factor-beta and the downregulation in interleukin-10. CUR NP-treated joints also decreased the mRNA expression of nuclear factor-kappa B and inducible nitric oxide synthase and the protein expression of matrix metalloproteinase-13 and caspase-3. Finally, CUR-loaded PLGA NP treatment mitigated the loss of type II collagen, which resulted in a significant reduction in malondialdehyde level and increased the glutathione content and superoxide dismutase activity compared with that of the OA group. *Conclusion.* This study demonstrated that the administration of CUR NPs could provide effective protection against MIA-induced OA and knee joint histological deteriorated changes due to its anti-inflammatory, antioxidant, and antiapoptotic properties.

1. Introduction

Osteoarthritis (OA) is a progressive and degenerative illness that happens in the whole joint and can result in articular cartilage degeneration, subchondral bone thickening, synovium inflammation, osteophyte formation, and meniscal degeneration [1]. Treatments for OA are mainly divided into three categories: nonpharmacological treatments, pharmacological treatments limited to analgesics and/or nonsteroidal anti-inflammatory drugs (NSAIDs), and surgical treatments [2]. Current available medications for OA, except joint replacement surgery, are essentially palliative and cannot hinder articular cartilage degradation [3]. Furthermore, long-term use of NSAIDs can cause adverse gastrointestinal,

renal, and cardiovascular effects [4]. This calls for the development of a structural OA disease drug that is safe, provides symptomatic relief, and hinders the progression of cartilage degeneration.

Curcumin (CUR) (diferuloylmethane), a polyphenol compound obtained from turmeric, is a naturally available molecule that has robust anticatabolic, antioxidant, anti-inflammatory, and antirheumatic properties [5–7]. Accordingly, CUR seems to be a promising approach in OA therapy. Nevertheless, the therapeutic efficiency of CUR is extremely restricted because of its low water solubility and limited oral bioavailability [8]. Nevertheless, studies have reported that CUR's biological activity could be efficiently enhanced using nanotechnology-based drug delivery [9, 10]. Various studies have explored CUR nanoparticles (NPs) and CUR encapsulation with various substances such as liposomes and polymers to overcome its inherent drawbacks [11, 12]. Polylactic-co-glycolic acid (PLGA) is considered as an effective biodegradable polymeric NPs that was authorized by US Food and Drug Administration for use in drug delivery systems due to its low toxicity, controlled and sustained-release properties, and biocompatibility with tissue and cells [13, 14].

On the other hand, the intra-articular route for drug delivery has significant potency and fewer systemic side effects compared to that of oral delivery [15]. Accordingly, this study was designed to explore the possible feasibility of the intra-articular injections (IAIs) of CUR-loaded PLGA NPs to treat monosodium iodoacetate- (MIA-) induced knee OA in a rat model.

2. Materials and Methods

2.1. Animals. This study used mature male Wistar rats weighing 130–150 g, which were kept in a standard 12 : 12 light/dark cycle in well-ventilated rooms. One week before initiating the experiments, the rats were housed in sterilized cages to be adapted to the laboratory with free access to water and pellets. All methods for handling, use, and euthanasia of the animals in this study were certified by the Experimental Animal Ethics Committee of Faculty of Science, Beni-Suef University, Egypt, and the ethical authorization number is BSU/FS/2018/15.

2.2. Induction of OA. MIA was obtained from Sigma-Aldrich (St. Louis, MO, USA) and dispersed in sterile saline. Under diethyl ether anesthesia, all rats, except the normal control group, received a single intra-articular injection of 50 μL of saline containing MIA (2 mg) into the left side knee joint, as previously described by Ragab et al. [16].

2.3. Preparation of CUR-Loaded PLGA NPs. PLGA, which is poly (D, L-lactide-co-glycolide) with lactide: glycolide 50 : 50, molecular weight (24,000), inherent viscosity (1.13 dL/g), and formula $[C_3H_4O_2]_x[C_2H_2O_2]y$, was obtained from Sigma-Aldrich (St. Louis, MO, USA). Besides, curcumin, chloroform, polyvinyl alcohol (PVA; MW 30,000–70,000), and ethanol were all purchased from Sigma-Aldrich (St. Louis, MO, USA) as well.

CUR-loaded PLGA NPs were synthesized by solvent solid-in-oil-in-water emulsion (s/o/w) evaporation based on the method published by Niazvand et al. [17]. The PLGA/chloroform solution (oil phase) was prepared by dissolving 60 mg of PLGA in 1 mL of chloroform. Then, 6 mg of CUR was added to the solution and sonicated, resulting in a solid/oil emulsion. Thereafter, ethanol and 2% PVA (1 : 1) was added to the emulsion and sonicated for 10 min to produce a solid/oil/weight (s/o/w) emulsion. The s/o/w emulsion was further sonicated and agitated by a magnetic stirrer for 5–6 h to evaporate the solvent (chloroform). The sample was subsequently centrifuged for 10 min at 15,000 g before being rinsed three times using distilled water. The sample was allowed to freeze-dry for 24 h to get a dry powder. The obtained NPs were kept at 4°C.

2.4. Characterization of CUR-Loaded PLGA NPs. The surface morphology of CUR-loaded PLGA NPs was investigated with a scanning electron microscope (Zeiss Sigma 500 VP Analytical FE-SEM, Carl Zeiss Germany) and X-ray diffraction (XRD) analysis (model no: 202964, Pananlytical Empyrean company). In addition, their zeta potential and size were detected by Malvern (Malvern Instruments Ltd) following the method by Moaty et al. [18].

2.5. Experimental Design. As described in Figure 1, the rats were randomly allocated into three groups ($n = 6$). At 0, 14, 18, 22, and 26 days, the normal control group took IAIs of 50 μL of saline into the left side knee joint, whereas the other two groups received IAIs of MIA (2 mg) into the left side knee joints on day 0. Then, rats in the OA control group were given saline IA injections on days 14, 18, 22, and 26, while the treatment group (MIA+CUR-loaded PLGA NPs) received intra-articular injections of CUR-loaded PLGA NPs at a dose of 200 mg/kg. MIA and CUR-loaded PLGA NPs injection doses were based on the previous studies by Ragab et al. [16] and Niazvand et al. [17], respectively.

2.6. Knee Diameter Measurement (Swelling). A manual caliper was used to assess the variations in the anterior-posterior diameter values of the knee joints among all groups [19]. The measurements were obtained on days 0, 7, 14, 21, and 28 after MIA injection.

2.7. X-Ray Examination. On day 30 post-MIA injection, animals from all groups were anesthetized using diethyl ether, and both hind limbs were extended and fixed on the table with tape. Radiographs of the left knees (anterior-posterior position) were captured using an X-ray device with a 60 cm focal film distance at 55 kV and 3 mA.

2.8. ELISA Evaluation. Inflammatory status was evaluated in all groups by measuring the serum proinflammatory cytokines, tumor necrosis factor-α (TNF-α) (cat# MBS697379), transforming growth factor-beta (TGF-β) (cat # MBS8819920), interleukin- (IL-) 6 (cat# MBS7727039), and IL-1β (cat# MBS697409) and the anti-inflammatory cytokine IL-10 (cat# MBS2707969) using MyBioSource Inc., San Diego, CA, USA, following the manufacturer's instructions.
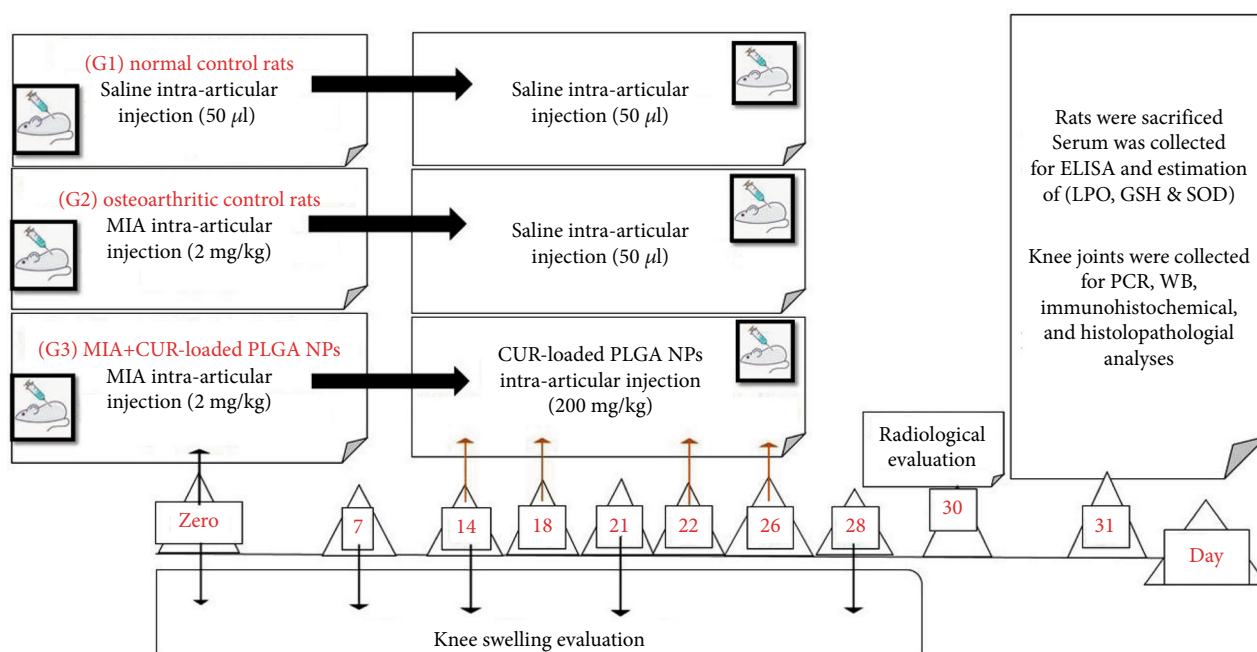
FIGURE 1: Timeline of the experiment showing the animal groupings, osteoarthritis (OA) induction on day 0, treatment on days 14, 18, 22, and 26, and animal euthanasia on day 31.

2.9. Evaluation of Antioxidant Markers and Oxidative Stress

2.9.1. Determination of Lipid Peroxidation Level.
Malondialdehyde (MDA) that was generated through the breakdown of polyunsaturated fatty acids was used as an index for assessment of the extent of lipid peroxidation in serum following the method of Preuss et al. [20].

2.9.2. Determination of Glutathione (GSH) Content and Superoxide Dismutase (SOD) Activity.
GSH content in serum was assayed following the procedure of Beutler et al. [21], while the detection of serum SOD relied on the enzyme's capacity to prevent the phenazine methosulphate-mediated decrease of nitroblue tetrazolium dye according to Nishikimi et al. [22].

2.10. Quantitative Reverse Transcription Polymerase Chain Reaction (qRT-PCR) Assay.
The mRNA levels of nuclear factor-kappa B (NF-κB), type II collagen, and inducible nitric oxide synthase (iNOS) were determined by real-time qRT-PCR, for which the Qiagen tissue extraction kit (Qiagen, USA) was applied for the total RNA isolation. Then, 0.5–2 μg total RNA was applied for cDNA synthesis utilizing a Fermentas kit (USA). Applied Biosystem software version 3.1 (StepOne, USA) was utilized for real-time qPCR amplification and analysis. The qRT-PCR assay was done with primer sets optimized for the annealing temperature. The sequences of the primers are listed in Table 1.

2.11. Western Blot Assay.
The impact of CUR-loaded PLGA NPs on the protein expression levels of NF-κB50 and NF-κB65 and cleaved caspase-3 was investigated using knee samples maintained at 80°C. Briefly, all samples were homogenized in a radio-immunoprecipitation (RIPA) buffer supplemented with proteinase inhibitors and centrifuged, and the protein concentration was assayed with Bradford assay in the obtained clear supernatant. Proteins (30 mg) were separated on SDS-PAGE, moved to nitrocellulose membranes, and blocked with TRIS using 3% bovine serum albumin and a Tween 20 (TBST) buffer at ambient temperature for 1 hour. Subsequently, membranes were left in the incubator with primary antibodies against NFκBp50 (Cat# 14-6732-81; eBioscience), NF-κBp65 (Cat# 14-6731-81, eBioscience), and cleaved caspase-3 (cat # PA5-114687, Thermo Fisher Scientific). Following the washing with TBST, the prepared membranes were left in the incubator with the corresponding secondary antibodies, after which a chemiluminescence kit (BIORAD, USA) was applied. The developed blots were scanned, and image analysis software was utilized to measure the obtained band intensity of the targeted proteins against the control sample after being normalized by beta-actin on a Chemi Doc MP imager.

2.12. Histopathological Analysis.
The left knee joints were assembled from all groups, followed by fixing in 10% neutral buffered formalin for 48 hours, and then decalcified using 20% EDTA for two weeks. The joints were excised sagittal and processed to get 4–6 μm paraffin-embedded sections. Obtained sections were then stained using hematoxylin and eosin (H&E) before being examined under a light microscope.

2.13. Immunohistochemistry Analysis.
The sections were stained following the streptavidin-biotin-peroxidase staining method [23]. Paraffin tissue sections (4–6 μm) were deparaffinized in xylene and then rehydrated in ethanol.

TABLE 1: Primer sequences for NF-κB, iNOS, and type II collagen mRNA.

Target gene	Primer sequence
NF-κB	Forward primer: 5′-CATTGAGGTGTATTTCACGG-3′ Reverse primer: 5′-GGCAAGTGGCCATTGTGTTC-3′
iNOS	Forward primer: 5′-GACCAGAAACTGTCTCACCTG-3′ Reverse primer: 5′-CGAACATCGAACGTCTCACA-3′
Type II collagen	Forward primer: 5′-GAGTGGAAGAGCGGAGACTACTG-3′ Reverse primer: 5′-CTCCATGTTGCAGAAGACTTTCA-3′
Beta-actin	Forward primer: 5′-TGTTTGAGACCTTCAACACC-3′ Reverse primer: 5′-CGCTCATTGCCGATAGTGAT-3′

There were six samples in each group, and data are described as means ± SEM. For each parameter, means (which have different superscript symbols) are statistically significant at $P < 0.05$.

(a)   (b)
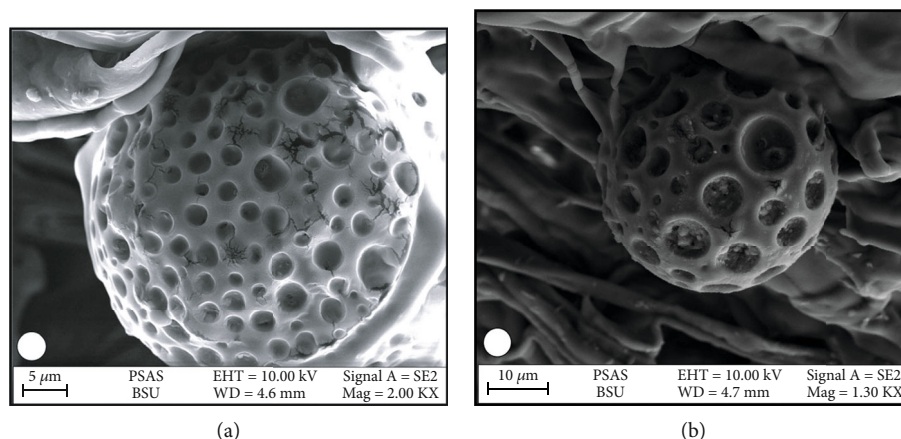
FIGURE 2: Scanning electron micrograph showing (a) PLGA and (b) CUR-loaded PLGA NPs.

Endogenous peroxidase and nonspecific binding sites for antibodies were suppressed by treating the sections for 10 min with hydrogen peroxide (0.3%) and for 20 min with 5% normal bovine serum (1 : 5 diluted tris buffer saline [TRIS]) at ambient temperature, respectively. Obtained sections were rinsed with PBS, and then, 10% normal goat serum was applied for 30 min to minimize nonspecific binding. Obtained sections were then incubated in anti MMP13 primary antibody (cat no: GB11247; Servicebio, China) for 1 h, followed by incubation in streptavidin horseradish peroxidase (Dako-K0690) and biotinylated secondary antibody (Dako Universal LSAB Kit) for 15 min and then incubated in 3-diaminobenzidine tetrahydrochloride (Sigma-D5905; Sigma-Aldrich Company Ltd., Gillingham, UK) substrate kit for 10 min to achieve immunolabelling. Afterward, the nuclei were stained using Harry's hematoxylin stain, dehydrated ethanol, cleared in xylene, and then mounted in DPX. Antibody binding was observed with high-power light microscopy.

2.14. Statistical Analysis. Statistical analyses were performed using SPSS software version 25.0 (SPSS Inc., Chicago, IL, USA). All results are presented as means (M) ± standard errors of means (SEMs), with $P < 0.05$ meaning a statistically significant difference.
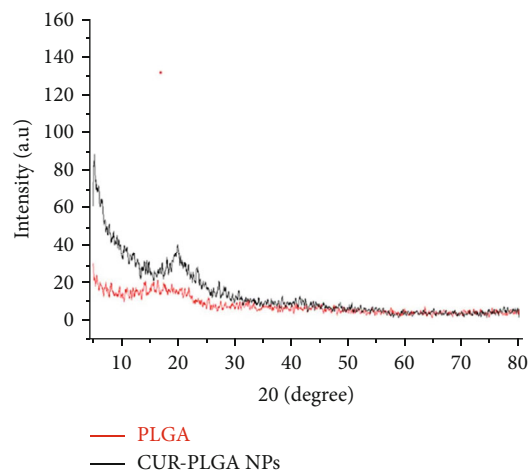
FIGURE 3: XRD of PLGA and CUR-loaded PLGA NPs.

3. Results

3.1. Characterization of CUR-Loaded PLGA NPs. In this study, the prepared CUR-loaded PLGA NPs were shown using a scanning electron microscope micrograph (Figure 2), which were spherically shaped. Meanwhile, the XRD pattern of CUR-loaded PLGA NPs (Figure 3) showed an absence of
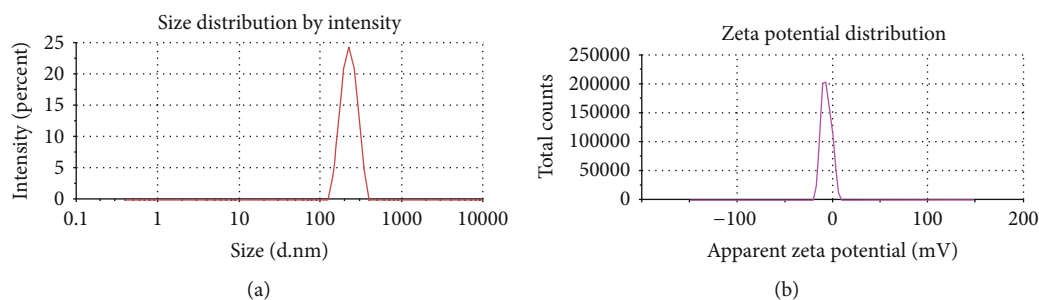
FIGURE 4: Illustration of the (a) size and (b) zeta potential of CUR-loaded PLGA nanoparticles.
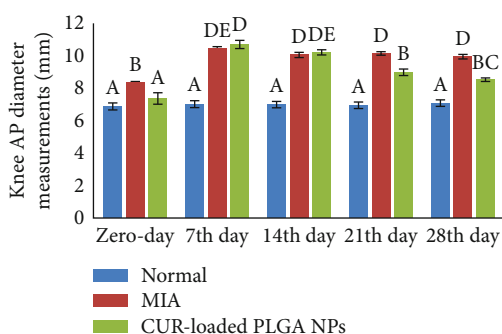
FIGURE 5: Knee anterior-posterior diameter measurements in the normal control, monosodium iodoacetate (MIA), and MIA+CUR-loaded PLGA NP groups. At each period, the means, which have different symbols (letters), are significantly different at $P < 0.05$.

marked crystalline domains in CUR-loaded PLGA NPs, implying that these NPs were in the disordered-crystalline phase or the amorphous or the solid-state solubilized form in the polymer matrix. Further, the average size (Figure 4(a)) and zeta potential (Figure 4(b)) of the CUR-loaded PLGA NPs were 265.2 nm and −6.86 mV, respectively.

3.2. Effect of CUR-Loaded PLGA NPs on Swelling (Knee Diameter Measurements). As shown in Figure 5, MIA induced an increase in the knee diameters of the OA control and treatment groups when compared to the measurements before the injection. Nevertheless, two weeks of CUR-loaded PLGA NP IAIs markedly reduced swelling in the left knee joints.

3.3. Effect of CUR-Loaded PLGA NPs Using X-Ray Imaging. Radiographic detection was carried out to observe changes in the knee joints after CUR-loaded PLGA NP treatment. Compared to that of the normal control group (Figure 6(a)), knee joints in the OA group (Figure 6(b)) had a narrow joint space and deformed articular surface. Meanwhile, the CUR-loaded PLGA NP treatment considerably hindered MIA-induced knee OA progression and attenuated joint destruction, in that the joints of the treated group (Figure 6(c)) showed a little degree of narrowing, and no obvious sclerosis and osteophyte formation was detected.

3.4. Effect of CUR-Loaded PLGA NPs on the Serum Levels of TNF-a, IL-1β, IL-6, TGF-β, and IL-10. The MIA-treated group (Table 2) showed a significant increase in serum TNF-a, IL-6, IL-1β, and TGF-β levels and a decrease in IL-10 levels compared to those of the normal control group ($P < 0.05$). Meanwhile, the OA knee joints from the treatment group showed a marked reduction in TNF-a, IL-6, IL-1β, and TGF-β levels, along with an elevation in IL-10 levels as compared to those of the OA group.

3.5. Effect of CUR-Loaded PLGA NPs on Lipid Peroxidation and Antioxidant Status. The enhanced level of serum lipid peroxidation product (MDA) in MIA-treated knee joints was accompanied by a substantial reduction in GSH level and SOD activity. Meanwhile, CUR-loaded PLGA NP IAIs significantly lowered the level of MDA and boosted the GSH content and SOD activity (Table 3).

3.6. Effect of CUR-Loaded PLGA NPs on NF-κB, iNOS, and Type II Collagen mRNA Expression. OA knee joints showed a marked ($P < 0.05$) elevation in the mRNA expression levels of NF-κB and iNOS, along with a significant decline in type II collagen compared with those of the normal group (Table 4). Moreover, OA knee joints treated with CUR exhibited a significant ($P < 0.05$) downregulation in NF-κB and iNOS levels and inhibited the loss of type II collagen mRNA expression level in comparison with that in OA control rats.

3.7. Effect of CUR-Loaded PLGA NPs on the Protein Expression Levels of NF-κB p50 and NF-κB p65. Western blot analysis shows that the protein expression levels of NF-κB p50 and NF-κB p65 (Figures 7) were elevated post-MIA administration when compared with the normal control. However, CUR-loaded PLGA NP treatment significantly diminished the protein expression of NF-κB p50 and NF-κB p65 in the OA knee joints as compared to the MIA group.

3.8. Effect of CUR-Loaded PLGA NPs on Cleaved Caspase-3 Protein Expression. The protein level of cleaved caspase-3 (Figure 8) in the knee joint was estimated with western blotting. OA rats demonstrated a marked increase in cleaved caspase-3 level relative to those in the normal control group, while OA rats injected with CUR-loaded PLGA NPs revealed a marked downregulation in the cleaved caspase-3 level compared with those in the OA control group.

3.9. Effect of CUR-Loaded PLGA NPs on the Histopathological Evaluation. H&E sections of the articular

(a)

(b)

(c)
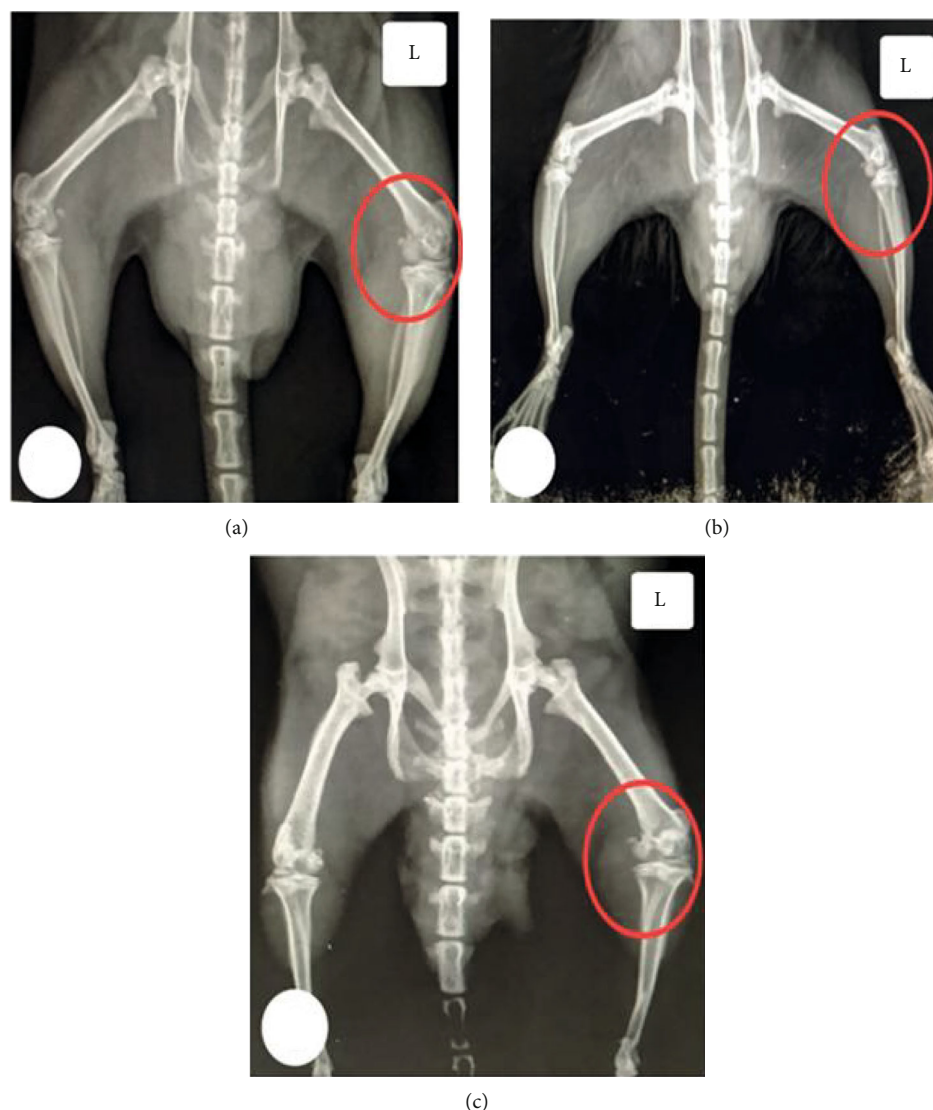
FIGURE 6: X-ray image showing the left knee joints (L) of all groups: (a) the normal knee joints; (b) MIA-treated knee joints depicting radiographic alternations such as erosion of the cartilage surface, osteophytes, and joint space narrowing; and (c) MIA+CUR-loaded PLGA NP-treated group, with joints nearly similar to those of the normal control.

TABLE 2: Effect of CUR-loaded PLGA NPs on the serum levels of TNF-α, IL-1β, IL-6, TGF-β, and IL-10 in MIA-induced OA in rats.

Groups	Parameters				
	TNF-α (pg/mL)	IL-1β (pg/mL)	IL-6 (pg/mL)	TGF-β (pg/mL)	IL-10 (pg/mL)
Normal control	20.22 ± 1.1[a]	47.05 ± 2.96[a]	62.78 ± 2.92[a]	115.36 ± 1.36[a]	324.67 ± 10.28[c]
MIA	261.19 ± 3.47[c]	136.07 ± 4.17[c]	188.9 ± 1.1[c]	260.55 ± 5.26[c]	122.87 ± 4.04[a]
MIA+CUR-loaded PLGA NPs	57.02 ± 1.23[b]	65.57 ± 2.92[b]	94.88 ± 2.62[b]	146.25 ± 5.61[b]	283.57 ± 4.36[b]

There were six samples in each group, and data are described as means ± SEM. For each parameter, means, which have different superscript symbols, are statistically significant at $P < 0.05$.

cartilage showed that chondrocytes in the normal control group were placed neatly, and the dyeing was uniform (Figure 9(a)). In the OA control group, obtained sections had a myriad of pathological alternations such as cracks, fibrillation, disorderly arranged cells, empty lacunae, hyperchromatic nuclei, and a magnificent reduction in the number of chondrocytes (Figures 9(b)–9(d)). In contrast, the MIA +CUR-loaded PLGA NP group (Figures 9(e)) showed a notable decrease in the severity of cartilage degradation, as the CUR treatment offered effective protection against OA progression. MIA+CUR-loaded PLGA NP-treated cartilage appeared to have a smooth surface, orderly arranged chondrocytes, less loss of cells, and intact subchondral bone compared to those of MIA-treated cartilages without treatment.

TABLE 3: Effect of CUR-loaded PLGA NPs on the serum MDA and GSH levels and SOD activity in MIA-induced OA rats.

| Groups | Parameters | | |
	MDA (nmol/mL)	GSH (mg/dL)	SOD (U/mL)
Normal control	0.84 ± 0.07^a	210.70 ± 10.40^c	263.11 ± 11.71^c
MIA	2.095 ± 0.37^c	9.2213 ± 0.66^a	55.09 ± 9.97^a
MIA+CUR-loaded PLAGA NPs	0.89 ± 0.11^b	41.46 ± 5.99^b	111.16 ± 6.28^b

There were six samples in each group, and data are described as means ± SEM. For each parameter, means, which have different superscript symbols, are statistically significant at $P < 0.05$.

TABLE 4: Effect of CUR-loaded PLGA NPs on mRNA relative expression of NF-κB, iNOS, and type II collagen of MIA-induced OA rats.

| Groups | Parameters | | |
	NF-κB	iNOS	Type II collagen
Normal control	0.094 ± 0.0095^a	1 ± 0.0106^a	1.05 ± 0.01^c
MIA	6.72 ± 0.33^c	5.64 ± 0.28^c	0.25 ± 0.06^a
MIA+CUR-loaded PLGA NPs	1.94 ± 0.16^b	2.13 ± 0.18^b	0.5 ± 0.04^b

There were six samples in each group, and data are described as means ± SEM. For each parameter, means, which have different superscript symbols, are statistically significant at $P < 0.05$.
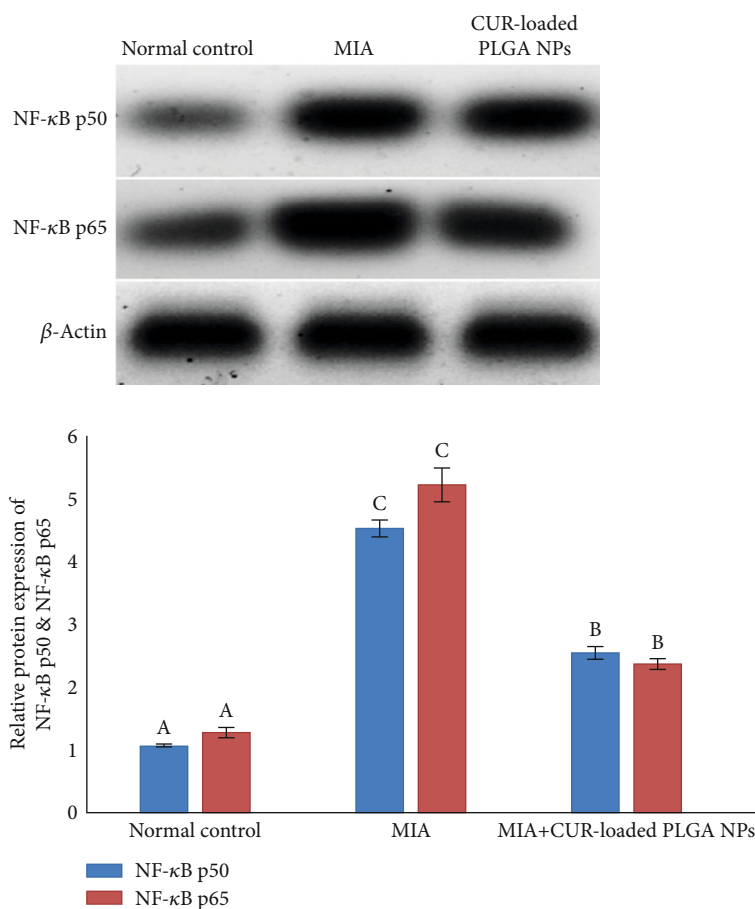
FIGURE 7: Effect of CUR-loaded PLGA NPs on the relative protein expression levels of NF-κB p50 and NF-κB p65 of MIA-induced OA rats. Means, which have different symbols (letters), are significantly different at $P < 0.05$.

3.10. Effect of CUR-Loaded PLGA NPs on the Matrix Metalloproteinase-13 (MMP-13) Expression. MMP-13, a key catabolic enzyme, was immunohistochemically stained in the chondrocytes of the articular cartilage to assess its protein expression. When compared with the normal control group, which almost had no positive staining for
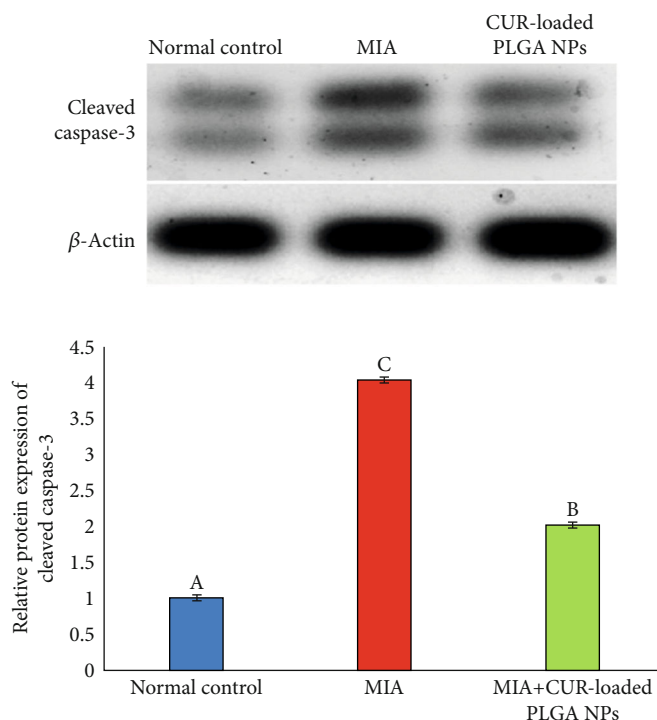
FIGURE 8: Effect of CUR-loaded PLGA NPs on the relative protein expression level of cleaved caspase-3 of MIA-induced OA rats. Means, which have different symbols (letters), are significantly different at $P < 0.05$.

MMP13 (Figure 10(a)), MIA induced an elevation in MMP-13 content in the articular cartilage of the OA control group (Figure 10(b)). However, sections (Figure 10(c)) showed that the MMP-13 content was notably diminished in the articular cartilage of the MIA+CUR-loaded PLGA NP group as compared to that of the OA control group.

Additionally, our results (Figure 10) demonstrate an increase in cell staining positive for MMP-13 in the articular cartilage following MIA injection compared with that of the normal control group (10.39 ± 0.22 vs. 1.01 ± 0.23, $P < 0.05$, respectively). However, osteoarthritic rats treated with CUR-loaded PLGA NPs exhibited a marked reduction in MMP-13-positive chondrocytes compared with that of the MIA-treated group without any treatment (5.26 ± 0.74 vs. 10.39 ± 0.22, $P < 0.05$).

4. Discussion

Currently, evidence shows that there is a significant correlation between the incidence and progression of OA and inflammation, oxidative stress, and excessive catabolic activity [24].

In the current work, we utilized MIA to generate histological and biochemical changes in the articular cartilage that resemble OA conditions in humans [25]. Moreover, in search of inexpensive and beneficial treatments against OA, we prepared CUR-loaded PLGA NPs and investigated their potency against inflammatory mediators, oxidative stress, and chondrocyte apoptosis in MIA-induced OA in a rat model (Figure 11).

The sizes of the CUR-loaded PLGA NP detected in our study were smaller than 300 nm and were consistent with those reported by Gonzales et al. [26]. While the XRD pattern in our study displayed no typical CUR peaks when entrapped in NPs, Khan et al. [27] elucidated that the absence of any noticeable crystalline domains of CUR implies that CUR loaded on PLGA NPs is in the disordered-crystalline phase or the amorphous or the solid-state solubilized form in the polymer matrix. This disordered-crystalline phase, or CUR, inside the polymeric matrix, allows for a controlled release of the encapsulated drug from the NPs.

Following Yabas et al. [28], our radiographic results revealed that CUR NP intra-articular administration markedly lessened the MIA-induced radiographic abnormalities in the knee joints of the treated rats represented by normal joint space and smooth surface of articular cartilage.

The NF-κB signaling pathway is claimed to be one of the main signaling pathways that promote the progression of OA [29]. Although NF-κB stays inactive in the cytoplasm under normal conditions, upon adequate stimulation, e.g., by inflammatory cytokines or the inflammatory microenvironment, IκB kinase (IKK) activity phosphorylates IκB proteins and causes their degeneration, which allows free NF-κB complexes to translocate from the cytoplasm into the nucleus and stimulate a variety of inflammation-related genes. Furthermore, it triggers extracellular matrix degradation, chondrocyte apoptosis, pannus formation, and, eventually, pathological cartilage destruction (Figure 11) [5, 30].

Alternatively, various studies assumed that CUR hinders OA-related inflammation by blocking the NF-κB signaling

(a) (b) (c)

(d) (e) (f)
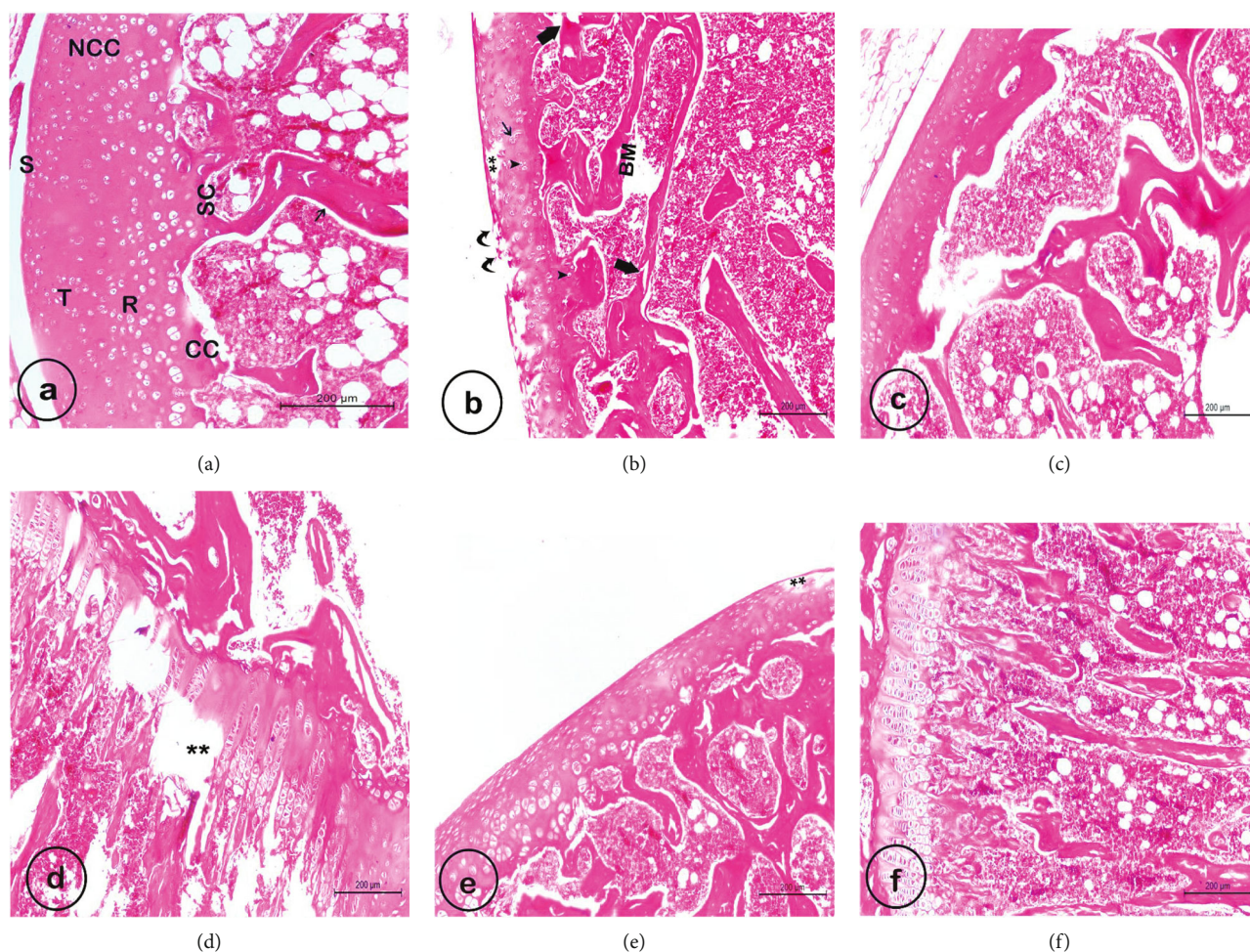
FIGURE 9: Photomicrographs of hematoxylin and eosin- (H&E-) stained sections of the left knee joints. (a) shows the normal control group with the normal architecture of the articular cartilage that consists of a noncalcified (NCC) region, which is arranged into superficial (S), transitional (T), and radial (R) zones and calcified (CC) region with a clear intact tidemark in between (scale bar = 200 μm). It also shows subchondral bone (SC) with well-oriented bony trabeculae (arrow). (b)–(d) show the MIA-treated group (osteoarthritic rats), wherein (b) depicts fissures, surface fibrillation (curved arrows), chondrocytes with hyperchromatic nuclei (arrowheads), chondrocytes clusters (thin arrow), marked loss of (matrix and chondrocytes), and degenerated and disorganized bone trabeculae (thick arrows); (c) shows a decrease in articular cartilage thickness, unclear tidemark, an abnormal subchondral with an increase in trabecular thickness, and bone marrow space (BM) containing fewer hematopoietic cells; and (d) shows degeneration (asterisk) and heterogeneous distribution of chondrocytes in the growth plate. (e) and (f) show the treatment group (MIA+CUR-loaded PLGA NPs), wherein (e) displays a marked restoration of the normal structure of articular cartilage with an intact surface, except for some damaged parts (**) and a few hyperchromatic nuclei, an increase in cellularity, a partial improvement in tidemark integrity, and nearly normal bone marrow space (BM) relative to the MIA group (scale bar = 200 μm), and (f) demonstrates neatly and properly aligned and oriented chondrocytes of the growth plate (scale bar = 200 μm).

pathway and preventing chondrocyte apoptosis [31, 32]. As a result, OA-related inflammation is suppressed and progression is slowed [11, 33, 34].

Subsequently, our study discussed the effect of CUR-loaded PLGA NP IAIs on NF-κB gene and NF-κB-regulated genes participating in inflammation, such as TNF-α, IL-6, IL-1β, and TGF-β. Our data in harmony with Alhusaini et al. [30] propose that CUR administration blocked NF-κB activation by inhibiting IκB degradation and phosphorylation and suppressing the translocation of NF-κB into the nucleus, thereby impeding the inflammatory response of the cells.

Additionally, in agreement with [35], our presented data revealed that CUR considerably boosted the serum levels of IL-10, a robust anti-inflammatory immunosuppressive and chondroprotective cytokine, indicating its potent anti-inflammatory capacity.

Furthermore, CUR-loaded PLGA NP treatment during OA inhibited the expression of iNOS, which is an inflammation-induced enzyme that catalyzes the production of the proinflammatory mediator nitric oxide (NO), further demonstrating its anti-inflammatory effects. Several *in vivo* and *in vitro* studies [36, 37] have shown that CUR treatment reduces iNOS production in various inflammatory diseases.

(a)   (b)   (c)
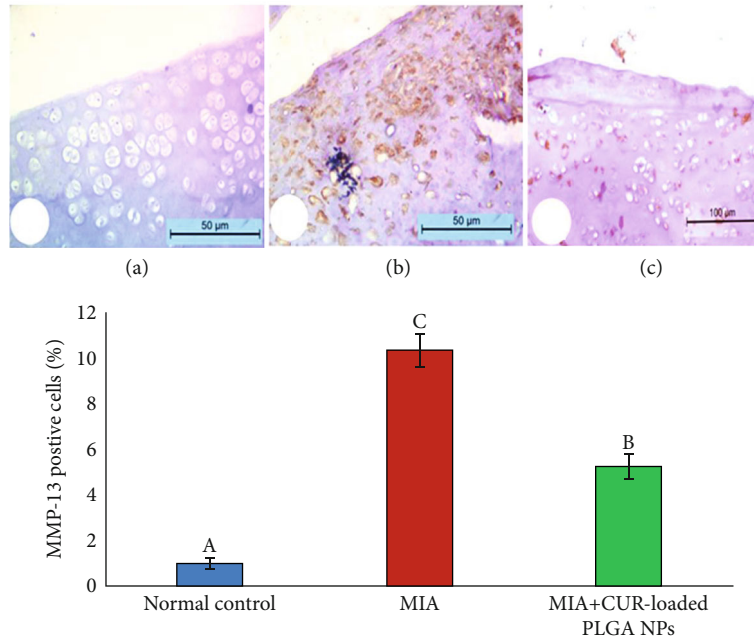
FIGURE 10: Photomicrograph showing immunostaining results of matrix metalloproteinase-1 (MMP-13) expression in cartilage tissue in the (a) normal control group, (b) MIA-treated group, and (c) MIA+CUR-loaded PLGA NP group. Stained cells (brown) were counted, and the percentage of positive cells is expressed as mean ± standard error of the mean (SEM), where $n = 6$ and $P < 0.05$.
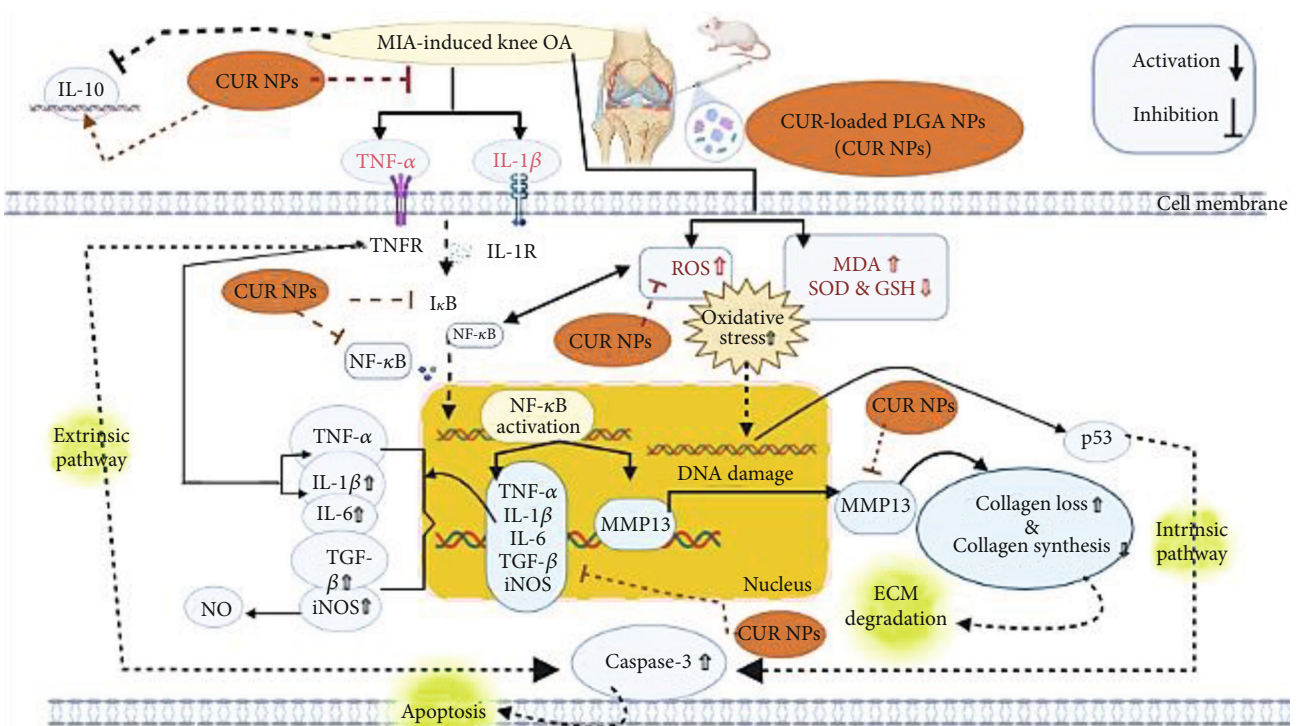
FIGURE 11: Therapeutic effect of CUR-loaded PLGA NPs against cartilage damage due to inflammation, extracellular matrix (ECM) degradation, and apoptosis in MIA-induced knee OA.

Most recently, Cheragh-Birjandi et al. [37] postulated that CUR administration can regulate NO levels by suppressing the activation of the N-terminal kinase (JNK), p38, and NF-κB pathways.

NF-κB pathway activation not only upregulates proinflammatory mediators but additionally mediates the chondrocyte activation triggered by the released extracellular matrix (ECM) products, e.g., fibronectin fragments, which

in turn promote the expression of a variety of matrix-degrading enzymes, including metalloproteinases (MMPs) [38–40]. In the early stage of OA, high upregulation of MMP-13 expression, a prominent catabolic enzyme, leads to severe deterioration of cartilage as it induces type II collagen, which is a reason for nearly 90% of the ECM. The loss of type II collagen is a critical stage that determines the irreversible progression of OA (Figure 11) [41]. Therefore, this study explored MMP-13 and collagen type II expression levels as indicators of the anticatabolic activity of CUR NPs in the OA knee joint.

Herein, IAIs of CUR NPs prevented OA exacerbation by diminishing MMP-13 expression [42] and the degradation of type II collagen [6]. Kumar et al. [43] posited that CUR possesses a suppressing effect on MMPs and variable cellular signaling pathways, e.g., Janus kinase STAT and NF-κB/mitogen-activated protein kinase/phosphoinositide 3-kinase, which eventually ameliorate OA and prevent the further damage of the cartilage.

Further, the effect of CUR treatment on cell death in knee OA has also been elucidated. Although apoptosis is a crucial process in keeping the homeostasis of several tissues, the high rate of chondrocyte death is a well-known pathological feature of OA [44]. MIA-induced TNF-α activates the tumor necrosis factor receptor (TNFR) or death receptors, eventually triggering the extrinsic pathway of apoptosis (Figure 11). While Ding et al. [45] postulated that in MIA-induced OA, the intrinsic pathway of apoptosis can be triggered by reactive oxygen species (ROS). ROS accumulation could induce oxidative stress, thus altering mitochondrial function and promoting the excretion of cytochrome c and activation of proapoptotic factors, e.g., caspase-3 [44, 46]. Moreover, mitochondrial impairment was shown to enhance the response to cytokine-induced chondrocyte inflammation by producing ROS and activating NF-κB [47].

Conversely, CUR has been shown to restore mitochondrial functions, scavenge free radicals and ROS [48, 49], and suppress lipid peroxidation [50]. CUR also enhances the activity of other antioxidants such as SOD, catalase, GSH, and glutathione peroxidase in various diseases [30, 51]. Based on these studies, we scrutinized the role of CUR-loaded PLGA NPs in suppressing the activation of the apoptosis mediators related to OA. Our data confirmed the antioxidant efficacy of CUR NPS as they considerably averted the increase in MDA lipid peroxidation product and enhanced the antioxidant status (GSH concentration and SOD activity). Moreover, consistent with the results of Buhrman et al. [52], our results revealed the antiapoptotic efficacy of CUR NPS, as they notably hindered upregulation in caspase-3 levels. The antioxidant, anticatabolic, and antiapoptotic potency can be mostly attributed to the hydroxyl, methoxy, α, β-unsaturated carbonyl, or diketone groups present in CUR [53].

MIA-induced knee OA inflammation led to severe histopathological alterations in the architecture of the articular cartilage, such as clefts, disorderly arranged cells, hyperchromatic, and a significant reduction in chondrocyte number [31]. Whereas CUR-loaded PLGA NP treatment did not affect the regeneration of the cells, it halted OA progression by reducing inflammation and chondrocytes apoptosis which is depicted by milder tissue defects and pronounced articular cartilage and subchondral bone integrity. Our findings are consistent with Yabas et al. [28], which revealed that CUR lessened OA severity by restoring the architecture of the knee joint. Wang et al. [54] postulated that CUR moderately enhanced the integrity of the articular cartilage by blocking the NF-κB/hypoxia-inducible factor 2α signaling pathway.

Therefore, current findings suggest that OA-related deteriorations and progression are halted due to the ability of CUR-loaded PLGA NPs to modulate various mediators such as NF-κB, MMP-13, and oxidative stress.

5. Conclusion

Overall, this study demonstrates that intra-articular treatment with CUR-loaded PLGA nanoparticles is a compelling candidate for improving joint health in knee OA due to their anti-inflammatory, anticatabolic, and antioxidant characteristics. However, for clinical applications, further research studies with a longer treatment period and bigger sample size should be carried out to explore its underlying mechanisms.

Abbreviations

Cur:	Curcumin
CUR-loaded PLGA NPs:	Curcumin-loaded polylactic-co-glycolic acid nanoparticles
ECM:	Extracellular matrix
GSH:	Reduced glutathione
IAIs:	Intra-articular injections
IFN-γ:	Interferon-γ
IL:	Interleukin
iNOS:	Inducible nitric oxide synthase
MDA:	Malondialdehyde
MIA:	Monosodium iodoacetate
MMP-13:	Matrix metalloproteinase-1
NF-κB:	Nuclear factor-kappa B
NO:	Nitric oxide
NPs:	Nanoparticles
NSAIDs:	Nonsteroidal anti-inflammatory drugs
OA:	Osteoarthritis
PLGA:	Polylactic-co-glycolic acid
PVA:	Polyvinyl alcohol
RIPA:	Radio-immunoprecipitation assay
ROS:	Reactive oxygen species
SDS-PAGE:	Sodium dodecyl sulfate-polyacrylamide gel electrophoresis
STAT:	Janus kinase signal transduction and activation transcription
TBA:	Thiobarbituric acid
TGF-β:	Transforming growth factor-beta
TNFR:	Tumor necrosis factor receptors
TNF-α:	Tumor necrosis factor-α.

Data Availability

The authors confirmed that all data generated or analyzed during this study are included in this published article.

Consent

Informed consent was obtained from all subjects involved in the study.

Conflicts of Interest

The authors declare no conflict of interest.

Authors' Contributions

RRA, SRG, and MA conceived and designed the experiments. HMH performed the experiments and analyzed the data. IAN, BSA, and OMA provided experimental technical support and assisted in completing the study at different stages. HMH drafted the manuscript. RRA, SRG, and MA finalized the paper. All authors are in agreement with the contents of the manuscript. All authors read and approved the final manuscript.

Acknowledgments

References

[1] Z. Zhang, C. Huang, Y. Cao et al., "2021 revised algorithm for the management of knee osteoarthritis—the Chinese viewpoint," *Aging Clinical and Experimental Research*, vol. 33, no. 8, pp. 2141–2147, 2021.

[2] O. Bruyère, G. Honvo, N. Veronese et al., "An updated algorithm recommendation for the management of knee osteoarthritis from the European Society for Clinical and Economic Aspects of Osteoporosis, Osteoarthritis and Musculoskeletal Diseases (ESCEO)," *Seminars in Arthritis and Rheumatism*, vol. 49, no. 3, pp. 337–350, 2019.

[3] Z. Wang, S. Wang, K. Wang, X. Wu, C. Tu, and C. Gao, "Stimuli-sensitive nanotherapies for the treatment of osteoarthritis," *Macromolecular Bioscience*, vol. 21, no. 11, article e2100280, 2021.

[4] C. Cooper, R. Chapurlat, N. Al-Daghri et al., "Safety of oral non-selective non-steroidal anti-inflammatory drugs in osteoarthritis: what does the literature say?," *Drugs & Aging*, vol. 36, Supplement 1, pp. 15–24, 2019.

[5] Y. Henrotin, A. L. Clutterbuck, D. Allaway et al., "Biological actions of curcumin on articular chondrocytes," *Osteoarthritis and Cartilage*, vol. 18, no. 2, pp. 141–149, 2010.

[6] J. Wang, J. Ma, J. H. Gu et al., "Regulation of type II collagen, matrix metalloproteinase-13 and cell proliferation by interleukin-1β is mediated by curcumin via inhibition of NF-κB signaling in rat chondrocytes," *Molecular Medicine Reports*, vol. 16, no. 2, pp. 1837–1845, 2017.

[7] M. Alagawany, M. Farag, S. Abdelnour, M. Dawood, S. Elnesr, and K. Dhama, "Curcumin and its different forms: a review on fish nutrition," *Aquaculture*, vol. 532, article 736030, 2021.

[8] L. Shen, C. C. Liu, C. Y. An, and H. F. Ji, "How does curcumin work with poor bioavailability? Clues from experimental and theoretical studies," *Scientific Reports*, vol. 6, no. 1, article 20872, 2016.

[9] P. Anand, A. B. Kunnumakkara, R. A. Newman, and B. B. Aggarwal, "Bioavailability of curcumin: problems and promises," *Molecular Pharmaceutics*, vol. 4, no. 6, pp. 807–818, 2007.

[10] A. Karthikeyan, K. N. Young, M. Moniruzzaman et al., "Curcumin and its modified formulations on inflammatory bowel disease (IBD): the story so far and future outlook," *Pharmaceutics*, vol. 13, no. 4, p. 484, 2021.

[11] S. Bisht, G. Feldmann, S. Soni et al., "Polymeric nanoparticle-encapsulated curcumin ("nanocurcumin"): a novel strategy for human cancer therapy," *Journal of Nanobiotechnology*, vol. 5, no. 1, p. 3, 2007.

[12] S. Shome, A. D. Talukdar, M. D. Choudhury, M. K. Bhattacharya, and H. Upadhyaya, "Curcumin as potential therapeutic natural product: a nanobiotechnological perspective," *Journal of Pharmacy and Pharmacology*, vol. 68, no. 12, pp. 1481–1500, 2016.

[13] F. S. Tabatabaei Mirakabad, K. Nejati-Koshki, A. Akbarzadeh et al., "PLGA-based nanoparticles as cancer drug delivery systems," *Asian Pacific Journal of Cancer Prevention : APJCP*, vol. 15, no. 2, pp. 517–535, 2014.

[14] R. Varela-Fernández, C. Bendicho-Lavilla, M. Martin-Pastor et al., "Design, optimization, and in vitro characterization of idebenone-loaded PLGA microspheres for LHON treatment," *International Journal of Pharmaceutics*, vol. 616, article 121504, 2022.

[15] M. Cristiano, A. Mancuso, E. Giuliano, D. Cosco, D. Paolino, and M. Fresta, "EtoGel for intra-articular drug delivery: a new challenge for joint diseases treatment," *Journal of Functional Biomaterials*, vol. 12, no. 2, p. 34, 2021.

[16] G. H. Ragab, F. M. Halfaya, O. M. Ahmed et al., "Platelet-rich plasma ameliorates monosodium iodoacetate-induced ankle osteoarthritis in the rat model via suppression of inflammation and oxidative stress," *Evidence-based Complementary and Alternative Medicine*, vol. 2021, Article ID 6692432, 13 pages, 2021.

[17] F. Niazvand, L. Khorsandi, M. Abbaspour et al., "Curcumin-loaded poly lactic-co-glycolic acid nanoparticles effects on mono-iodoacetate -induced osteoarthritis in rats," *Veterinary Research Forum*, vol. 8, no. 2, pp. 155–161, 2017.

[18] S. A. Moaty, A. Farghali, M. Moussa, and R. Khaled, "Remediation of waste water by Co-Fe layered double hydroxide and its catalytic activity," *Journal of the Taiwan Institute of Chemical Engineers*, vol. 71, pp. 441–453, 2017.

[19] A. A. Badawi, H. M. El-Laithy, D. I. Nesseem, and S. S. El-Husseney, "Pharmaceutical and medical aspects of hyaluronic acid–ketorolac combination therapy in osteoarthritis treatment: radiographic imaging and bone mineral density," *Journal of Drug Targeting*, vol. 21, no. 6, pp. 551–563, 2013.

[20] H. G. Preuss, S. T. Jarrell, R. Scheckenbach, S. Lieberman, and R. A. Anderson, "Comparative effects of chromium, vanadium and Gymnema sylvestre on sugar-induced blood pressure elevations in SHR," *Journal of the American College of Nutrition*, vol. 17, no. 2, pp. 116–123, 1998.

[21] E. Beutler, O. Duron, and B. M. Kelly, "Improved method for the determination of blood glutathione," *The Journal of Laboratory and Clinical Medicine*, vol. 61, pp. 882–888, 1963.

[22] M. Nishikimi, N. Appaji, and K. Yagi, "The occurrence of superoxide anion in the reaction of reduced phenazine metho-sulfate and molecular oxygen," *Biochemical and Biophysical Research Communications*, vol. 46, no. 2, pp. 849–854, 1972.

[23] K. Petrosyan, R. Tamayo, and D. Joseph, "Sensitivity of a novel biotin-free detection reagent (Powervision+™) for immuno-histochemistry," *Journal of Histotechnology*, vol. 25, no. 4, pp. 247–250, 2002.

[24] K. W. Park, K. M. Lee, D. S. Yoon et al., "Inhibition of microRNA-449a prevents IL-1β-induced cartilage destruction via SIRT1," *Osteoarthritis and Cartilage*, vol. 24, no. 12, pp. 2153–2161, 2016.

[25] S. V. Naveen, R. E. Ahmad, W. J. Hui et al., "Histology, glycos-aminoglycan level and cartilage stiffness in monoiodoacetate-induced osteoarthritis: comparative analysis with anterior cru-ciate ligament transection in rat model and human osteoar-thritis," *International Journal of Medical Sciences*, vol. 11, no. 1, pp. 97–105, 2014.

[26] C. M. Gonzales, L. F. Dalmolin, K. A. da Silva et al., "New insights of turmeric extract-loaded PLGA nanoparticles: development, characterization and in vitro evaluation of anti-oxidant activity," *Plant Foods for Human Nutrition*, vol. 76, no. 4, pp. 507–515, 2021.

[27] M. Khan, S. Ahmad, I. Ahmad, and M. Rizvi, "Anti-Prolifera-tive Activity of Curcumin Loaded PLGA Nanoparticles for Prostate Cancer," in *Nanotechnology Applied To Pharmaceuti-cal Technology*, pp. 267–278, Springer, Cham, 2017.

[28] M. Yabas, C. Orhan, B. Er et al., "A next generation formula-tion of curcumin ameliorates experimentally induced osteoar-thritis in rats via regulation of inflammatory mediators," *Frontiers in Immunology*, vol. 12, article 609629, 2021.

[29] F. Wang, Z. Guo, and Y. Yuan, "STAT3 speeds up progression of osteoarthritis through NF-κB signaling pathway," *Experi-mental and Therapeutic Medicine*, vol. 19, no. 1, pp. 722–728, 2020.

[30] A. Alhusaini, L. Fadda, I. H. Hasan, E. Zakaria, A. M. Alenazi, and A. M. Mahmoud, "Curcumin ameliorates lead-induced hepatotoxicity by suppressing oxidative stress and inflamma-tion, and modulating Akt/GSK-3β signaling pathway," *Bio-molecules*, vol. 9, no. 11, p. 703, 2019.

[31] Y. Zhang and Y. Zeng, "Curcumin reduces inflammation in knee osteoarthritis rats through blocking TLR4 /MyD88/NF-κB signal pathway," *Drug Development Research*, vol. 80, no. 3, pp. 353–359, 2019.

[32] A. Nakahata, A. Ito, R. Nakahara et al., "Intra-articular injec-tions of curcumin monoglucuronide TBP1901 suppresses articular cartilage damage and regulates subchondral bone alteration in an osteoarthritis rat model," *Cartilage*, vol. 13, Supplement 2, pp. 153s–167s, 2021.

[33] P. Anand, H. B. Nair, B. Sung et al., "Design of curcumin-loaded PLGA nanoparticles formulation with enhanced cellu-lar uptake, and increased bioactivity in vitro and superior bio-availability in vivo," *Biochemical Pharmacology*, vol. 79, no. 3, pp. 330–338, 2010.

[34] X.-H. Wang, W. Li, X.-H. Wang et al., "Water-soluble sub-stances of wheat: a potential preventer of aflatoxin B1-induced liver damage in broilers," *Poultry Science*, vol. 98, no. 1, pp. 136–149, 2019.

[35] N. Salah, L. Dubuquoy, R. Carpentier, and D. Betbeder, "Starch nanoparticles improve curcumin-induced production of anti-inflammatory cytokines in intestinal epithelial cells,"

International Journal of Pharmaceutics: X, vol. 4, article 100114, 2022.

[36] H. Y. Kim, E. J. Park, E. H. Joe, and I. Jou, "Curcumin sup-presses Janus kinase-STAT inflammatory signaling through activation of Src homology 2 domain-containing tyrosine phosphatase 2 in brain microglia," *The Journal of Immunology*, vol. 171, no. 11, pp. 6072–6079, 2003.

[37] S. Cheragh-Birjandi, M. Moghbeli, F. Haghighi et al., "Impact of resistance exercises and nano-curcumin on synovial levels of collagenase and nitric oxide in women with knee osteoar-thritis," *Translational Medicine Communications*, vol. 5, pp. 1–6, 2020.

[38] M. B. Goldring, "Chondrogenesis, chondrocyte differentiation, and articular cartilage metabolism in health and osteoarthri-tis," *Therapeutic Advances in Musculoskeletal Disease*, vol. 4, no. 4, pp. 269–285, 2012.

[39] K. Yamamoto, H. Okano, W. Miyagawa et al., "MMP-13 is constitutively produced in human chondrocytes and co-endocytosed with ADAMTS-5 and TIMP-3 by the endocytic receptor LRP1," *Matrix Biology*, vol. 56, pp. 57–73, 2016.

[40] Q. H. Zhao, L. P. Lin, Y. X. Guo et al., "Matrix metalloprotein-ase-13, NF-κB p65 and interleukin-1β are associated with the severity of knee osteoarthritis," *Experimental and Therapeutic Medicine*, vol. 19, no. 6, pp. 3620–3626, 2020.

[41] M. B. Goldring and M. Otero, "Inflammation in osteoarthri-tis," *Current Opinion in Rheumatology*, vol. 23, no. 5, pp. 471–478, 2011.

[42] S. Yang, J.-H. Ryu, H. Oh et al., "NAMPT (visfatin), a direct target of hypoxia-inducible factor-2α, is an essential catabolic regulator of osteoarthritis," *Annals of the Rheumatic Diseases*, vol. 74, no. 3, pp. 595–602, 2015.

[43] D. Kumar, M. Kumar, C. Saravanan, and S. K. Singh, "Curcu-min: a potential candidate for matrix metalloproteinase inhib-itors," *Expert Opinion on Therapeutic Targets*, vol. 16, no. 10, pp. 959–972, 2012.

[44] H. S. Hwang and H. A. Kim, "Chondrocyte apoptosis in the pathogenesis of osteoarthritis," *International Journal of Molec-ular Sciences*, vol. 16, no. 11, pp. 26035–26054, 2015.

[45] L. Ding, E. Heying, N. Nicholson et al., "Mechanical impact induces cartilage degradation via mitogen activated protein kinases," *Osteoarthritis and Cartilage*, vol. 18, no. 11, pp. 1509–1517, 2010.

[46] C. Vaamonde-García, R. R. Riveiro-Naveira, M. N. Valcárcel-Ares, L. Hermida-Carballo, F. J. Blanco, and M. J. López-Armada, "Mitochondrial dysfunction increases inflammatory responsiveness to cytokines in normal human chondrocytes," *Arthritis and Rheumatism*, vol. 64, no. 9, pp. 2927–2936, 2012.

[47] D. D'Lima, J. Hermida, S. Hashimoto, C. Colwell, and M. Lotz, "Caspase inhibitors reduce severity of cartilage lesions in experimental osteoarthritis," *Arthritis and Rheumatism*, vol. 54, no. 6, pp. 1814–1821, 2006.

[48] N. Sreejayan and M. N. Rao, "Free radical scavenging activity of curcuminoids," *Arzneimittel-Forschung*, vol. 46, no. 2, pp. 169–171, 1996.

[49] T. Ak and I. Gülçin, "Antioxidant and radical scavenging properties of curcumin," *Chemico-Biological Interactions*, vol. 174, no. 1, pp. 27–37, 2008.

[50] M. Soto-Urquieta, E. Franco-Robles, I. Zúñiga-Trujillo, A. Campos-Cervantes, V. Perez-Vazquez, and J. Ramírez-Emiliano, "Curcumin decreases oxidative stress in mitochon-dria isolated from liver and kidneys of high-fat diet-induced

obese mice," *Journal of Asian Natural Products Research*, vol. 15, no. 8, pp. 905–915, 2013.

[51] M. Alizadeh and S. Kheirouri, "Curcumin reduces malondialdehyde and improves antioxidants in humans with diseased conditions: a comprehensive meta-analysis of randomized controlled trials," *Biomedicine (Taipei)*, vol. 9, no. 4, pp. 23–23, 2019.

[52] C. Buhrmann, A. Mobasheri, U. Matis, and M. Shakibaei, "Curcumin mediated suppression of nuclear factor-κB promotes chondrogenic differentiation of mesenchymal stem cells in a high-density co-culture microenvironment," *Arthritis Research & Therapy*, vol. 12, no. 4, p. R127, 2010.

[53] G. Liang, S. Yang, H. Zhou et al., "Synthesis, crystal structure and anti-inflammatory properties of curcumin analogues," *European Journal of Medicinal Chemistry*, vol. 44, no. 2, pp. 915–919, 2009.

[54] P. Wang, Y. Ye, W. Yuan, Y. Tan, S. Zhang, and Q. Meng, "Curcumin exerts a protective effect on murine knee chondrocytes treated with IL-1β through blocking the NF-κB/HIF-2α signaling pathway," *Annals of Translational Medicine*, vol. 9, no. 11, pp. 940–940, 2021.

Review Article

Role of the Neutrophil to Lymphocyte Ratio in Guillain Barré Syndrome: A Systematic Review and Meta-Analysis

Shirin Sarejloo,[1] Shokoufeh Khanzadeh,[2] Samaneh Hosseini,[3] Morad Kohandel Gargari,[4] Brandon Lucke-Wold,[5] Seyedarad Mosalamiaghili [ID],[6] Pouria Azami,[1] Sanaz Oftadehbalani [ID],[7] and Shahram Sadeghvand [ID][8]

[1]*Cardiovascular Research Center, Shiraz University of Medical Sciences, Shiraz, Iran*
[2]*Student Research Committee, Tabriz University of Medical Sciences, Tabriz, Iran*
[3]*Neurosciences Research Center, Tabriz University of Medical Sciences, Tabriz, Iran*
[4]*Tabriz University of Medical Sciences, Tabriz, Iran*
[5]*University of Florida, Department of Neurosurgery, USA*
[6]*Student Research Committee, Shiraz University of Medical Sciences, Shiraz, Iran*
[7]*Fatemeh Zahra Hospital, Iran University of Medical Sciences, Tehran, Iran*
[8]*Department of Pediatrics, Tabriz University of Medical Sciences, Tabriz, Iran*

Correspondence should be addressed to Sanaz Oftadehbalani; faridehmousavi3@yahoo.com
and Shahram Sadeghvand; shahram.sadeghvand@yahoo.com

In this study, we conducted a systematic review and meta-analysis regarding the role of the neutrophil to lymphocyte ratio (NLR) in Guillain Barré syndrome (GBS). The most recent update to the search was on July 18, 2022, through the databases of Web of Science, PubMed, Embase, and Scopus. The Newcastle-Ottawa scale was used for quality assessment of included studies. Finally, 14 studies were included in the review, and among them, ten studies were included in the meta-analysis. Our results showed that NLR levels were significantly increased in the patients with GBS compared with healthy controls (SMD = 1.05; 95%CI = 0.59 to 1.50, $P < 0.001$). After treatment, NLR levels were decreased to the extent that they became similar to healthy controls (SMD = −0.03, 95%CI = −0.29 to 0.22, $P = 0.204$). Moreover, NLR was a stable predictor of outcome or response to treatment in such patients (SMD = 1.01, 95%CI = 0.65 to 1.37, $P < 0.001$); the higher the NLR, the worse the outcome. In addition, patients who underwent mechanical ventilation had higher levels of NLR compared to those who did not (SMD = 0.93, 95%CI = 0.05 to 1.82, $P = 0.03$). However, NLR levels were not different among distinct GBS subtypes, so it could not distinguish among them. In conclusion, our analysis indicates that the NLR levels are highly elevated in patients with GBS. Therefore, the NLR has the potential to be used as a biomarker to inform diagnosis, prognosis, or treatment responses in GBS, and future studies are warranted.

1. Introduction

Guillain Barré syndrome (GBS) is a peripheral nervous system immune-mediated disorder marked by muscle weakness [1]. Acute inflammatory demyelinating polyradiculoneuropathy (AIDP) is the most prevalent form of GBS, followed by acute motor axonal neuropathy (AMAN) and acute motor-sensory axonal neuropathy (AMSAN)

[1]. The disease has a prevalence of one to two cases per 100,000 people per year, with the majority of patients having an infection prior to the onset of the disorder [2]. Although it is widely assumed that GBS is caused by post-infectious immunological dysfunction that mediates demyelination of the peripheral nervous system, the exact etiology of the disease is yet unknown [2]. Indeed, it is an immunopathologically and clinically complex disorder

with a limited number of effective immunomodulatory therapies [3].

Furthermore, there are no biomarkers that can be used to help with disease diagnosis, categorization, or prognosis [4]. These characteristics often contribute to misdiagnosis, overtreatment, treatment failure, and unsatisfactory outcomes. This thereby necessitates identification of disease biomarkers to improve GBS diagnostic and therapeutic outcomes [4]. The neutrophil to lymphocyte ratio (NLR) is a new, inexpensive, simple, widely available, and fast-responding biomarker of cellular immune activation. In addition, it is a valid index of stress and systemic inflammation that has opened a new outlook for clinical medicine. It allows for a better understanding of the biology of inflammation and the coupling between adaptive and innate immunity [5]. During disease, the NLR is disrupted with a shift in balance between adaptive (lymphocytes) and innate (neutrophils) immune responses [5]. Its diagnostic and prognostic usefulness has been investigated in a variety of conditions, including cancer [6], cardiovascular disease [7], and neurological disorders [8, 9]. Several researchers have now looked into the link between NLR and GBS [10–16]. NLR may play a diagnostic and prognostic role in GBS, according to the results of these studies. NLR levels were found to be higher in patients with GBS compared to healthy controls in several studies [10, 12–14]. On the other hand, one recent study found no significant alterations in this marker between GBS patients and controls [11]. In addition, two previous studies declared that NLR could come into use when distinguishing between GBS subtypes [13, 16], while other studies found totally opposite findings [10–12]. This introduces the concept that timing of the test may be important. Furthermore, some previous studies show that early testing may predict the outcome of patients with GBS [11–13]. According to the contradictions in the current data, a systematic review and meta-analysis is required. In this study, we conducted a systematic review of the literature on the role of NLR in GBS and used a meta-analysis to pool the individual data from several studies.

2. Method

2.1. Search Strategy.
In compliance with the Preferred Reporting Items for Systematic Review and Meta-Analyses (PRISMA) standards, we performed a comprehensive review and meta-analysis to collect all published papers (Figure 1).

Two reviewers, who were entirely blind to the journal and author details, independently carried out a systematic literature search throughout the online databases of Web of Science, Scopus, PubMed, and Embase. The search strategy was as follows: ((guillain-barre AND syndrome) OR (guillain AND barre AND syndrome) OR GBS) AND ((neutrophil AND lymphocyte AND ratio) OR (neutrophil-to-lymphocyte) OR NLR).

The most recent update to the search was on July 18, 2022. We did not limit our search to a particular language or year of release. To find possibly suitable studies, researchers combed through the reference lists of related reviews and papers. Additionally, the Prospero Registry

was combed for information on unpublished and continuing investigations. Because most of the identified papers were conducted in China, we also conducted a rapid nonsystematic search in Google Scholar as a secondary database in English and Chinese to identify grey literature and more relevant studies.

2.2. Inclusion and Exclusion Criteria.
The following were the criteria for inclusion: (1) studies that are cross-sectional, case-control, or cohort and (2) studies comparing NLR data from GBS patients to healthy controls or studies using NLR data to predict the outcome. Good outcome was defined as Hughes disability score (HDS) < 3 after treatment. The following were the criteria for exclusion: (1) reviews, letters to editors, animal studies, case series, and case reports and (2) studies with similar data.

2.3. Extraction of Data and Quality Assessment.
Two authors independently investigated the titles/abstracts of the publications obtained. The entire texts of relevant papers were then separately examined for eligibility by the same two authors. A third independent author handled any disagreements between reviewers in both steps.

The first author, year of publication, language, study location, study design, age group (adult or children), total sample size, and the number of cases and controls were collected. NLR level data in GBS cases and controls were all extracted. When there were disagreements, a third author was consulted to reach a consensus.

Two writers independently assessed the quality of the studies included using the Newcastle-Ottawa scale, which has three sections: selection (4 items), comparability (2 items), and outcome (3 items), with a total grade of 0 to 9. Any differences were finally settled by a third author through arbitration.

2.4. Statistical Analysis.
NLR differences among GBS patients and healthy controls were evaluated using a standardized mean difference (SMD) with a 95% confidence interval (CI). The methods introduced by Wan et al. [17] were used to calculate the mean and SD from the median, range, or IQR. The chi-squared (χ^2) test and the I^2 statistic were used to determine the degree of heterogeneity between study results, and the I^2 statistic was used to quantify inconsistency throughout studies. $I^2 \geq 75\%$ and P value of χ^2 test ≤ 0.05 were considered significant. The random-effects meta-analysis was chosen in this study because both between-study heterogeneities were significant.

Subgroup analysis was performed according to age group (adults vs. children), study location (Turkey vs. other countries including China and Egypt), and sample size (large studies vs. small studies). We considered studies with sample size of 200 or more as large studies.

For detection of potential publication bias, Funnel plot and Egger's linear-regression test were used, and those with P value ≤ 0.05 were considered to have significant publication bias. For statistical analysis, STATA 12.0 software (Stata Corporation, College Station, TX, USA) was used. Statistical significance was defined as a P value of less than 0.05.
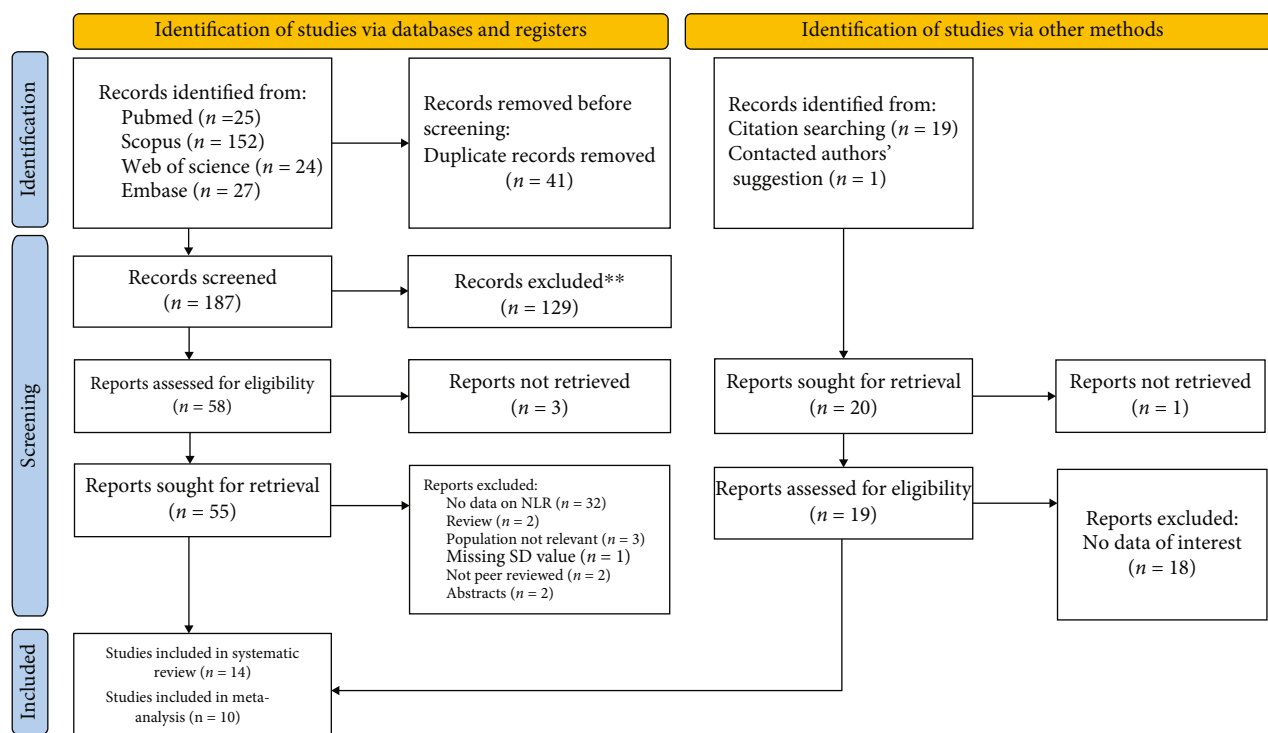
FIGURE 1: Flowchart of search and study selection.

3. Results

3.1. Literature Search and Selection. Figure 1 shows the process of identifying and selecting research evidence in this systematic review. In addition to the 228 studies found from the initial database search, 20 further studies were identified through reference lists of relevant articles and Google Scholar and were added. After screening, 14 studies were included in the review [10–16, 18–23]. Among them, ten studies had sufficient data to be included in the meta-analysis [10–16, 22, 24, 25].

3.2. Characteristics of the Included Studies. Of the ten studies included in this meta-analysis [10–16, 22, 24, 25], eight studies were retrospective [10–12, 14–16, 24, 25], and two studies were prospective [13, 22]. Concerning document language, all of the documents were in English. Overall, 522 healthy controls and 1207 GBS patients were enrolled in the selected studies. The general characteristics of the selected studies are presented in Table 1. Although the quality assessment of selected studies assessed with the Newcastle-Ottawa scale had different scores ranging from 4 to 9, we included all of them in the meta-analysis (Table 1).

Of the ten studies, five studies compared pretreatment NLR levels in patients with GBS and those of controls [10–14], three studies compared posttreatment NLR levels in patients with GBS and those of controls [11–13], four studies compared pre- and posttreatment NLR levels in patients with GBS [11–13, 15], three studies provided NLR data for both good and poor outcome patients [11–13],

and three studies reported association of NLR with mechanical ventilation [22, 24, 25]. Additionally, five studies declared the differences in NLR levels between AIDP and axonal types [10–13, 16], of which three studies showed the differences in NLR levels among AIDP, AMAN, and AMSAN [12, 13, 16].

3.3. Meta-Analysis of Differences between GBS Patients and Healthy Controls in NLR Level. Before treatment, NLR levels in GBS patients were compared with those of controls in five studies [10–14] with 412 patients with GBS and 522 controls. Compared with the control group, the GBS patients' NLR levels before treatment were significantly higher (random-effects model, SMD = 1.05; 95%CI = 0.59 to 1.50, $P < 0.001$) (Figure 2).

In subgroup analysis according to age group, there were four studies [10, 12–14], including solely the adult participants consisting of 344 patients with GBS and 459 controls. One study [11] included 36 adult and 32 pediatric participants and reported the mean ± SD for both groups. The pooled results showed that the NLR levels in adults with GBS were significantly higher than those in healthy controls (random-effects model, SMD = 1.61, 95%CI = 0.57 to 1.47, $P < 0.001$). The NLR levels of children with GBS in comparison with those of healthy controls showed no significant difference (random-effects model, SMD = 0.00, 95%CI = − 0.50 to 0.50) (Figure 3).

In subgroup analysis according to study location, we found that the NLR levels in patients with GBS were significantly higher than those in healthy controls in both Turkey

TABLE 1: General characteristics of studies included in the meta-analysis.

First author	Year	Design	Region	Age group	Comparison between cases and controls					Comparison between GBS types						Comparison between GBS cases with good and bad outcome						Comparison between GBS cases with and without mechanical ventilation				NOS score
					Healthy control		GBS cases			AIDP type		AMAN		Axonal type AMSAN		Total		Good outcome		Bad outcome		MV		Non-MV		
					N	NLR	N	Pretreatment NLR	Posttreatment NLR	N	NLR	N	NLR	N	NLR	N	NLR	N	NLR	N	NLR	N	NLR	N	NLR	
Geyik	2016	R	Turkey	Adult	101	2.53 ± 0.94	94	5.43 ± 3.98	2.61 ± 0.69	64	5.41 ± 3.09	16	5.82 ± 3.09	14	7.04 ± 3.98	30	6.38 ± 3.50	78	4.67 ± 3.57	16	9.01 ± 3.89	—	—	—	—	6
Ozdemir	2016	R	Turkey	Adult	—	—	62	—	—	35	5.78 ± 5.23	12	3.36 ± 1.20	15	2.15 ± 0.54	27	2.24 ± 0.83	—	—	—	—	—	—	—	—	8
Ethemoglu	2018	R	Turkey	Adult and children	63	2.70 ± 1.17	68	2.93 ± 1.53	2.75 ± 1.35	40	2.53 ± 1.44	—	—	—	—	28	3.08 ± 1.32	15	1.97 ± 0.87	53	2.98 ± 1.45	—	—	—	—	5
Huang	2018	R	China	Adult	217	1.51 ± 0.56	117	2.90 ± 1.81	—	—	—	—	—	—	—	—	—	—	—	—	—	—	—	—	—	6
Huner	2018	R	Turkey	Children	—	—	27	3.29 ± 4.30	1.37 ± 0.71	—	—	—	—	—	—	—	—	—	—	—	—	—	—	—	—	8
Bedel	2019	R	Turkey	Adult	101	1.29 ± 0.52	98	3.77 ± 2.13	—	59	3.94 ± 2.27	—	—	—	—	39	3.51 ± 1.89	—	—	—	—	—	—	—	—	6
Ning	2019	R	China	Adult	—	—	—	—	—	—	—	—	—	—	—	—	—	—	—	—	—	74	7.33 ± 5.42	352	2.92 ± 1.91	6
Hashim	2020	P	Egypt	Adult	40	2.58 ± 0.85	35	3.95 ± 1.34	2.27 ± 0.76	18	3.47 ± 1.04	7	4.04 ± 1.85	10	4.94 ± 1.08	17	4.56 ± 1.39	26	3.60 ± 1.18	9	5.11 ± 1.78	—	—	—	—	6
Tiwari	2020	P	India	Children	—	—	—	—	—	—	—	—	—	—	—	—	—	—	—	—	—	9	1.37 ± 0.89	37	1.91 ± 1.27	7
Cheng	2022	R	China	Adult	—	—	—	—	—	—	—	—	—	—	—	—	—	—	—	—	—	30	7.72 ± 8.58	204	2.77 ± 1.53	7

AIDP: acute inflammatory demyelinating polyradiculoneuropathy; AMAN: acute motor axonal neuropathy; AMSAN: acute motor-sensory axonal neuropathy; R: retrospective; P: prospective; NLR: neutrophil to lymphocyte ratio; MV: mechanical ventilation.

FIGURE 2: Meta-analysis of differences in NLR levels between GBS patients before treatment and healthy controls.
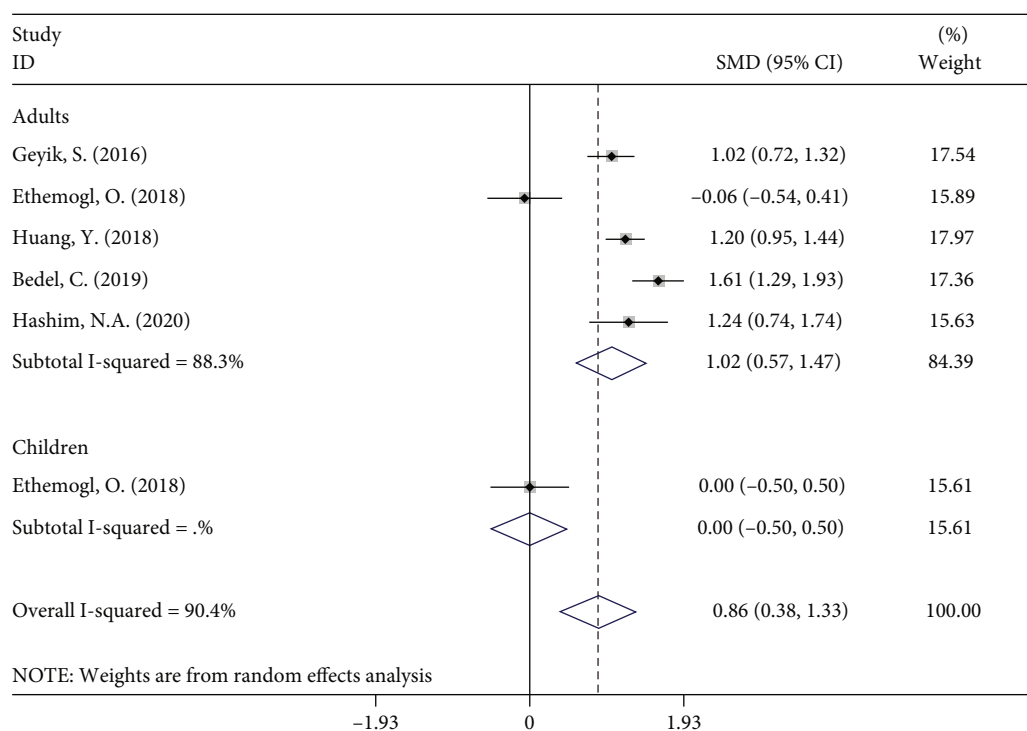
FIGURE 3: Subgroup analysis of differences in NLR levels between GBS patients before treatment and healthy controls according to age group.

(SMD = 0.91, 95%CI = 0.73 to 1.10, $P < 0.001$) and other countries (SMD = 1.21, 95%CI = 0.99 to 1.42, $P < 0.001$) (Figure 4).

Subgroup analysis according to age group showed that the NLR levels in patients with GBS were significantly higher than those in healthy controls in either small (SMD = 1.13, 95%CI = 0.94 to 1.31, $P < 0.001$) or large studies (SMD = 1.61, 95%CI = 0.57 to 1.47, $P < 0.001$) (Figure 5).

3.4. Association of NLR with Treatment in Patients with GBS. In the next step, we conducted a comparison of pre- and posttreatment NLR levels of GBS patients based on studies for whom the data (pre- and posttreatment NLR levels) was available. Four studies [11–13, 15], including 224 GBS cases, had sufficient data. The pooled results showed that pretreatment NLR levels were significantly higher than posttreatment NLR levels (random-
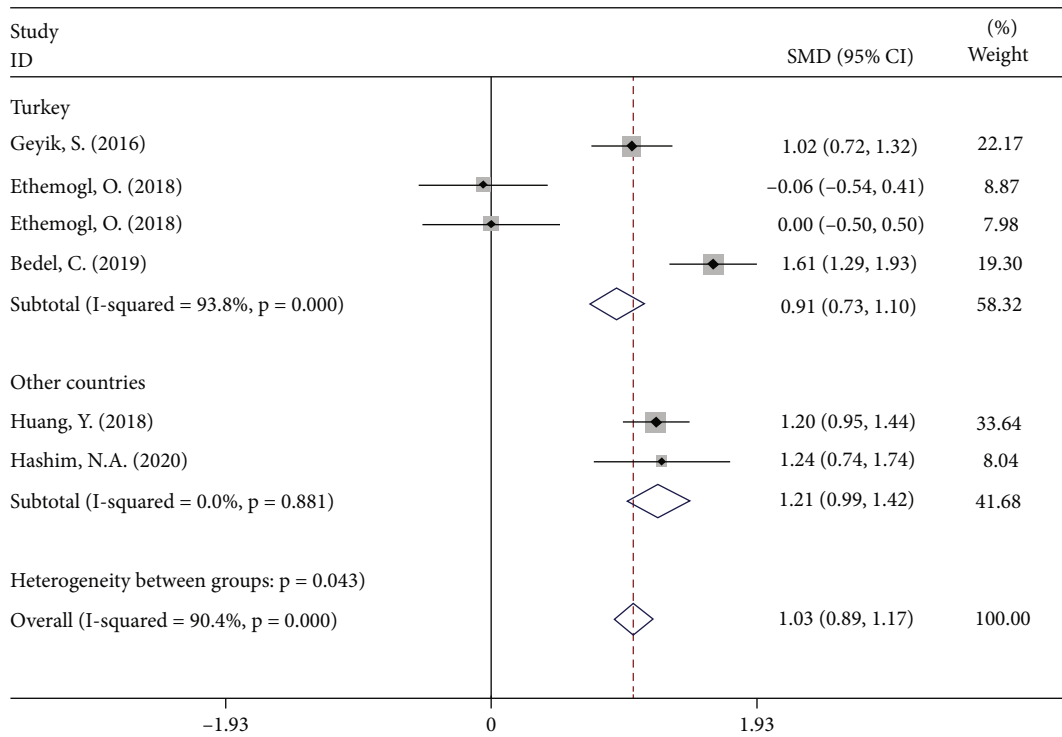
FIGURE 4: Subgroup analysis of differences in NLR levels between GBS patients before treatment and healthy controls according to study location.
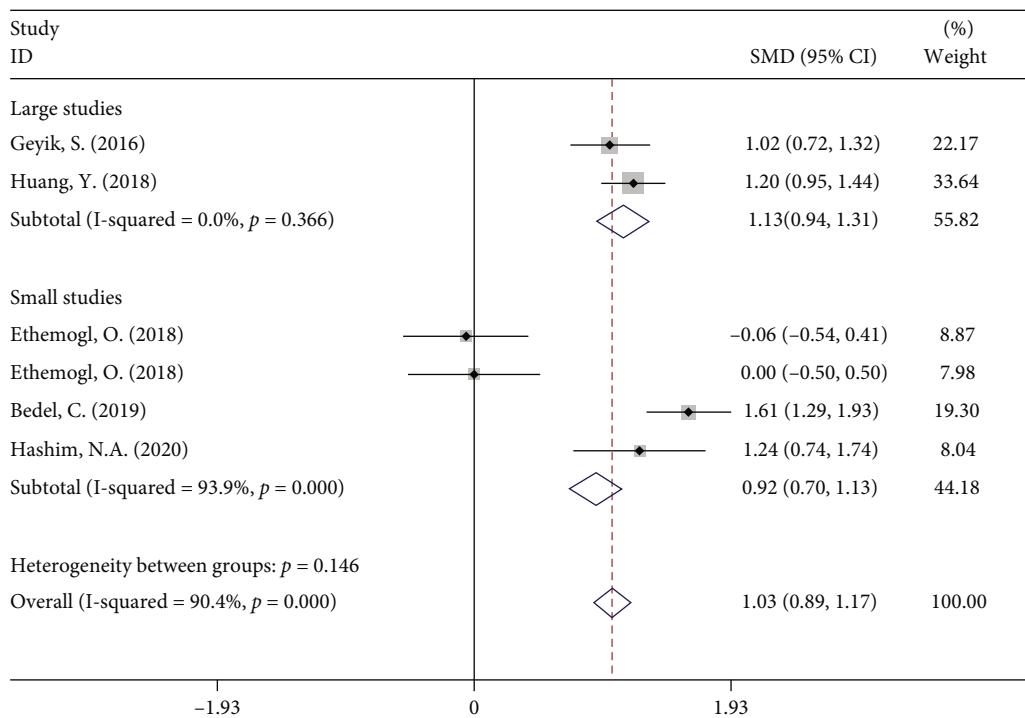
FIGURE 5: Subgroup analysis of differences in NLR levels between GBS patients before treatment and healthy controls according to sample size.

Study ID	SMD (95% CI)	(%) Weight
Geyik et al. (2016)	0.99 (0.68, 1.29)	26.98
Ethemogl et al. (2018)	0.12 (−0.21 0.46)	26.53
Huner et al. (2018)	0.62 (0.08, 1.17)	23.15
Hashim et al. (2020)	1.54 (1.01, 2.08)	23.34
Overall I-squared = 87.6%	0.80 (0.22, 1.38)	100.00

NOTE: Weights are from random effects analysis

−2.08   0   2.08
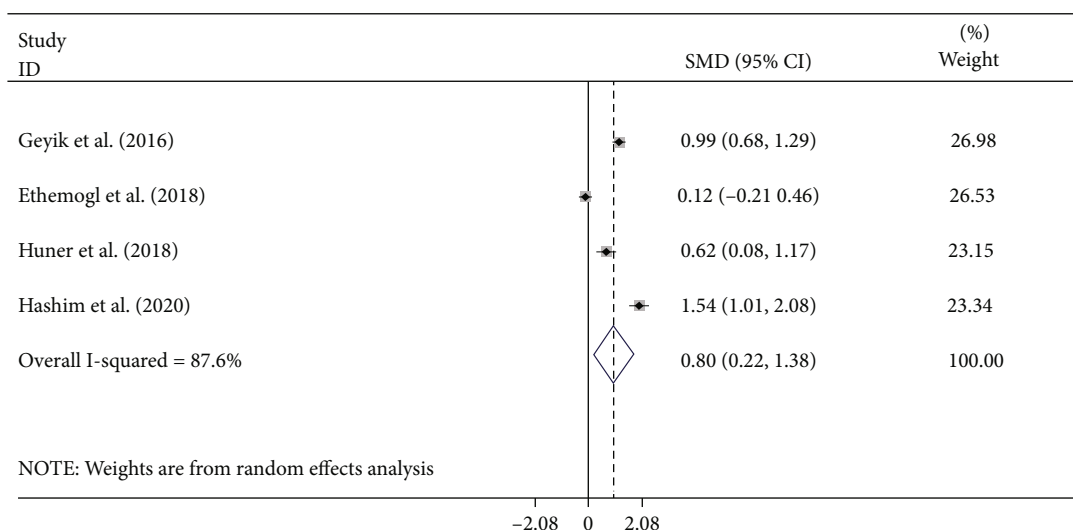
FIGURE 6: Meta-analysis of differences in NLR levels between pre- and posttreatment GBS.

effects model, SMD = 0.80, 95%CI = 0.22 to 1.38, $P < 0.001$) (Figure 6).

In addition, NLR levels of GBS patients after treatment became similar to those of controls (fixed-effects model, SMD = −0.04, 95%CI = −0.23 to 0.16, $P = 0.71$) based on three studies [11–13] comprising 197 patients and 204 controls (Figure 7).

3.5. Association of NLR with Prognosis in Patients with GBS.
Three of the ten studies [11–13] comprising 197 patients evaluated the relationship between NLR and outcome after treatment in patients with GBS. The pooled results showed that patients with bad outcomes had higher levels of NLR compared with good outcome patients after treatment (fixed-effects model, SMD = 1.02, 95%CI = 0.65 to 1.38, $P < 0.001$) (Figure 8). In other words, patients with lower NLR had a better response to treatment in comparison with those with higher NLR.

3.6. Association of NLR with Mechanical Ventilation in Patients with GBS.
Three of the ten studies comprising 706 patients evaluated the relationship between NLR and outcome after treatment in patients with GBS. The pooled results showed that patients who underwent mechanical ventilation had higher levels of NLR compared to those who did not (random-effects model, SMD = 0.93, 95%CI = 0.05 to 1.82, $P = 0.03$) (Figure 9). In other words, patients with lower NLR had a better response to treatment in comparison with those with higher NLR.

3.7. Differences in NLR Levels among GBS Subtypes.
Of the ten studies, five studies [10–13, 16], including 357 patients with GBS, reported the differences in NLR levels between axonal subtypes (including AMAN and AMSAN) and AIDP. Of the five studies, three more detailed studies [12, 13, 16] included 191 patients with GBS, including 117 cases with AIDP subtype and 74 cases with axonal subtype comprising 35 with AMAN and 39 AMSAN and compared these subgroups two-by-two. The pooled results showed that there

was no significant difference in NLR levels between AIDP and axonal subtypes (random-effects model, SMD = −0.08, 95%CI = −0.60 to 0.45, $P = 0.772$), AIDP and AMAN (random-effects model, SMD = 0.08, 95%CI = −0.59 to 0.75, $P = 0.807$), AIDP and AMSAN (random-effects model, SMD = −0.33, 95%CI = −1.53 to 0.67, $P = 0.588$), and AMAN and AMSAN (random-effects model, SMD = 0.19, 95%CI = −0.28 to 0.67, $P = 0.427$) (Figures 10–13).

3.8. Publication Bias and Small Study Effect.
The results of studies on either difference in NLR levels between GBS cases and controls [10–14] (Figure 14(a)) or differences between pre- and posttreatment NLR levels in GBS cases [11–13, 15] (Figure 14(b)) showed no statistically significant publication bias (Egger's test P value = 0.98 and 0.52, respectively).

4. Discussion

Our results showed that NLR levels were significantly increased in the patients with GBS compared with healthy controls. After treatment, NLR levels were decreased to the extent that they became similar to healthy controls. Moreover, NLR was a good predictor of outcome or response to treatment in such patients; the higher the NLR, the worse the outcome. In addition, NLR could predict the need for mechanical ventilation. Interestingly, NLR levels were not different among distinct GBS subtypes, so it could not distinguish among them.

In addition to the findings of our meta-analysis, previous studies mentioned some other roles for NLR in GBS. For example, it has been shown that the NLR correlates with disability scores in GBS such as the HDS and the medical research council (MRC) sum scale [12, 13, 18, 20–23]. Sahin et al. revealed that NLR was a predictor of facial diplegia [21] in GBS patients. Also, they mentioned that NLR had a statistically significant correlation with worse nerve conduction studies (NCS) findings such as changes in distal latency, main F latency, conduction velocity, and amplitude [21]. Kim et al. reported that GBS patients who fully recovered
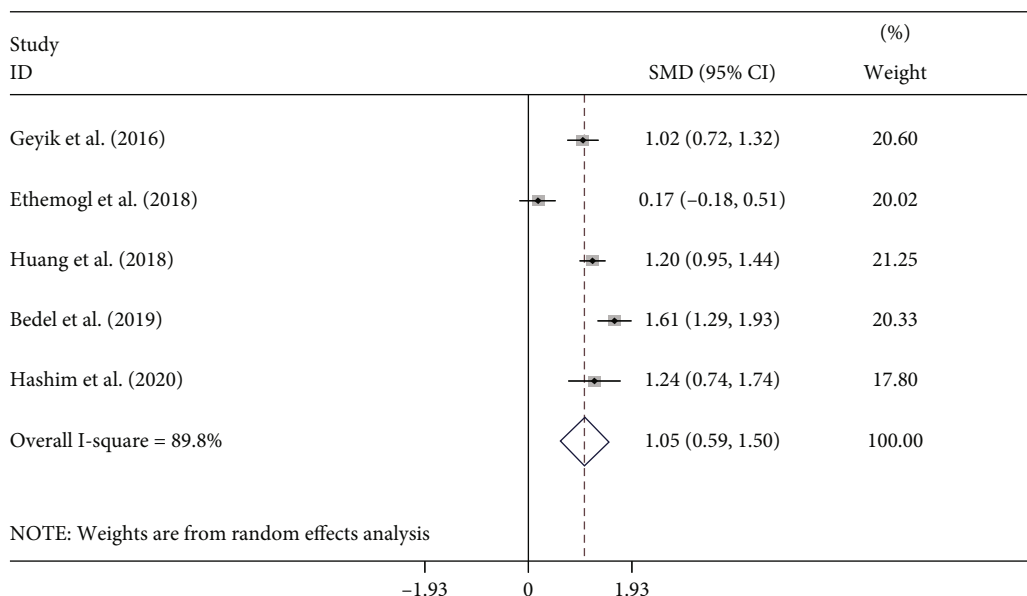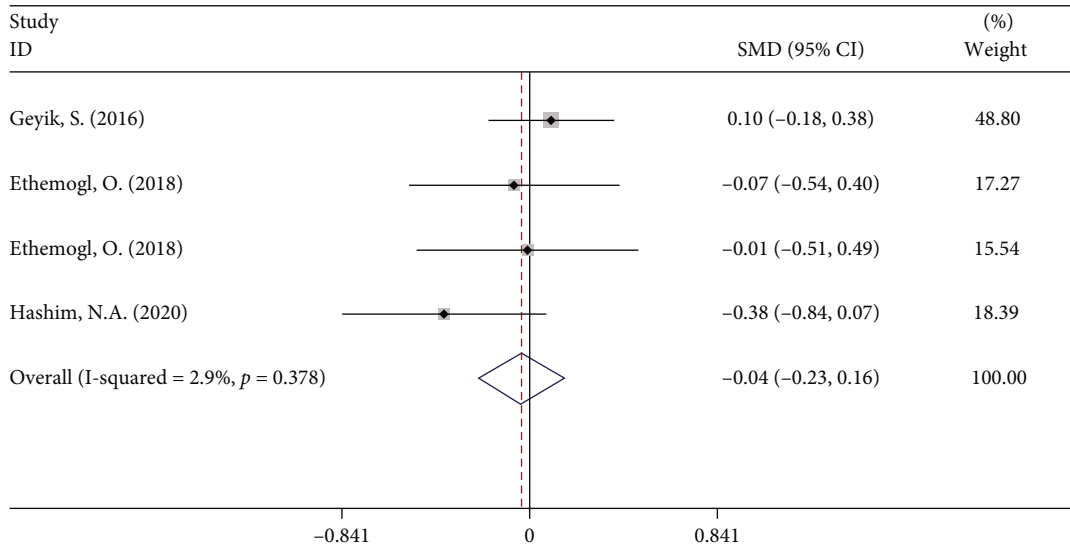
FIGURE 7: Meta-analysis of differences in NLR levels between GBS patients after treatment and healthy controls.
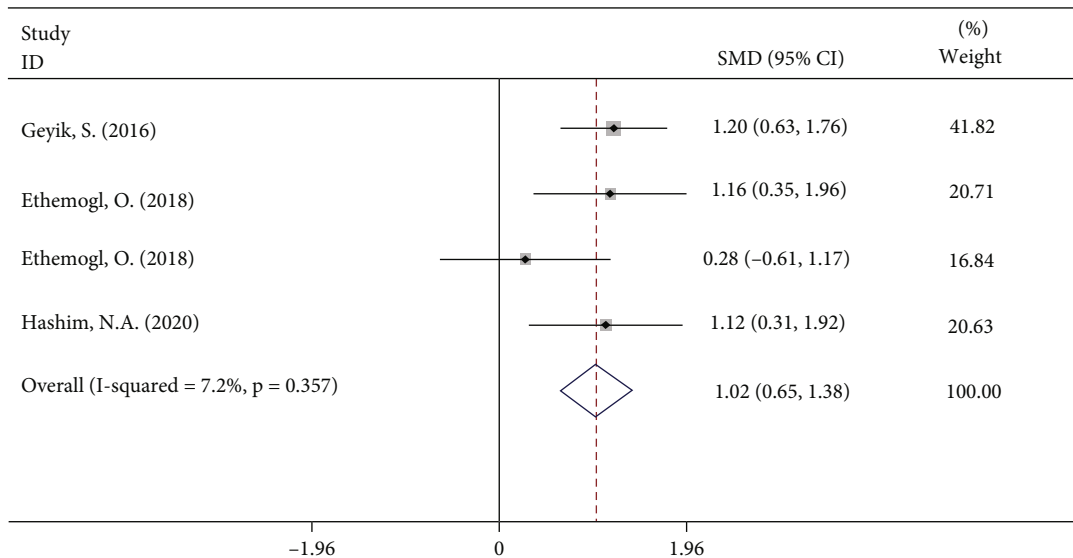
FIGURE 8: Meta-analysis of differences in NLR levels between GBS patients with good and bad outcome.

without any residual symptoms, compared to those with residual symptoms more than six months after the onset of disease, had significantly lower levels of NLR [19].

NLR is an established marker of inflammation and may reflect an underlying proinflammatory state, as well as immunologic dysfunction, in patients with GBS. Specifically, an elevated NLR may reflect an immune system imbalance [5]. As a brief explanation, neutrophils are a central component of the innate immune system which serves to enhance proinflammatory immune responses to fight pathogens and rid the body of foreign material [26]. On the other hand, lymphocytes are central players in the adaptive immune system, which serves to attenuate proinflammatory responses and regulate immunologic reactions [27]. A relative reduction in adaptive immunity, as reflected by an elevated NLR

value, could lead to unregulated proinflammatory responses which contribute in GBS development.

GBS is the leading cause of acute flaccid paralysis. Although the clinical features are varied, patients often present with sensory symptoms and weakness in the legs that advance to the central core muscles and arms [2]. In the absence of adequately specific and sensitive biomarkers, GBS is diagnosed based on the patient's medical history and electrophysiological, neurological, and cerebrospinal fluid investigation [1].

Throughout outbreaks of infectious diseases that cause GBS, the disease prevalence might rise [1]. For example, the COVID-19 virus epidemics have lately been connected to an upsurge in the number of people diagnosed with GBS [28]. Indeed, the outbreak of COVID-19 virus highlighted the lack
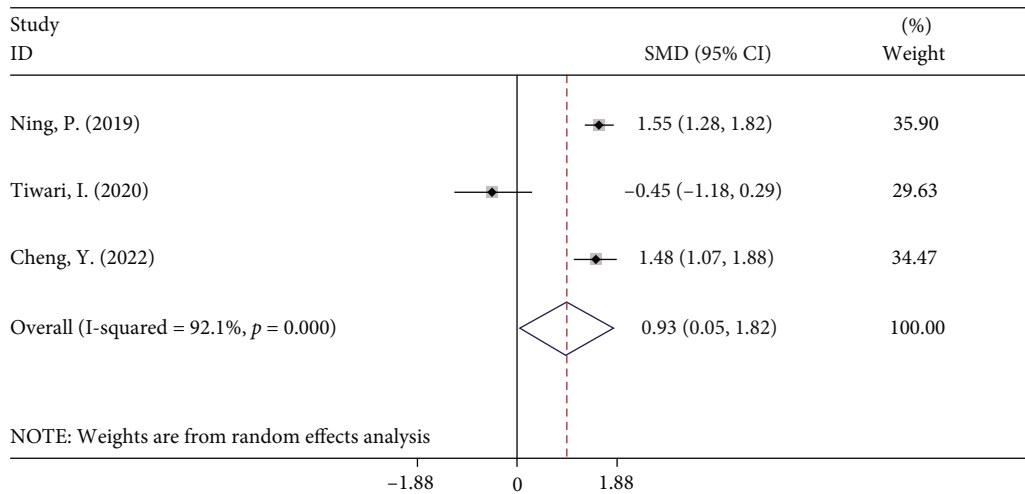
FIGURE 9: Meta-analysis of differences in NLR levels between GBS patients who underwent mechanical ventilation and those who did not.
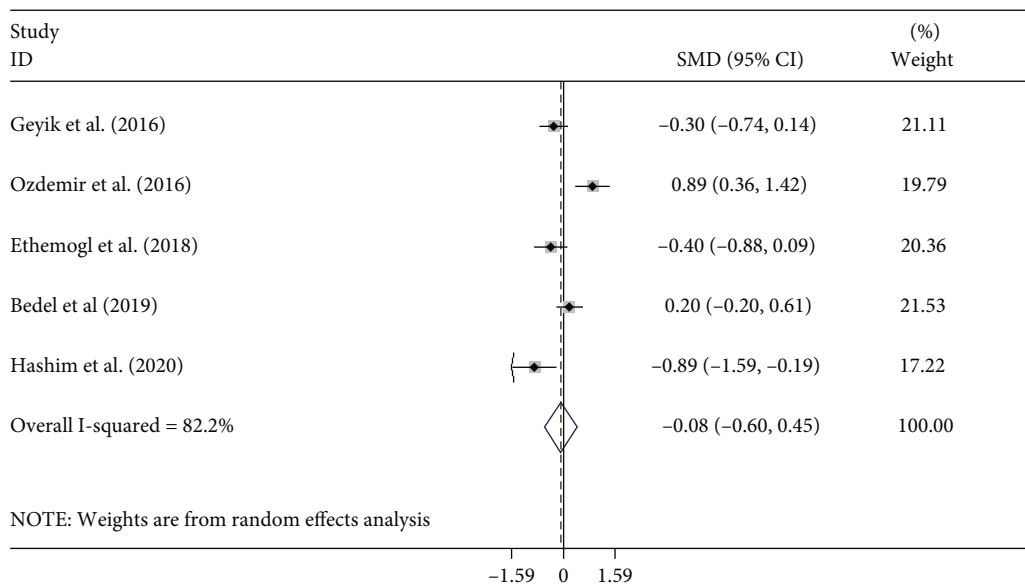
FIGURE 10: Meta-analysis of differences in NLR levels between patients with AIDP and axonal GBS.

of universally applicable criteria for the diagnosis and treatment of GBS. It showed the need for more research on this relatively poorly understood disorder [29]. Such investigations are necessary because the diagnosis of GBS is still challenging due to the lack of highly specific and sensitive diagnostic biomarkers, an extensive differential diagnosis, and heterogeneity in clinical presentation [1]. Furthermore, because illness development and outcome differ widely, prognostic indicators for GBS patients must be found [1].

Accordingly, among GBS patients, the role of some biomarkers such as tumor necrosis factor, hypocretin-1, neuron-specific enolase, myelin basic protein, neurofilaments, anti-ganglioside antibodies, neuron-specific enolase, neurofilaments, hypocretin-1, myelin basic protein, chemokines, and complements in disease prognosis and pathology has been established [11]. Furthermore, a recent meta-

analysis found that Th1-, Th2-, and Th17-related cytokines were all significantly higher in GBS patients [30]. Although the pathophysiology of GBS is unknown, these findings can be explained by the fact that GBS is caused by an abnormal immune response to infectious pathogens that lead to peripheral nerve injury [30]. Asbury and colleagues explored the role of the inflammatory process in GBS for the very first time in 1969 [31]. They discovered that lymphocyte infiltrates in the nerves in many GBS patients. They also discovered that even in individuals who had healed, persistent inflammation was present, leading them to believe that this is a potential cause of relapse [31]. Since then, a lot of effort has gone into figuring out how the immune system plays a role in inflammation. T cells have been found in the epineurium and endoneurium in sural nerve biopsies of GBS patients, and both CD8+ and CD4+ phenotypes have been

Study ID	SMD (95% CI)	(%) Weight
Geyik et al. (2016)	−0.13 (−0.68, 0.42)	38.57
Ethemogl et al. (2016)	0.75 (0.77, 1.42)	34.09
Hashim et al. (2020)	−0.44 (−1.32, 0.44)	27.34
Overall I-squared = 64.6%	0.80 (−0.59, 0.75)	100.00

NOTE: Weights are from random effects analysis

−1.42   0   1.42
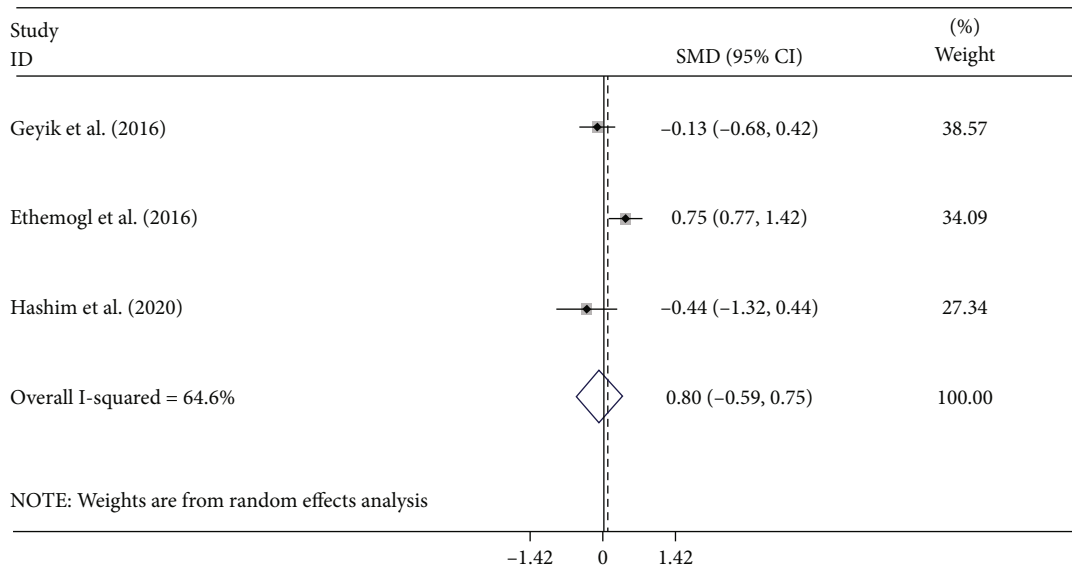
FIGURE 11: Meta-analysis of differences in NLR levels between patients with AIDP and AMAN GBS.

Study ID	SMD (95% CI)	(%) Weight
Geyik et al. (2016)	−0.50 (−1.08, 0.08)	34.48
Ozdermir et al. (2016)	0.82 (0.20, 1.45)	34.06
Hashim et al. (2020)	−1.39 (−2.26, −0.53)	31.46
Overall I-squared = 89.3%	−0.33 (−1.53, 0.87)	100.00

NOTE: Weights are from random effects analysis

−2.26   0   2.26
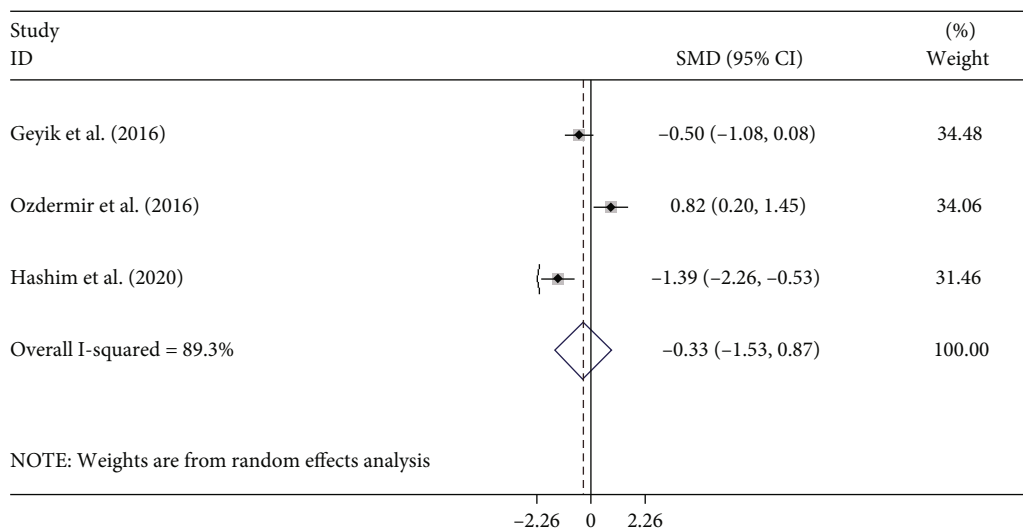
FIGURE 12: Meta-analysis of differences in NLR levels between patients with AIDP and AMSAN GBS.

detected in these infiltrating T cells [4]. In addition to T cells, there is an elevation in the number of macrophages in the epineurium and endoneurium of these nerves [4].

Furthermore, Yoshii and Shinohara discovered that natural killer cell function was lower in GBS than in the control group [4]; the authors suggested that natural killer cell activity deficiencies could leave people vulnerable to GBS because these cells suppress the immune system [4]. The majority of GBS studies, on the other hand, have concentrated on the diagnostic and prognostic role of cytokines [30]. Not surprisingly, because of the robust immune response, there are changes in cytokine and inflammatory biomarkers' levels in GBS [4].

Considering the involvement of inflammatory processes in hematopoietic multiple-lineage alterations, NLR can be used as an affordable and readily available marker for systemic inflammation [5, 32]. It is, in fact, the number of neutrophils divided by the total number of lymphocytes and is widely employed as a reliable and easily accessible biomarker for multiple conditions [5, 32]. The average range of NLR in adults is 1-2, with values greater than 3.0 and less than 0.7 being abnormal [5]. NLR in the 2.3-3.0 range may act as an early warning sign for pathological conditions or processes such as cancer, atherosclerosis, mental disorders, and neurologic illnesses [5]. It has also been proven in multiple studies to be a highly sensitive sign for infection [33], inflammation, and sepsis [34]. In critical illness or acute disease, NLR should be evaluated on a daily basis, with absolute values and dynamic course being monitored [5]. It should be utilized on a regular basis in emergency rooms, intensive
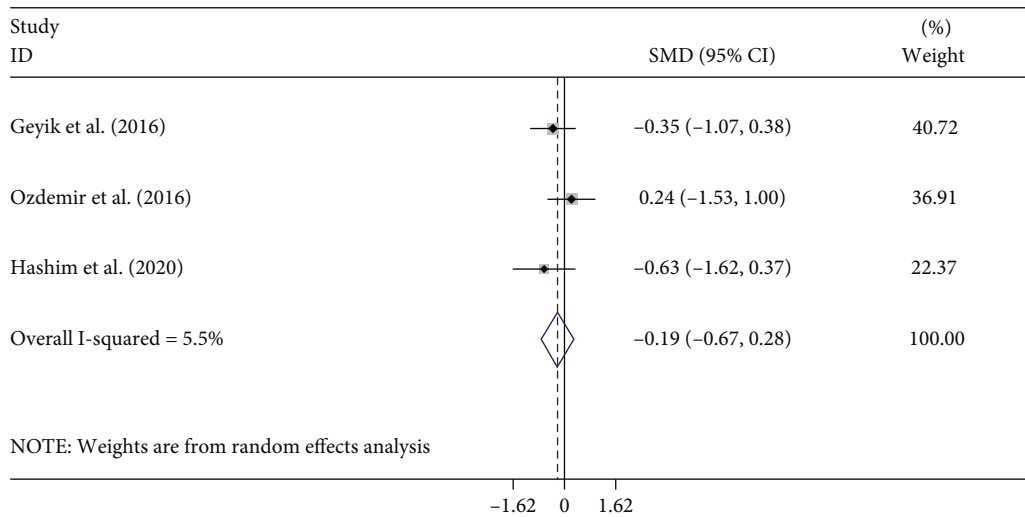
FIGURE 13: Meta-analysis of differences in NLR levels between patients with AMSAN and AMSAN GBS.
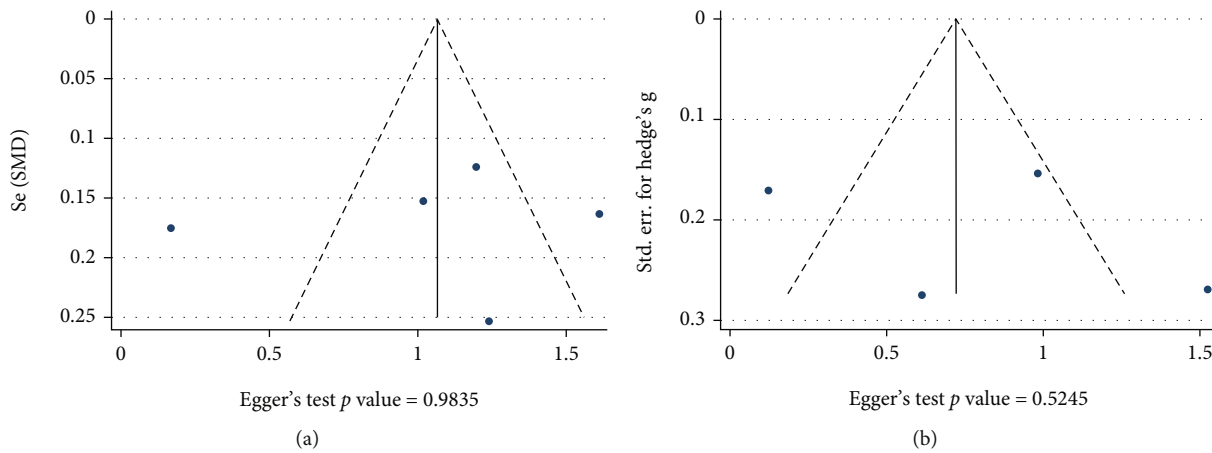
FIGURE 14: Publication bias between studies on (a) differences in NLR levels between GBS cases and controls and (b) differences between pre- and posttreatment NLR levels in GBS cases.

care units, and acute medicine settings such as surgery, orthopedics, traumatology, cardiology, neurology, psychiatry, and even on cancer wards [5].

Zahorec, in 2021, postulated that elevated NLR values are secondary to a multifactorial process involving neuroendocrine and immunologic input [5]. Stress and severe illness can activate the hypothalamic-pituitary-adrenal (HPA) axis leading to elevations in cortisol that stimulate neutrophil demargination and maturation, as well as lymphocyte apoptosis [35–39]. Immunologically, severe illness increases the production of neutrophils from the bone marrow and can lead to lymphopenia via various proposed mechanisms [40–42]. Ultimately, a relative neutrophilia and lymphopenia can result, leading to an elevated NLR.

The findings in this report are subject to at least four restrictions. First, there was significant statistical heterogeneity across studies, as previously stated. This is most likely due to variations in study inclusion criteria, recruiting condi-

tions, and target population. Furthermore, the majority of the studies included did not give information on the stage of GBS. As a result, the varied phases of patients across studies may have contributed to the between-study heterogeneity reported in this meta-analysis (Table 2).

Nonetheless, these findings underscore the necessity for ongoing research into the NLR level in GBS patients, as well as the control of pertinent clinical and methodological variables. This should be done in order to better understand the disease's cause. Another limitation was that the data retrieved from the relevant papers did not allow for the testing of the relationship between NLR and facial diplegia (a common symptom of GBS) and patients' mortality. As a result, these are critical topics that should be investigated further.

In conclusion, this is the first systematic review and meta-analysis to assess the NLR levels in patients with GBS. Our analysis indicates that the NLR levels are highly

TABLE 2: General characteristics of studies included merely in qualitative review.

First author	Year	Design	Region	Age group	Main findings	NOS score
Gumusyayla	2017	R	Turkey	Adults	NLR were found to be significantly higher in GBS patients participating in the study than healthy volunteers. In addition, NLR was positively correlated with the Hughes score and negatively correlated with the MRC sum score calculated at the time of admission and three months after admission.	6
Sahin	2017	R	Turkey	Adults	NLR was a predictor of facial diplegia in GBS patients. Also, NLR had a statistically significant correlation with MRC and NCS findings such as distal latency, main F latency, conduction velocity, and amplitude.	6
Kim	2019	R	Korea	Children	NLR was not different between GBS patients with full recovery and those with functional deficit after treatment.	6
Tunc	2019	R	Turkey	Adults	NLR was significantly correlated with HDS at the end of the first month after GBS.	7

R: retrospective; P: prospective; NLR: neutrophil to lymphocyte ratio; NCS: nerve conduction studies; HDS: Hughes disability score; A: adults; C: children.

elevated in patients with GBS. Therefore, the NLR has the potential to be used as biomarkers to inform diagnosis, prognosis, or treatment responses in GBS, and future studies are necessary to validate this hypothesis.

Abbreviations

GBS: Guillain Barré syndrome
AIDP: Acute inflammatory demyelinating
            polyradiculoneuropathy
AMSAN: Acute motor-sensory axonal neuropathy
NLR: Neutrophil to lymphocyte ratio
PRISMA: Preferred Reporting Items for Systematic Review
            and Meta-Analyses
HDS: Hughes disability score
NOS: Newcastle-Ottawa scale
SMD: Standardized mean difference
95% CI: 95% confidence interval
MRC: Medical research council
NCS: Nerve conduction studies.

Data Availability

The dataset supporting the conclusions of this article is included within the article.

Conflicts of Interest

The authors declare that they have no competing interests.

Authors' Contributions

All authors contributed to the design of the study. ShKh undertook the initial searches and screened articles for inclusion. Then, SO wrote the initial draft of the manuscript. Finally, ShKh edited the initial draft and all authors approved the final manuscript.

References

[1] S. E. Leonhard, M. R. Mandarakas, F. A. Gondim et al., "Diagnosis and management of Guillain-Barre syndrome in ten steps," *Nature Reviews Neurology.*, vol. 15, no. 11, pp. 671–683, 2019.

[2] N. Abbassi and G. Ambegaonkar, "Guillain-Barre syndrome: a review," *Paediatrics and Child Health*, vol. 29, no. 11, pp. 459–462, 2019.

[3] L. Querol and C. Lleixà, "Novel immunological and therapeutic insights in Guillain-Barré syndrome and CIDP," *Neurotherapeutics*, vol. 18, no. 4, pp. 2222–2235, 2021.

[4] K. M. Hagen and S. S. Ousman, "The neuroimmunology of Guillain-Barré syndrome and the potential role of an aging immune system," *Frontiers in Aging Neuroscience*, vol. 12, p. 492, 2021.

[5] R. Zahorec, "Neutrophil-to-lymphocyte ratio, past, present and future perspectives," *Bratislavske Lekarske Listy.*, vol. 122, no. 7, pp. 474–488, 2021.

[6] C. Kumarasamy, S. Sabarimurugan, R. M. Madurantakam et al., "Prognostic significance of blood inflammatory biomarkers NLR, PLR, and LMR in cancer—a protocol for systematic review and meta-analysis," *Medicine*, vol. 98, no. 24, p. e14834, 2019.

[7] T. Angkananard, T. Anothaisintawee, M. McEvoy, J. Attia, and A. Thakkinstian, "Neutrophil lymphocyte ratio and cardiovascular disease risk: a systematic review and meta-analysis," *BioMed Research International*, vol. 2018, Article ID 2703518, 11 pages, 2018.

[8] S.-Y. Song, X.-X. Zhao, G. Rajah et al., "Clinical significance of baseline neutrophil-to-lymphocyte ratio in patients with ischemic stroke or hemorrhagic stroke: an updated meta-analysis," *Frontiers in Neurology*, vol. 10, p. 1032, 2019.

[9] L. Muñoz-Delgado, D. Macías-García, S. Jesús et al., "Peripheral immune profile and neutrophil-to-lymphocyte ratio in Parkinson's disease," *Movement Disorders*, vol. 36, no. 10, pp. 2426–2430, 2021.

[10] C. Bedel and M. Korkut, "The clinical significance of neutrophil lymphocyte ratio, monocyte lymphocyte ratio and platelet lymphocyte ratio in patients with Guillain-Barré syndrome," *Medical Journal Of Haydarpaşa Numune Training and Research Hospital*, vol. 61, no. 3, 2020.

[11] O. Ethemoglu and M. Calik, "Effect of serum inflammatory markers on the prognosis of adult and pediatric patients with Guillain–Barré syndrome," *Neuropsychiatric Disease and Treatment*, vol. 14, pp. 1255–1260, 2018.

[12] S. Geyik, H. Bozkurt, M. Neyal, R. Yigiter, S. Kuzudisli, and S. Kul, "The clinical significance of the neutrophil-to-

lymphocyte ratio in patients with Guillain-Barré syndrome independent of infection," *Medical Science and Discovery.*, vol. 3, no. 8, pp. 305–311, 2016.

[13] N. A. Hashim, W. S. Mohamed, and E. M. Emad, "Neutrophil–lymphocyte ratio and response to plasmapheresis in Guillain–Barré syndrome: a prospective observational study," *The Egyptian Journal of Neurology, Psychiatry and Neurosurgery*, vol. 56, no. 1, pp. 1–6, 2020.

[14] Y. Huang, Z. Ying, W. Quan et al., "The clinical significance of neutrophil-to-lymphocyte ratio and monocyte-to-lymphocyte ratio in Guillain–Barré syndrome," *International Journal of Neuroscience.*, vol. 128, no. 8, pp. 729–735, 2018.

[15] E. A. Hüner, A. I. Dai, and A. T. Demiryürek, "Association of neutrophil/lymphocyte ratio with intravenous immunoglobulin treatment in children with Guillain-Barré syndrome," *Journal of Child Neurology*, vol. 33, no. 2, pp. 164–167, 2018.

[16] H. H. Ozdemir, "Analysis of the albumin level, neutrophil-lymphocyte ratio, and platelet-lymphocyte ratio in Guillain-Barré syndrome," *Arquivos de neuro-psiquiatria.*, vol. 74, no. 9, pp. 718–722, 2016.

[17] X. Wan, W. Wang, J. Liu, and T. Tong, "Estimating the sample mean and standard deviation from the sample size, median, range and/or interquartile range," *BMC Medical Research Methodology*, vol. 14, no. 1, pp. 1–13, 2014.

[18] Ş. Gümüşyayla and G. Vural, "The predictive value of neutrophil-lymphocyte ratio in disability of Gullain-Barr⊠ syndrome," *Bakirkoy Tip Dergisi*, vol. 15, no. 3, pp. 187–192, 2019.

[19] S. H. Kim, F. Samadov, A. Mukhamedov et al., "Clinical characteristics and prognostic factors of children with Guillain-Barré syndrome," *Annals of Child Neurology*, vol. 27, no. 4, pp. 113–119, 2019.

[20] P. Ning, B. Yang, X. Yang et al., "A nomogram to predict mechanical ventilation in Guillain-Barré syndrome patients," *Acta Neurologica Scandinavica.*, vol. 142, no. 5, pp. 466–474, 2020.

[21] S. Sahin, N. Cinar, and S. Karsidag, "Are cerebrospinal fluid protein levels and plasma neutrophil/lymphocyte ratio associated with prognosis of Guillain Barré syndrome," *Neurology International*, vol. 9, no. 2, pp. 21–24, 2017.

[22] I. Tiwari, A. Alam, C. Kanta et al., "Clinical profile and predictors of mechanical ventilation in Guillain-Barre syndrome in North Indian children," *Journal of Child Neurology*, vol. 36, no. 6, pp. 453–460, 2021.

[23] A. Tunç, "Early predictors of functional disability in Guillain–Barré Syndrome," *Acta Neurologica Belgica.*, vol. 119, no. 4, pp. 555–559, 2019.

[24] Y. Cheng, K. Liu, C. Li, W. Zhang, X. Wu, and S. Fang, "Risk factors for mechanical ventilation in patients with Guillain–Barré syndrome," *Neurocritical Care*, vol. 37, no. 1, pp. 121–128, 2022.

[25] P. Ning, B. Yang, X. Yang et al., "Lymphocyte-based ratios for predicting respiratory failure in Guillain-Barre syndrome," *Journal of Neuroimmunology*, vol. 353, p. 577504, 2021.

[26] K. Ley, H. M. Hoffman, P. Kubes et al., "Neutrophils: new insights and open questions," *Science Immunology*, vol. 3, no. 30, p. eaat4579, 2018.

[27] F. A. Bonilla and H. C. Oettgen, "Adaptive immunity," *The Journal of Allergy and Clinical Immunology*, vol. 125, no. 2, pp. S33–S40, 2010.

[28] L. Palaiodimou, M. I. Stefanou, A. H. Katsanos et al., "Prevalence, clinical characteristics and outcomes of Guillain–Barré syndrome spectrum associated with COVID-19: a systematic review and meta-analysis," *European Journal of Neurology*, vol. 28, no. 10, pp. 3517–3529, 2021.

[29] I. Hasan, K. Saif-Ur-Rahman, S. Hayat et al., "Guillain-Barré syndrome associated with SARS-CoV-2 infection: a systematic review and individual participant data meta-analysis," *Journal of the Peripheral Nervous System.*, vol. 25, no. 4, pp. 335–343, 2020.

[30] T. Sun, X. Chen, S. Shi, Q. Liu, and Y. Cheng, "Peripheral blood and cerebrospinal fluid cytokine levels in Guillain Barré syndrome: a systematic review and meta-analysis," *Frontiers in Neuroscience*, vol. 13, p. 717, 2019.

[31] A. K. Asbury, B. G. Arnason, and R. D. Adams, "The inflammatory lesion in idiopathic polyneuritis," *Medicine*, vol. 48, no. 3, pp. 173–215, 1969.

[32] P. Forget, C. Khalifa, J.-P. Defour, D. Latinne, M.-C. Van Pel, and M. De Kock, "What is the normal value of the neutrophil-to-lymphocyte ratio?," *BMC Research Notes*, vol. 10, no. 1, pp. 1–4, 2017.

[33] X. Li, C. Liu, Z. Mao et al., "Predictive values of neutrophil-to-lymphocyte ratio on disease severity and mortality in COVID-19 patients: a systematic review and meta-analysis," *Critical Care.*, vol. 24, no. 1, pp. 1–10, 2020.

[34] Z. Huang, Z. Fu, W. Huang, and K. Huang, "Prognostic value of neutrophil-to-lymphocyte ratio in sepsis: a meta-analysis," *The American Journal of Emergency Medicine*, vol. 38, no. 3, pp. 641–647, 2020.

[35] D. M. Cavalcanti, C. M. Lotufo, P. Borelli et al., "Adrenal deficiency alters mechanisms of neutrophil mobilization," *Molecular and Cellular Endocrinology*, vol. 249, no. 1-2, pp. 32–39, 2006.

[36] S. Ronchetti, E. Ricci, G. Migliorati, M. Gentili, and C. Riccardi, "How glucocorticoids affect the neutrophil life," *International Journal of Molecular Sciences*, vol. 19, no. 12, p. 4090, 2018.

[37] L. H. Ramaekers, P. M. Theunissen, and K. Went, "Acute lymphopenia, stress, and plasma cortisol," *Archives of Disease in Childhood*, vol. 50, no. 7, pp. 555–559, 1975.

[38] D. Zierath, P. Tanzi, D. Shibata, and K. J. Becker, "Cortisol is more important than metanephrines in driving changes in leukocyte counts after stroke," *Journal of Stroke and Cerebrovascular Diseases*, vol. 27, no. 3, pp. 555–562, 2018.

[39] R. Zahorec, "Ratio of neutrophil to lymphocyte counts–rapid and simple parameter of systemic inflammation and stress in critically ill," *Bratislavské Lekárske Listy*, vol. 102, no. 1, pp. 5–14, 2001.

[40] T. Suwa, J. C. Hogg, D. English, and S. F. Van Eeden, "Interleukin-6 induces demargination of intravascular neutrophils and shortens their transit in marrow," *American Journal of Physiology. Heart and Circulatory Physiology*, vol. 279, no. 6, pp. H2954–H2960, 2000.

[41] D. Xiao, Z. Zhao, J. Liu et al., "Diagnosis of invasive meningioma based on brain-tumor interface radiomics features on brain MR images: a multicenter study," *Frontiers in Oncology*, vol. 11, 2021.

[42] C. Summers, S. M. Rankin, A. M. Condliffe, N. Singh, A. M. Peters, and E. R. Chilvers, "Neutrophil kinetics in health and disease," *Trends in Immunology*, vol. 31, no. 8, pp. 318–324, 2010.

Research Article

Development and Validation of a Novel Nomogram to Predict the Risk of Intervertebral Disc Degeneration

Fudong Li [iD],[1] **Xiaofei Sun** [iD],[1] **Yuan Wang** [iD],[1] **Lu Gao** [iD],[2] **Jiangang Shi** [iD],[1] **and Kaiqiang Sun** [iD][3]

[1]*Department of Orthopedic Surgery, Shanghai Changzheng Hospital, Navy Medical University, Shanghai 200003, China*
[2]*Department of Physiology, Navy Medical University, Shanghai 200433, China*
[3]*Department of Orthopaedic Surgery, Naval Medical Center, Navy Medical University, Shanghai 200433, China*

Correspondence should be addressed to Lu Gao; lu.gao@smmu.edu.cn, Jiangang Shi; changzhengspine@smmu.edu.cn, and Kaiqiang Sun; 15721570551@163.com

Intervertebral disc degeneration (IVDD) has been a complex disorder resulted from genetic and environmental risk factors. The aim of this study was to identify the risk factors associated with IVDD in orthopaedic patients and develop a prediction model for predicting the risk of IVDD. A total of 309 patients were retrospectively included in the study and randomly divided into the training group and the validation group. The least absolute shrinkage and selection operator regression (LASSO) and the univariate logistic regression analysis were used to optimize factors selection for the IVDD risk model. Multivariable logistic regression analysis was used to establish a predicting nomogram model incorporating the factors. In addition, discrimination, calibration, and clinical usefulness of the nomogram model were evaluated via the C-index, receiver operating characteristic (ROC) curve, calibration plot, and decision curve analysis (DCA). Then, based on the results above, the relationship between IVDD and angiotensin II (AngII) level in peripheral blood was examined prospectively. The predictors of the nomogram include age, sex, hypertension, diabetes, gout, working posture, and exercising hours per week. The C-index values of the training and validation groups were 0.916 (95% CI, 0.876-0.956) and 0.949 (95% CI, 0.909-0.989), respectively, which indicated that the model displayed good discrimination. In addition, the area under the curve (AUC) values of the ROC curve of the training and the validation group were 0.815 (95% CI, 0.759-0.870) and 0.805 (95% CI, 0.718-0.892), respectively, revealing the satisfactory discrimination performance of the model. The prospective investigation showed that the average AngII level in the degenerated group (97.62 ± 44.02 pg/mL) was significantly higher than that in the nondegenerated group (52.91 ± 9.01 pg/mL) ($p < 0.001$). This present study explored the risk factors for IVDD and established a prediction model, which would effectively predict the risk of IVDD. In addition, based on the prediction model, AngII was revealed to be a potentially auxiliary clinical diagnostic marker for IVDD.

1. Introduction

Low back pain (LBP) is one of the major causes of disability worldwide, which often leads to bad quality of life. It was estimated that up to 80% of the individuals experienced LBP at some point during their entire lifetime [1]. In addition, it was reported that the lifetime morbidity of neck-related pain was more than 65% [2]. These conditions above impose a huge socioeconomic burden on the society [3]. LBP and neck-related pain are both symptoms resulted from intervertebral disc degeneration (IVDD). IVDD, an ageing-related disorder, is one of the most common diseases in clinical practice. IVDD is widely recognized as a contributor to spinal degenerative diseases, which is characterized by the loss of nucleus pulposus cells and the degradation of extracellular matrix (ECM).
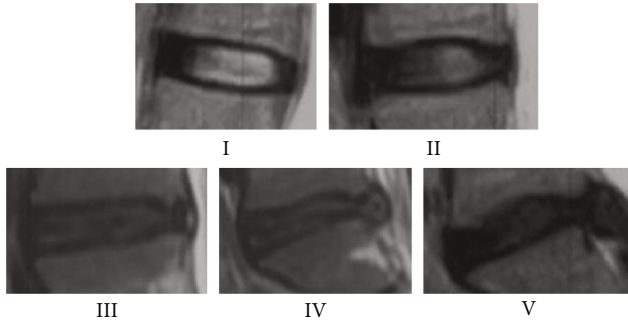
Figure 1: The degree of IVDD is evaluated by the Pfirrmann grade system. The discs with Pfirrmann grades I or II are nondegenerative discs, and the discs with grades III, IV, and V are taken as degenerative discs.

It is widely recognized that IVDD is caused by both environmental and genetic factors. While genetic factors play a critical role in IVDD, it cannot be ignored that environmental factors including living conditions, lifestyle characteristics, and chronic diseases tend to be closely associated with the risk of disc degeneration [4]. Kuisma et al. reported that Modic change was closely associated with IVDD [5]. In addition, IVDD was associated with metabolic diseases such as diabetes and hyperlipidemia [6, 7]. Our previous study revealed that the degenerated IVD tissue showed excessively activated the tissue renin-angiotensin system (tRAS) that can lead to nucleus pulposus cell (NPC) senescence, apoptosis, oxidative stress, and inflammatory reaction [8]. The activation of renin-angiotensin system (RAS) including both the systemic RAS and the tRAS has long been considered an essential part during the development of hypertension [9]. Therefore, we deduced that hypertension may be a potential risk factor for IVDD. What is more, manual handling and postures of the trunk were associated with IVDD. Yuya et al. reported that exercise can attenuate LBP and result in epigenetic alterations in IVDD [10]. In a cross-sectional case-control study, Elke et al. revealed that long-term physical inactivity was significantly associated with IVDD [11]. And it was reported that pain was alleviated and cell proliferation was promoted by running exercise in a rat model of IVDD [12]. Collectively, it is essential to comprehensively understand the clinical characteristics of patients with IVDD to identify the risk factors, which may provide novel insight into future treatment of IVDD.

Nomograms are graphical statistical models that are designed to integrate significant risk factors in numerous diseases and to predict the probability of certain clinical events [13]. It can integrate multiple risk factors into a reliable risk model and visualize the results. Based on potential risk factors, nomograms are superior to other available decision aids for more accurately predicting outcomes in various diseases [14]. Early identification of risk factors for IVDD can facilitate prevention and early intervention for high-risk populations, thereby reducing the socioeconomic burden and surgery-related complications. However, there is only one report on the application of nomogram for the development of IVDD, and its predictive factors were only

restricted to blood lipid-metabolism-related genes [15]. In addition, the limited samples in the GEO series can bring about statistical errors, and the data in their study did not contain necessary clinical information of patients. These aspects decreased the predictive power of the model. Taken together, it is imperative to establish a reliable risk prediction model for IVDD. In this study, orthopaedic patients were selected as a specific population to assess the risk factors and to develop a predictive nomogram model of IVDD. The present study is aimed at establishing a valid and simple predictive model to assess the risk of IVDD via assessing controllable environmental factors.

2. Methods

2.1. Patients and Data Collection. The clinical and imaging data of patients were derived from Shanghai Changzheng Hospital from January 2019 to September 2020. The study was approved by the Ethics Committee of the Shanghai Changzheng Hospital (approval No. CZ20181113). The inclusion criteria include (a) patients with complete medical records; (b) patients with complete imaging data including x-rays, computed tomography (CT), and magnetic resonance imaging (MRI) of the lumbar spine; and (c) patients over 18 years of age. The exclusion criteria include (a) patients who underwent spine surgery before the admission and (b) patients lack of contacting details. According to the criteria, a total of 309 participants were finally enrolled. Data of patients were collected, which included age, sex, smoking, drinking, BMI, hypertension, diabetes, hyperlipidemia, gout, marital status, working posture, exercising hours per week, education level, Modic changes, osteophytes, Ca^{2+}, hemoglobin, the history of lumbar puncture, and lumbar Pfirrmann grades.

2.2. Assessment of Intervertebral Disc Degeneration. The Pfirrmann grade system was used to evaluate the degree of disc degeneration on the T2-weighted MRI (Figure 1). Details of the Pfirrmann grading system can be found in Reference [16]. Pfirrmann grades I and II were taken as nondegenerative discs, whereas grades III, IV, and V were considered degenerative discs [16]. Based on the Pfirrmann grading system, patients were classified into group N (nondegenerative discs in lumbar) and group D (degenerative discs in lumbar). Two spine surgeons independently evaluated the grades of IVD. If there is disagreement between the two surgeons, it would be discussed and the results were ultimately confirmed by the corresponding author.

2.3. Enzyme-Linked Immunosorbent Assay (ELISA). The samples of peripheral blood from 108 patients with IVDD and of 92 individuals without IVDD were collected between November 2020 and March 2022. The informed consent was signed by the patients. The inclusion criteria of patients with IVDD are as follows: (1) patients with Pfirrmann grades III, IV, and V in the lumbar and cervical spine; (2) patients without hypertension; (3) patients with abnormal motor and sensory function of the upper or lower limbs; (4) patients who agreed to participate in the study; and (5)

TABLE 1: Characteristics of participants in the training group and the validation group.

Variables	No. (%) Training group (217)	Validation group (92)	χ^2	p value
IVDD				
No	125 (57.60)	52 (56.52)	0.031	0.86
Yes	92 (42.40)	40 (43.48)		
Age, year				
≤30	71 (32.72)	27 (29.35)	2.184	0.336
>30 and ≤60	82 (37.79)	30 (32.61)		
>60	64 (29.49)	35 (38.04)		
Sex				
Male	115 (53.00)	42 (45.65)	1.394	0.238
Female	102 (47.00)	50 (54.35)		
Smoking				
No	117 (53.92)	51 (55.43)	0.060	0.807
Yes	100 (46.08)	41 (44.57)		
Drinking				
No	122 (56.22)	49 (53.26)	0.229	0.632
Yes	95 (43.78)	43 (46.74)		
BMI				
<18.5	36 (16.59)	13 (14.13)	5.985	0.112
≥18.5 and<24	63 (29.03)	35 (38.04)		
≥24 and <28	75 (34.56)	35 (38.04)		
≥28	43 (19.82)	9 (9.78)		
Hypertension				
No	148 (68.20)	70 (76.09)	3.712	0.294
Mild	24 (11.06)	5 (5.43)		
Moderate	18 (8.29)	9 (9.78)		
Severe	27 (12.44)	8 (8.70)		
Diabetes				
No	162 (74.65)	62 (67.39)	1.709	0.191
Yes	55 (25.35)	30 (32.61)		
Gout				
No	172 (79.26)	74 (80.43)	0.055	0.815
Yes	45 (20.74)	18 (19.57)		
Marital status				
No	111 (51.15)	46 (50.00)	0.034	0.853
Yes	106 (48.85)	46 (50.00)		
Working posture				
Immobilized	138 (63.59)	62 (67.39)	0.408	0.523
Mobilized	79 (36.41)	30 (32.61)		
Exercising hours/week				
≤0.5	55 (25.35)	24 (26.09)	0.897	0.826
	58 (26.73)	20 (21.74)		
>1.5 and ≤3	49 (22.58)	23 (25.00)		
>3	55 (25.35)	25 (27.17)		

TABLE 1: Continued.

Variables	No. (%) Training group (217)	Validation group (92)	χ^2	p value
Education level				
High school	82 (37.79)	31 (33.70)	1.606	0.448
Bachelor degree	99 (45.62)	49 (53.26)		
Graduate degree	36 (16.59)	12 (13.04)		
Modic changes				
No	153 (70.51)	66 (71.74)	0.048	0.827
Yes	64 (29.49)	26 (28.26)		
Osteophytes				
No	152 (70.05)	63 (68.48)	0.075	0.784
Yes	65 (29.95)	29 (31.52)		
Ca^{2+}				
Normal	153 (70.51)	67 (72.83)	0.269	0.874
Low	36 (16.59)	15 (16.30)		
High	28 (12.9)	10 (10.87)		
Hb				
Normal	171 (78.80)	69 (75.00)	3.288	0.193
Low	33 (15.21)	12 (13.04)		
High	13 (5.99)	11 (11.96)		
Lumbar puncture				
No	166 (76.50)	71 (77.17)	0.017	0.898
Yes	51 (23.50)	21 (22.83)		

patients without neuroendocrine dysfunction or adrenal disorders. The inclusion criteria of individuals without IVDD are as follows: (1) individuals without Pfirrmann grades III, IV, and V in the lumbar and cervical spine; (2) individuals without hypertension; and (3) individuals who volunteered to participate in the study. The level of AngII in human peripheral blood was measured using the human Ang-II ELISA Kit (Westang, Shanghai, F00070) according to the manufacturer's instruction.

2.4. Statistical Analysis. The demographic and clinical characteristic data in this study were expressed as frequency and percentage. Continuous numeric variables were presented as the mean ± SD. Categorical variables were compared by the χ^2 test or Fisher's exact test. Statistical analysis was carried out with the R software (version R-3.4.3) and SPSS (version 25.0). The data were randomized to the training set and the validation set at the ratio of 7 : 3. The training group was applied to establish the prediction model, and the validation group was used to validate the model. The least absolute shrinkage and selection operator (LASSO) method was used to optimize the features used for multivariate logistic regression analysis. In the LASSO model, variables with nonzero coefficients were selected [17]. Univariate logistic analysis was performed for all the involved independent variables. To avoid missing important factors, we included parameters with $p < 0.1$ into the multivariate analysis [18]. The features

TABLE 2: Univariate logistic regression analysis of the training set.

Variables	IVDD ($n = 92$)	Non-IVDD ($n = 125$)	χ^2/Z	P value
Age (year)				
≤30	20 (21.74)	51 (40.80)	-3.548	<0.001
>30 and ≤60	37 (40.22)	45 (36.00)	2.147	0.032
>60	35 (38.04)	29 (23.20)	3.086	0.002
Sex				
Male	49 (53.26)	66 (52.80)	-1.579	0.114
Female	43 (46.74)	59 (47.20)	-0.067	0.946
Smoking				
No	44 (47.83)	61 (48.80)	-1.931	0.054
Yes	48 (52.17)	64 (51.20)	0.442	0.659
Drinking				
No	52 (56.52)	60 (48.00)	-1.265	0.206
Yes	40 (43.48)	65 (52.00)	-0.630	0.529
BMI				
<18.5	17 (18.48)	19 (15.20)	-0.333	0.739
≥18.5 and <24	23 (25.00)	40 (32.00)	-1.042	0.297
≥24 and <28	33 (35.87)	42 (33.60)	-0.319	0.749
≥28	19 (20.65)	24 (19.20)	-0.270	0.787
Hypertension				
No	48 (52.17)	100 (80.00)	-4.18	<0.001
Mild	9 (9.78)	15 (12.00)	0.489	0.625
Moderate	12 (13.04)	6 (4.80)	2.693	0.007
Severe	23 (25.00)	4 (3.20)	4.360	<0.001
Diabetes				
No	55 (59.78)	107 (85.60)	-4.011	<0.001
Yes	37 (40.22)	18 (14.40)	4.177	<0.001
Gout				
No	71 (77.17)	101 (80.80)	-2.276	0.023
Yes	21 (22.83)	24 (19.20)	0.650	0.515
Marital status				
No	47 (51.09)	64 (51.20)	-1.607	0.108
Yes	45 (48.91)	61 (48.80)	0.016	0.987
Working posture				
Immobilized	75 (81.52)	63 (50.40)	1.020	0.308
Mobilized	17 (18.48)	62 (49.60)	-4.549	<0.001
Exercising hours/week				
≤0.5	42 (45.65)	13 (10.40)	3.695	<0.001
>0.5 and ≤1.5	36 (39.13)	22 (17.60)	-1.631	0.103
>1.5 and ≤3	9 (9.78)	40 (32.00)	-5.475	<0.001
>3	5 (5.43)	50 (40.00)	-6.137	<0.001
Education level				
High school	31 (33.7)	51 (40.80)	-2.186	0.029
Bachelor degree	46 (50.00)	53 (42.40)	1.171	0.242
Graduate degree	15 (16.30)	21 (16.80)	0.396	0.692

TABLE 2: Continued.

Variables	IVDD ($n = 92$)	Non-IVDD ($n = 125$)	χ^2/Z	P value
Modic changes				
No	67 (72.83)	86 (68.80)	-1.532	0.126
Yes	25 (27.17)	39 (31.20)	-0.642	0.521
Osteophytes				
No	64 (69.57)	88 (70.40)	-1.938	0.053
Yes	28 (30.43)	37 (29.60)	0.133	0.895
Ca^{2+}				
Normal	64 (69.57)	89 (71.20)	-2.012	0.044
Low	14 (15.22)	22 (17.60)	-0.322	0.747
High	14 (15.22)	14 (11.20)	0.800	0.424
Hb				
Normal	73 (79.35)	98 (78.40)	-1.905	0.057
Low	14 (15.22)	19 (15.20)	-0.028	0.977
High	5 (5.43)	8 (6.40)	-0.297	0.766
Lumbar puncture				
No	75 (81.52)	91 (72.80)	-1.240	0.215
Yes	17 (18.48)	34 (27.20)	-1.490	0.136

selected through the univariate logistic analysis and the LASSO were applied for the multivariate logistic analysis. The independent risk factors of IVDD, which were determined by the multivariate logistic regression analysis, were included to develop a prediction model for IVDD. The nomogram was utilized to visualize the model.

Based on the prediction model, the performance of the nomogram model was assessed in both the training and validation groups. The area under the curve (AUC) of the receiver operating characteristic (ROC) curve and the Harrell's C-index were applied to assess prediction power of the model. An AUC of 0.5 implicated no prediction performance; an AUC value ≤ 0.7 indicates poor predictive performance; an AUC value greater than 0.7 but lower than 0.9 indicates moderate predictive performance; and an AUC value greater than 0.9 indicates excellent predictive performance. The C-index value of 0.5 suggests that the model is almost random chance in predicting the risk, whereas a value of 1.0 indicates perfect discrimination. The calibration process examines whether the predicted risks and the observed risks are consistent. To assess the clinical utility of the model, decision curve analysis (DCA) was used to evaluate the benefit. $p < 0.05$ was regarded statistically significant.

3. Result

3.1. Demographic and Clinical Characteristics. Details of the patients are shown in Table 1. A total of 309 participants were included. They were randomly divided into the training group ($n = 217$) and the validation group ($n = 92$). The training group was used to establish the nomogram for predicting the risk of IVDD. The validation group was used for

(a)

(b)
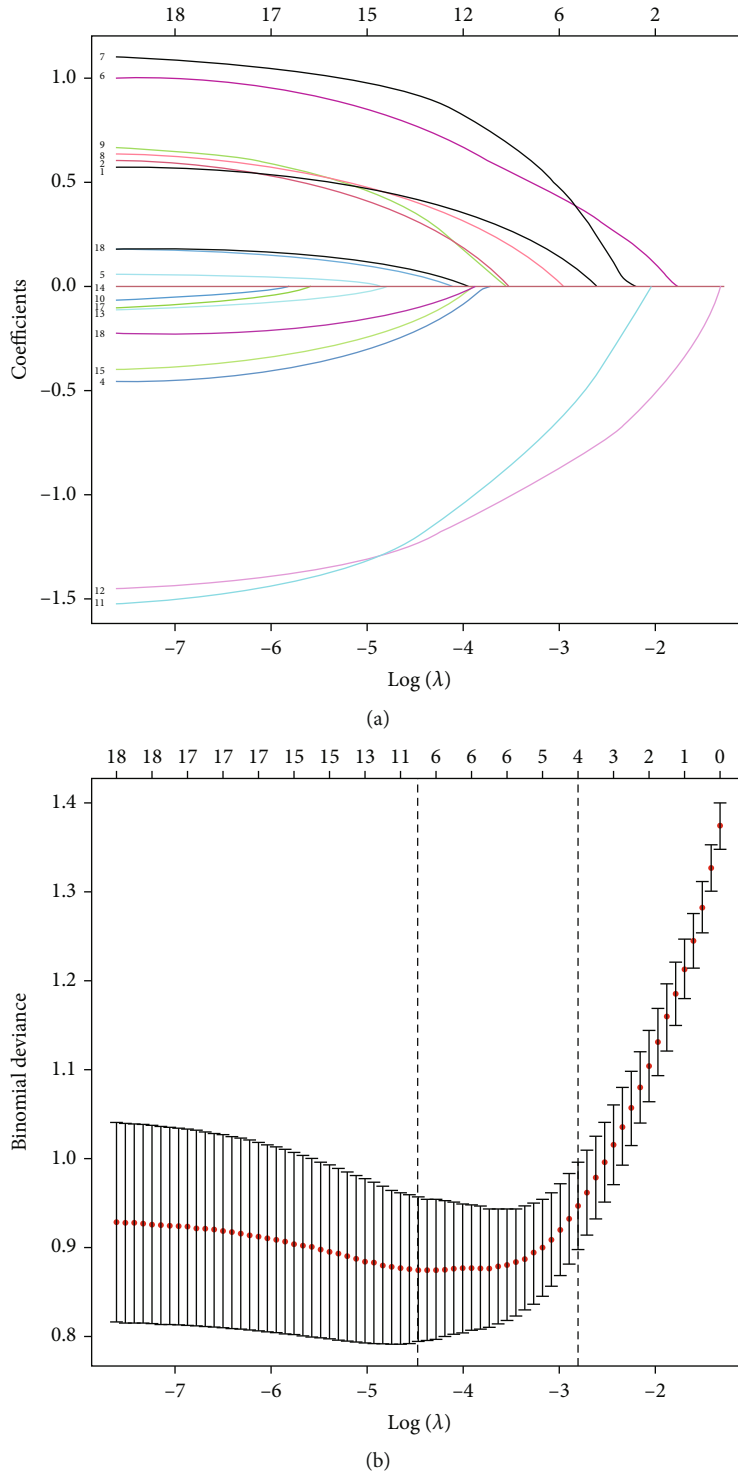
FIGURE 2: Results of the LASSO regression analysis. (a) LASSO coefficient profiles of the 18 features. (b) Feature selection in the LASSO. Dotted vertical lines were drawn at the optimal values.

validation. There were 92 (42.40%) and 40 (43.48%) patients with IVDD in the training cohort and the validation cohort, respectively. No significant differences were observed regarding the basic parameters between the two groups.

3.2. Selection of Independent Variables. IVDD occurred in 92 (42.40%) of the 217 patients in the nomogram development

cohort. Univariate logistics regression and LASSO regression analysis were used for the selection of potential predictors. In this present study, parameters with p values less than 0.1 in the univariate logistic analysis were regarded as potential predictors for the nomogram model, which included age, smoking, hypertension, diabetes, gout, working posture, exercising hours per week, education level, osteophytes,

TABLE 3: Multivariable logistic regression analysis of the training group.

Intercept and variable	Prediction model		
	β	OR (95% CI)	p value
Intercept	-0.157	0.855 (0.201-3.555)	0.829
Age			
≤30			
>30 and ≤60	0.876	2.402 (0.878-6.843)	0.092
>60	1.029	2.798 (0.953-8.656)	0.065
Sex			
Male			
Female	0.873	2.394 (0.971-6.231)	0.064
Smoking			
No			
Yes	-0.276	0.759 (0.296-1.887)	0.556
Drinking			
No			
Yes	-0.448	0.639 (0.243-1.627)	0.351
Hypertension			
No			
Mild	1.111	3.038 (0.772-12.407)	0.113
Moderate	1.842	6.309 (1.466-32.023)	0.018
Severe	3.587	36.113 (5.765-346.302)	<0.001
Diabetes			
No			
Yes	1.085	2.960 (1.045-8.918)	0.046
Gout			
No			
Yes	0.924	2.520 (0.902-7.395)	0.083
Working posture			
Immobilized			
Mobilized	-1.553	0.212 (0.080-0.517)	<0.001
Exercising hours/week			
≤0.5			
>0.5 and ≤1.5	-0.742	0.476 (0.160-1.354)	0.170
>1.5 and ≤3	-3.263	0.038 (0.009-0.134)	<0.001
>3	-4.305	0.013 (0.002-0.058)	<0.001
Education level			
High school			
Bachelor degree	0.434	1.543 (0.565-4.315)	0.399
Graduate degree	0.184	1.201 (0.394-3.669)	0.745
Osteophytes			
No			
Yes	-0.513	0.598 (0.229-1.517)	0.284
Ca2+			
Normal			
Low	-0.032	0.968 (0.275-3.354)	0.959
High	0.715	2.044 (0.596-7.368)	0.260
Hb			
Normal			

TABLE 3: Continued.

Intercept and variable	Prediction model		
Low	-0.084	0.919 (0.290-2.816)	0.884
High	-0.340	0.711 (0.108-4.291)	0.713
Lumbar puncture			
No			
Yes	-0.078	0.925 (0.332-2.567)	0.880

Ca^{2+}, and Hb (Table 2). LASSO regression analysis helped decrease the dimensionality that was associated with the decreased predictive power and increased the accuracy of the nomogram model. Variables in the LASSO regression analysis, which included age, sex, drinking, hypertension, diabetes, gout, working posture, exercising hours per week, education level, osteophytes, Ca^{2+}, and lumbar puncture, were selected as potential predictors (Figure 2). Finally, the results in both the univariate logistics regression and LASSO regression analysis were used for multivariable logistic regression analysis and revealed seven risk factors with $p < 0.1$, namely, age, sex, hypertension, diabetes, gout, working posture, and exercising hours per week (Table 3).

3.3. Establishment and Evaluation of Nomogram for Predicting the Risk of IVDD. The selected seven independent predictors above were used to establish the predictive nomogram (Figure 3). A comprehensive evaluation of the nomogram was carried out. The AUC of ROC curve of the nomogram model was 0.815 (95% CI, 0.759-0.870), indicating that the discrimination performance of the nomogram model was satisfactory (Figure 4(a)). Meanwhile, the favorable discrimination of the nomogram was confirmed by the C-index (0.916, (95% CI, 0.876-0.956)). In addition, the calibration plot revealed great agreement of the observed results and the predicted probability in this study (Figure 4(b)). To identify the clinical benefit of the predictive nomogram, the clinical practicability of it was also evaluated through DCA. The DCA (in a range of risk thresholds 0.01 to 1.00) indicated that the nomogram had a high net benefit (Figure 4(c)).

3.4. Validation of the Nomogram Prediction Model. The data of the validation group were utilized to validate the nomogram above. In the validation cohort, the AUC of nomogram model was 0.805 (95% CI, 0.718-0.892) (Figure 5(a)) and the C-index of nomogram was 0.949 (95% CI, 0.909-0.989). Consistently, the calibration plot also indicated a great consistency with the results (Figure 5(b)). Furthermore, the DCA results demonstrated that when the nomogram was used to assess the validation set, the model also showed good net benefit (Figure 5(c)).

3.5. Exploring the Relationship between the Severity of IVDD and the AngII Level. The AngII plays a pivotal role in the RAS. Aberrant activation of the RAS system can increase the level of AngII in the peripheral blood, which may enter the degenerated discs after vascular ingrowth. Based on the above results indicating the close relationship between
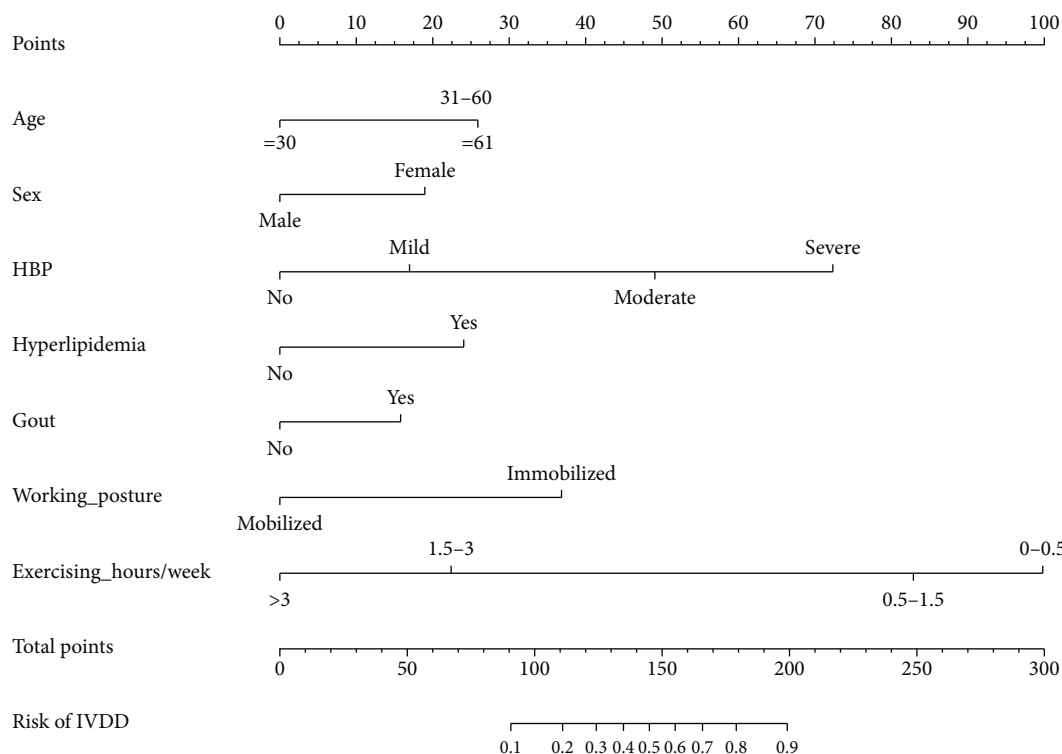
FIGURE 3: The IVDD nomogram. The predicting nomogram was developed with factors including age, sex, hypertension, diabetes, gout, working posture, and exercising hours per week.

IVDD and hypertension, we wonder whether IVDD and AngII are independently related. Our previous study found that AngII can lead to the dysfunction of nucleus pulposus cells. To explore whether AngII is an independent risk factor for IVDD, the peripheral blood samples of 108 patients with IVDD and of 92 university students without IVDD were collected (Figure 6(a)). Characteristics of the participants (108 patients and 92 students) were summarized in table 4. Despite significant difference in the age, no significant difference was observed in any other parameters. And the AngII levels in the peripheral blood of patients with various Pfirrmann grades were detected through ELISA. The results revealed that the average level of AngII in the nondegenerated group was 52.91 ± 9.01 pg/mL, whereas the average AngII level in the degenerated group (97.62 ± 44.02 pg/mL) was significantly higher ($p < 0.001$) (Figure 6(b)). In addition, we explored the relationship between the severity of IVDD and the AngII level. The results of Pearson's correlation revealed that the severity of IVDD was closely associated with the AngII level. The severity of IVDD was correlated with AngII level (Pearson's $R^2 = 0.4478$, $p < 0.001$) (Figure 6(c)). Additionally, the AUC of the ROC curve was 0.9172 ($p < 0.001$), indicating that the AngII level in the peripheral blood was an excellent predictor of IVDD (Figure 6(d)). The above results revealed that the AngII level was closely associated with the severity of IVDD, indicating that the AngII in the peripheral blood could be applied as the auxiliary diagnostic index of IVDD.

4. Discussion

Although there are complex and multifactorial causes for the development of LBP, it is widely accepted that IVDD is the major contributor to LBP [19]. IVDD can be affected by both genetic and environmental factors. However, environmental factors, such as lifestyles and dietary habits that are closely relevant to metabolic diseases and systemic diseases, can be consciously controlled and modified to improve human's health. Adverse lifestyle-related factors including high BMI, lack of physical activity and smoking can lead to or aggregate IVDD [20]. In addition, previous studies reported that metabolic diseases such as diabetes and obesity were associated with the development of IVDD [6]. In addition, metabolic disease is a kind of systemic disease that can affect many organ systems including intervertebral disc [21]. All these risk factors above should be emphasized in the prevention and control of IVDD.

To prevent and curb the development of IVDD, it is essential to establish a model to predict the potential risk factors. Several blood lipid-metabolism-related genes were previously selected as candidate predictive biomarkers for IVDD [15]. However, a comprehensive and useful predictive model for IVDD is still lacking. In this present study, based on potential risk factors, a predictive nomogram for IVDD was established. A total of 309 patients were included in this study, and seven independent predictors including age, sex, hypertension, diabetes, gout, working posture, and
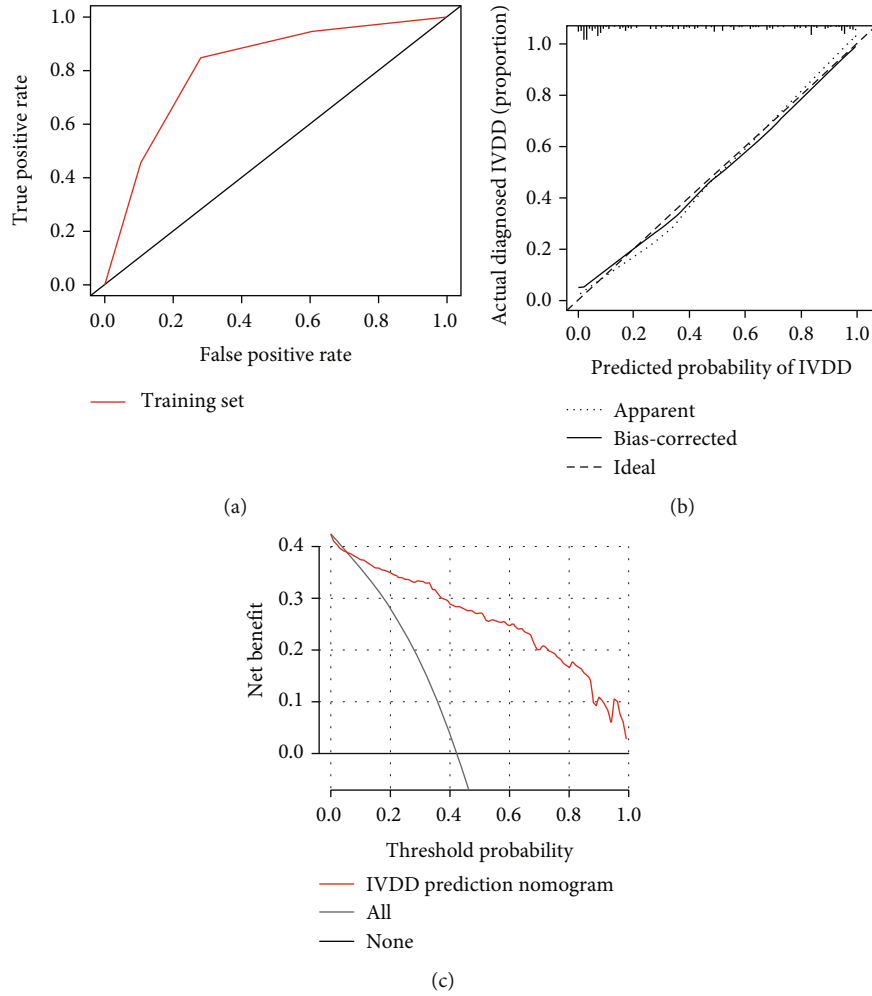
(a)

(b)

(c)

FIGURE 4: The ROC curve, calibration curve. and DCA curve of the training group. (a) The ROC curve of the nomogram model. (b) The calibration curve of the training group. (c) The decision curve of the training group.

exercising hours per week were selected to construct the predictive nomogram. The AUC of the model was 0.815 (95% CI, 0.759-0.870), which indicated good discrimination ability. Hypertension and the weight of exercising hours per week were the highest power factors shown in the nomogram, followed by working posture, diabetes, gout, age, and sex.

Hypertension is one of the major chronic metabolic diseases. It has long been known that the renin-angiotensin system (RAS) is essential in the development of hypertension [22]. In addition, local tissue RAS (tRAS) was observed in many tissues such as the brain, kidney, pancreas, and adipose tissue [23]. Local tRAS is not only associated with hypertension but also relevant to degeneration- or inflammation-related diseases in many tissues. Our previous study revealed that the activation of tRAS in the nucleus pulpous tissues was significantly associated with the development of IVDD [8]. In addition, we revealed that AngII could induce the degeneration and fibrosis of NPCs [8]. To verify the role of AngII in the development of IVDD, the spontaneously hypertensive rat (SHR) was used in our previous study [8]. The results revealed that the local tRAS was

also activated in SHR nucleus pulposus tissue, accompanied by higher level of angiotensin-converting enzyme (ACE). In addition, the results of immunofluorescence demonstrated higher level of MMP 3 and lower level of collagen type II in SHR nucleus pulposus tissue. The above findings in previous studies indicated that hypertension may correlate with IVDD. Consistently, the nomogram of this present study indicated that individuals with hypertension tend to have greater points and the higher the blood pressure is, the higher the points for predicting IVDD. Alternatively, previous studies reported that patients with osteoarthritis, a similar disease to IVDD, tend to have relatively higher risk of cardiovascular diseases including hypertension than those without osteoarthritis [24]. In a meta-analysis, Lo et al. also pointed that hypertension resulted in a 62% increase in knee osteoarthritis [25]. In addition, the results of the meta-analysis revealed that hypertension is a harmful factor rather than protective factor in the development of osteoarthritis [25]. Interestingly, a growing number of researches revealed a close relationship between metabolic diseases and osteoarthritis [26, 27]. Because of physiological similarities between the articular cartilage and the intervertebral disc cartilage

(a)

(b)

(c)
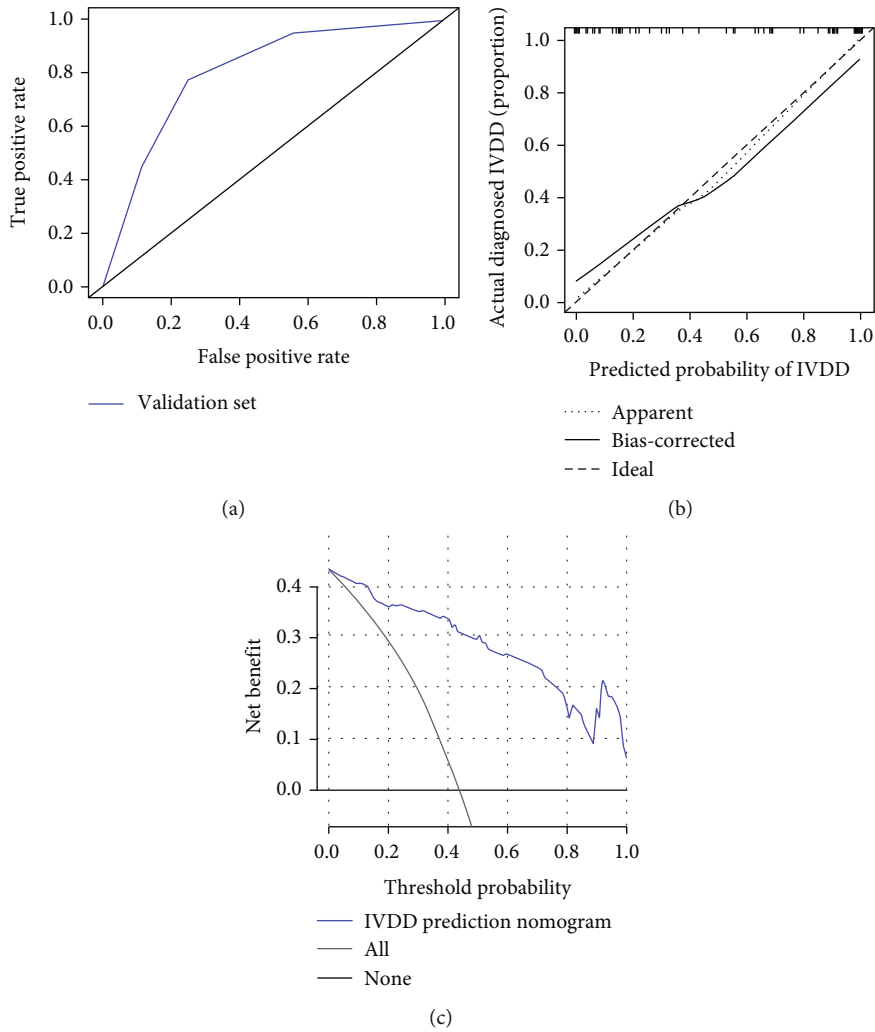
FIGURE 5: The ROC curve, calibration curve, and DCA curve of the validation group. (a) The ROC curve of the validation group. (b) The calibration curve of the validation group. (c) The decision curve of the validation group.

[28], it may be plausible to assume that hypertension is one of the risk factors for IVDD Consistently, this present study indicated that the p value of both diabetes and hypertension was less than 0.05 in the multivariate logistic regression analysis, indicating that diabetes was another potential risk factor of IVDD. Zheng et al. reported that in the condition of diabetes, human islet amyloid polypeptide (hIAPP) oligomers can promote the expression of IL-1β that is responsible for intervertebral disc degeneration [29]. Besides, Russo et al. reported that diabetes can lead to IVDD through promoting ECM degradation and cell apoptosis. The results of our study are consistent with previously reported findings. Although both hypertension and diabetes are systemic metabolic diseases, the results in the present study showed that patients with moderate or severe hypertension were at relatively higher risk of IVDD than patients with diabetes. More studies are still required to validate the exact effects of metabolic diseases on IVDD.

AngII is the major mediator to hypertension [30]. A previous study reported that AngII can result in a series of pathological changes including oxidative stress, inflammation,

and fibrosis [31]. Therefore, we want to explore whether AngII is an independent risk factor for IVDD. The peripheral blood samples of participants with or without IVDD but not hypertension were collected. Our prospective exploration results revealed that the mean AngII level in the peripheral blood of patients with IVDD was remarkably higher than that of individuals without IVDD. Pearson's correlation analysis indicated a remarkable correlation between AngII level and the severity of IVDD. And the AUC of the ROC curve was 0.9172, indicating that AngII level showed a good predictive power for IVDD. In the prospective exploration, nonhypertensive patients were included for two main purposes: first is to rule out medication effect; second is to seek out hypertension-independent risk factors. The results of the study suggested that AngII may be developed to be a potential predictive factor for IVDD.

Physical activity plays an important role in maintaining human's body health. Liu et al. reported that exercises can increase endurance and muscle strength [32]. The muscles can provide support to the spine, which can be strengthened

(a)

(b)

(c)

(d)
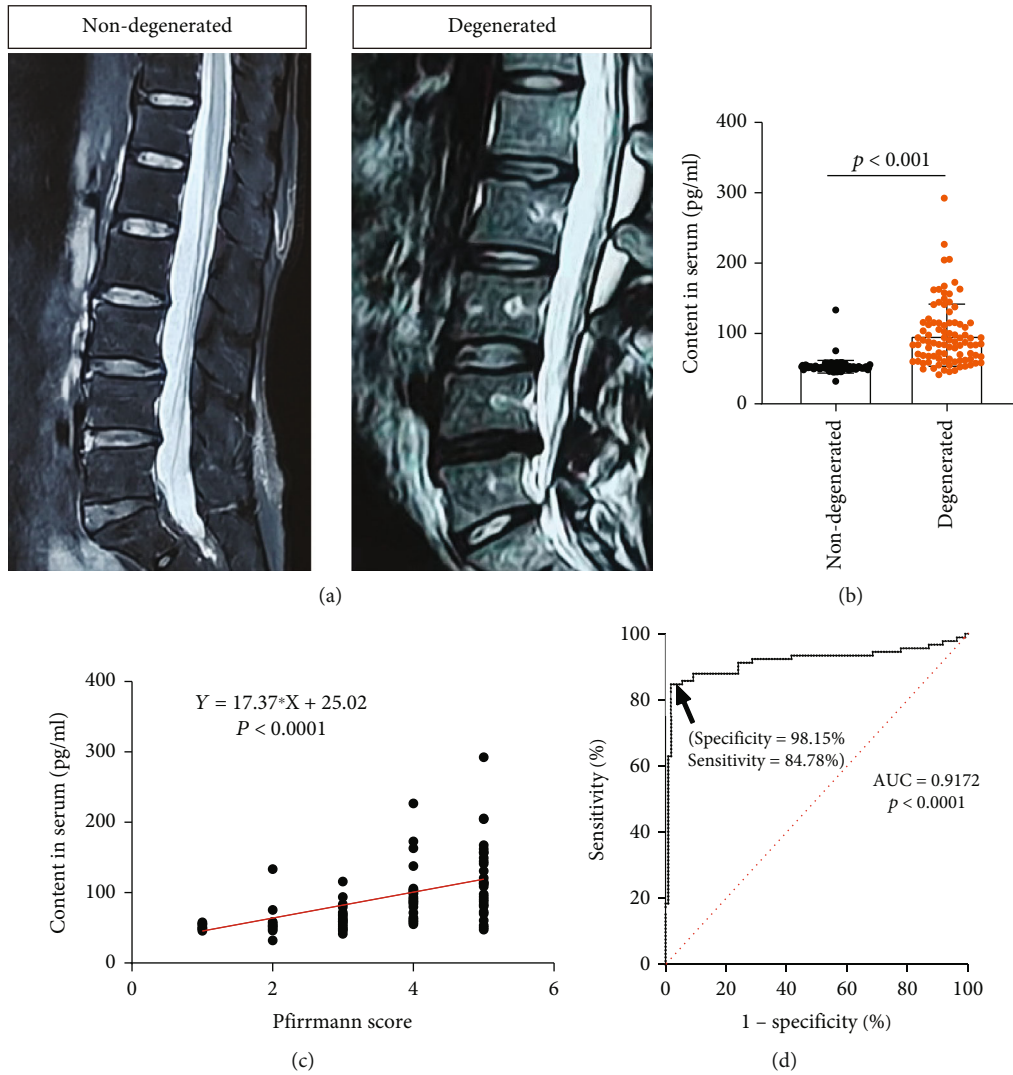
FIGURE 6: The relationship between the severity of IVDD and the AngII level in the peripheral blood. (a) The MRI results of non-degenerated patients and degenerated patients. (b) The level of AngII in peripheral blood of patients in the two groups. (c) Correlation analysis between AngII level in peripheral blood and the severity of IVDD. (d) The ROC curve analysis was used to test the ability of the AngII level to predict the risk of IVDD.

TABLE 4: Characteristics of the participants involved in exploring the relationship between IVDD and AngII.

Variables	IVDD ($n = 108$)	Non-IVDD ($n = 92$)	T value	p value
Age	41.36 ± 13.44	28.97 ± 4.01	8.525	<0.001
Sex, female (%)	55 (50.93)	45 (48.91)	0.081	0.777
Smoking, yes (%)	52 (48.15)	45 (48.91)	0.012	0.914
Drinking, yes (%)	49 (45.37)	44 (47.83)	0.120	0.729
BMI	23.43 ± 4.26	23.13 ± 4.29	0.490	0.625

through exercises. However, lack of exercises can result in poor physical condition with decreased muscle strength. Iki et al. reported that regular exercise is beneficial for bone health [33]. In their study, patients with poor trunk muscle strength and lack of exercise showed greater risk for bone loss. In contrast, participants who have regular exercises tend to be at relatively lower risk of osteoporosis. It is widely accepted that the decreased bone mineral density can negatively affect the biomechanics of the spinal column, which subsequently induce the damage to the nucleus pulposus and annulus fibrosus [34]. In this present study, the exercising hours per week was graded into four categories: ≤0.5 hours, >0.5 and ≤1.5 hours, >1.5 and ≤3 hours, and >3 hours. The results uncovered that individuals who spent less time in exercises tended to have higher points in the nomogram and people with more than 3 hours of exercises every week had the least points, indicating that regular exercises can help lower the risk of IVDD. This may be because exercise can promote blood circulation to the intervertebral disc and strengthen the endurance and flexibility of the spinal muscle that helps maintain the spine stability and protect against IVDD. As for the immobilized working posture,

one of the risk factors in the nomogram, Park et al. reported that adversely fixed working postures of dentists can cause musculoskeletal diseases especially in the lower back and neck [35]. This was in line with our results. As a result, regular exercises may help delay or attenuate the incidence of IVDD.

Moreover, other factors in the nomogram, which included old age, female gender, and gout, were also potential risk factors of IVDD. IVDD is an ageing-related disease. With the increase in age, the number of the nucleus pulposus cells and the content of water and ECM in the intervertebral disc will be reduced. This can impair the ability of intervertebral disc to absorb shock and stress, which might aggravate the process of IVDD. The results of the nomogram showed that women had higher risk in the risk evaluation of IVDD than men. Despite the protective effects of estrogen on musculoskeletal structures such as IVD [21], the high morbidity of IVDD in women may be due to pregnancy, menopause, and relatively weak spinal muscular strength. Although it was reported that IVDD was relevant to high BMI [20], the results of the present study showed that BMI was not statistically significant in univariate logistics regression analysis and not the strongest predictors in the LASSO regression analysis. Gout as a metabolic disease was also one of the potential risk factors in the development of IVDD. Patients with gout were reported with the accumulation of urate crystals in the bone joints, kidneys, and subcutaneous sites [36]. The results of this study revealed that IVDD was associated with gout. We speculated that this may be because urate crystal deposits in the IVD and its surrounding structures such as muscles and ligaments.

Based on the potential risk factors for IVDD, a prediction nomogram model was developed. The accuracy of the prediction model was assessed by various methods, and the results showed that this model could effectively predict the risk of IVDD. In addition, based on the model, AngII was revealed to be a possible diagnostic indicator of the IVDD.

4.1. *Limitations.* There are also several limitations in the present study. First and foremost, patients with severe metabolic diseases, such as hypertension, tend to be treated with medication, but the effects of medication on IVDD were not considered in the study. Further studies about the direct or indirect effects of medication on the process of IVDD are still required. Besides, biased results could be caused by a limited sample size. In addition, cases were collected over a short period of time and a relatively geographic area. Hence, a multicenter prospective study with a larger sample size is required to investigate other factors. What is more, majority of hypertensive patients require various kinds of RAS antagonists to control the blood pressure. But the present study cannot prove that RAS antagonists can attenuate IVDD or reduce the frequency of IVDD-related surgeries. Future research needs to be carried out from the perspective of cardiology. This can be confirmed through longitudinal, large sample size, cohort studies. Finally, in this study, 92 individuals without IVDD were relatively younger than those with IVDD. In a future study, the comparison between age-matched groups should be performed using a pair-sample t-test because age is also a potential risk factor for IVDD.

Abbreviations

LBP: Low back pain
IVDD: Intervertebral disc degeneration
IVD: Intervertebral disc
LASSO: Least absolute shrinkage and selection operator regression
ROC: Receiver operating characteristic
DCA: Decision curve analysis
AUC: Area under the curve
tRAS: Tissue renin-angiotensin system
RAS: Renin-angiotensin system
CT: Computed tomography
MRI: Magnetic resonance imaging
SHR: Spontaneously hypertensive rat
NP: Nucleus pulpous
AngII: Angiotensin II.

Data Availability

The dataset of this article is available on request from the corresponding authors.

Ethical Approval

This study was reviewed and approved by the Ethics Committee of the Shanghai Changzheng Hospital.

Conflicts of Interest

We declare there are no conflicts of interests.

Authors' Contributions

FDL, XFS, and YW collected and analyzed the data. FDL drafted the manuscript. KQS, JGS, and LG supervised the project and reviewed the manuscript. FDL, XFS, and KQS collected the blood samples of the patients. All authors read and approved the final manuscript. Fudong Li, Xiaofei Sun, and Yuan Wang contributed equally to this work and should be considered co-first authors.

References

[1] B. F. Walker, "The prevalence of low back pain: a systematic review of the literature from 1966 to 1998," *Journal of Spinal Disorders*, vol. 13, no. 3, pp. 205–217, 2000.

[2] M. V. Risbud and I. M. Shapiro, "Role of cytokines in intervertebral disc degeneration: pain and disc content," *Nature Reviews. Rheumatology*, vol. 10, no. 1, pp. 44–56, 2014.

[3] B. I. Martin, R. A. Deyo, S. K. Mirza et al., "Expenditures and health status among adults with back and neck problems," *Journal of the American Medical Association*, vol. 299, no. 6, pp. 656–664, 2008.

[4] S. R. Pye, D. M. Reid, J. E. Adams, A. J. Silman, and T. W. O'Neill, "Influence of weight, body mass index and lifestyle factors on radiographic features of lumbar disc degeneration,"

Annals of the Rheumatic Diseases, vol. 66, no. 3, pp. 426-427, 2007.

[5] M. Kuisma, J. Karppinen, M. Haapea et al., "Are the determinants of vertebral endplate changes and severe disc degeneration in the lumbar spine the same? A magnetic resonance imaging study in middle-aged male workers," *BMC Musculoskeletal Disorders*, vol. 9, no. 1, p. 51, 2008.

[6] E. Y. Park and J. B. Park, "Dose- and time-dependent effect of high glucose concentration on viability of notochordal cells and expression of matrix degrading and fibrotic enzymes," *International Orthopaedics*, vol. 37, no. 6, pp. 1179–1186, 2013.

[7] X. Li, X. Wang, Z. Hu et al., "Possible involvement of the oxLDL/LOX-1 system in the pathogenesis and progression of human intervertebral disc degeneration or herniation," *Scientific Reports*, vol. 7, no. 1, p. 7403, 2017.

[8] K. Sun, X. Sun, J. Sun et al., "Tissue renin-angiotensin system (tRAS) induce intervertebral disc degeneration by activating oxidative stress and inflammatory reaction," *Oxidative Medicine and Cellular Longevity*, vol. 2021, Article ID 3225439, 25 pages, 2021.

[9] Y. Zhao, C. Wang, C. Wang et al., "An essential role for Wnt/β-catenin signaling in mediating hypertensive heart disease," *Scientific Reports*, vol. 8, no. 1, p. 8996, 2018.

[10] Y. Kawarai, S. H. Jang, S. Lee et al., "Exercise attenuates low back pain and alters epigenetic regulation in intervertebral discs in a mouse model," *The Spine Journal*, vol. 21, no. 11, pp. 1938–1949, 2021.

[11] E. Maurer, C. Klinger, R. Lorbeer et al., "Long-term effect of physical inactivity on thoracic and lumbar disc degeneration–an MRI-based analysis of 385 individuals from the general population," *The Spine Journal*, vol. 20, no. 9, pp. 1386–1396, 2020.

[12] S. Luan, Q. Wan, H. Luo et al., "Running exercise alleviates pain and promotes cell proliferation in a rat model of intervertebral disc degeneration," *International Journal of Molecular Sciences*, vol. 16, no. 1, pp. 2130–2144, 2015.

[13] A. Makkouk, V. Sundaram, C. Chester et al., "Characterizing CD137 upregulation on NK cells in patients receiving monoclonal antibody therapy," *Annals of Oncology*, vol. 28, no. 2, pp. 415–420, 2017.

[14] S. F. Shariat, U. Capitanio, C. Jeldres, and P. I. Karakiewicz, "Can nomograms be superior to other prediction tools," *BJU International*, vol. 103, pp. 492–495, 2009.

[15] W. Li, Z. Ding, H. Zhang et al., "The roles of blood lipid-metabolism genes in immune infiltration could promote the development of IDD," *Frontiers in Cell and Developmental Biology*, vol. 10, article 844395, 2022.

[16] A. M. Hollenberg, N. Maqsoodi, A. Phan et al., "Bone morphogenic protein-2 signaling in human disc degeneration and correlation to the Pfirrmann MRI grading system," *The Spine Journal*, vol. 21, no. 7, pp. 1205–1216, 2021.

[17] H. Guo, J. Cai, X. Wang et al., "Prognostic values of a novel multi-mRNA signature for predicting relapse of cholangiocarcinoma," *International Journal of Biological Sciences*, vol. 16, no. 5, pp. 869–881, 2020.

[18] X. Liu, N. Li, Y. Gao et al., "Development and validation of a nomogram to predict chronic postoperative pain in elderly orthopedic patients," *Annals of Palliative Medicine*, vol. 10, no. 11, pp. 11868–11883, 2021.

[19] J. Ge, Y. Wang, Q. Yan et al., "FK506 induces the TGF-β1/Smad 3 pathway independently of calcineurin inhibition to prevent intervertebral disk degeneration," *Frontiers in Cell and Developmental Biology*, vol. 8, article 608308, 2020.

[20] S. Salo, H. Hurri, T. Rikkonen, R. Sund, H. Kröger, and J. Sirola, "Association between severe lumbar disc degeneration and self-reported occupational physical loading," *Journal of Occupational Health*, vol. 64, article e12316, 2022.

[21] Q. Liu, X. Wang, Y. Hua et al., "Estrogen deficiency exacerbates intervertebral disc degeneration induced by spinal instability in rats," *Spine*, vol. 44, no. 9, pp. E510–E519, 2019.

[22] J. Zicha, Z. Dobešová, M. Behuliak, M. Pintérová, J. Kuneš, and I. Vaněčková, "Nifedipine-sensitive blood pressure component in hypertensive models characterized by high activity of either sympathetic nervous system or renin-angiotensin system," *Physiological Research*, vol. 63, no. 1, pp. 13–26, 2014.

[23] M. Pahlavani, N. S. Kalupahana, L. Ramalingam, and N. Moustaid-Moussa, "Regulation and functions of the renin-angiotensin system in white and brown adipose tissue," *Comprehensive Physiology*, vol. 7, no. 4, pp. 1137–1150, 2017.

[24] T. Kendzerska, P. Jüni, L. K. King, R. Croxford, I. Stanaitis, and G. A. Hawker, "The longitudinal relationship between hand, hip and knee osteoarthritis and cardiovascular events: a population-based cohort study," *Osteoarthritis and Cartilage*, vol. 25, no. 11, pp. 1771–1780, 2017.

[25] K. Lo, M. Au, J. Ni, and C. Wen, "Association between hypertension and osteoarthritis: a systematic review and meta-analysis of observational studies," *Journal of Orthopaedic Translation*, vol. 32, pp. 12–20, 2022.

[26] Q. Zhuo, W. Yang, J. Chen, and Y. Wang, "Metabolic syndrome meets osteoarthritis," *Nature Reviews. Rheumatology*, vol. 8, no. 12, pp. 729–737, 2012.

[27] S. Konstari, K. Sääksjärvi, M. Heliövaara et al., "Associations of metabolic syndrome and its components with the risk of incident knee osteoarthritis leading to hospitalization: a 32-year follow-up study," *Cartilage*, vol. 13, 1_supplement, pp. 1445S–1456S, 2021.

[28] T. Miyamoto, T. Muneta, T. Tabuchi et al., "Intradiscal transplantation of synovial mesenchymal stem cells prevents intervertebral disc degeneration through suppression of matrix metalloproteinase-related genes in nucleus pulposus cells in rabbits," *Arthritis Research & Therapy*, vol. 12, no. 6, p. R206, 2010.

[29] X. Zheng, P. Liu, C. Yang, and X. Wu, "Amyloid protein aggregation in diabetes mellitus accelerate intervertebral disc degeneration," *Medical Hypotheses*, vol. 141, article 109739, 2020.

[30] S. Mathieu, N. El Khoury, K. Rivard, P. Paradis, M. Nemer, and C. Fiset, "Angiotensin II overstimulation leads to an increased susceptibility to dilated cardiomyopathy and higher mortality in female mice," *Scientific Reports*, vol. 8, no. 1, p. 952, 2018.

[31] E. Braunwald, "The path to an angiotensin receptor antagonist-neprilysin inhibitor in the treatment of heart failure," *Journal of the American College of Cardiology*, vol. 65, no. 10, pp. 1029–1041, 2015.

[32] P. Liu, M. A. Konstam, and T. Force, "Highlights of the 2004 scientific sessions of the Heart Failure Society of America, Toronto, Canada, September 12 to 15, 2004," *Journal of the American College of Cardiology*, vol. 45, no. 4, pp. 617–625, 2005.

[33] M. Iki, Y. Saito, E. Kajita, H. Nishino, and Y. Kusaka, "Trunk muscle strength is a strong predictor of bone loss in postmenopausal women," *Clinical Orthopaedics and Related Research*, vol. 443, pp. 66–72, 2006.

[34] H. Song, Y. Luo, W. Wang et al., "Effects of alendronate on lumbar intervertebral disc degeneration with bone loss in ovariectomized rats," *The Spine Journal*, vol. 17, no. 7, pp. 995–1003, 2017.

[35] H. S. Park, J. Kim, H. L. Roh, and S. Namkoong, "Analysis of the risk factors of musculoskeletal disease among dentists induced by work posture," *Journal of Physical Therapy Science*, vol. 27, no. 12, pp. 3651–3654, 2015.

[36] Y. Wu, C. Lu, N. Pan et al., "Serum lactate dehydrogenase activities as systems biomarkers for 48 types of human diseases," *Scientific Reports*, vol. 11, no. 1, Article ID 12997, pp. 1–8, 2021.

Hindawi

Research Article

The Reliability of Computer-Assisted Three-Dimensional Surgical Simulation of Posterior Osteotomies in Thoracolumbar Kyphosis Secondary to Ankylosing Spondylitis Patients

Yiqi Zhang [iD],[1] Yong Hai [iD],[1] Yuzeng Liu [iD],[1] Xinuo Zhang [iD],[1] Yangpu Zhang [iD],[1] Chaofan Han [iD],[1] Jingwei Liu [iD],[1,2] and Lijin Zhou [iD][1]

[1]Department of Orthopedics, Beijing Chaoyang Hospital, Capital Medical University, Gongtinanlu 8#, Chaoyang District, Beijing 100020, China
[2]Department of Orthopedics, Beijing Hospital, Peking University, DongdandahuaLu 1#, Dongcheng District, Beijing 100005, China

Correspondence should be addressed to Yong Hai; yong.hai@ccmu.edu.cn and Lijin Zhou; doctorzhoulijin@163.com

Objectives. The study was aimed at investigating the reliability of computer-assisted three-dimensional surgical simulation (CA3DSS) of posterior osteotomies in thoracolumbar kyphosis secondary to ankylosing spondylitis (TLKAS) patients. *Methods*. Eligible TLKAS patients who underwent posterior correction surgery with posterior osteotomies were consecutively included. Simulated posterior osteotomies were performed in Mimics and 3-Matic Medical software. Coronal and sagittal angle and alignment parameters were measured in preoperative full-length X-ray, preoperative original 3D spine (Pre-OS), simulated 3D spine (SS), and postoperative original 3D spine (Post-OS). Reliability was tested by both intraclass correlation coefficients (ICCs) and Bland-Altman analysis. *Results*. A total of 30 TLKAS patients were included. Excellent consistency of radiological parameters was shown between preoperative X-ray and Pre-OS model. In SS and Post-OS models, excellent reliabilities were shown in global kyphosis (ICC 0.832, 95% CI 0.677-0.916), thoracic kyphosis (ICC 0.773, 95% CI 0.577-0.885), and lumbar lordosis (ICC 0.896, 95% CI 0.794-0.949) and good reliabilities were exhibited in the main curve (ICC 0.680, 95% CI 0.428-0.834) and sagittal vertical axis (ICC 0.619, 95% CI 0.338-0.798). ICCs of correction angle achieved by pedicle subtraction osteotomy (PSO) was 0.754 (95% CI 0.487-0.892), and that of posterior column osteotomies (PCO) was 0.703 (95% CI 0.511-0.829). Bland-Altman analysis also showed good agreement for both Cobb angle and distance measurements in Pre-OS and SS models, and good reliabilities were shown in PCO and PSO in real spine and SS models. *Conclusions*. CA3DSS can provide an accurate measurement, and it is a reliable and effective method to conduct proper simulation for correction surgery with posterior osteotomies in TLKAS patients. This trial is registered with Chinese Clinical Trial Registry ChiCTR2100053808.

1. Introduction

Thoracolumbar kyphosis is commonly caused by untreated ankylosing spondylitis (AS), which is a chronic inflammatory disease involving ankylosis of the sacroiliac joint and ossification of the spinal ligament and joint [1–3]. Besides the kyphotic deformity, AS may lead to spinal pseudarthrosis on account of trauma, delayed ossification, severe pain, and neurologic symptoms caused by fibro-osseous tissue progress around the lesion [4, 5]. Thus, correction surgery

is desired with the aim to restore the normal sagittal balance and generally performed with posterior osteotomies including pedicle subtraction osteotomy (PSO), Smith-Petersen osteotomy (SPO), and Ponte osteotomy [6, 7].

Both posterior column osteotomies (PCO) and 3-column osteotomies (3CO) are widely applied in kyphotic deformity correction and can achieve adequate and satisfying outcomes in the aspect of radiography and cosmetic [8, 9], nevertheless, the risk of perioperative complications could not be ignored and might be catastrophic in certain
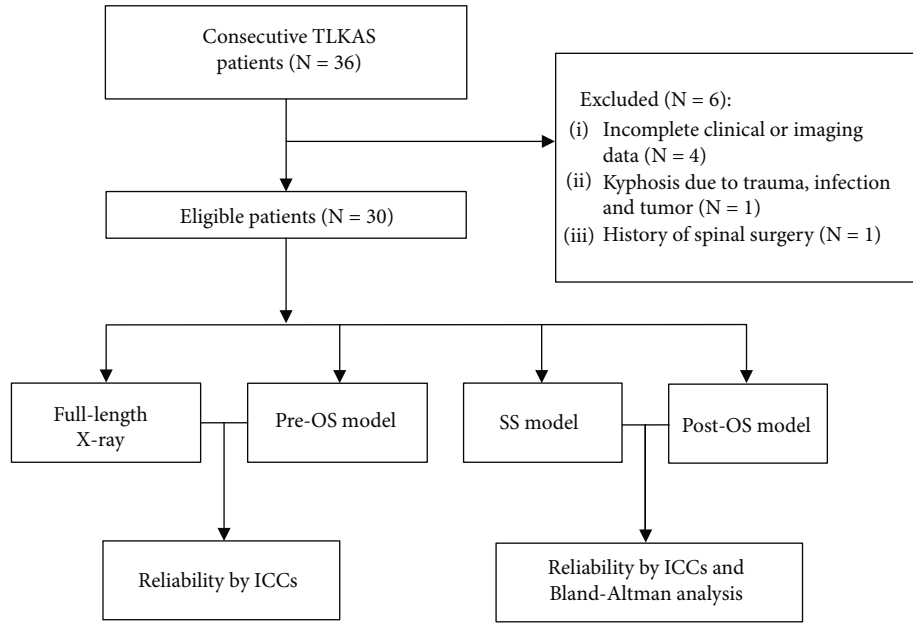
FIGURE 1: The flowchart. TLKAS: thoracolumbar kyphosis secondary to ankylosing spondylitis; Pre-OS: preoperative original 3D spine; SS: simulated 3D spine; Post-OS: postoperative original 3D spine.
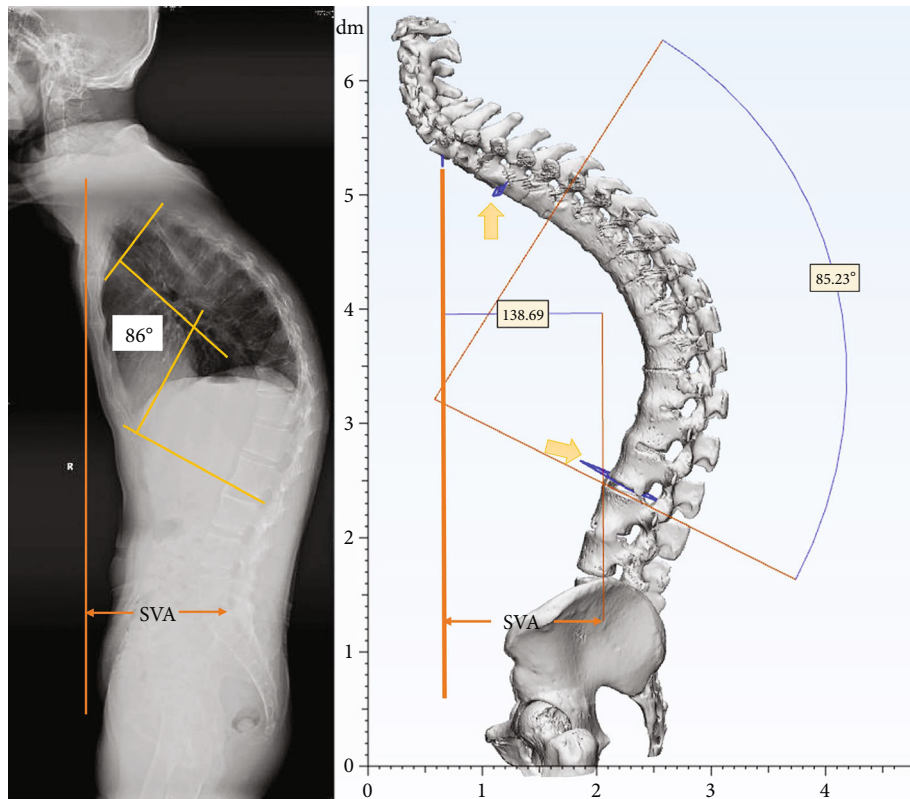
FIGURE 2: Measurements in Pre-OS. Yellow arrows indicated that planes paralleling to the end plates were used for Cobb angle measurement.

circumstance [10, 11]. Therefore, it is essential to make a meticulous preoperative surgical plan for osteotomy in correction surgery.

Several studies have reported 2D correction simulation to predict designed osteotomy plan based on sagittal or coronal X-ray, and the feasibility of 2D simulation in PSO has

(a)

(b)

(c)

FIGURE 3: 3D simulation of multilevel PCO. (a) Sagittal view of the 3D spine models. (b) Partial view of PCO simulation. (c) Intra-op photographs. Yellow arrows indicated osteotomy parts.

been reported [12, 13]. Although 2D simulation provided a reference about osteotomy location based on X-ray, most spinal deformities are 3D malformation of the spine. Thus, it might be more essential to design osteotomy plan with more anatomical details in 3D view to avoid iatrogenic injury. Multilevel PCO is an important correction technique for TLKAS patients, but 2D simulation was scarcely performed in multilevel PCO which may be due to the faint identification of posterior elements in X-ray.

Recently, researches have confirmed the application of 3D reconstruction technique with Mimics Medical software in hip trauma, orthopedic oncology, and cervical spine surgery for parameter measurement and 3D printing technology [14–16]. 3D simulation better allows the surgeon to improve the visualization of the patient's anatomy and perform the procedures through virtual omnidirectional feedback. The technique could compensate the deficiency of

2D simulation caused by faint identification of posterior elements [17]. Therefore, we presumed that it is more beneficial for TLKAS patients to accept 3D simulation, especially for patients who plan to undergo multilevel PCO. Nevertheless, the reliability of 3D simulation in posterior osteotomy simulation for TLKAS remains unknown yet. Given the paucity of the data in this field, we intended to initially explore the Mimics Medical and related software to provide an accurate, flexible, and intuitive 3D simulation to make surgical plan for posterior osteotomies based on CT scan data and aimed to investigate the reliability of CA3DSS for posterior osteotomies in TLKAS.

2. Materials and Methods

2.1. Patients. Eligible TLKAS patients were consecutively included in the study from January 2017 to November

(a)

(b)

(c)
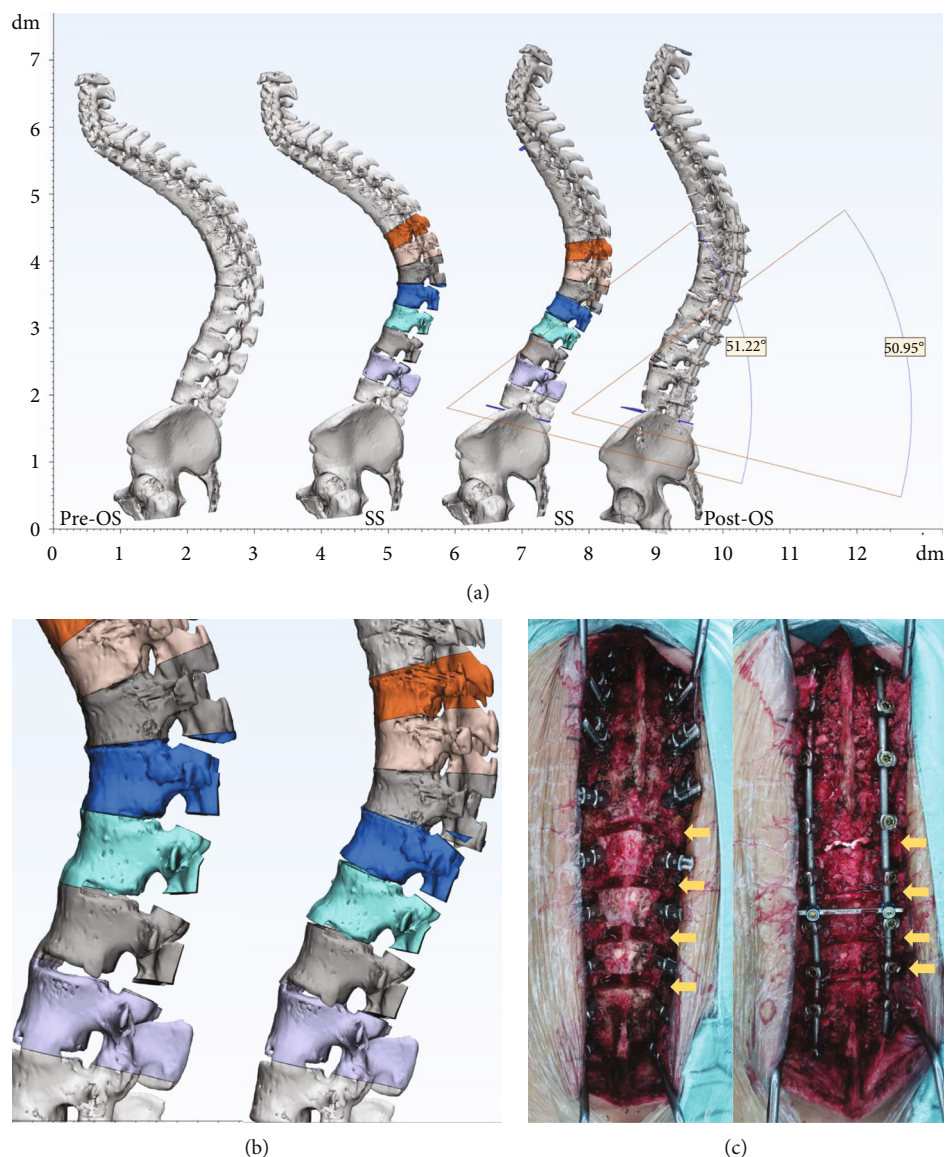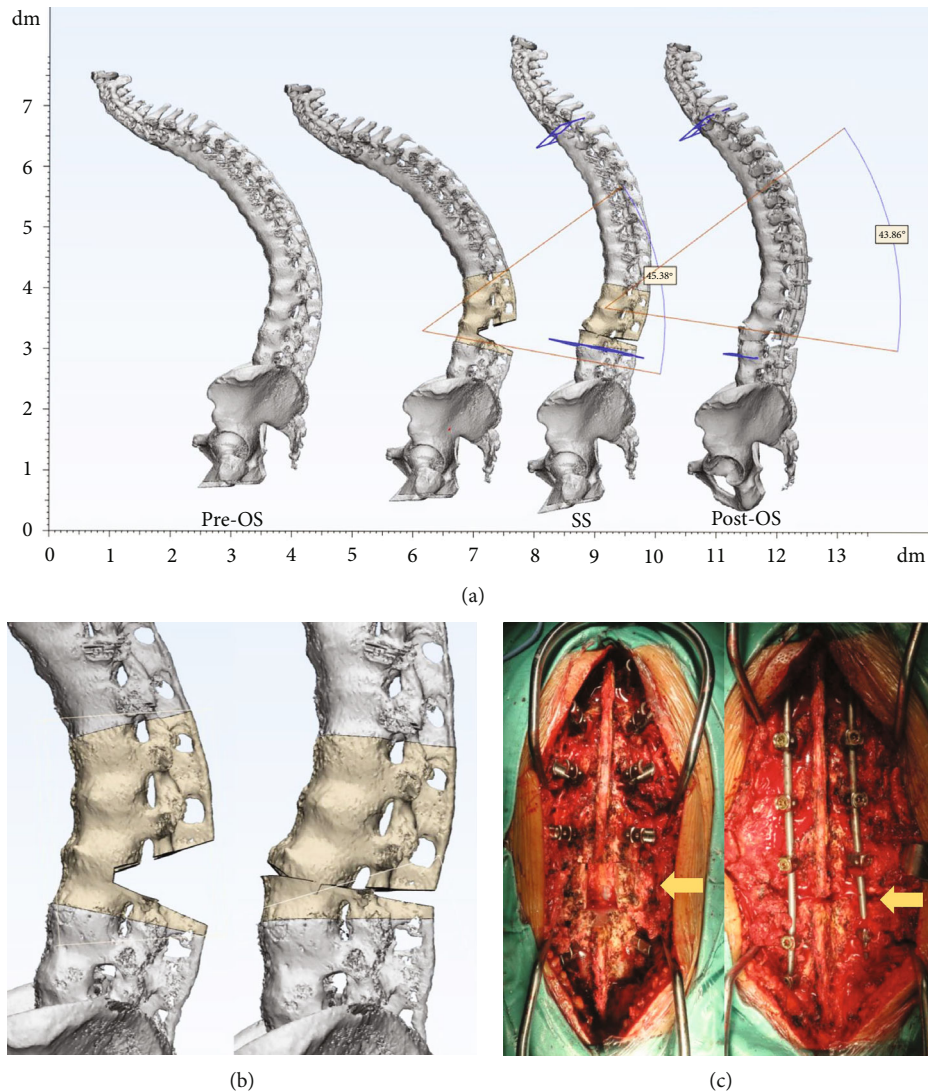
FIGURE 4: 3D simulation of PSO. (a) Sagittal view of the 3D spine models. (b) Partial view of PSO simulation. (c) Intra-op photographs and yellow arrows indicated L3 PSO.

2021. Inclusion criteria were as follows: (1) patients were diagnosed as AS by laboratory tests, radiological features, and clinical manifestations guided by the New York criteria [18] and (2) all the patients received one-stage posterior correction surgery due to kyphosis with pedicle screw fixation and posterior osteotomies at thoracolumbar spine by the same surgeon in the institution. Exclusion criteria were (1) patients with incomplete clinical or imaging data; (2) AS patients progressed kyphosis because of trauma, infection, and tumor; and (3) the patient had a history of spinal surgery. The study was approved by the institutional review board of our institution.

2.2. 3D Spine Model Reconstruction. Patients' CT scan data of the whole spine were collected with Digital Imaging and Communications in Medicine (DICOM) format (DICOM format data from Siemens CT machine, SOMATOM Sensa-

tion 16, Siemens AG, Forchheim, Germany). All the tomographic pictures were imported into Mimics Medical 21.0 (Materialise NV, Leuven, Belgium), and 3D spine model was established with threshold of 226-3071HU. Further parameter measurement and surgical planning were calculated and simulated in 3-Matic Medical 13.0 (Materialise NV, Leuven, Belgium) after importing the created 3D model.

Patients' radiological data were collected and analyzed. The measurement consistency was evaluated between X-ray and preoperative original 3D spine (Pre-OS) models. The results of osteotomy simulation by CA3DSS were evaluated by the measurement in simulated 3D spine (SS) and postoperative original 3D spine (Post-OS) models. The reliability of angle change by different posterior osteotomies was also assessed. Pre-OS model was the 3D spine model reconstructed with preoperative CT scan data, and SS model was the one that Pre-OS model underwent osteotomy

(a)

(b)

(c)
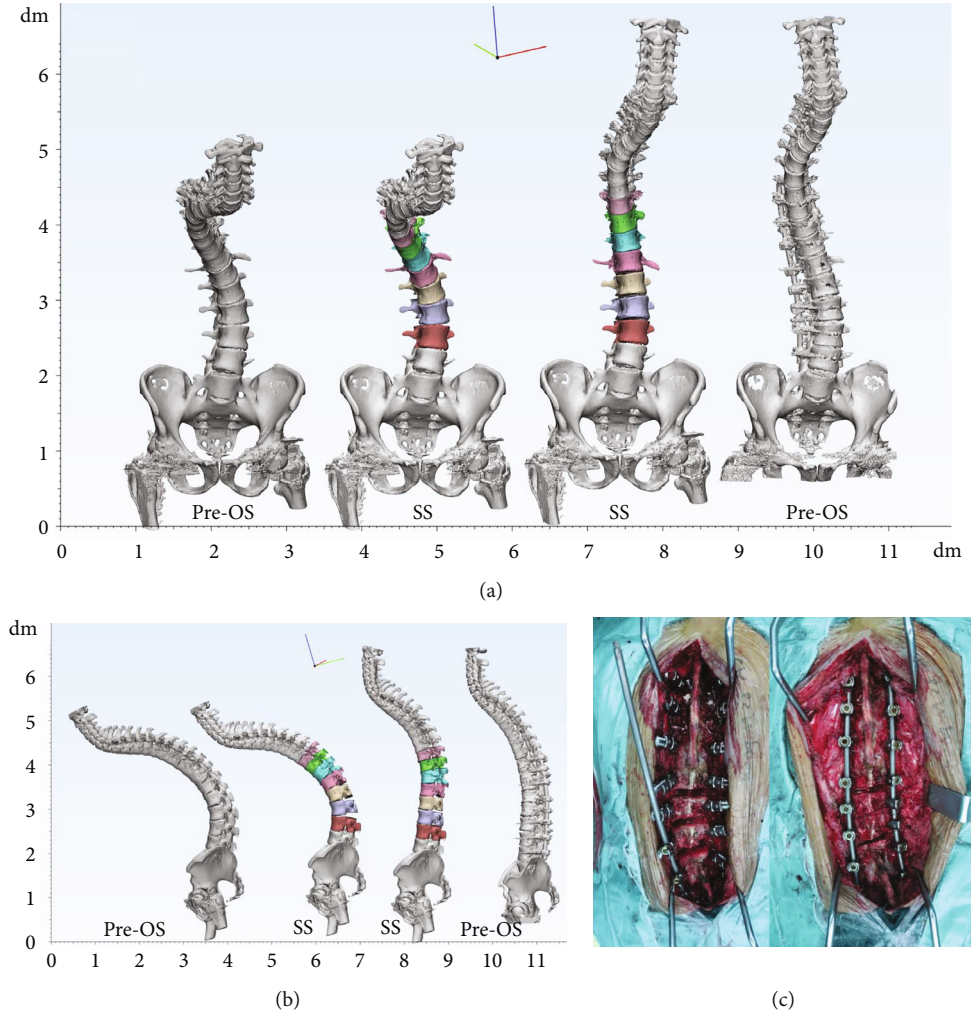
FIGURE 5: 3D simulation of multilevel PCO for TLKAS patient with scoliosis. (a) Coronal view of the 3D spine models. (b) Sagittal view of the 3D spine models. (c) Intra-op photographs of multilevel PCO and yellow arrows indicated PCO at T12/L1, L1/2, and L2/3.

TABLE 1: Results of ICCs for measurement in preoperative full-spine X-ray and Pre-OS models.

Parameters	X-ray	Pre-OS	ICC (95% CI)
GK (°)	87.86 ± 13.25	85.36 ± 13.14	0.942 (0.882-0.972)
TK (°)	65.67 ± 11.17	62.7 ± 10.85	0.954 (0.907-0.978)
LL (°)	5.15 ± 11.33	6.64 ± 12.00	0.955 (0.908-0.978)
MC (°)	2.60 (0.75-10.15)	2.55 (0.00-9.00)	0.992 (0.983-0.996)
SVA (cm)	6.95 (5.77-12.73)	7.80 (5.85-12.15)	0.965 (0.928-0.983)

GK: global kyphosis; TK: thoracic kyphosis; LL: lumbar lordosis; MC: main curve; SVA: sagittal vertical axis; Pre-OS: preoperative original 3D spine.

simulation. Post-OS model was reconstructed 3D spine model with postoperative CT scan data. The flowchart is depicted in Figure 1.

2.3. Parameter Measurement. For 2D radiological measurement, preoperative full-length anteroposterior and lateral spine X-ray were collected. Coronal and sagittal parameters were documented including global kyphosis (GK), thoracic kyphosis (TK), lumbar lordosis (LL), sagittal vertical axis

(SVA), and main curve (MC). GK was defined as the largest Cobb angle in sagittal plane, and MC was defined as the Cobb angle of the main curve in coronal plane.

For 3D radiological measurement, the mentioned parameters were documented with measuring tools in 3-Matic Medical 13.0 in Pre-OS, SS, and Post-OS models. To maintain an accurate data, the 3D spine model was initially adjusted to the same position as full-length AP view X-ray according to the pelvic position in sagittal plane. The Cobb

TABLE 2: Results of ICCs and Bland-Altman analysis for radiological measurement in Post-OS and SS models.

Parameters	Post-OS	SS	ICC analysis ICC (95% CI)	Bland-Altman analysis Mean bias	Bland-Altman analysis LOA (95% CI)
GK (°)	60.03 ± 8.02	56.63 ± 8.83	0.832 (0.677-0.916)	3.400	-6.183-12.98
TK (°)	49.70 ± 5.55	45.47 ± 5.27	0.773 (0.577-0.885)	4.233	-3.256-11.72
LL (°)	25.39 ± 10.05	27.73 ± 9.12	0.896 (0.794-0.949)	-0.2330	-15.12-10.46
MC	0.00 (0.50-1.25)	0 (0.00-0.00)	0.680 (0.428-0.834)	—	—
SVA (cm)	4.10 (3.05-6.72)	3.85 (2.10-5.58)	0.619 (0.338-0.798)	0.727	-2.902-4.356

MC and SVA were exhibited as medians with interquartile range. SS: simulated 3D spine; Post-OS: postoperative original 3D spine.

angle was achieved by angle measurement with two planes paralleling to upper and lower end plate according to the end vertebras settled in X-ray. SVA was measured by the vertical distance from posterior upper margin of S1 to the vertical plane settled by middle point of C7 (Figure 2).

2.4. Posterior Osteotomy Simulation. Posterior osteotomy simulation was performed in 3-Matic Medical 13.0 with cut tool and trim tool in Pre-OS model based on intra-op pictures and operation records. During the simulation process, the operators were blinded to Post-OS model. After trimming the targeted posterior element, the rotation tool was used to achieve the wedge closing process. PCO and PSO simulations were accomplished following the literatures [7, 8] and surgeon's experience (Figures 3 and 4). For patients with coronal curve, coronal correction simulation was achieved after sagittal procedure (Figure 5). The osteotomy angle was assessed in Pre-OS, SS, and Post-OS models by angle calculation according to the angle change of upper and lower end plate in targeted vertebras.

Both 2D and 3D radiological measurements were performed by two experienced surgeons, and any discrepancy was solved by reevaluation and discussion between them. The reliability of CA3DSS was assessed by global measurement and local measurement. Global measurement included GK, TK, LL, MC, and SVA. Local measurement included the angle change of different posterior osteotomies.

2.5. Statistics Analysis. Quantitative data were listed as means ± SD or as medians with interquartile range when the data presented a nonnormal distribution. The reliability of the parameters documented in X-ray, Pre-OS, SS, and Post-OS models were determined by intraclass correlation coefficients (ICCs). Reliabilities below 0.40 were considered as poor, 0.40 to 0.75 were fair to good, and >0.75 were characterized as excellent. All statistical analysis were calculated by SPSS Statistics 20 (IBM Corp, Armonk, New York, United States). Bias of the data conforming to normal distribution were analyzed using Bland-Altman analysis to evaluate the agreement between the mentioned corresponding parameters by GraphPad Prism 6 (GraphPad Software, La Jolla, CA).

3. Results

After screening 36 patients, a total of 30 eligible TLKAS patients were finally included in the study. All patients

underwent posterior pedicle screw fixation and posterior osteotomies for correction. The average age was 40 ± 5.8 years old. One-level PSO osteotomy was performed in 11 patients and two-level PSO osteotomy in 2 patients. Multi-PCO and hybrid osteotomy (PSO + multi − PCO) were performed in 11 patients and 6 patients, respectively.

3.1. Consistency between 2D and 3D Measurements. For preoperative measurement in both full-length X-ray and Pre-OS, excellent reliabilities were exhibited in GK (ICC 0.942, 95% CI 0.882-0.972), TK (ICC 0.954, 95% CI 0.907-0.978), LL (ICC 0.955, 95% CI 0.908-0.978), MC (ICC 0.992, 95% CI 0.983-0.996), and SVA (ICC 0.965, 95% CI 0.928-0.983) (Table 1).

3.2. Reliability of 3D Simulation by Global Measurement. For postoperative radiological parameters between Post-OS and SS models, excellent reliabilities were exhibited in GK (ICC 0.832, 95% CI 0.677-0.916), TK (ICC 0.773, 95% CI 0.577-0.885), and LL (ICC 0.896, 95% CI 0.794-0.949) and good reliabilities were shown in MC (ICC 0.680, 95% CI 0.428-0.834) and SVA (ICC 0.619, 95% CI 0.338-0.798) (Table 2). Bland-Altman analysis indicated acceptable agreement for GK, TK, LL, and SVA in SS and Post-OS models (Figure 6).

3.3. Reliability of 3D Simulation by Local Measurement. For measurement of posterior osteotomies, PCO showed 6.39° ± 1.45° for each level in real spine, and the consistency was good with an ICC value of 0.703 (95% CI 0.511-0.829). PSO procedure showed 20.84° ± 5.16° correction in each vertebra and achieved an excellent reliability (ICC 0.754, 95% CI 0.487-0.892) (Table 3). Bland-Altman analysis indicated good reliabilities for PCO and PSO in real spine and SS models (Figure 6).

4. Discussion

Approximately 30% of the AS patients will develop into thoracolumbar kyphosis [1]. Generally, the surgical target is to restore sagittal balance from flexed trunk with posterior osteotomies including PSO and PCO. Posterior osteotomies have been widely used in spinal deformity correction surgery and can provide an adequate correction and clinical outcomes especially for patients with kyphotic deformity [5–7, 19]. Whereas complications associated with posterior osteotomies should not be ignored, literatures have disclosed that the total complication rates were 43% and 28% for SPO and
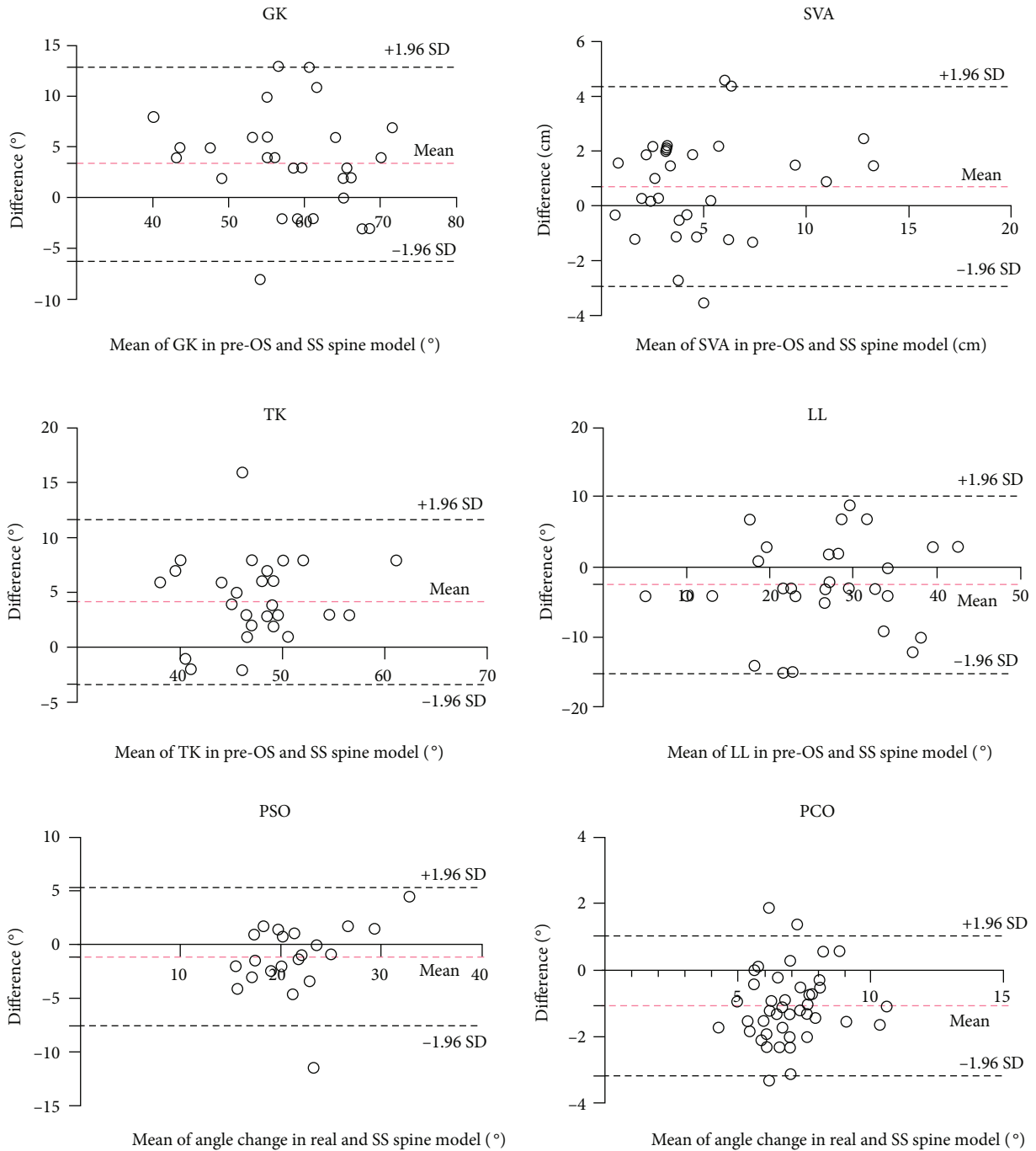
Figure 6: Bland-Altman analysis of radiological parameters. Red dashed lines indicated the mean difference with the corresponding 95% CI, and black dashed lines indicated the limits of agreement with the corresponding 95% CI.

Table 3: Results of ICCs and Bland-Altman analysis for the angle changes in real and simulated osteotomies.

Type of osteotomy	Real spine	Simulation	ICC analysis ICC (95% CI)	Bland-Altman analysis	
				Mean bias	LOA (95% CI)
PCO (°, $n = 42$)	6.39 ± 1.45	7.45 ± 1.33	0.703 (0.511-0.829)	-1.062	-3.167-1.043
PSO (°, $n = 21$)	20.84 ± 5.16	21.90 ± 4.17	0.754 (0.487-0.892)	-1.052	-7.499-5.394

PCO: posterior column osteotomy; PSO: pedicle subtraction osteotomy.

PSO, respectively, and the rates of neurological deficits were 6% for SPO and 5% for PSO [20]. To ensure patients to achieve an accurate, safe, and sufficient correction, computer-assisted surgical planning has been widely used in the application of preoperative osteotomy planning for AS patients [13, 21, 22]. Zhang et al. [21] have reported the application of Surgimap software in two-level PSO in kyphosis after AS and considered it was a feasible, safe, and effective method for individual treatment. Langella et al. [23] demonstrated the ability of Surgimap in prediction of proper alignment for sagittal imbalance. Previous studies have reported single-level posterior osteotomy simulation, and few have paid attention to multilevel PCO, which would be difficult with 2D simulation due to faint identification of posterior elements in X-ray. The simulation based on full-length X-ray could also bring difficulty in identifying where or how to perform the osteotomy procedure in detail [13, 24]. In addition, spinal deformities are 3D malformation of the spine, and in clinical work, we found that both sagittal imbalance and coronal imbalance could impact AS patients. 2D simulation could not show coronal and sagittal views in the same time. Hence, a real 3D and simulation is demanded.

In the present study, we have explored the reliability of Mimics and related software in TLKAS. The results showed proper predictive abilities in both angle and alignment. Considering the stiffness of spinal change in AS, we thought there might be no much difference in standing and supine radiographs, compared to a deviation of 8.8° magnitude in idiopathic scoliosis [25]. On the comparison of measurement, we noticed that there was a 1-3° magnitude between X-ray and 3D spine in Cobb angle, which just verified our mentioned assumption. And this also verified the feasibility of angle and alignment measurements in 3D spine model. The results also demonstrated an excellent consistency between SS and Post-OS models in sagittal parameters. The coronal parameter of MC showed slightly lower ICC value, but it was still in the reliable reference. Due to the abnormal distribution of the data, we did not perform Bland-Altman analysis of MC. Most of the simulated osteotomies were performed firstly in the sagittal plane, and then, coronal closing process would be performed which would affect the accuracy of coronal parameters, which might cause the lower ICC value of MC. In the cohort, the results of SS model showed 2°-4° deviation of GK compared to Post-OS, and we thought that the deviation occurred in osteotomy closing process. In PSO procedure, a 25°-35° correction of lordosis would be achieved though vertebral body wedge shorten after posterior element removal [8, 26, 27]. In the present study, we demonstrated a 20.8° correction for PSO procedure, and ICCs showed good agreement in SS model as 21.9°. For PCO procedure, literatures demonstrated a 5°-10° correction achieved with posterior element resection and gap closings, and multilevel PCO could acquire outstanding and safe outcomes [3, 7, 28, 29]. The efficacy of PCO in our study showed a 6.39° correction in each level and 7.45° as a result of simulation. The consistency was marginally worse compared to PSO procedure, and the reason we thought were as listed. First, PCO theoretically achieved a 5°-10° angle change while we could not ignore the measure error for 1°-3° as researches reported [30, 31]. Second, we found hardly that the closure of posterior elements could be matched exactly in real closing process, a desired closure could not be achieved in real although we simulated a relatively matched closure, and this also occurred in PSO simulation. However, a multilevel PCO tended to magnify the margin, and thus, a marginally worse result was indicated compared to PSO simulation. Despite the reliability of simulated PCO was not superior compared to simulated PSO, both of the simulated osteotomies demonstrated good predictability.

Computer-assisted virtual surgical planning has been widely used in 3D measurement and 3D printing technique [16, 32, 33]. The technique allows the surgeon to visualize the patient's anatomy thoroughly. In the present study, we demonstrated a 3D visual, flexible, and highly consistent simulation with the software for posterior osteotomies in TLKAS patients. This technique can provide intuitive reference and comprehension of posterior osteotomy, and we believed the technique can bring surgeons anatomy measurement and correction design preoperatively and further studies may be applied in other spinal deformities.

The limitations of the present study include that it was a retrospective study and the sample size was small. The simulation was calculated based on preoperative and postoperative supine position CT data, and SVA bias may exist in patients with mobilizable hip joint in upright position after its compensation compared to postoperative stand X-ray. This limitation exists in all the 2D and 3D simulation software, which is hard to overcome at present. So far, we believed this study can provide a great reference for further research.

5. Conclusions

The results of radiological measurements with CA3DSS are almost the same compared to 2D measurement. CA3DSS is reliable for posterior osteotomy simulation in TLKAS patients. The application of the technique is effective and would help surgeons verify the osteotomy location preoperatively and evaluate the magnitude for osteotomy procedure.

Data Availability

The datasets used and/or analyzed during the current study are not publicly available due to the data being confidential; however, they are available from the corresponding author on a reasonable request.

Ethical Approval

The study was approved by the institutional review board of our hospital. The present study was guided by the Declaration of Helsinki. The study was registered at Chinese Clinical Trial Registry as ChiCTR2100053808.

Consent

Informed consent was obtained from all patients.

Conflicts of Interest

We do not have a financial or personal relationship with a third party. On behalf of all authors, the corresponding author states that there is no conflict of interest.

Authors' Contributions

Yiqi Zhang was responsible for the software, validation, and formal analysis; collected and analyzed the data; designed the study; and wrote, reviewed, and edited the manuscript. Yong Hai performed the surgeries and designed and supervised the study. Yuzeng Liu was responsible for the methodology and designed the study. Xinuo Zhang was responsible for the methodology and supported the foundation. Yangpu Zhang was responsible for the software, validation, and methodology and wrote, reviewed, and edited the manuscript. Chaofan Han was responsible for the software and investigation. Jingwei Liu was responsible for the validation and methodology and collected and analyzed the data. Lijin Zhou was responsible for the methodology and designed and supervised the study. The authors read and approved the final manuscript.

References

[1] E. N. Kubiak, R. Moskovich, T. J. Errico, and P. E. Di Cesare, "Orthopaedic management of ankylosing spondylitis," *The Journal of the American Academy of Orthopaedic Surgeons*, vol. 13, no. 4, pp. 267–278, 2005.

[2] J. Braun and J. Sieper, "Ankylosing spondylitis," *Lancet (London, England)*, vol. 369, no. 9570, pp. 1379–1390, 2007.

[3] Y. S. Park, H. S. Kim, and S. W. Baek, "Spinal osteotomy in ankylosing spondylitis: radiological, clinical, and psychological results," *The Spine Journal*, vol. 14, no. 9, pp. 1921–1927, 2014.

[4] K. T. Kim, S. H. Lee, K. S. Suk, J. H. Lee, and Y. J. Im, "Spinal pseudarthrosis in advanced ankylosing spondylitis with sagittal plane deformity," *Spine (Phila Pa 1976)*, vol. 32, no. 15, pp. 1641–1647, 2007.

[5] W. Zhong, Z. Chen, Y. Zeng et al., "Two-level osteotomy for the corrective surgery of severe kyphosis from ankylosing spondylitis," *Spine (Phila Pa 1976)*, vol. 44, no. 23, pp. 1638–1646, 2019.

[6] K. H. Lee, K. T. Kim, Y. C. Kim, J. W. Lee, and K. Y. Ha, "Radiographic findings for surgery-related complications after pedicle subtraction osteotomy for thoracolumbar kyphosis in 230 patients with ankylosing spondylitis," *Journal of Neurosurgery. Spine*, vol. 33, no. 3, pp. 366–372, 2020.

[7] A. Ponte, G. Orlando, and G. L. Siccardi, "The true Ponte osteotomy: by the one who developed it," *Spine Deform*, vol. 6, no. 1, pp. 2–11, 2018.

[8] M. C. Gupta, S. Gupta, M. P. Kelly, and K. H. Bridwell, "Pedicle subtraction osteotomy," *JBJS Essential Surgical Techniques*, vol. 10, no. 1, p. e0028, 2020.

[9] C. Yang, Z. Zheng, H. Liu, J. Wang, Y. J. Kim, and S. Cho, "Posterior vertebral column resection in spinal deformity: a systematic review," *European Spine Journal*, vol. 25, no. 8, pp. 2368–2375, 2016.

[10] J. M. Buchowski, K. H. Bridwell, L. G. Lenke et al., "Neurologic complications of lumbar pedicle subtraction osteotomy," *Spine (Phila Pa 1976)*, vol. 32, no. 20, pp. 2245–2252, 2007.

[11] J. Qiao, L. Xiao, X. Sun et al., "Vertebral subluxation during three-column osteotomy in surgical correction of adult spine deformity: incidence, risk factors, and complications," *European Spine Journal*, vol. 27, no. 3, pp. 630–635, 2018.

[12] W. Hu, X. Zhang, J. Yu, F. Hu, H. Zhang, and Y. Wang, "Vertebral column decancellation in Pott's deformity: use of Surgimap spine for preoperative surgical planning, retrospective review of 18 patients," *BMC Musculoskeletal Disorders*, vol. 19, no. 1, p. 13, 2018.

[13] B. J. van Royen, "Preoperative planning and the use of free available software for sagittal plane corrective osteotomies of the lumbar spine in ankylosing spondylitis," *Orthopedic Research and Reviews*, vol. 12, pp. 171–182, 2020.

[14] A. Senkoylu, I. Daldal, and M. Cetinkaya, "3D printing and spine surgery," *Journal of Orthopaedic Surgery (Hong Kong)*, vol. 28, no. 2, p. 230949902092708, 2020.

[15] Y. Chen, X. Jia, M. Qiang, K. Zhang, and S. Chen, "Computer-assisted virtual surgical technology versus three-dimensional printing technology in preoperative planning for displaced three and four-part fractures of the proximal end of the humerus," *The Journal of Bone and Joint Surgery. American Volume*, vol. 100, no. 22, pp. 1960–1968, 2018.

[16] P. A. J. Pijpker, J. M. A. Kuijlen, J. Kraeima, and C. Faber, "Three-dimensional planning and use of individualized osteotomy-guiding templates for surgical correction of kyphoscoliosis: a technical case report," *World Neurosurgery*, vol. 119, pp. 113–117, 2018.

[17] S. P. Prabhu, "3D modeling and advanced visualization of the pediatric brain, neck, and spine," *Magnetic Resonance Imaging Clinics of North America*, vol. 29, no. 4, pp. 655–666, 2021.

[18] S. van der Linden, H. A. Valkenburg, and A. Cats, "Evaluation of diagnostic criteria for ankylosing spondylitis," *Arthritis and Rheumatism*, vol. 27, no. 4, pp. 361–368, 1984.

[19] J. C. Huang, B. P. Qian, Y. Qiu, B. Wang, Y. Yu, and M. Qiao, "What is the optimal postoperative sagittal alignment in ankylosing spondylitis patients with thoracolumbar kyphosis following one-level pedicle subtraction osteotomy," *The Spine Journal*, vol. 20, no. 5, pp. 765–775, 2020.

[20] H. Liu, C. Yang, Z. Zheng et al., "Comparison of Smith-Petersen osteotomy and pedicle subtraction osteotomy for the correction of thoracolumbar kyphotic deformity in ankylosing spondylitis: a systematic review and meta-analysis," *Spine (Phila Pa 1976)*, vol. 40, no. 8, pp. 570–579, 2015.

[21] N. Zhang, H. Li, Z. K. Xu, W. S. Chen, Q. X. Chen, and F. C. Li, "Computer simulation of two-level pedicle subtraction osteotomy for severe thoracolumbar kyphosis in ankylosing spondylitis," *Indian Journal of Orthopaedics*, vol. 51, no. 6, pp. 666–671, 2017.

[22] Y. S. Park, H. S. Kim, S. W. Baek, and J. H. Oh, "Preoperative computer-based simulations for the correction of kyphotic deformities in ankylosing spondylitis patients," *The Spine Journal*, vol. 14, no. 10, pp. 2420–2424, 2014.

[23] F. Langella, J. H. Villafañe, M. Damilano et al., "Predictive accuracy of Surgimap surgical planning for sagittal imbalance: a cohort study," *Spine*, vol. 42, pp. E1297–E1304, 2017.

[24] M. Akbar, J. Terran, C. P. Ames, V. Lafage, and F. Schwab, "Use of Surgimap spine in sagittal plane analysis, osteotomy planning, and correction calculation," *Neurosurgery Clinics of North America*, vol. 24, no. 2, pp. 163–172, 2013.

[25] G. Torell, A. Nachemson, K. Haderspeck-Grib, and A. Schultz, "Standing and supine Cobb measures in girls with idiopathic scoliosis," *Spine (Phila Pa 1976)*, vol. 10, no. 5, pp. 425–427, 1985.

[26] K. H. Bridwell, S. J. Lewis, A. Rinella, L. G. Lenke, C. Baldus, and K. Blanke, "Pedicle subtraction osteotomy for the treatment of fixed sagittal imbalance. Surgical technique," *The Journal of Bone and Joint Surgery. American*, vol. 86, Supplement 1, pp. 44–50, 2004.

[27] K. H. Bridwell, S. J. Lewis, L. G. Lenke, C. Baldus, and K. Blanke, "Pedicle subtraction osteotomy for the treatment of fixed sagittal imbalance," *The Journal of Bone and Joint Surgery. American Volume*, vol. 85, no. 3, pp. 454–463, 2003.

[28] B. P. Qian, J. C. Huang, Y. Qiu et al., "Complications of spinal osteotomy for thoracolumbar kyphosis secondary to ankylosing spondylitis in 342 patients: incidence and risk factors," *Journal of Neurosurgery. Spine*, vol. 30, pp. 91–98, 2019.

[29] M. N. Smith-Petersen, C. B. Larson, and O. E. Aufranc, "Osteotomy of the spine for correction of flexion deformity in rheumatoid arthritis," *Clinical Orthopaedics and Related Research*, vol. 66, no. 1, pp. 6–9, 1969.

[30] J. Wang, J. Zhang, R. Xu, T. G. Chen, K. S. Zhou, and H. H. Zhang, "Measurement of scoliosis Cobb angle by end vertebra tilt angle method," *Journal of Orthopaedic Surgery and Research*, vol. 13, no. 1, p. 223, 2018.

[31] F. Alrehily, P. Hogg, M. Twiste, S. Johansen, and A. Tootell, "The accuracy of Cobb angle measurement on CT scan projection radiograph images," *Radiography*, vol. 26, pp. e73–e77, 2020.

[32] J. C. Sun, K. Q. Sun, S. X. Sun et al., "Computer-assisted virtual operation planning in anterior controllable anterior-displacement and fusion surgery for ossification of the posterior longitudinal ligament based on actual computed tomography data," *Clinical Neurology and Neurosurgery*, vol. 177, pp. 86–91, 2019.

[33] X. Jia, K. Zhang, M. Qiang, Y. Wu, and Y. Chen, "Association of computer-assisted virtual preoperative planning with postoperative mortality and complications in older patients with intertrochanteric hip fracture," *JAMA Network Open*, vol. 3, no. 8, p. e205830, 2020.

Research Article

High Systemic Immune-Inflammation Index and Body Mass Index Are Independent Risk Factors of the Thoracic Ossification of the Ligamentum Flavum

Yongzhao Zhao [1,2,3] **Qian Xiang,** [1,2,3] **Jialiang Lin,** [1,2,3] **Shuai Jiang,** [1,2,3] **and Weishi Li** [1,2,3]

[1]*Department of Orthopaedics, Peking University Third Hospital, Beijing, China*
[2]*Beijing Key Laboratory of Spinal Disease Research, Beijing, China*
[3]*Engineering Research Center of Bone and Joint Precision Medicine, Ministry of Education, Beijing, China*

Correspondence should be addressed to Weishi Li; puh3liweishi@163.com

Background. Inflammation has been considered to play an important role in the pathogenesis of the thoracic ossification of the ligamentum flavum (OLF). However, the inflammation-related risk factors of thoracic OLF have not been fully investigated to date. *Methods*. A total of 95 patients (48 in the OLF group and 47 in the control group) were included in this retrospective study to explore the independent risk factors of thoracic OLF. The following demographic and clinical variables were compared between the two groups: gender, age, body mass index (BMI), coexistence of hypertension or diabetes, and inflammation-related variables. Multivariate logistic regression analysis was utilized to determine the independent risk factors. *Results*. High systemic immune-inflammation index (SII) (≥ 621) (odds ratio [OR] = 12.16, 95% confidence interval [CI] = 2.95 – 50.17, $p < 0.01$) and BMI ($\geq 25 \, \text{kg/m}^2$) (OR = 9.17, 95%CI = 3.22 – 26.08, $p < 0.01$) were independent risk factors of thoracic OLF. SII ($R = 0.38$, $p < 0.01$) and BMI ($R = 0.46$, $p < 0.01$) were positively associated with OLF score. *Conclusion*. High SII and BMI were the independent risk factors of thoracic OLF. Multicenter prospective studies with a large population should be conducted in the future to verify our findings.

1. Background

The thoracic ossification of the ligamentum flavum (OLF) has become the leading cause of thoracic spinal stenosis, which can compress the spinal cord and lead to thoracic myelopathy [1, 2]. Patients with OLF-induced thoracic spinal stenosis often ask for help with the complaints of weakness and the paraesthesia of the lower limbs, paraesthesia of the trunk, and loss of bladder or bowel control [2]. A position for the conservative treatment for thoracic OLF does not exist because of unsatisfactory results [2]. Posterior laminectomy is the standard treatment for thoracic spinal stenosis caused by OLF; however, its surgical process is challenging and associated with the high risk of perioperative complications [3, 4]. Therefore, seeking relevant biomarkers for thoracic OLF is necessary to improve the mechanistic investigation and therapy of this disease.

Thoracic OLF has been considered as a multifactorial disease, and several pathogenic factors, including genetic inheritance, metabolic disorders, inflammation, and mechanical stress, contribute to its onset and development [5–7]. Several studies have been conducted to identify the risk factors of thoracic OLF to further explore its underlying mechanisms [8–12]. Zhang et al. found that age and body mass index (BMI) were independent risk factors of thoracic OLF [8]. Tang et al. reported that new OLF was associated with high BMI and that the size progression of OLF was related to high BMI and smoking [9]. Liang et al. found that large thoracic kyphosis, lumbar lordosis, and sacral slope were associated with thoracic OLF; these associations indicated that mechanical stress might contribute to the development of OLF [10].

Inflammation is another important pathogenic factor of OLF, and several inflammatory cytokines, such as IL-6 and TNF-α, promote the onset and development of OLF [11, 12]. However, no inflammation-related risk factor of OLF has been identified to date.

Systemic inflammatory responses have been demonstrated to be associated with several nonimmunological diseases, including cancer [13, 14], intervertebral disc degeneration [15], and ectopic ossification [16]. Several clinical models consisting of leukocytes from the circulatory system were constructed for the further investigation of the role of systemic inflammatory responses in diseases and have been proven to have satisfactory diagnostic or prognostic value in human diseases [17–20]. Neutrophil-to-lymphocyte ratio (NLR), platelet-to-lymphocyte ratio (PLR), monocyte-to-lymphocyte ratio (MLR), and systemic immune-inflammation index (SII) are the most commonly used inflammatory biomarkers among existing models and have been verified to play an unfavorable role in the prognosis of several human diseases, especially cancers [21–23]. However, the relationship between inflammatory biomarkers and the development of OLF has not been investigated until now.

In this study, we compared the demographics and clinical variables of patients with thoracic OLF with those of patients without thoracic OLF to determine the inflammation-related risk factors of OLF.

2. Materials and Methods

2.1. General Information. This study was approved by the Ethics Committee of Peking University Third Hospital. Informed consent was not needed given the retrospective design of this study. Patients receiving posterior laminectomy for thoracic OLF from March 2021 to October 2021 at our hospital were included in the OLF group. Inflammation and abnormal immunity have been demonstrated to play important roles in the pathogenesis of degenerative musculoskeletal diseases, such as intervertebral disc degeneration and osteoarthritis [24, 25]. Furthermore, patients with fractures suffer from severe inflammation caused by their fractures [26, 27]. Therefore, patients receiving herniorrhaphy for reducible inguinal or femoral hernia from March 2020 to March 2021 at our hospital were selected as the controls in the control group. The following patients were excluded from this study: (1) patients with trauma, immune diseases (e.g., ankylosing spondylitis, and rheumatoid arthritis), infection, or tumors affecting the spine; (2) patients with the ossification of the posterior longitudinal ligament or thoracic disc herniation; (3) patients with incarcerated hernia or strangulated hernia; and (4) patients lacking the clinical variables of interest. The diagnosis of thoracic OLF was based on the radiographic findings in thoracic computerized tomography (Figure 1). Finally, 95 patients (48 in the OLF group and 47 in the control group) were included in this retrospective study.

2.2. Collection of Demographic and Clinical Variables. The following variables were collected for each included patient: gender; age; BMI; coexistence of hypertension or diabetes;
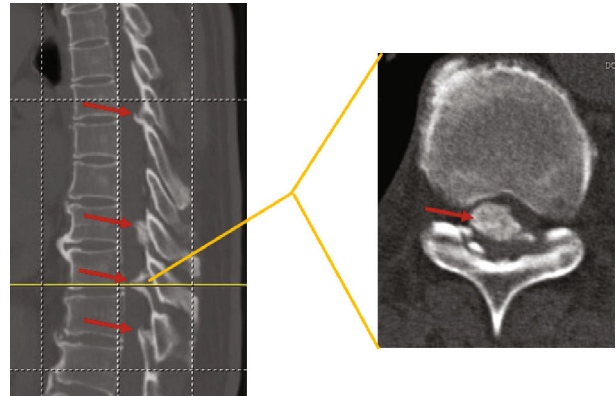

FIGURE 1: Ossified ligamentum flavum (red arrow) in thoracic spine.

and preoperative peripheral blood cells, including neutrophils, platelets, monocytes, and lymphocytes. The indexes of interest were calculated as follows: NLR = neutrophil counts/lymphocyte counts, PLR = platelet counts/lymphocyte counts, MLR = monocyte count/lymphocyte counts, and SII = platelet counts × neutrophil counts/lymphocyte counts. The OLF score of patients with thoracic OLF referred to the sum of segments affected by the ossified ligamentum flavum as previously reported [28]. The cut-off values of NLR and SII were set as 2.42 (Figure 2(a)) and 621 (Figure 2(b)), respectively, on the basis of the ROC curve. The cut-off value of age was set as 60 years old to distinguish between the young and elderly. The cut-off value of BMI was set as 25 kg/m^2 to distinguish between overweight patients and patients with normal weight.

2.3. Statistical Analysis. All analyses in this study were conducted by using the SPSS 22.0 software package (SPSS, IBM, Chicago, IL, USA). Continuous variables, including age, BMI, NLR, PLR, MLR, and SII, were compared between two groups by using the independent samples t-test. Dichotomous variables, including gender and the coexistence of hypertension or diabetes, were compared between two groups by using the χ^2 test. Variables with $p < 0.10$ in univariate analysis were included in the multivariate logistic regression analysis for further analysis. Variables with $p < 0.05$ in multivariate logistic regression analysis were considered as the independent risk factors of thoracic OLF and shown in the form of odds ratio (OR) with the corresponding 95% confidence interval (CI). The correlation between OLF score and BMI or SII was analyzed by using Spearman's correlation test. Here, $p < 0.05$ indicated a statistically significant result.

3. Results

3.1. General Information. The demographics of the included patients are listed in Table 1. Ninety-five patients consisting of 56 males and 39 females were included in this study. The mean age and BMI of the included patients were 51.78 ± 16.18 years and 25.31 ± 5.48 kg/m^2, respectively. Moreover,
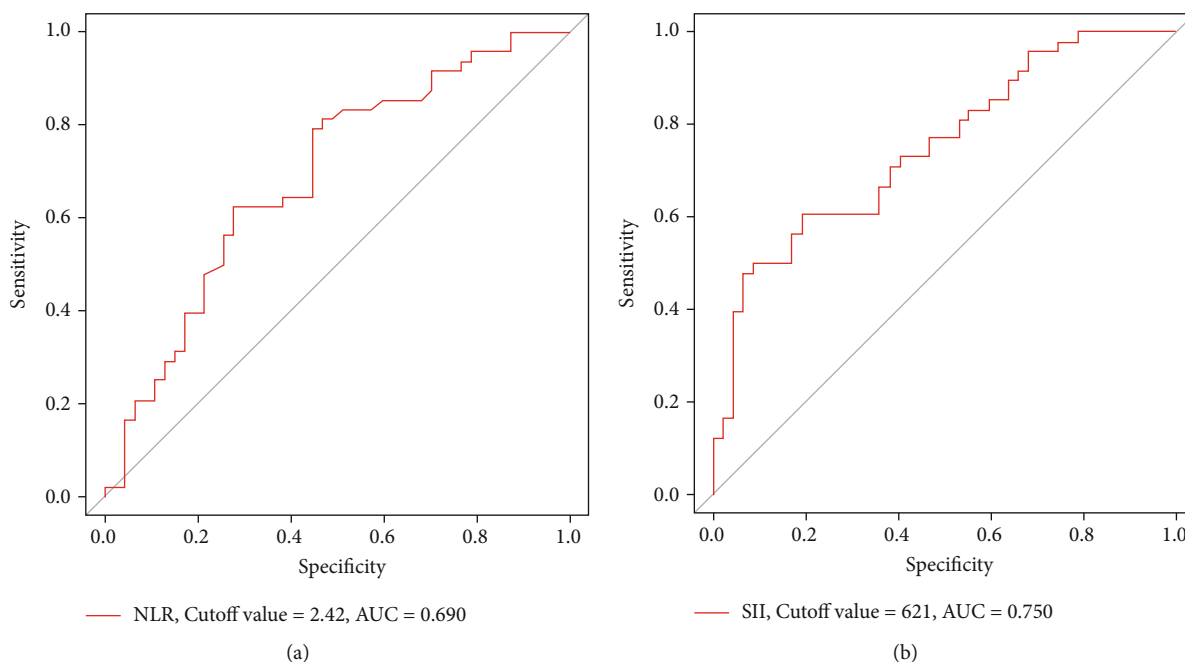
FIGURE 2: Determination of cut-off values. (a) NLR. (b) SII.

TABLE 1: Demographics of included patients.

Variables	Patients ($n = 95$)
Gender (n/%)	
Male	56 (59%)
Female	39 (41%)
Age (mean ± SD), (year)	51.78 ± 16.18
BMI (mean ± SD), (kg/m^2)	25.31 ± 5.48
Coexistence of hypertension or diabetes (n/%)	
No	71 (75%)
Yes	24 (25%)
Groups	
OLF patients	48 (51%)
Control patients	47 (49%)

SD: standard deviation; BMI: body mass index.

24 patients had coexisting hypertension or diabetes. The OLF and control groups comprised 48 and 47 patients, respectively.

3.2. Univariate Analysis for Potential Risk Factors.
As listed in Table 2, 95 patients (56 males and 39 females) were finally included in this research. In terms of demographic variables, the OLF group had a significantly higher age (55.23 years versus 48.19 years, $p = 0.03$) and BMI (27.67 versus 22.89, $p < 0.01$) than the control group. For inflammation-related variables, the OLF group had an obviously higher NLR (2.66 versus 2.16, $p < 0.01$) and SII (636.14 versus 435.25, $p < 0.01$) than the control group. The two groups showed no significant differences in terms of gender ($p = 0.26$),

TABLE 2: Univariate analysis for potential risk factors of thoracic OLF.

Variables	OLF group ($n = 48$)	Control group ($n = 47$)	p
Gender			0.26
Male	31/65%	25/53%	
Female	17/35%	22/47%	
Age (year)	55.23 ± 10.67	48.19 ± 10.82	0.03*
BMI (kg/m^2)	27.67 ± 6.05	22.89 ± 3.47	<0.01*
Coexistence of hypertension or diabetes			0.38
No	34/70%	37/79%	
Yes	14/30%	10/21%	
NLR	2.66 ± 0.88	2.16 ± 0.87	<0.01*
PLR	134.35 ± 46.56	142.45 ± 44.18	0.39
MLR	0.21 ± 0.07	0.24 ± 0.10	0.11
SII	636.14 ± 288.16	435.25 ± 150.12	<0.01*

OLF: ossification of the ligamentum flavum; BMI: body mass index; NLR: neutrophil-to-lymphocyte ratio; PLR: platelet-to-lymphocyte ratio; MLR: monocyte-to-lymphocyte ratio; SII: systemic immune inflammation index. *Variables with $p < 0.10$ were further included into the multivariate logistic regression analysis.

the coexistence of hypertension or diabetes ($p = 0.38$), PLR ($p = 0.39$), or MLR ($p = 0.11$).

3.3. Multivariate Logistic Regression Analysis for Independent Risk Factors.
Variables with $p < 0.10$ in univariate analysis were further included in multivariate logistic regression analysis to determine the independent risk factors of thoracic OLF. As listed in Table 3, high BMI (≥ 25 kg/m^2)

TABLE 3: Multivariate analysis for independent risk factors of thoracic OLF.

Variables	OR (95% CI)	p
Age (year) (≥60 versus <60)	2.14 (0.67-6.85)	0.20
BMI (kg/m^2) (≥25 versus <25)	9.17 (3.22-26.08)	<0.01*
NLR (≥2.42 versus <2.42)	1.58 (0.45-5.58)	0.48
SII (≥621 versus <621)	12.16 (2.95-50.17)	<0.01*

OLF: ossification of the ligamentum flavum; OR: odds ratio; CI: confidence interval; BMI: body mass index; NLR: neutrophil-to-lymphocyte ratio; PLR: platelet-to-lymphocyte ratio; MLR: monocyte-to-lymphocyte ratio; SII: systemic immune inflammation index. *Variables with $p < 0.05$ were considered as independent risk factors.

(OR = 9.17, 95%CI = 3.22 – 26.08, $p < 0.01$) and SII (≥621) (OR = 12.16, 95%CI = 2.95 – 50.17, $p < 0.01$) were independent risk factors of thoracic OLF. However, age ($p = 0.20$) and NLR ($p = 0.48$) were not significantly related to thoracic OLF after adjusting for all variables.

Correlation analysis between OLF score and BMI or SII was performed to determine the relationship of SII and BMI with OLF further. As shown in Figure 3, BMI ($R = 0.38$, $p < 0.01$) (Figure 3(a)) and SII ($R = 0.46$, $p < 0.01$) (Figure 3(b)) were significantly and positively related to OLF score.

4. Discussion

OLF has become the leading cause of thoracic spinal stenosis [1, 2]. Inflammation has been proven to play important roles in the pathogenesis of OLF, and the development of OLF is associated with several inflammatory cytokines, such as IL-6 and TNF-α [12, 29]. However, these inflammatory cytokines are rarely examined in clinical practice. Clinical models based on peripheral blood cells have been validated to have good clinical application in human diseases [17, 22, 23]. In the current study, we discovered that high SII (≥621) and BMI (≥25 kg/m^2) are independent risk factors of OLF. To the best of our knowledge, we are the first to demonstrate that high SII (≥621) is an independent risk factor of OLF.

SII was introduced as an indicator of the systemic inflammatory status in the body and has attracted increasing attention from researchers [30]. SII can serve as a valuable index for predicting the clinical outcomes of human diseases, especially cancers [31–33]. High SII is associated with the poor prognosis of several types of cancer, such as bladder cancer [31], cervical cancer [34], oral cancer [35], gastric cancer [36], and breast cancer [36]. In the current study, for the first time, we found that high SII is an independent risk factor of OLF and that SII is positively associated with OLF score. The underlying mechanism of inflammation in the pathogenesis of OLF has not been fully investigated. Inflammatory cells have been proven to execute important functions in ectopic ossification [37–44]. For example, Herath et al. showed that neutrophils could significantly promote the osteogenesis of osteoblasts [37] and found that autologous neutrophils could facilitate new bone formation in rabbits with calvarial bone defects [38]. Zhang and Wang

reported that in tendons subjected to repetitive mechanical loading, the increase in PGE2 might induce the ossification of tendon tissues [39]. They also considered that neutrophils participated in ectopic ossification because a large proportion of PGE2 originated from neutrophils [40]. Xia et al. discovered that platelet lysate could improve the osteogenic capability of bone marrow-derived mesenchymal stem cells [41]. Karakayali et al. reported that platelet-rich plasma could promote regenerated bone consolidation and increase bone mineral density during distraction osteogenesis [42]. Ranganathan et al. found that the development of ectopic ossification was attenuated in mice deficient in B- and T-lymphocytes [43]. Kanai and Kakiuchi observed that the response levels of peripheral lymphocytes to the anti-CD3 monoclonal antibody differed between the continuous-type and the segmental-type ossification of the posterior longitudinal ligament; this difference indicated that lymphocytes might play important roles in ectopic ossification [44]. SII is calculated on the basis of the counts of platelets, neutrophils, and lymphocytes. Although researchers have attempted to explore the role of inflammatory cells in osteogenesis [37–44], how neutrophils, platelets, and lymphocytes promote the development of OLF remains unclear. Future studies should further explore the role of neutrophils, platelets, and lymphocytes in the pathogenesis of OLF.

High BMI (≥25 kg/m^2) is another independent risk factor of OLF. Obesity or overweight is involved in the development of several human diseases, including OLF [9, 45–47]. Chang et al. reported that patients with thoracic OLF had a higher BMI than those without thoracic OLF ($p < 0.01$) [45]. Similarly, Endo et al. observed a higher BMI in the thoracic OLF group than in the control group ($p < 0.01$) and detected a significantly positive relationship between BMI and OLF score [46]. Moreover, Tang et al. reported that new OLF was usually observed in patients with high BMI; notably, reduced BMI was observed in patients with OLF disappearance within the 5-year follow-up ($p < 0.01$) [9]. In this study, we also discovered that BMI is associated with the development of OLF, and the subsequent multivariate logistic regression analysis revealed that BMI is an independent risk factor of OLF. Moreover, we observed a significantly positive relationship between BMI and OLF score. Although numerous studies have identified the unfavorable role of high BMI in the pathogenesis of OLF, the underlying mechanism of this role remains unclear. The leptin secreted by adipose tissue might be a potential reason for the tendency of patients with high BMI to develop OLF. An increased level of leptin was observed in patients with OLF, and leptin could promote ligamentum flavum cells via the activation of STAT3, JNK, and ERK1/2 [47]. Future studies should focus on the mechanistic investigation of the role of high BMI in the pathogenesis of OLF.

Some limitations should be considered when interpreting our findings. First, this study had a retrospective design and small sample size that might reduce the accuracy of its results. Second, we selected patients with reducible hernia as the control individuals. However, patients with reducible hernia are not same as the healthy population. This situation might affect the generalizability of our findings. Third,
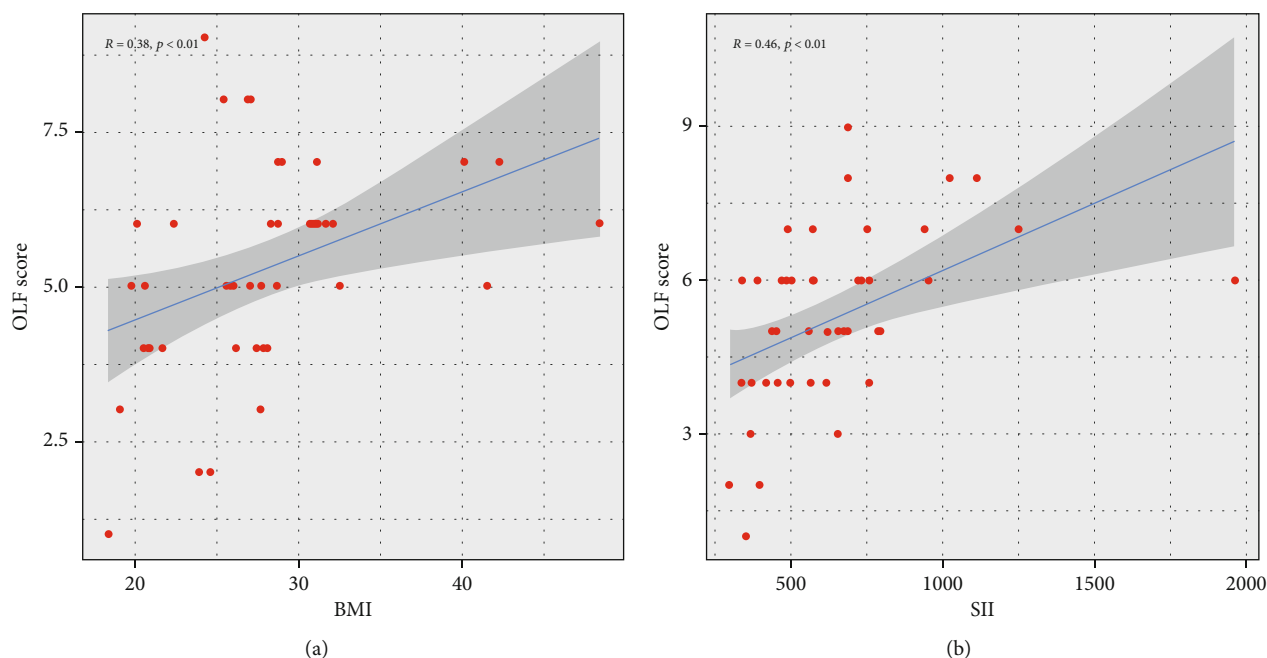
Figure 3: Spearman correlation analysis. (a) BMI and OLF score. (b) SII and OLF score.

inflammatory cells in peripheral blood are easily influenced by the external environment, such as bacterial or viral infections. Fourth, blood samples were collected preoperatively, and the change in SII during the pathogenesis of OLF was not confirmed given the retrospective design of this study. Fifth, some of the included patients were diagnosed with hypertension or diabetes, which might affect the SII results [48, 49]. Multicenter prospective studies with strict methodologies and large populations should be conducted to further determine the relationship between SII and OLF and explore its underlying mechanism.

5. Conclusion

High SII and BMI are independent risk factors of OLF. SII and BMI are positively associated with OLF score. Inflammation and obesity might contribute to the pathogenesis of OLF.

Abbreviations

OLF: Ossification of the ligamentum flavum
BMI: Body mass index
NLR: Neutrophil-to-lymphocyte ratio
PLR: Platelet-to-lymphocyte ratio
MLR: Monocyte-to-lymphocyte ratio
SII: Systemic immune-inflammation index.

Data Availability

The original contributions presented in the study are included in the article, and further inquiries can be directed to the corresponding author/s.

Ethical Approval

This study has been approved by the Ethics Committee of Peking University Third Hospital.

Consent

The written informed consent was not necessary for the retrospective design.

Conflicts of Interest

The authors declared no potential conflicts of interest with respect to the research, authorship, and/or publication of this article.

Authors' Contributions

Weishi Li designed and supervised the study. Yongzhao Zhao, Qian Xiang, and Shuai Jiang extracted and assembled the data. Yongzhao Zhao and Jialiang Lin analyzed the data. Yongzhao Zhao and Qian Xiang wrote the manuscript. All authors read, edited, and approved the manuscript. Yongzhao Zhao and Qian Xiang contributed equally to this work.

Acknowledgments

References

[1] G. Chen, T. Fan, X. Yang, C. Sun, D. Fan, and Z. Chen, "The prevalence and clinical characteristics of thoracic spinal stenosis: a systematic review," *European spine journal: official publication of the European Spine Society, the European Spinal Deformity Society, and the European Section of the Cervical Spine Research Society*, vol. 29, no. 9, pp. 2164–2172, 2020.

[2] Z. Q. Chen, C. G. Sun, and the Spine Surgery Group of Chinese Orthopedic Association, "Clinical guideline for treatment of symptomatic thoracic spinal stenosis," *Orthopaedic Surgery*, vol. 7, no. 3, pp. 208–212, 2015.

[3] C. Sun, Z. Chen, G. Chen et al., "A new "de-tension"-guided surgical strategy for multilevel ossification of posterior longitudinal ligament in thoracic spine: a prospective observational study with at least 3-year follow-up," *The spine journal: official journal of the North American Spine Society*, vol. 22, no. 8, pp. 1388–1398, 2022.

[4] L. Wang, H. Wang, Z. Chen, C. Sun, and W. Li, "Surgical strategy for non-continuous thoracic spinal stenosis: one- or two-stage surgery?," *International Orthopaedics*, vol. 45, no. 7, pp. 1871–1880, 2021.

[5] Q. Xiang, Y. Zhao, J. Lin, S. Jiang, and W. Li, "Epigenetic modifications in spinal ligament aging," *Ageing Research Reviews*, vol. 77, p. 101598, 2022.

[6] D. K. Ahn, S. Lee, S. H. Moon, K. H. Boo, B. K. Chang, and J. I. Lee, "Ossification of the ligamentum flavum," *Asian spine journal*, vol. 8, no. 1, pp. 89–96, 2014.

[7] Y. Zhao, B. Yuan, L. Cheng et al., "Cyclic tensile stress to rat thoracolumbar ligamentum flavum inducing the ossification of ligamentum flavum: an in vivo experimental study," *Spine*, vol. 46, no. 17, pp. 1129–1138, 2021.

[8] H. Zhang, N. Deng, L. Zhang, L. Zhang, and C. Wang, "Clinical risk factors for thoracic ossification of the ligamentum flavum: a cross-sectional study based on spinal thoracic three-dimensional computerized tomography," *Risk management and healthcare policy*, vol. Volume 15, pp. 1065–1072, 2022.

[9] C. Y. K. Tang, K. M. C. Cheung, D. Samartzis, and J. P. Y. Cheung, "The natural history of ossification of yellow ligament of the thoracic spine on MRI: a population-based cohort study," *Global spine journal*, vol. 11, no. 3, pp. 321–330, 2021.

[10] H. Liang, G. Liu, S. Lu et al., "Epidemiology of ossification of the spinal ligaments and associated factors in the Chinese population: a cross-sectional study of 2000 consecutive individuals," *BMC Musculoskeletal Disorders*, vol. 20, no. 1, p. 253, 2019.

[11] L. Ren, H. Hu, X. Sun, F. Li, J. J. Zhou, and Y. M. Wang, "The roles of inflammatory cytokines in the pathogenesis of ossification of ligamentum flavum," *American Journal of Translational Research*, vol. 5, no. 6, pp. 582–585, 2013.

[12] C. Zhang, Z. Chen, X. Meng, M. Li, L. Zhang, and A. Huang, "The involvement and possible mechanism of pro-inflammatory tumor necrosis factor alpha (TNF-α) in thoracic ossification of the ligamentum flavum," *Plo S one*, vol. 12, no. 6, article e0178986, 2017.

[13] C. I. Diakos, K. A. Charles, D. C. McMillan, and S. J. Clarke, "Cancer-related inflammation and treatment effectiveness," *The Lancet Oncology*, vol. 15, no. 11, pp. e493–e503, 2014.

[14] A. Sharabi, M. G. Tsokos, Y. Ding, T. R. Malek, D. Klatzmann, and G. C. Tsokos, "Regulatory T cells in the treatment of disease," *Nature Reviews Drug Discovery*, vol. 17, no. 11, pp. 823–844, 2018.

[15] Y. Zhao, Q. Xiang, J. Lin, S. Jiang, and W. Li, "Oxidative stress in intervertebral disc degeneration: new insights from bioinformatic strategies," *Oxidative Medicine and Cellular Longevity*, vol. 2022, Article ID 2239770, 27 pages, 2022.

[16] Y. Huang, X. Wang, D. Zhou, W. Zhou, F. Dai, and H. Lin, "Macrophages in heterotopic ossification: from mechanisms to therapy," *NPJ Regenerative medicine*, vol. 6, no. 1, p. 70, 2021.

[17] S. Chen, L. Zhang, G. Yan et al., "Neutrophil-to-lymphocyte ratio is a potential prognostic biomarker in patients with ovarian cancer: a meta-analysis," *Bio Med research international*, vol. 2017, article 7943467, 7 pages, 2017.

[18] Y. Zhou, S. Cheng, A. H. Fathy, H. Qian, and Y. Zhao, "Prognostic value of platelet-to-lymphocyte ratio in pancreatic cancer: a comprehensive meta-analysis of 17 cohort studies," *Onco Targets and therapy*, vol. Volume 11, pp. 1899–1908, 2018.

[19] G. Eraslan Doganay and M. O. Cirik, "Are neutrophil-lymphocyte, platelet-lymphocyte, and monocyte-lymphocyte ratios prognostic indicators in patients with chronic obstructive pulmonary disease in intensive care units?," *Cureus*, vol. 14, no. 3, article e23499, 2022.

[20] J. Zhang, X. Lu, S. Wang, and H. Li, "High neutrophil-to-lymphocyte ratio and platelet-to-lymphocyte ratio are associated with poor survival in patients with hemodialysis," *BioMed Research International*, vol. 2021, Article ID 9958081, 6 pages, 2021.

[21] Q. Li, X. Ma, Q. Shao et al., "Prognostic impact of multiple lymphocyte-based inflammatory indices in acute coronary syndrome patients," *Frontiers in cardiovascular medicine*, vol. 9, p. 811790, 2022.

[22] Y. Gao, W. Guo, S. Cai et al., "Systemic immune-inflammation index (SII) is useful to predict survival outcomes in patients with surgically resected esophageal squamous cell carcinoma," *Journal of Cancer*, vol. 10, no. 14, pp. 3188–3196, 2019.

[23] Q. Li, P. Chen, S. Shi et al., "Neutrophil-to-lymphocyte ratio as an independent inflammatory indicator of poor prognosis in IgA nephropathy," *International Immunopharmacology*, vol. 87, p. 106811, 2020.

[24] C. Ruiz-Fernández, V. Francisco, J. Pino et al., "Molecular relationships among obesity, inflammation and intervertebral disc degeneration: are adipokines the common link," *International Journal of Molecular Sciences*, vol. 20, no. 8, p. 2030, 2019.

[25] H. Zhang, D. Cai, and X. Bai, "Macrophages regulate the progression of osteoarthritis," *Osteoarthritis and Cartilage*, vol. 28, no. 5, pp. 555–561, 2020.

[26] S. A. Walsh and T. A. Davis, "Key early proinflammatory signaling molecules encapsulated within circulating exosomes following traumatic injury," *Journal of Inflammation (London, England)*, vol. 19, no. 1, p. 6, 2022.

[27] D. Ragipoglu, J. Bülow, K. Hauff et al., "Mast cells drive systemic inflammation and compromised bone repair after trauma," *Frontiers in Immunology*, vol. 13, p. 883707, 2022.

[28] Y. Kawaguchi, M. Nakano, T. Yasuda, S. Seki, T. Hori, and T. Kimura, "Ossification of the posterior longitudinal ligament in not only the cervical spine, but also other spinal regions," *Spine*, vol. 38, no. 23, pp. E1477–E1482, 2013.

[29] B. Wang, Z. Chen, X. Meng, M. Li, X. Yang, and C. Zhang, "iTRAQ quantitative proteomic study in patients with thoracic

ossification of the ligamentum flavum," *Biochemical and Biophysical Research Communications*, vol. 487, no. 4, pp. 834–839, 2017.

[30] B. Hu, X. R. Yang, Y. Xu et al., "Systemic immune-inflammation index predicts prognosis of patients after curative resection for hepatocellular carcinoma," *Clinical Cancer Research: An Official Journal of the American Association for Cancer Research*, vol. 20, no. 23, pp. 6212–6222, 2014.

[31] J. Li, D. Cao, Y. Huang et al., "The prognostic and clinicopathological significance of systemic immune-inflammation index in bladder cancer," *Frontiers in Immunology*, vol. 13, p. 865643, 2022.

[32] M. B. Vatan, A. C. Çakmak, S. Ağaç, E. Eynel, and H. Erkan, "The systemic immune-inflammation index predicts impaired myocardial perfusion and short-term mortality in ST-segment elevation myocardial infarction patients," *Angiology*, vol. 33197221106886, p. 000331972211068, 2022.

[33] Y. Yilmaz, S. Kelesoglu, D. Elcik, R. Ozmen, and N. Kalay, "Predictive values of systemic immune-inflammation index in new-onset atrial fibrillation following coronary artery bypass grafting," *Brazilian Journal of Cardiovascular Surgery*, 2022.

[34] P. Liu, Y. Jiang, X. Zheng, B. Pan, H. Xiang, and M. Zheng, "Pretreatment systemic immune-inflammation index can predict response to neoadjuvant chemotherapy in cervical cancer at stages IB2-IIB," *Pathology oncology research: POR*, vol. 28, p. 1610294, 2022.

[35] K. Kubota, R. Ito, N. Narita et al., "Utility of prognostic nutritional index and systemic immune-inflammation index in oral cancer treatment," *BMC Cancer*, vol. 22, no. 1, p. 368, 2022.

[36] K. He, L. Si, X. Pan et al., "Preoperative systemic immune-inflammation index (SII) as a superior predictor of long-term survival outcome in patients with stage I-II gastric cancer after radical surgery," *Frontiers in Oncology*, vol. 12, p. 829689, 2022.

[37] T. D. K. Herath, A. Larbi, S. H. Teoh, C. J. Kirkpatrick, and B. T. Goh, "Neutrophil-mediated enhancement of angiogenesis and osteogenesis in a novel triple cell co-culture model with endothelial cells and osteoblasts," *Journal of Tissue Engineering and Regenerative Medicine*, vol. 12, no. 2, pp. e1221–e1236, 2018.

[38] T. D. K. Herath, L. Saigo, B. Schaller et al., "In vivo efficacy of neutrophil-mediated bone regeneration using a rabbit calvarial defect model," *International Journal of Molecular Sciences*, vol. 22, no. 23, p. 13016, 2021.

[39] J. Zhang and J. H. Wang, "Production of PGE (2) increases in tendons subjected to repetitive mechanical loading and induces differentiation of tendon stem cells into non-tenocytes," *Journal of orthopaedic research: official publication of the Orthopaedic Research Society*, vol. 28, no. 2, pp. 198–203, 2010.

[40] H. L. Wright, R. J. Moots, R. C. Bucknall, and S. W. Edwards, "Neutrophil function in inflammation and inflammatory diseases," *Rheumatology (Oxford, England)*, vol. 49, no. 9, pp. 1618–1631, 2010.

[41] W. Xia, H. Li, Z. Wang et al., "Human platelet lysate supports ex vivo expansion and enhances osteogenic differentiation of human bone marrow-derived mesenchymal stem cells," *Cell Biology International*, vol. 35, no. 6, pp. 639–643, 2011.

[42] M. Karakayalı, Y. Alpay, and B. Sarısözen, "Effect of platelet-rich plasma on bone regenerate consolidation in distraction osteogenesis: an experimental study in rabbits," *Acta Orthopaedica et Traumatologica Turcica*, vol. 56, no. 1, pp. 8–13, 2022.

[43] K. Ranganathan, S. Agarwal, D. Cholok et al., "The role of the adaptive immune system in burn-induced heterotopic ossification and mesenchymal cell osteogenic differentiation," *The Journal of Surgical Research*, vol. 206, no. 1, pp. 53–61, 2016.

[44] Y. Kanai and T. Kakiuchi, "Response of peripheral lymphocytes from patients with ossification of posterior longitudinal ligament," *Clinical Orthopaedics and Related Research*, vol. 389, no. 389, pp. 79–88, 2001.

[45] S. Y. Chang, Y. Kim, J. Kim et al., "Sagittal alignment in patients with thoracic myelopathy caused by the ossification of the ligamentum flavum: a retrospective matched case-control study," *Spine*, vol. 46, no. 5, pp. 300–306, 2021.

[46] T. Endo, Y. Koike, Y. Hisada et al., "Aggravation of ossified ligamentum flavum lesion is associated with the degree of obesity," *Global Spine Journal*, p. 219256822110315, 2021.

[47] D. Fan, Z. Chen, Y. Chen, and Y. Shang, "Mechanistic roles of leptin in osteogenic stimulation in thoracic ligament flavum cells," *The Journal of Biological Chemistry*, vol. 282, no. 41, pp. 29958–29966, 2007.

[48] Z. Zhang and Z. Chen, "Higher systemic immune-inflammation index is associated with higher likelihood of peripheral arterial disease," *Annals of Vascular Surgery*, 2021.

[49] A. Elbeyli, B. E. Kurtul, S. C. Ozcan, and D. Ozarslan Ozcan, "The diagnostic value of systemic immune-inflammation index in diabetic macular oedema," *Clinical & Experimental Optometry*, pp. 1–5, 2021.

Research Article

Grape Seed Proanthocyanidins Exert a Neuroprotective Effect by Regulating Microglial M1/M2 Polarisation in Rats with Spinal Cord Injury

Wen-zhao Liu [1,2] **Zhan-jun Ma,**[1,3] **Ji-he Kang,**[1,2] **Ai-xin Lin,**[1,2] **Zhao-heng Wang,**[1,2]
Hai-wei Chen [1,2] **Xu-dong Guo,**[1,2] **Xue-gang He,**[1,2] **and Xue-wen Kang** [1,2,4]

[1]*The Second Clinical Medical College, Lanzhou University, Lanzhou, Gansu 730030, China*
[2]*Department of Orthopedics, Lanzhou University Second Hospital, Lanzhou, Gansu 730030, China*
[3]*Louvain Drug Research Institute, Advanced Drug Delivery and Biomaterials, Université Catholique de Louvain, UCLouvain,*
 1200 Brussels, Belgium
[4]*The International Cooperation Base of Gansu Province for the Pain Research in Spinal Disorders, Gansu 730000, China*

Correspondence should be addressed to Xue-wen Kang; ery_kangxw@lzu.edu.cn

Spinal cord injury (SCI) is a highly disabling disorder for which few effective treatments are available. Grape seed proanthocyanidins (GSPs) are polyphenolic compounds with various biological activities. In our preliminary experiment, GSP promoted functional recovery in rats with SCI, but the mechanism remains unclear. Therefore, we explored the protective effects of GSP on SCI and its possible underlying mechanisms. We found that GSP promoted locomotor recovery, reduced neuronal apoptosis, increased neuronal preservation, and regulated microglial polarisation *in vivo*. We also performed *in vitro* studies to verify the effects of GSP on neuronal protection and microglial polarisation and their potential mechanisms. We found that GSP regulated microglial polarisation and inhibited apoptosis in PC12 cells induced by M1-BV2 cells through the Toll-like receptor 4- (TLR4-) mediated nuclear factor kappa B (NF-κB) and phosphatidylinositol 3-kinase/serine threonine kinase (PI3K/AKT) signaling pathways. This suggests that GSP regulates microglial polarisation and prevents neuronal apoptosis, possibly by the TLR4-mediated NF-κB and PI3K/AKT signaling pathways.

1. Introduction

Spinal cord injury (SCI) is a serious neurological disorder worldwide, with devastating effects [1]. The pathological processes of SCI can be divided into primary and secondary injury. Primary injury refers to injury caused by external forces acting directly on the spinal cord [2, 3], whereas secondary SCI is progressive and delayed, including inflammation, ischemia, apoptosis, oedema, and local reactive gliosis [4, 5]. As the primary injury is irreversible, current treatments mainly focus on the symptoms of secondary injury, such as serious neuroinflammation [6].

Microglial activation is the key to the pathogenesis of secondary inflammatory injuries [7, 8]. Activated microglia are very important for repairing central nervous system (CNS) injuries [9, 10]. When unstimulated, microglia are of great significance for monitoring and regulating CNS homeostasis, neuronal regeneration, and proliferation [11]. Microglia can differentiate into two different phenotypes (M1/M2) to cope with the interference of various microenvironments [12]. Overactivation of M1 microglia prevents neuronal regeneration and leads to neuronal damage [13]. M1 microglia can release proinflammatory factors that can aggravate injury and hinder cell repair after CNS injury and disorders. Alternatively, M2 microglia release anti-inflammatory factors [14–16]. Therefore, inhibition of M1 microglial activation is an effective therapeutic strategy for SCI. However, researchers have recently found that

inhibition of M1 polarisation alone does not provide overall benefits. A more promising approach is to convert overactivated M1 microglia to the M2 phenotype following SCI [17].

Toll-like receptor 4 (TLR4), a transmembrane receptor, is highly expressed in microglia in the CNS [18, 19]. Stimulation with various ligands, including lipopolysaccharide (LPS), can activate downstream molecules. LPS can bind to LPS-binding protein (LBP), which is mainly produced by the liver. The LPS–LBP complex forms a larger complex with cluster of differentiation 14 (CD14) and activates the TLR4/myeloid differentiation factor 2 (MD2) complex, following which the intracellular part of TLR4 can activate its downstream myeloid differentiation primary reactive protein 88 (MyD88) and NF-κB and inhibit the PI3K/AKT pathway via MyD88 recruitment [20]. Activated NF-κB affects the transcription of proinflammatory cytokines, leading to neuroapoptosis and neuroinflammation [21–24]. Therefore, a viable therapeutic strategy for treating SCI involves inhibiting neuroapoptosis and neuroinflammation by inactivating this signaling pathway.

Proanthocyanidins, which are complex flavonoid polymers (Figure 1), are natural polyphenols found in many foods and beverages. The most abundant source is grape (*Vitis vinifera*) seeds, yielding grape seed proanthocyanidins (GSP) [25–28]. Proanthocyanidins have anti-inflammatory, antiapoptotic, antioxidant, and free-radical-scavenging properties [29–31]. In 2017, a study showed that proanthocyanidins had a positive effect on LPS-induced depression-like behavior [32]. In 2022, GSP was reported to have a promising role in modulating bisphenol A-induced neurotoxicity and neuroinflammation [33]. Nevertheless, whether GSP regulates microglial polarisation remains unclear.

Our study suggests that GSP promotes microglial M2 polarisation by targeting TLR4, thus promoting the recovery of locomotor function in rat models of SCI. These findings indicate a promising therapeutic target for SCI treatment.

2. Materials and Methods

2.1. Materials. GSP with a purity ≥ 95% was obtained from Solarbio (Beijing, China). LPS was obtained from Sigma-Aldrich. High-glucose DMEM and fetal bovine serum (FBS) were obtained from Gibco/BRL (Grand Island, NY, USA). CCK-8, fluorescein isothiocyanate/propidium iodide (FITC/PI), and nitric oxide (NO) assay kits were purchased from Beyotime (Shanghai, China). Antibodies against CD86 and CD206 were obtained from Santa Cruz Biotechnology (Dallas, TX, USA). Antibodies against GFAP, NeuN, IκBα, Iba1, TLR4, MyD88, p-IκBα, p-NF-κB p65, p-PI3K, PI3K, p-AKT, NF-κB p65, and AKT were purchased from Cell Signalling Technology (Danvers, MA, USA). Antibodies against β-actin, ARG1, BCL-2, inducible nitric oxide synthase (iNOS), BAX, IL-10, TNF-α, and cleaved caspase-3 were purchased from Proteintech Group Inc. (Chicago, IL, USA).

2.2. Animal Model of SCI and GSP Administration. Sixty specific pathogen-free adult Sprague-Dawley rats (female, 230 ± 20 g) were obtained from the Animal Experimental
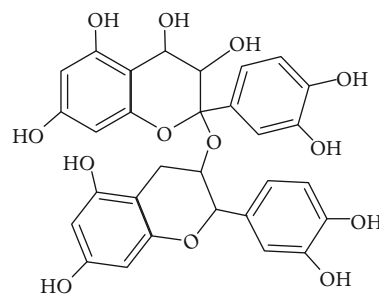

FIGURE 1: The chemical structure of GSP.

Centre of Lanzhou University. All rats were housed in separate cages under controlled housing conditions ($23°C \pm 2°C$, $50\% \pm 5\%$ humidity, and 12-h light-dark cycle). The animals were randomly divided into three groups (Figure 2): (1) sham, (2) SCI, and (3) SCI+40 mg/kg GSP ($n = 20$ per group). The modified Allen method was adopted to establish the SCI models [34]. Briefly, rats were anesthetized with pentobarbital (1%, 40 mg/kg). An approximately 2.0 cm midline incision was made, and the paraspinal muscles over the area of the vertebral T8–10 level were bluntly dissected. A T9 vertebral laminectomy was subsequently performed, and a spinal cord impactor was used to injure the rats using a 10 g rod falling freely from a height of 10 cm. In the sham rats, the spinal cord was only exposed without causing SCI. The injured rats exhibited involuntary hind limb spasms and apnoea and wriggled tails, indicating that the SCI models were successful. The rats were voided twice a day. In addition, the rats in the GSP-treated group were intraperitoneally injected with GSP (40 mg/kg or 67.34 μM/kg) once a day, and GSP was absorbed through the mesenteric vein. The remaining rats received the same volume of saline. All animal care and husbandry procedures were approved by the Animal Ethics Committee of Lanzhou University Second Hospital and were performed in accordance with the National Institutes of Health Guide for the Care and Use of Laboratory Animals guidelines.

2.3. Locomotor Recovery Assessment. The Basso, Beattie, and Bresnahan (BBB) scale was used to evaluate the extent of locomotor recovery experienced by rats following SCI [35], with scores in the range of 0-21. A score below 21 indicates impaired locomotor ability. Footprint analysis was adopted to evaluate motor coordination by immersing the hindlimb and forelimb in red and purple dyes, respectively. The results were obtained as the rats passed through a runway lined with white paper. The aforementioned tests were performed by two trained investigators who were blinded to the treatment regimens.

2.4. Terminal Deoxynucleotidyl Transferase dUTP Nick-End Labelling (TUNEL) Assay. Cellular apoptosis levels were determined using a TUNEL assay kit (Beyotime) according to the manufacturer's instructions. The cells were processed as previously described. The number of TUNEL-positive apoptotic cells was determined by calculating the mean of three randomly selected fields.
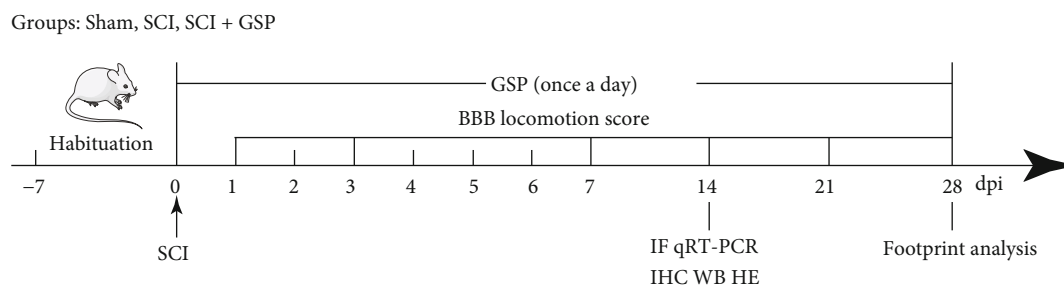
Groups: Sham, SCI, SCI + GSP

Figure 2: Timeline of the experimental protocol.

Table 1: Primer sequences for qRT-PCR.

Gene	Forward primer sequence	Reverse primer sequence
COX-2	TCATAAGCGAGGACCTGG	GGTGGCATACATCATCAGAC
iNOS	CACCGAGATTGGAGTTCG	GGAGCACAGCCACATTG
TNF-α	TGGAACTGGCAGAAGAGG	GAACTGATGAGAGGGAGGC
Arg-1	TGGCAGAGGTCCAGAAGTG	GGAGTGTTGATGTCAGTGTGAGC
IL-10	TGCTATGCTGCCTGCTC	TGGCTGAACCAAGGAGACG
TGF-β	TGGCTGAACCAAGGAGAC	CTCTGTGGAGCGTTGATTTCC
GAPDH	TGTGTCCGTCGTGGATCTGA	TGGCTGTTGAAGTAGCAGGAG

2.5. Annexin V-FITC/PI Assays. The cells were treated and centrifuged at $300 \times g$ for 5 min and subsequently washed three times with precooled phosphate-buffered saline (PBS). Following which the cells were centrifuged at $300 \times g$ at 4°C for 5 min after each wash. PBS was discarded, and the cells were resuspended in $100 \mu L$ of binding buffer. Next, Annexin V-FITC ($5 \mu L$) and PI ($10 \mu L$) solutions were sequentially added, and cells were stained at room temperature in the dark for 15 min. The cells were detected using flow cytometry.

2.6. Cell Viability and Morphological Analysis. BV2 cells were treated with 3.125, 6.25, 12.5, 25, 50, 100, and $200 \mu M$ GSP for 24 h. Another batch of cells was treated with LPS (100 ng/mL) for 24 h, followed by treatment with different concentrations of GSP for 24 h. CCK-8 solution ($10 \mu L$) was added to each well and maintained for 90 min. Finally, absorbance at 450 nm was measured using a microplate reader (Bio-Rad, Hercules, CA, USA). For morphological analysis, the cells were photographed using an EVOS XL Core Cell Imaging System (Semefeld, Waltham, MA, USA) at a magnification of ×100.

2.7. BV2 Cell Culture and Treatment. BV2 cells were cultured in MEM containing 10% FBS (Gibco) and 1% penicillin/streptomycin in a humidified 5% CO_2 atmosphere. They were passaged with 0.25% trypsin at approximately 80% confluence. BV2 cells were pretreated with 100 ng/mL of LPS for 24 h, followed by treatment with different concentrations of GSP (3.125, 6.25, and 12.5 μM) for 24 h. To explore the underlying mechanism of GSP, the TLR4-specific inhib-

itor TAK242 (1 μM, 60 min) was added to the BV2 cells before adding GSP.

2.8. Microglia/Neuron Coculture. A Transwell coculture system (0.4 μm pores; Corning, USA) incubated in a 24-well plate was employed in this study. PC12 cells were cultured in DMEM. BV2 cells were pretreated with 100 ng/mL LPS for 24 h, followed by treatment with 12.5 μM GSP for 24 h. BV2 cells were then seeded into inserts, placed on the PC12 monolayer at the bottom of the well, and cultured for 24 h.

2.9. Western Blotting (WB). Spinal cord tissues or cultured cells were lysed in RIPA buffer supplemented with phosphatase inhibitors and protease. The lysates were centrifuged at 12,000 rpm (4°C, 30 min), and the supernatants were collected. Protein concentrations were determined using a bicinchoninic acid kit. Proteins were separated by 10% or 12% sodium dodecyl polyacrylamide gel electrophoresis and transferred onto PVDF membranes. After blocking with 5% nonfat milk, the membranes were incubated overnight at 4°C with the following primary antibodies: iNOS (anti-rabbit, 1 : 1250), Arg1 (anti-rabbit, 1 : 1000), TNF-α (anti-rabbit, 1 : 1000), IL-10 (anti-rabbit, 1 : 1000), cleaved caspase-3 (anti-rabbit, 1 : 1000), Bax (anti-mouse, 1 : 1000), Bcl-2 (anti-mouse, 1 : 2000), and β-actin (anti-mouse, 1 : 1000) from Proteintech; CD86 (anti-mouse, 1 : 1000) and CD206 (anti-mouse, 1 : 1000) from Santa Cruz Biotechnology; and p-NF-κ B-p65 (anti-rabbit, 1 : 1000), NF-κB-p65 (anti-rabbit, 1 : 1000), IκBα (anti-rabbit, 1 : 1000), p-IκBα (anti-rabbit, 1 : 1000), PI3K (anti-rabbit, 1 : 1000), p-PI3K (anti-rabbit, 1 : 1000), AKT (anti-rabbit, 1 : 1000), and p-AKT (anti-
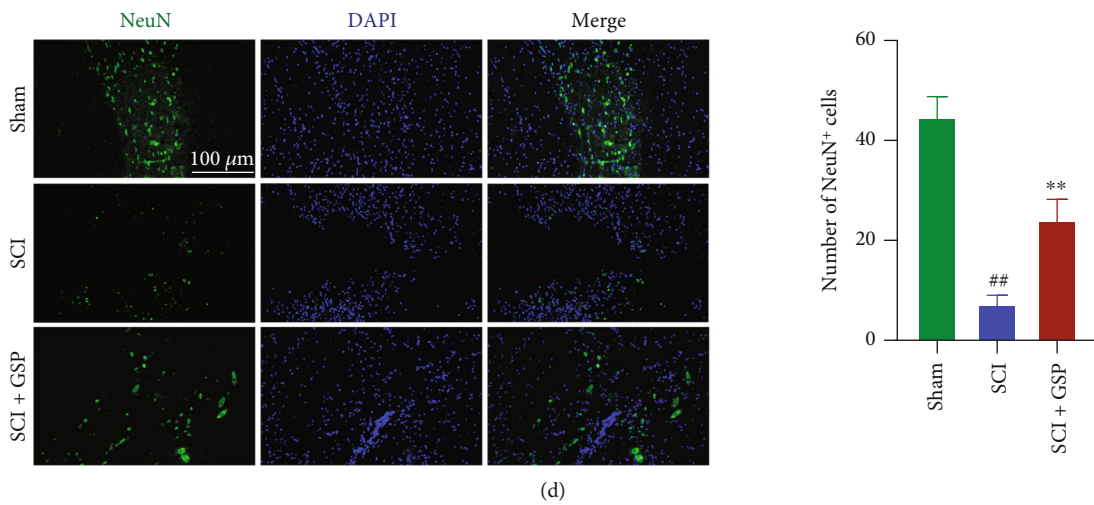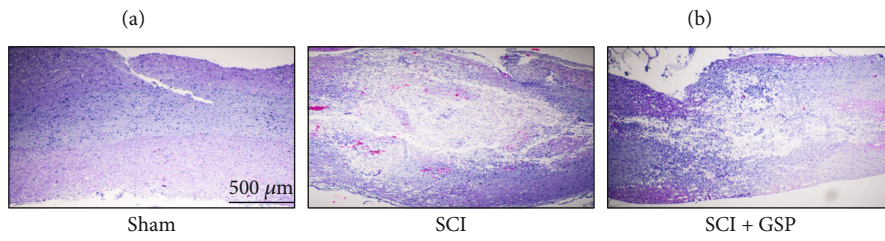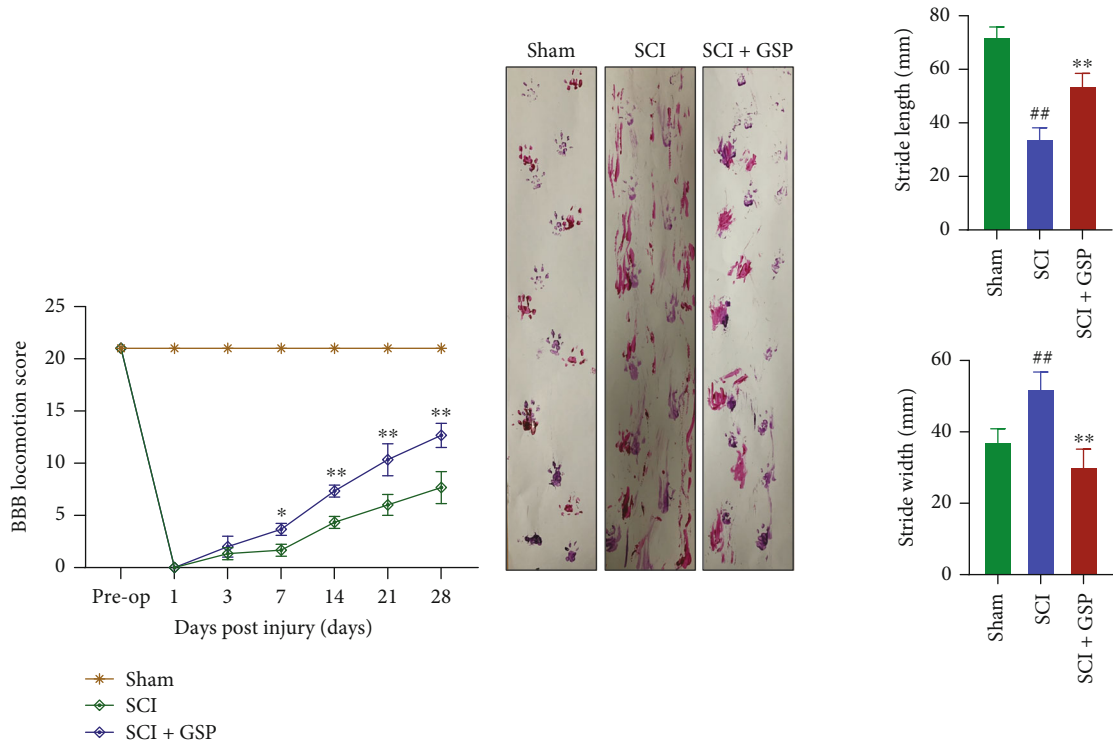
(a)

(b)

(c)

(d)

FIGURE 3: Continued.

(e)

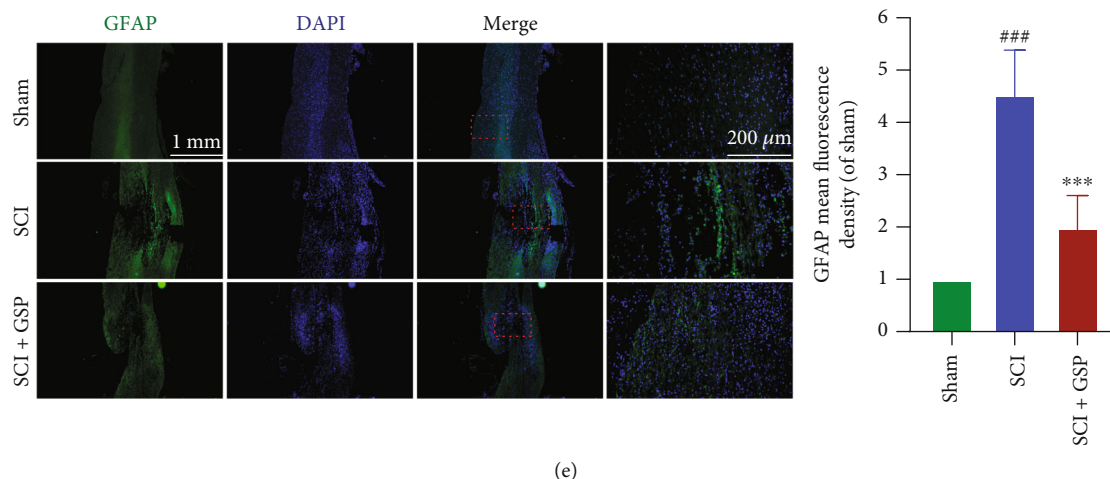FIGURE 3: Effect of GSP on locomotor function recovery in SCI rats. (a) BBB score in the three groups at 28 dpi ($n = 6$/group). (b) Footprints and their quantification analysis in each rat at 28 dpi. Purple: frontpaw; Red: hindpaw ($n = 5$/group). (c) Representative HE staining images. ($n = 3$/group). (d) IF and quantitative data for NeuN (green) at 14 dpi ($n = 3$/group). (e) IF and quantitative data for GFAP (green) at 14 dpi. ($n = 3$/group). $^{##}p < 0.01$, $^{###}p < 0.001$ vs. sham group, $^{**}p < 0.01$, $^{***}p < 0.001$ vs. SCI group.

rabbit, 1 : 1000) from Cell Signalling Technology. The membranes were incubated with goat anti-rabbit/mouse antibody (1 : 4000; Proteintech) and labeled with horseradish peroxidase for 1.5 h the next day. The protein signals were detected using an imaging system.

2.10. NO Assay. The ability of microglia to produce NO was evaluated by measuring the release of nitrite from the culture supernatant. BV2 cells were pretreated with 100 ng/mL LPS for 24 h, followed by treatment with different concentrations of GSP for 24 h. A NO assay kit (Beyotime) was used to detect NO production according to the manufacturer's instructions.

2.11. Immunofluorescence Staining (IF). Spinal cord tissues were removed, embedded in paraffin, and cut into longitudinal 4 μm-thick sections. After being blocked with 10% goat serum, the tissue sections were incubated overnight at 4°C with the following primary antibodies: anti-NeuN (1 : 200), anti-GFAP (1 : 300), anti-Iba1 (1 : 300), anti-CD86 (1 : 200), and anti-CD206 (1 : 200). For cell IF, the cells were placed on slides, fixed in 4% paraformaldehyde, and infiltrated with 0.5% Triton X-100. The cells were blocked with 10% goat serum and then incubated with anti-iNOS (1 : 250), anti-CD206 (1 : 250), anti-p-NF-κB-p65 (1 : 300), and p-AKT (1 : 300) primary antibodies overnight at 4°C. The next day, the tissue sections or cells on the slides were treated with the secondary antibodies for 2 h, stained with DAPI, and photographed under a fluorescence microscope.

2.12. Quantitative Real-Time Polymerase Chain Reaction (qRT-PCR). RNA was extracted from spinal cord tissue using TRIzol Reagent (Qiagen, CA, USA). A reverse transcription kit (Takara, China) was used to synthesize complementary DNA (cDNA) following a standard protocol with the LC96 System (Roche, Pleasanton, CA, USA) and quantified with SYBR Green (Takara). The relative expression

levels of the different genes were normalized to GAPDH using the $2^{-\Delta\Delta Ct}$ approach. Each experiment was performed in triplicate. The sequences of the primers are listed in Table 1.

2.13. Hematoxylin and Eosin (HE) Staining. The processed tissue sections were stained with hematoxylin for 70 s, differentiated in 1% hydrochloric acid, and stained with eosin for 100 s. Images were obtained under a light microscope.

2.14. Immunohistochemistry (IHC). After dewaxing, the paraffin tissue sections were subjected to antigen retrieval with sodium citrate buffer, blocked with 10% serum, and incubated with anti-cleaved caspase-3 antibody (1 : 100) overnight at 4°C. The following day, sections were rinsed with PBS three times, followed by treatment with secondary antibody for 1.5 h at 37°C. Diaminobenzidine and hematoxylin were used to visualize the antibody staining. Images were obtained using a light microscope.

2.15. Statistical Analysis. All experiments in this study were repeated at least three times. All data are presented as mean ± standard deviation and were analyzed using SPSS software (version 22.0; IBM, Armonk, NY, USA). When comparing two groups, the unmatched Student's t-test was used. One-way analysis of variance (ANOVA) and Tukey's multiple comparisons test were used for more than two groups.

3. Results

3.1. Effect of GSP on the Recovery of Locomotion in SCI Rats. To determine whether GSP can exert positive effects on functional recovery, rats were subjected to BBB score and footprint analysis. We found that hindlimb function in rats was lost immediately following SCI and gradually recovered over time (Figure 3(a)). At 28 days postinjury (dpi), the BBB scores of the SCI and GSP-treated groups were 8 and 13,
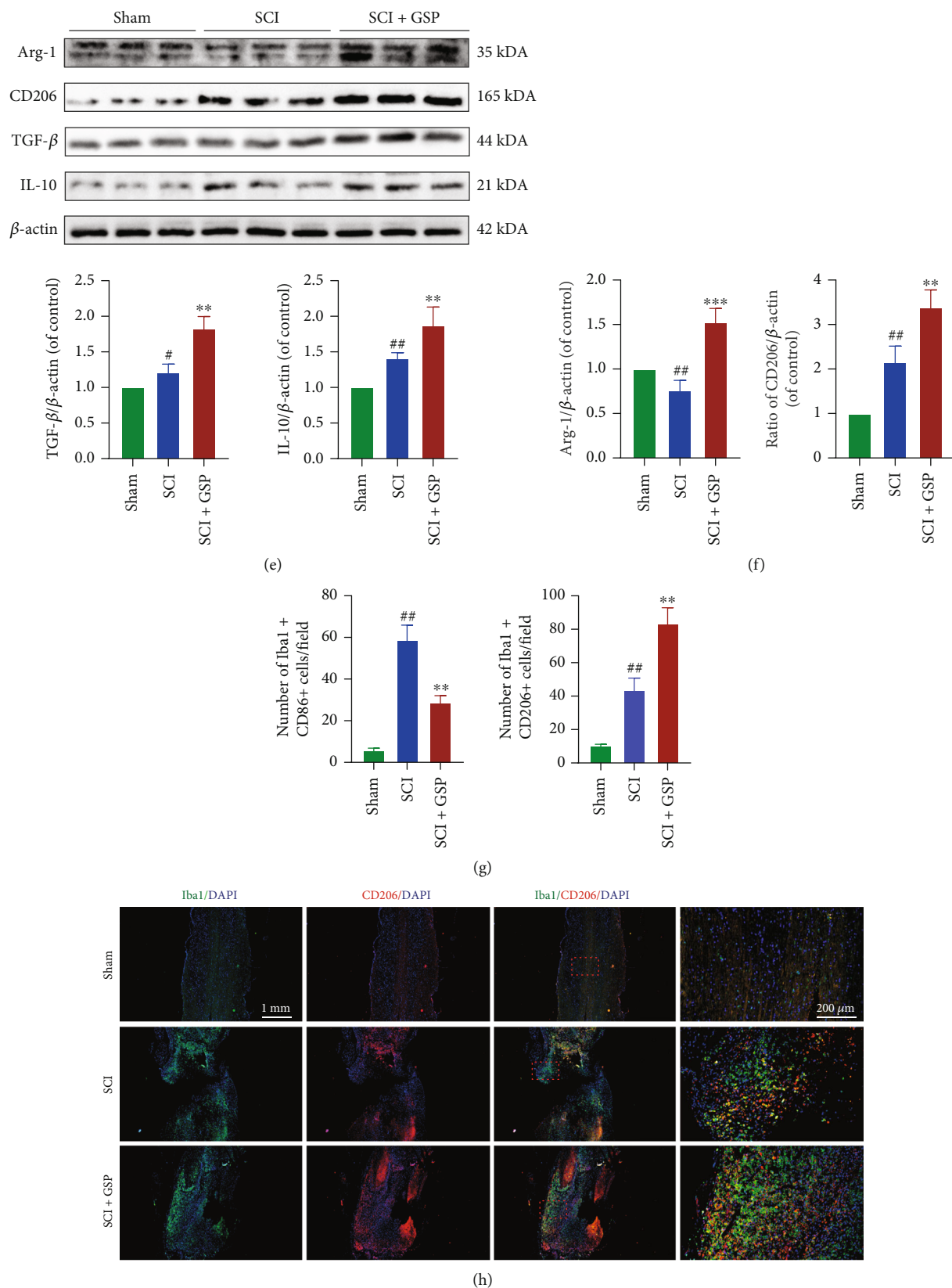
(a)

(b)
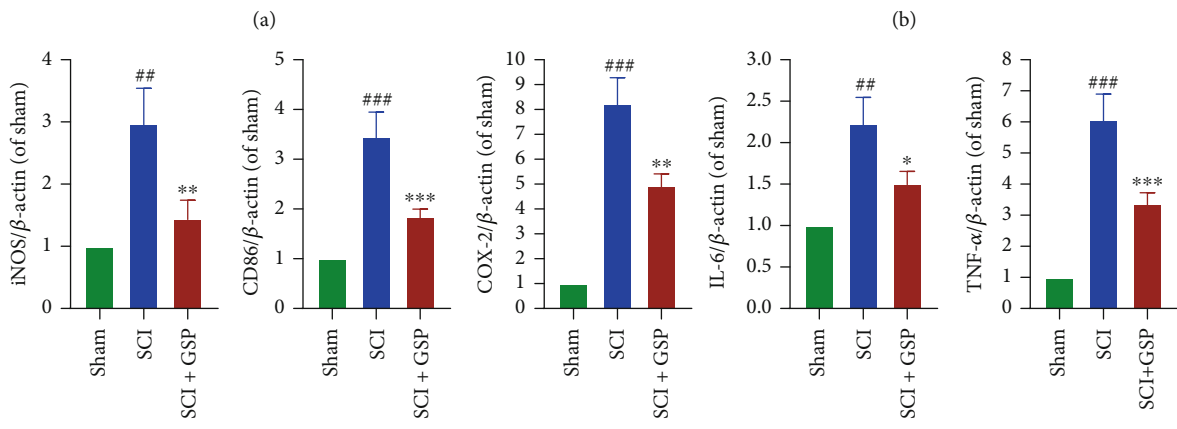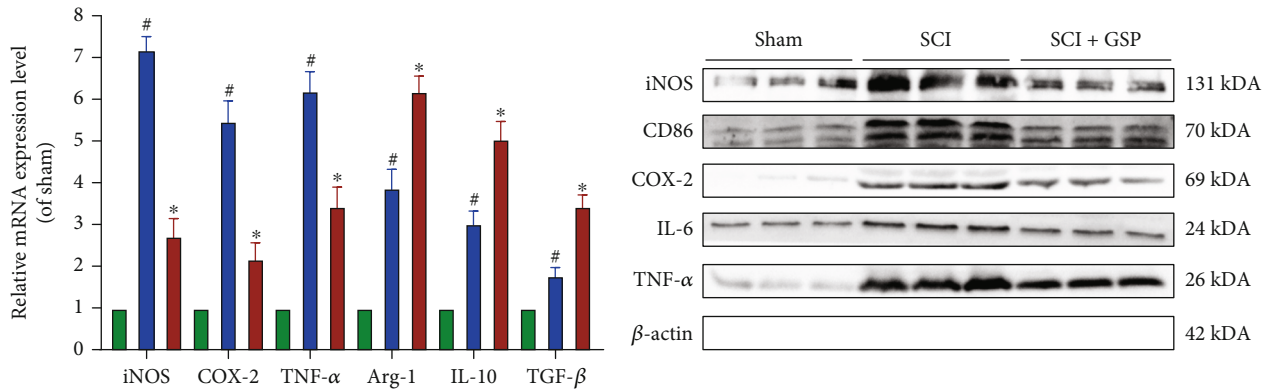
(c)
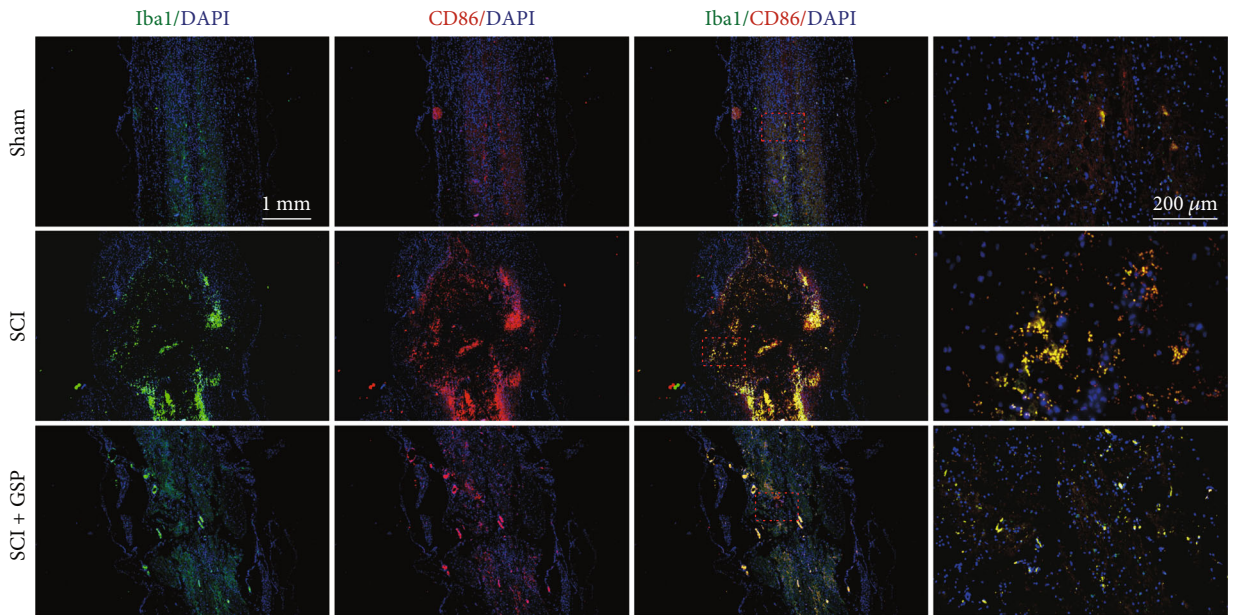
(d)

Figure 4: Continued.

FIGURE 4: Effect of GSP on microglial polarisation *in vivo*. (a) The M1/M2-related mRNA expressions were measured by qRT-PCR ($n = 3$/group). (b, c, e, f) Representative WB and quantitative data of M1/M2-related protein levels in each group. ($n = 3$/group). (d, g, h) Representative IF and quantitative data of CD86/CD206 at 14 dpi and ($n = 3$/group). [#]$p < 0.05$, [##]$p < 0.01$ vs. sham group. [*]$p < 0.05$, [**]$p < 0.01$, or [***]$p < 0.001$ vs. SCI group.
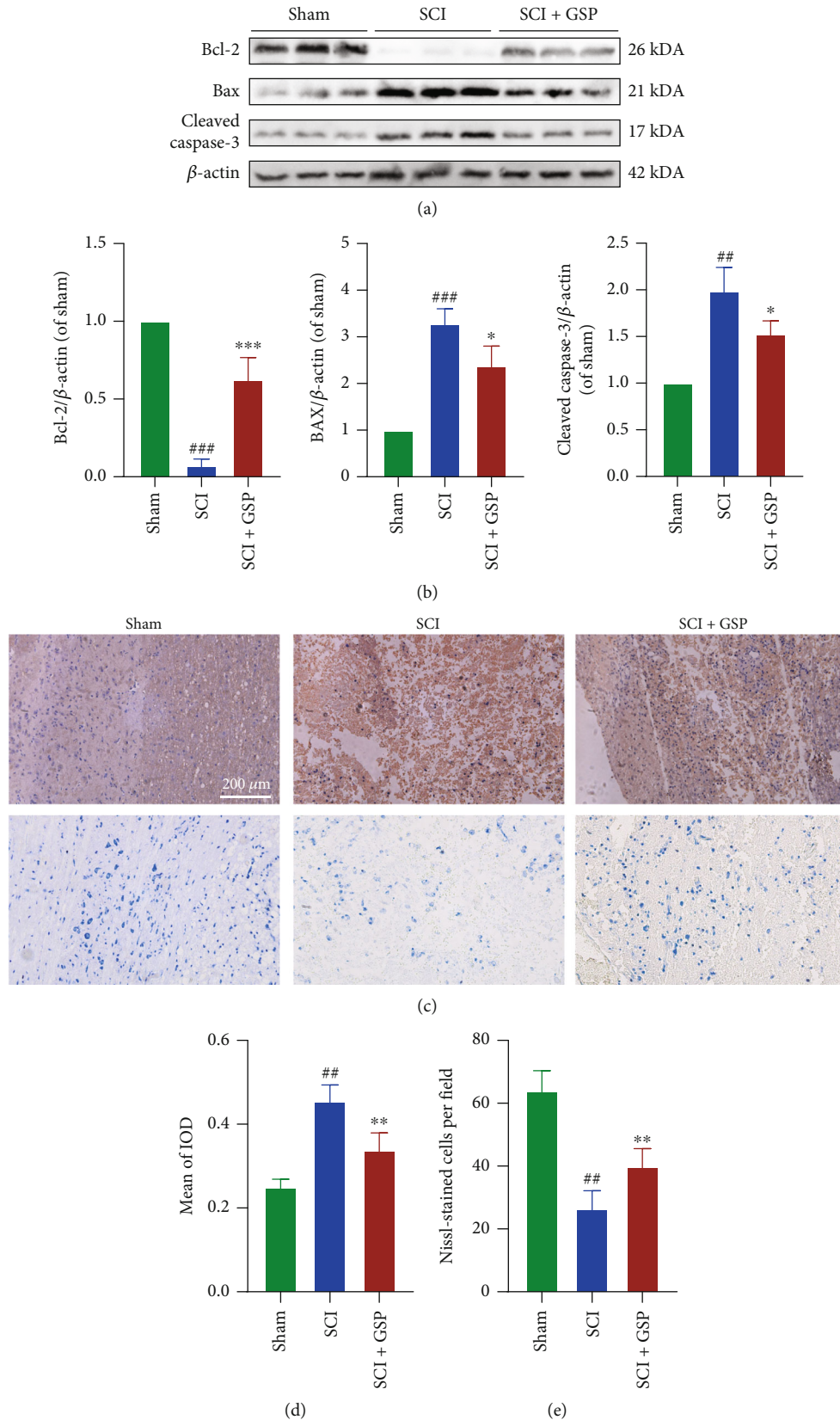
Figure 5: GSP inhibit apoptosis *in vivo*. (a, b) Representative WB and quantitative data of Bax, Bcl-2, and cleaved caspase-3 in the different groups at 14 dpi ($n = 3$ rats in each group). (c, d) Representative IHC staining and Nissl staining in the different groups at 14 dpi. (d) Quantitative data of cleaved caspase-3. ($n = 3$, with 5 images for each rat). (e) Quantitative data of the number of Nissl-stained cells at 14 days after SCI ($n = 3$ rats in each group). $^{##}p < 0.01$ or $^{###}p < 0.001$ vs. sham group. $^{*}p < 0.05$, $^{**}p < 0.01$, or $^{***}p < 0.001$ vs. SCI group.
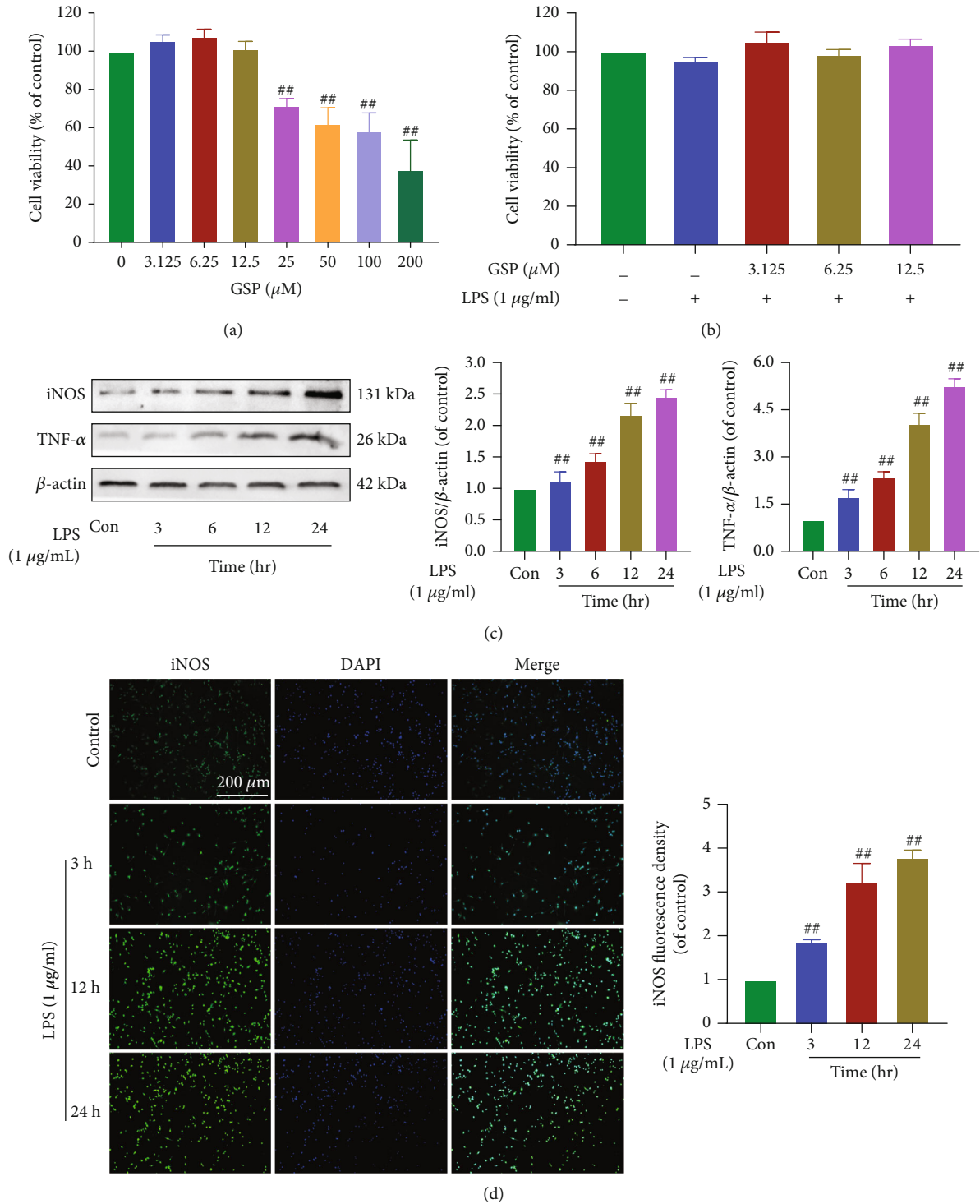
(a)

(b)

(c)

(d)

FIGURE 6: Effect of GSP on the viability and effect of LPS on microglial polarisation. (a) Effects of on cell viability. (b) Effects of GSP and LPS on cell viability. (c) Representative WB and quantitative data of iNOS and TNF-α in each group. (d) IF and quantitative data of iNOS. ##$p < 0.01$ vs. control group.

respectively. Starting at 7 dpi, the score of the GSP-treated group was remarkably higher than that of the SCI group. Consistent with this, our footprint analysis results (Figure 3(b)) showed that the hindlimb movement of rats in the GSP-treated group was relatively coordinated, whereas the SCI rats showed obvious hindlimb dragging.

These data indicate that GSP can improve locomotor function in SCI rats.

3.2. Effect of GSP on Neural Function In Vivo. Histological and morphological changes in rats were evaluated by HE and IF staining. We found that the spinal cords in the SCI
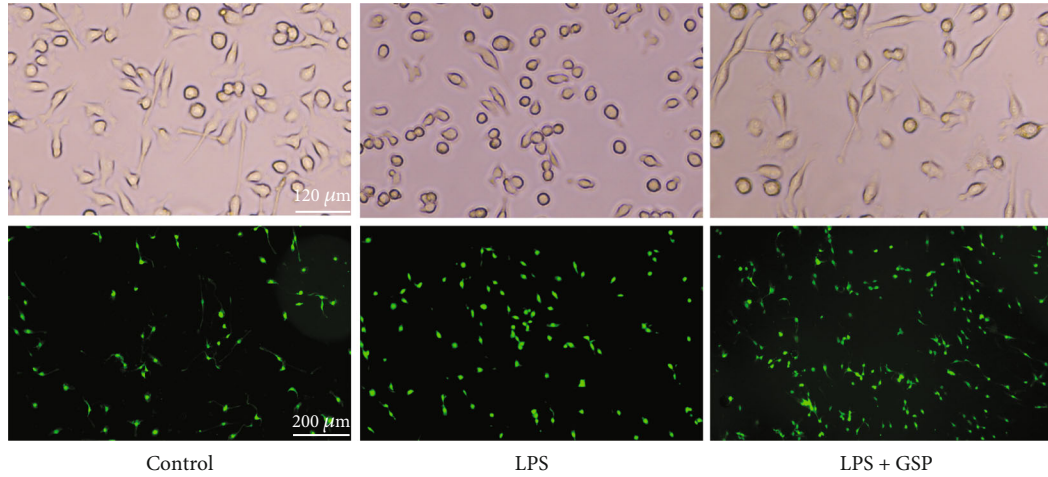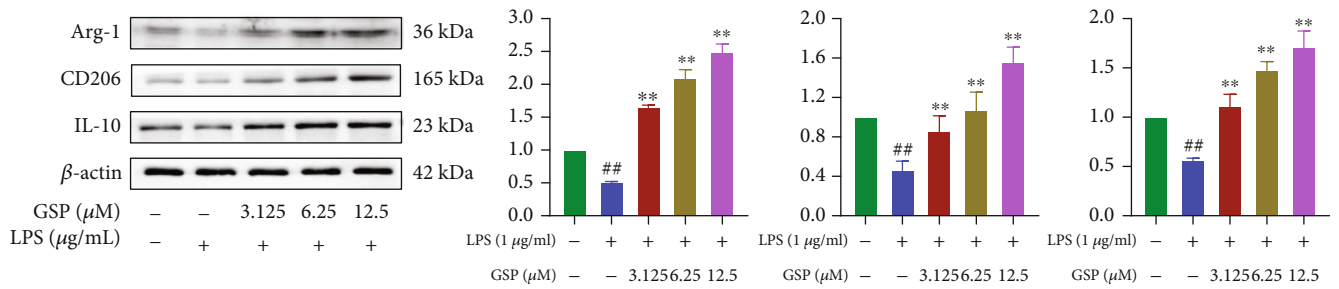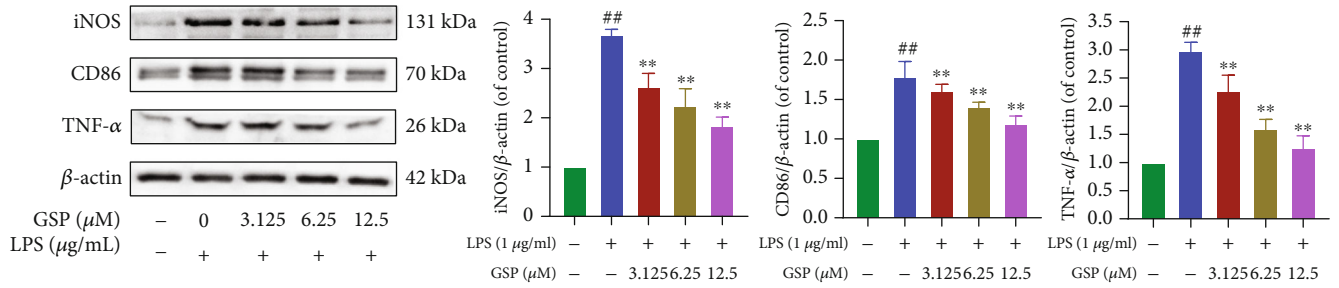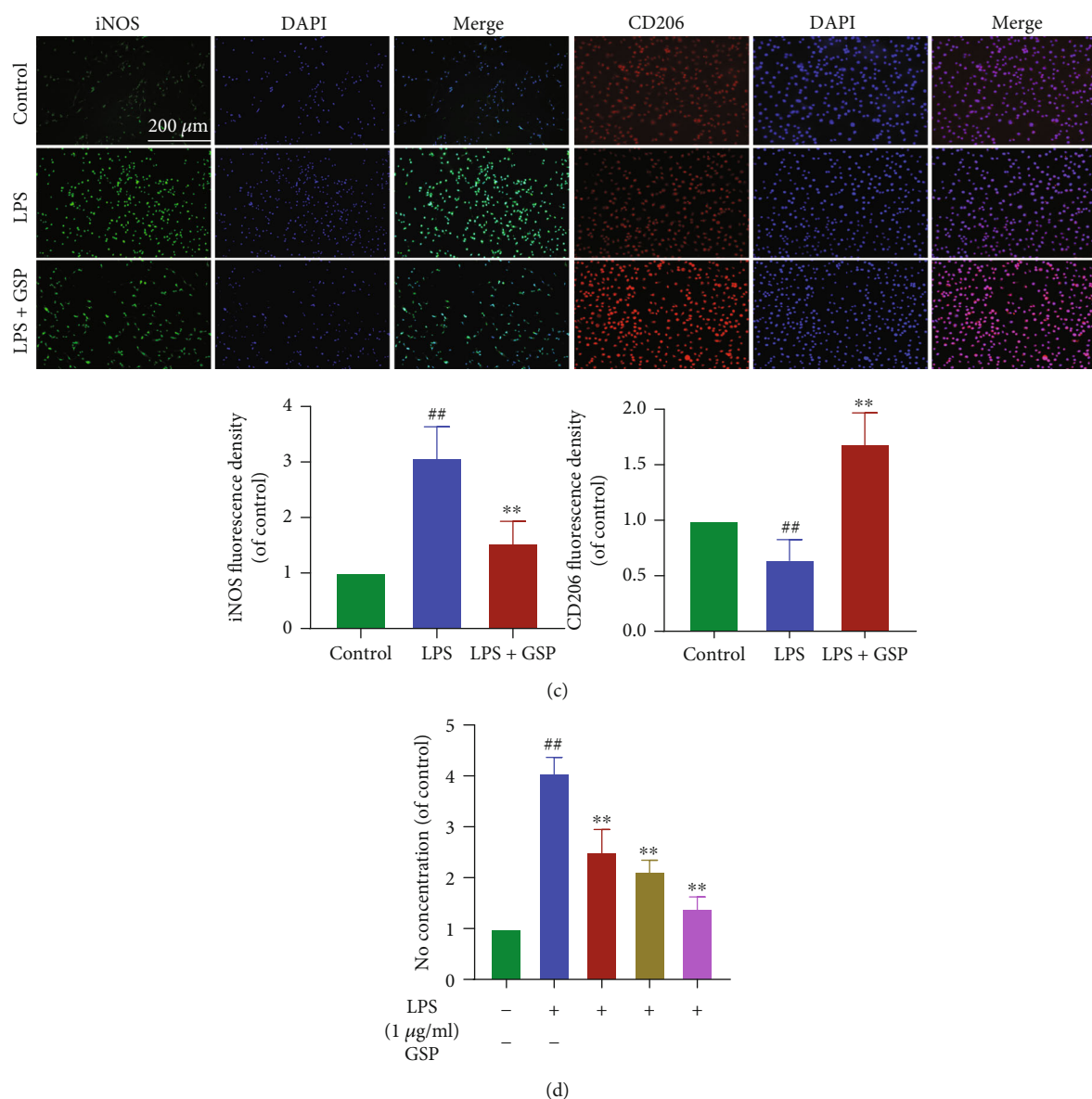
(a)

(b)

FIGURE 7: Continued.

(c)

(d)

Figure 7: Effect of GSP on microglial polarisation *in vitro*. (a) Morphological results and IF for Iba1 in each group. Scale bar = 200 μm. (b) Representative WB and quantitative data of M1/M2-related proteins. (c) IF and quantitative data of iNOS and CD206 in each group. (d) NO concentration of each group. $^{##}p < 0.01$ vs. control group. $^{**}p < 0.01$ vs. LPS-treated group.

group had large cavities that were significantly narrowed by GSP (Figure 3(c)). Next, we stained the cells for NeuN (a neuronal marker) to investigate the effects of GSP on the neurons. As shown in Figure 3(d), more NeuN-positive cells were observed in the GSP-treated group. GFAP was used to assess astrocyte activation. We observed increased GFAP expression in the SCI group, and this increase was markedly attenuated by GSP (Figure 3(e)). These results suggest that GSP can increase neuronal survival and inhibit astrocyte activation following SCI.

3.3. Effect of GSP on Microglia Polarisation In Vivo. At 14 dpi, qRT-PCR was used to detect the mRNA expression of inflammatory cytokines in the spinal cord tissues. GSP significantly decreased the expression of proinflammatory cytokines (TNF-α, iNOS, and COX-2) and elevated the expression of anti-inflammatory cytokines (Arg-1, TGF-β, and IL-10) (Figure 4(a)). Next, we investigated whether GSP could regulate microglial polarisation following SCI as microglia have two different phenotypes. The expressions of iNOS, CD86, TNF-α, IL-6, COX-2, Arg1, TGF-β, CD206, and IL-10 were analyzed by WB (Figures 4(b), 4(c), 4(e), and 4(f)). The GSP-treated group showed lower M1-related protein expression and higher M2-related protein expression than the SCI group. We used CD86, CD206, and Iba1 (a specific marker of microglia) for IF to evaluate microglial polarisation in each group (Figures 4(d) and 4(h)). As shown in Figure 4(g), the GSP-treated group tended to have more CD206-positive and fewer CD86-positive microglia than the SCI group at 14 dpi. These results
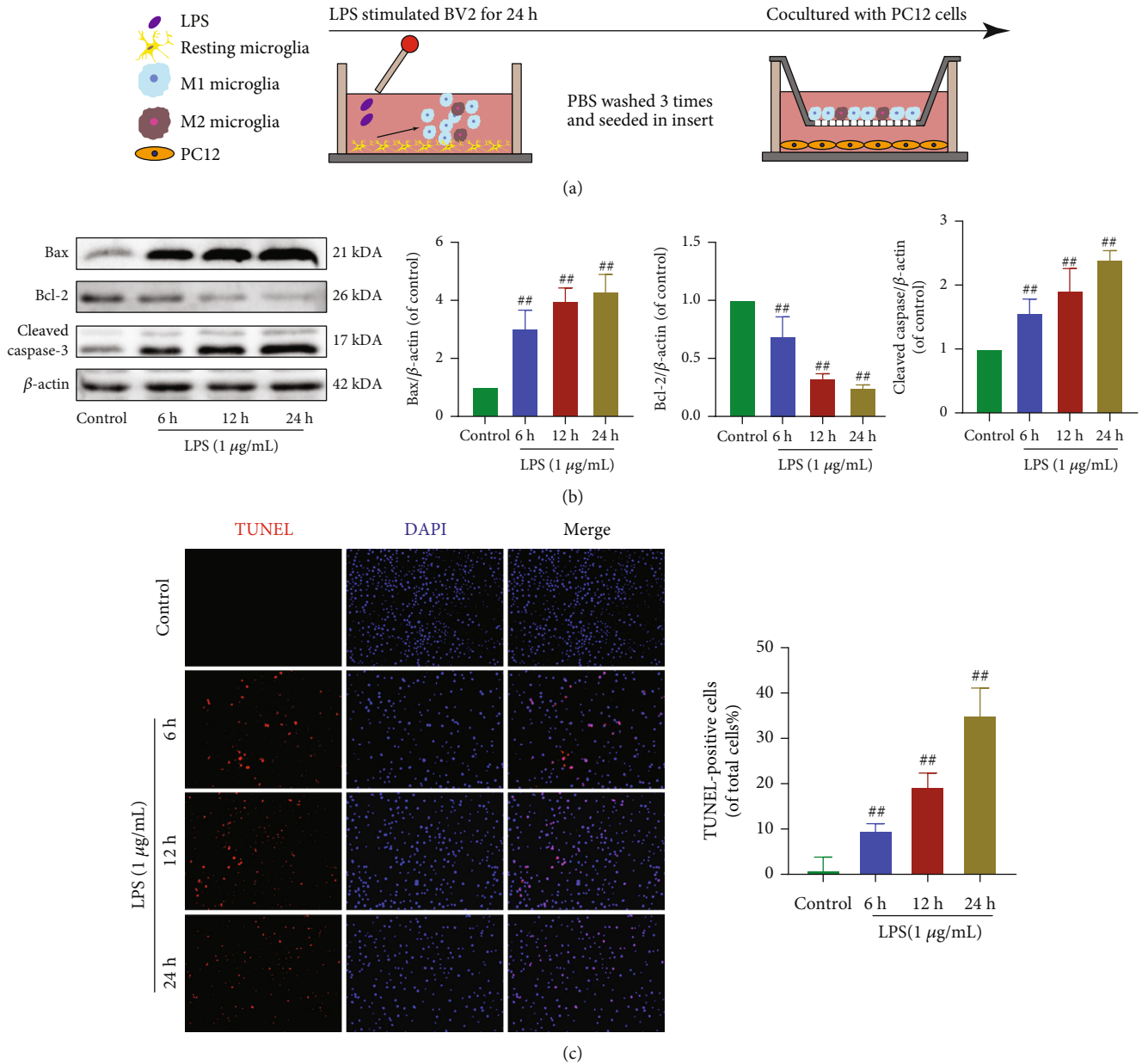
(a)

(b)

(c)

FIGURE 8: Effect of M1 microglia on neuronal apoptosis. (a) Schematic of cell treatments. (b) Representative WB and quantitative data of apoptosis-related proteins. (c) Apoptosis of PC12 was detected by TUNEL (scale bar: 200 μm). $^{\#\#}p < 0.01$ vs. control group.

suggest that GSP has a significant anti-inflammatory effect and can polarise M1 to M2 microglia in rats following SCI.

3.4. GSP Suppressed Neuronal Apoptosis In Vivo. The relationship between neuronal apoptosis and local inflammation has been previously reported [36]. Sustained microglial activation can cause neurological impairments by inducing neuronal apoptosis [37]. To determine the apoptosis of neurons and whether GSP prevents neuronal apoptosis in rats with SCI, we assayed the levels of apoptosis-related proteins. The WB results (Figures 5(a) and 5(b)) suggested that the expression of antiapoptotic Bcl-2 was downregulated, but proapoptotic Bax and cleaved caspase-3 were upregulated in the SCI versus sham group, all of which could be reversed

by GSP treatment. The results of IHC for cleaved caspase-3 (Figures 5(c) and 5(d)) were consistent with those of WB, suggesting that GSP could prevent neuronal apoptosis after SCI in rats.

3.5. Effect of GSP on BV2 Cell Viability. To determine whether GSP has a similar therapeutic effect in vitro as observed in vivo, LPS was added to induce an inflammatory microenvironment and simulate SCI in vitro. The CCK-8 assay was used to determine whether GSP affected the viability of BV2 cells. The results (Figure 6(a)) showed that GSP at concentrations lower than 25 μM caused no detectable cytotoxicity in BV2 cells. Therefore, we employed GSP concentrations of 3.125–12.5 μM in subsequent experiments. BV2

(a)

(b)

FIGURE 9: Continued.

(c)
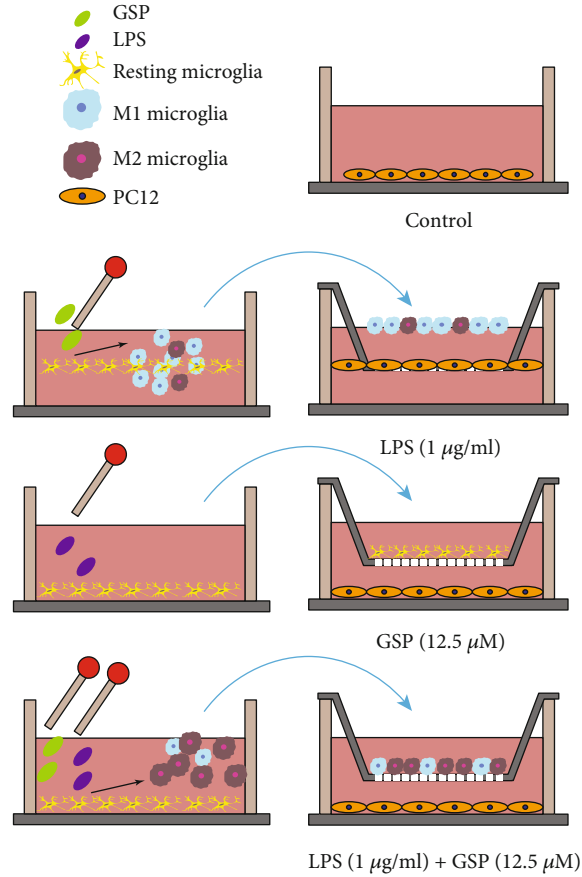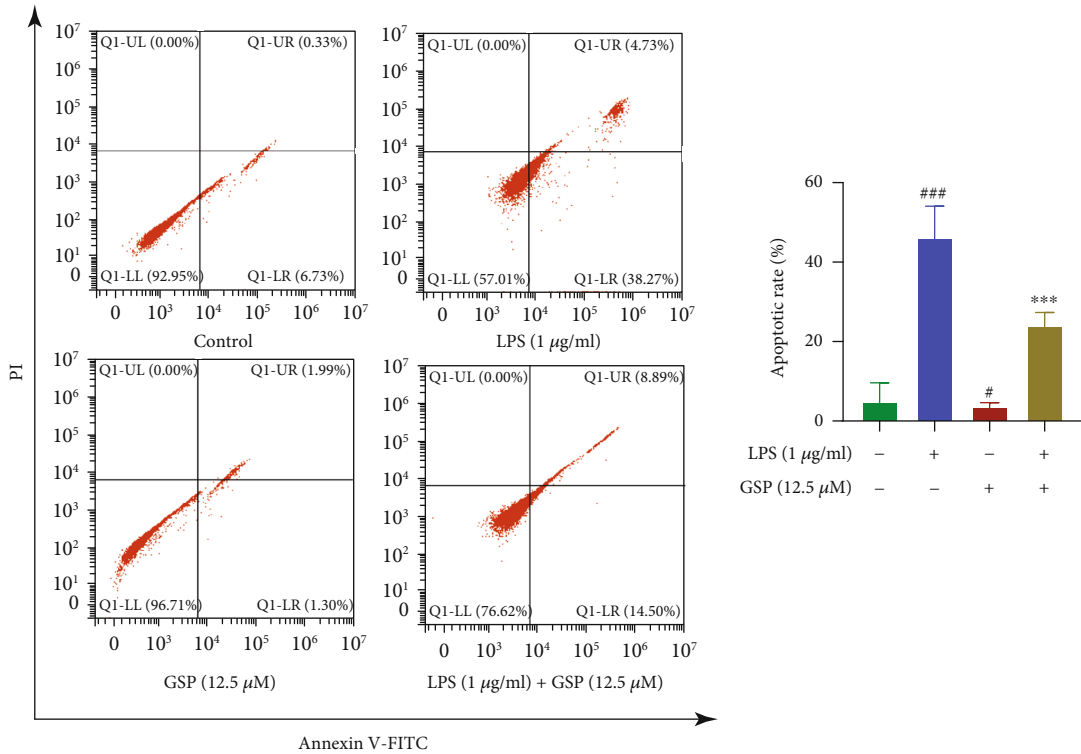
FIGURE 9: The antiapoptotic effect of GSP. (a) BV-2 cell treatments and the coculture system. (b) Apoptosis rates were measured by flow cytometry. (c) Representative WB and quantitative data of apoptosis-related proteins 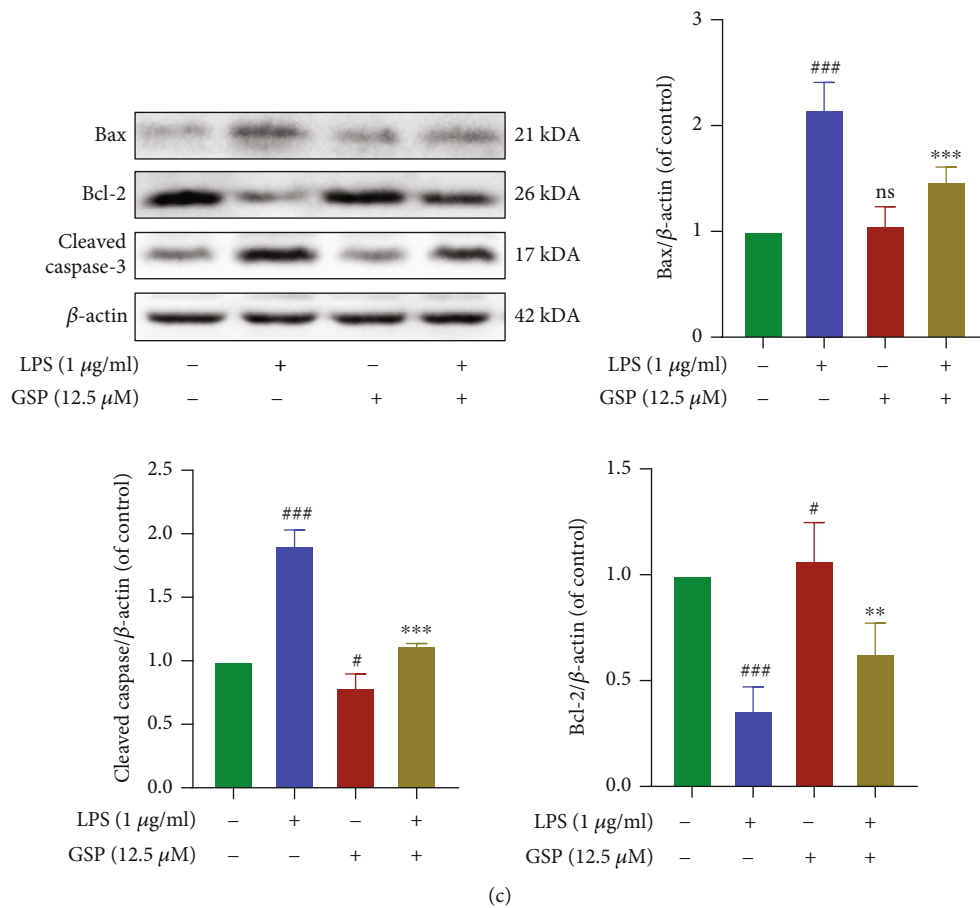in each group. $^{\#}p < 0.05$ or $^{\#\#\#}p < 0.001$ vs. control group. $^{**}p < 0.01$ or $^{***}p < 0.001$ vs. LPS-treated group.

cells were sequentially treated with LPS (100 ng/mL, 24 h) and various concentrations of GSP (3.125, 6.25, 12.5, and 24 h). The results (Figure 6(b)) indicated that after being treated with 3.125, 6.25, and 12.5 μM GSP and 100 ng/mL LPS, the viability of BV2 cells showed no significant difference.

3.6. Effects of LPS on Microglial Polarisation and Release of Proinflammatory Mediators.
Several previous studies have demonstrated that LPS (100 ng/mL) can induce neuroinflammation and polarise microglia to the M1 phenotype [38, 39]. Therefore, in the follow-up experiment, we chose to use LPS at 100 ng/mL. Our results (Figures 6(c) and 6(d)) suggest that the expression levels of TNF-α and iNOS increased in a time-dependent manner after LPS stimulation. Moreover, the iNOS expression detected by IF was consistent with that observed using WB (Figure 6(e)). Since 100 ng/mL LPS was sufficient to induce M1 polarisation of microglia, we used 100 ng/mL LPS to treat BV2 cells in subsequent experiments.

3.7. Effect of GSP on Microglia Polarisation In Vitro.
Morphological changes and IF for Iba1 were used to evaluate

the effects of GSP (12.5 μM) on LPS-induced microglia. We found that resting BV2 cells had small cell bodies and long processes, showed a spindle shape, and acquired an amoeba-like morphology with short and thick cell bodies after LPS treatment. Nonetheless, these changes could be reversed by GSP (Figure 7(a)). To further investigate whether GSP (12.5 μM) had the same effects in vitro, the expression levels of M1/M2-related markers in each group were measured (Figure 7(b)). GSP treatment reduced the expression of M1 microglial markers, similar to the effect of IF on iNOS (Figure 7(c)) and NO production (Figure 7(d)). GSP significantly upregulated the M2 microglial markers (Figure 7(b)). Similarly, the immunofluorescence intensity of CD206 (Figure 7(c)) was lower following LPS treatment but became stronger after GSP treatment. These in vitro results indicate that GSP can polarise microglia from the M1 to M2 phenotype, confirming the results observed in vivo.

3.8. Effect of GSP on M1 Microglia-Induced Neuronal Apoptosis In Vitro.
To determine the relationship between microglial polarisation and neuronal apoptosis, we cocultured LPS-BV2 and PC12 cells. The cells were then treated as shown in Figure 8(a). The results of TUNEL and WB
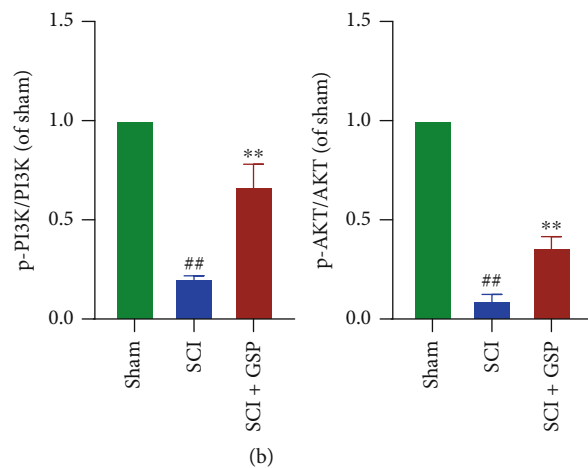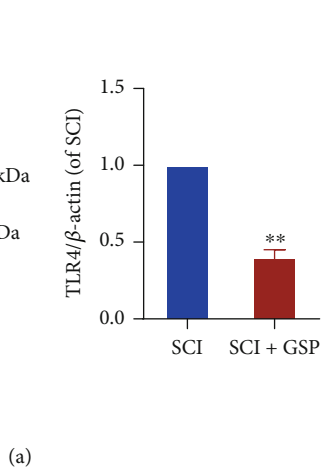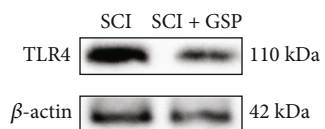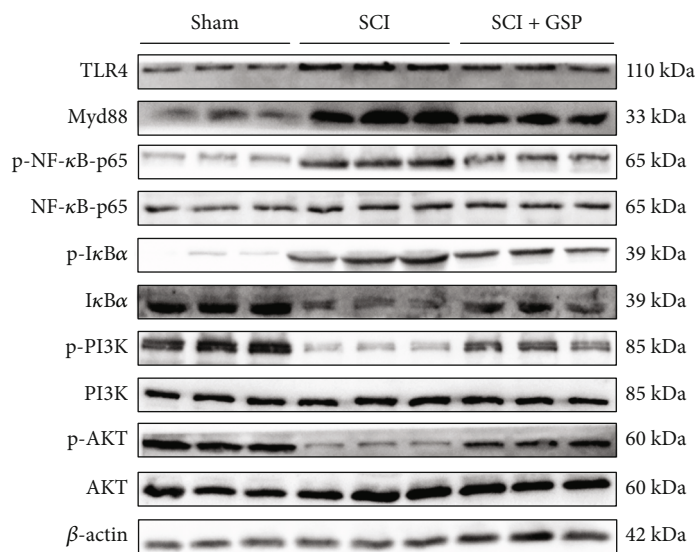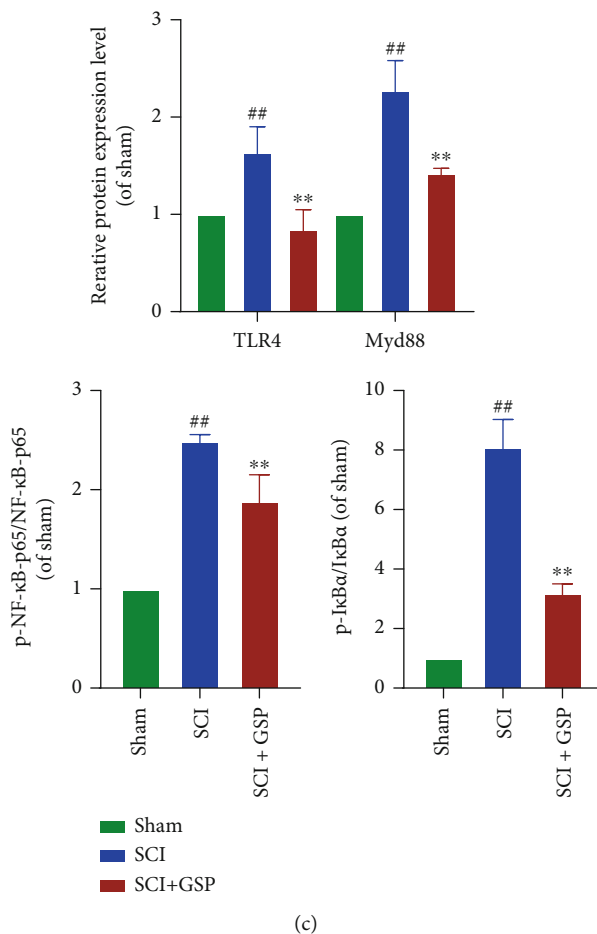
(a)

(b)

FIGURE 10: Continued.

(c)

FIGURE 10: Effect of GSP on TLR4/NF-κB/PI3K/AKT signaling cascades *in vivo*. (a) Representative WB and quantitative analysis of TLR4. (b, c) Representative WB and quantitative analysis of TLR4/MyD88/NF-κB/PI3K/AKT signaling cascades in each group. $^{\#\#}p < 0.01$ vs. sham group. $^{**}p < 0.01$ vs. SCI group.

analyses of apoptosis-related proteins (Figures 8(b) and 8(c)) showed that apoptosis of PC12 cells was induced by M1-BV2 cells.

To evaluate whether GSP affects M1 microglia-induced neuronal apoptosis, we cocultured PC12 cells with differentially treated BV2 cells (Figure 9(a)). The apoptotic rate in monocultured PC12 cells was 7.05%, which decreased to 3.29% when cocultured with GSP-pretreated BV2 cells. When cocultured with LPS-treated BV2 cells, the apoptosis rate of PC12 cells increased significantly to 42.09% and recovered to 23.39% when BV2 cells were pretreated with GSP (Figure 9(b)). Similar trends were observed in WB analysis of apoptosis-related proteins (Figure 9(c)). Taken together, these results indicate that GSP can attenuate apoptosis of neurons induced by M1 microglia.

3.9. GSP Regulates Microglial Polarisation by Targeting TLR4-Mediated Signaling. Both *in vivo* and *in vitro* studies revealed that GSP promotes functional recovery and shifts microglial polarisation from the M1 to M2 phenotype. To elucidate the mechanisms underlying the effects of GSP, we determined the expression of TLR4 after SCI. The WB results suggested that the expression of TLR4 was upregu-

lated in the SCI group but downregulated following GSP treatment. This indicated that GSP could inhibit TLR4. NF-κB and PI3K/AKT are downstream molecules of TLR4. Therefore, we determined the effects of GSP after SCI. In our *in vivo* study, the WB results showed that p-NF-κB-p65 was remarkably inhibited, but p-PI3K and p-AKT (downstream targets of p-PI3K) were activated in the GSP-treated group compared to the SCI group (Figures 10(b) and 10(c)).

In our *in vitro* study, TAK242 was used to explore the potential crosstalk between these two pathways after GSP treatment. First, we evaluated whether TAK242 affected BV2 cell viability and found that when the TAK242 concentration was below 500 nM, there was no obvious cytotoxicity (Figure 11(a)). In our preliminary experiment, TAK242 (100 nM) could not polarise BV2 to the M1 or M2 phenotype (Figure 11(b)). Therefore, in the follow-up experiments, we added TAK242 (100 nM) to BV2 cells for 1 h before GSP treatment and found that LPS significantly upregulated the expression of TLR4, MyD88, and p-NF-p65 and downregulated the expression of p-PI3K and p-AKT. However, both GSP (12.5 μM) and TAK242 reversed this trend, and the effect in the inhibitor group was more obvious

(a)

(b)
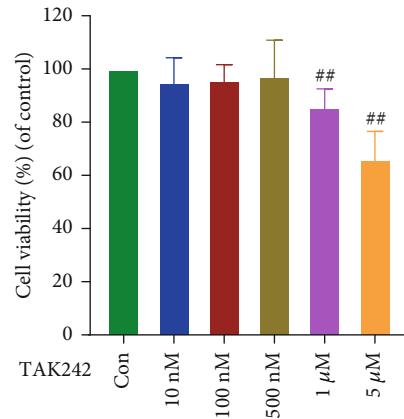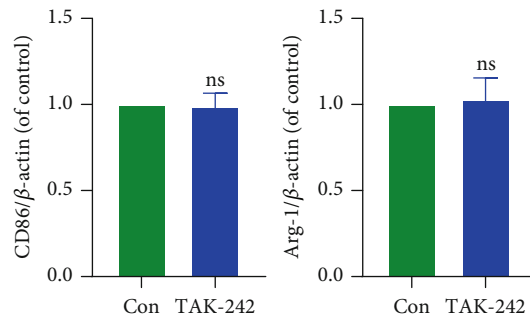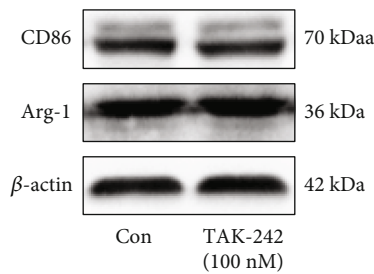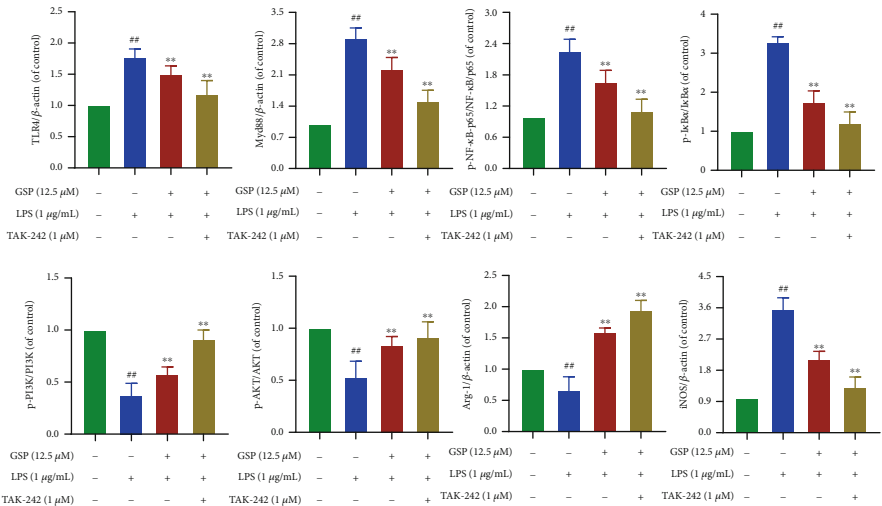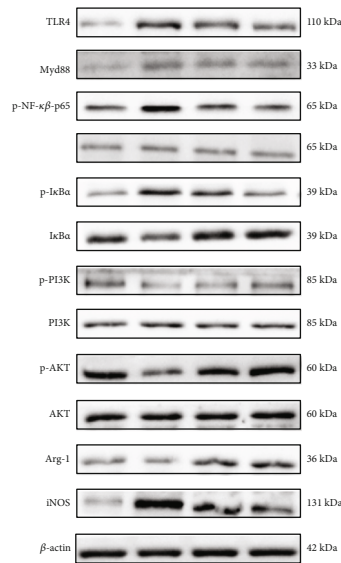
(c)

Figure 11: Continued.

(d)
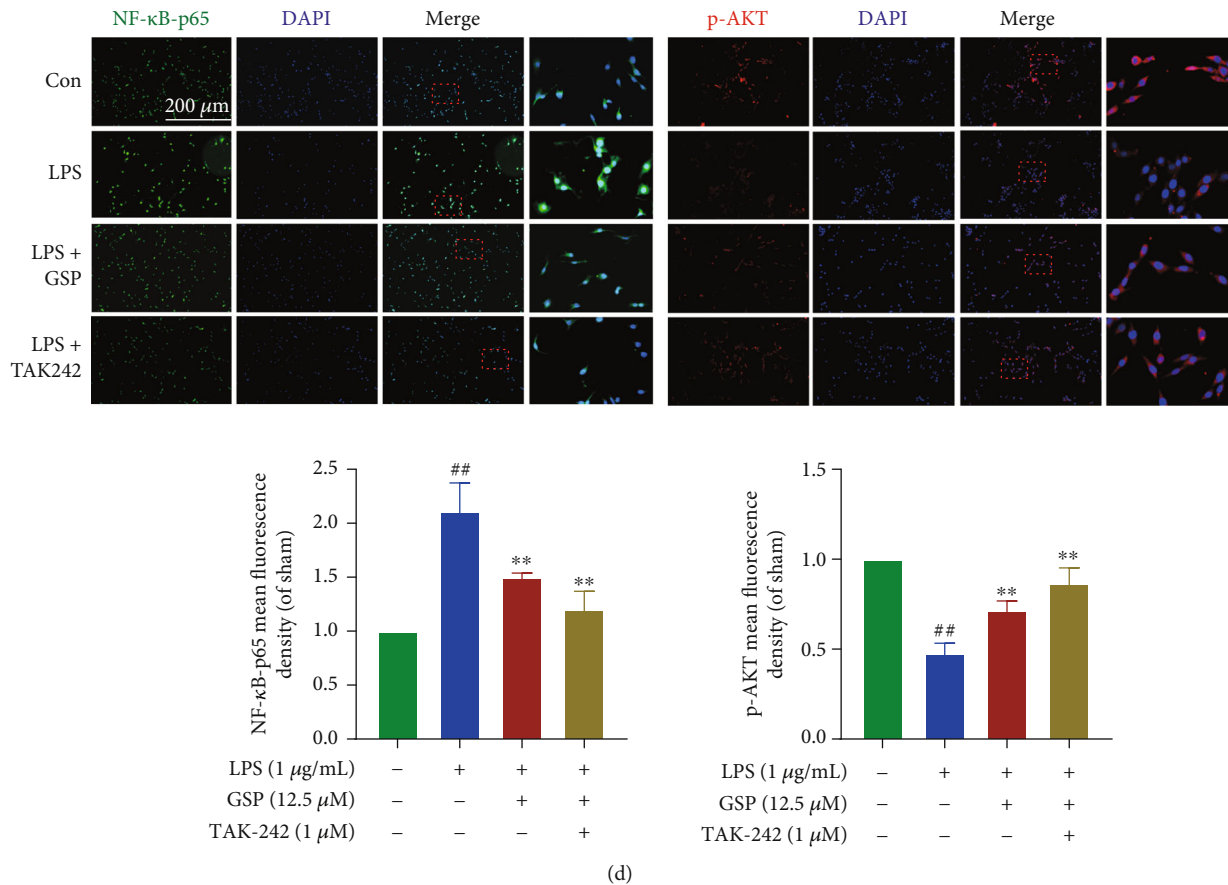
FIGURE 11: Effect of GSP on TLR4/NF-κB/PI3K/AKT signaling cascades *in vitro*. (a) Effects TAK242 on cell viability. (b) Representative WB and quantitative analysis of CD86 and Arg-1. (c) Representative WB and quantitative data of TLR4/MyD88/NF-κB/PI3K/AKT signaling cascades in each group. (d) IF and quantitative data of p-NF-κB-p65 and p-AKT in each group. $^{##}p < 0.01$ vs. control group. $^{**}p < 0.01$ vs. LPS-treated group.

(Figure 11(c)). Moreover, the IF results were consistent with those obtained using WB (Figure 11(d)). Hence, the above data demonstrates that GSP could promote the polarisation of BV2 cells to the M2 phenotype by targeting the TLR4/Myd88/NF-κB/PI3K/AKT signaling cascades, thus playing a neuroprotective role.

4. Discussion

SCI remains a major medical problem worldwide because of its high disability and mortality rates and remains a heavy burden on the patient's family and society. The complexity of the pathological process of SCI has created significant obstacles for the current treatments. Current treatment methods focus on inhibiting neuroinflammation in the secondary injury, thus creating a beneficial microenvironment for neurogenesis and axonal regeneration. Currently, SCI treatment cannot completely restore impaired function. The good news is that most SCI cases involve contusions, traction, or compression injuries rather than physical transection of the spinal cord, and these incomplete SCI can be treated [40].

Proanthocyanidins are pluripotent molecules that can be isolated from many plant species and have been shown to promote health and prevent disease [41–44]. After being metabolized, proanthocyanidins can cross the blood-brain/spinal barrier that prevent most drugs from reaching the CNS [45, 46]. Zhou et al. found that proanthocyanidins could promote functional recovery following SCI by inhibiting ferroptosis [47]. Our previous study demonstrated that proanthocyanidins could inhibit H_2O_2-induced apoptosis in PC12 cells [48]. Nonetheless, to date, no study has evaluated the potential effects of proanthocyanidins on microglial polarisation following SCI. Therefore, this study is aimed at exploring whether GSP has a protective effect against SCI and its potential mechanism. We established a rat model of SCI and hypothesized that GSP has a therapeutic effect. First, we evaluated locomotor function recovery in rats. We found that GSP significantly promoted functional recovery. The number of NeuN-positive cells decreased remarkably after SCI; however, this neuronal loss was reduced after GSP treatment. Activated astrocytes can cause glial scarring and affect axonal regeneration. Our IF results indicated that the GFAP expression was upregulated after SCI, and this phenomenon was markedly attenuated by GSP. Taken
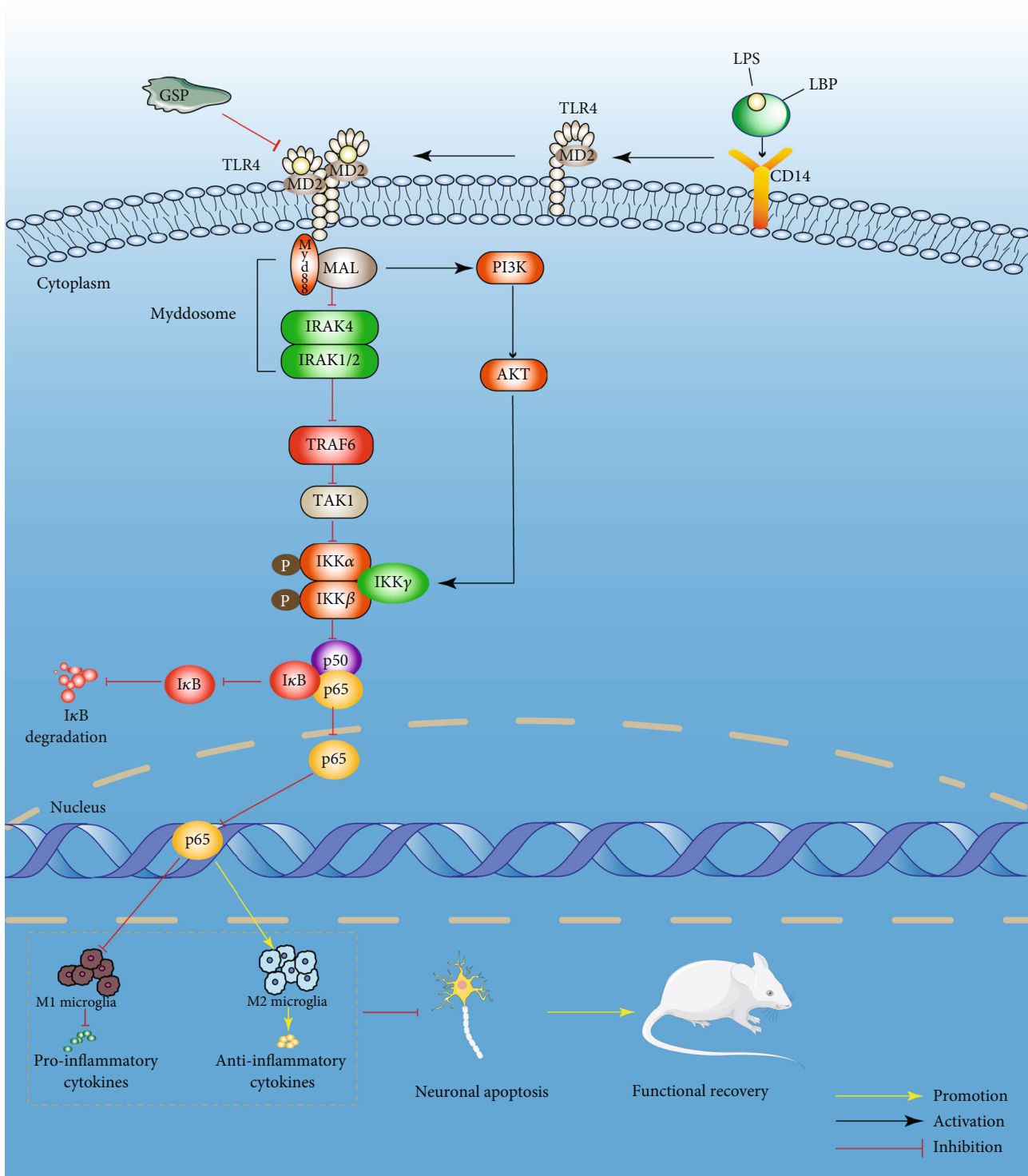
FIGURE 12: Schematic diagram of GSP regulate microglial polarisation through TLR4/NF-κB/PI3K/AKT signaling pathway.

together, the findings of our preliminary *in vivo* studies demonstrated that GSP could eliminate astrocyte activation and promote functional behavioral recovery in rats following SCI.

As a resident cell type of the CNS, microglia are very important for achieving CNS homeostasis and maintaining normal neuronal function under healthy conditions and are key regulators of SCI and repair. Like macrophages, microglia, as a type of highly plastic cell, can differentiate into M1 and M2 phenotypes. The M1 phenotype expresses various proinflammatory factors (TNF-α, NO, and iNOS). The M2 phenotype is characterized by the expression of anti-inflammatory mediators such as IL-10, Arg1, and CD206 [49–51]. Microglia can create a microenvironment

conducive to SCI recovery by modulating M1/M2 polarisation. Because microglia can cause neurotoxic or neuroprotective effects by dynamically switching between M1 and M2 phenotypes following stimulation, inhibiting overactivated M1 polarisation seems to be a feasible strategy for neuroprotection. However, there is evidence that inhibition of the M1 phenotype alone is unlikely to provide overall benefits [52, 53]. Compared to simply inhibiting M1 polarisation, the timely conversion of M1 to M2 microglia is considered a more promising strategy for treating SCI [54]. In our *in vivo* study, we used M1/M2-related markers to characterize microglial polarisation. We found that the M1 marker expression decreased, whereas the M2 marker expression increased, indicating that GSP could regulate microglial polarisation after SCI.

In the secondary injury of SCI, in addition to neurons, apoptosis also occurs in other cells in the CNS that leads to further loss of neurological function, thus creating obstacles to repair. Inhibition of neuronal apoptosis can promote functional and pathological recovery and prevent permanent neurological impairments [55]. The BCL-2 family of proteins is essential apoptosis regulatory proteins, including proapoptotic (e.g., Bax and cleaved caspase-3) and antiapoptotic (e.g., Bcl-2) proteins. Higher Bax/Bcl-2 ratios can form ion channels that activate cleaved caspase-3, which induces apoptosis [56]. Our *in vivo* results showed that GSP inhibited neuronal apoptosis.

To determine whether GSP has a similar therapeutic effect *in vitro* as observed *in vivo*, we used BV2 cells to simulate primary microglia for follow-up experiments. The rationale of BV-2 as a substitute for primary microglia has been verified previously [57]. Activated microglia can induce apoptosis in surrounding neurons [58–60]. Since we found that GSP inhibited neuronal apoptosis *in vivo*, we wondered whether it was mediated, at least partially, by inhibiting the activation of M1 microglia. Therefore, we evaluated the effects of M1 microglia on neuronal apoptosis *in vitro* using a coculture system and found that GSP alleviated neuronal apoptosis by inhibiting M1 polarisation in microglia.

LPS, a component of the outer membrane of gram-negative bacteria, is a classical TLR4 agonist that polarises microglia to the proinflammatory M1 phenotype and reduces M2 polarisation, thus aggravating inflammation [16, 61]. LPS-induced microglial models have been widely adopted in studies on microglial polarisation [62, 63]. Therefore, we stimulated BV2 cells with LPS to simulate neuroinflammation *in vitro* and found that LPS caused NO release and increased the expression of TNF-α, CD86, and iNOS in BV2 cells. Nevertheless, GSP reversed this trend and significantly upregulated M2-related markers, which suggested that GSP could polarise microglia from the M1 to the M2 phenotype.

TLR4 is mainly expressed in microglia of the CNS [64, 65]. TLR4-dependent microglial activation is crucial in SCI [66, 67]. The biological effects mediated by TLR4 are mainly related to its downstream signaling pathway, and the activation of TLR4 is essential for microglial M1 polarisation [67]. In our *in vivo* study, the expression of TLR4 decreased significantly after GSP treatment. This indicated that GSP

may inhibit the TLR4-mediated signaling pathway. Taken together, these results suggest that the effects of GSP on microglia-induced neuroinflammation or neuroapoptosis may be related to the TLR4-mediated signaling pathway.

After binding to TLR4, LPS induces downstream signaling pathways of TLR4, such as NF-κB [68]. NF-κB normally binds to IκB and remains in the cytoplasm in its inactive state. Upon activation, the rapid degradation of IκB leads to its dissociation from the NF-κB dimer (p65/p50). The dissociation of IκB from the NF-κB dimer can expose the DNA binding signal on the p65 subunit and the translocation signal on the p50 subunit, which results in p65/p50 dimer translocation from the cytoplasm to the nucleus [69, 70]. The PI3K/AKT pathway is another major regulator of neuroinflammation. When activated, it contributes to functional recovery following SCI [71] and promotes microglial polarisation towards the M2 phenotype [72]. There is growing evidence of crosstalk between the TLR4/Myd88/NF-κB and PI3K/AKT signaling pathways [73, 74]. Moreover, activation of PI3K/AKT signaling can inhibit the TLR4/NF-κB signaling pathway (Figure 12) [75]. Our results strongly indicate that GSP can regulate microglia towards the M2 phenotype, which may involve the two signaling pathways.

The results *in vivo* suggested that the NF-κB pathway was strongly activated following SCI, whereas PI3K/AKT pathway activity was inhibited. This trend was reversed by GSP treatment. To further explore the effects of GSP on these two pathways, we detected changes in related protein levels *in vitro*. Compared to the LPS group, the NF-κB pathway was inhibited, and the PI3K/AKT pathway was activated after GSP treatment. One strategy for inhibiting LPS-mediated signaling pathways is to block their receptors. Therefore, we blocked TLR4 with TAK242. We found that both TAK242 and GSP effectively reduced the high activity of NF-κB induced by LPS and upregulated PI3K/AKT signaling-related protein expression. Compared to TAK242, the regulation of GSP is limited or milder but sufficient to reduce LPS-induced neuroinflammation. We demonstrated that GSP regulates microglial polarisation by inhibiting the TLR4-mediated NF-κB and PI3K/AKT signaling pathways. Nevertheless, further experiments should be performed to explain the precise underlying mechanism of crosstalk between TLR4/NFκB and PI3K/AKT signaling pathways.

In summary, GSP can regulate microglial polarisation, thereby reducing neuronal apoptosis and improving functional recovery after SCI by inhibiting TLR4. Therefore, the TLR4/MyD88/NF-κB/PI3K/AKT signaling cascade is a suitable target for treating SCI. However, this study did not explore the long-term side effects of GSP, and the exact mechanism needs to be further explored.

5. Conclusion

GSP inhibited neuroinflammation and neuronal apoptosis by regulating microglial polarisation. Thus, GSP plays a neuroprotective role, which may be achieved by inhibiting the NF-κB signaling pathway and activating the PI3K/AKT signaling pathway mediated by TLR4. This study demonstrated the potential of GSP as a therapeutic SCI drug.

Data Availability

The data generated in this study can be obtained from the corresponding author upon request.

Conflicts of Interest

The authors declare that this study does not involve any conflicts of interest.

Acknowledgments

References

[1] R. J. Giger, E. R. Hollis 2nd, and M. H. Tuszynski, "Guidance molecules in axon regeneration," *Cold Spring Harbor Perspectives in Biology*, vol. 2, no. 7, article a001867, 2010.

[2] G. D. Carlson and C. Gorden, "Current developments in spinal cord injury research," *The Spine Journal*, vol. 2, no. 2, pp. 116–128, 2002.

[3] H. Kumar, A. E. Ropper, S. H. Lee, and I. Han, "Propitious therapeutic modulators to prevent blood-spinal cord barrier disruption in spinal cord injury," *Molecular Neurobiology*, vol. 54, no. 5, pp. 3578–3590, 2017.

[4] M. Nakamura, R. A. Houghtling, L. MacArthur, B. M. Bayer, and B. S. Bregman, "Differences in cytokine gene expression profile between acute and secondary injury in adult rat spinal cord," *Experimental Neurology*, vol. 184, no. 1, pp. 313–325, 2003.

[5] A. Ulndreaj, J. C. Chio, C. S. Ahuja, and M. G. Fehlings, "Modulating the immune response in spinal cord injury," *Expert Review of Neurotherapeutics*, vol. 16, no. 10, pp. 1127–1129, 2016.

[6] S. Thuret, L. D. Moon, and F. H. Gage, "Therapeutic interventions after spinal cord injury," *Nature Reviews. Neuroscience*, vol. 7, no. 8, pp. 628–643, 2006.

[7] J. Lin, X. Pan, C. Huang et al., "Dual regulation of microglia and neurons by Astragaloside IV-mediated mTORC1 suppression promotes functional recovery after acute spinal cord injury," *Journal of Cellular and Molecular Medicine*, vol. 24, no. 1, pp. 671–685, 2020.

[8] W. Liu, B. Xu, W. Xue et al., "A functional scaffold to promote the migration and neuronal differentiation of neural stem/progenitor cells for spinal cord injury repair," *Biomaterials*, vol. 243, p. 119941, 2020.

[9] Q. Q. Yang and J. W. Zhou, "Neuroinflammation in the central nervous system: symphony of glial cells," *Glia*, vol. 67, no. 6, pp. 1017–1035, 2019.

[10] D. Nayak, T. L. Roth, and D. B. McGavern, "Microglia development and function," *Annual Review of Immunology*, vol. 32, no. 1, pp. 367–402, 2014.

[11] E. Shobin, M. P. Bowley, L. I. Estrada et al., "Microglia activation and phagocytosis: relationship with aging and cognitive impairment in the rhesus monkey," *Geroscience*, vol. 39, no. 2, pp. 199–220, 2017.

[12] K. A. Kigerl, J. C. Gensel, D. P. Ankeny, J. K. Alexander, D. J. Donnelly, and P. G. Popovich, "Identification of two distinct macrophage subsets with divergent effects causing either neurotoxicity or regeneration in the injured mouse spinal cord," *The Journal of Neuroscience*, vol. 29, no. 43, pp. 13435–13444, 2009.

[13] F. O. Martinez and S. Gordon, "The M1 and M2 paradigm of macrophage activation: time for reassessment," *F1000Prime Rep*, vol. 6, p. 13, 2014.

[14] Y. Dong, X. Li, J. Cheng, and L. Hou, "Drug development for Alzheimer's disease: microglia induced neuroinflammation as a target?," *International Journal of Molecular Sciences*, vol. 20, no. 3, p. 558, 2019.

[15] C. S. Subhramanyam, C. Wang, Q. Hu, and S. T. Dheen, "Microglia-mediated neuroinflammation in neurodegenerative diseases," *Seminars in Cell & Developmental Biology*, vol. 94, pp. 112–120, 2019.

[16] S. David and A. Kroner, "Repertoire of microglial and macrophage responses after spinal cord injury," *Nature Reviews. Neuroscience*, vol. 12, no. 7, pp. 388–399, 2011.

[17] X. Hu, R. K. Leak, Y. Shi et al., "Microglial and macrophage polarization—new prospects for brain repair," *Nature Reviews. Neurology*, vol. 11, no. 1, pp. 56–64, 2015.

[18] H. Shi, L. Dong, J. Jiang et al., "Chlorogenic acid reduces liver inflammation and fibrosis through inhibition of toll-like receptor 4 signaling pathway," *Toxicology*, vol. 303, pp. 107–114, 2013.

[19] Y. Wang, S. Wu, X. Yu et al., "Dexmedetomidine protects rat liver against ischemia-reperfusion injury partly by the α2A-adrenoceptor subtype and the mechanism is associated with the TLR4/NF-κB pathway," *International Journal of Molecular Sciences*, vol. 17, no. 7, p. 995, 2016.

[20] Y. Yang, J. Lv, S. Jiang et al., "The emerging role of toll-like receptor 4 in myocardial inflammation," *Cell Death & Disease*, vol. 7, no. 5, article e2234, 2016.

[21] S. I. Miller, R. K. Ernst, and M. W. Bader, "LPS, TLR4 and infectious disease diversity," *Nature Reviews. Microbiology*, vol. 3, no. 1, pp. 36–46, 2005.

[22] N. N. Kuzmich, K. V. Sivak, V. N. Chubarev, Y. B. Porozov, T. N. Savateeva-Lyubimova, and F. Peri, "TLR4 signaling pathway modulators as potential therapeutics in inflammation and sepsis," *Vaccine*, vol. 5, no. 4, p. 34, 2017.

[23] H. Shi, X. L. Wang, H. F. Quan et al., "Effects of betaine on LPS-stimulated activation of microglial M1/M2 phenotypes by suppressing TLR4/NF-κB pathways in N9 cells," *Molecules*, vol. 24, no. 2, p. 367, 2019.

[24] S. J. Kim and H. M. Kim, "Dynamic lipopolysaccharide transfer cascade to TLR4/MD2 complex via LBP and CD14," *BMB Reports*, vol. 50, no. 2, pp. 55–57, 2017.

[25] A. F. Cerbaro, V. S. B. Rodrigues, M. Rigotti et al., "Grape seed proanthocyanidins improves mitochondrial function and reduces oxidative stress through an increase in sirtuin 3 expression in EA.hy926 cells in high glucose condition," *Molecular Biology Reports*, vol. 47, no. 5, pp. 3319–3330, 2020.

[26] M. L. Cádiz-Gurrea, I. Borrás-Linares, J. Lozano-Sánchez, J. Joven, S. Fernández-Arroyo, and A. Segura-Carretero, "Cocoa and grape seed byproducts as a source of antioxidant

and anti-inflammatory proanthocyanidins," *International Journal of Molecular Sciences*, vol. 18, no. 2, p. 376, 2017.

[27] M. Sintara, Y. Wang, L. Li et al., "Quantification of cranberry proanthocyanidins by normal-phase high-performance liquid chromatography using relative response factors," *Phytochemical Analysis*, vol. 31, no. 6, pp. 874–883, 2020.

[28] A. Morissette, C. Kropp, J. P. Songpadith et al., "Blueberry proanthocyanidins and anthocyanins improve metabolic health through a gut microbiota-dependent mechanism in diet-induced obese mice," *American Journal of Physiology. Endocrinology and Metabolism*, vol. 318, no. 6, pp. E965–e980, 2020.

[29] E. H. Wang, Z. L. Yu, G. F. Ping, and S. Zhai, "Grape seed procyanidin extract attenuate sodium fluoride-induced oxidative damage and apoptosis in rat kidneys," *Biomedical and Environmental Sciences*, vol. 33, no. 6, pp. 454–457, 2020.

[30] Q. Q. Wang, H. Gao, R. Yuan et al., "Procyanidin A2, a polyphenolic compound, exerts anti-inflammatory and antioxidative activity in lipopolysaccharide-stimulated RAW264.7 cells," *PLoS One*, vol. 15, no. 8, article e0237017, 2020.

[31] Y. X. Zeng, S. Wang, L. Wei, Y. Y. Cui, and Y. H. Chen, "Proanthocyanidins: components, pharmacokinetics and biomedical properties," *The American Journal of Chinese Medicine*, vol. 48, no. 4, pp. 813–869, 2020.

[32] X. Jiang, J. Liu, Q. Lin et al., "Proanthocyanidin prevents lipopolysaccharide-induced depressive-like behavior in mice via neuroinflammatory pathway," *Brain Research Bulletin*, vol. 135, pp. 40–46, 2017.

[33] H. M. Abdou, H. A. E. Abd Elkader, A. H. El-Gendy, and S. M. Eweda, "Neurotoxicity and neuroinflammatory effects of bisphenol A in male rats: the neuroprotective role of grape seed proanthocyanidins," *Environmental Science and Pollution Research International*, vol. 29, no. 6, pp. 9257–9268, 2022.

[34] S. H. Koozekanani, W. M. Vise, R. M. Hashemi, and R. B. McGhee, "Possible mechanisms for observed pathophysiological variability in experimental spinal cord injury by the method of Allen," *Journal of Neurosurgery*, vol. 44, no. 4, pp. 429–434, 1976.

[35] D. M. Basso, M. S. Beattie, and J. C. Bresnahan, "A sensitive and reliable locomotor rating scale for open field testing in rats," *Journal of Neurotrauma*, vol. 12, no. 1, pp. 1–21, 1995.

[36] W. Hu, X. Wu, D. Yu et al., "Regulation of JNK signaling pathway and RIPK3/AIF in necroptosis-mediated global cerebral ischemia/reperfusion injury in rats," *Experimental Neurology*, vol. 331, p. 113374, 2020.

[37] L. Peferoen, M. Kipp, P. van der Valk, J. M. van Noort, and S. Amor, "Oligodendrocyte-microglia cross-talk in the central nervous system," *Immunology*, vol. 141, no. 3, pp. 302–313, 2014.

[38] T. Gaojian, Q. Dingfei, L. Linwei et al., "Parthenolide promotes the repair of spinal cord injury by modulating M1/M2 polarization via the NF-κB and STAT 1/3 signaling pathway," *Cell Death Discovery*, vol. 6, no. 1, p. 97, 2020.

[39] C. Li, C. Zhang, H. Zhou et al., "Inhibitory effects of betulinic acid on LPS-induced neuroinflammation involve M2 microglial polarization via CaMKKβ-dependent AMPK activation," *Frontiers in Molecular Neuroscience*, vol. 11, p. 98, 2018.

[40] C. D. Thompson, J. C. Zurko, B. F. Hanna, D. J. Hellenbrand, and A. Hanna, "The therapeutic role of interleukin-10 after spinal cord injury," *Journal of Neurotrauma*, vol. 30, no. 15, pp. 1311–1324, 2013.

[41] R. A. Dixon, D. Y. Xie, and S. B. Sharma, "Proanthocyanidins – a final frontier in flavonoid research?," *The New Phytologist*, vol. 165, no. 1, pp. 9–28, 2005.

[42] J. Yamakoshi, S. Kataoka, T. Koga, and T. Ariga, "Proanthocyanidin-rich extract from grape seeds attenuates the development of aortic atherosclerosis in cholesterol-fed rabbits," *Atherosclerosis*, vol. 142, no. 1, pp. 139–149, 1999.

[43] A. Subarnas and H. Wagner, "Analgesic and anti-inflammatory activity of the proanthocyanidin shelleguea in a from Polypodium feei METT," *Phytomedicine*, vol. 7, no. 5, pp. 401–405, 2000.

[44] R. Corder, W. Mullen, N. Q. Khan et al., "Oenology: red wine procyanidins and vascular health," *Nature*, vol. 444, no. 7119, p. 566, 2006.

[45] J. Wang, M. G. Ferruzzi, L. Ho et al., "Brain-targeted proanthocyanidin metabolites for Alzheimer's disease treatment," *The Journal of Neuroscience*, vol. 32, no. 15, pp. 5144–5150, 2012.

[46] M. M. Abd El Mohsen, "Uptake and metabolism of epicatechin and its access to the brain after oral ingestion," *Free Radical Biology & Medicine*, vol. 33, no. 12, pp. 1693–1702, 2002.

[47] H. Zhou, C. Yin, Z. Zhang et al., "Proanthocyanidin promotes functional recovery of spinal cord injury via inhibiting ferroptosis," *Journal of Chemical Neuroanatomy*, vol. 107, p. 101807, 2020.

[48] X. He, X. Guo, Z. Ma et al., "Grape seed proanthocyanidins protect PC12 cells from hydrogen peroxide-induced damage via the PI3K/AKT signaling pathway," *Neuroscience Letters*, vol. 750, p. 135793, 2021.

[49] A. Cianciulli, R. Calvello, C. Porro, T. Trotta, R. Salvatore, and M. A. Panaro, "PI3k/Akt signalling pathway plays a crucial role in the anti-inflammatory effects of curcumin in LPS-activated microglia," *International Immunopharmacology*, vol. 36, pp. 282–290, 2016.

[50] F. Wu, T. Luo, Y. Mei et al., "Simvastatin alters M1/M2 polarization of murine BV2 microglia via Notch signaling," *Journal of Neuroimmunology*, vol. 316, pp. 56–64, 2018.

[51] B. Zhang, Y. Z. Wei, G. Q. Wang, D. D. Li, J. S. Shi, and F. Zhang, "Targeting MAPK pathways by naringenin modulates microglia M1/M2 polarization in lipopolysaccharide-stimulated cultures," *Frontiers in Cellular Neuroscience*, vol. 12, p. 531, 2019.

[52] S. Côté, P. H. Carmichael, R. Verreault, J. Lindsay, J. Lefebvre, and D. Laurin, "Nonsteroidal anti-inflammatory drug use and the risk of cognitive impairment and Alzheimer's disease," *Alzheimers Dement*, vol. 8, no. 3, pp. 219–226, 2012.

[53] S. Lehrer and P. H. Rheinstein, "Is Alzheimer's disease autoimmune inflammation of the brain that can be treated with nasal nonsteroidal anti-inflammatory drugs?," *American Journal of Alzheimer's Disease and Other Dementias*, vol. 30, no. 3, pp. 225–227, 2015.

[54] X. Jin, M. Y. Liu, D. F. Zhang et al., "Baicalin mitigates cognitive impairment and protects neurons from microglia-mediated neuroinflammation via suppressing NLRP3 inflammasomes and TLR4/NF-κB signaling pathway," *CNS Neuroscience & Therapeutics*, vol. 25, no. 5, pp. 575–590, 2019.

[55] X. Li, S. Chen, L. Mao et al., "Zinc improves functional recovery by regulating the secretion of granulocyte colony stimulating factor from microglia/macrophages after spinal cord injury," *Frontiers in Molecular Neuroscience*, vol. 12, p. 18, 2019.

[56] W. Lin, J. Xie, N. Xu et al., "Glaucocalyxin a induces G2/M cell cycle arrest and apoptosis through the PI3K/Akt pathway in human bladder cancer cells," *International Journal of Biological Sciences*, vol. 14, no. 4, pp. 418–426, 2018.

[57] A. Henn, S. Lund, M. Hedtjärn, A. Schrattenholz, P. Pörzgen, and M. Leist, "The suitability of BV2 cells as alternative model system for primary microglia cultures or for animal experiments examining brain inflammation," *ALTEX*, vol. 26, no. 2, pp. 83–94, 2009.

[58] M. L. Block, L. Zecca, and J. S. Hong, "Microglia-mediated neurotoxicity: uncovering the molecular mechanisms," *Nature Reviews. Neuroscience*, vol. 8, no. 1, pp. 57–69, 2007.

[59] G. C. Brown and A. Vilalta, "How microglia kill neurons," *Brain Research*, vol. 1628, no. Part B, pp. 288–297, 2015.

[60] J. Y. Kim, N. Kim, and M. A. Yenari, "Mechanisms and potential therapeutic applications of microglial activation after brain injury," *CNS Neuroscience & Therapeutics*, vol. 21, no. 4, pp. 309–319, 2015.

[61] K. Saijo and C. K. Glass, "Microglial cell origin and phenotypes in health and disease," *Nature Reviews. Immunology*, vol. 11, no. 11, pp. 775–787, 2011.

[62] C. J. Henry, Y. Huang, A. Wynne et al., "Minocycline attenuates lipopolysaccharide (LPS)-induced neuroinflammation, sickness behavior, and anhedonia," *Journal of Neuroinflammation*, vol. 5, no. 1, p. 15, 2008.

[63] Y. Xu, Y. Xu, Y. Wang et al., "Telmisartan prevention of LPS-induced microglia activation involves M2 microglia polarization via CaMKKβ-dependent AMPK activation," *Brain, Behavior, and Immunity*, vol. 50, pp. 298–313, 2015.

[64] K. A. Kigerl, W. Lai, S. Rivest, R. P. Hart, A. R. Satoskar, and P. G. Popovich, "Toll-like receptor (TLR)-2 and TLR-4 regulate inflammation, gliosis, and myelin sparing after spinal cord injury," *Journal of Neurochemistry*, vol. 102, no. 1, pp. 37–50, 2007.

[65] A. Heiman, A. Pallottie, R. F. Heary, and S. Elkabes, "Toll-like receptors in central nervous system injury and disease: a focus on the spinal cord," *Brain, Behavior, and Immunity*, vol. 42, pp. 232–245, 2014.

[66] A. Ahmad, R. Crupi, M. Campolo, T. Genovese, E. Esposito, and S. Cuzzocrea, "Absence of TLR4 reduces neurovascular unit and secondary inflammatory process after traumatic brain injury in mice," *PLoS One*, vol. 8, no. 3, article e57208, 2013.

[67] H. Capiralla, V. Vingtdeux, H. Zhao et al., "Resveratrol mitigates lipopolysaccharide- and Aβ-mediated microglial inflammation by inhibiting the TLR4/NF-κB/STAT signaling cascade," *Journal of Neurochemistry*, vol. 120, no. 3, pp. 461–472, 2012.

[68] S. Nair, K. S. Sobotka, P. Joshi et al., "Lipopolysaccharide-induced alteration of mitochondrial morphology induces a metabolic shift in microglia modulating the inflammatory response in vitro and in vivo," *Glia*, vol. 67, no. 6, pp. 1047–1061, 2019.

[69] G. Z. Zhang, M. Q. Liu, H. W. Chen et al., "NF-κB signalling pathways in nucleus pulposus cell function and intervertebral disc degeneration," *Cell Proliferation*, vol. 54, no. 7, article e13057, 2021.

[70] M. S. Hayden and S. Ghosh, "Shared principles in NF-kappaB signaling," *Cell*, vol. 132, no. 3, pp. 344–362, 2008.

[71] P. Zhang, L. Zhang, L. Zhu et al., "The change tendency of PI3K/Akt pathway after spinal cord injury," *American Journal of Translational Research*, vol. 7, no. 11, pp. 2223–2232, 2015.

[72] J. Peng, J. Pang, L. Huang et al., "LRP1 activation attenuates white matter injury by modulating microglial polarization through Shc1/PI3K/Akt pathway after subarachnoid hemorrhage in rats," *Redox Biology*, vol. 21, p. 101121, 2019.

[73] F. Hua, T. Ha, J. Ma et al., "Protection against myocardial ischemia/reperfusion injury in TLR4-deficient mice is mediated through a phosphoinositide 3-kinase-dependent mechanism," *Journal of Immunology*, vol. 178, no. 11, pp. 7317–7324, 2007.

[74] S. Fernandez-Lizarbe, M. Pascual, and C. Guerri, "Critical role of TLR4 response in the activation of microglia induced by ethanol," *Journal of Immunology*, vol. 183, no. 7, pp. 4733–4744, 2009.

[75] E. Vergadi, E. Ieronymaki, K. Lyroni, K. Vaporidi, and C. Tsatsanis, "Akt signaling pathway in macrophage activation and M1/M2 polarization," *Journal of Immunology*, vol. 198, no. 3, pp. 1006–1014, 2017.

Hindawi

Research Article

The Effects of Bone Cement Volume in Percutaneous Vertebroplasty for Thoracolumbar Junction Vertebral Compression Fractures: A Clinical Comparative Study

Meng Wang [1,2] **Bo Li,**[1] **Yuren Wang,**[1] **Shengdan Jiang** [1] **Gen Wen,**[2] **Leisheng Jiang** [1] **and Xinfeng Zheng** [1]

[1]*Department of Clinic of Spine Center, Xinhua Hospital, Shanghai Jiaotong University School of Medicine, Shanghai 200092, China*
[2]*Department of Orthopaedic Surgery, Shanghai Jiao Tong University Affiliated Sixth People's Hospital, Shanghai 200233, China*

Correspondence should be addressed to Leisheng Jiang; jiangleisheng@xinhuamed.com.cn
and Xinfeng Zheng; zhengxinfeng@xinhuamed.com.cn

We compared the outcomes of patients treated with different volumes of polymethyl methacrylate bone cement during percutaneous vertebroplasty (PVP) for thoracolumbar vertebral compression fractures. We performed a comparative, retrospective study of 316 patients who underwent PVP for a single-level thoracolumbar vertebral compression fracture. Patients were divided into two groups: group A (≤ 5 mL; $n = 146$) and group B (> 5 mL; $n = 170$). The visual analogue scale (VAS) for pain and the Roland-Morris Disability Questionnaire (RDQ) scores were compared between the two groups at 1 week and at 1, 6, 12, and 24 months after PVP. The incidence of cement leakage into the intervertebral discs was evaluated by a postoperative lateral radiograph assessment. Patients were evaluated for new fractures 1 and 2 years after PVP or when new fractures were suspected. Among the 316 patients enrolled, 245 completed the clinical research. No difference between groups A and B in terms of the VAS, RDQ, and rate of complications at all time points after surgery was observed. The presence of intervertebral disc leakage was a relative risk (RR) for subsequent total vertebral fracture (RR, 6.42; 95% confidence interval (CI), 2.72-14.19; $P < 0.0001$) and adjacent vertebral fracture (RR, 8.03; 95% CI, 2.74-23.54; $P = 0.0001$). A high volume of bone cement may increase the rate of subsequent total and adjacent vertebral fractures. However, the occurrence of intervertebral disc leakage is the principal risk factor for these negative outcomes of PVP.

1. Introduction

Percutaneous vertebroplasty (PVP) is a minimally invasive technique that involves percutaneous injection of polymethyl methacrylate or calcium phosphate cement into the involved vertebral body under C-arm fluoroscopy. For patients with an osteoporotic vertebral compression fracture (VCF), PVP can provide rapid pain relief and restore vertebral height, as well as improve function and mobility, which decreases the risk of mortality and incidence of complications. The efficacy of PVP has been proven in a series of clinical studies and a few randomized, controlled trials [1–8]. However, there were studies indicating that when the patients with VCFs were under PVP, the probability

of subsequent vertebral fractures was from 2.4% to 23% [9, 10] and 2/3 of them occurred in the adjacent vertebra [11, 12]. The volume of bone cement used is the most important factor to consider with regard to the therapeutic effect of PVP. *In vitro* biomechanical studies have not identified a benefit of a higher volume of cement in restoring vertebral stiffness and strength [13, 14] or the height of the vertebra [14]. In fact, asymmetric injection of a high volume of cement negatively transforms the biological characteristics of the vertebra [13]. In clinical reports, amounts of cement ranging from 1 to 12 mL have been used for PVP treatment of VCFs [15–17]. However, the appropriate volume of cement to be used remains unclear. For balloon kyphoplasty, Röder et al. [18] reported that a

cement volume > 4.5 mL was more effective than ≤4.5 mL. Of note, Jin et al. [19] reported that a high volume of cement during PVP increased the risk of subsequent adjacent vertebral fractures, and a volume of 4.9 mL was the most appropriate to minimize this risk. Based on this information, we conducted a retrospective, comparative study to determine if PVP performed with a low volume of cement provided the same clinical outcomes as PVP performed with a high volume of cement for the treatment of osteoporotic VCFs.

2. Materials and Methods

Eligible patients were those who underwent PVP for osteoporotic VCFs in the Department of Orthopedic Surgery at Xinhua Hospital Affiliated with Shanghai Jiaotong University School of Medicine between January 2008 and December 2013. The inclusion criteria were as follows: age ≥ 50 years and a single, acute, or subacute, painful osteoporotic VCF with a clinical onset < 3 months or a chronic, unhealed, painful, osteoporotic VCF with a clinical onset ≥ 3 months confirmed by spinal radiography and by magnetic resonance or emission computed tomography imaging. The exclusion criteria were as follows: pathological fractures from myeloma, metastatic tumor, or infection; history of coagulation disorders; disruption of the posterior wall of the fractured vertebral body; presence of any neurological symptom; severe cardiopulmonary comorbidity; suspected underlying malignant disease; diseases affecting bone metabolism; and history of glucocorticoid or antiosteoporosis drugs. The level of the VCF was classified as thoracic (T6-T9), thoracolumbar (T10-L2), or lumbar (L3-L5). All the patients included in this study were required to undergo dual-energy X-ray absorptiometry examination to determine bone mineral density scores of the lumbar vertebrae (L1–4). Fractured vertebrae were excluded at T-score evaluation when the fracture was at L1-L4.

Patient follow-up was conducted at 1 week after PVP and at 1, 6, 12, and 24 months after PVP. Patient-reported scores on the visual analogue scale (VAS) for back pain and the Roland-Morris Disability Questionnaire (RDQ) for functional recovery were obtained at baseline before PVP and at each follow-up. A 10-point VAS was used to quantify pain intensity with anchors at "0" (no pain) and "10" (worst possible pain). The RDQ was used for scoring activities of daily life on a 23-point scale with physical disability worsening as the score increased. Cement leakage into the intervertebral disc was evaluated on a postoperative lateral radiograph (see Figure 1).

Evaluation for a new VCF was performed by magnetic resonance or radioisotope imaging at 1 and 2 years after PVP or when suspected from the clinical presentation.

A 5 mL volume of cement was used as the cut-off, which was based on the report by Jin et al. [19], to compare the low- and high-volume groups. Patients were classified into the appropriate group for analysis: a low-volume group (group A) received a volume of cement ≤ 5 mL, and a high-volume group (group B) received a volume of cement > 5 mL.

FIGURE 1: Cement leakage into the intervertebral disc on direct postoperative radiograph.

Continuous variables were reported as the mean and standard deviation (SD) or 95% confidence interval (CI), and categorical variables were reported as a number and percentage. For dichotomous variables, the risk ratio (RR) and 95% CI were calculated. The Student t-test was used to evaluate between-group differences for continuous variables, and the chi-squared (χ^2) test was used for categorical variables. A P value < 0.05 was considered statistically significant.

The present study was approved by Xinhua Hospital, Shanghai Jiaotong University School of Medicine (approval number: XHEC-D-2020-071). Written informed consent was obtained from the patients.

3. Results

3.1. Baseline Characteristics. A total of 539 patients from January 2008 to December 2013 were eligible for the study, and 387 of these patients met the inclusion criteria. The distribution of fractures was as follows: thoracic, $n = 17$; thoracolumbar, $n = 316$; and lumbar, $n = 54$. Owing to the small number of cases, thoracic and lumbar fractures were not included in our analysis to reduce the risk of bias (see Figure 2). The 316 patients with thoracolumbar fractures included 61 males and 255 females with an average age of 77.0 (range, 52 to 96) years; however, only 245 patients completed the 2-year follow-up from beginning to end (see Figure 2). The relevant characteristics of these patients, classified into groups A (≤5 mL) and B (>5 mL), are presented in Table 1.

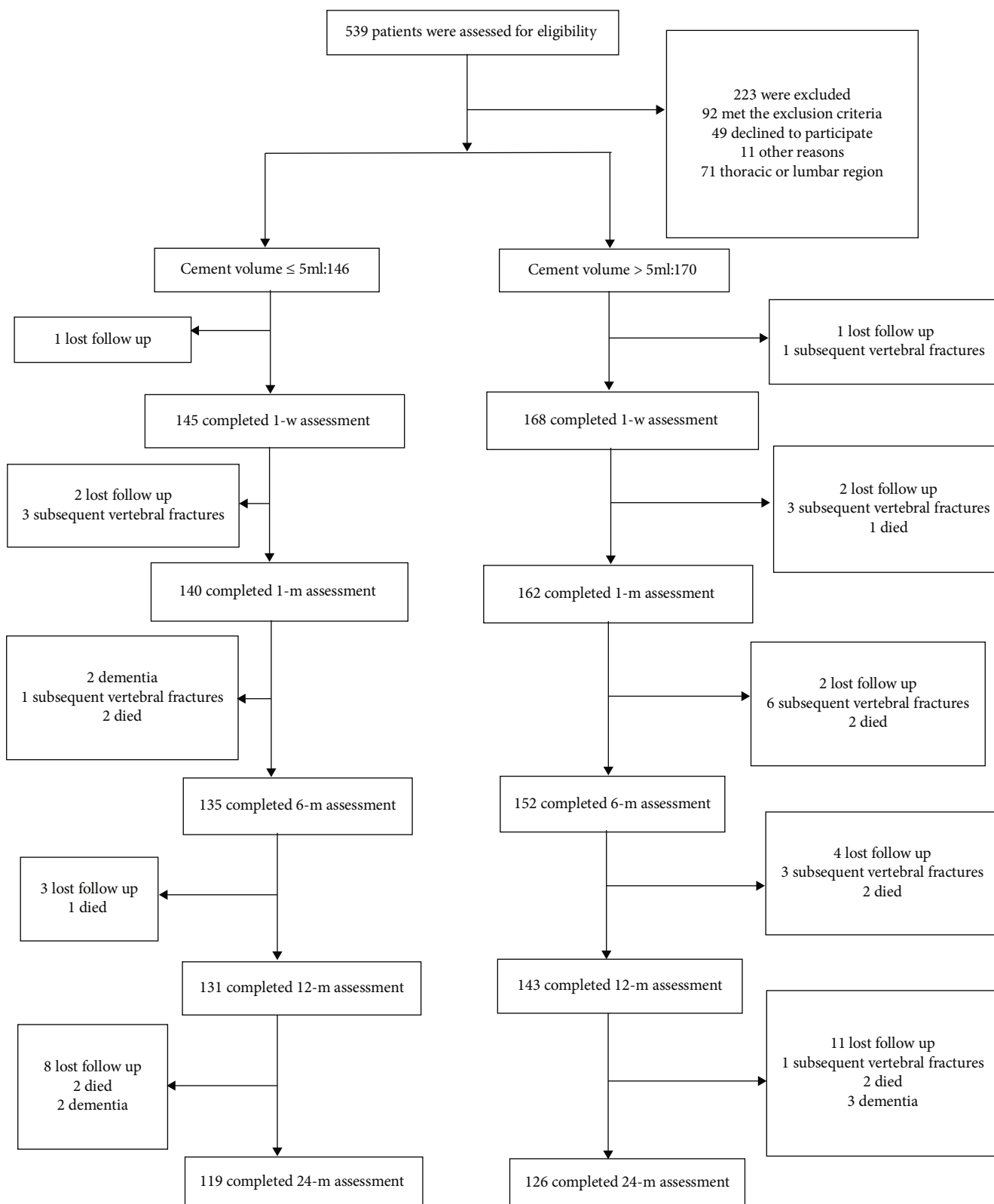Figure 2: Flow chart of including, excluding, and dividing cases and 2-year follow-up.

3.2. VAS and RDQ. No difference between groups A and B with regard to the VAS and RDQ scores at each time point of measurement was observed (see Table 2).

3.3. Intervertebral Leakage and Subsequent Vertebral Fractures. A total of 35 (11.1%) patients had intervertebral disc leakage, 18 (5.7%) patients had subsequent total

TABLE 1: Baseline characteristics of the 316 patients with thoracolumbar OVCFs treated with different volumes of cement.

	Low dose (≤5 mL)	High dose (>5 mL)	P value
Number of patients	146	170	
Sex, female; N (%)	116 (79.5%)	139 (81.8%)	0.606
Age, years; mean (SD)	77.1 (8.4)	76.2 (8.5)	0.305
BMD (T-value); mean (SD)	-2.7 (0.6)	-2.8 (0.7)	0.062
BMI (kg/m^2); mean (SD)	22.5 (2.8)	23.1 (3.7)	0.112
Cement volume, mL; mean (SD)	4.4 (0.8)	6.0 (0.6)	<0.01
Cement volume; N			
2.1-4.0 mL		43	
4.1-5.0 mL		103	
5.1-6.0 mL		151	
6.1-8.0 mL		14	
8.1-10.0 mL		5	

BMD: bone mineral density; BMI: body mass index; OVCFs: osteoporotic vertebral compression fractures.

TABLE 2: The VAS and RDQ scores at the different time points of measurement.

	Low-dose (≤5 mL)		High-dose (>5 mL)		P value
	N	Mean (SD)	N	Mean (SD)	
VAS at different periods					
Initial	146	7.7 ± 1.1	170	7.6 ± 1.0	0.489
1 w	145	4.8 ± 1.6	168	4.8 ± 1.8	0.686
1 m	140	4.2 ± 1.9	162	3.9 ± 1.7	0.179
6 m	135	3.8 ± 2.0	152	3.6 ± 1.7	0.255
12 m	131	3.5 ± 1.7	143	3.8 ± 1.8	0.182
24 m	119	3.6 ± 1.5	126	3.5 ± 1.3	0.291
RDQ at different periods					
Initial	146	19.0 ± 1.8	170	18.9 ± 2.0	0.689
1 w	145	14.1 ± 2.8	168	13.7 ± 3.2	0.249
1 m	140	12.6 ± 4.1	162	12.0 ± 3.8	0.193
6 m	135	11.8 ± 3.4	152	11.5 ± 3.4	0.383
12 m	131	11.5 ± 4.0	143	11.1 ± 4.0	0.417
24 m	119	11.4 ± 4.0	126	11.6 ± 4.1	0.570

VAS: visual analogue scale; RDQ: Roland-Morris Disability Questionnaire.

TABLE 3: The IDL, STVF, and SAVF in respective groups with different volumes of cement.

	≤5 mL	>5 mL	RR	P value
IDL	13/146	22/170	1.45	0.250
STVF	4/146	14/170	3.01	0.036
SAVF	2/146	10/170	4.29	0.029

IDL: intervertebral disc leakage; STVF: subsequent total vertebral fracture; SAVF: subsequent adjacent vertebral fracture; RR: relative risk.

TABLE 4: The independent risk factor analysis of intervertebral disc leakage for subsequent vertebral fracture.

	With IDL	Without IDL	RR	P value
STVF	8/35	10/281	6.42	P < 0.0001
SAVF	6/35	6/281	8.03	P = 0.0001

IDL: intervertebral disc leakage; STVF: subsequent total vertebral fracture; SAVF: subsequent adjacent vertebral fracture; RR: relative risk.

adjacent vertebral fracture, 6 (17.1%) and 6 (2.1%), respectively (RR, 8.03; 95% CI, 2.74 to 23.54; P = 0.0001) (see Table 4).

4. Discussion

A consensus regarding the effects of bone cement volume on the clinical efficacy of PVP for thoracolumbar VCFs does not exist. In our study, both low and high volumes of bone cement effectively relieved pain and promoted early recovery of function. Although a high volume of cement was associated with a high rate of subsequent total and adjacent vertebral fractures, the risk for these fractures was actually associated with the incidence of intervertebral leakage after surgery.

The effects of bone cement on the biomechanics of vertebrae have previously been reported. Belkoff et al. [20] reported that 2 mL of cement increased the strength of fractured vertebrae at the thoracic, lumbar, and thoracolumbar level; however, improvement in the rigidity of the vertebrae was specific to the level: 4 mL was required at the thoracic

vertebral fracture, and 12 (3.8%) patients had subsequent adjacent vertebral fractures. The differences in these outcomes between groups A and B were as follows: intervertebral leakage, 13 (8.9%) and 22 (12.9%), respectively (P = 0.250); subsequent total vertebral fracture, 4 (2.7%) and 14 (8.2%), respectively (P = 0.036); and subsequent adjacent vertebral fracture, 2 (1.4%) and 10 (5.9%), respectively (P = 0.029) (see Table 3).

3.4. A Risk Factor to Subsequent Vertebral Fractures. Intervertebral disc leakage (n = 35) increased the risk of subsequent fractures. The difference between those patients with and without leakage was as follows: subsequent total vertebral fracture, 8 (22.9%) and 10 (3.6%), respectively (RR, 6.42; 95% CI, 2.72 to 15.19; P < 0.0001), and subsequent

level, 4-6 mL was required at the lumbar level, and 4-8 mL was required at the thoracolumbar level, with the volume dependent on the cement materials used. Molloy et al. [14] reported that, although 3.5 mL of bone cement was sufficient to strengthen a vertebral fracture, a 7.0 mL volume was more effective; again, both volumes of bone cement failed to effectively repair the rigidity of vertebrae. Moreover, the effects of bone cement on osteoporotic bone tissue and, ultimately, on fracture repair have been an issue of long-standing controversy. In an animal study, Hu et al. [21] demonstrated that bone cement might not cause permanent injury to the bone tissue but could prolong the repair cycle of the bone surface.

The mechanism by which PVP yields its analgesic effects remains uncertain, although several hypotheses have been proposed and are worth exploring [22–24]. The first is that bone cement immediately solidifies the vertebra after injection and provides fixation to the fracture, which eliminates the fracture-site micromovements that stimulate sensory nerve endings. The second is that the heat effect of bone cement and cytotoxicity of monomers damage the sensory nerve endings, thus decreasing pain. The third is that the pain relief could be mediated by the local anesthetics used during PVP. The fourth is the possibility that PVP provides a placebo effect. Obviously, the last three hypotheses do not have an association with the volume of bone cement used. As such, the first hypothesis would clarify the association between pain improvement and postoperative vertebral strength. *In vitro* studies have proven that a low volume of bone cement is not inferior to a high volume for restoring the strength of a vertebra [13, 14, 20], which would explain why the volume of cement is not associated with the pain relief effect of PVP. In the same way, recovery of daily function depends on both the improvement of pain and restoration of vertebral strength and, thus, the volume of cement would have little effect on recovery of function. In contrast, the findings of Nieuwenhuijse et al. [22] showed that the degree of pain relief after PVP was related to the volume of bone cement, and a volume equivalent to 24% of the volume of the vertebral body provided the optimal effect. In our experience, alleviation of pain can be achieved effectively using both a low and high volume of cement. Luo et al. [23] reported that a 3.5 mL volume of cement maximizes recovery of normal stress distribution across both the fractured and adjacent vertebrae.

Several studies have confirmed that, compared to conservative treatment, vertebroplasty does not increase the incidence of subsequent fractures [24–29], but other studies have concluded the opposite [1, 30]. We note that a low volume of cement was used in two of the studies that reported the risk of subsequent fractures from PVP [25, 29]. In addition, we note that, in another study that reported an increased risk of subsequent fractures from PVP, the volume of cement was not specifically stated but the description provided was a fractured vertebra "fully filled" with bone cement [30]. The systematic review by Han et al. [31] reported that the volume of bone cement had no effect on the incidence of subsequent fractures. However, the studies included in Han et al.'s systematic review had wide variations in the volume of cement used, which resulted in high heterogeneity and an inability to conclusively determine the differential effects of a low or high volume. We further note that there is little evidence regarding the effect of different volumes on thoracolumbar VCFs after PVP. The volume of the vertebral body varies greatly across different segments of the spine; therefore, the possible differential effects of the volume of cement used must be examined at each level of the spine. We know that certain factors influence the incidence of subsequent fractures after PVP, namely, bone mineral density, body mass index, and bone cement intervertebral disc leakage [32, 33]. Our study adds to these findings by providing evidence that intervertebral disc leakage after PVP is a significant risk factor for subsequent vertebral fractures.

Our study shows that the incidence of intervertebral disc leakage after PVP is higher when a high volume of bone cement is used than when a low volume of bone cement is used, but the difference was not significant. Our study did confirm, however, that intervertebral disc leakage of bone cement is a risk factor for subsequent fractures.

Liu et al. [34] proposed that subsequent vertebral fractures after PVP reflected the natural progression of osteoporosis; this could explain the association between higher volumes of bone cement and an increased risk of subsequent fracture of adjacent but not distal vertebrae [35]. Syed et al. [36] confirmed that the use of a low volume of cement did not correlate with the distribution of subsequent vertebral fractures or incidence of intervertebral disc leakage. Of clinical importance, the volume of bone cement used plays an important role in improving the kyphotic deformity that results from VCFs of the thoracic spine.

The effects of bone cement on the stress of intervertebral discs have also been a controversial issue. Although bone cement intervertebral disc leakage is an important factor for subsequent fractures, the *in vitro* study by Aquarius et al. [37] indicated that bone cement does not increase peak stress of the lamina terminalis and, thus, would not cause an adverse change in the stress on adjacent vertebrae. However, Zhao et al. [38] indicated that bone cement could induce intervertebral disc degeneration, and both a higher volume of bone cement and longer time lapse since PCP resulted in more severe intervertebral disc degeneration; moreover, their research indicated more severe disc degeneration with the use of polymethyl methacrylate than with calcium phosphate cement.

Our study has several limitations. Foremost is the retrospective design of the study, which prevents an inference of any causality. Second is the limited number of cases of thoracic and lumbar VCFs, which prevented us from including these spinal levels in our analysis. Therefore, our findings are only applicable for thoracolumbar VCFs. Future research is warranted to examine the differential outcomes for thoracic and lumbar VCFs. Regarding our study design, we used a pairwise observation instead of a factor analysis and, thus, the specific effects of the volume of bone cement on measured outcomes require further analysis. Large, multicenter, randomized, controlled trials are needed to provide the necessary evidence regarding the optimal volume of bone cement on the efficacy of PVP for VCFs.

No clear difference between the use of low and high volumes of bone cement on the clinical outcomes of PVP for thoracolumbar VCFs was observed in our study. The volume of bone cement used did not influence the incidence of cement leakage into the intervertebral disc. However, intervertebral disc leakage was identified as a specific risk factor for adjacent vertebral fractures.

5. Conclusions

Both low and high volumes of bone cement effectively relieved pain and promoted early recovery of function in our study. A high volume of bone cement may increase the rate of subsequent total and adjacent vertebral fractures. However, the occurrence of intervertebral disc leakage is the principal risk factor for these negative outcomes of PVP.

Data Availability

The data used to support the findings of this study are included within the article.

Ethical Approval

The present study was approved by Xinhua Hospital, Shanghai Jiaotong University School of Medicine (approval number: XHEC-D-2020-071).

Consent

Written informed consent was obtained from the patients.

Conflicts of Interest

The authors declare that there is no conflict of interest regarding the publication of this paper.

Authors' Contributions

Meng Wang and Bo Li contributed equally to this work.

References

[1] J. Blasco, A. Martinez-Ferrer, J. Macho et al., "Effect of vertebroplasty on pain relief, quality of life, and the incidence of new vertebral fractures: a 12-month randomized follow-up, controlled trial," *Journal of Bone and Mineral Research*, vol. 27, no. 5, pp. 1159–1166, 2012.

[2] R. Rousing, K. L. Hansen, M. O. Andersen, S. M. Jespersen, K. Thomsen, and J. M. Lauritsen, "Twelve-months follow-up in forty-nine patients with acute/semiacute osteoporotic vertebral fractures treated conservatively or with percutaneous Vertebroplasty," *Spine*, vol. 35, no. 5, pp. 478–482, 2010.

[3] C. A. Klazen, P. N. Lohle, J. de Vries et al., "Vertebroplasty versus conservative treatment in acute osteoporotic vertebral compression fractures (Vertos II): an open-label randomised trial," *Lancet*, vol. 376, no. 9746, pp. 1085–1092, 2010.

[4] M. R. Farrokhi, E. Alibai, and Z. Maghami, "Randomized controlled trial of percutaneous vertebroplasty versus optimal medical management for the relief of pain and disability in acute osteoporotic vertebral compression fractures," *Journal of Neurosurgery Spine*, vol. 14, no. 5, pp. 561–569, 2011.

[5] B. S. Kim, B. Hum, J. C. Park, and I. S. Choi, "Retrospective review of procedural parameters and outcomes of percutaneous vertebroplasty in 673 patients," *Interventional Neuroradiology*, vol. 20, no. 5, pp. 564–575, 2014.

[6] F. Omidi-Kashani, E. G. Hasankhani, M. H. Ebrahimzadeh, A. R. Kachooei, M. Hasani, and A. Moradi, "Percutaneous vertebroplasty in Iranian patients with osteoporotic vertebral fractures," *Archives of Bone and Joint Surgery*, vol. 1, no. 1, pp. 9–13, 2013.

[7] W. C. Peh, L. A. Gilula, and D. D. Peck, "Percutaneous vertebroplasty for severe osteoporotic vertebral body compression fractures," *Radiology*, vol. 223, no. 1, pp. 121–126, 2002.

[8] J. K. McGraw, J. A. Lippert, K. D. Minkus, P. M. Rami, T. M. Davis, and R. F. Budzik, "Prospective evaluation of pain relief in 100 patients undergoing percutaneous vertebroplasty: results and follow-up," *Journal of Vascular and Interventional Radiology*, vol. 13, no. 9, pp. 883–886, 2002.

[9] J. D. Barr, M. S. Barr, T. J. Lemley, and R. M. McCann, "Percutaneous vertebroplasty for pain relief and spinal stabilization," *Spine*, vol. 25, no. 8, pp. 923–928, 2000.

[10] U. Berlemann, S. J. Ferguson, L. P. Nolte, and P. F. Heini, "Adjacent vertebral failure after vertebroplasty," *The journal of bone and joint surgery British volume*, vol. 84-B, no. 5, pp. 748–752, 2002.

[11] F. Grados, C. Depriester, G. Cayrolle, N. Hardy, H. Deramond, and P. Fardellone, "Long-term observations of vertebral osteoporotic fractures treated by percutaneous vertebroplasty," *Rheumatology*, vol. 39, no. 12, pp. 1410–1414, 2000.

[12] A. A. Uppin, J. A. Hirsch, L. V. Centenera, B. A. Pfiefer, A. G. Pazianos, and I. S. Choi, "Occurrence of new vertebral body fracture after percutaneous vertebroplasty in patients with osteoporosis," *Radiology*, vol. 226, no. 1, pp. 119–124, 2003.

[13] M. A. Liebschner, W. S. Rosenberg, and T. M. Keaveny, "Effects of bone cement volume and distribution on vertebral stiffness after vertebroplasty," *Spine*, vol. 26, no. 14, pp. 1547–1554, 2001.

[14] S. Molloy, L. H. Riley, and S. M. Belkoff, "Effect of cement volume and placement on mechanical-property restoration resulting from vertebroplasty," *AJNR. American Journal of Neuroradiology*, vol. 26, no. 2, pp. 401–404, 2005.

[15] J. F. Chen, S. T. Lee, T. N. Lui, C. T. Wu, and C. C. Liao, "Percutaneous vertebroplasty for the treatment of osteoporotic vertebral compression fractures: a preliminary report," *Chang Gung Medical Journal*, vol. 25, no. 5, pp. 306–314, 2002.

[16] M. H. Voormolen, P. N. Lohle, L. E. Lampmann et al., "Prospective clinical follow-up after percutaneous vertebroplasty in patients with painful osteoporotic vertebral compression fractures," *Journal of Vascular and Interventional Radiology*, vol. 17, no. 8, pp. 1313–1320, 2006.

[17] K. Kobayashi, K. Shimoyama, K. Nakamura, and K. Murata, "Percutaneous vertebroplasty immediately relieves pain of osteoporotic vertebral compression fractures and prevents prolonged immobilization of patients," *European Radiology*, vol. 15, no. 2, pp. 360–367, 2005.

[18] C. Röder, B. Boszczyk, G. Perler, E. Aghayev, F. Külling, and G. Maestretti, "Cement volume is the most important modifiable predictor for pain relief in BKP: results from SWISSspine, a nationwide registry," *European Spine Journal*, vol. 22, no. 10, pp. 2241–2248, 2013.

[19] Y. J. Jin, S. H. Yoon, K. W. Park et al., "The volumetric analysis of cement in vertebroplasty: relationship with clinical outcome and complications," *Spine*, vol. 36, no. 12, pp. E761–E772, 2011.

[20] S. M. Belkoff, J. M. Mathis, L. E. Jasper, and H. Deramond, "The biomechanics of vertebroplasty," *Spine*, vol. 26, no. 14, pp. 1537–1541, 2001.

[21] Z. Hu, G. Zhao, L. Wang et al., "Related biological research in the interface between bone cement and bone after percutaneous vertebroplasty," *International Journal of Endocrinology*, vol. 2013, Article ID 109784, 7 pages, 2013.

[22] M. J. Nieuwenhuijse, L. Bollen, A. R. van Erkel, and P. D. Dijkstra, "Optimal intravertebral cement volume in percutaneous vertebroplasty for painful osteoporotic vertebral compression fractures," *Spine*, vol. 37, no. 20, pp. 1747–1755, 2012.

[23] J. Luo, L. Daines, A. Charalambous, M. A. Adams, D. J. Annesley-Williams, and P. Dolan, "Vertebroplasty," *Spine*, vol. 34, no. 26, pp. 2865–2873, 2009.

[24] R. Rousing, M. O. Andersen, S. M. Jespersen, K. Thomsen, and J. Lauritsen, "Percutaneous vertebroplasty compared to conservative treatment in patients with painful acute or subacute osteoporotic vertebral fractures," *Spine*, vol. 34, no. 13, pp. 1349–1354, 2009.

[25] R. Buchbinder, R. H. Osborne, P. R. Ebeling et al., "A randomized trial of vertebroplasty for painful osteoporotic vertebral fractures," *The New England Journal of Medicine*, vol. 361, no. 6, pp. 557–568, 2009.

[26] H. K. Wang, K. Lu, C. L. Liang et al., "Comparing clinical outcomes following percutaneous vertebroplasty with conservative therapy for acute osteoporotic vertebral compression fractures," *Pain Medicine*, vol. 11, no. 11, pp. 1659–1665, 2010.

[27] J. Thillainadesan, G. Schlaphoff, K. A. Gibson, G. M. Hassett, and H. P. McNeil, "Long-term outcomes of vertebroplasty for osteoporotic compression fractures," *Journal of Medical Imaging and Radiation Oncology*, vol. 54, no. 4, pp. 307–314, 2010.

[28] L. Alvarez, M. Alcaraz, A. Pérez-Higueras et al., "Percutaneous vertebroplasty: functional improvement in patients with osteoporotic compression fractures," *Spine*, vol. 31, no. 10, pp. 1113–1118, 2006.

[29] D. Chen, Z. Q. An, S. Song, J. F. Tang, and H. Qin, "Percutaneous vertebroplasty compared with conservative treatment in patients with chronic painful osteoporotic spinal fractures," *Journal of Clinical Neuroscience*, vol. 21, no. 3, pp. 473–477, 2014.

[30] K. Chosa, A. Naito, and K. Awai, "Newly developed compression fractures after percutaneous vertebroplasty: comparison with conservative treatment," *Japanese Journal of Radiology*, vol. 29, no. 5, pp. 335–341, 2011.

[31] S. L. Han, S. L. Wan, Q. T. Li et al., "Is vertebroplasty a risk factor for subsequent vertebral fracture, meta-analysis of published evidence?," *Osteoporosis International*, vol. 26, no. 1, pp. 113–122, 2015.

[32] Z. Zhang, J. Fan, Q. Ding, M. Wu, and G. Yin, "Risk factors for new osteoporotic vertebral compression fractures after vertebroplasty," *Journal of Spinal Disorders & Techniques*, vol. 26, no. 4, pp. E150–E157, 2013.

[33] D. G. Lee, C. K. Park, C. J. Park, D. C. Lee, and J. H. Hwang, "Analysis of risk factors causing new symptomatic vertebral compression fractures after percutaneous vertebroplasty for painful osteoporotic vertebral compression fractures: a 4-year follow-up," *Journal of Spinal Disorders & Techniques*, vol. 28, no. 10, pp. E578–E583, 2015.

[34] W. G. Liu, S. C. He, G. Deng et al., "Risk factors for new vertebral fractures after percutaneous vertebroplasty in patients with osteoporosis: a prospective study," *Journal of Vascular and Interventional Radiology*, vol. 23, no. 9, pp. 1143–1149, 2012.

[35] Y. A. Li, C. L. Lin, M. C. Chang, C. L. Liu, T. H. Chen, and S. C. Lai, "Subsequent vertebral fracture after vertebroplasty," *Spine*, vol. 37, no. 3, pp. 179–183, 2012.

[36] M. I. Syed, N. A. Patel, S. Jan, M. S. Harron, K. Morar, and A. Shaikh, "Intradiskal extravasation with low-volume cement filling in percutaneous vertebroplasty," *AJNR. American Journal of Neuroradiology*, vol. 26, no. 9, pp. 2397–2401, 2005.

[37] R. Aquarius, A. M. van der Zijden, J. Homminga, N. Verdonschot, and E. Tanck, "Does bone cement in percutaneous vertebroplasty act as a stress riser?," *Spine*, vol. 38, no. 24, pp. 2092–2097, 2013.

[38] H. Zhao, C. F. Ni, J. Huang et al., "Effects of bone cement on intervertebral disc degeneration," *Experimental and Therapeutic Medicine*, vol. 7, no. 4, pp. 963–969, 2014.

Hindawi

Research Article

Vericiguat Modulates Osteoclast Differentiation and Bone Resorption via a Balance between VASP and NF-*κ*B Pathways

Kaiqiang Sun [iD],[1] **Fanqi Kong** [iD],[1] **Feng Lin** [iD],[2] **Fudong Li** [iD],[1] **Jingchuan Sun** [iD],[1] **Changzhen Ren** [iD],[3] **Bing Zheng** [iD],[1] **and Jiangang Shi** [iD][1]

[1]*Department of Orthopedic Surgery, Spine Center, Changzheng Hospital, Naval Medical University, No. 415 Fengyang Road, Shanghai, 200003, China*
[2]*Department of Orthopedic Surgery, The Affiliated Yantai Yuhuangding Hospital of Qingdao University, Shandong, China*
[3]*Department of General Practice, The 960th Hospital of PLA, Jinan, China*

Correspondence should be addressed to Changzhen Ren; renchangzhen90@163.com, Bing Zheng; 546552786@126.com, and Jiangang Shi; shijiangangspine@163.com

Bone homeostasis has been a dynamic equilibrium between osteoclasts (OCs) and osteoblasts (OBs). However, excessive activation of OCs could disturb the bone homeostasis. As a result, effective medical interventions for patients are greatly demanding. NO/guanylate cyclase (GC)/cGMP signaling cascade has been previously reported to regulate bone metabolism, and GC plays a significantly critical role. Vericiguat, as a novel oral soluble guanylate cyclase (sGC) stimulator, has been firstly reported in 2020 to treat patients with heart failure. Nevertheless, the biological effects of Vericiguat on the function of OCs have not yet been explored. In this present study, we found that Vericiguat with the concentration between 0 and 8 μM was noncytotoxic to bone marrow-derived monocyte-macrophage lineage (BMMs). Vericiguat could enhance the differentiation of OCs at concentration of 500 nM, whereas it inhibited OC differentiation at 8 μM. In addition, Vericiguat also showed dual effects on OC fusion and bone resorption in a dose-dependent manner. Furthermore, a molecular assay suggested that the dual regulatory effects of Vericiguat on OCs were mediated by the bidirectional activation of the IκB-α/NF-κB signaling pathway. Taken together, our present study demonstrated the dual effects of Vericiguat on the formation of functional OCs. The regulatory effects of Vericiguat on OCs were achieved by the bidirectional modulation of the IκB-α/NF-κB signaling pathway, and a potential balance between the IκB-α/NF-κB signaling pathway and sGC/cGMP/VASP may exist.

1. Introduction

Bone tissue consistently undergoes dynamic changes, by means of new bone formation by osteoblasts (OBs) and aging bone elimination by osteoclasts (OCs) [1, 2]. On the contrary, excessive activation of OCs will trigger a disequilibrium between OCs and OBs and thus cause osteolytic bone diseases, such as osteoporosis [3]. Collectively, agents targeting the suppression of the activation of OCs are still clinically demanding.

Osteoclastogenesis is significantly necessary for bone resorption. Normally, OCs are differentiated from bone marrow-derived monocyte-macrophage lineage (BMMs), under the stimulation of macrophage colony-stimulating factor (MCSF) and receptor activator of nuclear factor-κ B ligand (RANKL) [3, 4]. MCSF combined with RANKL will further activate downstream signaling pathways, mitogen-activated protein kinases (MAPK), NF-κB pathways, and PI3K/AKT pathways [5, 6]. Then, the activated pathways can activate nuclear factor of activated T cell cytosolic 1 (NFATc1) and c-Fos. These two factors induce the expression of OC-specific markers, including tartrate resistant acid phosphatase (TRAP), cathepsin K (CTSK), calcitonin receptor (CTR), and dendritic cell-specific transmembrane protein (DC-STAMP) [7]. Thus, mature OCs will produce a tight sealing zone via the formation of F-actin and secrete related enzymes into its sealing zone to accomplish the bone resorption [7]. As a result, agents targeting RANKL/RANK

signaling cascades are effective strategy to treat OC-related bone diseases.

Previous studies have suggested that NO is widely involved in regulating bone metabolism via directly activating guanylate cyclase (GC). Rangaswami et al. ever reported that mechanical stimulation could induce OB proliferation via NO/sGC/cGMP(cGMP) signaling cascades [8]. Furthermore, NO was demonstrated to regulate the mobility and detachment of OCs in a concentration-dependent manner via cGMP [9]. Nevertheless, the activated oxidative stress mediated by NO has limited its clinical application [10]. Therefore, regulating the activity of cellular GC may provide a novel perspective into the treatment of osteoporosis. In fact, animal experiment by Joshua et al. has suggested that treatment with soluble GC (sGC) activators could attenuate estrogen deficiency-induced bone loss [11]. A recent study reported that pharmacologically activating sGC in an NO- or heme-independent manner could be a new therapeutic strategy to suppress cementum loss [12]. Vericiguat, a novel oral soluble guanylate cyclase (sGC) stimulator, has been firstly reported to reduce the death incidence from cardiovascular causes or hospitalization for heart failure patients in 2020 [13, 14]. However, the effects of Vericiguat on the function of OCs remain elusive.

Therefore, this present study was aimed at investigating the biological effects of Vericiguat on OC differentiation and potential molecular mechanisms, which will provide novel reference for future treatment of bone loss-related diseases.

2. Materials and Methods

All animal experiments in this study complied with the ARRIVE guidelines and were carried out in accordance with the National Research Council's Guide for the Care and Use of Laboratory Animals.

2.1. Bone Marrow-Derived Macrophage (BMM) Isolation.
This method has been described in detail in our previous study [15]. Briefly, the whole bone marrow fluid was flushed from the mice femurs and tibias using a sterile 5 ml syringe with complete α-MEM (30 ng/ml M-CSF) and then grown in a T-25 cm^2 flask for 5 days. Adherent cells were BMMs. The harvested BMMs were used for the subsequent experiments.

2.2. Cell Viability Assay.
This method has been described in detail in our previous study [15]. Vericiguat used in this present study was purchased from MedChemExpress (HY-16774). The cytotoxicity of Vericiguat on BMMs was examined by using the CCK-8 assay kit (Dojindo Institute of Biotechnology, Kumamoto, Japan). Briefly, BMMs were seeded in a 96-well plate (4-5 × 10^3 cells/well) for 24 hours. Then, BMMs were added with Vericiguat (0, 10, 20, 50, 100, 200, and 500 nM and 1, 2, 4, 8, and 10 μM) for another 24 hours. Subsequently, BMMs were incubated with 100 μl CCK-8 test solution in a 37°C incubator for 2-3 h. The absorbance was detected at a wavelength of 450 nm.

2.3. OC Differentiation Assay In Vitro.
BMMs were cultured with density of 10000 cells/well in a 96-well plate. RANKL (50 ng/ml) without or with Vericiguat (0, 100 μM, 500 nM, 1 μM, 2 μM, 4 μM, and 8 μM) was added at the second day for 6 d. Recombinant mouse-derived M-CSF and RANKL were purchased from Novoprotein Scientific Inc. (Pudong New District, China). The identification of OC was evaluated by TRAP staining using a tartrate resistant acid phosphatase staining kit (Sigma-Aldrich Institute of Biotechnology, St. Louis, MO, USA). TRAP-positive cells were observed and imaged using light microscopy (Nikon, Tokyo, Japan).

2.4. F-actin Ring Assay and Bone Resorption Pit Assay.
These two methods have been described in detail in our previous study [15]. Briefly, matured OCs were fixed using 4% paraformaldehyde for 10 minutes, followed by permeabilization in 0.1% Triton X-100 for another 10 minutes and then incubation with phalloidin diluted solution (G1028, Servicebio, Wuhan, China) for 2 h in the dark. Nuclei were stained with DAPI staining. The F-actin belt was detected using fluorescence microscopy.

For the bone resorption assay, after BMMs fused, an equal number of fused OCs were transplanted onto Corning Osteo Assay Surface Multiple Well Plate (Corning, Inc., Corning, NY, USA). After OC adhesion, the cells were treated with 0 and 500 nM and 8 μM Vericiguat for 2-3 days. Subsequently, the cells on the plates were eliminated. The percentage of the resorbed region was randomly measured in totally three resorption sites from three independent experiments using ImageJ (National Institutes of Health, Bethesda, MD).

2.5. Real-Time Quantitative PCR (qRT-PCR).
This method has been described in detail in our previous study [15]. Total cellular RNA was harvested using the RNA extraction kit (Magen, Inc., Guangzhou, China). The acquired mRNA was then reversed using HiScript® III RT SuperMix for qPCR Kit (R323-01, Vazyme, Nanjing, China). Subsequently, the mRNA expression levels were detected by qRT-PCR using the SYBR qPCR Master Mix (Q711-02, Vazyme, Nanjing, China). The reaction conditions were reported in our previous study as follows: one cycle at 95°C for 30 s (step 1), followed by 40 cycles at 95°C for 10 s and at 60°C for 30 s (step 2). All experiments were repeated for 3 times, and GAPDH was used as the internal reference. The primer sequences used for qRT-PCR analysis are shown in Table 1.

2.6. Western Blot.
To investigate the effects of Vericiguat on osteoclastogenesis-related signaling pathways, pre-OCs were pretreated with α-MEM (nonserum and M-CSF) for 2 hours followed by Vericiguat (0, 100 nM, 200 nM, 500 nM, 2 μM, and 8 μM) for 3-4 hours, and then, BMM cells were incubated with RANKL (50 ng/ml) for another 30 minutes. In terms of the protein expression level of c-Fos and NFATc1, RANKL (50 ng/ml) with Vericiguat (0, 100 nM, 500 nM, 1 μM, 2 μM, 4 μM, 6 μM, and 8 μM) was added to BMMs for 3 days. In addition, to confirm the effects of Vericiguat

TABLE 1: Primers used for quantitative PCR.

| Targeted gene	Forward (5'-3')	Reverse (3'-5')
GAPDH	TGACCACAGTCCATGCCATC	GACGGACACATTGGGGGTAG
c-Fos	CCAGTCAAGAGCATCAGCAA	AAGTAGTGCAGCCCGGAGTA
NFATc1	CCGTTGCTTCCAGAAAATAACA	TGTGGGATGTGAACTCGGAA
TRAP	CTGGAGTGCACGATGCCAGCGACA	TCCGTGCTCGGCGATGGACCAGA
CTR	TGGTTGAGGTTGTGCCCA	CTCGTGGGTTTGCCTCATC
CTSK	CTTCCAATACGTGCAGCAGA	TCTTCAGGGCTTTCTCGTTC
DC-STAMP	TCCTCCATGAACAAACAGTTCCAA	AGACGTGGTTTAGGAATGCAGCTC
VASP	GTGCGGAAGGAGCTACAGA	AGGCAGGGAAAGCAGGT

(a)

(b)

(c)

(d)

(e)
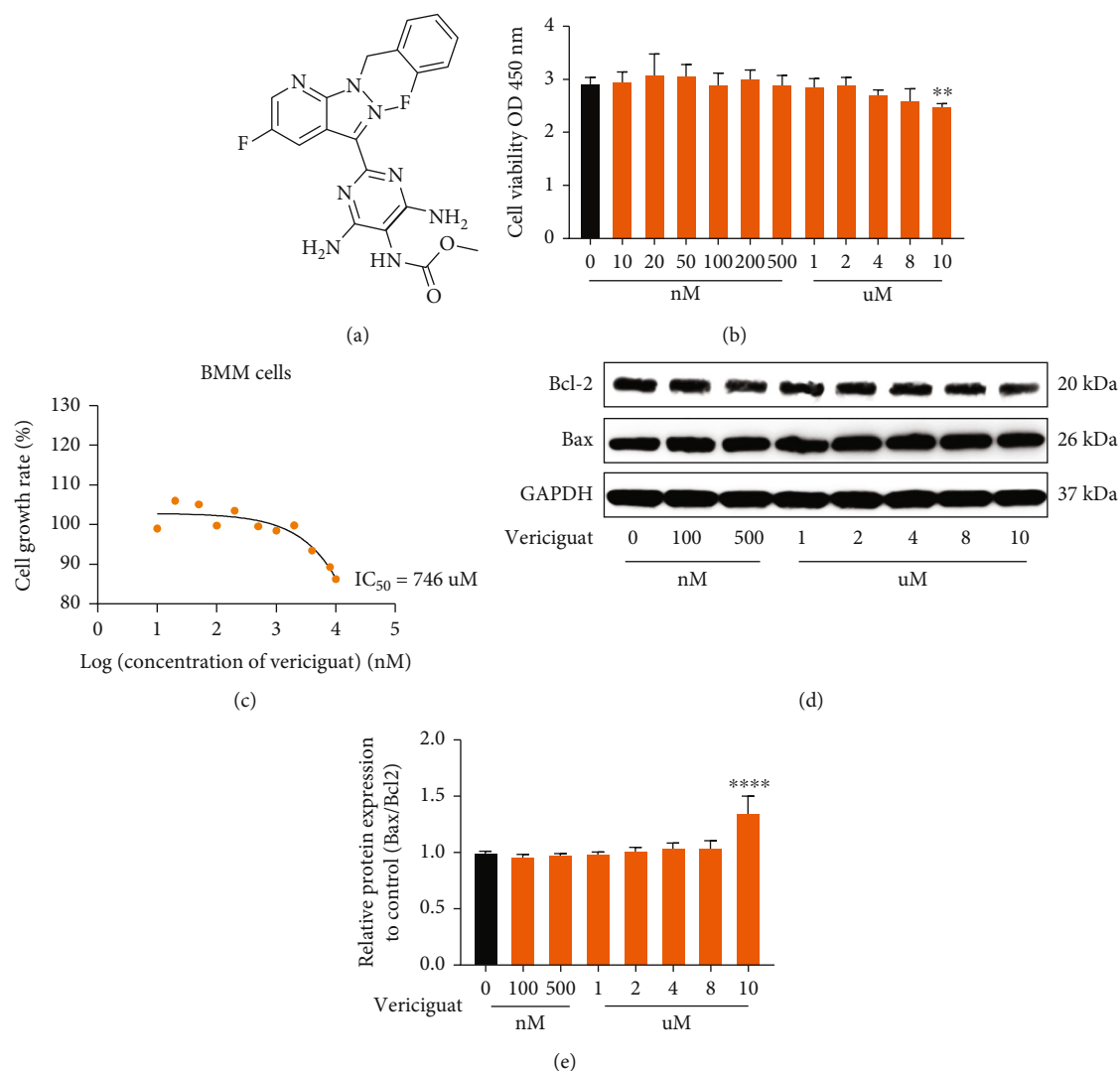
FIGURE 1: Molecular structure and cytotoxicity of Vericiguat on bone marrow-derived monocyte-macrophage lineage (BMMs). (a) Molecular structure of Vericiguat; (b) BMM cell viability as detected by CCK-8 assay after treatment with indicated concentrations of Vericiguat for 24 h. Data are presented as mean ± standard deviation ($n = 5$). (c) The IC_{50} values of Vericiguat against BMMs. (d, e) The effect of Vericiguat on apoptosis-related markers, Bax and Bcl-2, in BMMs and quantitative results ($n = 3$). ∗ indicated a comparison with the control group (0 nM): $^*p < 0.05$, $^{**}p < 0.01$, $^{***}p < 0.001$, and $^{****}p < 0.0001$.
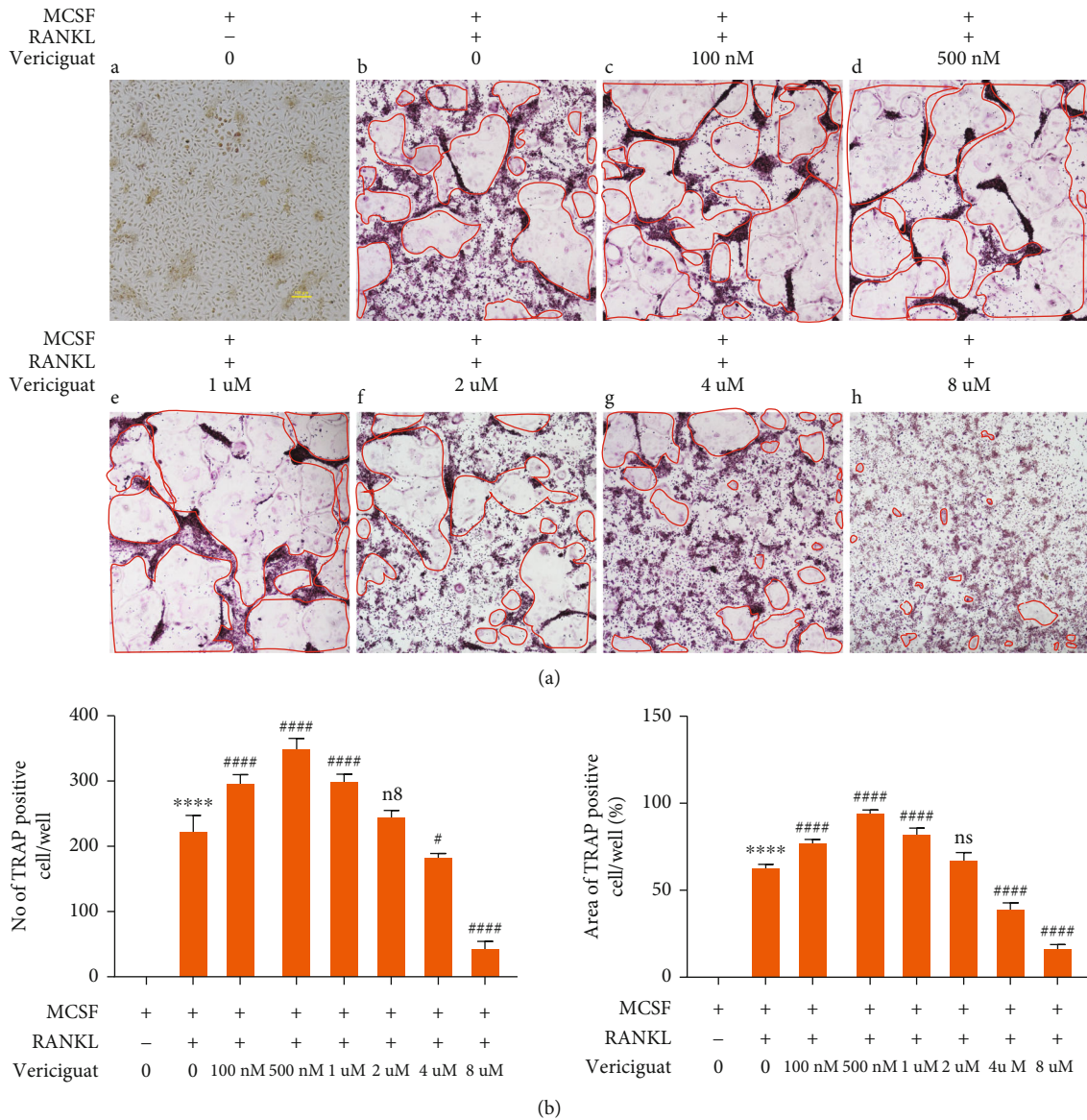
(a)

(b)

FIGURE 2: Vericiguat dually regulated RANKL-triggered osteoclast formation in vitro. (a) Representative images of TRAP-positive osteoclasts (red circles) after stimulation with RANKL and indicated concentrations of Vericiguat ($n = 3$). Image was used as the negative control (BMMS without RANKL). (b) The number and the size of TRAP$^+$ multinucleated osteoclasts were quantified. $n = 3$ means three independent experiments. * indicated a comparison with the control group (without RANKL and Vericiguat): $^*p < 0.05$, $^{**}p < 0.01$, $^{***}p < 0.001$, and $^{****}p < 0.0001$. # indicated a comparison between the group with RANKL only and the group with RANKL and Vericiguat: $^#p < 0.05$, $^{##}p < 0.01$, $^{###}p < 0.001$, and $^{####}p < 0.0001$. ns: not statistically significant. Scar bar = 100 μm.

(500 nM and 8 μM) on the protein expression of NFATc1 and c-Fos, we also evaluated the cytoplasmic and nuclear protein expression of NFATc1 for 0, 2, and 4 days, respectively.

The method of protein extraction has been described in detail in our previous study [15]. Briefly, BMMs were lysed in RIPA on the ice, and the protein amount was quantified using the protein measurement kit (Beyotime Institute of Technology, Shanghai, China). A total of 20-30 μg protein per lane was separated by means of electrophoresis (10% sodium dodecyl sulphate polyacrylamide gel, 80 V, 110 min). Subsequently, the isolated protein bands were transferred onto the polyvinylidene fluoride membrane

(EMD Millipore, Billerica, MA, USA) for 100 minutes, with the voltage of 100 V. Next, blocking was conducted by using 5% nonfat milk (Invitrogen, San Diego, CA, USA) dissolving in Tris-buffered saline-Tween for 3 hours at appropriately 28°C. Then, the PVDF membranes were washed for three times (5 min per time) using TBST. The membranes were then immersed in specific primary antibodies at 4°C for one night. On the second day, the membranes were submerged in the secondary antibodies (goat against rabbit or mouse, 1 : 1000-5000) for 2-3 hours at appropriately 28°C. Finally, the protein bands were captured using the Imaging System (version 5200, Tanon Science & Technology Co., Ltd., Shanghai, China).
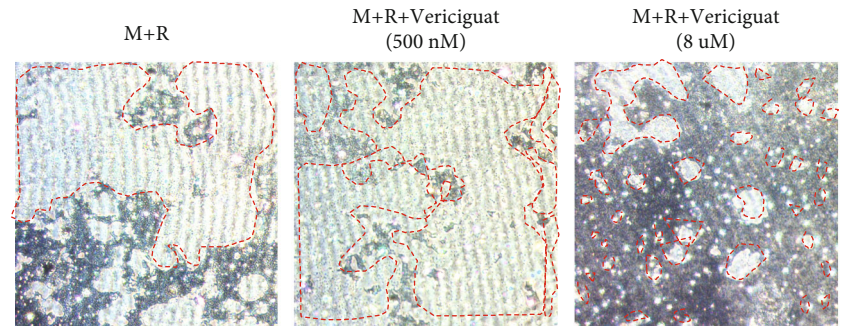
(a)

(b)
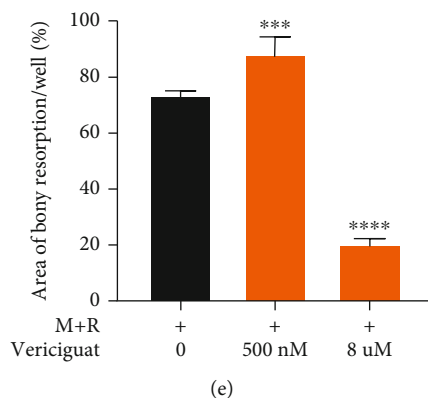

(c)

(d)

Figure 3: Continued.

(e)
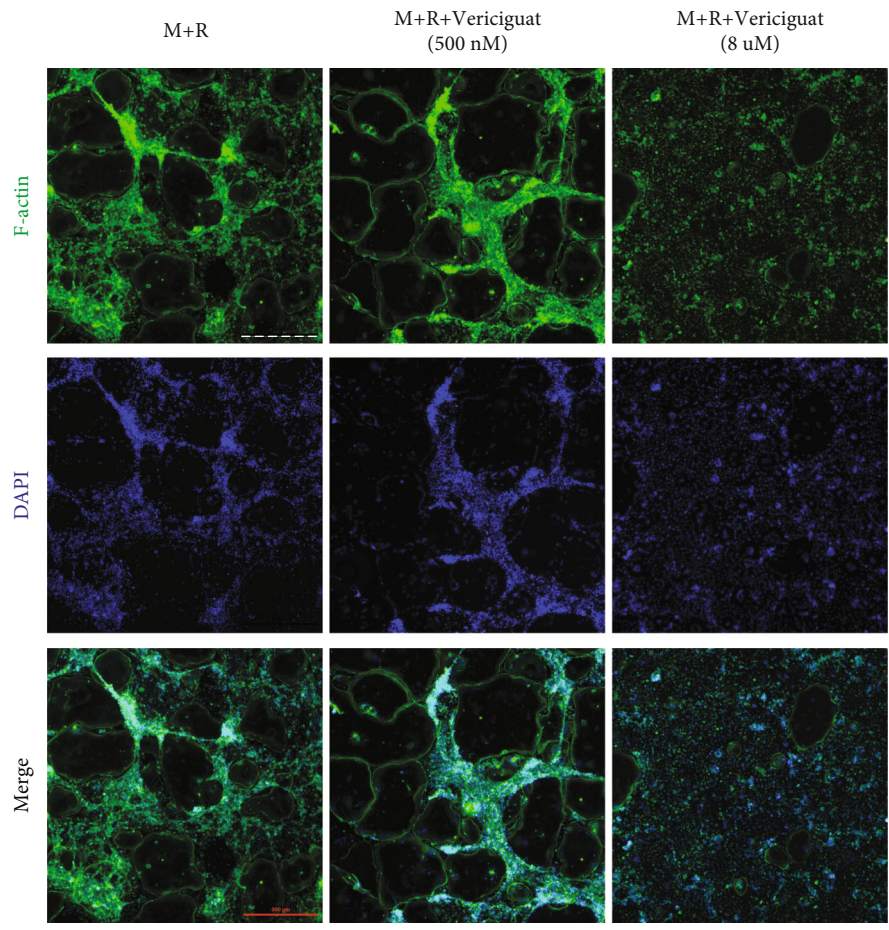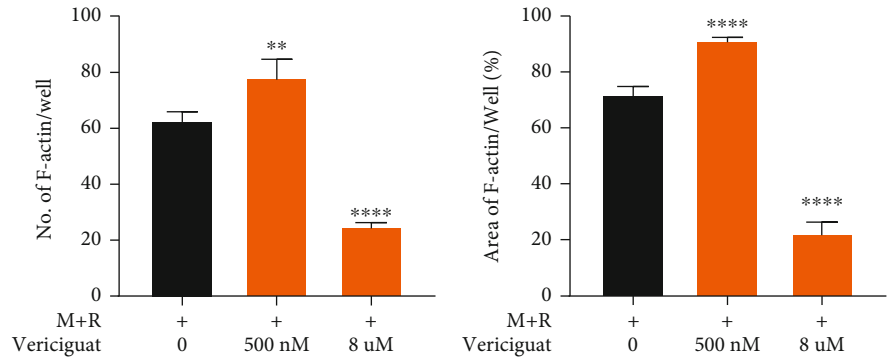
Figure 3: Vericiguat dually regulated the formation of F-actin ring and bony resorption of osteoclasts. (a) Representative images of F-actin-stained osteoclasts under the stimulation of RANKL for 7 d with 500 nM and 8 μM Vericiguat, respectively. (b) The average number and area of F-actin ring (c) ($n = 3$). (d) Representative images of bony resorption (white area circled by a red dotted line) by mature osteoclasts. (e) The bony resorption area was quantified. Values are presented as the mean $\pm$ standard deviation ($n = 3$). $*$ indicated a comparison with the control group (Vericiguat, 0 nM): $*p < 0.05$, $**p < 0.01$, $***p < 0.001$, and $****p < 0.0001$. Scale bar = 500 μm.

Specific primary antibodies in this study mainly included Bax (342772, 17 kDa; Zenbio, Chengdu, China, 1 : 500), Bcl-2 (250198, 26 kDa; Zenbio, Chengdu, China, 1 : 500), NF-κB p65 (D14E12, #8242, Cell Signaling Technology, Inc., 3 Trask Lane, Danvers, USA), p-p65 (Ser536; #3033, Cell Signaling Technology, Inc., 3 Trask Lane, Danvers, USA), Ik-Ba (380682, 35 kDa; Zenbio, Chengdu, China, 1 : 1,000), p-Ik-Ba (340776, 35 kDa; Zenbio, Chengdu, China, 1 : 1,000), ERK1/2 (201245-4A4, 42/44 kDa; Zenbio, Chengdu, China, 1 : 1,000), p-ERK1/2 (301245, 42/44 kDa; Zenbio, Chengdu, China, 1 : 1,000), p38 (200782, 43 kDa; Zenbio, Chengdu, China, 1 : 500), p-p38 (310069, 43 kDa; Zenbio, Chengdu, China, 1 : 1,000), JNK (381100, 46/54 kDa; Zenbio, Chengdu, China, 1 : 1,000), p-JNK (380556, 46/54 kDa; Zenbio, Chengdu, China, 1 : 1,000), c-Fos (9F6, #2250, Cell Signaling Technology, Inc., 3 Trask Lane, Danvers, USA), NFATc1 (#8032; D15F1, Cell Signaling Technology, Inc., 3 Trask Lane, Danvers, USA), AKT (#4691; D15F1, Cell Signaling Technology, Inc., 3 Trask Lane, Danvers, USA), p-AKT (#4060; D15F1, Cell Signaling Technology, Inc., 3 Trask Lane, Danvers, USA), mTOR (380411, 289 kDa; Zenbio, Chengdu, China, 1 : 500), p-mTOR (381548, 289 kDa; Zenbio, Chengdu, China, 1 : 500), GAPDH (#5174, D16H11, Cell Signaling Technology, Inc., 3 Trask Lane, Danvers, USA), and histone H3 (250182, 15 kDa; Zenbio, Chengdu, China, 1 : 1,000).

2.7. Nuclear Translocation of the NF-κB p65 Assay. This method has been described in detail in our previous study [15]. Briefly, BMMs were incubated with α-MEM (without serum and M-CSF) for 2 hours, and then, the wells were added with Vericiguat (0, 500 nM, and 8 μM) for 3 hours, followed by stimulation with or without RANKL (50 ng/ml) for 30 minutes. Subsequently, the BMMs were fixed for 30 minutes using 4% paraformaldehyde and permeabilized for another 30 minutes in 0.1% Triton X-100. Next, cells were immerged in nonfat milk (5%) in PBST for 2-3 hours, followed by incubation with the p65 primary antibody for one night at 4°C. Finally, cells were added with

FITC-conjugated goat anti-rabbit IgG (Servicebio, Wuhan, China) for 50 minutes, and then, the nucleus was stained with DAPI (Sigma; St. Louis, MO, USA) for 5 minutes. Cells were washed three times using PBS and imaged using a laser scanning confocal microscope.

2.8. Transfection of si-VASP. The siRNA of VASP was designed and purchased from GenePharma (Shanghai, China). si-RNA was transfected into cells by means of Lipofectamine 3000 (Thermo Fisher Scientific, USA). The expression of mRNA and protein was evaluated after 24 h and 48 h, respectively. The highest efficiency for knockdown of VASP was as follows: forward (GAGCCAAACUCAGG AAAGUTT) and reverse (ACUUUCCUGAGUUUGGCUC TT).

2.9. Molecular Modeling Experiments. Molecular modeling experiments were performed using the Schrödinger Maestro 9.0 package. Receptor docking (Glide), combined with the protein structure prediction, was used to analyze ligand and receptor flexibility based on the program Prime. In order to prepare protein, the program Protein Preparation Wizard was used to prepare the IKKβ cocrystal structure by means of the Schrödinger Maestro suite prior to performing docking experiments. Water molecules were firstly removed from the crystal structure, followed by adding the hydrogen atoms, and then, the resultant structure was refined using OPLS_2005 force field. The minimization ended with hydrogens. Subsequently, the Receptor Grid Preparation option present in Glide was utilized to produce the protein grid, and the protein grid was subsequently applied to docking experiments. The van der Waals radius scaling factor was set to 1.0 (the partial charge cutoff was 0.25). The ligand was prepared with LigPrep in Maestro 9.0 and the OPLS_2005 force field. Epika was used to produce possible states at target pH 7.00 ± 3.00. Ligand docking options were used in Glide for the first round of docking experiments. In terms of setting, XP (extra precision), "dock flexibly," "sample nitrogen inversions," "sample ring
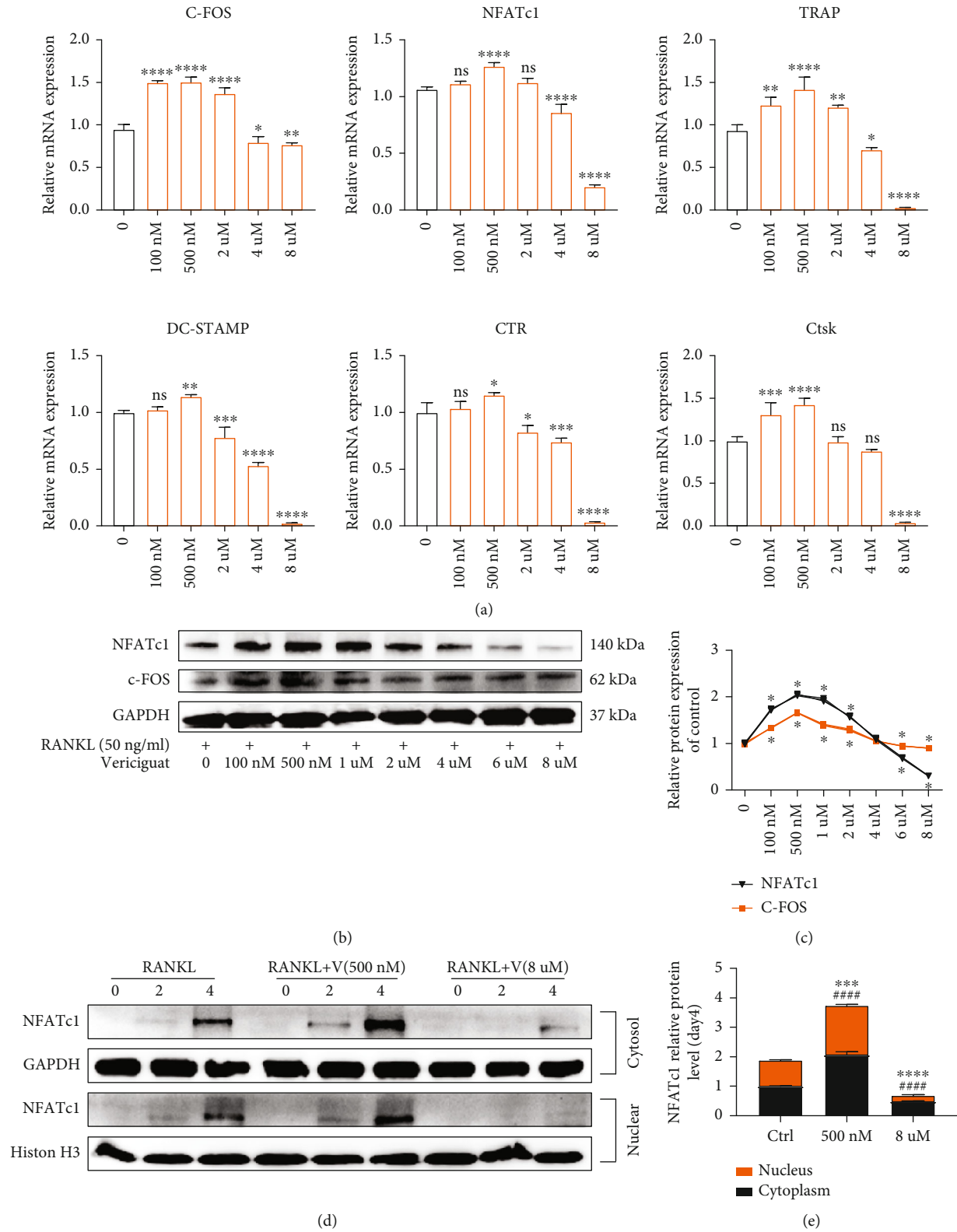
(a)

(b)

(c)

(d)

(e)

FIGURE 4: Continued.

NFATc1/DAPI/Merge

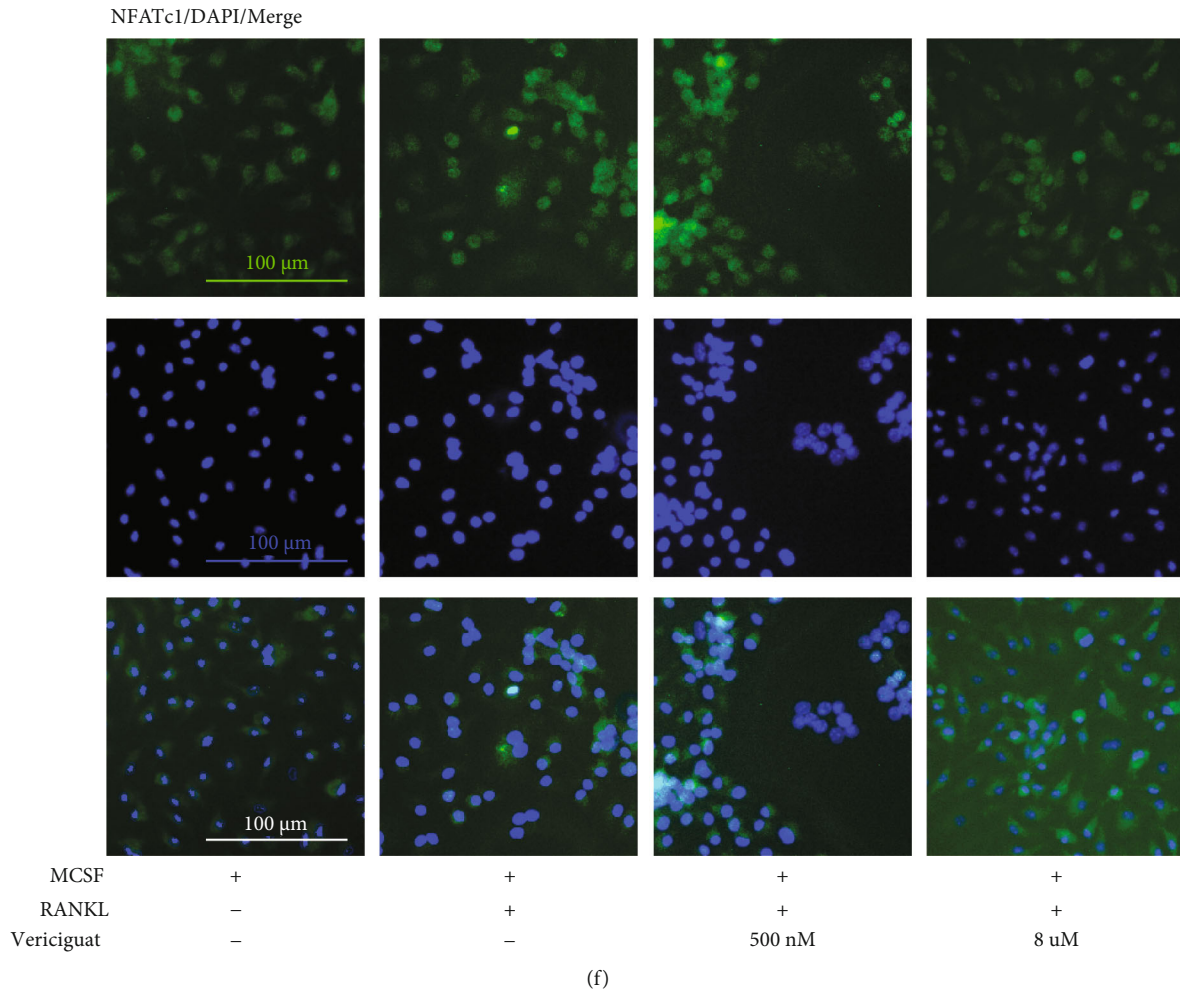| MCSF | + | + | + | + |
| RANKL | − | + | + | + |
| Vericiguat | − | − | 500 nM | 8 uM |

(f)

FIGURE 4: Vericiguat dually regulated RANKL-triggered osteoclast-specific gene expression in osteoclast formation. (a) The relative mRNA expression of osteoclast marker genes (c-Fos, NFATc1, TRAP, CTSK, CTR, and DC-STAMP) in BMMs treated with RANKL+MCSF, as well as indicated concentrations of Vericiguat, for three days was quantified by qRT-PCR ($n = 3$). Values are presented as the mean ± standard deviation. ∗ indicated a comparison with the control group (Vericiguat, 0 nM): $^*p < 0.05$, $^{**}p < 0.01$, $^{***}p < 0.001$, and ∗∗∗ ∗p < 0.0001. (b, c) Western blot analysis results on the protein expression levels of OC-related markers including c-Fos and NFATc1 in BMM cells stimulated with RANKL for 5 d without or with Vericiguat with indicated concentrations and quantitative results ($n = 3$). ∗ indicated a comparison with the control group (Vericiguat, 0 nM): $^*p < 0.05$, $^{**}p < 0.01$, $^{***}p < 0.001$, and $^{****}p < 0.0001$. (d, e) The cytoplasmic and nuclear fractions of the BMMs treated with 30 ng/mL M-CSF, 50 ng/mL RANKL, and Vericiguat (500 nM and 8 μM) for 0, 2, and 4 d, respectively, were analyzed by western blotting and quantitative results. GAPDH and histone H3 were used as nuclear and cytoplasmic loading controls, respectively ($n = 3$). ∗ indicated a comparison with the control group (Vericiguat, 0 nM) regarding the protein expression of NFATc1 within the cytosol at day 4 after stimulation: $^{***}p < 0.001$ and $^{****}p < 0.0001$. # indicated a comparison with the control group (Vericiguat, 0 nM) regarding the protein expression of NFATc1 within the nucleus at day 4 after stimulation: $^{####}p < 0.0001$. (f) Immunofluorescence results of the nuclear translocation of NFATc1 at day 4 after stimulation showed that Vericiguat at low concentration promoted the nuclear translocation of NFATc1, whereas high-concentration Vericiguat suppressed this effect. ns: not statistically significant. Scale bar = 100 μm.

conformation," and "Epik state penalties" were selected to the docking score.

2.10. Establishment of the Ovariectomy- (OVX-) Induced Bone Loss Model In Vivo and Evaluation of the Therapeutic Effects of Vericiguat. This procedure has been reported in our previous study [15]. According to the study design, the C57BL/6 was randomly divided into four groups ($n = 5$): sham group (mock operation with DMSO injection), OVX group (OVX with DMSO injection), low-dose group (OVX with low-dose Vericiguat, 5 μg/kg/day), and high-dose group (OVX with high-dose Vericiguat, 10 μg/kg/day). After ending the experiment, the femurs were collected for microcomputed tomography (micro-CT) analysis [15]. In addition, after μCT analysis, the bone samples were further decalcified in EDTA solution (10%) for another 4 weeks and then embedded in paraffin blocks for subsequent sectioning. Sections were then stained with hematoxylin eosin or TRAP
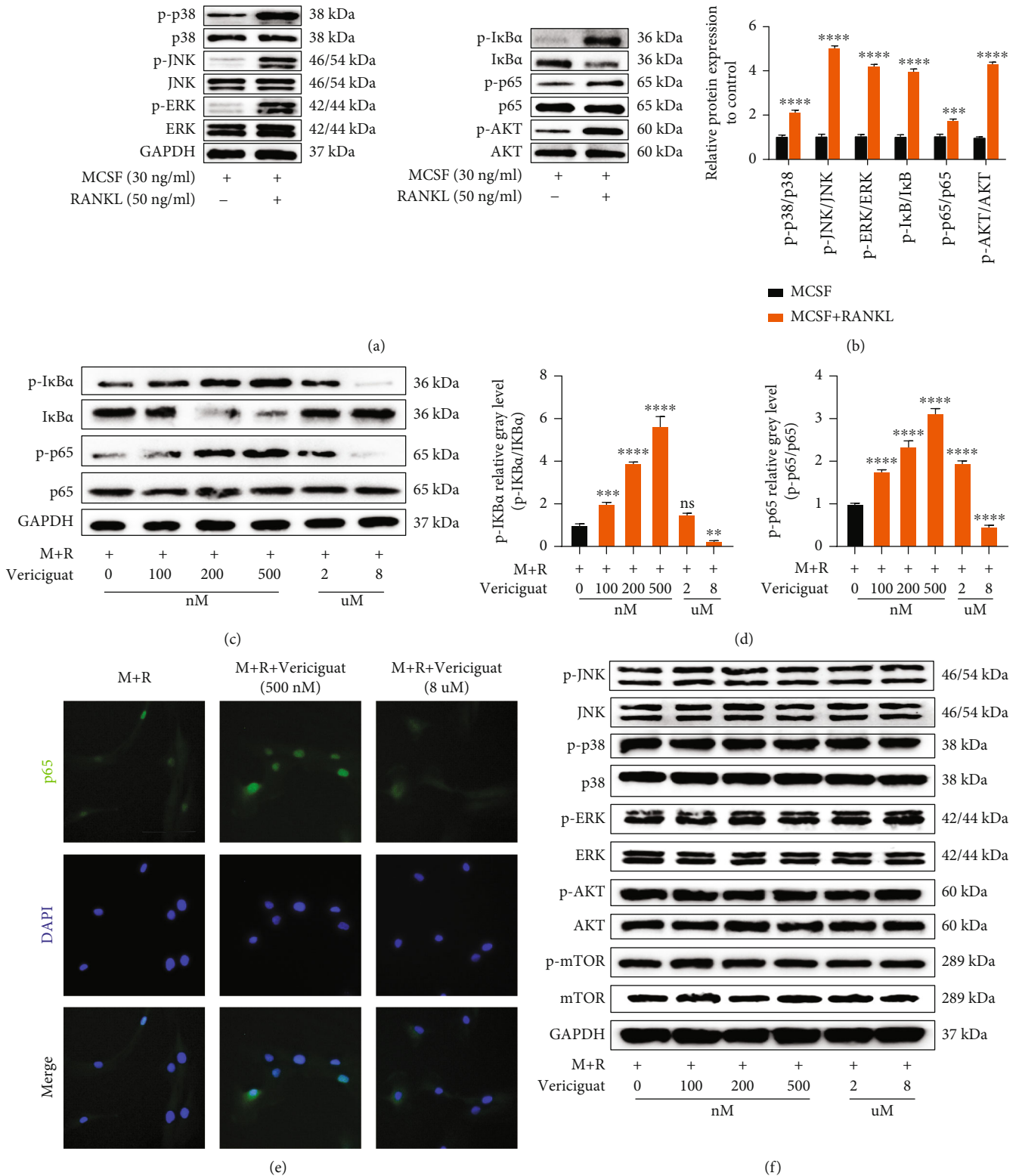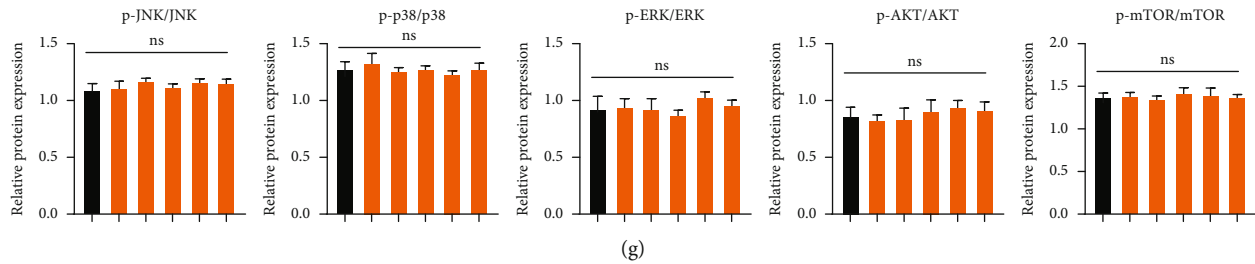
(a)

(b)

(c)

(d)

(e)

(f)

Figure 5: Continued.

(g)

Figure 5: Vericiguat dually regulated RANKL-triggered activation of IκB-α/NF-κB signaling pathway. (a, b) Western blot results of the expression of osteoclast-related signaling pathways (NF-κB, AKT, and MAPK) with or without RANKL stimulation ($n = 3$). ∗ indicated a comparison with the control group without RANKL. (c, d) Western blot results of the expression of IκB-α and NF-κB in BMMs after treatment with RANKL (50 ng/ml) for 30 min followed by Vericiguat with indicated concentrations. (e) Immunofluorescence staining of RANKL-induced P65 nuclear translocation with or without Vericiguat with indicated concentrations. (f, g) Western Blot and quantified results of MAPK and AKT in BMMs after treatment with RANKL (50 ng/ml) for 30 min followed by Vericiguat with indicated concentrations. $n = 3$ means three independent experiments. ∗ indicated a comparison with the control group (Vericiguat, 0 nM): $^*p < 0.05$, $^{**}p < 0.01$, $^{***}p < 0.001$, and $^{****}p < 0.0001$. ns: not statistically significant. Scale bar = 100 μm.

staining. The area and the number of OCs were quantified using the ImageJ software (National Institutes of Health, Bethesda, MD) [15].

3. Statistical Analysis

Statistical analyses were carried out by means of GraphPad Prism 8 (GraphPad Software Inc.; La Jolla, CA). The quantified data were presented as mean ± standard deviation. All experiments were repeated independently at least for three times. One-way analysis of variance (ANOVA) was performed, followed by the Student–Neuman–Keuls as the post hoc test. A p value < 0.05 was considered to indicate statistical difference.

4. Results

4.1. Cytotoxicity Effect of Vericiguat on BMMs. Figure 1 shows the chemical structure of Vericiguat (Figure 1(a)). The cell viability was detected using the CCK-8 viability assay, and we found that Vericiguat below 8 μM showed no cytotoxicity to BMMs, with the IC_{50} being 746 μM (Figures 1(b) and 1(c)). In addition, we evaluated the expression of apoptosis-related markers, Bax and Bcl-2, and found similar results to those of the CCK-8 assay (Figures 1(d) and 1(e)). The results above indicated that the concentration range of Vericiguat between 0 and 8 μM was noncytotoxic to BMMs.

4.2. Dual Effects of Vericiguat on RANKL-Induced Osteoclastogenesis In Vitro. According to the results above, we explored the effects of Vericiguat on RANKL-induced functional OCs in vitro. As shown in Figure 2(a), Vericiguat enhanced differentiation of OCs at concentrations of 100 nM, 500 nM, and 1 μM, but it inhibited differentiation at 4 μM and 8 μM in terms of the number and size of OCs (Figures 2(a) and 2(b)).

These results above indicated that Vericiguat showed dual effects on RANKL-induced osteoclastogenesis in vitro.

4.3. Vericiguat Dually Regulated RANKL-Mediated OC Formation and Bony Resorption in a Concentration-

Dependent Manner. The formation of the F-actin belt has been the most typical feature of mature OCs [15]. As shown in Figure 3, mature OCs have a typical F-actin ring (Figure 3(a)). However, the F-actin belt surrounding the OCs was increased under low concentration of Vericiguat (500 nM) but decreased when the concentration of Vericiguat was high (8 μM) (Figure 3(a)). The number and size of the F-actin belt also showed similar tendency to the FITC-phalloidin staining (Figures 3(b) and 3(c)).

In addition, we explored whether Vericiguat could affect the bony resorption of OCs. BMMs were grown onto the plate (M-CSF 30 ng/ml, RANKL 50 ng/ml) with Vericiguat of different concentrations. As suggested in Figure 3, the area of bone resorption was expanded under Vericiguat at low concentration (500 nM) but decreased when the concentration of Vericiguat was high (8 μM) (Figures 3(d) and 3(e)).

Collectively, Vericiguat showed dual effects on the RANKL-induced formation of the F-actin belt and bony resorption in a concentration-dependent manner.

4.4. Vericiguat Dually Regulated RANKL-Mediated OC Marker Gene Expression during Osteoclastogenesis. After treatment with Vericiguat (0, 100 nM, 500 nM, 2 μM, 4 μM, and 8 μM), the mRNA expression of OC marker genes was markedly upregulated in the low-concentration group (100 nM, 500 nM, and 2 μM) during osteoclastogenesis, including c-Fos, NFATc1, TRAP, DC-STAMP, CTR, and CTSK. On the contrary, the mRNA expression of those genes was significantly downregulated in the high-concentration group (4 μM and 8 μM) (Figure 4(a)).

RANKL leads to the induction and activation of NFATc1 and c-Fos, the two critical factors for osteoclastogenesis [16]. Resultantly, we explored the effects of Vericiguat on the protein expression of these two markers. Western blot results revealed that the expression of these two markers was enhanced at low concentration (100 nM-2 μM) but decreased at high concentration (8 μM), consistent with the results of qRT-PCR above (Figures 4(b) and 4(c)). NFATc1 nuclear translocation exerts a critical role in the regulation of the transcription of OC-related genes, such as DC-STAMP, TRAP, CTR, and CTSK [17]. Western blot
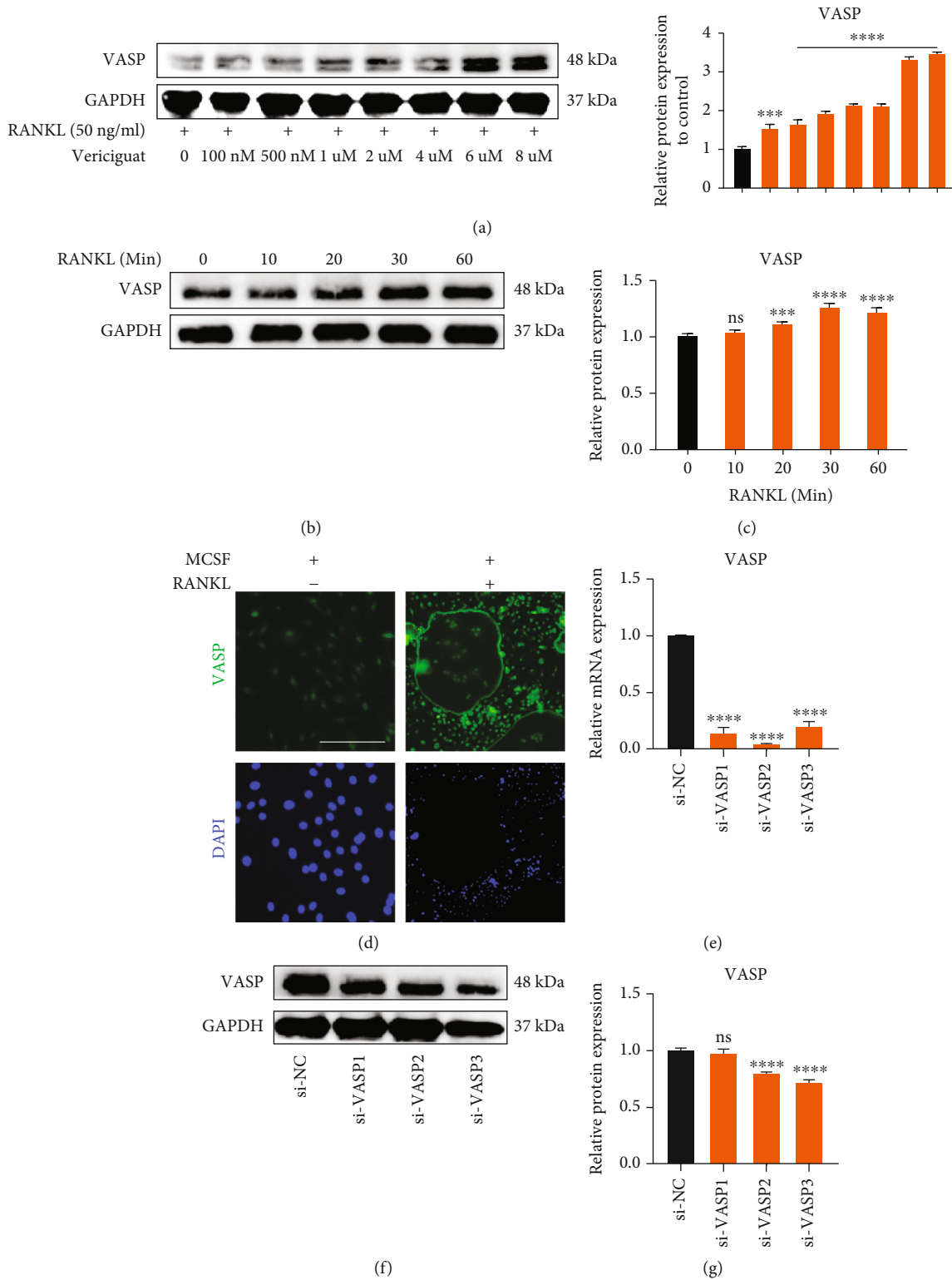
(a)

(b)

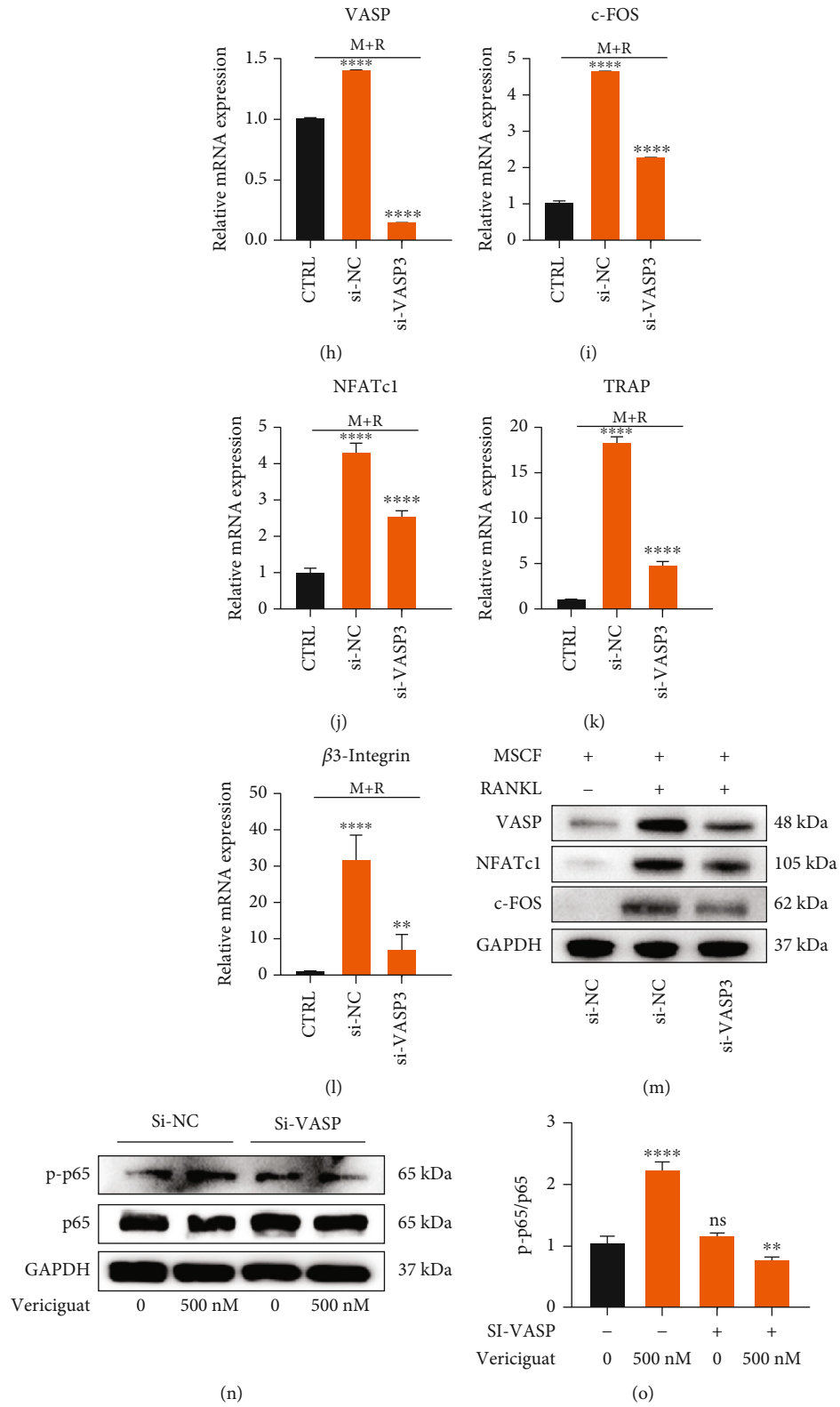(c)

(d)

(e)

(f)

(g)

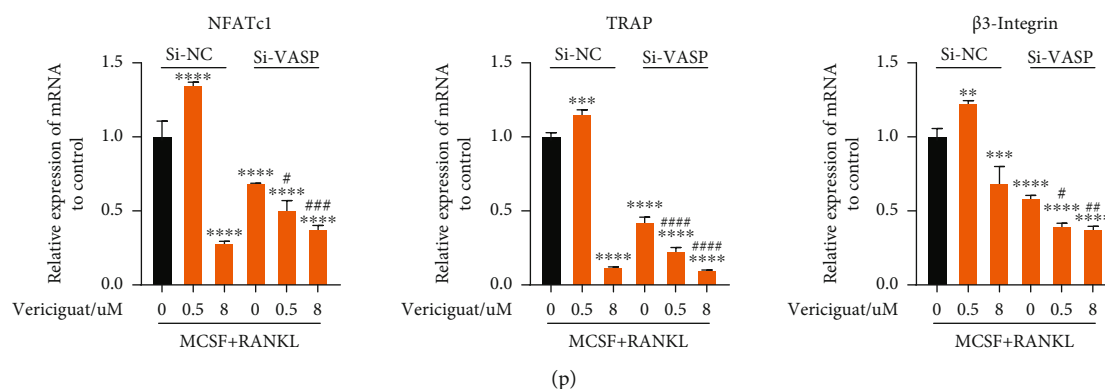FIGURE 6: Continued.

FIGURE 6: Continued.

(p)

FIGURE 6: VASP was essential to osteoclast differentiation, and the expression of VASP could be promoted by Vericiguat. (a) VEGT augmented the expression of VASP in a dosage-dependent manner ($n = 3$). (b, c) RANKL enhanced the expression of VASP in a dosage-dependent manner and quantitative results ($n = 3$). ∗ indicated a comparison with the control group without RANKL. (d) Immunofluorescence position of VASP in BMMs with or without RANKL. (e) The mRNA expression of VASP in BMMs after treatment with siRNA ($n = 3$); ∗ indicated a comparison with the control group (si-NC). (f, g) The protein expression of VASP in BMMs after treatment with siRNA and quantitative results ($n = 3$). ∗ indicated a comparison with the control group (si-NC). (h–l) The mRNA expression of OC-related genes in BMMs after treatment with siRNA ($n = 3$). ∗ indicated a comparison with the control group: $^*p < 0.05$, $^{**}p < 0.01$, $^{***}p < 0.001$, and $^{****}p < 0.0001$. # indicated a comparison between the group with si-VASP and the group with si-NC: $^\#p < 0.05$, $^{\#\#}p < 0.01$, $^{\#\#\#}p < 0.001$, and $^{\#\#\#\#}p < 0.0001$. (m) The protein expression of osteoclast-related genes in BMMs after treatment with siRNA and quantitative results ($n = 3$). (n, o) The expression of NF-κB protein in BMMs with or without siRNA-VASP treated with Vericiguat only ($n = 3$). (p) The mRNA expression of osteoclast-related genes (NFATc1, TRAP, and β3-Integrin) in siRNA-VASP-induced BMMs compared with siRNA-NC-induced BMMs ($n = 3$); ∗ indicated a comparison with the control group (Vericiguat, 0 nM) in the siRNA-NC group and si-VASP group, respectively: $^*p < 0.05$, $^{**}p < 0.01$, $^{***}p < 0.001$, and $^{****}p < 0.0001$. # indicated a comparison between the siNC-induced group and si-VASP-induced group at the same concentration of Vericiguat: $^\#p < 0.05$, $^{\#\#}p < 0.01$, $^{\#\#\#}p < 0.001$, and $^{\#\#\#\#}p < 0.0001$. Scale bar = 100 μm.

suggested that RANKL triggered NFATc1 translocation into the nucleus during OC differentiation in a time-dependent manner (Figures 4(d) and 4(e)). Vericiguat promoted the RANKL-induced nuclear translocation of NFATc1 in the low-concentration group (500 nM), whereas this effect was inhibited in the high-concentration group (8 μM) (Figures 4(d) and 4(e)). Immunofluorescence results of the nuclear translocation of NFATc1 at day 4 after stimulation showed similar tendency to the results of Western blot (Figure 4(f)).

Therefore, these results confirmed the dual effects of Vericiguat on RANKL-induced osteoclastogenesis in vitro.

4.5. Vericiguat Dually Regulated RANKL-Induced Activation of the NF-κB Signaling Cascade. As shown in Figure 5, RANKL significantly induced the activation of the NF-κB signaling pathway, MAPK signaling pathways (p38, JNK, and ERK), and AKT signaling pathway (Figures 5(a) and 5(b)). To identify the changes of those signaling pathways during OC development after stimulation with Vericiguat, we examined the activation of those critical pathways. As demonstrated in Figure 5, the activation of the IκB-α/p65 signaling pathway was dually regulated by Vericiguat in a concentration-dependent manner. The phosphorylation of IκB-α and p65 was enhanced in the low-concentration group (100 nM-2 μM) but decreased at high concentration (8 μM) (Figures 5(c) and 5(d)). In addition, the early nucleus translocation of p65 after RANKL stimulation with or without Vericiguat as determined by the immune-fluorescent staining suggested an increasing trend at low concentration and

a decreasing trend at high concentration (Figure 5(e)). However, the MAPK (p38, JNK, and ERK) signaling pathway and AKT signaling pathway were not affected by Vericiguat stimulation (Figures 5(f) and 5(g)).

Taken together, the results above suggested that Vericiguat was involved in OC differentiation via dually regulating the activation of the IκB-α/NF-κB signaling pathway.

4.6. VASP Was Essential to OC Differentiation, and the Expression of VASP Could Be Promoted by Vericiguat. The activated sGC would excessively induce the activation of the VASP (vasodilator-stimulated phosphoprotein) [18]. Therefore, we evaluated the expression of VASP in BMMs and found the increasing expression of VASP induced by a dose-dependent manner of Vericiguat with RANKL (Figure 6(a)). In order to investigate the potential dually regulative effects of Vericiguat on OC differentiation, we firstly evaluated the expression of VASP in BMMs induced by RANKL and found that RANKL could dose-dependently increase the expression of VASP (Figures 6(b) and 6(c)). In addition, mature OC also highly expressed VASP, and VASP protein was primarily distributed surrounding the cell membrane (Figure 6(d)). However, OC differentiation was significantly disturbed after silencing the expression of VASP via siRNA in BMMs, as shown by downregulated expression of OC-related marker genes (c-FOS, NFATc1, TRAP, and β3-integrin) (Figures 6(e)–6(m)). The results above suggested that VASP was essential to OC differentiation. However, the promotive effect of Vericiguat only on the amount of p-p65 was blocked by the silencing of VASP (Figures 6(n)
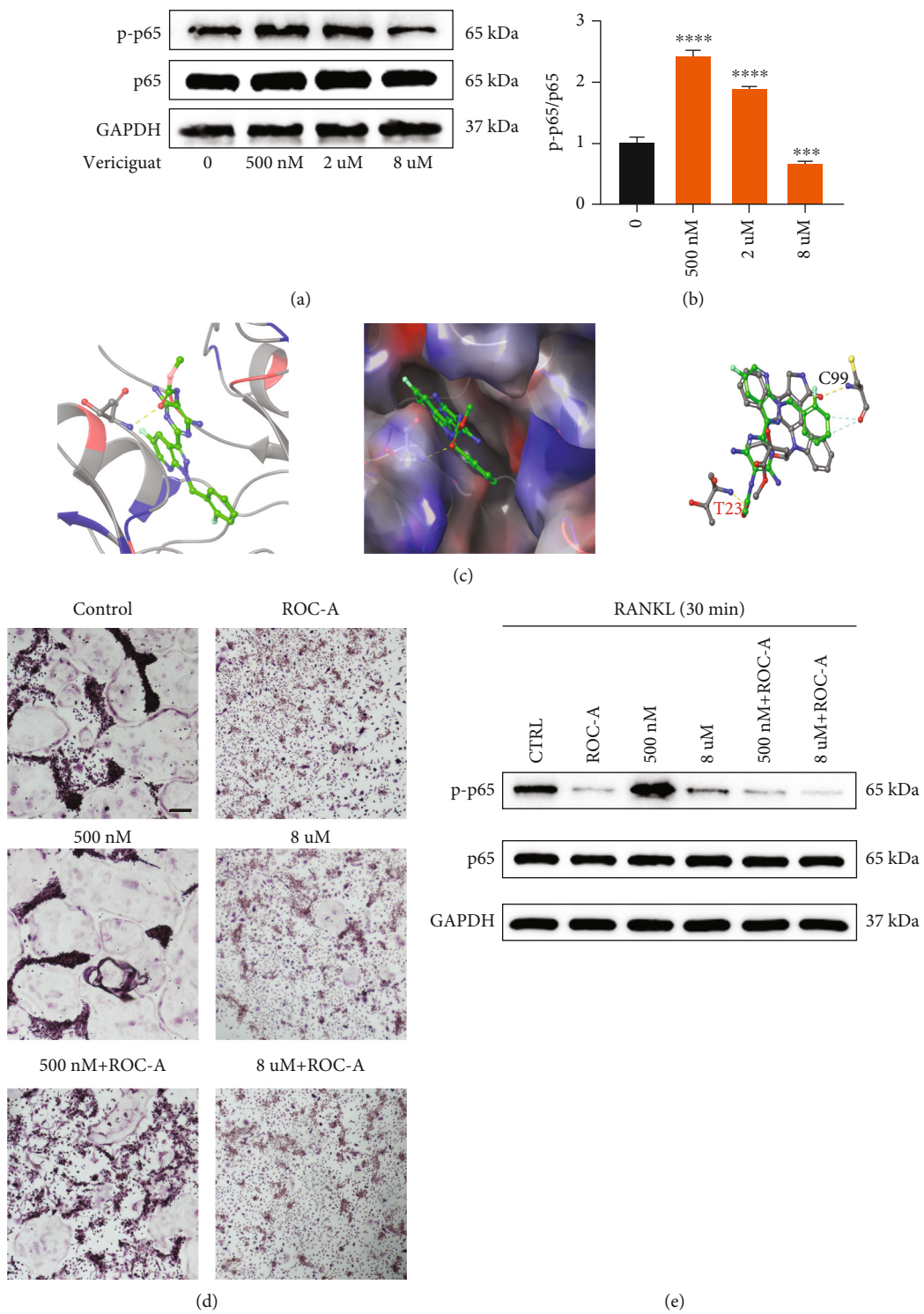
(a)

(b)

(c)
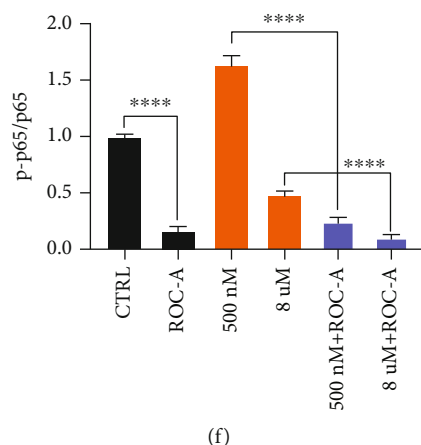

(d)

(e)

Figure 7: Continued.

(f)

FIGURE 7: Dual effects of Vericiguat on osteoclast differentiation and bone resorption via a balance between VASP and NF-κB. (a, b) The expression of NF-κB protein in BMMs treated with Vericiguat only ($n = 3$). $*$ indicated a comparison with the control group (Vericiguat, 0 nM). (c) (A) The predicted optimal binding manner of Vericiguat at the ATP binding site of IKKβ protein; hydrogen bonds (yellow lines). (B) MOLCAD representation showed the molecular lipophilic potential surface upon the bioactive pose of Vericiguat at the ATP binding site of IKKβ. The blue represented hydrophilic, red represented lipophilic, and gray represented neutral moiety. Hydrogen bonds were displayed as yellow lines. (C) The overlap analysis of Vericiguat and the ligand of IKKβ and the participating amino acid residue (Thr23) were marked. (d) TRAP staining of RANKL-induced BMMs treated with Vericiguat with or without the NF-κB inhibitor ROC-A. (e, f) The expression of NF-κB in RANKL-induced BMMs treated with Vericiguat with or without the NF-κB inhibitor ROC-A. Scale bar = 500 μm.

and 6(o)). Notably, in the presence of MCSF and RANKL, after silencing of VASP, the promotive effect of Vericiguat (500 μM) on OC differentiation was also blocked, whereas the suppressive effect of Vericiguat (8 μM) on osteoclast differentiation was enhanced (Figure 6(p)). The results above suggested that VASP could mediate the promotive effect of Vericiguat on the phosphorylation of p65 under low concentration with or without the presence of MCSF and RANKL.

4.7. Dual Bioeffects of Vericiguat on OC Formation and Bony Resorption via a Balance between VASP and NF-κB. However, the inhibitory effect of high-dose Vericiguat on OC differentiation remains unclear. Further, we explored the expression of the NF-κB signaling cascade in BMMs treated with Vericiguat only and found that Vericiguat could also dually regulate the activation of NF-κB without MCSF and RANKL (Figures 7(a) and 7(b)). Regarding the repressive effect of Vericiguat on OC differentiation at high concentration, we deduced that high-dose Vericiguat may directly disturb the activation of the NF-κB signaling cascade. Therefore, we introduced molecular modeling experiments and found that Vericiguat possessed similar molecular structure to the ligand of IKKβ and could directly bind to the ATP binding pocket of the IKKβ kinase domain function via hydrogen bond. However, the binding site was Thr23, but not the activated site, Cys99, which may be the reason for the inhibitory effect of Vericiguat on OC differentiation at high concentration (Figure 7(c)). In addition, blocking the activation of p65 could also disturb the promotive effect of Vericiguat on OC differentiation and enhance the suppressive effect of Vericiguat on OC differentiation (Figures 7(e) and 7(f)). Here, we hypothesized that Vericiguat may regulate OC differentiation via VASP/NF-κB signaling crosstalk.

Taken together, at low concentration, Vericiguat dominantly showed promotive effect on OC differentiation via the VASP/NF-κB signaling axis, whereas at high concentration, the increased binding of Vericiguat to IKKβ kinase would result in the deactivation of p65 and inhibit OC differentiation (Figure 8).

4.8. Validation of the Effects of Vericiguat on OVX-Induced Bone Loss In Vivo. As shown in Figure 9, the micro-CT results of BMD, BS/BV, BV/TV, Tb.N, Tb.Th, and Tb.Sp suggested that OVX mice exhibited obvious loss of trabecular bone, whereas this effect was restored by Vericiguat administration, either low or high dose (Figures 9(a) and 9(b)). However, the promotive effect of low-concentration Vericiguat on OC differentiation in vitro was not consistent with results in vivo. We deduced that there may be two reasons. Firstly, the low and high concentrations of Vericiguat in vitro cannot be considered equal to low and high doses in vivo. Secondly, cinaciguat, the same kind of Vericiguat, has been reported to promote OB differentiation and improve OVX-mediated bone loss [11]. Therefore, the proosteogenic effect of Vericiguat may in part offset the probony resorption at low concentration. Analysis of cortical bone parameters, BMD, BV/TV, Ct.th, Ct.Ar, Th.Ar, and Ct.Ar/Th.Ar, showed that OVX decreased the amount of cortical bone, whereas Vericiguat, especially at high doses, ameliorates the effect caused by OVX compared to the OVX group and sham group (Figures 9(c) and 9(d)). Collectively, the bioeffects of Vericiguat in vitro cannot be equal to those in vivo due to complex body environment.

As to histological analysis, H&E staining of the collected femurs suggested that the area of trabecular bone was markedly reduced in OVX mice, whereas mice treated with Vericiguat showed marked improvement of the trabecular bone
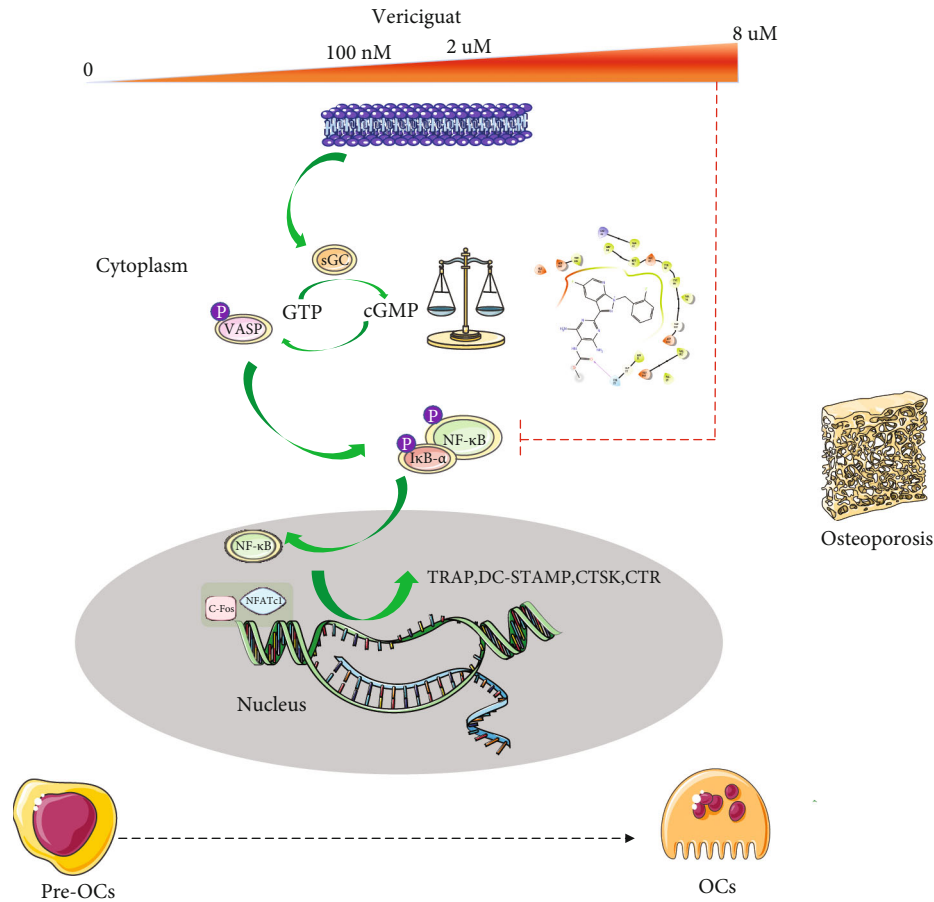
FIGURE 8: Dual effect of Vericiguat on RANKL-induced osteoclastogenesis and molecular mechanism. There may be a potential balance between the IκB-α/NF-κB signaling pathway and sGC/cGMP/VASP in BMMs. Vericiguat at low doses (0-2 μmol/l) enhanced RANKL-induced osteoclastogenesis dominantly through upregulation of the VASP/IκB-α/NF-κB signaling pathway, whereas Vericiguat at high doses (4 or 8 μmol/L) suppressed RANKL-induced osteoclastogenesis through directly inhibiting the IκB-α/NF-κB signaling pathway signaling cascade, which could disturb VASP-mediated activation of the IκB-α/NF-κB signaling pathway.

area (Figure 10(a)). TRAP staining showed obvious enhancement in the total number and area of TRAP$^+$ OCs along the trabecular bone in OVX mice, whereas Vericiguat decreased the area and the number of TRAP$^+$ OCs per bone surface area (Figure 10(b)).

5. Discussion

Excessive activation of OCs may contribute to various OC-related diseases, such as rheumatoid arthritis and osteoporosis [19–22]. Thus, timely medical therapy targeting OCs is necessary for treating OC-related diseases [23, 24]. This present study firstly showed that Vericiguat dually regulated OC differentiation and bony resorption in mouse BMMs via bidirectionally affecting the activation of the IκB-α/NF-κB signaling pathway and nuclear translocation of NFATc1 in a dose-dependent manner. In fact, there are plentiful agents reported to possess dual effects according to concentration [25]. For OCs, baicalin has been reported to exert dual effects on OC formation in a concentration-dependent manner [26]. Compounds with dual effects have important clinical applications. Consequently, analyzing the effects of

Vericiguat on the differentiation of OCs may deepen our understanding of the relationship between the pharmacological effects and dosage of Vericiguat on bone metabolism and also provide some medical references for future clinical application of Vericiguat to cardiovascular diseases.

The NO/GC/cGMP signaling cascade has been widely reported in regulating bone metabolism, and GC plays a significantly critical role [27, 28]. However, there exists controversy regarding the effect of NO/GC/cGMP on OCs [27–30]. Yaroslavskiy et al. ever reported NO-stimulated OC motility at low concentration, whereas at high concentrations, NO caused OC detachment and terminated resorption. And this effect was accomplished via the GC/cGMP/VASP cascade [9]. Another study from Joshua's team reported that cinaciguat (BAY 58–2667), a prototype of direct sGC activators, could reverse OVX-induced osteocyte apoptosis as efficiently as estradiol and promoted bone formation in vivo [11]. However, they found that the antiosteoporosis by cinaciguat was associated with enhancing function of OB, but not with the changes of OCs [11]. Nevertheless, Homer et al. found that oral administration of the sGC agonist could increase the number of OCs and bone resorption in the axial skeleton
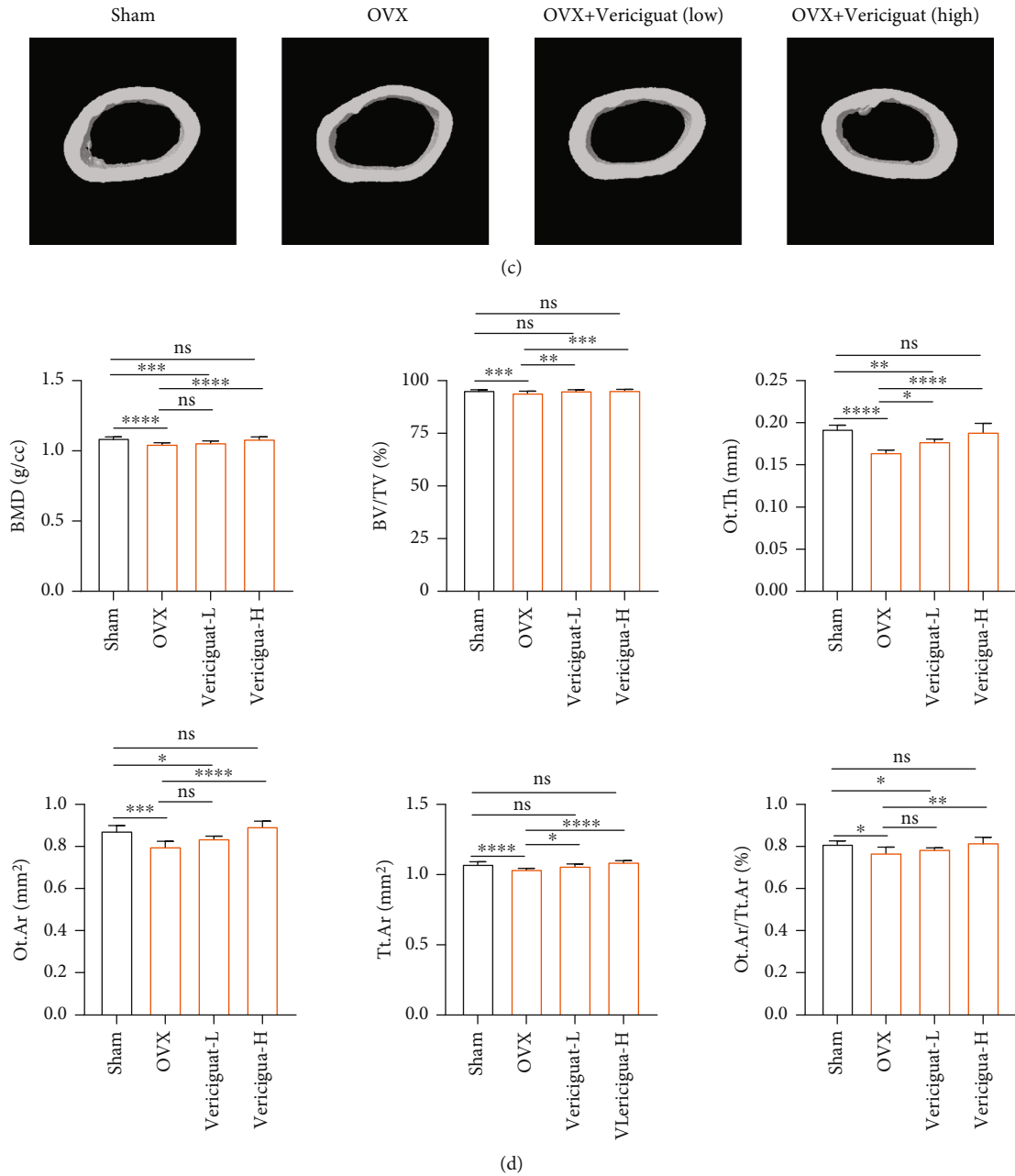
(a)

(b)

Figure 9: Continued.

(c)
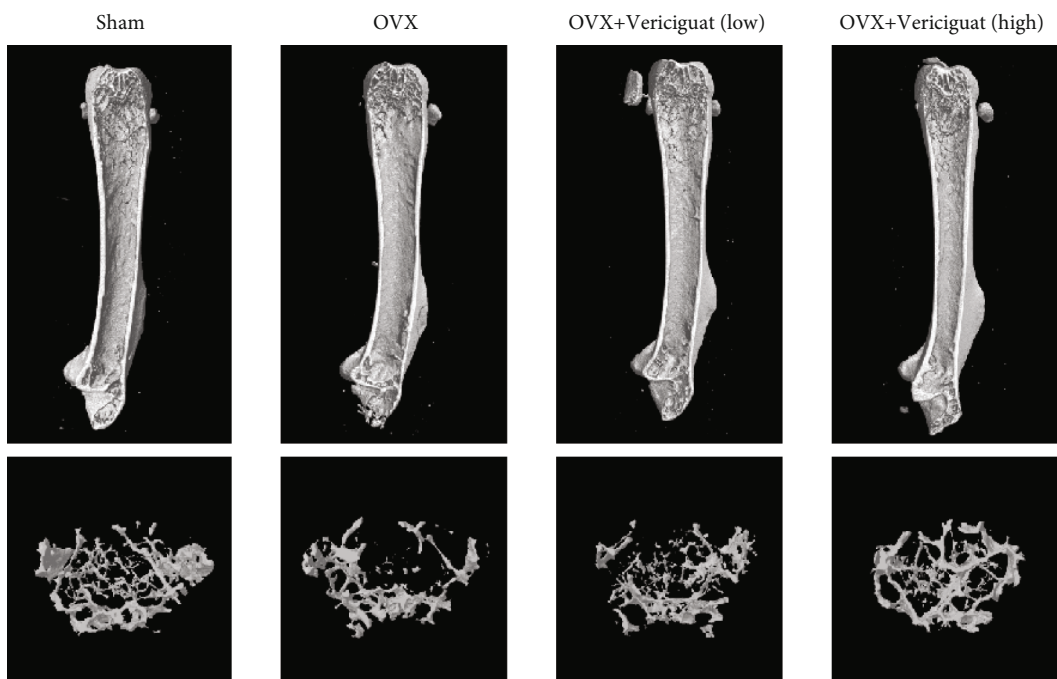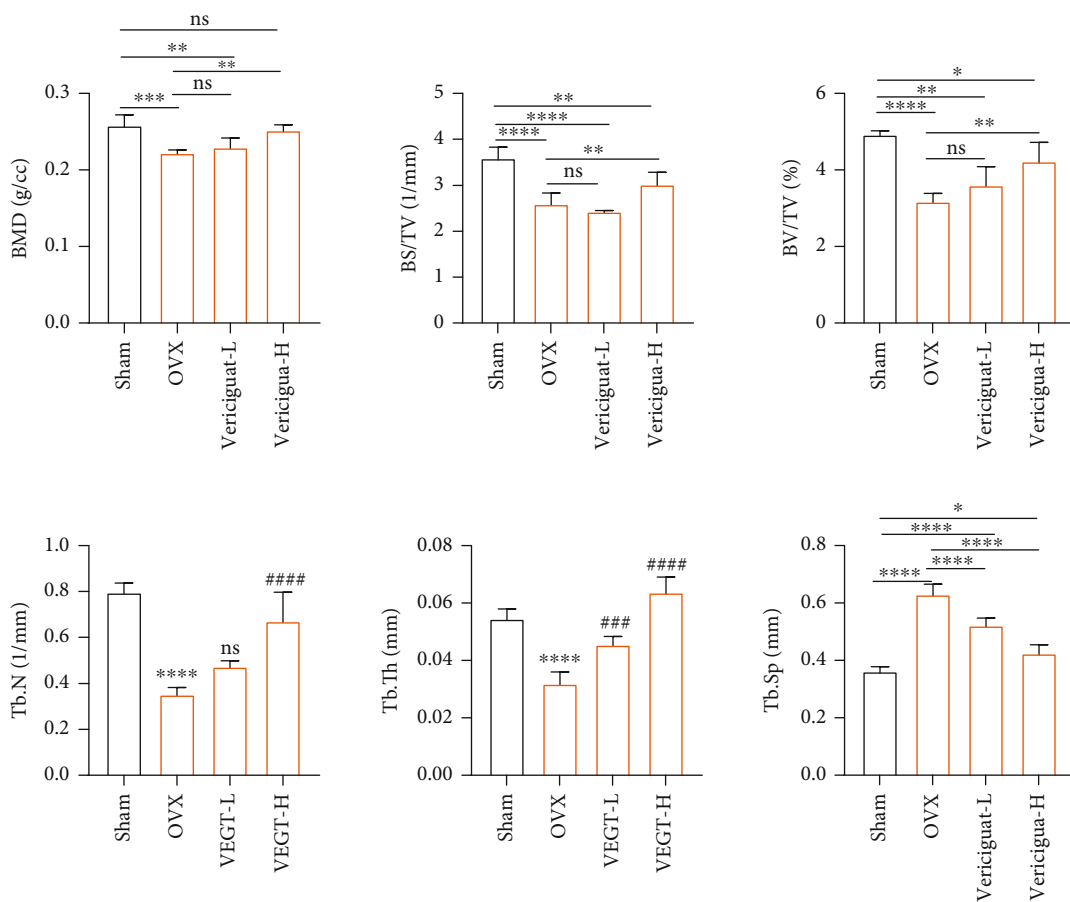
(d)

FIGURE 9: Validation of the effects of Vericiguat on OVX-induced bone loss in vivo indicated by microstructure analysis. (a) Representative 3-dimensional images of μCT for mouse femur from the sham group (mock operation with DMSO injection), OVX group (OVX with DMSO injection), low-dose group (OVX with low-dose Vericiguat, $5\,\mu$g/kg/day), and high-dose group (OVX with high-dose Vericiguat, $10\,\mu$g/kg/day) ($n = 5$). (b) Quantitative results of bone structural parameters, including trabecular bone mineral density (BMD, g/cc), bone surface area/total volume (BS/TV; %), bone volume/total volume (BV/TV; mm^{-1}), trabecular number (Tb.N; mm^{-1}), trabecular spacing (Tb.Sp; mm), and trabecular thickness (Tb.Th; mm) within the selected metaphyseal region ($n = 5$). (c) Representative 3-dimensional images of μCT for the mouse femur (cortical bone) from different groups above. (d) Quantitative results of bone structural parameters, including cortical bone mineral density (BMD; g/cc), bone volume/total volume (BV/TV; mm^{-1}), total cross-sectional area inside the periosteal envelope (Tt.Ar; mm^2), cortical bone area (Ct.Ar; mm^2), cortical area fraction (Ct.Ar/Tt. Ar; %), and average cortical thickness (Ct.Th; mm). $*$ indicated a comparison with the sham group: $***p < 0.001$ and $****p < 0.0001$. # indicated a comparison between the VEGT-L/H group and OVX group at the same concentration of Vericiguat: $^{\#\#}p < 0.01$, $^{\#\#\#}p < 0.001$, and $^{\#\#\#\#}p < 0.0001$. ns: not statistically significant.

of Sprague-Dawley rats [31]. In fact, after careful studying the figures presented in Joshua's research, we found the decreased tendency regarding the number of OCs and eroded surface in the OVX$^+$ cinaciguat group compared to the OVX group, although they demonstrated no statistical difference. Firstly, we deduced that the dose used in their mouse model ($10\,\mu$g/kg/day) may not reach the key point. In fact, the dose could be $10\,$mg/kg/day in animals [32].
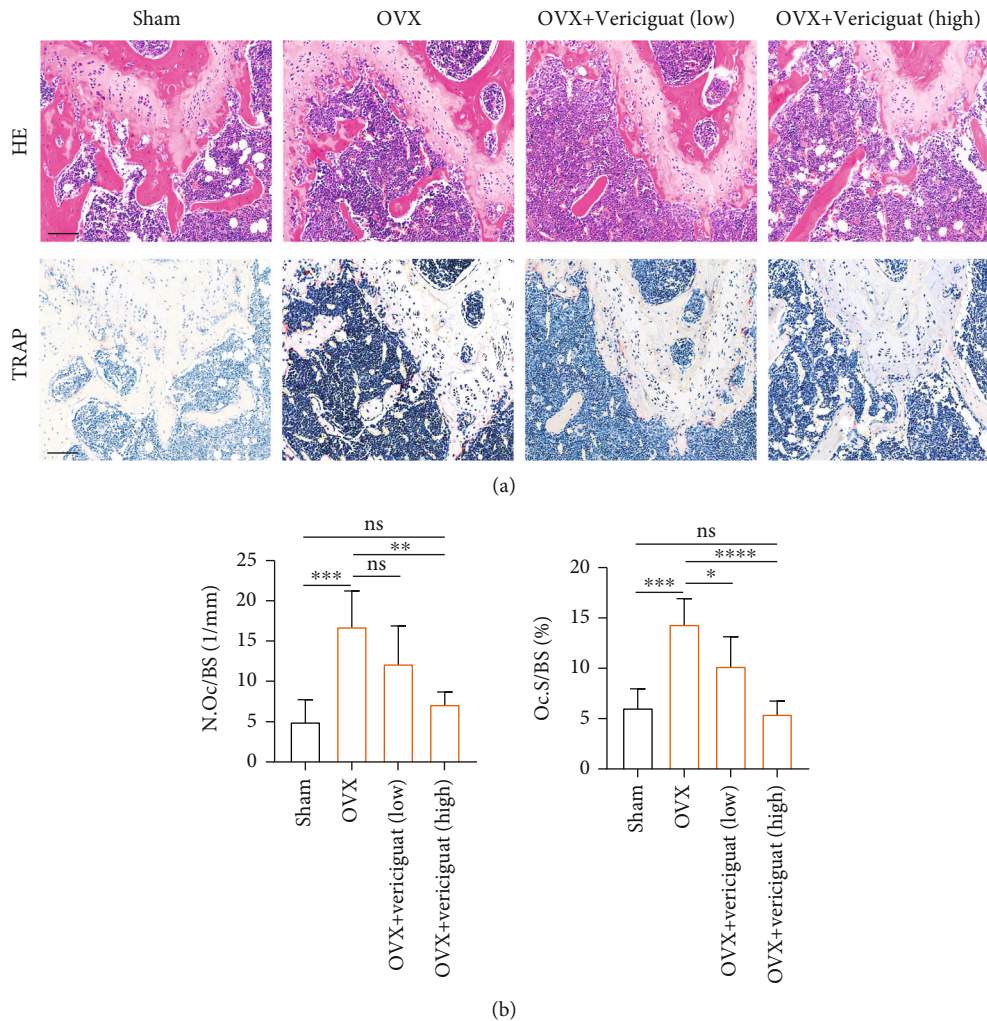
(a)

(b)

FIGURE 10: Validation of the effects of Vericiguat on OVX-induced bone loss in vivo indicated by histological analysis. (a) Representative images of H&E staining and TRAP staining within the selected metaphyseal region from the sham group, OVX group, low-dose group, and high-dose group ($n = 5$). (b) The number and area of TRAP$^+$ cells per bone surface were quantified. $^*p < 0.05$, $^{**}p < 0.01$, $^{***}p < 0.001$, and $^{****}p < 0.0001$. Scale bar = 100 μm.

Secondly, cinaciguat can be orally absorbed, but they chose ip injection. Thirdly, they did not perform the in vitro experiment regarding OCs. In addition, the abnormally high standard deviation regarding the number of OCs and eroded surface may also affect the real statistical results. Therefore, the exact mechanism of SC activators on OCs needs further investigation. In this present in vitro study, we found that Vericiguat could enhance RANKL-induced formation of functional OC under low concentration, whereas this effect was converted to inhibitory effect when BMMs were cocultured with Vericiguat at high concentration. What is more, Vericiguat also had dually regulatory effects on the RANKL-induced bone-resorbing ability. Collectively, these results suggested that Vericiguat dually regulated OC differentiation and bony resorption in mouse BMMs.

After RANKL binding to its receptor RANK on pre-OCs, RANKL would activate nuclear receptor NFATc1 and c-Fos [7]. NFATc1 has been one of the critical transcriptional regulators for RANKL-mediated OC differentiation [33]. After activation, NFATc1 will translocate into the nucleus and induce the expression of OC-specific genes, including DC-STAMP, TRAP, CTSK, and CTR [4, 34]. Our study suggested that Vericiguat dually regulated RANKL-induced expression of NFATc1 and its nuclear translocation during OC differentiation. In addition, the similar tendency regarding the mRNA expression changes of OC-specific genes (DC-STAMP, TRAP, CTSK, and CTR) also confirmed the bidirectional regulatory effects of Vericiguat on osteoclastogenesis. During osteoclastogenesis, c-Fos is also an essential mediator for osteoclastogenesis [4, 34]. Meanwhile, c-Fos is also involved in regulating the partial function of NFATc1 [4, 34]. In this present study, Vericiguat showed similar regulatory effects on RANKL-triggered expression of c-Fos under both mRNA and protein levels. Taken together, the results above indicated the dual effects of Vericiguat on RANKL-induced mature OC formation by regulating the transcriptional activity of c-Fos and NFATc1 and downstream critical OC-related gene expression.

During OC differentiation, NF-κB, MAPK (ERK, p38, and JNK), and AKT signaling pathways are critically

activated after RANKL stimulation [7]. Interestingly, in this present study, we found that Vericiguat dually regulated the phosphorylation of NF-κB and the nuclear translocation of p65 in a dosage-dependent manner, without affecting MAPK and AKT signaling pathways. sGC activators could increase the amount pf sGC, which would excessively induce the activation of the VASP [18]. To further expound the potential regulatory mechanism through which Vericiguat regulated the NF-κB pathway, we found increasing expression of VASP induced by either Vericiguat only or RANKL in a dose-dependent manner. Furthermore, in vitro experiment suggested that VASP was essential to OC differentiation, consistent with a recent study from Hu et al. [35]. Additionally, we found that Vericiguat only could also dually regulate the activation of NF-κB. However, the promotive effect of Vericiguat on the expression of p-p65 was blocked by knocking down VASP, indicating that VASP may participate in OC differentiation via increasing the activation of the NF-κB signaling cascade. However, with the increasing dose of Vericiguat imposed on BMMs, this promotive effect was missing. The results of molecular modeling experiments confirmed our hypothesis that high-dose Vericiguat may directly disturb the activation of the NF-κB signaling cascade. In fact, Flores-Costa et al. reported that another sGC stimulator, praliciguat, could also reduce the phosphorylation of IκB and NF-κB to exert anti-inflammatory effect [35]. We deduced that Vericiguat may dominantly activate the sGC/VASP/IκB-α/NF-κB signaling pathway at low concentration. Nevertheless, with the increasing dose imposed on BMMs, Vericiguat would directly bind to IKKβ to suppress nuclear factor-κB (NF-κB) activity. Thus, a delight balance between the IκB-α/NF-κB signaling pathway and sGC/cGMP/VASP may exist.

Despite these promising results above, there are several limitations in this present study. Firstly, this present study demonstrated the dual effects of Vericiguat on osteoclastogenesis, which was inconsistent with most of previous studies that NO/sGC/cGMP inhibits OC differentiation and maturation. We proposed a delight balance between the IκB-α/NF-κB signaling pathway and sGC/cGMP/VASP. At low concentration, the enhanced effect of RANKL-induced osteoclastogenesis by Vericiguat may be associated with the activated VASP/IκB-α/NF-κB signaling pathway. However, with the increasing concentration of Vericiguat, the direct inhibition of the IκB-α/NF-κB signaling pathway would dominantly counteract the promoting effect of VASP on the IκB-α/NF-κB signaling pathway and suppress osteoclastogenesis. However, the exact mechanism of Vericiguat on OC differentiation needs further investigation. Secondly, bone loss in vivo is a complex biological process related to various factors, such as estrogen deficiency, inflammatory condition, or aging [36–38]. We only used one model in this present study and confirmed the protective effect of Vericiguat on OVX-induced bone loss at a high dose. However, the promotive OC differentiation of low-concentration Vericiguat in vitro was not validated in vivo. Therefore, more bone loss model in vivo experiment will be required to confirm the dual effects of Vericiguat on bone loss, such as the LPS-induced inflammatory bone loss model. Thirdly, OBs

also play a critical role in bone metabolism. Therefore, the biological effects of Vericiguat on OBs in vitro and in vivo also need to be explored, although other sGC activator, such as cinaciguat, has been reported to increase the proliferation, differentiation, and survival of OBs [11]. Our study will further focus on the effect of Vericiguat on OB differentiation both in vivo and in vitro.

In conclusion, our present study demonstrated the dual effects of Vericiguat on the formation of functional OCs in a concentration-dependent manner. The regulatory effect of Vericiguat on OCs was achieved by the bidirectional activation of the IκB-α/NF-κB signaling pathway, and a potential balance between the IκB-α/NF-κB signaling pathway and sGC/cGMP/VASP may exist. However, the exact mechanism of Vericiguat on OC differentiation both in vitro and in vivo needs further investigation.

Data Availability

Data will be available when requested.

Disclosure

A preprint has previously been published with the link as follows: https://www.preprints.org/manuscript/202109.0151/v1 [39]. However, the content has been further improved in this submission.

Conflicts of Interest

All authors have disclosed no any financial and personal relationships with other people or organizations in this study.

Authors' Contributions

Kaiqiang Sun, Fanqi Kong, and Feng Lin contributed equally to this study and should be considered as co-first authors.

Acknowledgments

References

[1] R. Eastell and P. Szulc, "Use of bone turnover markers in postmenopausal osteoporosis," The Lancet Diabetes and Endocrinology, vol. 5, no. 11, pp. 908–923, 2017.

[2] J. He, X. Li, Z. Wang et al., "Therapeutic anabolic and anticatabolic benefits of natural Chinese medicines for the treatment of osteoporosis," Frontiers in Pharmacology, vol. 10, p. 1344, 2019.

[3] M. Asagiri and H. Takayanagi, "The molecular understanding of osteoclast differentiation," Bone, vol. 40, no. 2, pp. 251–264, 2007.

[4] W. J. Boyle, W. S. Simonet, and D. L. Lacey, "Osteoclast differentiation and activation," Nature, vol. 423, no. 6937, pp. 337–342, 2003.

[5] B. J. Kim, Y. S. Lee, S. Y. Lee et al., "Osteoclast-secreted SLIT3 coordinates bone resorption and formation," *The Journal of Clinical Investigation*, vol. 128, no. 4, pp. 1429–1441, 2018.

[6] H. S. Kim, S. T. Nam, S. H. Mun et al., "DJ-1 controls bone homeostasis through the regulation of osteoclast differentiation," *Nature Communications*, vol. 8, no. 1, p. 1519, 2017.

[7] D. S. Győri and A. Mócsai, "Osteoclast signal transduction during bone metastasis formation," *Frontiers in Cell and Development Biology*, vol. 8, p. 507, 2020.

[8] H. Rangaswami, R. Schwappacher, N. Marathe et al., "Cyclic GMP and protein kinase G control a Src-containing mechanosome in osteoblasts," *Science Signaling*, vol. 3, no. 153, p. ra91, 2010.

[9] B. B. Yaroslavskiy, Y. Zhang, S. E. Kalla et al., "NO-dependent osteoclast motility: reliance on cGMP-dependent protein kinase I and VASP," *Journal of Cell Science*, vol. 118, no. 23, pp. 5479–5487, 2005.

[10] J. D. Parker, "Nitrate tolerance, oxidative stress, and mitochondrial function: another worrisome chapter on the effects of organic nitrates," *The Journal of Clinical Investigation*, vol. 113, no. 3, pp. 352–354, 2004.

[11] J. Joshua, G. K. Schwaerzer, H. Kalyanaraman et al., "Soluble guanylate cyclase as a novel treatment target for osteoporosis," *Endocrinology*, vol. 155, no. 12, pp. 4720–4730, 2014.

[12] Y. Korkmaz, B. Puladi, K. Galler et al., "Inflammation in the human periodontium induces downregulation of the α1- and β1-subunits of the sGC in cementoclasts," *International Journal of Molecular Sciences*, vol. 22, no. 2, p. 539, 2021.

[13] M. Gheorghiade, S. J. Greene, J. Butler et al., "Effect of vericiguat, a soluble guanylate cyclase stimulator, on natriuretic peptide levels in patients with worsening chronic heart failure and reduced ejection fraction: the SOCRATES-REDUCED randomized trial," *Journal of the American Medical Association*, vol. 314, no. 21, pp. 2251–2262, 2015.

[14] P. W. Armstrong, B. Pieske, K. J. Anstrom et al., "Vericiguat in patients with heart failure and reduced ejection fraction," *The New England Journal of Medicine*, vol. 382, no. 20, pp. 1883–1893, 2020.

[15] K. Sun, J. Zhu, Y. Deng et al., "Gamabufotalin inhibits osteoclastgenesis and counteracts estrogen-deficient bone loss in mice by suppressing RANKL-induced NF-κB and ERK/MAPK pathways," *Frontiers in Pharmacology*, vol. 12, article 629968, 2021.

[16] W. F. Chiou, J. F. Liao, C. Y. Huang, and C. C. Chen, "2-Methoxystypandrone represses RANKL-mediated osteoclastogenesis by down-regulating formation of TRAF6–TAK1 signalling complexes," *British Journal of Pharmacology*, vol. 161, no. 2, pp. 321–335, 2010.

[17] Y. Jang, H. M. Sohn, Y. J. Ko, H. Hyun, and W. Lim, "Inhibition of RANKL-induced osteoclastogenesis by novel mutant RANKL," *International Journal of Molecular Sciences*, vol. 22, no. 1, p. 434, 2021.

[18] R. Flores-Costa, M. Duran-Güell, M. Casulleras et al., "Stimulation of soluble guanylate cyclase exerts antiinflammatory actions in the liver through a VASP/NF-κB/NLRP3 inflammasome circuit," *Proceedings of the National Academy of Sciences of the United States of America*, vol. 117, no. 45, pp. 28263–28274, 2020.

[19] J. McHugh, "Regulating the osteoclast workforce," *Nature Reviews Rheumatology*, vol. 13, no. 9, p. 514, 2017.

[20] D. Kurotaki, H. Yoshida, and T. Tamura, "Epigenetic and transcriptional regulation of osteoclast differentiation," *Bone*, vol. 138, article 115471, 2020.

[21] H. Kitaura, A. Marahleh, F. Ohori et al., "Osteocyte-related cytokines regulate osteoclast formation and bone resorption," *International Journal of Molecular Sciences*, vol. 21, no. 14, p. 5169, 2020.

[22] C. Liao, T. Cheng, S. Wang, C. Zhang, L. Jin, and Y. Yang, "Shear stress inhibits IL-17A-mediated induction of osteoclastogenesis via osteocyte pathways," *Bone*, vol. 101, pp. 10–20, 2017.

[23] M. Zhao, J. Liu, X. Zhang, L. Peng, C. Li, and S. Peng, "3D QSAR of novel estrogen-RGD peptide conjugates: getting insight into structural dependence of anti-osteoporosis activity and side effect of estrogen in ERT," *Bioorganic & Medicinal Chemistry*, vol. 17, no. 10, pp. 3680–3689, 2009.

[24] C. A. McHorney, J. T. Schousboe, R. R. Cline, and T. W. Weiss, "The impact of osteoporosis medication beliefs and side-effect experiences on non-adherence to oral bisphosphonates," *Current Medical Research and Opinion*, vol. 23, no. 12, pp. 3137–3152, 2007.

[25] A. S. Tarnawski and T. C. Caves, "Aspirin in the XXI century: its major clinical impact, novel mechanisms of action, and new safer formulations," *Gastroenterology*, vol. 127, no. 1, pp. 341–343, 2004.

[26] X. Lu, W. He, W. Yang et al., "Dual effects of baicalin on osteoclast differentiation and bone resorption," *Journal of Cellular and Molecular Medicine*, vol. 22, no. 10, pp. 5029–5039, 2018.

[27] Y. Korkmaz, M. A. Baumann, H. Schröder et al., "Localization of the NO-cGMP signaling pathway molecules, NOS III-phosphorylation sites, ERK1/2, and Akt/PKB in osteoclasts," *Journal of Periodontology*, vol. 75, no. 8, pp. 1119–1125, 2004.

[28] H. Kalyanaraman, N. Schall, and R. B. Pilz, "Nitric oxide and cyclic GMP functions in bone," *Nitric Oxide*, vol. 76, pp. 62–70, 2018.

[29] D. Nilforoushan, A. Gramoun, M. Glogauer, and M. F. Manolson, "Nitric oxide enhances osteoclastogenesis possibly by mediating cell fusion," *Nitric Oxide*, vol. 21, no. 1, pp. 27–36, 2009.

[30] J. Zhang, C. Ding, X. Meng, and P. Shang, "Nitric oxide modulates the responses of osteoclast formation to static magnetic fields," *Electromagnetic Biology and Medicine*, vol. 37, no. 1, pp. 23–34, 2018.

[31] B. L. Homer, D. Morton, C. M. Bagi et al., "Oral administration of soluble guanylate cyclase agonists to rats results in osteoclastic bone resorption and remodeling with new bone formation in the appendicular and axial skeleton," *Toxicologic Pathology*, vol. 43, no. 3, pp. 411–423, 2015.

[32] Y. Reinke, S. Gross, L. G. Eckerle et al., "The soluble guanylate cyclase stimulator riociguat and the soluble guanylate cyclase activator cinaciguat exert no direct effects on contractility and relaxation of cardiac myocytes from normal rats," *European Journal of Pharmacology*, vol. 767, pp. 1–9, 2015.

[33] H. Takayanagi, S. Kim, K. Matsuo et al., "RANKL maintains bone homeostasis through c-Fos-dependent induction of interferon-β," *Nature*, vol. 416, no. 6882, pp. 744–749, 2002.

[34] Y. Han, X. You, W. Xing, Z. Zhang, and W. Zou, "Paracrine and endocrine actions of bone–the functions of secretory proteins from osteoblasts, osteocytes, and osteoclasts," *Bone Res.*, vol. 6, no. 1, p. 16, 2018.

[35] H. Hu, C. Li, H. Zhang, G. Wu, and Y. Huang, "Role of vasodilator-stimulated phosphoprotein in RANKL-differentiated murine macrophage RAW264.7 cells: modulation of NF-κB, c-Fos and NFATc1 transcription factors," *Experimental and Therapeutic Medicine*, vol. 21, no. 5, p. 412, 2021.

[36] D. M. Black and C. J. Rosen, "Postmenopausal osteoporosis," *The New England Journal of Medicine*, vol. 374, no. 3, pp. 254–262, 2016.

[37] K. M. Prestwood, C. C. Pilbeam, and L. G. Raisz, "Treatment of osteoporosis," *Annual Review of Medicine*, vol. 46, no. 1, pp. 249–256, 1995.

[38] A. Qadir, S. Liang, Z. Wu, Z. Chen, L. Hu, and A. Qian, "Senile osteoporosis: the involvement of differentiation and senescence of bone marrow stromal cells," *International Journal of Molecular Sciences*, vol. 21, no. 1, p. 349, 2020.

[39] K. Sun, F. Kong, F. Lin et al., "Dual effects of vericiguat on osteoclast differentiation and bone resorption via a balance between VASP and NF-kappaB pathways," Link: https://www.preprints.org/manuscript/202109.0151/v1.